Biophysikalische und molekulare Grundlagen der Regulation des Kaliumtransports in Pflanzen

Habilitationsschrift

eingereicht an der

Mathematisch-Naturwissenschaftlichen Fakultät

der Universität Potsdam

zur Erlangung der Venia Legendi im Fach

Biophysik und Molekulare Pflanzenphysiologie

von

Dr. Ingo Dreyer

Institut für Biochemie und Biologie, Abteilung Molekularbiologie

Potsdam, Dezember 2005

Inhaltsverzeichnis

Abbildungsverzeichnis

Hinweis

Die im folgenden in **Fettdruck** zitierten Literaturangaben beziehen sich auf Artikel mit eigener Beteiligung. Die Artikel sind im Anhang beigefügt.

Zusammenfassung

Kaliumionen (K^+) sind die am häufigsten vorkommenden anorganischen Kationen in Pflanzen. Gemessen am Trockengewicht kann ihr Anteil bis zu 10% ausmachen. Kaliumionen übernehmen wichtige Funktionen in verschiedenen Prozessen in der Pflanze. So sind sie z.B. essentiell für das Wachstum und für den Stoffwechsel. Viele wichtige Enzyme arbeiten optimal bei einer K^+ Konzentration im Bereich von 100 mM. Aus diesem Grund halten Pflanzenzellen in ihren Kompartimenten, die am Stoffwechsel beteiligt sind, eine kontrollierte Kaliumkonzentration von etwa 100 mM aufrecht.

Die Aufnahme von Kaliumionen aus dem Erdreich und deren Transport innerhalb der Pflanze und innerhalb einer Pflanzenzelle wird durch verschiedene Kaliumtransportproteine ermöglicht. Die Aufrechterhaltung einer stabilen K^+ Konzentration ist jedoch nur möglich, wenn die Aktivität dieser Transportproteine einer strikten Kontrolle unterliegt. Die Prozesse, die die Transportproteine regulieren, sind bis heute nur ansatzweise verstanden. Detailliertere Kenntnisse auf diesem Gebiet sind aber von zentraler Bedeutung für das Verständnis der Integration der Transportproteine in das komplexe System des pflanzlichen Organismus.

In dieser Habilitationsschrift werden eigene Publikationen zusammenfassend dargestellt, in denen die Untersuchungen verschiedener Regulationsmechanismen pflanzlicher Kaliumkanäle beschrieben werden. Diese Untersuchungen umfassen ein Spektrum aus verschiedenen proteinbiochemischen, biophysikalischen und pflanzenphysiologischen Analysen. Um die Regulationsmechanismen grundlegend zu verstehen, werden zum einen ihre strukturellen und molekularen Besonderheiten untersucht. Zum anderen werden die biophysikalischen und reaktionskinetischen Zusammenhänge der Regulationsmechanismen analysiert. Die gewonnenen Erkenntnisse erlauben eine neue, detailliertere Interpretation der physiologischen Rolle der Kaliumtransportproteine in der Pflanze.

Woher bekommen Pflanzen ihre Masse?

Diese Frage beschäftigte die Naturforscher im 17. und 18. Jahrhundert. Ausgehend von verschiedenen Experimenten wuchs die Erkenntnis, dass Pflanzen von ihrer Umgebung abhängig sind. Für das Pflanzenwachstum werden sowohl Wasser als auch das umgebende Erdreich benötigt, das die Pflanzen mit essentiellen Nährstoffen versorgt. Darüber hinaus ist auch der Gasaustausch mit der Atmosphäre von entscheidender Wichtigkeit (Blatt, 2004b). Da Pflanzen nicht von einem ungünstigen Standort an einen anderen Ort wechseln können, der bessere Bedingungen für ihr Wachstum und Überleben bietet, müssen sie deshalb sehr flexibel auf Änderungen in ihrer Umgebung reagieren können. Im speziellen die Mechanismen der Nährstoffversorgung müssen sich an die jeweiligen Bedingungen anpassen. Seit dem 19. Jahrhundert wird die Nährstoffaufnahme und der Nährstofftransport in Pflanzen systematisch untersucht (von Liebig, 1840). Die Erkenntnisse, die an Pflanzen gewonnen wurden, inspirierte die Forscher im Verlauf des letzten Jahrhunderts, ihre Untersuchungen von Transportprozessen auch auf andere Organismen (Algen, Bakterien, Vertebrate und Invertebrate) auszuweiten.

Transportprozesse sind Grundlage des Lebens

Ein charakteristisches Merkmal aller lebender Organismen ist der Transport diverser verschiedenartiger organischer und anorganischer Moleküle über biologische Membranen. Diese Transportprozesse sind integriert in sehr unterschiedliche biologische Abläufe. Sie erlauben es erst den Zellen, mit ihrer Umgebung in Wechselwirkung zu treten. Transportprozesse dienen unter anderem der Ernährung, der Entgiftung und dem Austausch elektrischer und chemischer Signale.

Jede Zelle ist von einer Lipiddoppelschicht, der Zellmembran, umgeben. Diese stellt in der Regel eine Diffusionsbarriere für geladene oder polare Moleküle und Ionen dar. Den Transport dieser Substanzen über die Diffusionsbarriere übernehmen zum größten Teil[1] transmembrane Proteine, die in die Membran eingebettet sind und in der

[1] Neben dem transmembranen Transport, der durch integrale Membranproteine ermöglicht wird, können Zellen auch unter gewissen Bedingungen Stoffe mittels Exo- und Endozytose über die Diffusionsbarriere transportieren. Der massgebliche Einfluss der Exo- und Endozytose auf den Membrantransport besteht jedoch im kontrollierten Einbau von Transportproteinen in die Membran (Hurst et al., 2004).

Regel selektiv die Permeation von Teilchen einer bestimmte Substanzklasse gestatten. Die Regulation der Transportproteine erlaubt es den Zellen, transmembrane Konzentrationsgradienten zu etablieren und damit die Zusammensetzung des zellulären Milieus zu steuern.

Diese Zusammenhänge zeigen, dass das Verständnis biologischer Abläufe untrennbar mit dem umfassenden Verständnis zellulärer Transportphänomene verknüpft ist. Daher ist es von großer Bedeutung in der modernen Biologie, die molekulare Struktur eines Transportproteins aufzuklären, das Expressionsmusters seines Gens zu analysieren, seine physiologischen Funktion zu eruieren und seine Rolle in Stoffwechselwegen und in Signalkaskaden zu erforschen.

Membrantransport aus biophysikalischer Sicht

Die Aufnahme von Nährstoffen durch einzelne Zellen und deren Weiterleitung in einem Zellverbund ist in der Regel kein Vorgang, der spontan abläuft. Aus diesem Grund ist es sinnvoll, Transportprozesse an biologischen Membranen etwas genauer aus physikalischer Sicht zu betrachten.

Transportprozesse sind immer Ausgleichsprozesse, ganz gleich ob sie in einem lebenden System oder in toter Materie stattfinden. Die Grundvoraussetzung für einen Transport ist ein Potentialgradient. Dies kann z.B. ein Gradient im chemischen Potential, ein Gradient im elektrischen Potential, ein Druckgradient, oder ein Temperaturgradient sein. In Pflanzen spielen diese exemplarisch angeführten Gradienten die größte Bedeutung.

Der einfachste Transportprozess in lebenden Systemen oder in toter Materie ist die **Diffusion**. Durch Diffusion werden Konzentrationsgradienten ausgeglichen. Wie bereits erwähnt, ist die Zellmembran eine Diffusionsbarriere. Erst sie ermöglicht es den Zellen, - der Diffusion entgegengerichtet - unter Energieaufwand Konzentrationsgradienten aufzubauen.

Eine fundamentale Voraussetzung für den Aufbau von Konzentrationsgradienten ist die Energieumwandlung. Die Energie chemischer Verbindungen, die entweder über die Nahrung aufgenommen werden oder im Falle von photoautotrophen Organismen unter Ausnutzung der solare Strahlungsenergie synthetisiert werden, kann genutzt werden, um **aktive Transportprozesse** zu energetisieren. In Pflanzen zum Beispiel nutzen Protonenpumpen (H^+-ATPasen) die Energie aus der Hydrolyse von

Adenosintriphosphat (ATP) zu Adenosindiphosphat (ADP)[2], um Protonen aus dem Zytosol in den Extrazellulärraum oder in die Vakuole zu transportieren. Als Folge entsteht über die verschiedenen Membranen sowohl ein chemischer Protonengradient als auch ein elektrischer Gradient. Diese Gradienten können wiederum durch andere Transporterproteine genutzt werden, um ihrerseits andere Substanzen über die Membran zu transportieren. Das kann zum einen in einem gekoppelten Transport geschehen, zum anderen in einem passiven Transport. Der **gekoppelte Transport** verknüpft den Transport einer Substanz entgegen eines Potentialgradienten mit dem gleichzeitigen energieliefernden Transport einer anderen Substanz entlang ihres Potentialgradienten (z.B. Zucker-Protonen Symport über die Plasmamembran; Bush, 2004; oder Kalzium-Proton Antiport über die Vakuolenmembran; Hawkesford und Miller, 2004). Der **passive Transport** erfolgt durch Kanäle. Diese Membranproteine sind nur für bestimmte Substanzen permeabel und erleichtern dadurch die selektive Diffusion einzelner Substanzen. Handelt es sich bei den transportierten Substanzen um Ionen, so erfolgt der Transport nicht entlang der chemischen Gradienten dieser Substanzen sondern entlang der elektrochemischen Gradienten. In diesem Fall ist der transmembrane elektrische Potentialgradient (die Membranspannung) dem chemischen Gradienten überlagert und kann diesen unter bestimmten Bedingungen auch kompensieren. Dadurch ist es zum Beispiel einer Pflanzenzelle möglich, Kaliumionen über Kaliumkanäle aufzunehmen, obwohl die K^+ Konzentration in der Zelle größer ist als außerhalb.

Transportproteine in Pflanzen

In Pflanzen wurden Transportproteine für alle oben genannten Transportarten nachgewiesen (**Amtmann et al., 2004a**). Technische Entwicklungen - vor allem in den Bereichen Optik und Elektronik - ermöglichten im Laufe des vergangenen Jahrhunderts eine immer genauere Charakterisierung der Transporteigenschaften verschiedener pflanzlicher Transportproteine *in vivo*. Einen besonderen Schub an neuen und detaillierten Einsichten in die Biologie des Stofftransports in Pflanzen brachten aber vor allem die letzten 15 Jahre. Wie die meisten anderen Bereiche der Biologie wurde auch

[2] Neben H^+-ATPasen wurde in der Vakuole von Pflanzenzellen eine Protonen Pyrophosphatase identifiziert, die die Energie der Hydrolyse von Pyrophosphat zu Orthophosphat zum Transport von Protonen aus dem Zytosol ins Lumen der Vakuole nutzt (Sarafian et al., 1992; Übersicht in López-Maqués et al., 2004).

das Gebiet der Pflanzenwissenschaften durch die Entwicklung und Nutzung molekularbiologischer Techniken revolutioniert. Molekulargenetische Ansätze ermöglichten es erstmals, einzelne Transporter aus dem komplizierten Netzwerk der ganzen Pflanze zu separieren, um sie detailliert in Isolation zu studieren.

Die Klonierung pflanzlicher Gene und der zugehörigen cDNA ermöglichte es, pflanzliche Proteine in heterologen Expressionssystemen zu exprimieren (z.B. in *Escherichia coli*, Hefe, *Xenopus* Oozyten, Insektenzelllinien, Säugetierzelllinien; Details in **Dreyer et al., 1999**). Zunächst beschränkte sich die Analyse auf Transportproteine, die strukturell ähnlich waren zu bekannten Transportproteinen aus anderen Organismen, oder auf Transportproteine, die aufgrund ihrer Funktion isoliert wurden (**Dreyer et al., 1999**). Seit dem Jahr 2000 ist jedoch die komplette Sequenz des Genoms der Modellpflanze *Arabidopsis thaliana* verfügbar (Arabidopsis Genome Initiative, 2000) und somit für bioinformatorische Analysen zugänglich.

Ungefähr 20 % aller Protein-kodierenden Gene des *Arabidopsis* Genoms kodieren für Proteine mit zwei oder mehr transmembranen Domänen (**Dreyer et al., 2002**). Etwa ein Viertel dieser Proteine sind sehr wahrscheinlich Transportproteine. Anhand von Sequenzhomologien zu anderen, bereits bekannten Transportern aus Pflanzen oder Tieren können die vorhergesagten Gene, die vermutlich für ähnliche Transportproteine kodieren, klassifiziert werden (Maser et al., 2001; Ward, 2001). Die Ergebnisse dieser bioinformatorischen Analysen sind mittlerweile in diversen Datenbanken zusammengefasst (siehe z.B. **Dreyer et al., 2002**, für eine - nicht vollständige - Übersicht).

Kaliumtransport in Pflanzen

Kaliumionen (K^+) sind die am häufigsten vorkommenden anorganischen Kationen in Pflanzen. Gemessen am Trockengewicht kann ihr Anteil bis zu 10% ausmachen (Leigh und Wyn Jones, 1984). Kaliumionen haben essentielle Funktionen im Metabolismus, im Wachstum und in der Stressadaptation. Eine relativ hohe und stabile Kaliumkonzentration in bestimmten zellulären Kompartimenten ist wichtig für die Enzymaktivierung, Stabilisierung der Proteinsynthese, Neutralisierung negativer Ladungen an Proteinen und Aufrechterhaltung der zellulären pH Homöostase (Marschner, 1995). Die optimale K^+ Konzentration für Enzymaktivierung und Proteinsynthese liegt im Bereich von 100 mM (Wyn Jones und Pollard, 1983). Dies

bedeutet, dass für eine optimale metabolische Aktivität die Zellen eine kontrollierte Kaliumkonzentration von etwa 100 mM in den metabolisch aktiven Kompartimenten (Zytosol, Nucleus, Stroma des Chloroplasten und in der Matrix der Mitonchondrien) aufrechterhalten müssen.

Weiterhin nutzen Pflanzen die hohe Mobilität der K^+-Ionen. Dies wird besonders in schnellen osmotischen Prozessen deutlich: z.B. der Stomabewegung, dem Phototropismus, dem Gravitropismus oder dem Streckungswachstum. Hierbei werden K^+-Ionen zusammen mit Anionen (zur Ladungskompensation) in den Vakuolen akkumuliert. Das passiv nachströmenden Wasser erzeugt einen osmotischen und hydrostatischen Druck, der die Zellausdehnung bewirkt. Experimente haben gezeigt, dass K^+ in dieser Funktion nur durch wenige andere, ebenfalls hoch mobile Ionen (z.B. Na^+) ersetzt werden kann (Reckmann et al., 1990). Wenn das Streckungswachstum zum Stillstand gekommen ist, kann das osmotische Potential auch durch weniger mobile Substanzen, wie z.B. Zucker, aufrechterhalten werden. Die dadurch nicht mehr in großem Umfang benötigten K^+ Ionen können z.T. aus den Vakuolen zurückgewonnen werden und stehen damit der Pflanze für andere Prozesse (z.B. im Phloemtransport) zur Verfügung (Amtmann et al., 2004b).

Die genannten Beispiele verdeutlichen, dass die Kaliumhomöostase (= Aufrechterhaltung eines dynamischen Gleichgewichts in der K^+ Konzentration) für

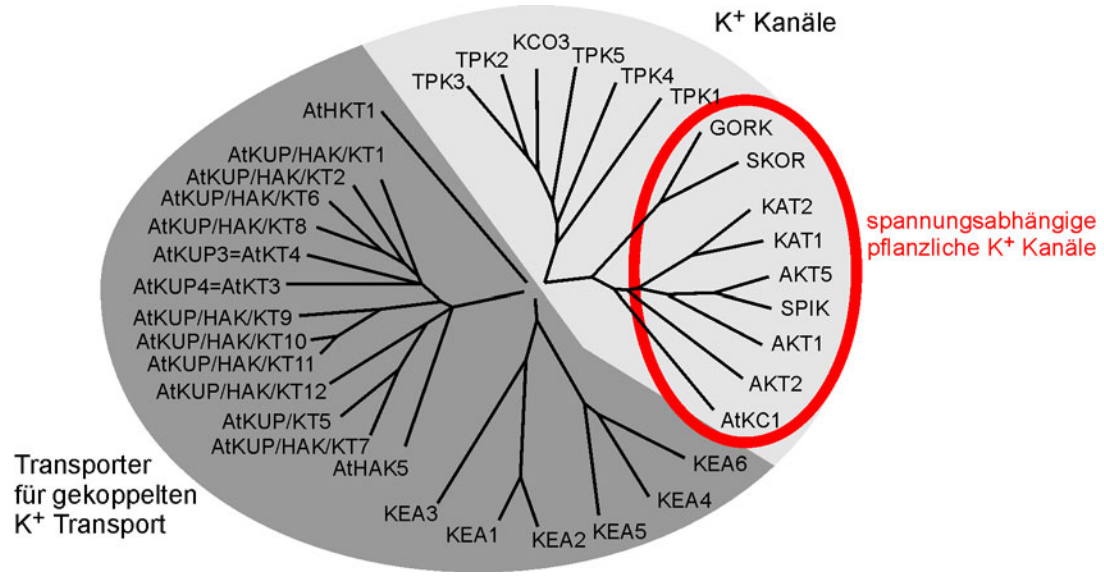

Abbildung 1. Kaliumtransportproteine in *Arabidopsis thaliana*.
Das Genom der Modellpflanze Arabidopsis thaliana enthält mindestens 35 Gene, die für (putative) K^+ Transportproteine kodieren. Diese Proteine vermitteln entweder einen gekoppelten K^+ Transport (dunkelgrau unterlegt) oder einen passiven K^+ Transport (K^+ Kanäle; hellgrau unterlegt). In der Klasse der Kaliumkanäle ist die Gruppe der spannungsabhängigen K^+ Kanäle noch besonders hervorgehoben. [Abbildung nach Maser et al. (2001)].

Pflanzen von zentraler Bedeutung ist. Aus diesem Grund ist es auch nicht verwunderlich, dass z.B. in der Modellpflanze *Arabidopsis thaliana* mindestens 35 Gene für Kaliumtransportproteine kodieren (Maser et al., 2001). Die Klassifizierung anhand struktureller Ähnlichkeiten zu bekannten Transportern ergab, dass die pflanzlichen K^+ Transportproteine zum einen den gekoppelten K^+ Transport ermöglichen (z.B. H^+/K^+ Symport, K^+/Na^+ Symport, H^+/K^+ Antiport; 20 Gene) zum anderen den passiven K^+ Transport (K^+ Kanäle; 15 Gene) (Abbildung 1).

In dieser Habilitationsschrift werden Arbeiten zur Gruppe der spannungsabhängigen pflanzlichen Kaliumkanäle vorgestellt (Abbildung 1, rote Markierung). Alle bislang untersuchten Kanäle dieses Typs sind in die Plasmamembran integriert und sind an der Steuerung des Kaliumtransports in die Zelle hinein und aus der Zelle heraus beteiligt.

Spannungsregulierte Kaliumkanäle in Pflanzen

Die ersten pflanzlichen Kaliumkanalgene wurden 1992 kloniert. Auf der Suche nach pflanzlichen Kaliumtransportern wurden cDNA-Bibliotheken aus *Arabidopsis thaliana* in mutierten Stämmen der Hefe *Saccharomyces cerevisiae* exprimiert. In diesen Hefen wurden die endogenen Kaliumaufnahmesysteme gezielt deletiert, so dass die Stämme nicht mehr auf Nährmedien wachsen konnten, die weniger als 1 mM K^+ enthielten. Zwei verschiedenen Arbeitsgruppen gelang es, zwei cDNA-Klone zu isolieren, die es den mutierten Hefen erlaubten, auch auf Medien mit niedriger K^+-Konzentration zu wachsen (Anderson et al., 1992; Sentenac et al., 1992). Diese cDNA-Klone kodierten die spannungsregulierten, *Shaker*-ähnlichen Kaliumkanäle AKT1 und KAT1.

Spannungsregulierte Kaliumkanäle in Pflanzen zeigen große Ähnlichkeit zu tierischen Kaliumkanälen der so genannten *Shaker* Superfamilie, deren Namensgebung auf die ersten molekular identifizierten Kaliumkanäle aus der Taufliege *Drosophila melanogaster* zurückgeht. Der *Shaker* locus in *Drosophila* kodiert für eine Gruppe spannungsregulierter Kaliumkanäle (Kamb et al., 1987; Papazian et al., 1987; Tempel et al., 1987; Iverson et al., 1988; Kamb et al., 1988; Pongs et al., 1988; Schwarz et al., 1988; Timpe et al., 1988a; Timpe et al., 1988b). Jüngste Kristallstrukturanalysen zeigten, dass spannungsregulierte Ionenkanäle von Prokaryoten und Eukaryoten große strukturelle Gemeinsamkeiten aufweisen (Jiang et al., 2003; Long et al., 2005a). Dies lässt darauf schließen, dass sich die grundlegende Struktur, die für die

spannungsabhängige Regulation verantwortlich ist, bereits vor mehr als 2 Milliarden Jahren entwickelt hat.

Kanäle der Superfamilie spannungsregulierter Kaliumkanäle besitzen eine tetramere Struktur (Abbildung 2A), wobei jede der vier Untereinheiten ein membranständiges Polypeptid ist. Eine Untereinheit besteht aus 6 transmembranspannenden Domänen (S1-S6) und einer amphiphilen Verbindungsdomäne P zwischen S5 und S6 (Uozumi et al., 1998) (Abbildung 2B). Die S5-P-S6 Bereiche der vier Untereinheiten sind so angeordnet, dass sie einen hydrophilen Permeationsweg durch die hydrophobe Membran bilden. Die amphiphile Verbindungsdomäne P verengt den Permeationsweg im Zytosol-abgewandten Drittel und das universelle Motiv TXXTXGYG des Selektivitätsfilters (Heginbotham et al., 1994) an der engsten Stelle ist verantwortlich für die Kaliumselektivität des Kanals (Uozumi et al., 1995; **Becker et al., 1996**; Nakamura et al., 1997; **Dreyer et al., 1998**) (Abbildung 3). Kristallstrukturanalysen am bakteriellen Kaliumkanal KcsA konnten zeigen, dass an dieser Engstelle die acht Wassermoleküle der inneren Hydrathülle des Kaliumions durch den polaren Sauerstoff des Peptidrückgrads der Aminosäuren TVGYG ersetzt werden (Abbildung 3C) (Doyle et al., 1998). Der Ersetzungsmechanismus erlaubt das Abstreifen der Hydrathülle unter minimalem Energieaufwand, so dass ein Kaliumion den Selektivitätsfilter in einer imitierten Hydrathülle passieren kann. Gleichzeitig werden kleinere monovalente Ionen, z.B.

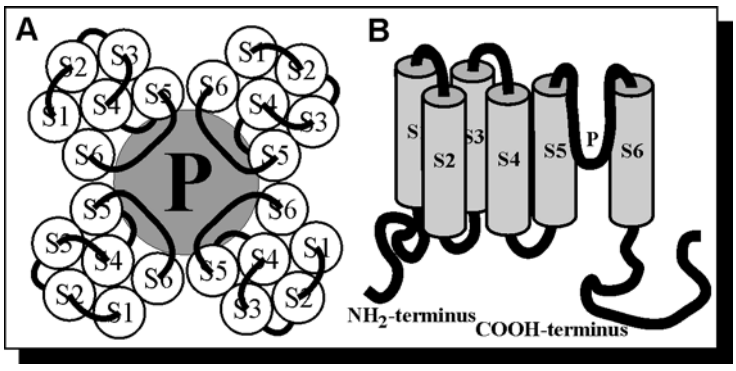

Abbildung 2. Schematisierte Struktur spannungsregulierter Kaliumkanäle.
(A) Ein spannungsregulierter Kaliumkanal ist aus vier α-Untereinheiten aufgebaut. Diese lagern sich symmetrisch aneinander und bilden in der zentralen Achse einen Permeationsweg (Pore, P, Selektivitätsfilter) für Kaliumionen. Hier ist ein Kanal schematisch in einer Aufsicht dargestellt. **(B)** Eine α-Untereinheiten besteht in einem sehr vereinfachenden Bild aus sechs transmembranen Domänen, die mit S1-S6 bezeichnet werden. Diese werden von zytosolischen NH_2-terminalen und COOH-terminalen Bereichen des Polypeptids flankiert. Die Region, die maßgeblich an der Bildung des Selektivitätsfilters beteiligt ist, liegt zwischen den transmembranen Domänen S5 und S6. Hier ist die Struktur in einer Seitenansicht skizziert, wobei die Membrane nicht mit dargestellt ist. [Abbildung aus **Dreyer et al. (2004a)**].

Natrium- und Lithium-Ionen, oder divalente Ionen, z.B. Kalziumionen, mit ihrer stärker gebundenen Hydrathülle an der Passage des Kanals gehindert. Neben Kaliumionen sind auch Rubidiumionen in der Lage, den Selektivitätsfilter von K^+-Kanälen zu passieren, wenngleich mit einer geringeren Effizienz (Hille, 2001). Aufgrund dieser Ähnlichkeit wurde und wird in Transportstudien in Ermangelung eines praktikablen radioaktiven Kaliumisotops das Rubidiumisotop ^{86}Rb eingesetzt. Auch das Ion des größten Elements der Alikaligruppe, das Caesiumion, kann in den Selektivitätsfilter von K^+-Kanälen eindringen. Jedoch ist die Permeation dieses Ions so sehr verlangsamt, dass Cs^+ effektiv die Pore verstopft (**Hedrich et al., 1995**; **Becker et al., 1996**; Hille, 2001).

Wie bereits eingangs erwähnt, wurden 1992 mit AKT1 und KAT1 die ersten Kaliumkanalgene einer Pflanze kloniert (Anderson et al., 1992; Sentenac et al., 1992). Diese Ergebnisse ermöglichten es erstmals, die Funktion des Kaliumtransports in Pflanzen mit einer DNA-Sequenz zu korrelieren, was wiederum in den folgenden Jahren die Klonierung ähnlicher Gene und deren zugehöriger cDNA aus anderen Pflanzen vereinfachte. Mittlerweile sind Volllängen-cDNAs von Genen, die für *Shaker*-ähnliche Kaliumkanäle kodieren, aus 15 unterschiedlichen Pflanzenspezies kloniert worden: Kartoffel (*Solanum tuberosum*; Mueller-Roeber et al., 1995), Mais (*Zea mays*; Philippar et al., 1999), Karotte (*Daucus carota*; Downey et al., 2000), Tomate (*Lycospersicon escelentum*; Hartje et al., 2000), Weizen (*Tritiucum aestivum*; Buschmann et al., 2000), Ackerbohne (*Vicia faba*; **Ache et al., 2001**), Pappel (*Populus tremula x tremuloides*; Langer et al., 2002), Regenbaum (*Samanea saman*; Moshelion et al., 2002), Weintraube

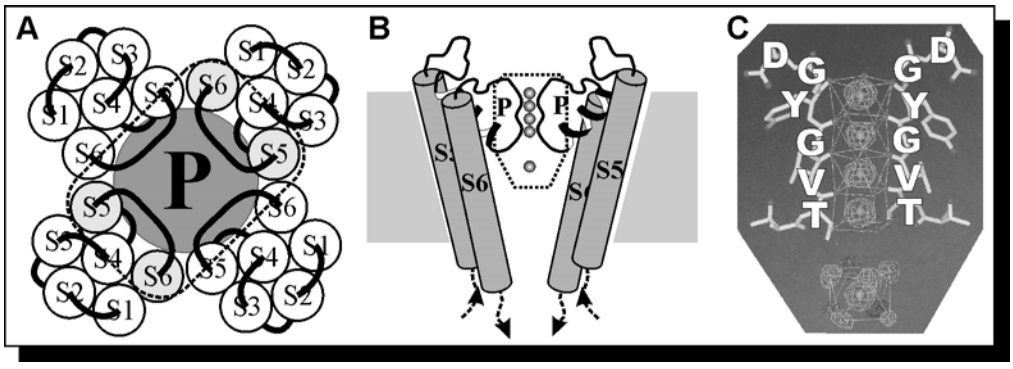

Abbildung 3. Der Selektivitätsfilter von Kaliumkanälen.
(A) Aufsicht auf einen Kaliumkanal. Der gestrichelte Bereich mit den Segmenten S5-P-S6 zweier gegenüberliegender Untereinheiten ist in (B) in der Seitenansicht dargestellt. **(B)** Seitenansicht des gestrichelten Bereichs in (A). Die P-Regionen bilden eine Engstelle im Permeationsweg. Die Kaliumionen sind als Kugeln angedeutet. **(C)** Detaillierte Darstellung des Selektivitätsfilters [gestrichelter Bereich in (B)]. Die Detailkenntnis resultiert aus der Röntgenstrukturanalyse eines kristallisierten Kaliumkanals. Das untere Kaliumion ist noch von seiner Hydrathülle (8 Wassermoleküle) umgeben. Die vier Kaliumionen in der Engstelle wurden beim Eintritt in den Selektivitätsfilter dehydratisiert. Die Sauerstoffreste des Peptidrückgrads der Sequenz TVGYG übernehmen die Funktion der abgestreiften Hydrathülle und koordinieren die Kaliumionen. [Abbildung nach **Dreyer et al. (2004a)**].

(*Vitis vinifera*; Pratelli et al., 2002), Reis (*Oryza sativa*; Golldack et al., 2003; Fuchs et al., 2005), Tabak (*Nicotiana paniculata* und *Nicotiana tabacum*), Eiskraut (*Mesembryanthemum crystallinum*), und Eukalyptus (*Eucalyptus camaldulensis*). Die detailliertesten Kenntnisse über diese Transporterfamilie gibt es jedoch für die Ackerschmalwand (*Arabidopsis thaliana*) – die Modellpflanze für pflanzengenetische Studien (Meinke et al., 1998). Das Genom von *Arabidopsis* enthält 9 Gene, die für *Shaker*-ähnliche Kaliumkanäle kodieren (Abbildung 1). Phylogenetische Untersuchungen an diesen 9 Kaliumkanälen aus *Arabidopsis* sowie an 30 weiteren aus anderen Pflanzenspezies lagen den Schluss nahe, dass die Familie der pflanzlichen *Shaker*-ähnlichen Kaliumkanäle in fünf Unterfamilien unterteilt werden kann (Abbildung 4, I-V) (Pilot et al., 2003b). Diese Einteilung in Unterfamilien spiegelt auch zum größten Teil die funktionellen Unterschiede der Kanalproteine wider.

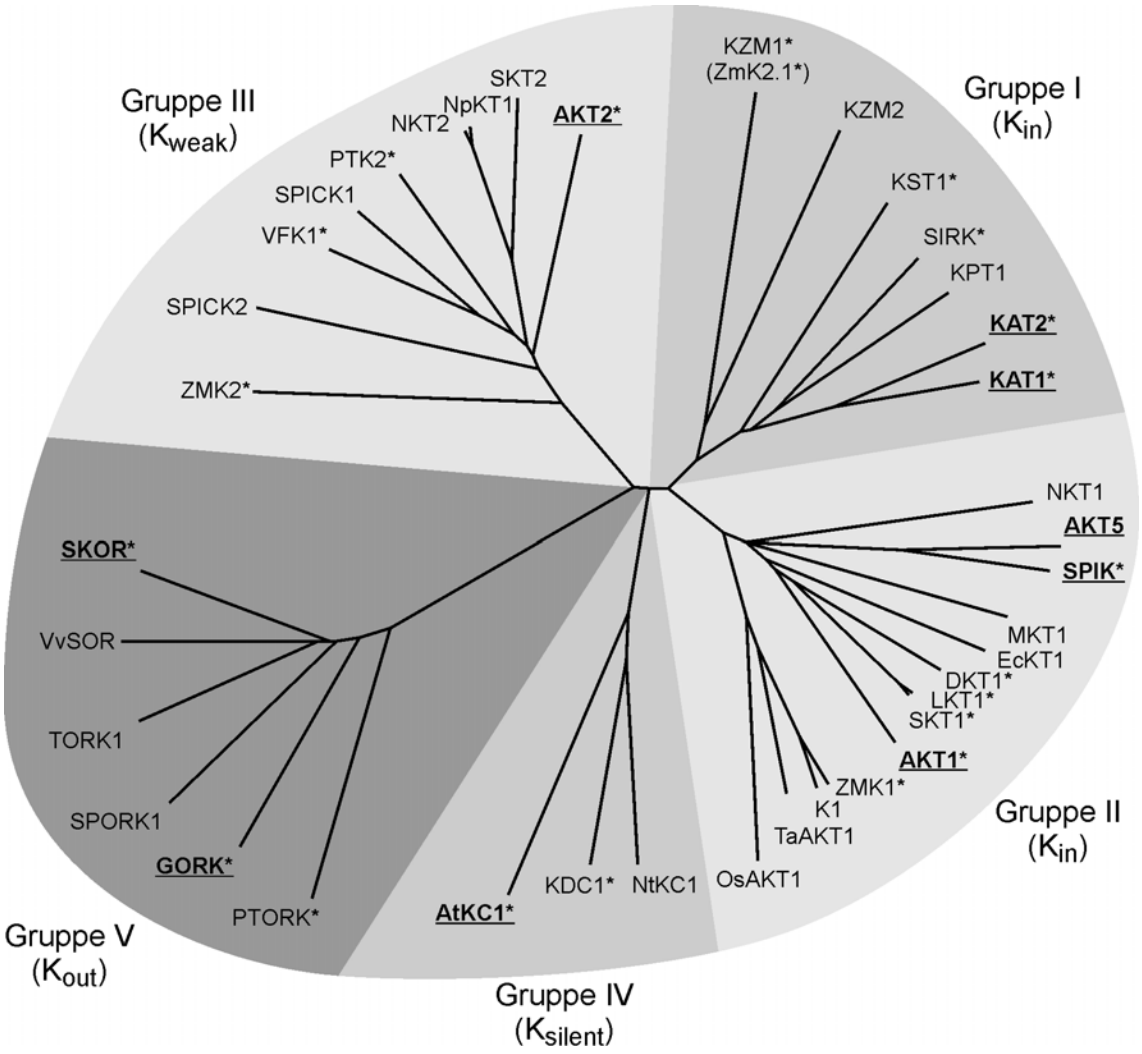

Abbildung 4. Unterteilung pflanzlicher *Shaker*-ähnlicher K^+-Kanäle in fünf Gruppen bzw. vier funktionelle Unterfamilien.
Insgesamt 39 verschiedene Volllängen-cDNAs, die für *Shaker*-ähnliche K^+-Kanaluntereinheiten in 15 verschiedenen Pflanzenspezies kodieren, wurden in der NCBI Datenbank gefunden (Stand 22.07.2005; http://www.ncbi.nlm.nih.gov/). Die Aminosäuresequenzen der abgeleiteten Proteine wurden mit dem Programm ClastalW (http://www.ebi.ac.uk/clustalw/) verglichen. Die verwandtschaftliche Beziehung zwischen den Proteinen wurde in einem wurzellosen phylogenetischen Baum dargestellt (Programm „treeview"; http://taxonomy.zoology.gla.ac.uk/rod/treeview.html). Die 39 Proteine wurden in 5 Gruppen (Gruppe I – Gruppe V) unterteilt. Die funktionelle Charakterisierung einiger Vertreter der einzelnen Gruppen in heterologen Expressionssystemen (*) erlaubt darüber hinaus eine Einteilung in die funktionellen Unterfamilien K_{in}, K_{out}, K_{weak} und K_{silent}. Die GenBank-Accession Nummern der Proteine lauten: *Arabidopsis thaliana* (unterstrichen): KAT1 (AAA32824), KAT2 (Q38849), AKT1 (Q38998), SPIK (Q8GXE6) AKT5 (Q9SCX5), AKT2 (Q38898), AtKC1 (P92960), SKOR (CAA11280), GORK (CAC17380); *Eucalyptus camaldulensis:* EcKT1 (AAL25648); *Daucus carota*: DKT1 (CAG27094), KDC1 (CAB62555); *Lycospersicon escelentum*: LKT1 (CAA65254); *Mesembryanthemum crystallinum*: MKT1 (AAF81249); *Nicotiana paniculata*: NpKT1 (BAA84085); *Nicotiana tabacum*: NKT1 (BAD81034), NKT2 (BAD81033), NtKC1 (BAD81035), TORK1 (BAD81036); *Oryza sativa*: OsAKT1 (NP_917226); *Populus tremula x Populus tremuloides*: KPT1 (CAC87141), PTK2 (CAC05489), PTORK (CAC05488); *Samanea saman*: SPICK1 (AAD16278), SPICK2 (AAD39492), SPORK1 (CAC10514); *Solanum tuberosum*: KST1 (CAA56175), SKT1 (CAA60016), SKT2 (CAA70870); *Tritiucum aestivum*: TaAKT1 (AAF36832); *Vicia faba*: VFK1 (CAA71598); *Vitis vinifera*: SIRK (AAL09479), VvSOR (CAD35400); *Zea mays*: KZM1 (CAD18901), ZmK2.1 (AAR21353) ist eine NH_2-terminal verkürzte Form von KZM1, ZmK1 (CAA68912), K1 (CAI77627), ZMK2 (CAB54856).

Funktionelle Vielfalt pflanzlicher *Shaker*-ähnlicher Kaliumkanäle

Spannungsregulierte pflanzliche Kaliumkanäle wurden mit verschiedenen elektrophysiologischen Techniken (Blatt, 2004a; Hills und Volkov, 2004) funktionell untersucht. Die methodische Bandbreite umfasst hierbei sowohl *in vivo* Untersuchungen der Kaliumkanäle im nativen Gewebe als auch *in vitro* Untersuchungen, d.h. nach funktioneller Expression in heterologen Expressionssystemen, wie z.B. Hefe, Insektenzellen, Säugetierzelllinien und Oozyten des südafrikanischen Krallenfroschs *Xenopus laevis* (**Dreyer et al., 1999**).

Anhand ihrer funktionellen Eigenschaften lassen sich pflanzliche *Shaker*-ähnliche Kaliumkanäle in 4 Gruppen unterteilen (Abbildung 4): einwärtsgleichrichtende Kaliumkanäle (K_{in} Kanäle), auswärtsgleichrichtende Kaliumkanäle (K_{out} Kanäle), schwach gleichrichtende Kaliumkanäle (K_{weak}) und modulierende Kanaluntereinheiten (K_{silent}), deren Funktionalität bislang nur in Kombination mit anderen K_{in} Kanaluntereinheiten nachgewiesen werden konnte.

K_{in} – Einwärtsgleichrichtende Kaliumkanäle

Die Gruppen I und II (Abbildung 4) bilden die Unterfamilie der einwärtsgleichrichtenden Kaliumkanäle (oder auch hyperpolarisierungsaktivierte K^+ Kanäle). K_{in} Kanäle sind nur bei Membranspannungen[3] negativ von ungefähr –100 mV aktiv (Abbildung 5), d.h. geöffnet. Bei positiveren Spannungen sind sie nicht aktiv, d.h.

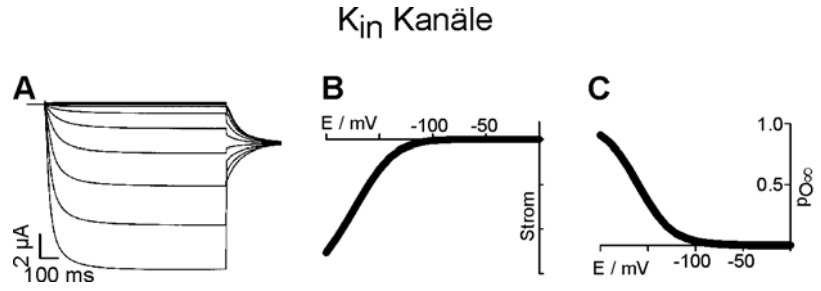

Abbildung 5. Charakteristika von K_{in} Känalen.
(A) Typische Stromantworten des K_{in} Kanals KAT1, exprimiert in *Xenopus* Oozyten, auf 1-s Aktivierungsspannungspulse. Die Aktivierungsspannung wurde ausgehend von einer Haltespannung von -20 mV im Bereich von +20 mV bis –160 mV in 15-mV Schritten variiert. **(B)** Strom-Spannungs-Kennlinie von K_{in} Kanälen im thermischen Gleichgewicht. **(C)** Spannungsabhängigkeit der Aktivität (Offenwahrscheinlichkeit $p_{O\infty}$) von K_{in} Kanälen im Gleichwicht. [Abbildung nach **Dreyer et al. (2004a)**].

[3] Gemessen als $E = \psi_{cyt.} - \psi_{ext.}$
$\psi_{cyt.}$: cytosolisches elektrisches Potential, $\psi_{ext.}$: extrazelluläres elektrisches Potential

geschlossen (**Dreyer et al., 2004a**). Unter physiologischen Bedingungen sind K_{in} Kanäle in der Regel nur geöffnet, wenn die treibende Kraft der Elektrodiffusion für Kalium in die Zelle hinein (=einwärts) gerichtet ist (Abbildung 5). Dies ist in der Regel bei sehr negativer Membranspannung der Fall, welche wiederum eine Folge der Aktivität von Plasmamembran H^+-ATPasen ist (López-Maqués et al., 2004). K_{in} Kanäle fungieren also als Kaliumaufnahmekanäle. Sie ermöglichen es den Pflanzenzellen, große Mengen an Kalium in relativ kurzer Zeit zu akkumulieren (Sentenac et al., 1992).

K_{out} – Auswärtsgleichrichtende Kaliumkanäle

Die Gruppe V (Abbildung 4) ist identisch mit der Unterfamilie der auswärtsgleichrichtenden Kaliumkanäle (oder auch depolarisierungsaktivierte K^+ Kanäle). K_{out} Kanäle öffnen nur, wenn die Membranspannung positiver als die Gleichgewichtsspannung für Kalium (Nernst-Spannung für K^+, E_K) ist. Bei negativeren Spannungen sind sie geschlossen (**Dreyer et al., 2004a**). Folglich sind K_{out} Kanäle nur geöffnet, wenn die treibende Kraft der Elektrodiffusion für Kalium aus der Zelle heraus (=auswärts) gerichtet ist. K_{out} Kanäle fungieren also als Kaliumeffluxkanäle. Sie ermöglichen es den Pflanzenzellen, Kalium an die zelluläre Umgebung abzugeben. Physiologisch ist dies vor allem bedeutsam beim Stomaschluss (**Hosy et al., 2003**) sowie bei der Beladung des Xylems mit K^+ Ionen (Gaymard et al., 1998). Eine besondere Eigenschaft von K_{out} Kanälen ist, dass sich ihre spannungsabhängige Aktivierung an die extrazelluläre K^+ Konzentration anpasst, indem sich die

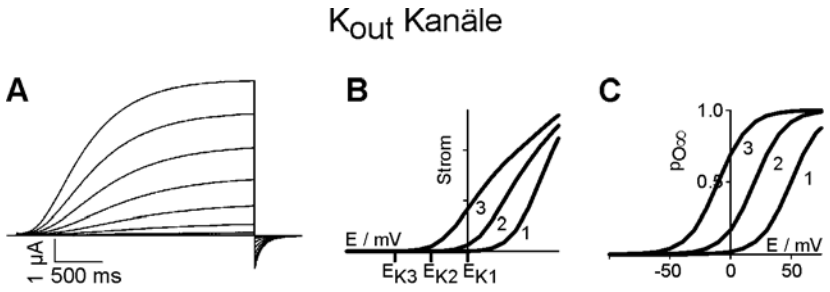

Abbildung 6. Charakteristika von K_{out} Känalen.
(A) Typische Stromantworten des K_{out} Kanals SKOR, exprimiert in *Xenopus* Oozyten, auf 2.5-s Aktivierungsspannungspulse. Die Aktivierungsspannung wurde ausgehend von einer Haltespannung von -100 mV im Bereich von -100 mV bis +50 mV in 15-mV Schritten variiert. **(B)** Strom-Spannungs-Kennlinie von K_{out} Kanälen im thermischen Gleichgewicht. **(C)** Spannungsabhängigkeit der Aktivität (Offenwahrscheinlichkeit $p_{O\infty}$) von K_{out} Kanälen im Gleichwicht. Die Aktivität von K_{out} Kanälen wird durch die extrazelluläre Kaliumkonzentration moduliert. Die verschiedenen Kurven (1-3) repräsentieren das Verhalten unter drei verschiedenen Bedingungen (E_K: Nernst-Potential für Kalium). [Abbildung nach **Dreyer et al. (2004a)**].

Aktivierungsschwelle mit E_K verschiebt (Abbildung 6). Erst dieser Mechanismus garantiert, dass K_{out} Kanäle nur als Kaliumeffluxkanäle fungieren, selbst wenn die extrazelluläre Kaliumkonzentration über einen Bereich von 10 nm bis 100 mM variiert (Blatt, 1988; Schroeder, 1989; Blatt und Gradmann, 1997; Roelfsema und Prins, 1997). Details zum K^+-abhängigen Schaltverhalten dieser Kanäle werden im Abschnitt „Der K+-Sensor von Kout Kanälen“, Seite 29, erläutert.

K_{weak} – schwach gleichrichtende Kaliumkanäle

Die Gruppe III (Abbildung 4) ist identisch mit der Unterfamilie der schwach gleichrichtenden Kaliumkanäle. Die Namensgebung dieser Unterfamilie beruht auf der Beobachtung, dass K_{weak} Kanäle im gesamten physiologischen Spannungsbereich aktiv sind, ihre Aktivität jedoch mit negativer werdender Membranspannung weiter zunimmt (Abbildung 7). Dies wird besonders in Spannungspulsexperimenten deutlich. In diesen Experimenten werden zwei unterschiedliche Stromkomponenten beobachtet (Marten et al., 1999; Lacombe et al., 2000; **Dreyer et al., 2001**). Zum einen reagiert der Strom instanstan auf den geänderten elektrochemischen Gradienten (Abbildung 7A, weißer Balken). Zum anderen wird eine zeit- und spannungsabhängig aktivierende Stromkomponente bei Membranspannungen negativ von –60 mV sichtbar (Abbildung 7A, grauer Balken). Aufgrund der schwachen Gleichrichtungseigenschaften können K_{weak} Kanäle den Zellen sowohl die Kaliumaufnahme als auch die Kaliumabgabe ermöglichen (**Dreyer et al., 2004a**). Details zum Mechanismus der schwachen

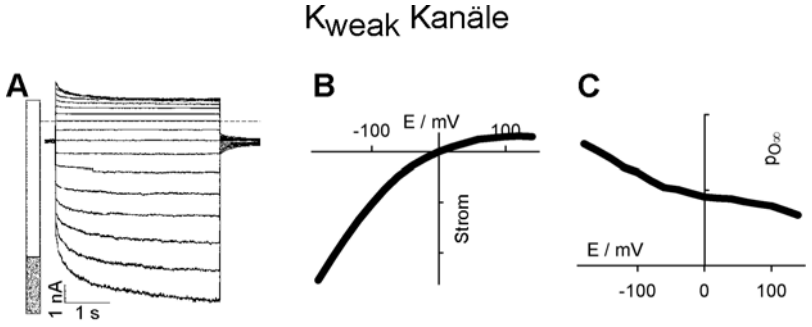

Abbildung 7. Charakteristika von K_{weak} Känalen.
(A) Typische Stromantworten des K_{weak} Kanals AKT2, exprimiert in COS Zellen, auf 3.5-s Aktivierungsspannungspulse. Die Aktivierungsspannung wurde ausgehend von einer Haltespannung von -40 mV im Bereich von -180 mV bis +140 mV in 20-mV Schritten variiert. Die Stromantwort zeigt zwei Komponenten: eine instantane Komponente und eine spannungs- und zeitabhängige Komponente. Die Verhältnisse der Komponenten sind als Balken dargestellt (instantan: weißer Bereich; zeitabhängig: grauer Bereich) **(B)** Strom-Spannungs-Kennlinie von K_{weak} Kanälen im thermischen Gleichgewicht. **(C)** Spannungsabhängigkeit der Aktivität (Offenwahrscheinlichkeit $p_{O\infty}$) von K_{weak} Kanälen im Gleichwicht. [Abbildung nach **Dreyer et al. (2001)**].

Gleichrichtung werden im Abschnitt „Kweak Kanäle reagieren sensitiv auf Phosphorylierungen“, Seite 23, dargestellt.

K_{silent} – modulierende Kanaluntereinheiten

Die Gruppe III (Abbildung 4) bildet die Unterfamilie der modulierenden Kanaluntereinheiten. Polypeptide diesen Typs bilden nach Expression in homologen und heterologen Expressionssystemen in der Regel keine funktionell nachweisbaren Kanäle in der Plasmamembran. Werden sie jedoch zusammen mit anderen Kaliumkanaluntereinheiten der K_{in} Unterfamilien exprimiert, so modulieren sie deren Eigenschaften (**Dreyer et al., 1997**; Ivashikina et al., 2001; Paganetto et al., 2001; Reintanz et al., 2002; Formentin et al., 2004; Picco et al., 2004). Aufgrund dieser Eigenschaften werden Polypeptide der Unterfamilie III auch als stille Untereinheiten (K_{silent}) bezeichnet. Bislang wurden zwei modulatorische Effekte von K_{silent} Untereinheiten beschrieben. Sie können zum einen die Aktivität von einwärtsgleichrichtenden Kaliumkanälen beeinflussen (Abbildung 8), zum anderen können sie deren Permeationseigenschaften verändern (**Dreyer et al., 1997**; Paganetto et al., 2001; Picco et al., 2004).

An dieser Stelle sollte angemerkt werden, dass in der Literatur in einer Publikation die Bildung funktioneller Kanäle nur aus K_{silent} Untereinheiten beschrieben wurde (Downey et al., 2000). In späteren Studien konnten die Ergebnisse von Downey et al. (2000) jedoch nicht reproduziert werden konnten (Paganetto et al., 2001; Formentin et al., 2004; Picco et al., 2004).

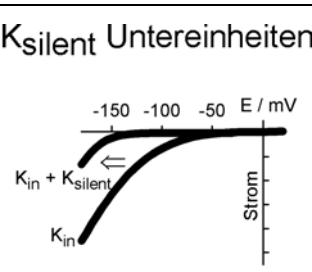

Abbildung 8. Ein Beispiel für die modulierenden Eigenschaften von K_{silent} Untereinheiten.
K_{silent} Untereinheiten bilden in der Regel keine funktionell nachweisbaren Kaliumkanäle. Jedoch moduliert die Präsenz von K_{silent} Untereinheiten die Eigenschaften von K_{in} Kanälen. In dem gezeigten Beispiel [K_{silent} = AtKC1, K_{in} = KAT1 oder KST1, (**Dreyer et al., 1997**)] verschiebt die K_{silent} Untereinheit die Aktivierungsschwelle der einwärtsgleichrichtenden Kaliumkanäle zu negativeren Spannungen.

Pflanzliche Kaliumkanaluntereinheiten können homo- und heteromere Kaliumkanäle bilden

In den vorhergehenden Abschnitten wurde bereits erwähnt, dass funktionelle pflanzlicher Kaliumkanäle multimere Proteine sind. Dies wurde erstmals 1997 nachgewiesen (**Dreyer et al., 1997**). Nach Koexpression einer mutierter Version der Kaliumkanaluntereinheit KAT1 mit der nicht mutierten Untereinheit (Wildtyp) wurden in *Xenopus* Oozyten Kanaleigenschaften gemessen, die sich nicht als Summe der Charakteristika der einzelnen Kanäle beschreiben ließen (Abbildung 9).

Der multimere Aufbau pflanzlicher Kaliumkanäle warf die Frage auf, ob diese Kanaluntereinheiten sich nur als Homomultimere (d.h. ein Kanal besteht nur aus identischen Untereinheiten) zusammenlagern können oder ob auch heteromultimere Kanäle gebildet werden können. Mit Hilfe gezielt ausgewählter Kanalmutanten konnten in Koexpressionsstudien in *Xenopus* Oozyten Kaliumkanälen nachgewiesen werden, die aus verschiedenen Untereinheiten aufgebaut waren (**Dreyer et al., 1997**). Im speziellen wurde gezeigt, dass verschiedenen Kanaluntereinheiten der Gruppen I untereinander, der Gruppe II untereinander, der Gruppen I und II miteinander und der Gruppen I und IV miteinander heteromere Kaliumkanäle bilden können. Dieser funktionelle Nachweis heteromerer Kaliumkanäle konnte in biochemischen Studien zunächst jedoch nicht bestätigt werden (Urbach et al., 2000). Nach Koexpression in Insektenzellen konnten keine heteromeren Kanalproteinkomplexe nachgewiesen werden. Mittlerweile wurden aber die 1997 publizierten Ergebnisse mit verschiedenen experimentellen Techniken

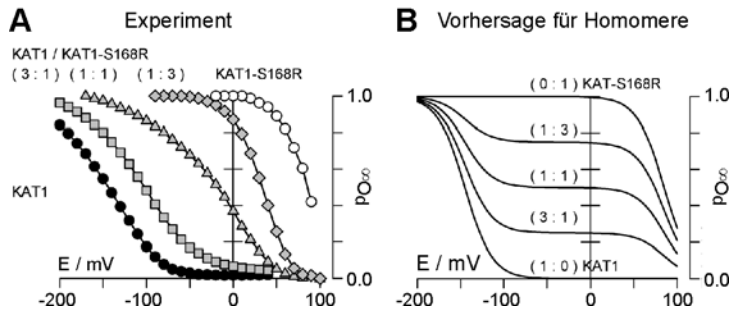

Abbildung 9. Pflanzliche Kaliumkanäle sind multimere Proteine.
(A) Koexpression des KAT1 Wildtyps und der Mutante KAT1-S168R in *Xenopus* Oozyten. Die Spannungsabhängigkeit der Kanäle (Offenwahrscheinlichkeit $p_{O\infty}$) wurde für verschiedene Expressionsverhältnisse bestimmt: KAT1 (schwarze Kreise), KAT1-S168R (weiße Kreise) sowie 3:1 (Quadrate), 1:1 (Dreiecke) und 1:3 (Rauten) Mischungen aus beiden. **(B)** Erwartete Ergebnisse für die Experimente in (A) für den Fall, dass pflanzliche Kaliumkanäle homomere Proteine sind. [Abbildung aus **Dreyer et al. (1997)**].

verifiziert (**Hedrich et al., 1998**; Baizabal-Aguirre et al., 1999; **Ache et al., 2001**; Ivashikina et al., 2001; Paganetto et al., 2001; Pilot et al., 2001; Zimmermann et al., 2001; Reintanz et al., 2002; Formentin et al., 2004; Obrdlik et al., 2004; Picco et al., 2004). Darüber hinaus wurde gezeigt, dass auch Kanaluntereinheiten der Gruppen I und III, der Gruppen II und III, sowie der Gruppen II und IV assemblieren können.

Interessanterweise wurde keine Heteromerbildung von Kanaluntereinheiten der Gruppe V mit z.B. Kanaluntereinheiten der Gruppe I festgestellt, sondern nur Heteromerbildung innerhalb der Gruppe V (Ache et al., 2000; **Dreyer et al., 2004b**). Dies deutet darauf hin, dass eine molekulare Barriere die Assemblierung von K_{in}- und K_{out}-Kanaluntereinheiten verhindert (**Dreyer et al., 2004b**). Jedoch liegen sowohl bei K_{in} Kanälen als auch bei K_{out} Kanälen die Domänen, die für die Formation funktioneller Kanäle verantwortlich sind, in der zytosolischen Carboxy-terminalen Region des Polypeptids (Daram et al., 1997; **Dreyer et al., 2004b**). In dieser Eigenschaft ähneln pflanzliche Kaliumkanäle den tierischen EAG-ähnlichen Kaliumkanälen (Ludwig et al., 1997), deren Assemblierung ebenfalls durch Bereiche in der zytosolischen Carboxy-terminalen Region zustande kommt, aber weniger den *Shaker* Kanälen, deren Assemblierung maßgeblich über eine Region im zytosolischen, Amino-terminalen Bereich bestimmt wird (Li et al., 1992).

Der multimere Aufbau pflanzlicher Kaliumkanäle wurde ausgenutzt, um die physiologische Rolle des K_{out} Kanals GORK in Schließzellen von *Arabidopsis thaliana* genauer zu untersuchen (**Hosy et al., 2003**). In einer dominant-negativ Strategie wurde *Arabidopsis* mit einem mutierten *GORK* Gen transformiert, das für eine modifizierte Kanaluntereinheit mit einer veränderten Porenregion P kodierte. In den transgenen Pflanzen wurden sowohl der GORK Wildtyp als auch die mutierte Kanaluntereinheit exprimiert und es wurden heteromere K_{out} Kanäle gebildet. Die veränderte Porenregion der Mutante bewirkte, dass die Kanäle, die eine mutierte GORK Untereinheit enthielten, nicht mehr funktionell waren. Die Expression der dominant-negativen Mutante reduzierte die Anzahl funktioneller GORK Kanäle so stark, dass der ABA[4]- und Dunkelheit-induzierte Stomaschluss in den transgenen Pflanzen beeinträchtigt wurde. Dies wurde noch deutlicher in Pflanzen, die kein funktionelles GORK Gen mehr hatten (T-DNA Insertion im *GORK* Gen). In dieser „knock-out“ Linie konnten keine auswärtsgleichrichtenden Kaliumkanäle in Schließzellen mehr nachgewiesen werden. Die physiologische Konsequenz des Verlustes des K_{out} Kanals GORK war eine

[4] Abscisinsäure

Veränderung der Stomabewegung. Die Stomata der „knock-out"-Pflanzen schlossen sich langsamer als die der Wildtyp-Pflanzen. Als Folge war die Transpirationsrate der „knock-out"-Pflanzen größer und damit auch deren Wasserverlust. Die Ergebnisse, die mit den dominant-negativen und „knock-out" Linien erzielt worden sind, deuteten darauf hin, (i) dass auswärtsgleichrichtende Kaliumkanäle wichtig sind, um größere Mengen an Kaliumionen in kurzer Zeit aus der Zelle zu entlassen, aber auch (ii) dass die Kaliumabgabe nicht nur durch K_{out} Kanäle erfolgt. Die Ergebnisse zeigten nämlich weiterhin, dass auswärtsgleichrichtenden Kaliumkanäle in Schließzellen von *Arabidopsis* homomere GORK Kanäle sind. Der Verlust des *GORK* Gens verhindert jedoch nicht den Stomaschluss, er verzögert ihn nur (**Hosy et al., 2003**).

Im Gegensatz zu K_{out} Kanälen in Schließzellen gibt es starke Indizien, dass einwärtsgleichrichtende Kaliumkanäle in Schließzellen, Geleitzellen und Wurzelzellen nicht nur als homomere Polypeptide vorliegen. Zum einen exprimieren diese Zellen nicht nur ein Gen, das für eine Kanaluntereinheit der Gruppen I, II, III, oder IV kodiert, sondern mehrere (Ivashikina et al., 2001; Szyroki et al., 2001; Pilot et al., 2001; Zimmermann et al., 2001; Reintanz et al., 2002; Ivashikina et al., 2003; Pilot et al., 2003a; Ivashikina et al., 2005). Für diese Untereinheitstypen wurde die Heteromerisierung in heterologen Expressionssystemen (*in vitro*) gezeigt (siehe oben). Zum anderen unterscheiden sich die Eigenschaften von K_{in} Kanälen *in vivo* fundamental von denen homomerer K_{in} Kanäle *in vitro*. Es wurden Unterschiede in den Permeationseigenschaften und in der Kanalregulation beobachtet (**Dietrich et al., 1998; Bruggemann et al., 1999b**). Die gesamte Datenlage lässt kaum noch Zweifel an der Existenz heteromultimerer K_{in} Kanäle *in vivo*.

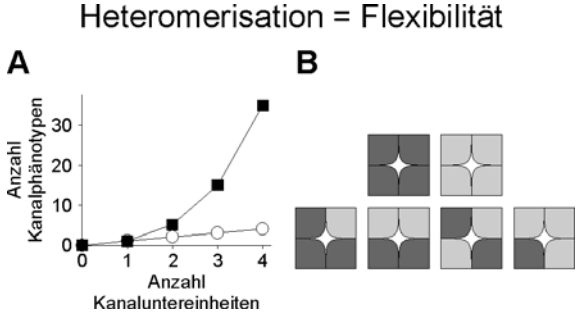

Abbildung 10. Das Potential heteromerer Kaliumkanäle.
(A) *Weiße Kreise*: Kaliumkanäle als Homomere, eine Zelle kann nur eine kleine Anzahl verschiedener Kanalphänotypen generieren. *Schwarze Quadrate*: Kaliumkanäle als Heteromere, selbst mit wenigen verschiedenen Kanaluntereinheiten kann eine Zelle eine große Bandbreite an Kanalphänotypen generieren. **(B)** Beispiel für eine Zelle mit zwei verschiedenen Kanaluntereinheiten. Falls keine Heteromerisierung möglich ist, werden nur zwei verschiedene Kanaltypen gebildet (*obere Zeile*). Falls die Heteromerisierung möglich ist, können darüber hinaus noch vier weitere Kanaltypen gebildet werden (*untere Zeile*). [Abbildung aus **Dreyer et al. (2002)**].

Die Bildung heteromerer Kaliumkanäle würde Pflanzen ein hohes Maß an Flexibilität in der Kontrolle des Kaliumtransports ermöglichen (Abbildung 10). Durch die Expression weniger verschiedener Untereinheiten (wobei jede über andere Kontrollmechanismen reguliert wird) könnte eine Bandbreite unterschiedlicher Kaliumkanäle erzeugt werden. Inwieweit das Potential der Heteromerisierung von Pflanzen genutzt wird, ist zur Zeit Gegenstand der Forschung in mehreren Arbeitsgruppen weltweit.

Regulation der Aktivität pflanzlicher *Shaker*-ähnlicher K^+ Kanäle

Ein wichtiger Aspekt der Kaliumhomöostase in Pflanzen ist die Regulation der verschiedenen, am Kaliumtransport beteiligten Transportproteine (Walker et al., 1996). Die Aktivität der Kaliumtransporter kann zum einen indirekt auf der Ebene der Expression reguliert werden (Pilot et al., 2003a; Véry und Sentenac, 2003), zum anderen direkt auf Proteinebene (**Dreyer et al., 2004a**). Die dieser Habilitationsschrift zugrundeliegenden Arbeiten fokussieren auf die direkte, post-translationale Regulation pflanzlicher Kaliumkanäle.

In **Dreyer et al. (2004a)** wird ein umfassender Überblick über mögliche post-translationale Regulationsmechanismen gegeben. Hierzu gehören z.B. Phosphorylierungen, Nitrosilierungen, aber auch die Wechselwirkung mit Kationen und Anionen, mit Hormonen, mit Lipiden und mit anderen Proteinen und Peptiden. Die Wechselwirkungen und Modifikationen beeinflussen die Aktivität der Kanäle, was wiederum weitreichende physiologische Auswirkungen haben kann. Somit ist das Verständnis der Regulation pflanzlicher Kaliumkanäle der Schlüssel zu einem tieferen Verständnis der physiologischen Rolle dieser Transportproteine.

Die Arbeiten, die im folgenden zusammengefasst dargestellt werden, haben maßgeblich dazu beigetragen, verschiedene post-translationale Regulationsmechanismen pflanzlicher Kaliumkanäle zu verstehen.

Die Spannungsabhängigkeit pflanzlicher Kaliumkanäle

Es wurde bereits eingangs erwähnt, dass pflanzliche *Shaker*-ähnliche Kaliumkanäle eine große funktionelle Vielfalt aufweisen. Obwohl sie die gleiche Struktur haben, fungieren sie als Kaliumaufnahmekanäle (K_{in}), als Kaliumabgabekanäle (K_{out}) oder als Kaliumaufnahme- und Kaliumabgabekanäle (K_{weak}) (Abbildung 11). Die Ursache für diese Funktionsunterschiede ist die unterschiedliche Spannungsabhängigkeit der Kanäle. K_{in} und K_{weak} Kanäle öffnen mit zunehmend negativ werdender Membranspannung und schließen mit zunehmend positiv werdender Spannung, während K_{out} Kanäle sich genau entgegengesetzt verhalten. Die genauen molekularen Ursachen dieser Unterschiede sind im Detail bislang noch nicht vollständig verstanden. Experimentelle Studien, die in den vergangenen Jahren durchgeführt wurden, erlauben jedoch erste Einblicke in die Mechanismen, die der Spannungsabhängigkeit zugrunde liegen.

Mutageneseexperimente an den beiden K_{in} Kanälen KAT1 und KST1 konnten zeigen, dass die vierte transmembrane Domäne des Polypeptids (S4) eine wichtige Rolle in der spannungsabhängigen Regulierung dieser Kanäle spielt (**Dreyer et al., 1997**; **Hoth et al., 1997b**; Marten und Hoshi, 1998; Zei und Aldrich, 1998). Das S4-Segment weist eine hohe Dichte an der positiv geladenen Aminosäure Arginin auf. Änderungen in der Membranspannung induzieren eine Bewegung des S4-Segments, wobei dieses dabei mit verschiedenen anderen Bereichen des Polypeptids interagiert

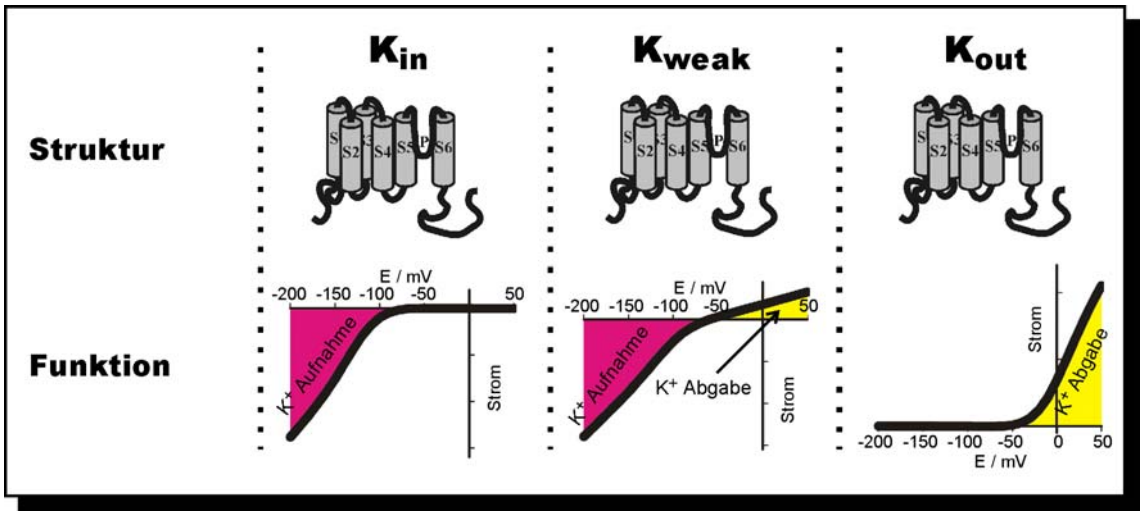

Abbildung 11. Die funktionelle Vielfalt pflanzlicher Kaliumkanäle.
Shaker-ähnliche pflanzliche Kaliumkanäle haben alle die gleiche Struktur, zeigen aber ein breites funktionales Spektrum. K_{in} Kanäle erlauben den Zellen die Kaliumaufnahme, K_{out} Kanäle die Kaliumabgabe. K_{weak} Kanäle können sowohl als Kaliumaufnahmekanäle als auch als Kaliumabgabekanäle fungieren.

(**Becker et al., 1996**; Marten und Hoshi, 1997; Marten und Hoshi, 1998; Latorre et al., 2003; Lai et al., 2005). Ähnliche Ergebnisse wurden auch an anderen spannungsabhängigen Kaliumkanälen aus Eukaryoten und Prokaryoten gewonnen (Übersicht in Swartz, 2004). Somit liegt der Schluss nahe, dass die Spannungsabhängigkeit der verschiedenen Kanäle auf dem gleichen Prinzip beruht. Zur Zeit werden zwei Modelle diskutiert, um die spannungsabhängige Aktivierung von Kaliumkanälen zu erklären: zum einen könnte der Spannungssensor (das S4-Segment) in Form einer α-Helix eine leichte Schraubenbewegung durchführen (Abbildung 12A) (Bezanilla, 2002; Cuello et al., 2004; Starace und Bezanilla, 2004), zum anderen könnte der Spannungssensor eine Klappbewegung durchführen (Abbildung 12B) (MacKinnon, 2004; Long et al., 2005b).

In beiden Fällen verursacht die Bewegung des Spannungssensors weiterreichende Konformationsänderungen des Kanalproteins, die schließlich zu einer Erweiterung bzw. Verengung der Pore an der zytosolischen Seite führen (Abbildung 12C) (Larsson, 2002; Bezanilla und Perozo, 2003; Swartz, 2004; Long et al., 2005b).

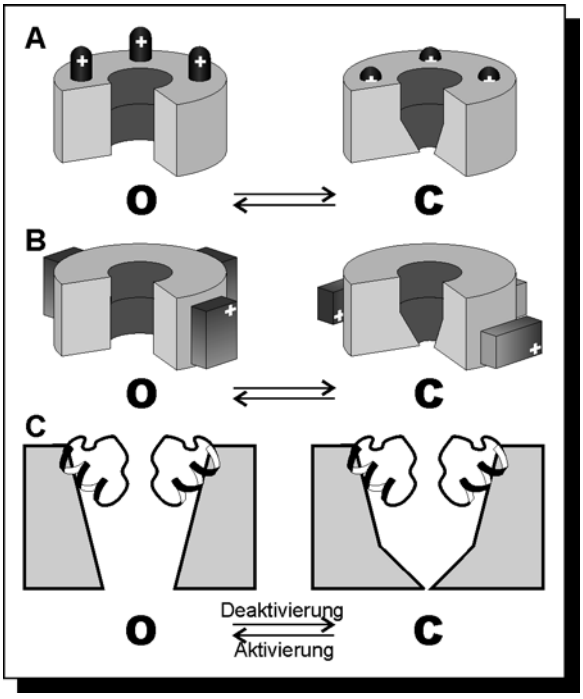

Abbildung 12. Modelle für die Bewegungen des Spannungssensors.
(A und B) Bestimmte Bereiche des Kanalproteins, die eine hohe Dichte geladener Aminosäuren aufweisen (angedeutet als „+“), sind in der Lage, auf die transmembrane Spannung zu reagieren. Die Position dieser Bereiche innerhalb des Kanalproteins ist abhängig von der Membranspannung. Derzeit werden zwei Modelle in der Literatur diskutiert: **(A)** Das S4-Segment liegt als α-Helix vor und vollzieht eine leichte schraubenförmige Bewegung; **(B)** Das S4 Segment bildet mit Teilen des S3 Segments eine Paddelstruktur und vollzieht eine Klappbewegung. **(C)** In beiden Fällen induziert die Bewegung des Spannungssensors weitere Konformationsänderungen, die den Permeationsweg am zytosolischen Ende der Pore entweder verschließen oder öffnen [Abbildungen nach **Dreyer et al. (2004a)**].

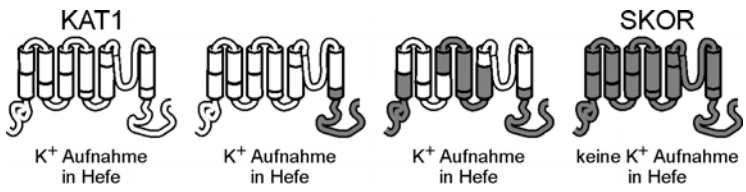

Abbildung 13. KAT1-SKOR Chimären erlauben Hefen die Kaliumaufnahme.
Der K_{in} Kanal KAT1 ermöglicht Hefezellen die K^+-Aufnahme (*links*). Der K_{out} Kanal SKOR ist nicht dazu in der Lage (*rechts*). KAT1 verliert diese Eigenschaften nicht, wenn der zytosolische Carboxyterminus gegen den von SKOR ausgetauscht wird (Mitte links), oder wenn sowohl der zytosolische Carboxyterminus, der zytosolische Aminoterminus als auch der Spannungssensor S4 ausgetauscht werden (*Mitte rechts*) [Abbildungen nach **Poree et al. (2005)**]

Für den K_{out} Kanal SKOR konnte kürzlich gezeigt werden, dass die letzte transmembrane Domäne S6 an diesem Verschlussmechanismus beteiligt ist (**Poree et al., 2005**). In dieser Studie wurden zunächst 256 Chimären zwischen dem K_{in} Kanal KAT1 und dem K_{out} Kanal SKOR hergestellt und in Hefezellen daraufhin untersucht, ob sie in der Lage waren, die Kaliumaufnahme zu ermöglichen. Im K_{in} Kanal KAT1 konnten der zytosolische Carboxyterminus, der zytosolische Aminoterminus und der Spannungssensor S4 durch die entsprechenden Gegenstücke aus dem K_{out} Kanal SKOR ersetzt werden, ohne dass die Eigenschaft der Kaliumaufnahme zerstört wurde

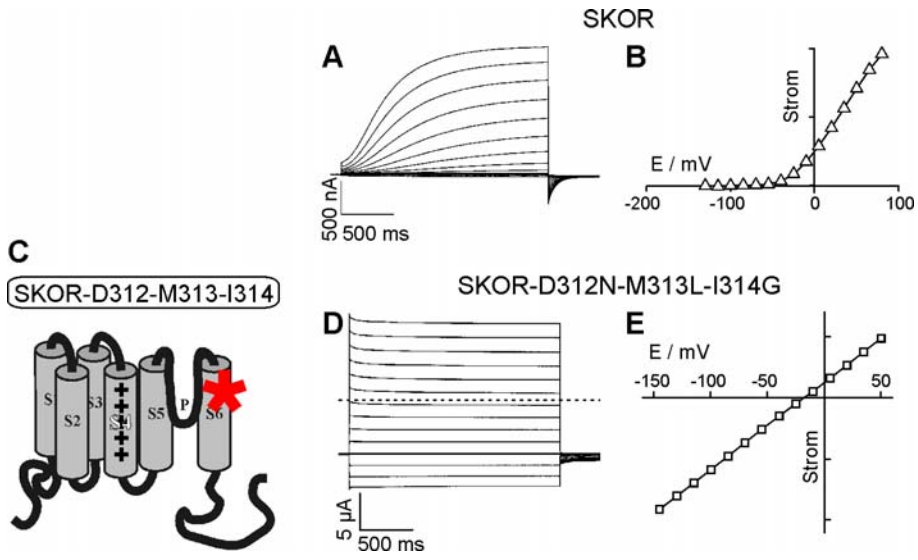

Abbildung 14. Eine wichtige Domäne für die Auswärtsgleichrichtung befindet sich im S6 Segment.
(A) Typische Stromantworten des K_{out} Kanals SKOR, exprimiert in *Xenopus* Oozyten, auf 2-s Aktivierungsspannungspulse. Die Aktivierungsspannung wurde ausgehend von einer Haltespannung von -100 mV im Bereich von -130 mV bis +80 mV in 15-mV Schritten variiert. **(B)** Strom-Spannungs-Kennlinie von SKOR im thermischen Gleichgewicht. (C - E) Die Mutante SKOR-D312N-M313L-I314G zeigt keine Auswärtsgleichrichtung mehr. **(C)** Schematische Darstellung der Lage des Motivs D312-M313-I314 innerhalb des SKOR-Polypeptids. **(D)** Typische Stromantworten von SKOR-D312N-M313L-I314G, exprimiert in *Xenopus* Oozyten, auf 4-s Aktivierungsspannungspulse. Die Aktivierungsspannung wurde ausgehend von einer Haltespannung von -100 mV im Bereich von -145 mV bis +50 mV in 15-mV Schritten variiert. **(E)** Strom-Spannungs-Kennlinie von SKOR-D312N-M313L-I314G. [Abbildung nach **Porree et al. (2005)**].

(Abbildung 13). Im Gegenzug wurden Bereiche in SKOR durch Bereiche von KAT1 ersetzt. Wurden drei Aminosäuren im S6 Segment von SKOR ersetzt, so verlor der Kanal seine Gleichrichtungseigenschaften (Abbildung 14). Die Chimäre war im untersuchten Spannungsbereich immer geöffnet, d.h. sie reagierte nicht mehr auf physiologische Spannungsänderungen (**Poree et al., 2005**).

K_{weak} Kanäle reagieren sensitiv auf Phosphorylierungen

Im Gegensatz zu den Unterschieden zwischen K_{in} und K_{out} Kanälen sind die molekularen Ursachen der schwachen Gleichrichtung von K_{weak} Kanälen -Dank neuester Studien am K_{weak} Kanal AKT2 **(Dreyer et al., 2001; Michard et al., 2005a; Michard et al., 2005b)**- relativ gut verstanden. Im Grunde sind K_{weak} Kanäle einwärtsgleichrichtende Kaliumkanäle, d.h. sie aktivieren mit negativ werdender Membranspannung und schließen mit positiv werdender Membranspannung. Die Besonderheit von K_{weak} Kanälen ist ihre Hypersensitivität gegenüber der

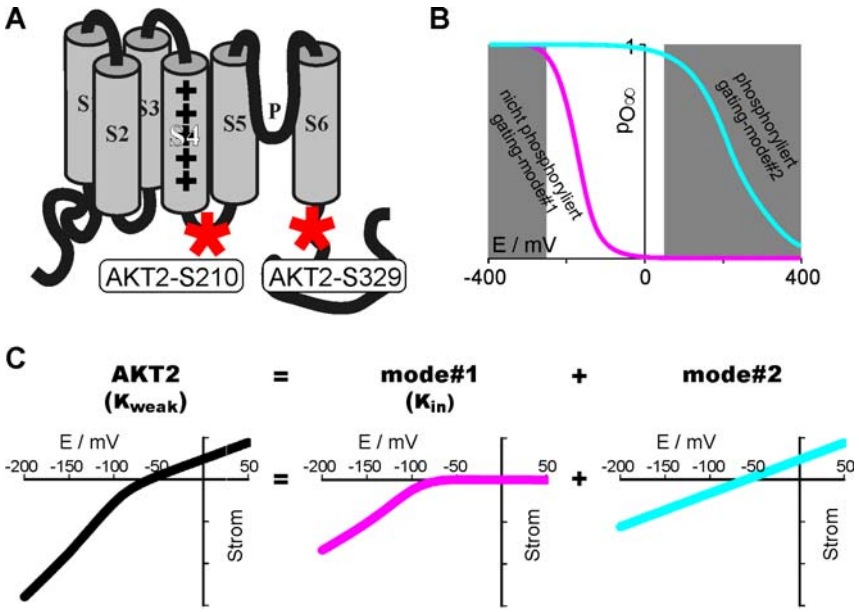

Abbildung 15. K_{weak} Kanäle reagieren sensitiv auf Phosphorylierungen.
(A) Zwei putative Phosphorylierungsstellen sind hoch konserviert in allen K_{weak} Kanälen. In AKT2 sind dies Serin 210 und Serin 329. **(B)** Sind beide Serine phosphoryliert, so aktiviert der Kanal bereits bei sehr hohen positiven Spannungen („gating-mode#2“, *blaue Kurve*). Im physiologischen Spannungsbereich (*weißer Bereich*) ist der Kanal offen. Sind die Serine nicht phosphoryliert, so aktiviert der Kanal wie ein gewöhnlicher Einwärtsgleichrichter (K_{in} Kanal) bei moderaten negativen Spannungen („gating-mode#1“, *violette Kurve*). **(C)** In einem Standardexperiment, z.B. in *Xenopus* Oozyten oder in COS-Zellen, besteht ein Gleichgewicht zwischen phosphorylierten und nicht-phosphorylierten K_{weak} Kanälen. Die Überlagerung der beiden unterschiedlichen Schaltverhalten („mode#1“ und „mode#2“) erzeugt das charakteristische Bild der schwachen Gleichrichtung. [Abbildung teilweise aus **Dreyer et al. (2002; 2004a)**].

Phosphorylierung bestimmter Aminosäuren im zytosolischen Bereich zwischen den transmembranen Domänen S4 und S5 und im zytosolischen Bereich kurz nach der sechsten transmembranen Domäne (Abbildung 15A) (**Michard et al., 2005a**). Die Phosphorylierung von Serinen in diesen beiden Bereichen induziert eine Änderung des Schaltverhaltens des Kanals (Änderung von „gating-mode#1“ zu „gating-mode#2). Physikalisch bedeutet dies eine Reduzierung der Energie, die nötig ist, den Kanal zu öffnen, um etwa 9 *kT* **(Michard et al., 2005b)**. Als Folge ist der phosphorylierte Kanal im gesamten physiologischen Spannungsbereich offen und schließt erst bei unphysiologisch hohen, positiven Spannungen (Abbildung 15B) (**Dreyer et al., 2001**).

Die Serine sind Bestandteil der Sequenz [R-X-S], die in *Xenopus* Oozyten und in COS Zellen von endogenen Proteinkinasen des Typs A erkannt wird. In einem gewöhnlichen Experiment, z.B. in *Xenopus* Oozyten, liegen daher K_{weak} Kanäle sowohl im phosphorylierten als auch im nicht-phosphorylierten Zustand vor. Die phosphorylierten Kanäle tragen einen instantan aktivierenden Strom mit einer nahezu linearen Stromspannungskennlinie, während die nicht-phosphorylierten Kanäle zeit- und spannungsabhängig aktivieren und eine einwärtsgleichrichtenden Stromspannungskennlinie aufweisen (**Dreyer et al., 2001**). Die ursprünglich beschriebene schwache Gleichrichtung von K_{weak} Kanälen kann durch die Überlagerung dieser beiden Stromkomponenten erklärt werden (Abbildung 15C; vergleiche mit Abbildung 7) (**Dreyer et al., 2001**).

K_{weak} Kanäle sind sehr sensitiv gegenüber Phosphorylierung der beiden genannten Stellen. Eine ähnlich ausgeprägte Sensitivität gegenüber Phosphorylierungsereignissen konnte für K_{in} oder K_{out} Kanäle bislang noch nicht nachgewiesen werden. Mittels vergleichender Analysen zwischen dem K_{weak} Kanal AKT2 und dem K_{in} Kanal KAT1 konnten **Michard et al. (2005b)** zeigen, dass der Spannungssensor von K_{weak} Kanälen eine besondere Rolle bei der Ausprägung der Sensitivität spielt. Die Phosphorylierungsstellen liegen in Bereichen, die beim Öffnen und Schließen des Kanals starke Konformationsänderungen durchführen (Long et al., 2005a). Im geschlossenen Zustand des Kanals (Abbildung 12) sind die Phosphorylierungsstellen nicht für Kinasen zugänglich. Erst die Bewegung des Spannungssensors induziert Konformationsänderungen, die die Phosphorylierungsstellen exponieren (**Michard et al., 2005a**). Die Phosphorylierung dieser Stellen blockiert den Spannungssensor im Offen-Zustand, so dass ein Schließen nur unter großem energetischen Aufwand möglich ist (d.h. bei sehr positiven Spannungen). **Michard et al. (2005b)** ersetzten im

Spannungssensor des K_{weak} Kanals AKT2 ein K_{weak}-spezifisches Lysin durch Serin und konnten dadurch die Blockierung im Offen-Zustand aufheben. Der mutierte Kanal zeigte das Aktivierungsverhalten eines K_{in} Kanals mit klassischen einwärtsgleichrichtenden Eigenschaften. Die biophysikalische Analyse zeigte, dass die Präsenz des Lysins im Spannungssensor den Effekt der Phosphorylierung des K_{weak} Kanals AKT2 um etwa 6 *kT* verstärkt **(Michard et al., 2005b)**.

Die physiologische Bedeutung der Phosphoregulation von K_{weak} Kanälen ist noch nicht erforscht. Es sollte jedoch erwähnt werden, dass beide charakteristischen Stromkomponenten von K_{weak} Kanälen in Protoplasten verschiedener Pflanzenzellen nachgewiesen wurden (Bauer et al., 2000; Ivashikina et al., 2005). Darüber hinaus wurde in *Arabidopsis thaliana* eine Phosphatase identifiziert, die spezifisch mit dem K_{weak} Kanal AKT2 interagiert (Chérel et al., 2002). Diese Phosphatase ist - wie AKT2 auch - unter anderem in Schließzellen exprimiert (Ivashikina et al., 2005), was erklären könnte, dass bislang in Schließzellen keine schwach-gleichrichtenden Kaliumkanäle nachgewiesen wurden **(Hedrich et al., 1995; Dietrich et al., 1998; Bruggemann et al., 1999b)**. Diese verschiedenen Ergebnisse lassen vermuten, dass in der Pflanze die Gleichrichtungseigenschaft von K_{weak} Kanälen stark kontrolliert wird. Wie **Michard et al. (2005b)** diskutieren, würde diese Kontrolle auch physiologisch durchaus Sinn machen. Im nicht-phosphorylierten Zustand („gating-mode#1“) sind K_{weak} Kanäle einwärtsgleichrichtende Kaliumkanäle. Im Zusammenspiel mit H^+-ATPasen ermöglichen sie es der Zelle, größere Mengen an K^+ zu akkumulieren (z.B. bei der Stomaöffnung; Ivashikina et al., 2005). Phosphorylierung ändert das Schaltverhalten von K_{weak} Kanälen, so dass die Kanäle auch bei Depolarisierungen nicht mehr schließen. Als Folge stabilisiert sich die Membranspannung in der Nähe der Nernst-Spannung für K^+-Ionen (Deeken et al., 2002). Darüber hinaus aktiviert die Phosphorylierung eine physiologisch wichtige „Kaliumbatterie“. Ein offener Kaliumkanal ermöglicht nämlich die Nutzung des transmembranen K^+-Gradienten (zusätzlich zum transmembranen Protonengradienten), um andere transmembrane Transportprozesse zu energetisieren. Interessanterweise haben **Ache et al. (2001)** nachgewiesen, dass K_{weak} Kanal Untereinheiten ihre besonderen Schalteigenschaften auch auf heteromere Kaliumkanäle (mit K_{in} Untereinheiten) übertragen können. Somit könnte eine Zelle über Phosphorylierung von K_{weak} Kanal Untereinheiten kontrollieren, ob sie die Kaliumbatterie lädt oder ausnutzt **(Michard et al., 2005b)**.

In *Arabidopsis* wird der K_{weak} Kanal AKT2 hauptsächlich im Phloemgewebe, in Mesophyllzellen und in Schließzellen erprimiert (Marten et al., 1999; Deeken et al., 2000; Lacombe et al., 2000; Dennison et al., 2001; Chérel et al., 2002; Deeken et al., 2002; Ivashikina et al., 2005). Aufgrund seiner eigentümlichen Eigenschaften könnte AKT2 somit am Zuckertransport im Phloem beteiligt sein. Er könnte aber auch eine wichtige Rolle in der elektrischen Signalverarbeitung und –weiterleitung spielen **(Michard et al., 2005b)**.

Der pH-Sensor von K_{in} Kanälen

Die Akkumulation größerer Mengen an K^+ realisieren Pflanzenzellen zu einem Teil über einen Proton-Kalium-Antiport. An diesem Prozess sind zwei verschiedene Transporter beteiligt: (i) Die Plasmamembrane H^+-ATPase (Abbildung 16, Pumpe, *gestrichelte graue Linie*) pumpt Protonen aus der Zelle und etabliert dadurch einen einwärtsgerichteten elektrischen Gradienten, d.h. die Membranspannung wird negativ. (ii) Ein einwärtsgleichrichtender Kaliumkanal (Abbildung 16, K_{in}, *gepunktete graue Linie*) öffnet bei negativen Spannungen und ermöglicht die Diffusion von K^+-Ionen entlang ihres elektrochemischen Gradienten. Im Gleichgewicht kompensiert die Ladung des K^+-Einstroms die Ladung des H^+-Ausstroms (Abbildung 16, *schwarze Line*, Schnittpunkt mit der Abszissenachse). Darüber hinaus baut dieser Transport einen chemischen Protonengradienten auf. Da das Zytoplasma stark gepuffert ist (Grabov und Blatt, 1997; Grabov und Blatt, 1998), verändert sich der zytosolische pH Wert kaum

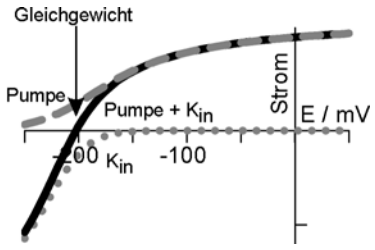

Abbildung 16. K^+-Aufnahme durch das Zusammenspiel von Pumpen und K_{in} Kanälen.
Virtuelle Strom-Spannungskennlinien der H^+-ATPase (*grau, gestrichelt*), des K_{in} Kanals (*grau, gepunktet*) und des kombinierten Systems aus beiden (*schwarz, durchgezogen*). Protonen-ATPasen (Pumpe) erzeugen durch den aktiven Transport von H^+ aus der Zelle einen positiven Pumpstrom (*gestrichelte graue Line*). Dadurch wird die Membranspannung negativ. Kaliumaufnahmekanäle (K_{in}) öffnen bei negativen Spannungen und erlauben den passiven Einstrom von K^+-Ionen in die Zelle (negativer Strom, *gepunktete graue Linie*). Durch diesen Einstrom wird die Membranspannung positiver. Im Gleichgewicht kompensieren sich die beiden Ströme (Schnittpunkt der schwarzen Linie mit der Abszisse). Der Netto-Ladungstransport ist Null. Das System tauscht Protonen gegen Kaliumionen. [Abbildung teilweise nach Blatt (1992) und **Dreyer et al. (2004a)**].

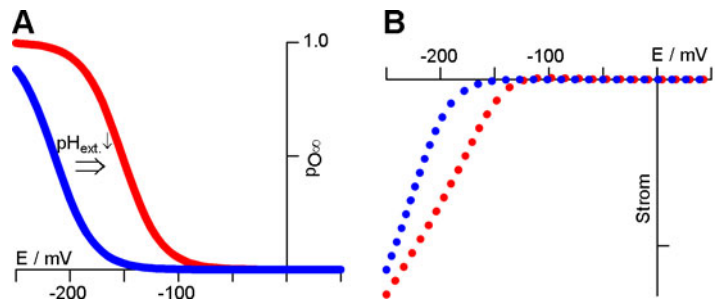

Abbildung 18. Extrazelluläre Ansäuerung aktiviert K_{in} Kanäle.
(A) Ein sinkender extrazellulärer pH-Wert verschiebt die Spannungsabhängigkeit der K_{in} Kanäle (Offenwahrscheinlichkeit $p_{O\infty}$) zu weniger negativen Spannungen. In diesem Fall sind die Verhältnisse für einen neutralen Apoplasten (pH7,0; *blaue Kurve*) und einen leicht säuerlichen Apoplasten (z.B. pH5,5; *rote Kurve*) dargestellt. **(B)** Als Konsequenz fließt bei gleicher Spannung ein größerer Kaliumstrom über die Membran. [Abbildung teilweise nach **Dreyer et al. (2002; 2004a)**].

(pH 7.0). Der extrazelluläre Raum wird durch die Aktivität der Pumpe jedoch angesäuert (~pH 5-6). K_{in} Kanäle reagieren auf diese apoplastische Ansäuerung mit einer Aktivierung (Blatt, 1992; **Hedrich et al., 1995**; Mueller-Roeber et al., 1995; **Hoth et al., 1997a; Dietrich et al., 1998; Bruggemann et al., 1999a; Bruggemann et al., 1999b**). Mit abnehmendem extrazellulären pH-Wert verringert sich die Energie, die nötig ist, einen Kanal zu öffnen. Die Aktivierungsschwelle der Kanäle verschiebt sich auf der Spannungsachse in positive Richtung (Abbildung 18A). Als Folge sind im sauren Milieu bei konstanter Spannung mehr K_{in} Kanäle aktiv als im neutralen, und damit ist auch die Stromamplitude größer (Abbildung 18B).

Im Zusammenspiel mit der Protonenpumpe hat diese Aktivierung entscheidende Auswirkungen. Die Gleichgewichtspannung, bei der der Protonenstrom den Kaliumstrom kompensiert, verschiebt sich bei sinkendem extrazellulärem pH-Wert zu weniger negativen Spannungen (Abbildung 17). Damit verbessert sich aber auch die

Abbildung 17. Extrazelluläre Ansäuerung optimiert die Energienutzung.
(A) Neutraler extrazellulärer pH: Der Kaliumeinstrom kompensiert den Protonenausstrom. Das System ist bei der durch den Pfeil gekennzeichneten Membranspannung im Gleichgewicht. **(B)** Ein sinkender extrazellulärer pH-Wert verschiebt die Spannungsabhängigkeit der K_{in} Kanäle (Abbildung 18) und aktiviert sie damit. Als Folge verschiebt sich die Gleichgewichtsmembranspannung zu weniger negativen Werten (*schwarzer Pfeil*). In der Konsequenz werden mehr K^+- und H^+-Ionen pro Zeiteinheit transportiert (Unterschied zwischen *blauer* und *roter gestrichelter Linie*).

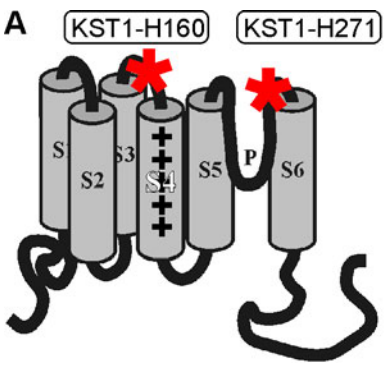

B

Position 160	Position 271: H	A	R	D
H	Vergleich	schwächer	invers	stärker
A	schwächer	insensitiv		
R	schwächer			
D	schwächer			

Abbildung 19. Extrazelluläre Histidine sind Bestandteil des pH-Sensors von KST1.
(A) Eine Untereinheit des K_{in} Kanals KST1 hat zwei extrazelluläre Histidine. Schematische Darstellung der Position im Polypeptid. **(B)** Der Austausch der Histidine durch die neutrale Aminosäure Alanin („A“), die positiv geladene Aminosäure Arginin („R“) und die negativ geladene Aminosäure Aspartat („D“) beeinflusst die Antwort auf extrazelluläre pH-Wert Änderungen. Zusammenfassende Darstellung der Ergebnisse aus **Hoth et al. (1997a)**.

Energieeffizienz der H^+-ATPase. Die Energie, die aus der Hydrolyse von ATP zu ADP gewonnen wird, muss weniger stark dafür eingesetzt werden, Protonen gegen den elektrischen Gradienten zu transportieren. Als Folge werden mehr Protonen und mehr Kaliumionen pro Zeiteinheit transportiert (Abbildung 17) (Blatt, 1992).

Auf der Suche nach der molekularen Ursache der pH-Regulation haben **Hoth et al. (1997a)** am Beispiel des K_{in} Kanals KST1 aus Schließzellen der Kartoffel Aminosäuren identifiziert, die an der pH-Regulation dieses Kanals beteiligt sind. Es handelte sich hierbei um zwei Histidine (Abbildung 19A). Eins ist im extrazellulären Bereich zwischen den transmembranen Segmenten S3 und S4 lokalsiert (KST1-H160), das andere am Carboxy-terminalen Ende der Porenregion (KST1-H271). Nach Ersetzen beider Histidine durch Alanine war der mutierte Kanal nicht mehr sensitiv gegenüber einer Änderung des extrazellulären pH-Werts (Abbildung 19). Eine Verschiebung der Aktivierungsschwelle konnte nicht mehr beobachtet werden (vgl. Abbildung 18A).

Wurde allein das Histidin an Position 160 gegen die ungeladene Aminsäure Alanin, gegen die negativ geladene Aminosäure Aspartat oder gegen die positiv geladene Aminosäure Arginin ausgetauscht, so war in allen drei Fällen der pH-Effekt abgeschwächt. D.h. trotz Gegenwart des Histidins in der Porenregion, induzierte eine extrazelluläre pH-Wert Änderung bei allen drei Mutanten eine geringere Verschiebung der Aktivierungsschwelle als im Wildtyp.

Ein differenzierteres Bild ergab sich, wenn allein das Histidin an Position 271 mutiert wurde. Während auch hier der pH-Effekt durch den Austausch des Histidins gegen die ungeladene Aminsäure Alanin abgeschwächt worden ist, wurde er durch den Austausch gegen die negativ geladene Aminosäure Aspartat sogar noch verstärkt. Der

Austausch des Histidins gegen die positiv geladene Aminosäure Arginin resultierte in einem inversen Verhalten des mutierten Kanals KST1-H271R gegenüber pH-Wert Änderungen **(Dreyer et al., 1997; Hoth et al., 1997a)**. Die Öffnung dieses Kanals wurde durch Ansäuerung des extrazellulären Mediums energetisch erschwert. Die Aktivierungsschwelle des mutierten Kanals verschob sich auf der Spannungsachse in negative Richtung (umgekehrt zu dem in Abbildung 18A gezeigten Verhalten).

Zusammenfassend, zeigen die Ergebnisse von **Hoth et al. (1997a)**, (i) dass beide Histidine an der Regulation von KST1 durch Protonen beteiligt sind, (ii) dass das Histidin an Position 160 maßgeblich die Stärke des pH-Effekts bestimmt, und (iii) dass das Histidin in der Porenregion an Position 271 dagegen weitestgehend „nur" modulierenden Charakter hat.

Der K^+-Sensor von K_{out} Kanälen

Auswärtsgleichrichtende Kaliumkanäle (K_{out}) besitzen die bemerkenswerte Eigenschaft, nur bei Membranspannungen zu öffnen, bei denen der elektrochemische Gradient auswärtsgerichtet ist, d.h. bei Spannungen, die positiver sind als die Gleichgewichtsspannung für K^+, E_K (Abbildung 6B). Dies bedeutet, dass das Schaltverhalten von K_{out} Kanälen nicht nur von der Membranspannung abhängt, sondern auch von der extrazellulären K^+ Konzentration (Blatt, 1991). Hierin unterscheiden sich K_{out} Kanäle fundamental von einwärtsgleichrichtenden Kaliumkanälen (K_{in}), deren Schaltverhalten insensitiv gegenüber Änderungen in der extrazellulären K^+ Konzentration ist **(Bruggemann et al., 1999a; Johansson et al., 2006)**.

Aus biophysikalischer Sicht modulieren extrazelluläre Kaliumionen das Schaltverhalten von K_{out} Kanälen, indem sie die Energie erhöhen, die nötig ist, einen Kanal zu aktivieren. Es bedarf daher bei hohen extrazellulären K^+ Konzentrationen einer größeren Membranspannung, um die Kanäle zu einem bestimmten Grad zu aktivieren, als bei niedrigeren. Die Aktivierungsschwelle der Kanäle verschiebt sich mit steigender extrazellulärer K^+ Konzentration auf der Spannungsachse in positive Richtung (Abbildung 6C). Aus physiologischer Sicht erlaubt dieser Mechanismus den K_{out} Kanälen, die extrazelluläre Kaliumkonzentration zu „fühlen". Dadurch wird garantiert, dass K_{out} Kanäle nur öffnen, wenn die treibende Kraft für einen netto K^+-Fluss auswärtsgerichtet ist. In Schließzellen zu Beispiel erleichtert diese Eigenschaft,

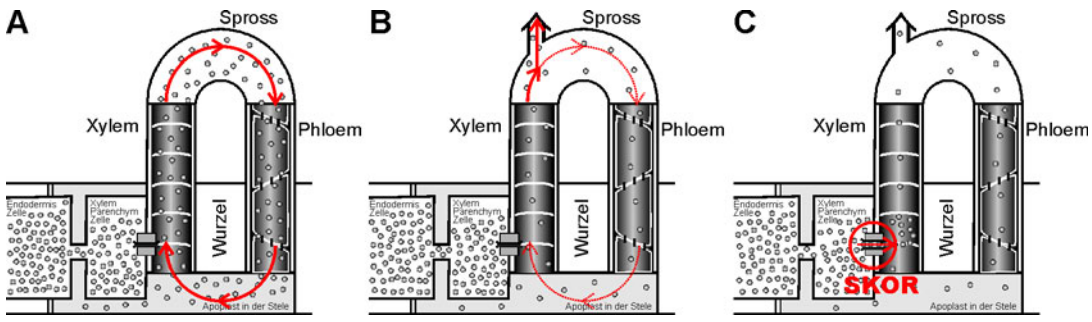

Abbildung 20. Einfaches Schema zur K^+ Zirkulation über Xylem und Phloem in der Pflanze.
(A) Kaliumionen werden in der Pflanze mit dem Transpirationsstrom von der Wurzel, dem Ort der Aufnahme, in den Spross transportiert. Im Gegenzug werden Kaliumionen im Phloem vom Spross zur Wurzel transportiert. **(B)** Durch die Entnahme von K^+ im Spross, z.B. beim Wachstum, reduziert sich die zurücktransportierte Kaliummenge. **(C)** Der K_{out} Kanal SKOR nimmt die reduzierte K^+ Konzentration im Apoplasten der Stele war und belädt das Xylem mit K^+ aus den Wurzelzellen. [Abbildung nach Wegner und de Boer (1997) und modifiziert nach **Johansson et al. (2006; animiertes Online Zusatzmaterial)**].

den Kaliumausfluss beim Stomaschluss aufrechtzuerhalten. Dadurch kann der Gasaustausch kontrolliert werden, selbst wenn die extrazelluläre K^+ Konzentration über eine Bandbreite von 10 nM bis 100 mM variiert (Blatt, 1988; Schroeder, 1989; Blatt und Gradmann, 1997; Roelfsema und Prins, 1997). Ein anderes Beispiel für die Effizienz K^+-regulierter K_{out} Kanäle ist die Xylembeladung. Hierbei ermöglicht der K^+-Sensor die regulierte K^+-Abgabe von Kaliumionen aus dem Parenchym in die Leitbündel (Roberts und Tester, 1995; Wegner und de Boer, 1997). Um die physiologische Bedeutung verständlicher zu machen, wird in Abbildung 20 der K^+-Fluss innerhalb einer Pflanze schematisch dargestellt. Ein großer Teil der Kaliumionen, die sich im Transpirationsstrom des Xylems bewegen, wird aus dem rückfließenden Phloem eingespeist (Abbildung 20A) (Kochian und Lucas, 1988). Somit spiegelt die apoplastische Kaliumkonzentration in der Stele die Re-Zirkulation von K^+ wider und damit die Nachfrage des Sprossgewebes nach diesem Ion (Abbildung 20B). Der K_{out} Kanal SKOR wird in der Stele von *Arabidopsis thaliana* exprimiert (Gaymard et al., 1998). SKOR „fühlt“ die apoplastische Kaliumkonzentration und entlässt K^+ Ionen in das Xylem, falls weniger Kalium über das Phloem re-zirkuliert wird (Abbildung 20C) (Engels und Marschner, 1992; Roberts und Tester, 1995; Wegner und de Boer, 1997).

Der molekulare Mechanismus, der es SKOR ermöglicht, die extrazelluläre K^+ Konzentration wahrzunehmen, wurde kürzlich von **Johansson et al. (2006)** aufgeklärt. In ausführlichen Mutagenesestudien wurden in verschiedenen Bereichen des Polypeptids einzelne Aminosäuren ausgetauscht, um ihre Bedeutung für das K^+-abhängige Schaltverhalten von SKOR zu überprüfen (Abbildung 21). Es stellte sich heraus, dass nur Änderungen bestimmter Aminosäuren in der Porenregion und in der

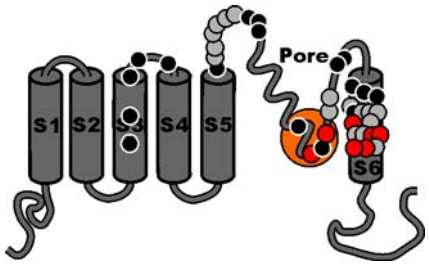

Abbildung 21. Überprüfte Bereiche auf der Suche nach dem K^+-Sensor von SKOR.
Es wurden Punktmutationen in weiten Bereichen des SKOR Polypeptids eingeführt. Jeder Punkt symbolisiert eine solche Mutation. Darüber hinaus wurde ein größerer Teile der Pore von SKOR durch den äquivalenten Bereich aus KAT1 ersetzt (größere Punkt in der Pore). Die Mutationen, die die K^+-Sensitivität von SKOR veränderten, sind durch rote Punkte gekennzeichnet. Die schwarzen Punkte bezeichnen die Mutationen, die die K^+-Sensitivität von SKOR nicht veränderten. Graue Punkte symbolisieren die Mutanten, die nicht mehr als funktioneller Kaliumkanal in Oozyten nachweisbar waren. [Abbildung nach **Johansson et al. (2006)**].

sechsten transmembranen Domäne die K^+-Abhängigkeit beeinflussten (Abbildung 21, *rote Punkte*). Mutationen in anderen Bereichen veränderten die Eigenschaften von SKOR entweder gar nicht (Abbildung 21, *schwarze Punkte*) oder waren anscheinend letal für die Kanalfunktion (Abbildung 21, *graue Punkte*).

Bei einer genaueren Analyse der wirksamen Mutationen in der Pore und im S6-Segment konnten diese in drei große Gruppen eingeteilt werden: (i) Zwei Mutationen in S6 verschoben allein die Aktivierungsschwelle des Kanals auf der Spannungsachse, eine in positive, die andere in negative Richtung. Die Mutanten wiesen aber immer noch die gleiche K^+-Sensitivität auf, wie der nicht mutierte SKOR Kanal (Abbildung 22, *gelb*). Aus biophysikalischer Sicht bedeutet dies, dass die Mutationen die Energien verändert haben, die nötig sind, die Kanäle zu aktivieren. Der Einfluss extrazellulärer Kaliumionen auf diese Energien blieb jedoch als additive Größe erhalten. (ii) Eine

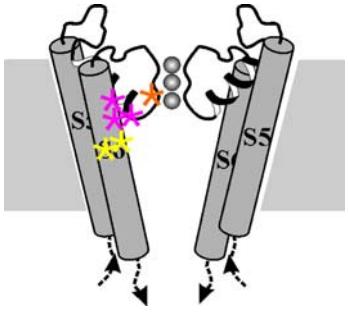

Abbildung 22. Unterschiedliche Wirkungen von Mutationen auf das Schaltverhalten von SKOR.
Punktmutationen in der Pore und im S6-Segment wirkten sich unterschiedlich auf das K^+-abhängige Schaltverhalten von SKOR aus. Mutationen an zwei Positionen in S6 (*gelb*) verschoben die Aktivierungsschwelle auf der Spannungsachse, ließen aber die K^+-Abhängigkeit unverändert. Mutationen an zwei Positionen in S6 und an einer Position in der Pore (*lila*) verschoben sowohl die Aktivierungsschwelle und änderten die K^+-Abhängigkeit. Die Mutation an einer Stelle in der Pore (orange) veränderte allein die K^+-Abhängigkeit, ließ aber die Aktivierungsschwelle unverändert. [Abbildung nach **Johansson et al. (2006)**].

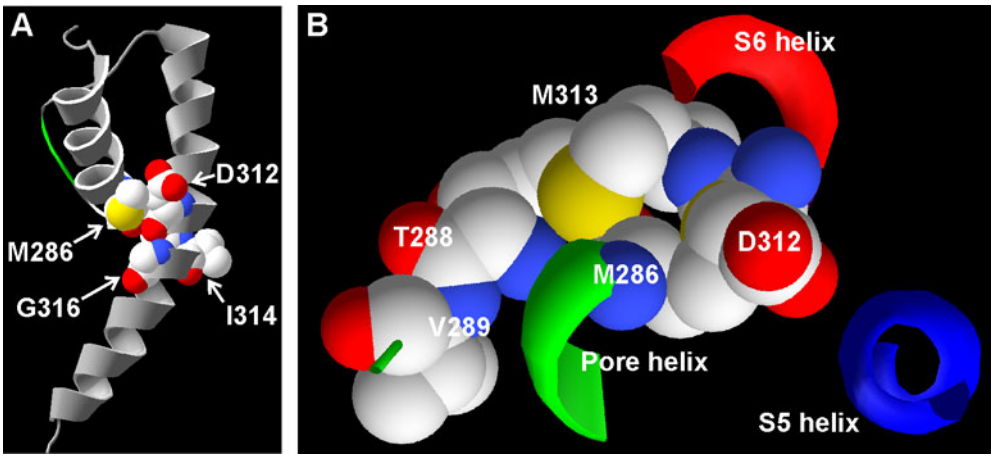

Abbildung 23. Direkter Kontakt zwischen Pore und S6-Segment im K_{out} Kanal SKOR.
Modellierung der SKOR Sequenz auf die Kristallstruktur des spannungsregulierten Kanals KvAP aus *Aeropyrum pernix*. **(A)** Der Ausschnitt aus der Porenregion und dem S6 Segment zeigt die Nachbarschaft zwischen den Aminosäuren M286 und D312 und M313 (verdeckt). Die Aminsäuren I314 und G316 korrespondieren mit den gelben Sternen in Abbildung 22. Der Selektivitätsfilter ist links in grün angedeutet. Die abgeleitete atomare Distanz zu M286(S_δ) beträgt: D312($O_\gamma^{(-)}$), 3.7Å; M313(S_δ), 3.4 Å; G316(C_α), 5.1 Å. **(B)** Darstellung von (A) in einer Aufsicht. Die Aminosäure V289 wurde in Abbildung 22 als oranger Stern dargestellt. [Abbildung aus **Johansson et al. (2006)**].

Mutation im Selektivitätsfilter der Pore hatte keinen Einfluss auf die Aktivierungsschwelle des Kanals, sofern diese mit dem nicht mutierten SKOR Kanal in niedrigen Kaliumkonzentrationen verglichen wurden. Der Einfluss extrazellulärer Kaliumionen auf die Aktivierungsschwelle - und damit auf die Aktivierungsenergie - war in der Mutante jedoch stark abgeschwächt (Abbildung 22, *orange*). (iii) Zwei Mutationen in S6 und eine Mutation in der Pore veränderten sowohl die Aktivierungsschwelle bei niedriger Kaliumkonzentration als auch den Einfluss extrazellulären Kaliumionen auf diese (Abbildung 22, *lila*). Die sehr ähnlichen Befunde in der letzten Gruppe konnten dadurch erklärt werden, dass sich die untersuchten Bereiche in räumlicher Nähe im dreidimensionalen Kanalprotein befinden. Eine Modellierung der SKOR Sequenz auf die Kristallstruktur des spannungsregulierten Kanals KvAP aus *Aeropyrum pernix* (Jiang et al., 2003) zeigte, dass die drei identifizierten Aminosäuren in direktem Kontakt zueinander stehen (Abbildung 23).

Aufbauend auf diese Resultate entwickelten **Johansson et al. (2006)** ein Modell, dass die modulierende Wirkung extrazellulärer Kaliumionen auf den SKOR Kanal erklären konnte. Die Grundideen dieses Modells sind in Abbildung 24 dargestellt. Ein geöffneter K_{out} Kanal (Abbildung 24A) schließt durch Konformationsänderungen im Caroxy-terminal Bereich des S6 segments. Dadurch wird der Zugang von Kaliumionen aus dem Zytosol in die Porenregion unterbunden. Der Zugang aus dem Extrazellulärraum ist jedoch weiterhin möglich (Abbildung 24B). Als Folge stellt sich

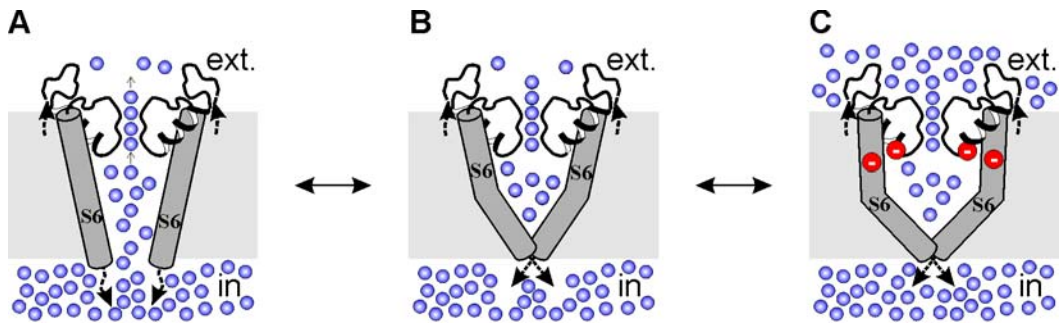

Abbildung 24. Die Grundprinzipien des K^+-Sensors von SKOR.
(A) Ein offener K_{out} Kanal erleichtert die Diffusion von Kaliumionen in den Extrazellulärraum. **(B)** Der Kanal schließt durch Konformationsänderungen im Carboxy-terminalen Bereich des S6-Segments. **(C)** Die Besetzung des Selektivitätsfilter durch K^+-Ionen induziert eine weitere Konformationsänderung und stabilisiert den Geschlossenzustand des Kanals [Abbildung nach **Johansson et al. (2006; animiertes Online Zusatzmaterial)**].

ein Gleichgewicht zwischen der extrazellulären Kaliumkonzentration und der K^+ Konzentration im Selektivitätsfilter und in der Pore ein. Ist der Selektivitätsfilter besetzt, so ist dieser starr (Zhou et al., 2001). Die Interaktion zwischen der Pore und dem S6 Segment induziert weitere Konformationsänderungen, die den Geschlossenzustand des Kanals stabilisieren (Abbildung 24C).

Basierend auf diese Grundideen wird im folgenden das gesamte Modell für die Modulation des Schaltverhaltens von SKOR durch K^+-Ionen vorgestellt (Abbildung 25). Ein offener K_{out} Kanal erleichtert die Diffusion von Kaliumionen in den Extrazellulärraum (A). Der Kanal schließt durch Konformationsänderungen im

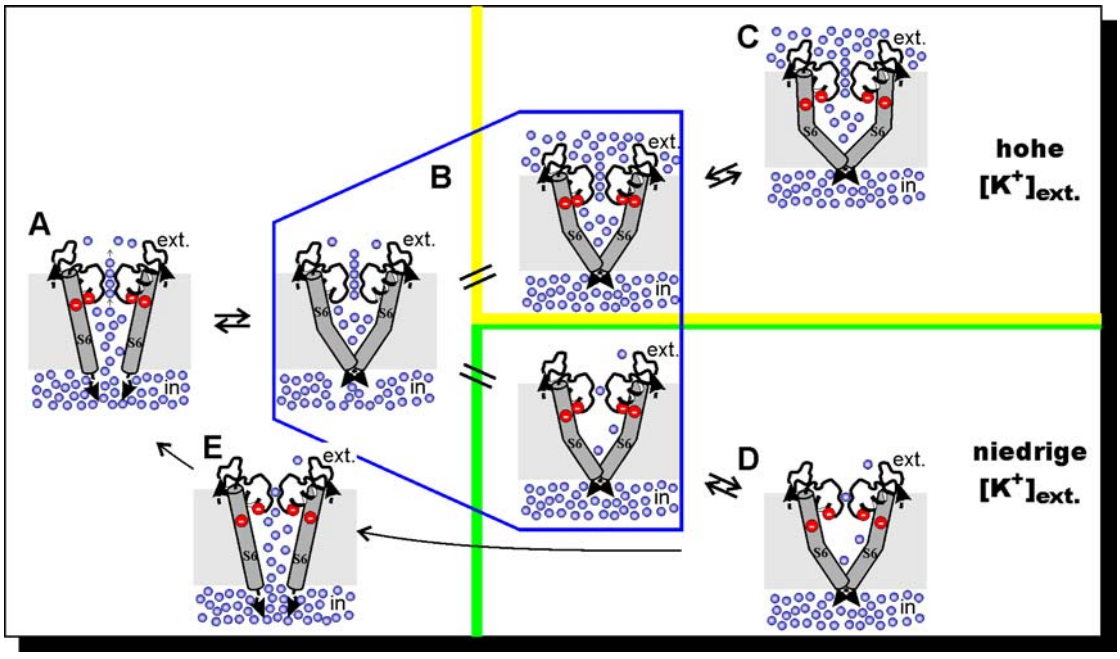

Abbildung 25. Modell für die Modulation des Schaltverhaltens von SKOR durch K^+-Ionen.
Erläuterungen im Text. [Abbildung nach **Johansson et al. (2006; animiertes Online Zusatzmaterial)**].

Carboxy-terminalen Bereich des S6-Segments. Die Kaliumkonzentration in der Pore hängt nur noch von der extrazellulären Kaliumkonzentration ab (B). Ist die extrazelluläre K^+ Konzentration hoch, so ist der Selektivitätsfilter durch K^+-Ionen besetzt und starr. Die Interaktion zwischen der Porenregion und dem S6 Segment (Abbildung 23) induziert eine weitere Konformationsänderung, die den Geschlossenzustand des Kanals stabilisiert (C). Ist die extrazelluläre K^+ Konzentration niedrig, so ist der Selektivitätsfilter nicht durch K^+-Ionen besetzt. Er nimmt in diesem Fall eine andere Struktur an (Zhou et al., 2001) (D). Es wird keine weitere Konformationsänderung in S6 induziert. Dadurch kann der Kanal einfacher wieder öffnen (E). Die aus dem Zytosol in die Pore einströmenden Kaliumionen ändern wieder die Struktur des Selektivitätsfilters und der Kanal erleichtert erneut die passive Diffusion von K^+ Ionen (A). **(Johansson et al., 2006; animiertes Online Zusatzmaterial)**.

Ausblick

Die strukturelle und mechanistische Aufklärung der verschiedenen Regulationen pflanzlicher Transportproteine ist die Grundlage für ein tieferes Verständnis ihrer physiologischen Rolle. Die gewonnenen Erkenntnisse ermöglichen Einblicke in die komplexen zellulären Signalnetzwerke und erlauben die Generierung neuer, weiterreichender Hypothesen. Weiterhin ist die Isolierung von mutierten Transportproteinen, die in ihren regulatorischen Eigenschaften verändert sind, von enormem experimentellem Wert. Sie eröffnen die Möglichkeit, die Auswirkungen von

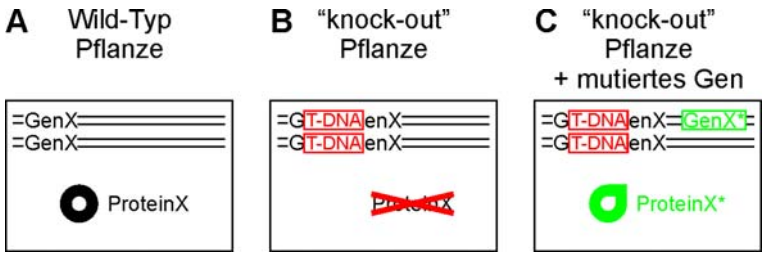

Abbildung 26. Schematische Darstellung einer Strategie zur gezielten Mutagenese *in planta*.
(A) Das Genom der Wild-Typ *Arabidopsis* Pflanze enthält zwei Allele des Gens X. Es wird das Protein X exprimiert. **(B)** Durch die Insertion einer T-DNA wird die Funktion des Gens gestört. Durch Selektion können homozygote Pflanzen isoliert werden, bei denen beide Allele des Gens eine T-DNA Insertion aufweisen. Im Großteil der Fälle wird kein funktionelles Protein mehr hergestellt. Diese Pflanzen werden „knock-out" Pflanzen genannt. **(C)** Die Transformation der „knock-out" Pflanze mit einem mutierten GenX* resultiert in der Expression eines mutierten Proteins X*. In dieser Pflanze wird nur das mutierte Protein exprimiert.

Defekten in der Regulation auch *in vivo* zu untersuchen. Die Strategie hierzu ist in Abbildung 26 dargestellt. Mittlerweile gibt es große Kollektionen von *Arabidopsis thaliana* Pflanzen, bei denen die Funktion bestimmter Gene durch den zufälligen Einbau einer T-DNA deletiert wurde (Abbildung 26 B). Es wurden zum Beispiel bereits für mindestens fünf der neun Gene, die für spannungsabhängige Kaliumkanäle kodieren, T-DNA Insertionslinien isoliert: *SKOR* (Gaymard et al., 1998), *GORK* (**Hosy et al., 2003**), *AKT2* (Dennison et al., 2001; Deeken et al., 2002), *AKT1* (Hirsch et al., 1998), *SPIK* (Mouline et al., 2002); für zwei weitere existieren *En-1* Transposon Linien: *AtKC1* (Reintanz et al., 2002), *KAT1* (Szyroki et al., 2001). In diese „knock-out" Pflanzen kann ein mutiertes Gen eingebracht werden, so dass ein gezielt verändertes Protein exprimiert wird (Abbildung 26 C). Aufbauend auf die Ergebnisse, die in dieser Habilitationsschrift vorgestellt wurden, wird die in Abbildung 26 vorgestellte Strategie zur Zeit für pflanzliche spannungsregulierte Kaliumkanäle angewandt. Ergebnisse zu diesen Studien werden in der nahen Zukunft erwartet.

Acknowledgements

Die Grundlagen großer Teile dieser Arbeit wurden während meines Auslandsaufenthalts am Laboratoire de Biochimie et Physiologie Moléculaires des Plantes am INRA in Montpellier, Frankreich, gelegt. Ich danke der Europäischen Union für die Förderung durch ein Marie-Curie Stipendium und den Leitern der AG „canaux ioniques", Drs. Hervé Sentenac und Jean-Baptiste Thibaud für die weitreichende Unterstützung. Weiterhin danke ich allen Mitgliedern im Labor für die phantastische Zusammenarbeit. Namentlich seinen erwähnt: Dr. Fabien Porée, Dr. Erwan Michard, Dr. Benoît Lacombe, Jossia Boucherez und Dr. Frédéric Gaymard. Begonnene Projekte konnte ich nach meiner Rückkehr nach Deutschland z.T. im altbewährten Team (F.P., E.M.) am Lehrstuhl Molekularbiologie der Universität Potsdam fortsetzen. Ich danke Herrn Prof. Dr. Bernd Müller-Röber, dass er mir dies ermöglicht hat. Ich danke ihm für das in mich gesetzte Vertrauen, die Freiheiten und die vielfältige Unterstützung. Erst dieses perfekte Umfeld ermöglichte es, langfristige Projekte weiterzuführen und sukzessive neue Projekte aufzubauen. Weiterhin danke ich allen Mitgliedern der AG Müller-Röber für die Unterstützung und das angenehme Arbeitsklima. Besonders erwähnen möchte ich Frau Antje Schneider, die mich nach Kräften im Labor unterstützt. Nicht zuletzt gilt mein Dank den Gutachtern für ihre Zeit und Mühen.

Literaturverzeichnis

Ache P., Becker D., Deeken R., Dreyer I., Weber H., Fromm J., Hedrich R. (2001). VFK1, a *Vicia faba* K^+ channel involved in phloem unloading. Plant J. **27,** 571-580.

Ache P., Becker D., Ivashikina N., Dietrich P., Roelfsema M.R., Hedrich R. (2000). GORK, a delayed outward rectifier expressed in guard cells of *Arabidopsis thaliana*, is a K^+-selective, K^+-sensing ion channel. FEBS Lett. **486,** 93-98.

Amtmann A., Armengaud P., Assmann S.M., Bibikova T.N., Boursiac Y., Blatt M.R., Bush D.R., Dominy P., Dreyer I., Gilroy S., Hawkesford M.J., Hills A., Homann U., Hurst A.C., Jakobsen M.K., Köhler B., López-Maqués R.L., Maathuis F.J., Maurel C., Miller T., Mueller-Roeber B., Palmgren M.G., Rosser S., Schiott M., Thiel G., Verdoucq L., Volkov V., Vander Willigen C. (2004a). Membrane Transport in Plants. Oxford, UK: Blackwell Publishing

Amtmann A., Armengaud P., Volkov V. (2004b). Potassium nutrition and salt stress. *In* Membrane Transport in Plants, M.R. Blatt, ed (Oxford: Blackwell), pp 316-348.

Anderson J.A., Huprikar S.S., Kochian L.V., Lucas W.J., Gaber R.F. (1992). Functional expression of a probable *Arabidopsis thaliana* potassium channel in *Saccharomyces cerevisiae*. Proc. Natl. Acad. Sci. U. S. A **89,** 3736-3740.

Arabidopsis Genome Initiative (2000). Analysis of the genome sequence of the flowering plant *Arabidopsis thaliana*. Nature **408,** 796-815.

Baizabal-Aguirre V.M., Clemens S., Uozumi N., Schroeder J.I. (1999). Suppression of inward-rectifying K^+ channels KAT1 and AKT2 by dominant negative point mutations in the KAT1 alpha-subunit. J. Membr. Biol. **167,** 119-125.

Bauer C.S., Hoth S., Haga K., Philippar K., Aoki N., Hedrich R. (2000). Differential expression and regulation of K^+ channels in the maize coleoptile: molecular and biophysical analysis of cells isolated from cortex and vasculature. Plant J. **24,** 139-145.

Becker D., Dreyer I., Hoth S., Reid J.D., Busch H., Lehnen M., Palme K., Hedrich R. (1996). Changes in voltage activation, Cs^+ sensitivity, and ion permeability in H5 mutants of the plant K^+ channel KAT1. Proc. Natl. Acad. Sci. U. S. A **93,** 8123-8128.

Bezanilla F. (2002). Voltage sensor movements. J. Gen. Physiol **120,** 465-473.

Bezanilla F., Perozo E. (2003). The voltage sensor and the gate in ion channels. Adv. Protein Chem. **63,** 211-241.

Blatt M.R. (1988). Potassium-dependent bipolar gating of potassium channels in guard cells. J. Membr. Biol. **102,** 235-246.

Blatt M.R. (1991). Ion channel gating in plants: physiological implications and integration for stomatal function. J. Membr. Biol. **124,** 95-112.

Blatt M.R. (1992). K^+ channels of stomatal guard cells. Characteristics of the inward rectifier and its control by pH. J. Gen. Physiol **99,** 615-644.

Blatt M.R. (2004a). Concepts and techniques in plant membrane physiology. *In* Membrane Transport in Plants, M.R. Blatt, ed (Oxford: Blackwell), pp 1-39.

Blatt M.R. (2004b). Preface. *In* Membrane Transport in Plants, M.R. Blatt, ed (Oxford: Blackwell Publishing), pp xvii-xx.

Blatt M.R., Gradmann D. (1997). K^+-sensitive gating of the K^+ outward rectifier in *Vicia* guard cells. J. Membr. Biol. **158,** 241-256.

Bruggemann L.I., Dietrich P., Becker D., Dreyer I., Palme K., Hedrich R. (1999a). Channel-mediated high-affinity K^+ uptake into guard cells from *Arabidopsis*. Proc. Natl. Acad. Sci. U. S. A **96,** 3298-3302.

Bruggemann L.I., Dietrich P., Dreyer I., Hedrich R. (1999b). Pronounced differences between the native K^+ channels and KAT1 and KST1 alpha-subunit homomers of guard cells. Planta **207,** 370-376.

Buschmann P.H., Vaidyanathan R., Gassmann W., Schroeder J.I. (2000). Enhancement of Na^+ uptake currents, time-dependent inward-rectifying K^+ channel currents, and K^+ channel transcripts by K^+ starvation in wheat root cells. Plant Physiol **122,** 1387-1397.

Bush D.R. (2004). Functional analysis of proton-coupled sucrose transport. *In* Membrane Transport in Plants, M.R. Blatt, ed (Oxford: Blackwell Publishing), pp 135-149.

Chérel I., Michard E., Platet N., Mouline K., Alcon C., Sentenac H., Thibaud J.B. (2002). Physical and functional interaction of the *Arabidopsis* K^+ channel AKT2 and phosphatase AtPP2CA. Plant Cell **14,** 1133-1146.

Cuello L.G., Cortes D.M., Perozo E. (2004). Molecular architecture of the KvAP voltage-dependent K^+ channel in a lipid bilayer. Science **306,** 491-495.

Daram P., Urbach S., Gaymard F., Sentenac H., Cherel I. (1997). Tetramerization of the AKT1 plant potassium channel involves its C-terminal cytoplasmic domain. EMBO J. **16,** 3455-3463.

Deeken R., Geiger D., Fromm J., Koroleva O., Ache P., Langenfeld-Heyser R., Sauer N., May S.T., Hedrich R. (2002). Loss of the AKT2/3 potassium channel affects sugar loading into the phloem of *Arabidopsis*. Planta **216,** 334-344.

Deeken R., Sanders C., Ache P., Hedrich R. (2000). Developmental and light-dependent regulation of a phloem-localised K^+ channel of *Arabidopsis thaliana*. Plant J. **23,** 285-290.

Dennison K.L., Robertson W.R., Lewis B.D., Hirsch R.E., Sussman M.R., Spalding E.P. (2001). Functions of AKT1 and AKT2 potassium channels determined by studies of single and double mutants of *Arabidopsis*. Plant Physiol **127,** 1012-1019.

Dietrich P., Dreyer I., Wiesner P., Hedrich R. (1998). Cation sensitivity and kinetics of guard-cell potassium channels differ among species. Planta **205,** 277-287.

Downey P., Szabo I., Ivashikina N., Negro A., Guzzo F., Ache P., Hedrich R., Terzi M., LoSchiavo F. (2000). KDC1, a novel carrot root hair K^+ channel. Cloning, characterization, and expression in mammalian cells. J. Biol. Chem. **275,** 39420-39426.

Doyle D.A., Morais C.J., Pfuetzner R.A., Kuo A., Gulbis J.M., Cohen S.L., Chait B.T., MacKinnon R. (1998). The structure of the potassium channel: molecular basis of K^+ conduction and selectivity. Science **280,** 69-77.

Dreyer I., Antunes S., Hoshi T., Mueller-Roeber B., Palme K., Pongs O., Reintanz B., Hedrich R. (1997). Plant K^+ channel alpha-subunits assemble indiscriminately. Biophys. J. **72,** 2143-2150.

Dreyer I., Becker D., Bregante M., Gambale F., Lehnen M., Palme K., Hedrich R. (1998). Single mutations strongly alter the K^+-selective pore of the K_{in} channel KAT1. FEBS Lett. **430,** 370-376.

Dreyer I., Horeau C., Lemaillet G., Zimmermann S., Bush D.R., Rodriguez-Navarro A., Schachtman D.P., Spalding E.P., Sentenac H., Gaber R.F. (1999). Identification and characterization of plant transporters using heterologous expression systems. J. Exp. Bot. **50,** 1073-1087.

Dreyer I., Michard E., Lacombe B., Thibaud J.B. (2001). A plant Shaker-like K^+ channel switches between two distinct gating modes resulting in either inward-rectifying or "leak" current. FEBS Lett. **505,** 233-239.

Dreyer I., Mueller-Roeber B., Köhler B. (2002). New challenges in plant ion transport research: From molecules to phenomena. *In* Recent Res. Devel. Mol. Cell. Biol. (Kerala, India: Research Signpost), pp 379-395.

Dreyer I., Mueller-Roeber B., Köhler B. (2004a). Voltage-gated ion channels. *In* Membrane Transport in Plants, M.R. Blatt, ed (Oxford: Blackwell Publishing), pp 150-192.

Dreyer I., Poree F., Schneider A., Mittelstädt J., Bertl A., Sentenac H., Thibaud J.B., Mueller-Roeber B. (2004b). Assembly of plant *Shaker*-like Kout channels requires two distinct sites of the channel alpha-subunit. Biophys. J. **87,** 858-872.

Engels C., Marschner H. (1992). Adaptation of potassium translocation into the shoot of maize (*Zea mays*) to shoot demand: evidence for xylem loading as a regulating step. Physiol. Plant. **86,** 263-268.

Formentin E., Varotto S., Costa A., Downey P., Bregante M., Naso A., Picco C., Gambale F., LoSchiavo F. (2004). DKT1, a novel K^+ channel from carrot, forms functional heteromeric channels with KDC1. FEBS Lett. **573,** 61-67.

Fuchs I., Stolzle S., Ivashikina N., Hedrich R. (2005). Rice K^+ uptake channel OsAKT1 is sensitive to salt stress. Planta **221,** 212-221.

Gaymard F., Pilot G., Lacombe B., Bouchez D., Bruneau D., Boucherez J., Michaux-Ferriere N., Thibaud J.B., Sentenac H. (1998). Identification and disruption of a plant shaker-like outward channel involved in K^+ release into the xylem sap. Cell **94,** 647-655.

Golldack D., Quigley F., Michalowski C.B., Kamasani U.R., Bohnert H.J. (2003). Salinity stress-tolerant and -sensitive rice (*Oryza sativa* L.) regulate AKT1-type potassium channel transcripts differently. Plant Mol. Biol. **51,** 71-81.

Grabov A., Blatt M.R. (1997). Parallel control of the inward-rectifier K^+ channel by cytosolic-free Ca^{2+} and pH in *Vicia* guard cells. Planta **201,** 84-95.

Grabov A., Blatt M.R. (1998). Co-ordination of signalling elements in guard cell ion channel control. Journal of Experimental Botany **49,** 351-360.

Hartje S., Zimmermann S., Klonus D., Mueller-Roeber B. (2000). Functional characterisation of LKT1, a K^+ uptake channel from tomato root hairs, and comparison with the closely related potato inwardly rectifying K^+ channel SKT1 after expression in *Xenopus* oocytes. Planta **210,** 723-731.

Hawkesford M.J., Miller A.J. (2004). Ion-coupled transport of inorganic solutes. *In* Membrane Transport in Plants, M.R. Blatt, ed (Oxford: Blackwell Publishing), pp 105-134.

Hedrich R., Hoth S., Becker D., Dreyer I., Dietrich P. (1998). On the structure and function of plant K^+ channels. *In* Cellular Integration of Signalling Pathways in Plant Development, F. LoSchiavo, R.L. Last, G. Morelli and N.V. Raikhel, eds (Berlin Heidelberg: Springer Verlag), pp 35-45.

Hedrich R., Moran O., Conti F., Busch H., Becker D., Gambale F., Dreyer I., Kuch A., Neuwinger K., Palme K. (1995). Inward rectifier potassium channels in plants differ from their animal counterparts in response to voltage and channel modulators. Eur. Biophys. J. **24,** 107-115.

Heginbotham L., Lu Z., Abramson T., MacKinnon R. (1994). Mutations in the K^+ channel signature sequence. Biophys. J. **66,** 1061-1067.

Hille B. (2001). Ionic Channels of Excitable Membranes. Sunderland, MA: Sinauer Press

Hills A., Volkov V. (2004). Electrophysiology equipment and software. *In* Membrane Transport in Plants, M.R. Blatt, ed (Oxford: Blackwell), pp 40-71.

Hirsch R.E., Lewis B.D., Spalding E.P., Sussman M.R. (1998). A role for the AKT1 potassium channel in plant nutrition. Science **280,** 918-921.

Hosy E., Vavasseur A., Mouline K., Dreyer I., Gaymard F., Poree F., Boucherez J., Lebaudy A., Bouchez D., Very A.A., Simonneau T., Thibaud J.B., Sentenac H. (2003). The *Arabidopsis* outward K^+ channel GORK is involved in regulation of stomatal movements and plant transpiration. Proc. Natl. Acad. Sci. U. S. A **100,** 5549-5554.

Hoth S., Dreyer I., Dietrich P., Becker D., Mueller-Roeber B., Hedrich R. (1997a). Molecular basis of plant-specific acid activation of K^+ uptake channels. Proc. Natl. Acad. Sci. U. S. A **94,** 4806-4810.

Hoth S., Dreyer I., Hedrich R. (1997b). Mutational analysis of functional domains within plant K^+ uptake channels. J. Exp. Bot. **48,** 415-420.

Hurst A.C., Thiel G., Homann U. (2004). Vesicle traffic and plasma membrane transport. *In* Membrane Transport in Plants, M.R. Blatt, ed (Oxford: Blackwell), pp 279-292.

Ivashikina N., Becker D., Ache P., Meyerhoff O., Felle H.H., Hedrich R. (2001). K^+ channel profile and electrical properties of *Arabidopsis* root hairs. FEBS Lett. **508,** 463-469.

Ivashikina N., Deeken R., Ache P., Kranz E., Pommerrenig B., Sauer N., Hedrich R. (2003). Isolation of AtSUC2 promoter-GFP-marked companion cells for patch-clamp studies and expression profiling. Plant J **36,** 931-945.

Ivashikina N., Deeken R., Fischer S., Ache P., Hedrich R. (2005). AKT2/3 subunits render guard cell K^+ channels Ca^{2+} sensitive. J. Gen. Physiol **125,** 483-492.

Iverson L.E., Tanouye M.A., Lester H.A., Davidson N., Rudy B. (1988). A-type potassium channels expressed from *Shaker* locus cDNA. Proc Natl Acad Sci U S A **85,** 5723-5727.

Jiang Y., Lee A., Chen J., Ruta V., Cadene M., Chait B.T., MacKinnon R. (2003). X-ray structure of a voltage-dependent K^+ channel. Nature **423,** 33-41.

Johansson I., Wulfetange K., Poree F., Michard E., Gajdanowicz P., Lacombe B., Sentenac H., Thibaud J.B., Mueller-Roeber B., Blatt M.R., Dreyer I. (2006). External $[K^+]$ modulates the activity of the *Arabidopsis* potassium channel SKOR via an unusual mechanism. Plant J. **Provisionally accepted,**

Kamb A., Iverson L.E., Tanouye M.A. (1987). Molecular characterization of *Shaker*, a *Drosophila* gene that encodes a potassium channel. Cell **50,** 405-413.

Kamb A., Tseng-Crank J., Tanouye M.A. (1988). Multiple products of the Drosophila *Shaker* gene may contribute to potassium channel diversity. Neuron **1,** 421-430.

Kochian L.V., Lucas W.J. (1988). Potassium transport in roots. Adv. Bot. Res. **15,** 93-178.

Lacombe B., Pilot G., Michard E., Gaymard F., Sentenac H., Thibaud J.B. (2000). A *Shaker*-like K^+ channel with weak rectification is expressed in both source and sink phloem tissues of *Arabidopsis*. Plant Cell **12,** 837-851.

Lai H.C., Grabe M., Jan Y.N., Jan L.Y. (2005). The S4 voltage sensor packs against the pore domain in the KAT1 voltage-gated potassium channel. Neuron **47,** 395-406.

Langer K., Ache P., Geiger D., Stinzing A., Arend M., Wind C., Regan S., Fromm J., Hedrich R. (2002). Poplar potassium transporters capable of controlling K^+ homeostasis and K^+-dependent xylogenesis. Plant J. **32,** 997-1009.

Larsson H.P. (2002). The search is on for the voltage sensor-to-gate coupling. J. Gen. Physiol **120,** 475-481.

Latorre R., Olcese R., Basso C., Gonzalez C., Munoz F., Cosmelli D., Alvarez O. (2003). Molecular coupling between voltage sensor and pore opening in the *Arabidopsis* inward rectifier K^+ channel KAT1. J. Gen. Physiol **122,** 459-469.

Leigh R.A., Wyn Jones R.G. (1984). A hypothesis relating critical potassium concentrations for growth to the distribution and functions of this ion in the plant cell. New Phytol. **97,** 1-13.

Li M., Jan Y.N., Jan L.Y. (1992). Specification of subunit assembly by the hydrophilic amino-terminal domain of the *Shaker* potassium channel. Science **257,** 1225-1230.

Long S.B., Campbell E.B., MacKinnon R. (2005a). Crystal structure of a mammalian voltage-dependent *Shaker* family K^+-channel. Science **309,** 897-903.

Long S.B., Campbell E.B., MacKinnon R. (2005b). Voltage sensor of Kv1.2: structural basis of electromechanical coupling. Science **309,** 903-908.

López-Maqués R.L., Schiott M., Jakobsen M.K., Palmgren M.G. (2004). Structure, function and regulation of primary H^+ and Ca^{2+} pumps. *In* Membrane Transport in Plants, M.R. Blatt, ed (Oxford: Blackwell), pp 72-104.

Ludwig J., Owen D., Pongs O. (1997). Carboxy-terminal domain mediates assembly of the voltage-gated rat ether-a-go-go potassium channel. EMBO J. **16,** 6337-6345.

MacKinnon R. (2004). Structural biology. Voltage sensor meets lipid membrane. Science **306,** 1304-1305.

Marschner H. (1995). Mineral Nutrition of higher plants. London: Academic Press

Marten I., Hoshi T. (1997). Voltage-dependent gating characteristics of the K^+ channel KAT1 depend on the N and C termini. Proc. Natl. Acad. Sci. U. S. A **94,** 3448-3453.

Marten I., Hoshi T. (1998). The N-terminus of the K channel KAT1 controls its voltage-dependent gating by altering the membrane electric field. Biophys. J. **74,** 2953-2962.

Marten I., Hoth S., Deeken R., Ache P., Ketchum K.A., Hoshi T., Hedrich R. (1999). AKT3, a phloem-localized K^+ channel, is blocked by protons. Proc. Natl. Acad. Sci. U. S. A **96,** 7581-7586.

Maser P., Thomine S., Schroeder J.I., Ward J.M., Hirschi K., Sze H., Talke I.N., Amtmann A., Maathuis F.J., Sanders D., Harper J.F., Tchieu J., Gribskov M., Persans M.W., Salt D.E., Kim S.A., Guerinot M.L. (2001). Phylogenetic relationships within cation transporter families of *Arabidopsis*. Plant Physiol **126,** 1646-1667.

Meinke D.W., Cherry J.M., Dean C., Rounsley S.D., Koornneef M. (1998). *Arabidopsis thaliana*: a model plant for genome analysis. Science **282,** 662, 679-682.

Michard E., Dreyer I., Lacombe B., Sentenac H., Thibaud J.B. (2005a). Inward rectification of the AKT2 channel abolished by voltage-dependent phosphorylation. Plant J. **44,** 783-797.

Michard E., Lacombe B., Poree F., Mueller-Roeber B., Sentenac H., Thibaud J.B., Dreyer I. (2005b). A unique voltage sensor sensitizes the potassium channel AKT2 to phosphoregulation. J. Gen. Physiol **126,** 605-617.

Moshelion M., Becker D., Czempinski K., Mueller-Roeber B., Attali B., Hedrich R., Moran N. (2002). Diurnal and circadian regulation of putative potassium channels in a leaf moving organ. Plant Physiol **128,** 634-642.

Mouline K., Very A.A., Gaymard F., Boucherez J., Pilot G., Devic M., Bouchez D., Thibaud J.B., Sentenac H. (2002). Pollen tube development and competitive ability are impaired by disruption of a *Shaker* K^+ channel in *Arabidopsis*. Genes Dev. **16,** 339-350.

Mueller-Roeber B., Ellenberg J., Provart N., Willmitzer L., Busch H., Becker D., Dietrich P., Hoth S., Hedrich R. (1995). Cloning and electrophysiological analysis of KST1, an inward rectifying K^+ channel expressed in potato guard cells. EMBO J. **14,** 2409-2416.

Nakamura R.L., Anderson J.A., Gaber R.F. (1997). Determination of key structural requirements of a K^+ channel pore. J. Biol. Chem. **272,** 1011-1018.

Obrdlik P., El-Bakkoury M., Hamacher T., Cappellaro C., Vilarino C., Fleischer C., Ellerbrok H., Kamuzinzi R., Ledent V., Blaudez D., Sanders D., Revuelta J.L., Boles E., André B., Frommer W.B. (2004). K^+ channel interactions detected by a genetic system optimized for systematic studies of membrane protein interactions. Proc Natl Acad Sci U S A **101,** 12242-12247.

Paganetto A., Bregante M., Downey P., LoSchiavo F., Hoth S., Hedrich R., Gambale F. (2001). A novel K^+ channel expressed in carrot roots with a low susceptibility toward metal ions. J. Bioenerg. Biomembr. **33,** 63-71.

Papazian D.M., Schwarz T.L., Tempel B.L., Jan Y.N., Jan L.Y. (1987). Cloning of genomic and complementary DNA from *Shaker*, a putative potassium channel gene from *Drosophila*. Science **237,** 749-753.

Philippar K., Fuchs I., Luthen H., Hoth S., Bauer C.S., Haga K., Thiel G., Ljung K., Sandberg G., Bottger M., Becker D., Hedrich R. (1999). Auxin-induced K^+ channel expression represents an essential step in coleoptile growth and gravitropism. Proc. Natl. Acad. Sci. U. S. A **96,** 12186-12191.

Picco C., Bregante M., Naso A., Gavazzo P., Costa A., Formentin E., Downey P., LoSchiavo F., Gambale F. (2004). Histidines are responsible for zinc potentiation of the current in KDC1 carrot channels. Biophys. J. **86,** 224-234.

Pilot G., Gaymard F., Mouline K., Cherel I., Sentenac H. (2003a). Regulated expression of *Arabidopsis Shaker* K^+ channel genes involved in K^+ uptake and distribution in the plant. Plant Mol. Biol. **51,** 773-787.

Pilot G., Lacombe B., Gaymard F., Cherel I., Boucherez J., Thibaud J.B., Sentenac H. (2001). Guard cell inward K^+ channel activity in *Arabidopsis* involves expression of the twin channel subunits KAT1 and KAT2. J. Biol. Chem. **276,** 3215-3221.

Pilot G., Pratelli R., Gaymard F., Meyer Y., Sentenac H. (2003b). Five-Group Distribution of the *Shaker*-like K^+ Channel Family in Higher Plants. J. Mol. Evol. **56,** 418-434.

Pongs O., Kecskemethy N., Muller R., Krah-Jentgens I., Baumann A., Kiltz H.H., Canal I., Llamazares S., Ferrus A. (1988). *Shaker* encodes a family of putative potassium channel proteins in the nervous system of *Drosophila*. EMBO J **7,** 1087-1096.

Poree F., Wulfetange K., Naso A., Carpaneto A., Roller A., Natura G., Bertl A., Sentenac H., Thibaud J.B., Dreyer I. (2005). Plant K_{in} and K_{out} channels: Approaching the trait of opposite rectification by analyzing more than 250 KAT1-SKOR chimeras. Biochem. Biophys. Res. Commun. **332,** 465-473.

Pratelli R., Lacombe B., Torregrosa L., Gaymard F., Romieu C., Thibaud J.B., Sentenac H. (2002). A grapevine gene encoding a guard cell K^+ channel displays developmental regulation in the grapevine berry. Plant Physiol **128,** 564-577.

Reckmann U., Scheibe R., Raschke K. (1990). Rubisco activity in guard cells compared with the solute requirement for stomatal opening. Plant Physiol **92,** 246-253.

Reintanz B., Szyroki A., Ivashikina N., Ache P., Godde M., Becker D., Palme K., Hedrich R. (2002). AtKC1, a silent *Arabidopsis* potassium channel alpha-subunit modulates root hair K^+ influx. Proc. Natl. Acad. Sci. U. S. A **99,** 4079-4084.

Roberts S.K., Tester M. (1995). Inward and outward K^+-selective currents in the plasma membrane of protoplasts from maize root cortex and stele. Plant J. **8,** 811-825.

Roelfsema M.R., Prins H.B. (1997). Ion channels in guard cells of *Arabidopsis thaliana* (L.) Heynh. Planta **202,** 18-27.

Sarafian V., Kim Y., Poole R.J., Rea P.A. (1992). Molecular cloning and sequence of cDNA encoding the pyrophosphate-energized vacuolar membrane proton pump of *Arabidopsis thaliana*. Proc. Natl. Acad. Sci. U. S. A **89,** 1775-1779.

Schroeder J.I. (1989). Quantitative analysis of outward rectifying K^+ channel currents in guard cell protoplasts from *Vicia faba*. J. Membr. Biol. **107,** 229-235.

Schwarz T.L., Tempel B.L., Papazian D.M., Jan Y.N., Jan L.Y. (1988). Multiple potassium-channel components are produced by alternative splicing at the *Shaker* locus in *Drosophila*. Nature **331,** 137-142.

Sentenac H., Bonneaud N., Minet M., Lacroute F., Salmon J.M., Gaymard F., Grignon C. (1992). Cloning and expression in yeast of a plant potassium ion transport system. Science **256,** 663-665.

Starace D.M., Bezanilla F. (2004). A proton pore in a potassium channel voltage sensor reveals a focused electric field. Nature **427,** 548-553.

Swartz K.J. (2004). Towards a structural view of gating in potassium channels. Nat. Rev. Neurosci. **5,** 905-916.

Szyroki A., Ivashikina N., Dietrich P., Roelfsema M.R., Ache P., Reintanz B., Deeken R., Godde M., Felle H., Steinmeyer R., Palme K., Hedrich R. (2001). KAT1 is not essential for stomatal opening. Proc. Natl. Acad. Sci. U. S. A **98,** 2917-2921.

Tempel B.L., Papazian D.M., Schwarz T.L., Jan Y.N., Jan L.Y. (1987). Sequence of a probable potassium channel component encoded at *Shaker* locus of *Drosophila*. Science **237,** 770-775.

Timpe L.C., Jan Y.N., Jan L.Y. (1988a). Four cDNA clones from the *Shaker* locus of *Drosophila* induce kinetically distinct A-type potassium currents in *Xenopus* oocytes. Neuron **1,** 659-667.

Timpe L.C., Schwarz T.L., Tempel B.L., Papazian D.M., Jan Y.N., Jan L.Y. (1988b). Expression of functional potassium channels from *Shaker* cDNA in *Xenopus* oocytes. Nature **331,** 143-145.

Uozumi N., Gassmann W., Cao Y., Schroeder J.I. (1995). Identification of strong modifications in cation selectivity in an *Arabidopsis* inward rectifying potassium channel by mutant selection in yeast. J. Biol. Chem. **270,** 24276-24281.

Uozumi N., Nakamura T., Schroeder J.I., Muto S. (1998). Determination of transmembrane topology of an inward-rectifying potassium channel from *Arabidopsis thaliana* based on functional expression in *Escherichia coli*. Proc. Natl. Acad. Sci. U. S. A **95,** 9773-9778.

Urbach S., Cherel I., Sentenac H., Gaymard F. (2000). Biochemical characterization of the *Arabidopsis* K^+ channels KAT1 and AKT1 expressed or co-expressed in insect cells. Plant J. **23,** 527-538.

Véry A.A., Sentenac H. (2003). Molecular mechanisms and regulation of K^+ transport in higher plants. Ann. Rev. Plant Biol. **54,** 575-603.

von Liebig J. (1840). Die Chemie in ihrer Anwendung auf Agrikultur und Physiologie. Leipzig: Wilhelm Engelmann

Walker D.J., Leigh R.A., Miller A.J. (1996). Potassium homeostasis in vacuolate plant cells. Proc. Natl. Acad. Sci. U. S. A **93,** 10510-10514.

Ward J.M. (2001). Identification of novel families of membrane proteins from the model plant *Arabidopsis thaliana*. Bioinformatics. **17,** 560-563.

Wegner L.H., de Boer A.H. (1997). Properties of two outward-rectifying channels in root xylem parenchyma cells suggest a role in K^+ homeostasis and long- distance signaling. Plant Physiol **115,** 1707-1719.

Wyn Jones R.G., Pollard A. (1983). Proteins, enzymes and inorganic ions. *In* Encyclopedia of Plant Physiology, A. Lauchli and A. Pirson, eds (Berlin: Springer), pp 528-562.

Zei P.C., Aldrich R.W. (1998). Voltage-dependent gating of single wild-type and S4 mutant KAT1 inward rectifier potassium channels. J. Gen. Physiol **112,** 679-713.

Zhou Y., Morais-Cabral J.H., Kaufman A., MacKinnon R. (2001). Chemistry of ion coordination and hydration revealed by a K^+ channel-Fab complex at 2.0 A resolution. Nature **414,** 43-48.

Zimmermann S., Hartje S., Ehrhardt T., Plesch G., Mueller-Roeber B. (2001). The K^+ channel SKT1 is co-expressed with KST1 in potato guard cells-- both channels can co-assemble via their conserved KT domains. Plant J. **28,** 517-527.

Originalarbeiten

Johansson, Wulfetange, Porée, Michard, Gajdanowicz, Lacombe, Sentenac, Thibaud, Mueller-Roeber, Blatt, **Dreyer** (2006) External [K^+] modulates the activity of the Arabidopsis potassium channel SKOR via an unusual mechanism. *Plant J.* in press..... Anhang [1]

Michard, Lacombe, Porée, Mueller-Roeber, Sentenac, Thibaud, **Dreyer** (2005) A unique voltage sensor sensitizes the potassium channel AKT2 to phosphoregulation. *J. Gen. Physiol.* 126:605-617. ..... Anhang [2]

Michard, **Dreyer**, Lacombe, Sentenac, Thibaud (2005) Inward rectification of the AKT2 channel abolished by voltage-dependent phosphorylation. *Plant J.* 44:783-797..... Anhang [3]

Porée, Wulfetange, Naso, Carpaneto, Roller, Natura, Bertl, Sentenac, Thibaud, **Dreyer** (2005) Plant K_{in} and K_{out} channels: Approaching the trait of opposite rectification by analyzing more than 250 KAT1-SKOR chimeras. *Biochem. Biophys. Res. Commun.* 332:465-473. ..... Anhang [4]

Riaño-Pachón, **Dreyer**, Mueller-Roeber (2005) Orphan transcripts in *Arabidopsis thaliana*: identification of several hundred previously unrecognised genes. *Plant J.* 43:205-212. ..... Anhang [5]

Dreyer, Porée, Schneider, Mittelstädt, Bertl, Sentenac, Thibaud, Mueller-Roeber (2004) Assembly of plant *Shaker*-like K_{out} channels requires two distinct sites of the channel alpha-subunit. *Biophys. J.* 87:858-872. ..... Anhang [6]

Hosy, Mouline, Vavasseur, **Dreyer**, Gaymard, Poree, Boucherez, Bouchez, Very, Simmonneau, Thibaud, Sentenac (2003) The *Arabidopsis* outward K^+ channel GORK is involved in regulation of stomatal movements and plant transpiration. *Proc. Natl. Acad. Sci. USA* 100:5549-5554..... Anhang [7]

Dreyer, Michard, Lacombe, Thibaud (2001) A plant *Shaker*-like K^+ channel switches between two distinct gating modes resulting in either inward-rectifying or 'leak' current. *FEBS Lett.* 505:233-239. ..... Anhang [8]

Ache, Becker, Deeken, **Dreyer**, Weber, Fromm, Hedrich (2001) VFK1, a *Vicia faba* K^+ channel involved in phloem unloading. *Plant J.* 27:571-580. ..... Anhang [9]

Brüggemann, Dietrich, Becker, **Dreyer**, Palme, Hedrich (1999) Channel-mediated high-affinity K^+ uptake into guard cells from *Arabidopsis*. *Proc. Natl. Acad. Sci. USA* 96:3298-3302. ..... Anhang [10]

Brüggemann, Dietrich, **Dreyer**, Hedrich (1999) Pronounced differences between the native K^+ channels and KAT1 and KST1 α-subunit homomers of guard cells. *Planta.* 207:370-376. ..... Anhang [11]

Dreyer, Becker, Bregante, Gambale, Lehnen, Palme, Hedrich (1998) Single mutations strongly alter the K^+-selective pore of the K_{in} channel KAT1. *FEBS Lett.* 430:370-376..... Anhang [12]

Dietrich, **Dreyer**, Wiesner, Hedrich (1998) Cation-sensitivity and kinetics of guard cell potassium channels differ among species. *Planta.* 205:277-287..... Anhang [13]

Hoth, **Dreyer**, Dietrich, Becker, Mueller-Roeber, Hedrich (1997) Molecular basis of plant-specific acid activation of K^+ uptake channels. *Proc. Natl. Acad. Sci. USA* 94:4806-4810. ..... Anhang [14]

Dreyer, Antunes, Hoshi, Mueller-Roeber, Palme, Pongs, Reintanz, Hedrich (1997) Plant K^+ channel α-subunits assemble indiscriminately. *Biophys. J.* 72:2143-2150..... Anhang [15]

Becker, **Dreyer**, Hoth, Reid, Busch, Lehnen, Palme, Hedrich (1996) Changes in voltage activation, Cs^+ sensitivity, and ion permeability in H5 mutants of the plant K^+ channel KAT1. *Proc. Natl. Acad. Sci. USA* 93:8123-8128. ..... Anhang [16]

Hedrich, Bregante, **Dreyer**, Gambale (1995) The voltage-dependent potassium-uptake channel of corn coleoptiles has permeation properties different from other K^+ channels. *Planta.* 197:193-199. ..... Anhang [17]

Hedrich, Moran, Conti, Busch, Becker, Gambale, **Dreyer**, Küch, Neuwinger, Palme (1995) Inward rectifier potassium channels in plants differ from their animal counterparts in response to voltage and channel modulators. *Eur. Biophys. J.* 24:107-115. ..... Anhang [18]

Buch- und Übersichtsartikel

Hoth, **Dreyer**, Hedrich (1997) Mutational analysis of functional domains within plant K^+ uptake channels. *J. Exp. Bot.* 48:415-420..... Anhang [19]

Hedrich, Hoth, Becker, **Dreyer**, Dietrich (1998) On the structure and function of plant K^+ channels. In: *Cellular integration of signalling pathways in plant developement*. F. Lo Schiavo, R.L. Last, G. Morelli, and N.V. Raikhel (eds.) *NATO ASI Series.* H 104:35-45. ..... Anhang [20]

Dreyer, Horeau, Lemaillet, Zimmermann, Bush, Rodríguez-Navarro, Schachtman, Spalding, Sentenac, Gaber (1999) Identification and characterization of plant transporters using heterologous expression systems. *J. Exp. Bot.* 50 (Special Issue):1073-1087..... Anhang [21]

Dreyer, Mueller-Roeber, Koehler (2002) New challenges in plant ion transport research: from molecules to phenomena. In: *Recent Research Developments in Molecular & Cellular Biology*. Research Signpost, Kerala, India. 3:379-395. ..... Anhang [22]

Dreyer, Mueller-Roeber, Koehler (2004) Voltage-gated ion channels. In: *Membrane Transport in Plants*. Blatt M.R. (ed). pp 150-192. Oxford, Blackwell. ..... Anhang [23]

Abschätzung des eigenen experimentellen Beitrags

Der jeweilige eigene experimentelle Beitrag zu den Publikationen [1], [2], [3], [4], [6], [8], [12], [13], [14], [15], und [16] beträgt 25% oder mehr. Der experimentelle Beitrag zu den Publikationen [7], [9], [10], [11] und [17] beträgt zwischen 10% und 25%. Der experimentelle Beitrag zu den Publikationen [5] und [18] beträgt weniger als 10%.

⇒ zurück zur Übersicht

2006

Johansson, Wulfetange, Porée, Michard, Gajdanowicz, Lacombe, Sentenac, Thibaud, Mueller-Roeber, Blatt, **Dreyer**

External [K^+] modulates the activity of the Arabidopsis potassium channel SKOR via an unusual mechanism.

Plant J. in press.

Pre-print of a manuscript in press in *The Plant Journal* (2006)

External [K^+] modulates the activity of the Arabidopsis potassium channel SKOR via an unusual mechanism

Ingela Johansson[1†], Klaas Wulfetange[2†‡], Fabien Porée[3], Erwan Michard[2,3§], Pawel Gajdanowicz[2], Benoît Lacombe[4], Hervé Sentenac[4], Jean-Baptiste Thibaud[4], Bernd Mueller-Roeber[2,3], Michael R. Blatt[1] and Ingo Dreyer[2,3,5]

[1] *Laboratory of Plant Physiology and Biophysics, IBLS Plant Sciences, Bower Building, University of Glasgow, Glasgow G12 8QQ, UK*

[2] *Universität Potsdam, Institut für Biochemie und Biologie, Abteilung Molekularbiologie, D-14476 Potsdam/Golm, Germany*

[3] *Max-Planck Institute of Molecular Plant Physiology, Cooperate Research Group, D-14476 Potsdam/Golm, Gemany*

[4] *Biochimie et Physiologie Moléculaires des Plantes, UMR 5004, Agro-M / CNRS / INRA / UM2, F-34060 Montpellier Cedex 1, France*

[*] For correspondence (fax: +49-331-977-2512; e-mail: dreyer@rz.uni-potsdam.de)

[†] These authors contributed equally to this work

[‡] Present address: FU Berlin, Institut für Biologie, Angewandte Genetik, 14195 Berlin

[§] Present address: Instituto Gulbenkian de Ciência, R. Quinta Grande 6, PT-2780-156 Oeiras, Portugal

Summary

Plant outward-rectifying K^+ channels mediate K^+ efflux from guard cells during stomatal closure and from root cells into the xylem for root-shoot allocation of potassium. Intriguingly, the gating of these channels depends on the extracellular K^+ concentration, although the ions carrying the current are derived from inside. This K^+-dependency confers a sensitivity to extracellular K^+ concentration that ensures the channels mediate K^+ efflux only, regardless of the [K^+] prevailing outside. We investigated the mechanism for K^+-dependent gating in the K^+ channel SKOR of *Arabidopsis* by site-directed mutagenesis. Mutations affecting the intrinsic K^+-dependence of gating were found to cluster in the pore and within the S6 transmembrane helix, identifying an 'S6 gating domain' deep within the membrane. Mapping the SKOR sequence to the KvAP K^+ channel crystal structure suggested interaction between the S6 gating domain and the base of the pore helix, a prediction supported by mutations at this site. These results offer an unique insight into the molecular basis for a physiologically important K^+-sensory process in plants.

Keywords: Arabidopsis / channel protein - cation interaction / channel protein structure / gating, K^+-dependent / K^+ channel, outward rectifier

Introduction

As the predominant, inorganic ion of plant cells, potassium plays a major role as an osmoticum contributing to cellular hydrostatic (turgor) pressure, growth and responses to the environment. Plants often confront large fluctuations in the ionic environment which affect both on K^+ uptake and the electrochemical driving force for K^+ diffusion and its release. Plant cells accommodate changes in the K^+ environment through a number of adaptations in their capacity for K^+ transport and its regulation, processes that rely on a variety of transport proteins (Very and Sentenac, 2003; Amtmann *et al*, 2004). An important role is played by voltage-gated K^+ channels of the so-called Shaker family (Pilot *et al*, 2003). This family is represented in plants by inward-rectifying channels which facilitate K^+ uptake into root cells and guard cells, weakly voltage-dependent channels which are thought to play a role in phloem (un)loading, and outward-rectifying channels which mediate K^+ efflux from guard cells during stomatal closure and from root cells into the xylem for root-shoot allocation of potassium.

Like the K^+ channels of animal cells, outward-rectifying K^+ channels in plants open on membrane depolarization. However, intriguingly, they do so only at membrane voltages positive of the equilibrium potential for potassium, E_K. Hence, their gating is sensitive both to membrane voltage and to the

prevailing extracellular K^+ concentration (Blatt, 1991). From a physiological standpoint, this ability to sense the prevailing K^+ concentration difference effectively guarantees that the channels open only when the driving force for net K^+ flux is directed outward. In stomatal guard cells, for example, these characteristics help ensure the K^+ efflux needed to drive stomatal closure and control gas exchange, even when the extracellular K^+ varies over concentrations from 10 nM to 100 mM (Blatt, 1988; Schroeder, 1989; Blatt and Gradmann, 1997; Roelfsema and Prins, 1997). And in xylem loading these characteristics underlie the tightly controlled K^+ release by stelar cells into the vessels (Roberts and Tester, 1995; Wegner and de Boer, 1997; see also the animated model in the Supplementary Material).

Although the physiological significance of K^+-dependency in plant outward-rectifying K^+ channels is well recognized as one element contributing to a complex web of homeostatic controls within the whole plant (Amtmann *et al*, 2004), little detail has come to light that could bear on the molecular mechanism for K^+-dependent gating of these unusual channels. One previous analysis of the outward-rectifying K^+ channels of *Vicia* guard cells indicated that gating was subject to control by K^+ binding to sites with characteristics similar to the pore itself (Blatt and Gradmann, 1997). An analogous gating dependence on K^+ is characteristic for the outward-rectifying K^+ channel TOK1/YKC1 of yeast. In this case, mutagenesis studies identified two exterior K^+-binding domains adjacent each of the pore loops (Vergani *et al*, 1998; Vergani and Blatt, 1999) as well as two intracellular domains that contribute to gating (Loukin *et al*, 1997; Loukin and Saimi, 1999). However, TOK1 is structurally unique among eukaryotes, thus raising questions about the extent to which these observations might bear on the mechanism for gating in the plant K^+ channels.

The *Arabidopsis* genome includes two genes, *GORK* and *SKOR*, that encode for *Shaker*-like, outward-rectifying K^+ channels (Gaymard *et al*, 1998; Ache *et al*, 2000). SKOR is expressed in the root stele and has been shown to play a major role in K^+ release to the xylem and therefore in the transport of potassium from roots towards shoots (Gaymard *et al*, 1998). GORK is the predominant outward-rectifying K^+ channel in guard cells and plays an important role in stomatal closure (Hosy *et al*, 2003). GORK and SKOR are structurally very similar, and both channels exhibit the canonical gating dependence on K^+ and membrane voltage of the plant outward-rectifiers. Thus, GORK senses the K^+ concentration in the guard-cell environment and SKOR the K^+ concentration in the stelar apoplast. In order to analyze the features of this physiologically important sensory process we took advantage from the expression in heterologous expression systems. We carried out site-directed mutagenesis, targeting domains throughout the SKOR K^+ channel that might contribute to such K^+-sensitivity, and analyzed the mutant currents. Remarkably, we uncovered a protein domain deep within the membrane that affects the K^+- and voltage-sensitivity of the channel. These results implicate a sophisticated coupling between K^+-sensitive gating and permeation and a highly efficient solution for K^+-sensing. The new molecular insights into the K^+-sensory process of SKOR allowed us to propose a working model which explains all relevant details of K^+-sensing of outward-rectifying plant K^+ channels (animated in the Supplementary Material).

Results

Alkali cations modulate SKOR activity from outside

When expressed in *Xenopus* oocytes, SKOR yields slowly-activating current with distinctly sigmoid kinetics on depolarizing voltage-clamp steps (Figure 1a) that are characteristic of this channel (Gaymard *et al*, 1998) and similar to outward-rectifying K^+ channels described previously in vivo (Schroeder, 1988; Blatt, 1988; Roelfsema and Prins, 1997; Wegner and de Boer, 1999). We found that increasing $[K^+]$ outside from 3 mM to 30 mM resulted in an increase in the halftime ($t_{1/2}$) for current activation (Figure 1b), it depressed the steady-state current (Figure 1c) at any one voltage, and it displaced the conductance-voltage curve to more positive voltages in parallel with the equilibrium potential for K^+, E_K (Figure 1d; see also Figure 5). The effect of K^+ on SKOR current and conductance was independent of the means to balance ionic strength when compensated by Na^+, Li^+ or NMDG; but Cs^+ and Rb^+ were almost equally effective as K^+ in suppressing the current and displacing the conductance-voltage curve to more positive voltages (Figure 1e,f). This K^+-sensitivity of SKOR was effected solely from the outside. We recorded SKOR current in whole-cell mode from COS cells expressing the channel with 10 mM and 150 mM K^+ outside after dialysis against either 75 mM or 150 mM K^+ inside the pipette (Figure 1g,h). In each case, increasing $[K^+]$ outside displaced the current-voltage curve to the right along the voltage axis. Similar effects were observed with Rb^+ and Cs^+ while substitutions with Na^+ and Li^+ outside had no effect on voltage-dependent SKOR gating. The *relative* steady-state current and conductance were virtually insensitive to the change in $[K^+]$ inside, unlike the yeast TOK1/YKC1 K^+ channel (Loukin and Saimi, 1999). In this context it should be noted that SKOR is not completely insensitive to changes in the internal K^+ concentration. Liu and co-workers show in this issue that SKOR senses internal $[K^+]$ in a voltage-*in*dependent manner. Alterations in $[K^+]$ inside do not affect the voltage-dependent gating but the number of channels which actively participate in the gating process (Liu et al., 2006).

Taken the result of Figure 1 together, like the outward-rectifying K^+ channels in vivo (Schroeder, 1988; Blatt, 1988; Roelfsema and Prins, 1997; Wegner

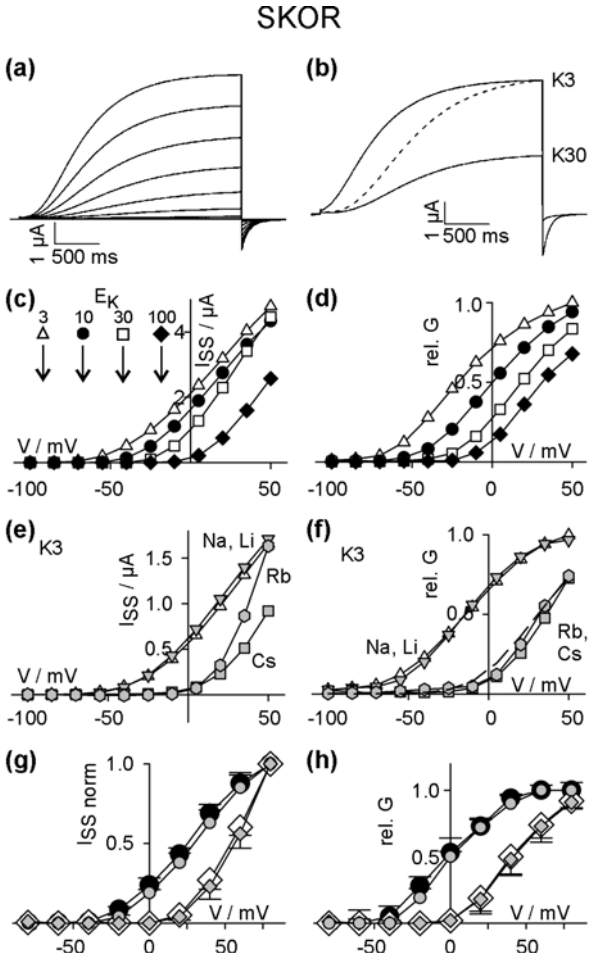

Figure 1. SKOR gating is modulated by extracellular, but not by intracellular K^+.
(a) Representative outward K^+ currents obtained from one oocyte injected with SKOR cRNA and recorded in 10 mM K^+ (K10). Currents elicited by 2.5-s voltage steps from a holding potential of –100 mV to voltages from -100 mV to +50 mV (15-mV increments).
(b) Comparison of current relaxations in 3 mM K^+ (K3) and in 30 mM K^+ (K30) at +35 mV. The dashed line indicates the current trace measured in K30 scaled to the maximum current measured in K3. Activation halftimes, in 3 mM K^+, 560 ms; in 30 mM K^+, 1 s.
(c) K^+-dependent shift in current activation. Steady state currents measured in 3 mM (*triangles*), 10 mM (*circles*), 30 mM (*squares*), and 100 mM K^+ (*diamonds*). The Nernst-potential for potassium, E_K, is indicated for all four conditions.
(d) Relative conductance determined as described in *Data analysis*. Symbols as in (c).
(e) Rb^+ and Cs^+ substitute for K^+ in modulating gating, but not Na^+ and Li^+. Steady state currents measured at the end of 2.5-s voltage steps as in (a) with 3 mM K^+ and 97 mM Na^+ (*white triangles*), 97 mM Li^+ (*gray triangles*), 97 mM Rb^+ (*gray hexagons*), and 97 mM Cs^+ (*gray squares*).
(f) Relative conductances determined as described in *Data analysis*. Symbols as in (e). The dashed line is the relative conductance in 100 mM K^+.
(g) Independence of SKOR from intracellular $[K^+]$. Current-voltage characteristics determined in SKOR-expressing COS cells at the end of 1.6-s steps from a holding voltage of -100 mV. Currents were recorded in 10 mM (*circles*) and 150 mM (*diamonds*) external K^+ and normalized to values measured at +80 mV. The internal (pipette) K^+ concentration was 150 mM (*white and black symbols*) and 75 mM (*gray symbols*). Data of 9 and 17 cells, respectively.
(h) Relative conductance-voltage characteristics. Symbols as in (g).

and de Boer, 1999), the gating of SKOR shows a pronounced sensitivity to voltage and external K^+. It

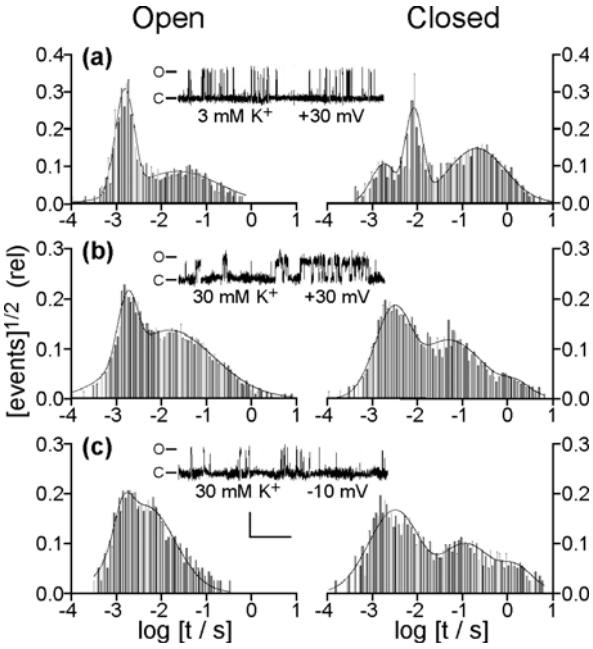

Figure 2. Increasing extracellular K^+ concentration introduces a long-lived closed state of the wild-type SKOR K^+ channel. Cumulative open (*left*) and closed (*right*) lifetime analysis of wild-type SKOR derived from 10-min recordings of single channels (cell-attached) at +30 mV with 3 mM (a) and 30 mM K^+ (b) at the outer face of the membrane, and with 30 mM K^+ at -10 mV (c). Clamp voltage corrected for the cell voltage of –40 mV (membrane voltage = cell voltage – pipette voltage). Representative trace segments as shown; C: closed state; O: open state. Dwell-time histograms were fitted by non-linear, least-squares analysis to Eqn [2], yielding component time constants (τ_i, < ±0.2%):

$[K^+]$	3 mM	30 mM	
	+30 mV	+30 mV	-10 mV
Open lifetime (ms)			
τ_1	1.55±0.02	1.85±0.05	1.54±0.02
τ_2	36±12	19±7	5±1
Closed lifetime (ms)			
τ_1	1.81±0.05	3.1±0.1	3.2±0.2
τ_2	8.3±0.3	48±9	112±8
τ_3	205±5	1190±40	1340±80

Representative trace segments of approx. 60 s are shown for each condition. Scale: vertical 1 pA; horizontal 10 s.

also shows a close similarity to permeation with a selectivity that discriminates among the alkali cations in favor of K^+, Rb^+ and Cs^+ over Li^+, Na^+. The effect of external $[K^+]$ on SKOR could be interpreted as an interaction of K^+-ions with a channel-intrinsic cation binding-site. As evidenced by triggered K^+-diffusion experiments this cation binding-site was accessible from the outside even when the channel was closed (Supplementary Material, Figure S1).

We used single-channel analysis to examine the gating kinetic components affected by K^+. Because single channel activity was lost rapidly upon patch excision (see also Liu *et al*, 2005) single channel experiments were carried out in the cell-attached configuration. Channel lifetime analysis for 10-min recording segments in 3 mM and 30 mM K^+ at +30 mV (Figure 2a,b) yielded open lifetimes that were well-fitted by a sum of two exponential components but showed little effect of $[K^+]$ on the time constants. By

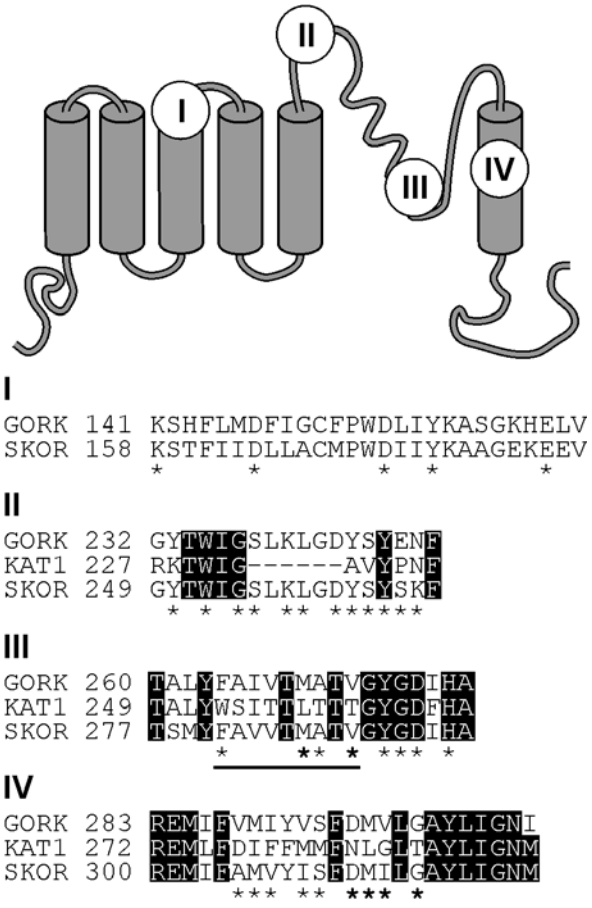

Figure 3. Domains of SKOR targeted for site-directed mutagenesis. In general, residues differing from KAT1, AKT1 and KST1 were targeted (*). Sequence alignments of GORK, KAT1 and SKOR are shown. (I) Mutations in the S1, and S3-segments and in the S3-S4 linker: T100G-K158R, D164N, D172N, Y175S, E182A. (II) Mutations in the region upstream the pore comprising additional amino acid residues compared to these inward-rectifying K^+ channels: Y250S, Y261H, Y261A, S262A. The following mutants were created for a cysteine-scanning approach: W252C, G254T-S255C, K257T-L258C, D260T-Y261C, S262T-Y263C, S264T-K265C. (III) Mutations in the pore region: SKOR-P_{KAT} (=SKOR-F281W-A282S-V283I-V284T-M286L-A287T-V289T), F281W, M286L, A287T, V289T, Y291C, G292D-D293S, H295A, H295K. (IV) Mutations in the S6 segment: A305D, M306I, V307F, I309M, S310L, D312A, D312E, D312N, D312R, D312Q, M313E, M313I, M313L, M313V, I314D, I314G, G316T. Note that SKOR-Y308 corresponds to AKT1-Y273 and KST1-Y284, and that SKOR-I303 aligns to AKT1-I268. Mutations that are described in detail in this study are marked with a bold asterisk.

contrast, closed lifetimes derived from the same recordings yielded two predominant exponential components for 3 mM K^+ and required an additional component with relaxation time constant near 2 s, to accommodate the data for 30 mM K^+ (Figure 2b). Similar results were obtained at -10 mV, with an increase principally in mean closed lifetimes of the longest-lived component and a decrease in the greater of the two time constants for the open lifetime (Figure 2c). Thus, in effect increasing [K^+] over this concentration range introduces a substantial, long-lived closed state of the channel and has little effect on the short-lived open and closed lifetimes of the channel.

Mutations in S6 affect voltage- and K^+-dependent gating

Extracellular cations affect the activity of several voltage-gated ion channels. Among these, components of mammalian Kv channel gating – so-called C-type inactivation – are influenced by extracellular [K^+] (Pardo *et al*, 1992; Baukrowitz and Yellen, 1995). Amino-acid substitutions at position 449, adjacent the *Shaker* K^+ channel pore, strongly affect the kinetics of C-type inactivation (Lopez-Barneo *et al*, 1993), and residues in the externally-exposed S5-pore linker similarly have been implicated in gating of the HERG K^+ channel (Torres *et al*, 2003) and in H^+- and K^+-modulated activation of AKT3 (Geiger *et al*, 2002). Activation of K^+ channels belonging to the *Drosophila* EAG subfamily is suppressed by elevating the concentration of Mg^{2+} and other divalent cations outside (Terlau *et al*, 1996), much as is SKOR by elevated [K^+]. In this case, mutations in the third transmembrane domain (S3) and externally-exposed (S3-S4) linker have been found to reduce or eliminate the Mg^{2+}-sensitivity of the channel (Schonherr *et al*, 1999; Silverman *et al*, 2000). Finally, the yeast YKC1/TOK1 K^+ channel is sensitive to both intracellular and extracellular [K^+] (Ketchum *et al*, 1995; Vergani *et al*, 1997; Loukin and Saimi, 1999) and its gating is affected by mutations in the externally-exposed pore linker regions (Vergani *et al*, 1998; Vergani and Blatt, 1999).

These and other results have suggested the existence of cation binding sites near the outer mouth of the pore of several K^+ channels which affect (in)activation, and they informed our hunt for domains that might contribute to the K^+-sensitivity of SKOR. We also compared the SKOR sequence with related K^+ channels of *Arabidopsis*, including KAT1, that do not show SKOR-like gating to help pinpointing specific residues unique to SKOR (Figure 3). Mutations at over 30 different sites within these domains – including cysteine-scanning mutagenesis and single residue substitutions with corresponding amino acids from KAT1 – failed to yield evidence of an effect on the K^+-sensitivity of SKOR (Table 1). Besides mutations close to the selectivity filter of the pore, only mutations clustered about residue M313, within the S6 transmembrane domain, either modified or eliminated the K^+-sensitivity of SKOR gating. In each case, the effects of mutation were without appreciable influence on the cation selectivity of the pore or the single-channel conductance as summarized below.

SKOR-M313L is virtually K^+-insensitive

The mutant SKOR-M313L conducted both outward and inward current at voltages positive of -100 mV, notably at [K^+] above 10 mM (Figure 4a and c). The SKOR-M313L current activated with both instantane-

Table 1 A summary of SKOR mutants analyzed in this study

SKOR region[a]	Mutation	Expressed current	Rectification (in/out/no)	K^+-sensitivity
I	T100G-K158R	yes	out	wt
	D164N	yes	out	wt
	D172N	yes	out	wt
	Y175S	yes	out	wt
	E182A	yes	out	wt
II	Y250S	yes	out	wt
	W252C	no		
	G254T-S255C	no		
	K257T-L258C	no		
	D260T-Y261C	no		
	Y261A	yes	out	wt
	Y261H	yes	out	wt
	S262A	yes	out	wt
	S262T-Y263C	no		
	S264T-K265C	no		
III	SKOR-P_{KAT}	yes	$out^{(-)}$	K^+-activated
	F281W	yes	out	wt
	M286L	yes	$out^{(-)}$	K^+-activated
	A287T	yes	out	wt
	V289T	yes	out	decreased
	Y291C	no		
	G292D-D293S	no		
	H295A	yes	out	wt
	H295K	yes	out	wt
IV	A305D	yes	out	wt
	M306I	yes	out	wt
	V307F	yes	out	wt
	I309M	no		
	S310L	yes	out	wt
	D312A	no		
	D312E	no		
	D312N	yes	out	K^+-activated
	D312Q	no		
	D312R	no		
	D312N-M313L-I314G	yes	no[b]	
	M313E	no		
	M313I	yes	$out^{(-)}$	~0
	M313L	yes	$out^{(-)}$	~0
	M313L-G316T	yes	$out^{(-)}$	~0
	M313V	no		
	I314D	no		
	I314G	yes	$out^{(-)}$	wt
	G316T	yes	$out^{(+)}$	wt

[a]See Figure 3
[b]Tested voltage range, -150 to +80 mV
$^{(-)}V_{1/2}$ displaced negative relative to wt
$^{(+)}V_{1/2}$ displaced positive relative to wt

ous and time-dependent components (Figure 4a) and increasing $[K^+]$ outside from 3 mM to 100 mM had a modest, but reduced effect on the $t_{1/2}$ following activation from a holding voltage of -120 mV (Figure 4b). Significantly, the steady-state current showed little evidence of a shift in the voltage-dependence for gating; instead, increasing $[K^+]$ led to increases in the amplitude of inward current carried by the channel at voltages positive of -100 mV (Figure 4c). Analysis of SKOR-M313L conductance using a two-step protocol confirmed the loss of any significant K^+-sensitivity to the conductance-voltage characteristic in the mutant (Figure 4d, see also Figure 5 and compare Figure 1d). These data also showed that the voltage-dependence of gating in the mutant was displaced to more negative voltages relative to wild-type SKOR (Figure 4d, *dotted line*, corresponding to the wild-type SKOR in 3 mM K^+). Substitution of K^+ with Rb^+, Li^+ and Na^+ had no effect on this voltage-dependence (not shown).

The voltage-dependence for gating aside, SKOR-M313L showed permeation characteristics very similar to that of the wild-type channel. Single-channel measurements yielded an unitary conductance that was virtually identical to that of the wild-type channel (Figure S2). We also examined the selectivity of the channel for alkali cations under bi-ionic conditions. Again, no significant difference from the wild-type could be determined (Table 2). Thus, the effect of mutation at residue M313 appeared to target specifically the K^+-sensitivity of the channel gate.

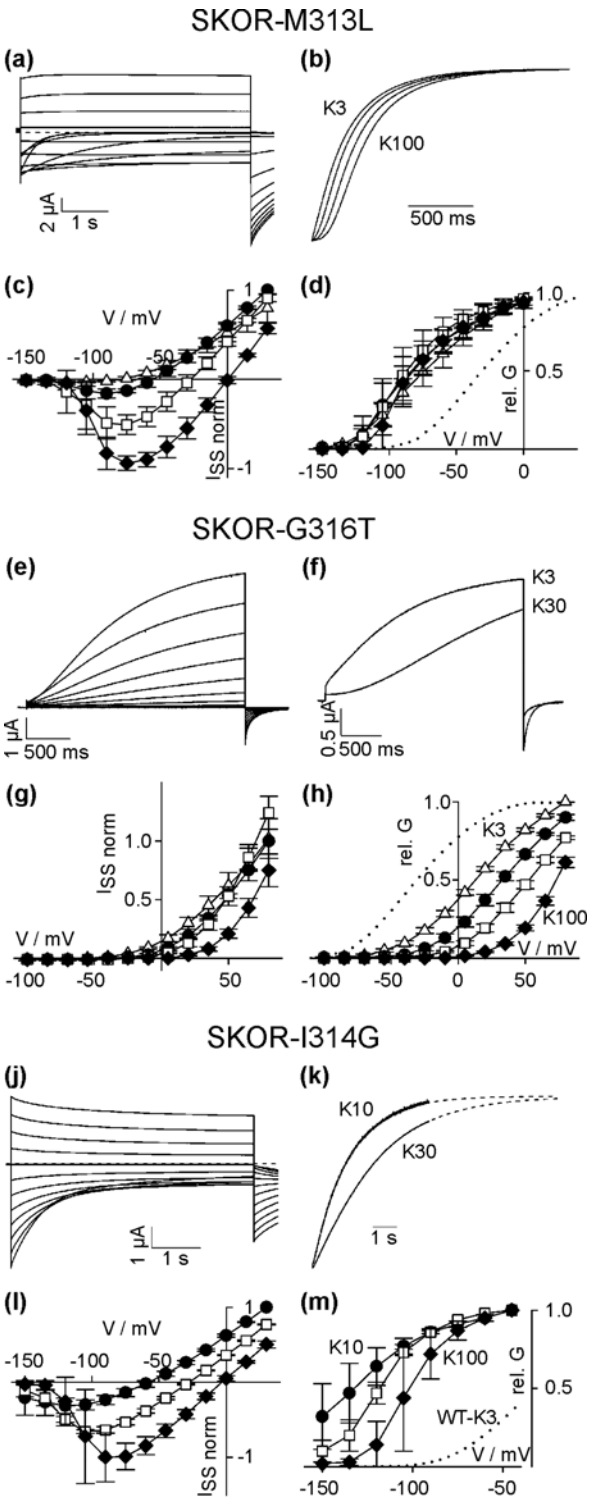

Figure 4. Mutations clustering in S6 affect gating control by K^+.
(a-d) Reduced K^+-sensitivity in the SKOR-M313L mutant.
(a) Representative inward and outward K^+ currents obtained from one oocyte injected with SKOR-M313L cRNA. Currents recorded in 30 mM K^+ and elicited in 5-s voltage steps from -45 mV to voltages between -150 mV and +30 mV (15-mV increments) followed by a further voltage step to -100 mV (zero current, *dashed line*).
(b) Current relaxations of SKOR-M313L recorded in 3, 10, 30, and 100 mM K^+ at +35 mV (from a holding potential of –120 mV) and scaled to a common amplitude. This mutant is characterized by a sigmoidicity that increases with external $[K^+]$. Activation halftimes: 3 mM K^+, 200 ms; 10 mM K^+, 260 ms; 30 mM K^+, 300 ms; 100 mM K^+, 370 ms.
(c) SKOR-M313L mediates inward and outward current. Steady-state current-voltage curves for 3 mM K^+ (*triangles*), 10 mM K^+ (*circles*), 30 mM K^+ (*squares*), and 100 mM K^+ (*diamonds*). Data of 4 cells normalized to values measured in 10 mM K^+ at +30 mV.
(d) SKOR-M313L gating is largely insensitive to K^+. Relative conductance determined as described in *Data analysis* from and cross-referenced with data in (c) by symbol (*dotted line*, relative conductance of wild-type SKOR in 3 mM K^+).
(e-h) Displaced activation threshold in the SKOR-G316T mutant.
(e) Representative K^+ currents obtained from one oocyte injected with SKOR-G316T cRNA. Currents recorded in 10 mM K^+ and elicited in 2.5-s voltage steps from -100 mV to voltages between -100 mV and +80 mV (15-mV increments) followed by a further voltage step to -100 mV.
(f) Current relaxations of SKOR-G316T recorded in 3 mM (K3) and 30 mM K^+ (K30) at +50 mV. This mutant is characterized by a profound sigmoidicity that increases with external $[K^+]$.
(g) SKOR-G316T mediates outward current only. Steady-state current-voltage curves for 3 mM K^+ (*triangles*), 10 mM K^+ (*circles*), 30 mM K^+ (*squares*), and 100 mM K^+ (*diamonds*). Data of 4 cells normalized to values measured in 10 mM K^+ at +80 mV.
(h) SKOR-G316T gating is sensitive to K^+, but displaced towards positive voltages compared with the wild-type. Relative conductance determined as described in *Data analysis* and cross-referenced with data in (g) by symbol (*dotted line*, relative conductance of wild-type SKOR in 3 mM K^+).
(j-m) Displaced activation threshold in the SKOR-I314G mutant.
(j) Representative K^+ currents obtained from one oocyte injected with SKOR-I314G cRNA. Currents recorded in 10 mM K^+ and elicited in 5-s voltage steps from -60 mV to voltages between -165 mV and 0 mV (15-mV increments) followed by a further voltage step to -100 mV.
(k) Current relaxations of SKOR-I314G recorded in 10 mM (K10) and 30 mM K^+ (K30) at -135 mV. Current relaxations approximate a simple exponential with an increase in the time constant for decay with $[K^+]$. Relaxations extrapolated and scaled to a common amplitude.
(l) SKOR-I314G mediates outward and inward current. Steady-state current-voltage curves for 10 mM K^+ (*circles*), 30 mM K^+ (*squares*), and 100 mM K^+ (*diamonds*). Data of 3 cells normalized to values measured in 10 mM K^+ at +30 mV.
(m) SKOR-I314G gating is sensitive to K^+, but displaced towards negative voltages compared with the wild-type. Relative conductance determined as described in *Data analysis* and cross-referenced with data in (l) by symbol (*dotted line*, relative conductance of wild-type SKOR in 3 mM K^+).

Mutations SKOR-G316T and SKOR-I314G affect the voltage-dependence for gating but not its sensitivity to K^+

Mutation of residues close to M313 also influenced the gating of SKOR. Like the wild-type, the mutant SKOR-G316T showed a pronounced sigmoidicity to current activation at positive voltages (Figure 4e) and a sensitivity to $[K^+]$ in $t_{1/2}$ for activation (Figure 4f), the steady-state current (Figure 4g) and conductance (Figure 4h). However, both the current- and conductance-voltage characteristics were strongly shifted positive relative to wild-type SKOR (Figure 4h). Quantitative analysis of the K^+- and voltage-dependence of SKOR-G316T yielded a slope of the $V_{1/2}$-log($[K^+]_{ext.}$)-curve identical to that of the wild-type, but the curve was displaced by roughly +35 mV (Figure 5, *white circles*). Like the wild-type SKOR, this effect of K^+ on gating in the mutant was mimicked by Rb^+ and Cs^+, but not by Na^+ or Li^+ (not shown). Again, single-channel records showed that the mutation did not affect unitary conductance (Figure S2), and the selectivity for permeation among alkali cations appeared unaffected (Table 2).

Table 2 Relative ionic selectivity for permeation of wild-type SKOR and selected mutants. Relative permeabilities, P_X/P_K, determined from the reversal voltage of tail currents under bi-ionic conditions using the Constant Field assumption. Data are from 3 - 6 experiments in each case.

	K^+	Rb^+	Cs^+	Li^+	Na^+
wild-type	1.00	0.43 ± 0.04	0.09 ± 0.04	<0.03	<0.03
M286L	1.00	0.39 ± 0.03	0.06 ± 0.04	<0.03	<0.03
V289T[a]	1.00	0.55 ± 0.02	n.d.	<0.03	<0.03
A305D	1.00	0.39 ± 0.04	0.09 ± 0.03	<0.03	<0.03
M306I	1.00	0.43 ± 0.08	n.d.	<0.03	<0.03
V307F	1.00	0.46 ± 0.04	0.11 ± 0.02	<0.03	<0.03
S310L	1.00	0.48 ± 0.04	0.13 ± 0.04	<0.03	<0.03
D312N	1.00	0.46 ± 0.03	0.09 ± 0.05	<0.03	<0.03
M313L	1.00	0.46 ± 0.07	0.07 ± 0.02	<0.03	<0.03
I314G	1.00	0.49 ± 0.05	0.10 ± 0.01	<0.03	<0.03
G316T	1.00	0.45 ± 0.04	0.11 ± 0.05	<0.03	<0.03

[a]The difference in the rubidium-permeability between the wild-type and the mutant V289T is statistically significant (t-test, P<0.005).

The mutant SKOR-I314G also retained a $[K^+]$-dependence to its gating while affecting the effective voltage range for channel activity. In this case, however, voltage clamp records yielded significant inward currents, even in 10 mM K^+ (Figure 4j-l). Analysis of SKOR-I314G conductance showed that gating was displaced strongly negative relative to wild-type SKOR (Figure 4m). The slope of the $V_{1/2}$-log($[K^+]_{ext.}$)-curve was virtually identical to that obtained for the wild-type, but the curve was displaced by roughly -120 mV relative to wild-type SKOR (Figure 5, *white squares*). Again, substitutions with Rb^+, but not with Na^+ or Li^+ mimicked the effect of K^+ (external Cs^+ blocked the inward component of the current, not shown), and the selectivity for permeation among alkali cations appeared unaffected (Table 2). Thus, the mutants SKOR-G316T and SKOR-I314G each affected the current, but only by displacing the voltage-dependence of the gate either positive or negative, respectively, relative to wild-type SKOR.

SKOR-D312N is activated by external K^+

For outward-rectifying K^+ channels like SKOR, the gating action of K^+ can be understood as a $[K^+]$-dependent block mediated by K^+ binding to the channel that is overcome by positive membrane voltage (Blatt and Gradmann, 1997). The only difference between wild-type SKOR, the SKOR-G316T and SKOR-I314G mutants was the effective voltage range for K^+ action (Figure 5). It might be argued that the SKOR-M313L mutation largely eliminated this $[K^+]$ dependence either by suppressing K^+ interaction with its binding site or by uncoupling K^+ binding from its action on the channel gate. The SKOR-D312N mutation, however, uncovered an entirely different perspective on the K^+-sensitivity of this channel. SKOR-D312N gave currents in 10 mM K^+ with a substantial instantaneous component that reached a new steady-state comparatively rapidly on depolarizing voltage steps (Figure 6a,b). No evidence of sigmoid activation kinetics was observed in the current activation, and increasing $[K^+]$ from 3 mM to 100 mM had no effect on the activation time $t_{1/2}$ (Figure 6b, *inset*). In patch recordings, the SKOR-D312N mutant showed no significant change in single-channel conductance, but a profound increase in openings at all voltages (Figure S2) consistent with a loss of longer-lived channel closed states (not shown). SKOR-D312N carried current both inward and outward, depending on the K^+ electrochemical gradient. Inward current was enhanced by increasing external K^+ (Figure 6c), and analysis of the relative conductance showed that high $[K^+]$ increased the activity of the channel, especially at voltages negative of E_K. This activation was mimicked by Rb^+, but not by Na^+ and Li^+ (Cs^+-ions blocked the inward current, not

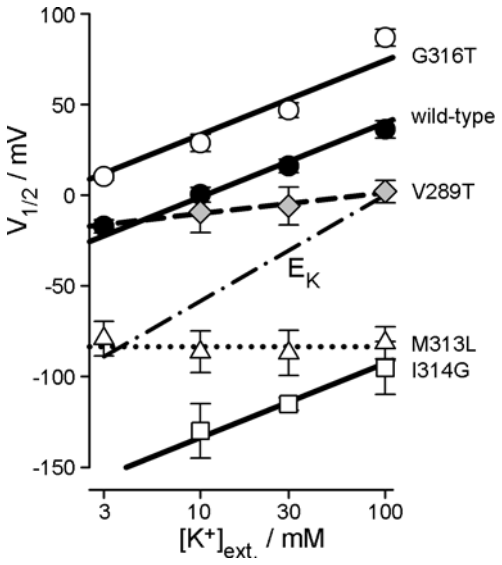

Figure 5. SKOR gating follows the apparent K^+ equilibrium voltage. Voltages ($V_{1/2}$) giving half-maximal conductances for wild-type SKOR and selected mutations. $V_{1/2}$ values determined from non-linear least-squares fittings to Eqn. [1]. Best results at all K^+ concentrations (Figures 1, 4, and 7) were obtained with δ held in common to a value near 1.4. Values are plotted together with the predicted K^+ equilibrium voltage (E_K) calculated assuming 120 mM K^+ inside (*dashed-dotted line*). Solid, dashed and dotted lines show linear regressions of the data. Note the shift along the vertical axis for the SKOR-G316T and -I314G mutants relative to the wild-type, the reduced K^+-sensitivity of the V289T mutant, and the loss of K^+-sensitivity for the M313L mutant. Each point represents data from 4-7 cells.

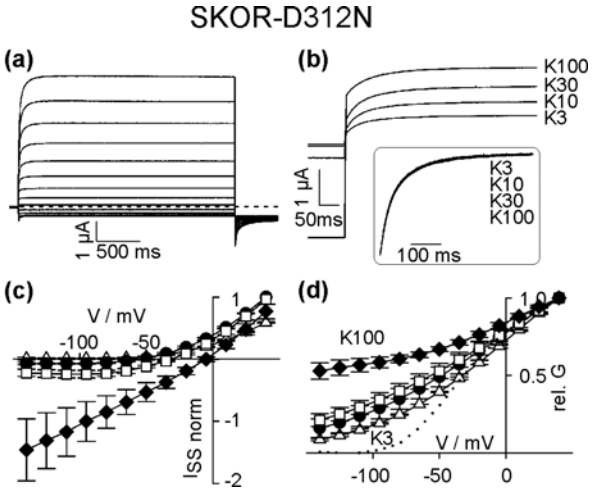

Figure 6. SKOR-D312N mutation in S6 reverses gating control by K^+.
(a) Representative outward K^+ currents obtained from an oocyte injected with SKOR-D312N cRNA. Currents recorded in 10 mM K^+ during 2.5-s steps from -45 mV to voltages between -100 mV and +80 mV (15-mV increments) followed by a final step to -100 mV (*dashed line*, zero-current level).
(b) Current relaxation of SKOR-D312N is K^+-independent. Comparison of the activation kinetics measured in 3 (K3), 10 (K10), 30 (K30), and 100 mM K^+ (K100) at +35 mV (starting from –100 mV). *Inset*: Current relaxations scaled to a common amplitude. Data of three repetitions in each case are superimposed.
(c) SKOR-D312N mediates both inward and outward current. Steady-state current-voltage curves for 3 mM (*triangles*), 10 mM (*circles*), 30 mM (*squares*), and 100 mM K^+ (*diamonds*) normalized between cells to the currents recorded in 10 mM K^+ at +45 mV. Data of 5 cells.
(d) SKOR-D312N conductance increases with extracellular $[K^+]$. Relative conductances estimated as described in the text (*dotted line*, relative conductance for wild-type SKOR in 3 mM K^+).

shown). Thus, by contrast with wild-type SKOR, substituting the aspartate at residue 312 with the uncharged asparagine reversed the effect of external K^+.

Mutation at the base of the pore loop affects K^+-dependent gating

The clustering of residues that affect gating properties between D312 and G316 poses an intriguing question about SKOR gating and the mechanism of its K^+-sensitivity. This cluster is positioned roughly 20 residues C-terminal to the GYGD K^+ channel signature sequence (=residues 290-293) and is predicted to situate centrally within the core of the S6 transmembrane helix and thus deep within the membrane. Yet our data indicated that each of the residues unique to SKOR is important for the control of gating by K^+ at the *outer* surface of the membrane. An in silico analysis offered one explanation. Mapping the SKOR sequence from residue D270 to G330 to the crystal structure for the *Aeropyrum* KvAP K^+ channel (Jiang *et al*, 2003a) suggested that residue M286, at the lower end of the pore helix, is situated close to the SKOR residues between D312 and G316 (see Discussion). Thus, steric and charge interactions with the pore helix of SKOR might couple the occupancy of the pore to the S6 residue cluster and therefore to gating.

To test this idea, we replaced the methionine in position 286 with the corresponding leucine of KAT1, anticipating that this mutation would similarly affect the current through altered dipole moment interactions and the scope for movement relative to the adjoining S6 residues. In fact, SKOR-M286L yielded a current that followed instantaneously all changes in clamp voltage without obvious, time-dependent activation/deactivation (Figure 7a). Like the SKOR-D312N mutant, the substitution at M286 carried current both inward and outward, depending on the K^+ electrochemical gradient, and with the inward current enhanced in high external K^+ (Figure 7b; compare Figure 6c). Virtually identical characteristics to that of SKOR-M286L were observed when a larger part of the pore of SKOR was replaced by the corresponding region of KAT1 (Figure S3).

To elucidate further the role of the pore in the K^+-sensing process we examined mutants in other positions of this region. Mutations in the outer rim of the pore at position SKOR-H295, within the pore helix at SKOR-F281 and at its C-terminal end at SKOR-A287 were indistinguishable from wild-type (not shown). Finally, we focused on the selectivity filter itself (permeation pathway-lining residues [T-V-G-Y-G-D]; Figure 3; Table 1). The mutants SKOR-Y291C and SKOR-G292D-D293S were not functional. By contrast, a current was observed with SKOR-V289T. At a first glance, this mutant showed characteristics analogous to the wild-type channel, including sigmoid activation kinetics and a selectivity for K^+ over Rb^+, albeit with a slight increase in Rb^+-permeability (Table 2). However, close inspection showed a reduced K^+-sensitivity of the gating characteristic (Figure 7c-f). Quantitative analyses revealed that the slope of the $V_{1/2}$-$\log([K^+]_{ext.})$-curve was reduced when compared with the wild-type giving an apparent K^+-sensitivity (slope) of 28% of the wild-type (Figure 5). As a consequence, this mutant carried significant inward currents negative of E_K when external $[K^+]$ was larger than 30 mM (Figure 7e). Thus, mutation at the pore residue V289 affected specifically the K^+-sensitivity of SKOR gating.

Discussion

The outward-rectifying K^+ channels of many plant cells are characterised by an unique gating dependence on both membrane voltage and K^+, a characteristic which has profound physiological implications (see e.g. the animation in the Supplementary Material). This K^+-dependent gating behavior is encapsulated in the potassium channel SKOR of *Arabidopsis* when expressed heterologously (Gaymard *et al*, 1998) which offers an unique opportunity to investigate the molecular details of this sensory process. Our study has identified structural elements of key importance for coupling the gating of SKOR to extracellular K^+: (i) The

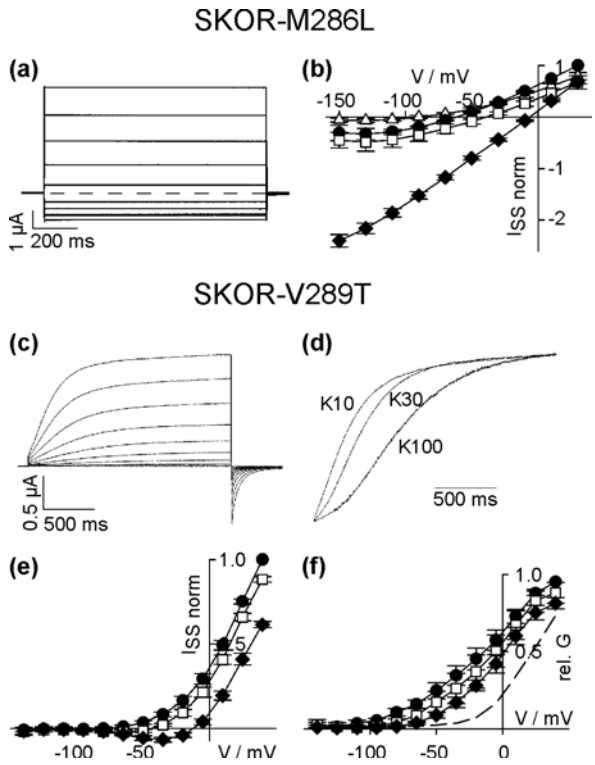

Figure 7. Mutations in the pore affect gating control by K^+.
(a-b) Pore helix mutation adjacent the S6 residue cluster yields current characteristics similar to SKOR-D312N.
(a) Representative K^+ currents obtained from one oocyte injected with SKOR-M286L cRNA. Currents recorded in 10 mM K^+ during 1-s voltage steps from -60 mV to voltages between -150 mV and +30 mV (20-mV increments) followed by a final step to -60 mV (*dashed line*, zero-current level).
(b) Steady-state current-voltage curves for SKOR-M286L recorded in 3 mM K^+ (*triangles*), 10 mM K^+ (*circles*), 30 mM K^+ (*squares*), and 100 mM K^+ (*diamonds*) normalized between experiments to values measured in 10 mM K^+ at +30 mV. Data of 4 cells.
(c-f) Reduced K^+-sensitivity in the SKOR-V289T mutant.
(c) Representative K^+ currents obtained from one oocyte injected with SKOR-V289T cRNA. Currents recorded in K10 during 2-s voltage steps from -100 mV to voltages between -115 mV and +50 mV (15-mV increments) followed by a final step to -140 mV.
(d) Current relaxations of SKOR-V289T recorded in 10 mM (K10), 30 mM (K30), and 100 mM K^+ (K100) at +35 mV (from a holding potential of -100 mV) and scaled to a common amplitude. This mutant is characterized by a sigmoidicity that increases with external $[K^+]$. Activation halftimes: 10 mM K^+, 290 ms; 30 mM K^+, 400 ms; 100 mM K^+, 700 ms.
(e) V289T mediates inward and outward current. Steady-state current-voltage curves for 10 mM K^+ (*circles*), 30 mM K^+ (*squares*), and 100 mM K^+ (*diamonds*). Data of 8 cells normalized to values measured in K10 at +40 mV. Note the inward currents in K100 at –35 mV.
(f) SKOR-V289T gating is slightly dependent on external $[K^+]$. Relative conductance determined as described in *Data analysis* and cross-referenced with data in (e) by symbol (*dashed line*, relative conductance of wild-type SKOR in 100 mM K^+).

efficacy among alkali cations in mediating gating closely matches with their abilities to enter the channel pore; (ii) Single site mutations at residues clustering within the S6 transmembrane helix adjacent the pore dramatically alter gating, affecting its voltage- and K^+-sensitivity; (iii) The most dramatic of these characteristics are mimicked by mutations within the pore helix at the putative interacting site opposing the S6 mutant cluster; a mutation near the base of the pore helix and selectivity filter reduces the K^+-sensitivity of gating; (iv) The K^+ binding-site is accessible from the outside even when the channel is closed; (v) Mutations in domains thought to be exposed to the outside failed to yield any evidence of a role in K^+-sensing, although the corresponding domains in other voltage-gated K^+ channels are known to contribute cation dependencies. These results point to local interactions between the cluster site within the S6 transmembrane helix and the base of the pore helix as a key element in coupling K^+ sensitivity and gating, and they imply a role for cation occupancy of the channel pore in this process.

Voltage- and K^+-dependent gating associates with a SKOR-specific residue cluster

A key finding was that mutations affecting the K^+-sensitivity of SKOR clustered near the mid-point of the S6 transmembrane helix and that these mutations were closely associated also with changes in the voltage-sensitivity of gating. Significantly, this cluster of mutations affecting SKOR gating coincides with motifs at the center of the S6 transmembrane helix that distinguish between the plant *Shaker*-like K^+ channels. Outward-rectifying K^+ channels like SKOR and GORK are characterized by a common [D-M-(I/V)-L-G] motif, whereas inward- and weakly-recitfying K^+ channels like KAT1, KAT2, AKT1, AKT2, AKT6 and SPIK1 share the sequence [N-L-G-L-T] (Figure S4). Each mutation at positions 312-316 (Figures 4 and 6) represents an exchange between the two motifs. Channels with alternative substitutions within this cluster (Table 1), were non-functional when expressed in oocytes and COS cells, suggesting that these positions are very sensitive to amino acid substitution. By contrast, other sites – corresponding to ones known to affect the gating of other K^+ channel types, and associated with an action of external cations – uniformly failed to yield any evidence of a role in the K^+-sensitivity of SKOR. Although we cannot fully rule out contributions from other domains within the SKOR sequence, it is clear that the cluster of residues within the S6 transmembrane helix – a structure of SKOR that we hereafter refer to as the S6 gating domain – marks a sequence of special importance in coupling gating to extracellular K^+. Interestingly, mutation of the corresponding region of the K^+-insensitive KAT1 channel did not alter significantly any feature of this inward-rectifier indicating (i) fundamental differences in the gating mechanisms of plant inward- and outward-rectifying K^+ channels and (ii) a close coupling of the K^+-sensing property to outward-rectification (Figure S5).

The location of this S6 gating domain corresponds to the so-called 'gating hinge' of bacterial K^+ channels (Jiang *et al*, 2002). Rotation around this hinge is thought to translate into a much larger movement at the inner face of the membrane, thereby opening an internal gate formed by the C-terminal half of the S6 helix (Jiang *et al*, 2002). Mutation of the hinge domain

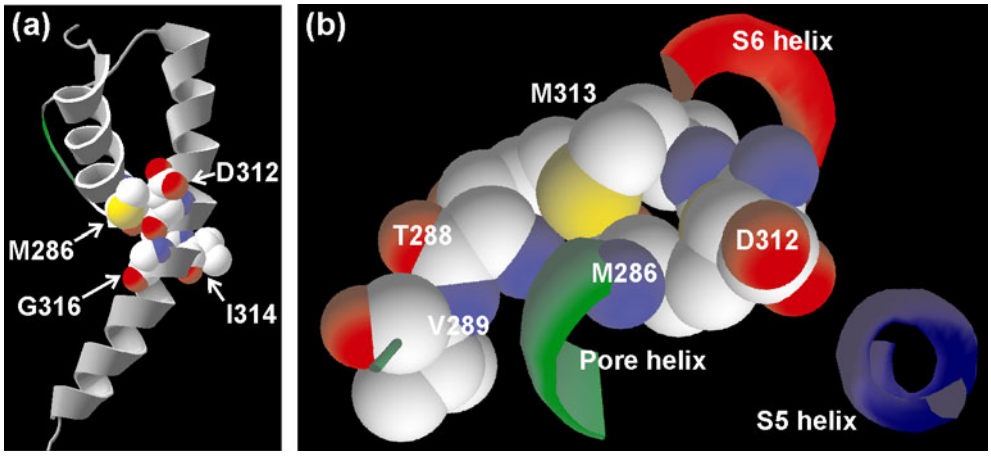

Figure 8. A molecular view on coupling of ion occupancy and gating.
(a) Juxtaposition of residues M286 and the S6 gating domain of the SKOR K^+ channel. Shown are SKOR residues from D270 through G330, including the pore helix, pore loop and S6 transmembrane helix of one subunit mapped by comparative modeling to the crystal structure of the corresponding sequence of the KvAP K^+ channel in the open conformation (Jiang *et al*, 2003a) using SWISS-MODEL (http://www.expasy.org/; Peitsch, 1995; Guex and Peitsch, 1997; Schwede *et al*, 2003). The selectivity filter (in green) is visible to the left and behind the pore helix (shorter helix on left) with the S6 helix as the dominant structure running from top right (outer membrane surface) to bottom left (inner membrane surface). Key residues in the S6 gating domain (D312, M313, I314, G316) and at the base of the pore helix (M286) are shown with atomic space filled to highlight their proximity and position relative to the pore. Residue M313 is situated on the far side of the S6 helix and is only just visible in this perspective. Predicted atomic distances from M286(S_δ): to D312($O_\gamma^{(-)}$), 3.7Å; to M313(S_δ), 3.4 Å; to G316(C_α), 5.1 Å.
(b) Proximity of the S6 gating domain and the pore illustrated in a top view. The transect view in (a) was pivoted on the medial axis with the upper (outer) part of the channel towards the viewer. Additionally the nearby S5-helix is indicated which is not displayed in (a). Residues M286 at the base of the pore helix, T288 and V289 in the neighboring selectivity filter, and D312 and M313 in the S6 gating domain are shown with atomic space filled. The permeation pathway (on the left) is lined by the hydroxyl-groups of the backbone of the TVGYGD selectivity filter (only T288 and V289 displayed). Additionally the nearby S5-helix is indicated.

in several mammalian K^+ channels, including Kir inward- (Alagem *et al*, 2003) and KCNQ outward-rectifying K^+ channels (Seebohm *et al*, 2003), suppresses channel closure by altering the mobility of the internal gate, effectively 'locking open' the internal gate (Webster *et al*, 2004). Such open-locked behavior appears to extend to the triple mutant SKOR-D312N-M313L-I314G (Liu *et al*, 2005; Poree *et al*, 2005). This mutant does not show significant rectification and behaves as a K^+ selective leak. However, this behavior does not extend to the single mutants SKOR-D312N, -M313L, and -I314G, each of which retains the voltage-dependence and depolarization-activated gating, albeit altered from the wild-type channel.

Gating and K^+-sensitivity require interactions between the pore and S6 gating domain

One outstanding feature of SKOR gating is its selectivity among alkali cations favoring K^+, Rb^+ and Cs^+ over other cations. This selectivity sequence is strikingly similar to the selectivity for ion entry into the pore. Both K^+ and Rb^+ readily permeate the channel, and Cs^+ blocks K^+ current in a voltage-dependent manner, indicating that it, too, must enter the pore (Gaymard *et al*, 1998). These observations raise the question whether the pore itself might function as a sensor for the extracellular cations in controlling gating. If the S6 gating domain interacted with the pore, it could explain why this cluster of residues situated deep within the membrane might be important for the control of gating by K^+ at the *outer* surface of the cell. To explore this hypothesis, we mapped the S5 linker, the pore helix and loop, and the complete S6 transmembrane domain of SKOR to the crystal structure of the KvAP channel (Jiang *et al*, 2003a) (Figures 3 and 8). This approach is limited, notably because it does not include explicitly contributions from the SKOR sequence outside these domains. Nonetheless, the analysis led us to suspect that the lower end of the pore helix and the S6 gating domain were sufficiently close to give rise to steric and charge interactions in the open channel (Figure 8). We tested the hypothesis, substituting M286 of the pore helix with leucine anticipating that the smaller hydration radius and concurrent loss of dipole moment with the leucine residue might similarly alter any pore helix - S6 gating domain interactions. Consistent with this interpretation, the M286L mutation mimicked characteristics of the D312N substitution in the S6 gating domain, most significantly reversing the apparent [K^+]-dependence of the steady-state current (Figure 7). Further support was provided by mutating the selectivity filter of SKOR. The mutation V289T increased the Rb^+ permeability and left the Na^+ and Li^+ permeability apparently unaffected (Table 2) indicating tiny changes in the structure of the selectivity filter. A closer look to the homology model indicated that residue V289 was not in direct contact with M286 or any residue in the S6 gating domain (Figure 8b). This spatial distance to the gating machinery might explain that the mutant V289T did not show the strong impairments in gating, as observed in M286L, D312N

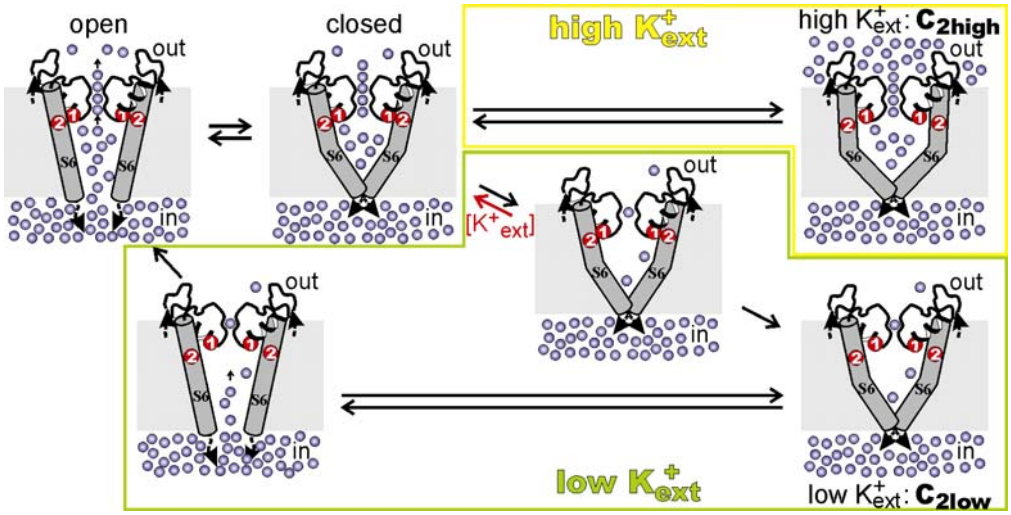

Figure 9. A mechanistic model for the K^+-sensitivity of SKOR. For clarity, only the pore loop, pore helix and S6 helix for two channel subunits are illustrated. Each channel is proposed to exist in four predominant states, open (O), a proximal closed state with the pore occupied (closed), and two distal closed states, one with the pore occupied ($C_{2,high}$) and one with it unoccupied ($C_{2,low}$). Additionally, two further intermediate states are shown. Domains ⌈ and ⌇ are proposed to interact in gating. For details, see the animated Supplementary Material.

and M313L. Nevertheless, the changes in the selectivity filter spread to the K^+-sensing mechanism resulting in a reduced K^+-sensitivity of SKOR-V289T.

So how might we explain the K^+-sensitivity of SKOR and its association with the S6 gating domain? Analogous interactions between the pore helix and the S6 helix are known to affect gating and inactivation of Kir and Kv K^+ channels (Seebohm *et al*, 2003; Alagem *et al*, 2003), and our observations are therefore particularly intriguing. The pores of all K^+ channels comprise four protein domains, each with a pore loop and two, flanking transmembrane helices (S5 and S6 in SKOR), one of which lines the pore (S6). These pore-lining helices form a 'diaphragm' or 'teepee'-like arrangement that results in a narrowing of the pore near the inner membrane surface and cuts off access to the TVGYGD selectivity filter from inside when closed (Figure 9; see also the animated model in the Supplementary Material). Opening of this internal gate depends on rotation of the pore-lining helices coupled to movement of the outer helix, and draws apart this pore diaphragm (Jiang *et al*, 2003b; Jiang *et al*, 2004; Fleishman *et al*, 2004). In mammalian K^+ channels, occupation of the TVGYGD filter favors open channel states, an effect that is thought to arise from interactions between the pore helix and the gating hinge of the S6 helix. In effect, cations within the pore of these K^+ channels can be thought to "push out" on the pore loop and helix and, via the S6 gating hinge, on the internal S6 gate to stabilize the open state [the so-called 'foot-in-the-door' hypothesis of Armstrong, see (Hille, 2001; Yellen, 2002)]. In SKOR, mutations within this domain of the S6 helix, like K^+, also affect channel stability, as evident in the voltage-dependence of gating and altered sensitivity to K^+. However, unlike the animal K^+ channels, interactions associated with K^+ appear to stabilize a long-lived *closed* state of the SKOR K^+ channel (Figures 1 and 2)! So the proximity of our cluster of residues to the S6 glycine hinge indicates an unusual and critical role in coupling the K^+-dependence of gating. Based on our data and the former considerations we developed a model which allows us to explain all relevant details of the K^+-sensory process of SKOR (Figure9; see also the animated model in the Supplementary Material for details).

In summary, we find that a major molecular determinant of K^+-dependent gating in the outward-rectifier K^+ channel SKOR resides in a region adjacent the pore and selectivity filter. Evidence has emerged previously of roles for the pore in the gating of various ion channels. Our data now offer strong evidence of gating by extracellular cations that depends on a proximal cluster of residues on the S6 helix. These residues are most likely situated deep within the transmembrane domain of the channel and interact with the pore helix and ion occupation of the selectivity filter. From a physiological standpoint, these findings implicate the stelar K^+ outward-rectifying channel SKOR senses the K^+-concentration in the stelar apoplast by an unusual mechanism and they offer key molecular insights into this process. The results presented here open the door to investigate in future studies the K^+-sensory process of plant outward-rectifying channels in vivo in further detail.

Experimental procedures

Molecular genetics and expression

SKOR mutation, expression and analysis used standard molecular genetic methods. Site mutations were generated

as outlined in detail in the Supplementary Material. All mutants were verified by sequencing. For expression, the coding regions of wild-type and mutant channels were cloned into the vector pGEMHE and cRNA was synthesized using T7 polymerase (mMessage mMachine, Ambion Europe Ltd, Huntingdon, UK).

For expression in oocytes, stage V and VI oocytes were taken from *Xenopus laevis* and maintained at 18°C in a modified Barth's medium containing (in mM) 96 NaCl, 2 KCl, 1 $CaCl_2$, 1 $MgCl_2$, 10 HEPES/NaOH (pH 7.4). Oocytes were defolliculated during 60-min collagenase treatment (2 mg/ml, type IA, Sigma, Taufkirchen, Germany, No.C9891). Defolliculated oocytes were injected with 40 ng (1 µg/µl) cRNA using a solid displacement injector (Picospritzer III, Parker Instrumentation, Fairfield, NJ) and kept at 18-20°C. Control oocytes were injected with 40 nl of deionized water. Culture and transfection of COS-7 cells were performed as described previously (Dreyer *et al*, 2001).

Electrophysiology

Whole-cell currents were measured under voltage clamp (Turbo TEC-10CX, npi electronic, Tamm, Germany) with a two-electrode clamp circuit and virtual ground. Voltage control, data acquisition, and data analyses were carried out using the Pulse/PulseFit software (HEKA, Lambrecht/Pfalz, Germany). Measurements were performed in bath solutions containing (in mM) 1 $CaCl_2$, 2 $MgCl_2$, buffered with 10 Tris/MES, pH7.4 with the addition of (in mM): K3: 3 KCl, 97 NaCl; K10: 10 KCl, 90 NaCl; K30: 30 KCl, 70 NaCl; K100: 100 KCl. For selectivity analysis monovalent cations were substituted to give: K3: 3 KCl, 97 NaCl; Li: 3 KCl, 97 LiCl; Rb: 3 KCl, 97 RbCl; Cs: 3 KCl, 97 CsCl; NMDG: 3 KCl, 97 N-methyl-D-glucamine(NMDG)-Cl. Measurements were repeated routinely at the end of each treatment with the addition of 10 mM Cs^+ to distinguish SKOR currents and any background, non-selective leak, and to set a baseline of relative conductance for mutants that showed little evidence of current relaxations. Whole-cell recordings from COS cells were performed as described previously (Dreyer *et al*, 2001). The bath solutions contained (in mM) 1 $CaCl_2$, 1.5 $MgCl_2$, 10 HEPES/NaOH (pH 7.4), 10 and 150 KCl. Pipette solutions contained (in mM) 1.5 $MgCl_2$, 3 EGTA, 2.5 MgATP, 10 HEPES/NaOH (pH 7.2), and 50, 75 and 150 KCl, respectively.

For single-channel measurements, the oocyte vitelline membrane was removed using forceps after exposure of the oocytes to hypertonic solution (in mM: 10 HEPES-NaOH, pH 7.4, 5 EGTA, 220 KCl, 200 NaCl, 1 $MgCl_2$). Patch pipettes were pulled using a Narishige (Tokyo, Japan) PP-83 puller modified for three-stage pulls and were fire-polished. Bath and pipette solutions were identical and consisted of (in mM) 5 HEPES-$Ca(OH)_2$, pH 7.4, 1 $MgCl_2$ with the addition of 3 KCl and 97 NaCl or 30 KCl and 70 NaCl. Currents were recorded with an Axopatch 200B patch amplifier (Axon instruments, CA, USA) after filtering at 1 kHz and sampled at 44 kHz for analysis. Subsequent filtering and analyses were performed using N-Pro (Y-Science, Glasgow, UK) and Tac (Bruxton, WA, USA) software.

Data analysis

In order to compare the features of the wild-type with those of the mutants in a standardized way, relative conductances were obtained in two-step tail-pulse experiments. In a first conditioning pulse (voltage V_C) channels were activated followed by a tail-pulse. The current measured at the end of the tail-pulse, steady-state current I_{SS}, can be expressed as $I_{SS}(V) = N \times i(V) \times popen(V)$, where V symbolizes the voltage of the tail-pulse, N the number of active channels in the membrane, i(V) the single-channel current at voltage V, and popen(V) the open probability of the channel in the steady-state at voltage V. The current measured at the onset of the tail-pulse, tail current I_T, can be expressed as $I_T(V) = N \times i(V) \times popen(V_C)$, where $popen(V_C)$ denotes the open probability of the channel at the end of the conditioning pulse (voltage V_C). The quotient $I_{SS}(V)/I_T(V)$ is proportional to the open probability popen(V). The resulting curves were fitted with a Boltzmann function such that

$$I_{ss}(V)/I_T(V) = g_{max}/(1+e^{(-\delta F/RT)(V-V1/2)}) \quad [1]$$

where g_{max} is the maximum conductance, V is the voltage of the tail pulse, $V_{1/2}$ is the voltage giving half-maximal conductance, δ is the apparent gating charge (voltage sensitivity coefficient) and *F*, *R* and *T* have their usual meanings. Fittings were carried out using a Marquardt-Levenberg algorithm (Marquardt, 1963) and the resulting values for g_{max} used to calculate relative conductances (rel $G = [I_{SS}(V)/I_T(V)]/g_{max}$). Current records were corrected for background current, estimated as a linear leak component from measurements between -130 and -160 mV after substituting Cs^+ for K^+ to block the K^+ channel. [Cs^+ substitution also served to identify the K^+ current and conductance for mutants with significant activity over the entire test voltage interval.] Measurements were discarded when the maximum leak current exceeded 5% of the maximum current in the steady-state. Results reported as means±SD where appropriate.

Open and closed lifetime distributions were determined from dwell-time histograms of opening and closing events from patch recordings showing evidence of only a single channel. Events were calculated using the Bayesian estimation of PANDORA! (YScience, Glasgow UK) and TacFit (HEKA, Lambrecht/Pfalz, Germany) and were derived from 10-min recording segments incorporating 5 or more independent experiments. Dwell-time histograms were subjected to non-linear, least-squares fitting (Colquhoun and Sigworth, 1995) to the function

$$f = \Sigma(w_i/\tau_i)\, e^{-t/ri} \quad [2]$$

to determine the number of identifiable states and the component time constants in each case. w_i is the fraction of the total number of events in the *i*th kinetic component (time constant τ_i).

Acknowledgements

This work was supported in part by an EU Marie Curie Fellowship to I.D. (Contract No. ERBBIO4CT985058), by a Life Science Fellowship "Ausländische Wissenschaftler für Brandenburg" of the Biotechologie Stiftung Berlin-Brandenburg and a Royal Society of Edinburgh travel grant to I.J., by the GABI-Génoplante joint programs (GABI FKZ 0312852, GENOPLANTE contract Nr. AF2001093), and by the UK Biotechnology and Biological Sciences Research Council (grants 17/C013599, 17/C09640 and 17/P013610).

Supplementary Material

The following supplementary material is available for this article online:

Figure S1. Slow K^+ exchange by triggered diffusion.

Figure S2. Representative single-channel currents from oocytes expressing SKOR, SKOR-M313L, SKOR-G316T, and SKOR-D312N.

Figure S3. The chimera SKOR-PKAT shows characteristics identical to the mutant SKOR-M286L.

Figure S4. Sequence comparison of the P-S6 regions of outward- and inward-rectifying K^+ channels of plants.

Figure S5. The quadruple mutant KAT1-L258M-N284D-L285M-G286I does not differ fundamentally from the KAT1 wild-type.
Figure S6. Generation of SKOR mutants.
Figure S7. Generation of KAT1 mutants.
Animation S8. A model to explain $[K^+]_{ext.}$-sensing of outward-rectifying plant K^+ channels.

References

Ache, P., Becker, D., Ivashikina, N., Dietrich, P., Roelfsema, M.R. and Hedrich, R. (2000) GORK, a delayed outward rectifier expressed in guard cells of *Arabidopsis thaliana*, is a K^+-selective, K^+-sensing ion channel. *FEBS Lett* **486,** 93-98.

Alagem, N., Yesylevskyy, S. and Reuveny, E. (2003) The pore helix is involved in stabilizing the open state of inwardly rectifying K^+ channels. *Biophys J* **85,** 300-312.

Amtmann, A., Armengaud, P. and Volkov, V. (2004) Potassium nutrition and salt stress. In *Membrane Transport in Plants* (Blatt, M.R., ed). Oxford: Blackwell, pp. 316-348.

Baukrowitz, T. and Yellen G. (1995) Modulation of K^+ current by frequency and external $[K^+]$: a tale of two inactivation mechanisms. *Neuron* **15,** 951-960.

Blatt, M.R. (1988) Potassium-dependent bipolar gating of potassium channels in guard cells. *J Membr Biol* **102,** 235-246.

Blatt, M.R. (1991) Ion channel gating in plants: physiological implications and integration for stomatal function. *J Membr Biol* **124,** 95-112.

Blatt, M.R. and Gradmann, D. (1997) K^+-sensitive gating of the K^+ outward rectifier in *Vicia* guard cells. *J Membr Biol* **158,** 241-256.

Colquhoun, D. and Sigworth, F.J. (1995) Fitting and statistical analysis of single-channel records. In *Single-Channel Recording*, (Sakmann, B. and Neher, E., eds). New York and London: Plenum Press, pp 483-587.

Dreyer, I., Michard, E., Lacombe, B. and Thibaud, J.B. (2001) A plant Shaker-like K^+ channel switches between two distinct gating modes resulting in either inward-rectifying or "leak" current. *FEBS Lett* **505,** 233-239.

Fleishman, S.J., Yifrach, O. and Ben Tal, N. (2004) An evolutionarily conserved network of amino acids mediates gating in voltage-dependent potassium channels. *J Mol Biol* **340,** 307-318.

Gaymard, F., Pilot, G., Lacombe, B., Bouchez, D., Bruneau, D., Boucherez, J., Michaux-Ferriere, N., Thibaud, J.B. and Sentenac, H. (1998) Identification and disruption of a plant shaker-like outward channel involved in K^+ release into the xylem sap. *Cell* **94,** 647-655.

Geiger, D., Becker, D., Lacombe, B. and Hedrich, R. (2002) Outer Pore Residues Control the H^+ and K^+ Sensitivity of the Arabidopsis Potassium Channel AKT3. *Plant Cell* **14,** 1859-1868.

Guex, N. and Peitsch, M.C. (1997) SWISS-MODEL and the Swiss-PdbViewer: an environment for comparative protein modeling. *Electrophoresis* **18,** 2714-2723.

Hille, B. (2001) *Ionic Channels of Excitable Membranes.* Sinauer Press, Sunderland, MA.

Hosy, E., Vavasseur, A., Mouline, K., Dreyer, I., Gaymard, F., Poree, F., Boucherez, J., Lebaudy, A., Bouchez, D., Very, A.A., Simonneau, T., Thibaud, J.B. and Sentenac, H. (2003) The *Arabidopsis* outward K^+ channel GORK is involved in regulation of stomatal movements and plant transpiration. *Proc Natl Acad Sci USA* **100,** 5549-5554.

Jiang, Q.X., Wang, D.N. and MacKinnon, R. (2004) Electron microscopic analysis of KvAP voltage-dependent K^+ channels in an open conformation. *Nature* **430,** 806-810.

Jiang, Y., Lee, A., Chen, J., Cadene, M., Chait, B.T. and MacKinnon, R. (2002) The open pore conformation of potassium channels. *Nature* **417,** 523-526.

Jiang, Y., Lee, A., Chen, J., Ruta, V., Cadene, M., Chait, B.T. and MacKinnon, R. (2003a) X-ray structure of a voltage-dependent K^+ channel. *Nature* **423,** 33-41.

Jiang, Y., Ruta, V., Chen, J., Lee, A. and MacKinnon, R. (2003b) The principle of gating charge movement in a voltage-dependent K^+ channel. *Nature* **423,** 42-48.

Ketchum, K.A., Joiner, W.J., Sellers, A.J., Kaczmarek, L.K. and Goldstein, S.A. (1995) A new family of outwardly rectifying potassium channel proteins with two pore domains in tandem. *Nature* **376,** 690-695.

Liu, K., Li, L. and Luan, S. (2005) An essential function of phosphatidylinositol phosphates in activation of plant shaker-type K^+ channels. *Plant J* **42,** 433-443.

Liu, K., Li, L. and Luan, S. (2006) Intracellular K^+ sensing of SKOR, a Shaker-type K^+ channel from *Arabidopsis*. *Plant J* **In press.**

Lopez-Barneo, J., Hoshi, T., Heinemann, S.H. and Aldrich, R.W. (1993) Effects of external cations and mutations in the pore region on C-type inactivation of Shaker potassium channels. *Receptors Channels* **1,** 61-71.

Loukin, S.H. and Saimi, Y. (1999) K^+-dependent composite gating of the yeast K^+ channel, Tok1. *Biophys J* **77,** 3060-3070.

Loukin, S.H., Vaillant, B., Zhou, X.L., Spalding, E.P., Kung, C. and Saimi, Y. (1997) Random mutagenesis reveals a region important for gating of the yeast K^+ channel Ykc1. *EMBO J* **16,** 4817-4825.

Marquardt, D.W. (1963) An algorithm for least squares estimation of nonlinear parameters. *J Soc Ind Appl Math* **11,** 431-441

Pardo, L.A., Heinemann, S.H., Terlau, H., Ludewig, U., Lorra, C., Pongs, O. and Stuhmer, W. (1992) Extracellular K^+ specifically modulates a rat brain K^+ channel. *Proc Natl Acad Sci USA* **89,** 2466-2470.

Peitsch, M.C. (1995) Protein modeling by E-mail. *Bio/Technology* **13,** 658-660.

Pilot, G., Gaymard, F., Mouline, K., Cherel, I. and Sentenac, H. (2003) Regulated expression of *Arabidopsis* shaker K^+ channel genes involved in K^+ uptake and distribution in the plant. *Plant Mol Biol* **51,** 773-787.

Poree, F., Wulfetange, K., Naso, A., Carpaneto, A., Roller, A., Natura, G., Bertl, A., Sentenac, H., Thibaud, J.B. and Dreyer, I. (2005) Plant K_{in} and K_{out} channels: Approaching the trait of opposite rectification by analyzing more than 250 KAT1-SKOR chimeras. *Biochem Biophys Res Commun* **332,** 465-473.

Roberts, S.K. and Tester, M. (1995) Inward and outward K^+-selective currents in the plasma membrane of protoplasts from maize root cortex and stele. *Plant J* **8,** 811-825.

Roelfsema, M.R. and Prins, H.B. (1997) Ion channels in guard cells of *Arabidopsis thaliana* (L.) Heynh. *Planta* **202,** 18-27.

Schonherr, R., Hehl, S., Terlau, H., Baumann, A. and Heinemann, S.H. (1999) Individual subunits contribute independently to slow gating of bovine EAG potassium channels. *J Biol Chem* **274,** 5362-5369.

Schroeder, J.I. (1988) K^+ transport properties of K^+ channels in the plasma membrane of *Vicia faba* guard cells. *J Gen Physiol* **92,** 667-683.

Schroeder, J.I. (1989) Quantitative analysis of outward rectifying K^+ channel currents in guard cell protoplasts from *Vicia faba*. *J Membr Biol* **107,** 229-235.

Schwede, T., Kopp, J., Guex, N. and Peitsch, M.C. (2003) SWISS-MODEL: An automated protein homology-modeling server. *Nucleic Acids Res* **31,** 3381-3385.

Seebohm, G., Sanguinetti, M.C. and Pusch, M. (2003) Tight coupling of rubidium conductance and inactivation in human KCNQ1 potassium channels. *J Physiol* **552,** 369-378.

Silverman, W.R., Tang, C.Y., Mock, A.F., Huh, K.B. and Papazian, D.M. (2000) Mg^{2+} modulates voltage-dependent

activation in ether-a-go-go potassium channels by binding between transmembrane segments S2 and S3. *J Gen Physiol* **116,** 663-678.

Terlau, H., Ludwig, J., Steffan, R., Pongs, O., Stuhmer, W. and Heinemann, S.H. (1996) Extracellular Mg^{2+} regulates activation of rat eag potassium channel. *Pflugers Arch* **432,** 301-312.

Torres, A.M., Bansal, P.S., Sunde, M., Clarke, C.E., Bursill, J.A., Smith, D.J., Bauskin, A., Breit, S.N., Campbell, T.J., Alewood, P.F., Kuchel, P.W. and Vandenberg, J.I. (2003) Structure of the HERG K^+ channel S5P extracellular linker: role of an amphipathic alpha-helix in C-type inactivation. *J Biol Chem* **278,** 42136-42148.

Vergani, P. and Blatt, M,R, (1999) Mutations in the yeast two pore K^+ channel YKC1 identify functional differences between the pore domains. *FEBS Lett* **458,** 285-291.

Vergani, P., Hamilton, D., Jarvis, S. and Blatt, M.R. (1998) Mutations in the pore regions of the yeast K^+ channel YKC1 affect gating by extracellular K^+. *EMBO J* **17,** 7190-7198.

Vergani, P., Miosga, T., Jarvis, S.M. and Blatt, M.R. (1997) Extracellular K^+ and Ba^{2+} mediate voltage-dependent inactivation of the outward-rectifying K^+ channel encoded by the yeast gene TOK1. *FEBS Lett* **405,** 337-344.

Very, A.A. and Sentenac, H. (2003) Molecular mechanisms and regulation of K^+ transport in higher plants. *Ann Rev Plant Biol* **54,** 575-603.

Webster, S.M., Del Camino, D., Dekker, J.P. and Yellen, G. (2004) Intracellular gate opening in Shaker K^+ channels defined by high-affinity metal bridges. *Nature* **428,** 864-868.

Wegner, L.H. and de Boer, A.H. (1997) Properties of two outward-rectifying channels in root xylem parenchyma cells suggest a role in K^+ homeostasis and long- distance signaling. *Plant Physiol* **115,** 1707-1719.

Wegner, L.H. and de Boer, A.H. (1999) Activation kinetics of the K^+ outward rectifying conductance (KORC) in xylem parenchyma cells from barley roots. *J Membr Biol* **170,** 103-119.

Yellen, G. (2002) The voltage-gated potassium channels and their relatives. *Nature* **419,** 35-42.

Figure S1

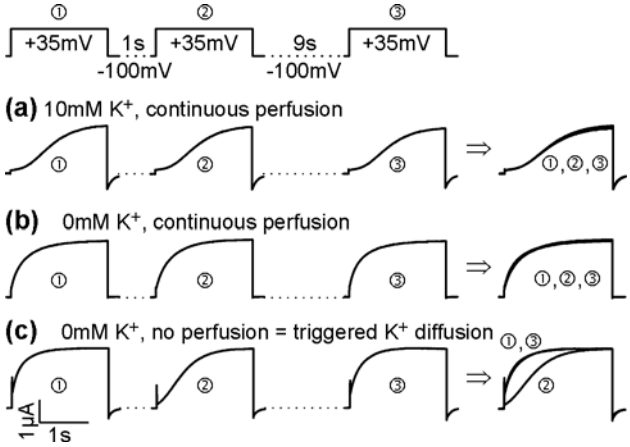

Figure S1. Slow K^+ exchange by triggered diffusion. SKOR-expressing oocytes were stimulated from a holding potential of –100 mV by repetitive 2-s pulses to +35 mV (pulse-protocol, *top panel*). The time-interval between the pulses was varied. Traces measured after > 30 s at –100 mV (initiating pulse ①), after 1 s at –100 mV (②), and after 9 s at –100 mV (③) are shown. Experimental conditions: (a) 10 mM K^+, 90 mM NDMG, continuous perfusion, (b) 10 mM Na^+, 90 mM NMDG, continuous perfusion, (c) 10 mM Na^+, 90 mM NMDG, stopped perfusion. Data are representative for 4 independent repeats.

Additional information to Figure S1: The effect of external [K^+] on SKOR could be interpreted as an interaction of K^+-ions with a channel-intrinsic cation binding-site. This cation binding-site was accessible from the outside even when the channel was closed as evidenced by triggered K^+-diffusion experiments (Figure S1). SKOR channels which were activated by a 2-s voltage pulse to +35 mV released about 40 picomoles of K^+-ions into the bath (triggered K^+-release). When the bath was continuously perfused this K^+-release did not influence local [K^+] in the close vicinity of the oocyte. Repeated stimulation following varying times of channel closure at –100 mV resulted in identical current activation time courses (Figure S1a,b). In contrast, when the perfusion was stopped, time courses depended on the resting time at -100 mV (Figure S1c). When SKOR channels were kept closed for about 1s, they activated in the following pulse with sigmoid kinetics (Figure S1c,②). When the resting time at -100 mV was increased to 9s, SKOR activated without sigmoid kinetics (Figure S1c,③). These results indicated (i) that the K^+-ions which were released during the preceding triggering pulse diffused slowly in the bath and (ii) that the K^+ binding-site equilibrated with the environment even when the channel was closed. Triggered K^+-diffusion experiments were only applicable in 0 mM K^+. When the bath contained 10 mM K^+ SKOR already activated with sigmoid kinetics (Figure S1a) and the differences could not be distinguished anymore.

Figure S2

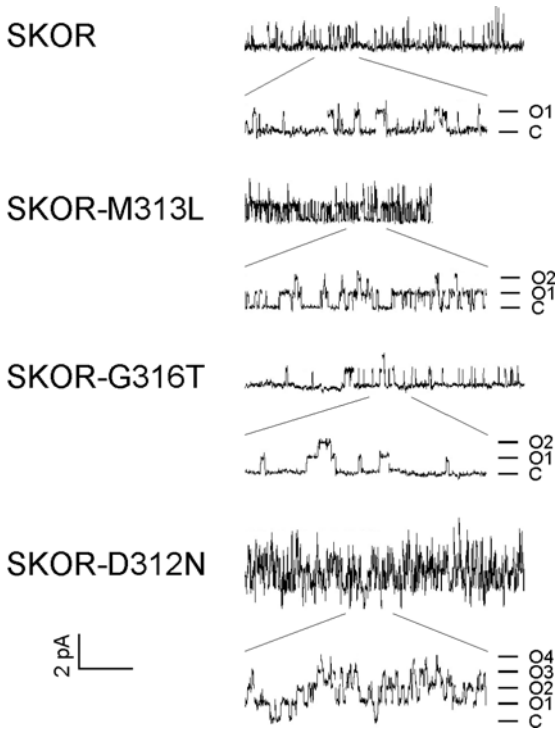

Figure S2. Representative single-channel currents (cell-attached) recorded at 0 mV from oocytes expressing SKOR, SKOR-M313L, SKOR-G316T, and SKOR-D312N. Clamp voltage corrected for the cell voltage of -40 mV (membrane voltage = cell voltage – pipette voltage). Both pipette and bath solutions contained 3 mM KCl. Mean unitary conductances were 12.0 ± 0.5 pS (SKOR wild-type), 11.0 ± 0.4 pS (SKOR-M313L), 12.0 ± 0.8 pS (SKOR-G316T), and 11.7 ± 0.4 pS (SKOR-D312N), calculated using an estimated value of E_K of -90 mV. C: closed state; O1, O2, …O*n*: open states of 1,2,..n channels. Horizontal scale: 5 s or 1 s (expanded traces).

Figure S3

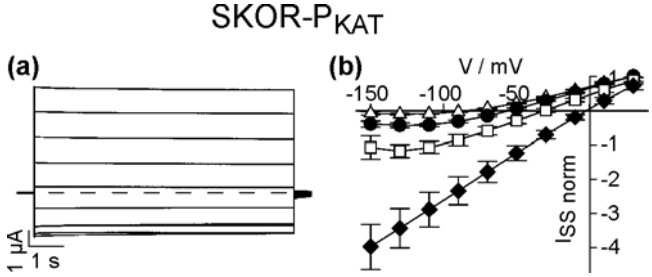

Figure S3. The chimera SKOR-PKAT shows characteristics identical to the mutant SKOR-M286L.
(a) Representative K^+ currents obtained from one oocyte injected with SKOR-P_{KAT} cRNA. Currents recorded in 10 mM K^+ during 1-s voltage steps from -55 mV to voltages between -150 mV and +30 mV (20-mV increments) followed by a final step to -55 mV (*dashed line*, zero-current level).
(b) Steady-state current-voltage curves for SKOR-P_{KAT} recorded in 3 mM K^+ (*triangles*), 10 mM K^+ (*circles*), 30 mM K^+ (*squares*), and 100 mM K^+ (*diamonds*) normalized between experiments to values measured in 10 mM K^+ at +30 mV. Data of 3 cells.

Additional information to Figure S3: Identical characteristics to that of the single pore mutant SKOR-M286L were observed when a SKOR-KAT1 chimera was expressed (see underlined sequence in Figure 3, III). In this case, substituting a major part of the pore loop and helix of SKOR with that of the KAT1 K^+ channel also showed near-instantaneous current transitions with voltage steps (Figure S3a), and increasing [K^+] outside enhanced inward current disproportionately in the steady-state (Figure S3b). This indicates that additional substitutions to give a KAT1-like pore loop and helix gave a current that showed no appreciable variation from that observed in M286L.

Figure S4

Figure S4. Sequence comparison of the P-S6 regions of outward-rectifying K^+ channels of plants and of the inward- and weakly-recitfying K^+ channels KAT1, KAT2, AKT1, SPIK1, AKT6, and AKT2 from *Arabidopsis thaliana*. NCBI-Accession codes: SKOR (Q9M8S6), GORK (Q94A76), KAT1 (S32816), KAT2 (Q38849), AKT1 (Q38998), SPIK (Q8GXE6), AKT6 (Q9SCX5), AKT2 (Q38898) from *Arabidopsis thaliana*, PTORK from *Populus tremula x Populus tremuloides* (CAC05488), SPORK1 from *Samanea saman* (CAC10514), VvSOR from *Vitis vinifera* (CAD35400), TORK1 from *Nicotiana tabacum* (BAD81036).

Additional information to Figure S4: It is worth noting that the [D-M-(I/V)-L-G] motif in the S6 gating domain together with the crucial methionine in the pore [M-A-T-V-G-Y-G-D] motif are preserved in several (putative) outward-rectifying K^+ channels of plants, including VvSOR from *Vitis vinifera*, SPORK1 from *Samanea saman*, PTORK from *Populus tremula x Populus tremuloides*, and TORK1 from *Nicotiana tabacum* (Figure S4) indicating that the association of these key residues with K^+-dependent gating was established early in evolution.

Figure S5

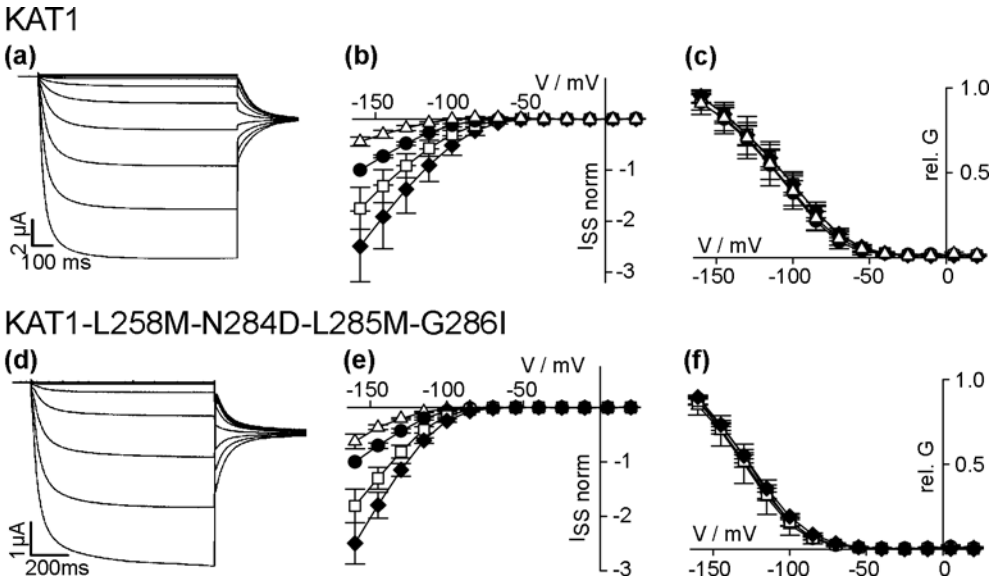

Figure S5. The quadruple mutant KAT1-L258M-N284D-L285M-G286I does not differ fundamentally from the KAT1 wild-type.
(a) Representative K^+ currents obtained from one oocyte injected with KAT1 cRNA. Currents recorded in 10 mM K^+ during 1-s voltage steps from -40 mV to voltages between -160 mV and +20 mV (15-mV increments) followed by a final step to -110 mV.
(b) Steady-state current-voltage curves for KAT1 recorded in 3 mM K^+ (*triangles*), 10 mM K^+ (*circles*), 30 mM K^+ (*squares*), and 100 mM K^+ (*diamonds*) normalized between experiments to values measured in 10 mM K^+ at -160 mV. Data of 4 cells.
(c) Relative conductance determined as described in *Data analysis*. Symbols as in (b).
(d) Representative K^+ currents obtained from one oocyte injected with KAT1-L258M-N284D-L285M-G286I cRNA. Currents recorded in 10 mM K^+ during 1-s voltage steps from -20 mV to voltages between -160 mV and +20 mV (15-mV increments) followed by a final step to -120 mV.
(e) Steady-state current-voltage curves for KAT1-L258M-N284D-L285M-G286I recorded in 3 mM K^+ (*triangles*), 10 mM K^+ (*circles*), 30 mM K^+ (*squares*), and 100 mM K^+ (*diamonds*) normalized between experiments to values measured in 10 mM K^+ at -160 mV. Data of 3 cells.
(f) Relative conductance determined as described in *Data analysis*. Symbols as in (e).

Additional information to Figure S5: The closest K^+-insensitive relatives of K^+-sensitive plant outward-rectifying channels are plant inward-rectifying and weak-rectifying K^+ channels. Mutations at the residue corresponding to SKOR-M286 in the pore of AKT2, a weakly rectifying K^+ channel of *Arabidopsis*, and in the inward-rectifying K^+ channel KST1 of potato do not confer K^+-sensitivity on these channels (Hoth et al, 2001, Plant Cell 13: 943-952). Likewise, also the quadruple mutant KAT1-L258M-N284D-L285M-G286I was not K^+-sensitive (Figure S5). Interestingly, the exchange of the three amino acids in the S6 segment of KAT1 did neither influence significantly the gating properties of this inward-rectifying channel, in contrast to the inverse mutations in the outward-rectifier SKOR (Figures 4 and 6; Poree et al., 2005; Biochem Biophys Res Commun 332: 465-473). This might point to differences in the gating mechanisms of KAT1 and SKOR and raises the question: “Is the domain corresponding to the S6 gating domain of SKOR also an essential gating domain of inward-rectifying channels, like KAT1?” With regard to these results the findings on SKOR emphasize the special role for M286 in a coupling between the pore and the gating machinery which appears to be unique to outward-rectifiers.

Generation of SKOR and KAT1 mutants

SKOR mutation, expression and analysis used standard molecular genetic methods (Ausubel et al., 1997, *Current protocols in molecular biology.* John Wiley & Sons, USA, New York). Mutants were created by PCR-based techniques and with the pAlter mutagenesis system (Promega, Charbonnières, France) using appropriate oligonucleotides to introduce the desired mutations. For expression, the coding regions of wild-type SKOR and the various mutants were cloned into the BamHI site and the coding regions of KAT1 and its mutants were cloned into the SmaI-XbaI sites of pGEMHE (Liman et al., 1992, Neuron 9: 861-871). Constructs were linearized by digestion with NheI, and G(5')ppp(5')G-capped cRNA was synthesized using T7 polymerase (mMessage mMachine, Ambion Europe Ltd, Huntingdon, UK).

Figure S6

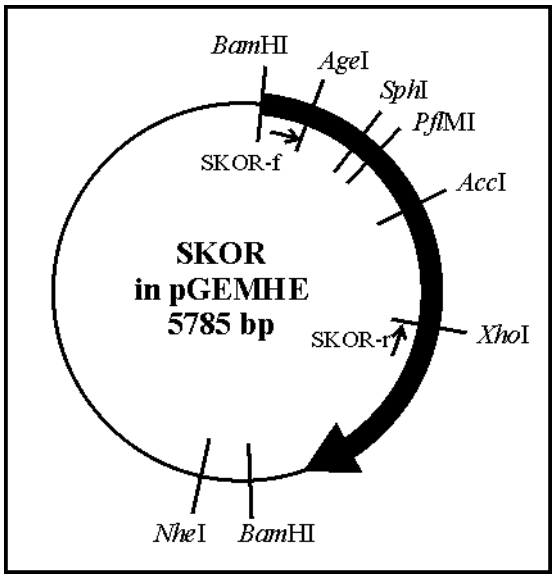

Figure S6. Generation of SKOR mutants. Vector map of the plasmid pGEMHE-SKOR. The coding sequence of SKOR is shown as black arrow. Additionally the restriction sites used in this study are displayed: The unique restriction sites for *Age*I, *Sph*I, *Pfl*MI, *Acc*I, *Xho*I, and *Nhe*I. The *Bam*HI sites were used to clone the SKOR-coding sequence into pGEMHE.

SKOR-mutations generated with the pAlter system

The *Sph*I-*Xho*I fragment of the SKOR coding region was cloned into the *Sph*I-*Sal*I sites of the vector pAlter-1. The mutagenesis reactions were performed according to the user manual of the pAlter mutagenesis system. To introduce the mutations the following oligonucleotides were used:

SKOR-Y175S: 5'-CgCCTgCAgCCTTggAgATTATATCCCATggCATgCAAg-3'
SKOR-Y250S: 5'-CCTAACTTCAAgCTTCCAATCCAAgTggATCCTTCTTgAgAAgCAggAAgCg-3'
SKOR-Y261H: 5'-CgATCTCTCTAAACTTCgAgTAACTgTgATCCCCgAgCTTCAAgCTTCCAATCCAAgTgTACC-3'
SKOR-Y261A: 5'-CgATCTCTCTAAACTTCgAgTAAgACgCgTCTCCTAACTTCAAgCTTCCAATCC-3'
SKOR-S262A: 5'-CgATCTCTCTAAACTTCgAgTACgCgTAATCTCCTAACTTCAAgCTTCC-3'
SKOR-W252C: 5'-CCTAACTTCAAgCTTCCAATgCACgTgTACCCTTCTTgAgAAgC-3'
SKOR-G254T-S255C: 5'-gTAATCTCCTAACTTCAAgCACgTgATCCAAgTgTACCCTTCTTg-3'
SKOR-K257T-L258C: 5'-CTTCgAgTAACTgTAATCTCCgCACgTgAggCTTCCAATCCAAgTgTACCC-3'
SKOR-D260T-Y261C: 5'-CTAAACTTCgAgTAACTgCACgTgCCTAACTTCAAgCTTCC-3'
SKOR-S262T-Y263C: 5'-CgATCTCTCTAAACTTCgAgCACgTgTAATCTCCTAACTTCAAgC-3'
SKOR-S264T-K265C: 5'-CCAgAgATCgATCTCTCTAAAgCACgTgTAACTgTAATCTCCTAACTTC-3'
SKOR-F281W: 5'-CCATAACCAACAgTTgCCATggTAACCACTgCCCAgTACATAgAAgTAgTgTATCg-3'
SKOR-A287T: 5'-CTCCATAACCAACAgTTgTCATggTAACCACTgCAAAgTACATAgAAg-3'

Subsequently the *Sph*I-*Acc*I cassette of the pGEMHE-SKOR plasmid was replaced by the respective mutagenised cassette.

To generate the double mutant T100G-K158R, the *Kpn*I fragment of pBlueScript-SKOR was cloned into the *Kpn*I site of the vector pAlter-1. The two oligonucleotides

SKOR-T100G: 5'-CCTgAAgAATCCgAATTCCAACggACCgAAgAAggAAgAATAAAgTgC-3'
SKOR-K158R: 5'-gCAAgTAAgTCAATTATAAAAgTTgACCTAAggTACCgTAAAgCAATTgAgC-3'

were annealed simultaneously during the mutagenesis reaction. Subsequently the *Age*I-*Sph*I cassette of the pGEMHE-SKOR plasmid was replaced by the respective mutagenised cassette.

SKOR-Mutations generated by PCR

The other mutants were generated by polymerase chain reaction using *Pfu* polymerase (Promega, Mannheim, Germany) in an one-step or in a two-step protocol. If the codon of interest was located downstream but still in close vicinity to the *Acc*I site (Figure S6), the primers introducing the mutations were designed to cover also this restriction site. A single polymerase chain reaction with the SKOR-specific reverse primer

SKOR-r: 5'-gCCgCACTATTCAACTTCAgAgCTAgTTCTgCCTCTTgTTTACTgATATg-3'

together with one of the following mutation-carrying primers allowed to generate a mutagenised cassette.

SKOR-I309M: 5'-ggTCTACATgTCATTCgATATgATTCTAgg-3'
SKOR-S310L: 5'-ggTCTACATTCTATTCgATATgATCCTAggAg-3'
SKOR-D312A: 5'-CgATggTCTACATAAgCTTCgCTATgATTC-3'
SKOR-D312E: 5'-CgATggTCTACATAAgCTTCgAgATgATTC-3'
SKOR-D312N: 5'-CgATggTCTACATAAgCTTCAATATgATTC-3'
SKOR-D312R: 5'-CgATggTCTACATAAgCTTCCgTATgATTC-3'
SKOR-D312Q: 5'-CgATggTCTACATAAgCTTCCAgATgATTC-3'
SKOR-M313E: 5'-ggTCTACATAAgCTTCgATgAgATTCTAgg-3'
SKOR-M313I: 5'-ggTCTACATAAgCTTCgATATCATTCTAgg-3'
SKOR-M313L: 5'-ggTCTACATAAgCTTCgATCTgATTCTAgg-3'
SKOR-M313V: 5'-ggTCTACATAAgCTTCgATgTgATTCTAgg-3'
SKOR-M313L-G316T: 5'-CgATggTCTACATAAgCTTCgATCTgATTCTAACAgCTTACTTgATTgg-3'
SKOR-I314D: 5'-ggTCTACATAAgCTTCgATATggATCTAggAgC-3'
SKOR-I314G: 5'-ggTCTACATAAgCTTCgATATgggTCTAggAgC-3'
SKOR-G316T: 5'-ggTCTACATAAgCTTCgATATgATTCTAACAgCTTACTTgATTgg-3'
SKOR-D312N-M313L-I314G: 5'-CgATggTCTACATAAgCTTCAATCTgggTCTAggAgCTTACTTg-3'

Subsequently the *Acc*I-*Xho*I cassette of the pGEMHE-SKOR plasmid was replaced by the respective mutagenised cassette.

If the codon of interest was located upstream but still in close vicinity to the *Acc*I site (Figure S6), the SKOR-specific forward primer

SKOR-f: 5'-CCgTCATTAATggAATCAgAgATATCTCC-3'

together with one of the following mutation-carrying reverse primers were used for PCR:

SKOR-A305D: 5'-gAAATgTAgACCATATCgAATATCATTTCC-3'
SKOR-M306I: 5'-gAAATgTAgACgATAgCgAATATCATTTCC-3'

Subsequently the *Age*I-*Acc*I cassette of the pGEMHE-SKOR plasmid was replaced by the respective mutagenised cassette.

If the codon of interest was located not close to an unique restriction site, or the desired mutation eliminated the restriction site, the mutagenised cassette was generated in two steps. At first, two PCRs were carried out using for one the SKOR-specific forward primer

SKOR-f: 5'-CCgTCATTAATggAATCAgAgATATCTCC-3'

together with one of the following mutation-carrying reverse primers

SKOR-D164N-r: 5'-gCATgCAAgTAAgTTAATTATAAAAgTTg-3'
SKOR-D172N-r: 5'-gATATTCCATggCATgCATgCAAgTAAgTC-3'
SKOR-E182A-r: 5'-gTACCTCACTTCTgCTTTTTCgCCTgCAgC-3'
SKOR-P_{KAT1}-r: 5'-CCATAACCAgTAgTTgTCAACgTAgTAATTgACCAgTACATAgAAgTAgTgTATCg-3'
SKOR-M286L-r: 5'-CCATAACCAACAgTTgCCAACgTTACAACTgCAAAgTACATAgAAg-3'
SKOR-V289T-r: 5'-CCATAACCAgTAgTTgCCATggTAACAACTgCAAAgTACATAgAAg-3'
SKOR-Y291C-r: 5'-gCgTgTATATCTCCACAACCAACAgTTgCCATggTAACAACTgC-3'
SKOR-G292D-D293S-r: 5'-gCgTgTATATCACTATCACCAACAgTTgCCATggTAACAACTgC-3'
SKOR-H295A-r: 5'-CATATTAACCgCggCTATATCTCC-3'
SKOR-H295K-r: 5'-CATATTAACCgCTTTTATATCTCC-3'
SKOR-V307F-r: 5'-gCTCCTAgAATCATATCgAAgCTTATgTAgAACATCgCgAATATCATTTCCC-3'

and for the other the SKOR-specific reverse primer

SKOR-r: 5'-gCCgCACTATTCAACTTCAgAgCTAgTTCTgCCTCTTgTTTACTgATATg-3'

together with one of the following mutation-carrying forward primers

SKOR-D164N-f: 5'-TAATTAACTTACTTgCATgCATgCCATggg-3'
SKOR-D172N-f: 5'-CATgCATgCCATggAATATCATCTACAAgg-3'
SKOR-E182A-f: 5'-gCAgAAgTgAggTACCTATTgTTgATAAgg-3'
SKOR-P_{KAT1}-f: 5'-CTTCTATgTACTggTCAATTACTACgTTgACAACTACTggTTATggAgATATACACgCgg-3'
SKOR-M286L-f: 5'-CTTCTATgTACTTTgCAgTTgTAACgTTggCAACTgTTggTTATgg-3'
SKOR-V289T-f: 5'-CTTCTATgTACTTTgCAgTTgTTACCATggCAACTACTggTTATgg-3'
SKOR-Y291C-f: 5'-gCAgTTgTTACCATggCAACTgTTggTTgTggAgATATACACgC-3'
SKOR-G292D-D293S-f: 5'-gCAgTTgTTACCATggCAACTgTTggTgATAgTgATATACACgC-3'
SKOR-H295A-f: 5'-ggAgATATAgCCgCggTTAATATg-3'
SKOR-H295K-f: 5'-ggAgATATAAAAgCggTTAATATg-3'
SKOR-V307F-f: 5'-gggAAATgATATTCgCgATgTTCTACATAAgCTTCgATATgATTCTAggAgC-3'

The PCR-products were purified, and corresponding pairs were used as templates for the second elongating step again by PCR employing the SKOR-f and SKOR-r flanking primers. Subsequently the *Age*I-*Acc*I or the *Age*I-*Xho*I cassette of the pGEMHE-SKOR plasmid was replaced by the respective mutagenised cassette.

Figure S7

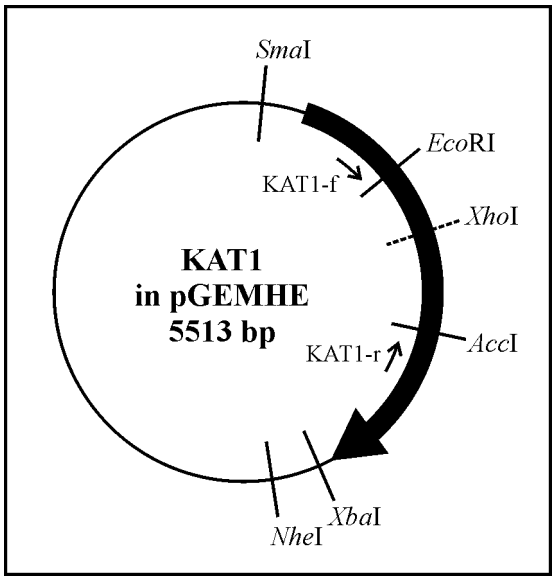

Figure S7. Generation of KAT1 mutants. Vector map of the plasmid pGEMHE-KAT1. The coding sequence of KAT1 is shown as black arrow. Additionally the restriction sites used in this study are displayed: The unique restriction sites for *Eco*RI, *Acc*I, *Xho*I (generated by silent mutagenesis), and *Nhe*I. The *Sma*I and *Xba*I sites were used to clone the KAT1-coding sequence into pGEMHE.

KAT1-mutations generated by PCR

The mutants were generated by polymerase chain reaction using *Pfu* polymerase (Promega, Mannheim, Germany) in a two-step protocol. At first, two PCRs were carried out using for one the KAT1-specific forward primer

KAT1-f: 5'-CCACTCCTATCTTCTAgTTgACAgTCC-3'

together with one of the following mutation-carrying reverse primers

KAT1-L258M-r: 5'-gAgggTTCTCAgCATgAAAATCTCCATATCCCgTggTCgTCATTgTCgTAATggACC-3'

KAT1-N284D-L285M-G286I-r:

5'-ATCATgTCgAACATCATgAAgAAAATgTCAAAAAgCATTTCTCgAgggTTCTCAgC-3'

and for the other the KAT1-specific reverse primer

KAT1-r: 5'-ATTgTTCATgATgACTCgTCCATCg-3'

together with one of the following mutation-carrying forward primers

KAT1-L258M-f: 5'-gACgACCACgggATATggAgATTTTCATgCTgAgAACCCTCgAgAAATgC-3'

KAT1-N284D-L285M-G286I-f:

5'-TCgAgAAATgCTTTTTgACATTTTCTTCATgATgTTCgACATgATTTTgACAgCTTACC-3'

The PCR-products were purified, and corresponding pairs were used as templates for the second elongating step again by PCR employing the KAT1-f and KAT1-r flanking primers. Subsequently the *Eco*RI-*Acc*I fragment of the pGEMHE-KAT1 plasmid was replaced by the respective mutagenised cassette. To generate the quadruple mutant KAT1-L258M-N284D-L285M-G286I the 0.3 kb *Eco*RI-*Xho*I fragment of pGEMHE-KAT1-N284D-L285M-G286I was replaced by the corresponding fragment of pGEMHE-KAT1-L258M.

All mutations were verified by sequencing the mutagenised cassette.

⇒ zurück zur Übersicht

2005

Michard, Lacombe, Porée, Mueller-Roeber, Sentenac, Thibaud, **Dreyer**

A unique voltage sensor sensitizes the potassium channel AKT2 to phosphoregulation.

J. Gen. Physiol. **126**:605-617.

A Unique Voltage Sensor Sensitizes the Potassium Channel AKT2 to Phosphoregulation

Erwan Michard,[1,2,3] Benoît Lacombe,[3] Fabien Porée,[1,2] Bernd Mueller-Roeber,[1,2] Hervé Sentenac,[3] Jean-Baptiste Thibaud,[3] and Ingo Dreyer[1,2,3]

[1]Universität Potsdam, Institut für Biochemie und Biologie, Abteilung Molekularbiologie, D-14476 Potsdam-Golm, Germany
[2]Max-Planck Institute of Molecular Plant Physiology, Cooperate Research Group, D-14424 Potsdam-Golm, Germany
[3]Laboratoire de Biochimie et Physiologie Moléculaire des Plantes, UMR 5004, Agro-M/CNRS/INRA/UM2, F-34000 Montpellier, France

Among all voltage-gated K^+ channels from the model plant *Arabidopsis thaliana*, the weakly rectifying K^+ channel (K_{weak} channel) AKT2 displays unique gating properties. AKT2 is exceptionally regulated by phosphorylation: when nonphosphorylated AKT2 behaves as an inward-rectifying potassium channel; phosphorylation of AKT2 abolishes inward rectification by shifting its activation threshold far positive (>200 mV) so that it closes only at voltages positive of +100 mV. In its phosphorylated form, AKT2 is thus locked in the open state in the entire physiological voltage range. To understand the molecular grounds of this unique gating behavior, we generated chimeras between AKT2 and the conventional inward-rectifying channel KAT1. The transfer of the pore from KAT1 to AKT2 altered the permeation properties of the channel. However, the gating properties were unaffected, suggesting that the pore region of AKT2 is not responsible for the unique K_{weak} gating. Instead, a lysine residue in S4, highly conserved among all K_{weak} channels but absent from other plant K^+ channels, was pinpointed in a site-directed mutagenesis approach. Substitution of the lysine by serine or aspartate abolished the "open-lock" characteristic and converted AKT2 into an inward-rectifying channel. Interestingly, phosphoregulation of the mutant AKT2-K197S appeared to be similar to that of the K_{in} channel KAT1: as suggested by mimicking the phosphorylated and dephosphorylated states, phosphorylation induced a shift of the activation threshold of AKT2-K197S by about +50 mV. We conclude that the lysine residue K197 sensitizes AKT2 to phosphoregulation. The phosphorylation-induced reduction of the activation energy in AKT2 is ~6 *kT* larger than in the K197S mutant. It is discussed that this hypersensitive response of AKT2 to phosphorylation equips a cell with the versatility to establish a potassium gradient and to make efficient use of it.

INTRODUCTION

Potassium is the predominant, inorganic ion of plant cells where it plays a major role as an osmoticum contributing to cellular hydrostatic (turgor) pressure, growth, and responses to the environment. The transport of potassium is accomplished by a variety of transport proteins (Véry and Sentenac, 2003; Amtmann et al., 2004). An important role is played by voltage-gated potassium channels of the so-called *Shaker* family (Pilot et al., 2003). *Shaker*-like plant potassium channels belong to the superfamily of voltage-gated K^+ channels (Yellen, 2002). A functional K^+ channel is a tetramer built up of four α subunits as indicated by coexpression studies (MacKinnon, 1991; Dreyer et al., 1997) and directly evidenced by the X-ray structure of a voltage-dependent *Shaker* K^+ channel (Long et al., 2005a). A single α-subunit shows a topology of six transmembrane domains (identified as S1–S6) flanked by cytosolic NH_2 and COOH termini, and a P (pore) loop and helix between S5 and S6 that contribute to the channel pore and ion selectivity filter. The voltage-sensing property of voltage-gated potassium channels is associated with the first four transmembrane domains and mainly with the S4 helix (Bezanilla, 2000; Männikkö et al., 2002; Latorre et al., 2003).

The family of plant voltage-gated potassium channels segregates into at least three functionally different subfamilies (Pilot et al., 2003): (1) hyperpolarization-activated, inward-rectifying K_{in} channels mediate potassium uptake, (2) depolarization-activated, outward-rectifying K_{out} channels mediate potassium release, and (3) weak-rectifying K_{weak} channels can mediate both potassium uptake and release. A model system for investigations of the properties of K_{weak} channels is the *Arabidopsis* K_{weak} channel AKT2 (Cao et al., 1995b; Ketchum and Slayman, 1996; Marten et al., 1999; Lacombe et al., 2000; Dreyer et al., 2001; Hoth et al., 2001; Chérel et al., 2002; Geiger et al., 2002; Michard et al., 2005). In literature this channel is also called AKT3 and AKT2/3. AKT3 refers to a truncated AKT2 protein lacking the first 15 amino acids. In order

Correspondence to Ingo Dreyer: dreyer@rz.uni-potsdam.de
E. Michard's present address is Instituto Gulbenkian de Ciência, R. Quinta Grande 6, PT-2780-156 Oeiras, Portugal.

to be consistent with the gene nomenclature (Cao et al., 1995b) we used in all cases the name AKT2 throughout this manuscript. AKT2 is predominantly expressed in the phloem and in guard cells and was proposed to fulfill different functions in these tissues. Among them is the control of the electrical membrane potential. Thereby, AKT2 may regulate sugar transport in the phloem and may play a role in electric cell signaling and membrane excitability. AKT2 was also proposed to be involved in the plant response to drought by adjusting potassium/sugar homeostasis (Marten et al., 1999; Lacombe et al., 2000; Deeken et al., 2002).

However, the results from recent biophysical approaches brought new aspects into the interpretation of the physiological function of AKT2-like channels and fueled the speculations on their diverse roles in the plant (Michard et al., 2005). Detailed electrophysiological analyses revealed an unexpected bimodal gating behavior of AKT2. It was particularly demonstrated that this channel, depending on its phosphorylation state, displays either the properties of a K_{in} channel or acts as a "potassium selective leak." Indeed, it was shown that the unique gating behavior of K_{weak} channels originates from the superimposition of two distinct gating modes (Dreyer et al., 2001): so-called gating mode#1 AKT2 channels activate at voltages more negative than −50 mV, whereas gating mode#2 channels are open in the entire physiological voltage interval (−250 mV to +50 mV). Interestingly, mode#2 channels are also voltage gated and close at nonphysiological voltages more positive than +100 mV, suggesting that the mechanistic difference between mode#1 and mode#2 channels is mainly a shifted activation threshold.

Further studies indicated that the setting of the gating mode is correlated with the phosphorylation status of the channel protein. One single channel can be converted from one mode into the other by phosphorylation/dephosphorylation events (Dreyer et al., 2001; Chérel et al., 2002; Michard et al., 2005). Two putative phosphorylation sites highly conserved among the K_{weak} subfamily and located in the S4–S5 linker and in the S6–COOH terminus linker of AKT2-like polypeptides (e.g., AKT2-S210 and AKT2-S329) were identified. When both serines in AKT2 were mutated to alanines, the mutant channel was inward rectifying and thus mimicked gating mode#1 channels, and when both serines were mutated to asparagines the mutant channel exhibited instantaneous currents only and thus mimicked gating mode#2 channels (Michard et al., 2005).

Phosphorylation appears to be a widely used process to regulate the activity of plant ion channels (Dreyer et al., 2004). For instance, biochemical approaches evidenced the phosphorylation of the K_{in} channel KAT1 in planta (Li et al., 1998; Mori et al., 2000). However, at the functional level the modulation of KAT1 activity (Berkowitz et al., 2000) and gating (Tang and Hoshi, 1999) by phosphorylation was far less pronounced (activation threshold shifted by around +50 mV) compared with the effects observed on AKT2 (activation threshold shifted by >+200 mV). Thus, although the concept of phosphoregulation allows to explain all our experimental observations on AKT2, so far it raises the following question. Which molecular peculiarities render the gating of K_{weak} channels highly sensitive to phosphorylation when compared with K_{in} channels?

In the present study we created chimeras between the K_{weak} channel AKT2 and the K_{in} channel KAT1. The results indicated that the regions upstream of the pore (from the NH_2 terminus to S4) contain sites crucial for weak rectification. We identified a K_{weak}-specific lysine residue in the voltage-sensing S4 helix that is essential for the weak rectification properties of AKT2. We conclude that the presence of this lysine residue strongly sensitizes AKT2 to phosphoregulation.

MATERIALS AND METHODS

Molecular Genetics

Standard molecular genetic methods were employed. Site-specific mutations were generated with the pAlter mutagenesis system (for details see online supplemental material, available at http://www.jgp.org/cgi/content/full/jgp.200509413/DC1). Mutants were verified by sequencing. For expression, the coding regions of the various channels were cloned into the mammalian expression vector pCI (Promega).

Expression and Electrophysiology

Culture and transfection of COS-7 cells as well as whole-cell and single channel recordings from COS cells were performed as described previously (Dreyer et al., 2001). The bath solution as well as the pipette solution in the cell-attached configuration contained (in mM) 150 KCl, 1 $CaCl_2$, 1.5 $MgCl_2$, 10 HEPES/NaOH (pH 7.4). The whole-cell pipette solution contained (in mM) 150 KCl, 1.5 $MgCl_2$, 3 EGTA, 10 HEPES/NaOH (pH 7.2), 2.5 MgATP. This ATP concentration had been shown to avoid channel activity rundown (Michard et al., 2005). Expression in *Xenopus* oocytes was performed as previously described (Dreyer et al., 2001). Measurements were repeated routinely at the end of each treatment with the addition of 10 mM Cs^+ to distinguish AKT2 currents and any background, nonselective leak, and to set a baseline of relative conductance. When 10 mM extracellular Cs^+ was applied, almost 100% of AKT2-mediated currents were blocked at voltages more negative than −150 mV (Lacombe et al., 2000).

Data Analyses

Data were analyzed according to common protocols (Sakmann and Neher, 1995; Blatt, 2004). Relative conductance (rel.G[V]) was obtained from tail current (I_0[V]) analyses with double-pulse voltage-clamp protocols in whole-cell recordings (Dreyer et al., 2001): after activating pulses in the −180 to +140 mV range, tail currents were recorded at voltage V_T (e.g., −40 mV). These tail currents displayed exponential deactivation kinetics. The instantaneous tail current (I_0) was obtained by extrapolating the kinetics to the time of the voltage jump to V_T and subsequently plotted against the voltage V applied during the preceding activating

pulse. $I_0(V)$ is proportional to the conductance (rel.G[V]) at the end of the activating pulse. For channels displaying two distinct gating modes (e.g., AKT2), a sum of two scaled Boltzmann functions was fitted to the resulting curves such that

$$I_0(V) = \frac{I_{max.mode\#1}}{1 + e^{-\delta_1 \frac{F}{RT}(V - V_{1/2,1})}} + \frac{I_{max.mode\#2}}{1 + e^{-\delta_2 \frac{F}{RT}(V - V_{1/2,2})}}, \quad (1)$$

where *F*, *R*, and *T* have their usual meaning, δ_1 and δ_2 denote the apparent gating charges, and $V_{1/2,1}$ and $V_{1/2,2}$ the half-activation voltages of the two modes. Because the $I_0(V)$ data in the experimentally accessible voltage interval from −180 to +140 mV were not sufficient to robustly fit all six free parameters independently, usually constraints were imposed on the parameters (details are outlined in the figure legends). Fittings were performed using a Marquardt-Levenberg algorithm (Marquardt, 1963) and the resulting values used to calculate relative conductance (rel.G) separately for the different gating modes:

$$rel.G_{mode\#1}(V) = \frac{I_0(V) - \frac{I_{max.mode\#2}}{1 + e^{-\delta_2 \frac{F}{RT}(V - V_{1/2,2})}}}{I_{max.mode\#1}} \quad (2)$$

$$rel.G_{mode\#2}(V) = \frac{I_0(V) - \frac{I_{max.mode\#1}}{1 + e^{-\delta_1 \frac{F}{RT}(V - V_{1/2,1})}}}{I_{max.mode\#2}}. \quad (3)$$

For AKT2 mutants displaying apparently only one gating mode Eq. 1 was applied with $I_{max.mode\#2} = \delta_2 = V_{1/2,2} = 0$. All results are reported as mean ± 1 SD where appropriate. To describe gating with a two state model and to quantify the energy difference between open and closed state, ΔG_{OC}, a Boltzmann function was fitted to the mean rel.G(V) values:

$$rel.G(V) = \frac{1}{1 + e^{-\left(\frac{\Delta G_{OC}}{kT}\right)}} = \frac{1}{1 + e^{-\delta \frac{F}{RT}(V - V_{1/2})}}, \quad (4)$$

resulting in $\Delta G_{OC} = \delta \times F/(RT) \times (V - V_{1/2}) \times kT$ values, which could be compared.

Single channel currents were low-pass filtered at 2.5 kHz and sampled at 10 kHz. Traces showing a stable baseline were used to generate histograms with bin width of 0.02 pA. Histograms were fitted with sums of Gauss functions:

$$histo(i_{bin}) = \sum_{k=0}^{N} \frac{A_k}{\sqrt{2\pi}\sigma_k} \exp\left[-\frac{(i_{bin} - i_k)^2}{2\sigma_k^2}\right]. \quad (5)$$

Each Gauss function is characterized by a mean value i_k, a variance σ_k, and an amplitude A_k. k = 0 represents the channel in the closed conformation, k = 1 one open channel, k = 2 two open channels, etc. Single channel amplitudes were deduced from the differences between the means: $I_{SC} = i_1 - i_0$. The channel open probability was calculated from the relations between the surfaces under the different Gauss curves. If a patch contained only one active channel ($N = 1$) p_{open} was calculated as $p_{open} = A_1/(A_1 + A_0)$. One patch out of seven contained three channels. In this case the binomial distribution was applied, i.e., p_{open} was deduced from fitting to the following set of four equations:

$$A_3/(A_0 + A_1 + A_2 + A_3) = (p_{open})^3 \quad (6.1)$$

$$A_2/(A_0 + A_1 + A_2 + A_3) = 3 \cdot (p_{open})^2 \cdot (1 - p_{open}) \quad (6.2)$$

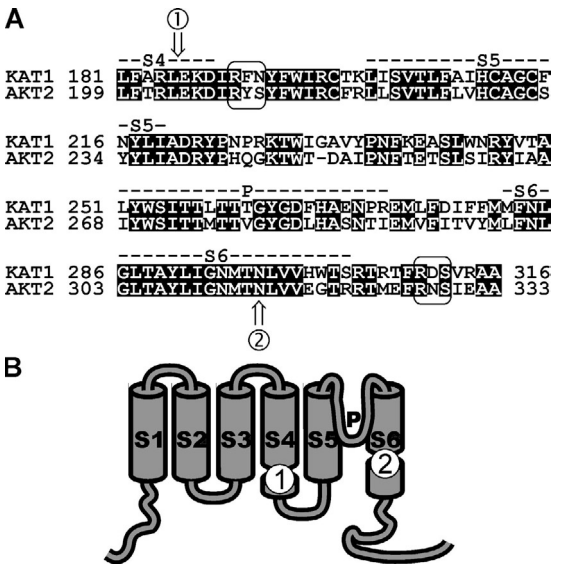

Figure 1. Sequence alignment to illustrate generation of chimeras. (A) Amino acid comparison of the S4–S6 regions of KAT1 and AKT2. The two pinpointed putative phosphoserines [RYS–210] and [RNS–329] together with the corresponding KAT1 motifs are labeled by boxes. The labels 1 (XhoI restriction site in the underlying plasmids) and 2 (BstXI restriction site in the underlying plasmids) indicate the sites used to swap domains. (B) Schematic representation of the topological location of the sites 1 and 2 in a channel subunit.

$$A_1/(A_0 + A_1 + A_2 + A_3) = 3 \cdot p_{open} \cdot (1 - p_{open})^2 \quad (6.3)$$

$$A_0/(A_0 + A_1 + A_2 + A_3) = (1 - p_{open})^3 \quad (6.4)$$

Online Supplemental Material

The online supplemental material (available at http://www.jgp.org/cgi/content/full/jgp.200509413/DC1) provides details on the cloning strategies and the primers used to generate mutants and chimeras.

RESULTS

The Region Upstream the S5 Segment Contains Elements Essential for Weak Rectification

Previous studies suggested that nonphosphorylated plant K_{weak} channels share functional similarities with K_{in} channels. After phosphorylation, however, their functional characteristics fundamentally diverge. Nonphosphorylated (mode#1) K_{weak} channels mediate time- and voltage-dependent inward potassium currents, whereas phosphorylated (mode#2) K_{weak} channels mediate instantaneous, leak-like potassium currents. Usually, in standard electrophysiological experiments, these two components superimpose and generate the impression of a weak rectification of the currents.

To understand the apparent differences in phosphoregulation between the K_{in} channel KAT1 and the K_{weak}

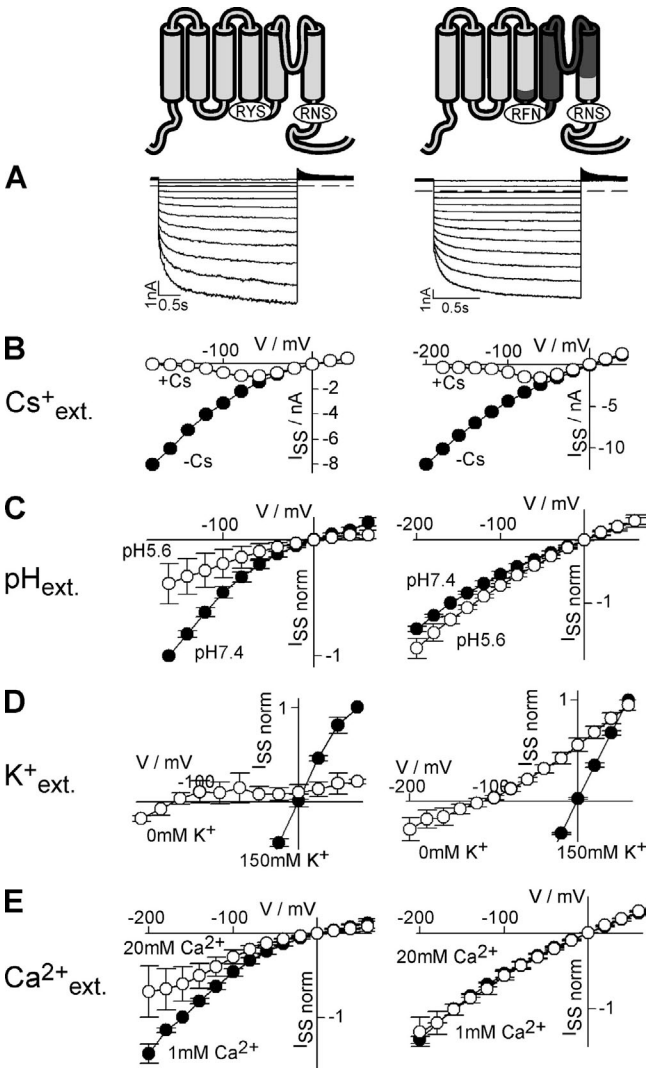

Figure 2. Exchange of the AKT2 pore by the KAT1 pore does not affect gating but alters the permeation properties of the chimeric channel. Characteristics of AKT2 (left) and the chimera AKT2-S5-P-S6-KAT1 (right) expressed in COS cells. In the chimera the fragment AKT2-E204_N314 was replaced by the fragment KAT1-E186_N297. (A) Currents elicited by voltage steps (AKT2: 3 s; chimera: 1.6 s) from a holding potential of +40 mV to voltages from +40 mV to −180 mV (20-mV decrements). The dashed lines indicate the zero current level. (B) Steady-state current–voltage characteristics. Currents were measured in standard solution (black circles) and after the addition of 10 mM Cs^+ to external standard solution (white circles). Data displayed in A and B are representative for at least three repeats. (C) Normalized current–voltage characteristics measured at pH 7.4 (black) and pH 5.6 (white). Currents were normalized to the current values measured at −160 mV at pH 7.4 (I_{SS}[−160 mV; pH 7.4] = −1). Data are displayed as mean ± SD (n = 3–8). (D) Normalized current–voltage characteristics measured in the presence (standard solution; black) and absence of external potassium (white; KCl in standard solution was replaced by NaCl). Currents were normalized to the current values measured at +60 mV in standard solution (I_{SS}[+60 mV; 150 mM K^+] = 1). Data are displayed as mean ± SD (n = 3). (E) Normalized current–voltage characteristics measured in bath solutions containing 1 mM Ca^{2+} (standard solution; black) and 20 mM Ca^{2+} (standard solution + 19 mM $CaCl_2$; white). Currents were normalized to the current values measured at −160 mV in 1 mM Ca^{2+} (I_{SS}[−160 mV; 1 mM Ca^{2+}] = −1). Data are displayed as mean ± SD (n = 3). It should be noted that, with respect to the permeation properties, the chimera behaved essentially like KAT1 (Hedrich et al., 1995; Véry et al., 1995; Becker et al., 1996; Hoth et al., 1997; Dreyer et al., 1998), the donor of the pore.

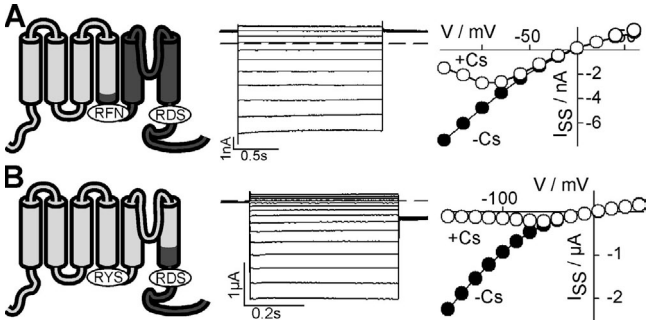

Figure 3. AKT2-KAT1 chimeras show "open-locked" behavior. Chimeras' structure (see also Fig. 1) is indicated (left). Parts originating from AKT2 are illustrated in light gray and parts from KAT1 in dark gray. Current traces (middle) and steady-state current–voltage characteristics (right) of the chimeras. Currents were measured in standard solution (black circles) and after the addition of 10 mM Cs^+ to external standard solution (white circles). The dashed lines indicate the zero current level. (A) Expression in COS cells. Currents elicited by 1.6-s voltage steps from a holding potential of +40 mV to voltages from +60 mV to −140 mV (20-mV decrements). (B) Expression in oocytes (100 mM KCl in the bath); 0.5-s voltage steps from 0 mV to voltages from +50 mV to −160 mV (15-mV decrements) followed by a step to −60 mV. Data displayed in A and B are representative for at least three repeats.

channel AKT2, we constructed recombinant chimeric channels between both. We swapped (a) the region between S4 and the COOH terminus comprising the P domain, (b) the COOH termini, and (c) the entire regions downstream the S4 segment (Figs. 1–4). The electrophysiological phenotypes of the chimeras were analyzed after expression in COS cells and *Xenopus* oocytes (Figs. 2–4). When the fragment between S4 and the COOH terminus of AKT2 was replaced by the corresponding region of KAT1, the chimera exhibited a voltage-dependent gating identical to the AKT2 wild-type characterized by the two K^+ current components: an instantaneous "leak-like" component and a hyperpolarization-activated time-dependent component (Fig. 2 A). The two current components of both channels were blocked by extracellular Cs^+ ions (Fig. 2 B). A more refined pharmacological fingerprint, however, unmasked the chimera. In contrast to wild-type AKT2, the chimera was neither blocked by protons (Fig. 2 C) nor sensitive to a reduction in the external K^+ concentration (Fig. 2 D). Additionally, the chimera was less Ca^{2+} sensitive when compared with AKT2 (Fig. 2 E). Consequently, with respect to its susceptibility toward

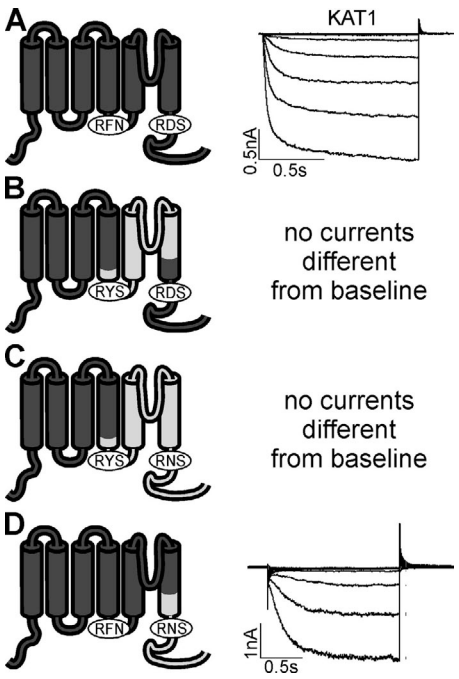

Figure 4. AKT2-KAT1 chimeras containing the NH_2 terminus and the first four membrane-spanning segments (S1–S4) of KAT1. (A) KAT1 mediates inward-rectifying currents. Currents were elicited in 1.2-s voltage steps from +40 mV to voltages between +40 mV and −160 mV (20-mV decrements). (B) No currents could be detected when the fragment KAT1-E186_N297 was replaced by the fragment AKT2-E204_N314. (C) No currents could be detected when the fragment KAT1-E186_N677 was replaced by the fragment AKT2-E204_I802. (D) The chimera KAT1-Ct_{AKT2} mediates inward currents. The fragment KAT1-N297_N677 was replaced by the fragment AKT2-N314_I802. Currents were elicited in 1.6-s voltage steps from +40 mV to voltages between +60 mV and −200 mV (20-mV decrements). Data in A–D are representatives from at least three independent repeats each.

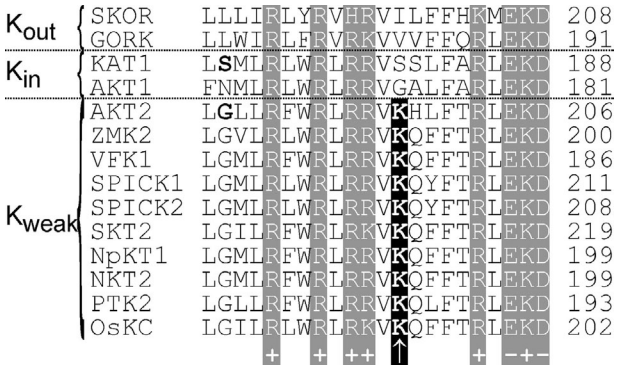

Figure 5. K_{weak} channels contain an additional lysine residue in S4. Sequence comparison of the putative voltage-sensing segment of AKT2 (GenBank/EMBL/DDBJ accession no. AAA97865) with those of other plant K^+ channels: the *Arabidopsis* K_{out} channels SKOR (Q9M8S6) and GORK (Q94A76), the *Arabidopsis* K_{in} channels KAT1 (AAA32824) and AKT1 (Q38998), and the (putative) K_{weak} channels ZMK2 (CAB54856) from *Zea mays*, VFK1 (CAA71598) from *Vicia faba*, SPICK1 (AAD16278) and SPICK2 (AAD39492) from *Samanea saman*, SKT2 (CAA70870) from *Solanum tuberosum*, NpKT1 (BAA84085) from *Nicotiana paniculata*, NKT2 (BAD81033) from *Nicotiana tabacum*, PTK2 (CAC05489) from *Populus tremula x Populus tremuloides*, and OsKC (AAS90668) from *Oryza sativa*. Charged residues present in all channels are marked. Residues AKT2-G186 (see Fig. 6) and KAT1-S168 are displayed in bold letters. Additionally, the K_{weak}-specific lysine residue is highlighted.

H^+, K^+, and Ca^{2+}, the chimera had the features of the KAT1 pore (Hedrich et al., 1995; Véry et al., 1995; Becker et al., 1996; Hoth et al., 1997; Dreyer et al., 1998) rather than the features of the AKT2 pore (Fig. 2, left; Hoth et al., 2001; Geiger et al., 2002). Thus, the replacement of the pore altered the properties of the permeation pathway. However, this exchange left the gating properties unaffected.

When the entire region downstream the S4 segment of AKT2 was replaced by that of KAT1, the resulting chimera mediated only instantaneously activating currents. A time-dependent component was not observable (Fig. 3 A). Similar results were obtained when only the COOH terminus was exchanged (Fig. 3 B), indicating that the COOH terminus of KAT1 is influencing the gating process differently compared with the AKT2 COOH terminus.

The inverse chimeras comprising the NH_2 terminus and the first four membrane-spanning segments (i.e., S1–S4) of KAT1 mediated either inward-rectifying currents or were electrically silent (Fig. 4). Interestingly, the exchange of the COOH termini did not alter the gating properties. The features of the chimera KAT1-Ct_{AKT2} (Fig. 4 D) were not fundamentally different from that of the KAT1 wild type (Fig. 4 A).

Taken together, the results indicated that the putatively voltage-sensing module of AKT2, i.e., the NH_2 terminus and the first four membrane-spanning segments, confers the weak rectification property on the chimeric channels (for comparison see Cao et al., 1995a). In the following we investigated further the role of the putative primary voltage sensor, the S4 segment, in AKT2 channel gating.

The S4 Segment Is Involved in AKT2 Gating

Voltage-dependent gating of diverse animal and plant voltage-gated channels has been shown to depend on the S4 segment carrying a high density of positive charges (Dreyer et al., 1999, 2004; Männikkö et al., 2002; Bezanilla and Perozo, 2003; Latorre et al., 2003; Swartz, 2004). Therefore, this region was proposed to be also involved in the gating of plant K_{weak} channels (Michard et al., 2005). To elucidate the role of the S4 segment (ranging from AKT2-L285 to AKT2-D206; Fig. 5) in AKT2 gating, we introduced an additional charge at position G186 by generating the mutation AKT2-G186R. The mutation did not alter the bimodal gating feature of the AKT2 channel (Fig. 6, A–C). Like the

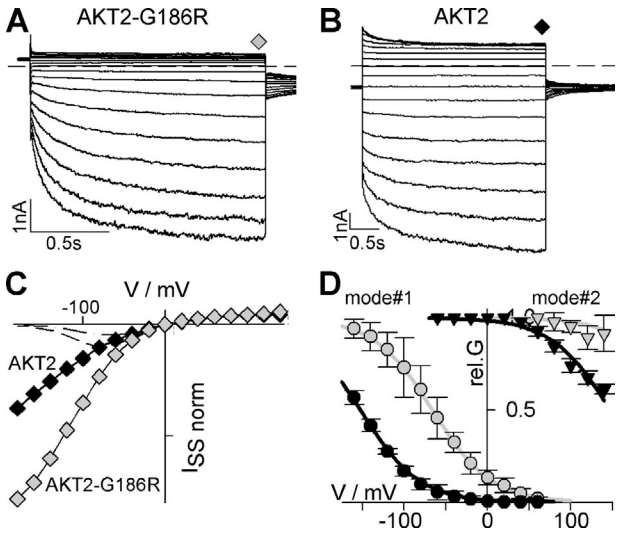

Figure 6. Mutation in S4 affects gating of AKT2. (A) Representative K^+ currents obtained from one COS cell expressing the mutant AKT2-G186R. Currents elicited by 1.6-s voltage steps from a holding potential of +40 mV to voltages from +140 mV to −180 mV (20-mV decrements) followed by a further voltage step to −40 mV (dashed line, zero-current level). (B) Representative K^+ currents obtained from one COS cell expressing the AKT2 wild type. Currents elicited by 3-s voltage steps from a holding potential of −40 mV to voltages from +140 mV to −180 mV (20-mV decrements; dashed line, zero-current level). (C) Normalized steady-state currents measured at the end of the voltage steps shown in A (AKT2-G186R, gray diamonds) and B (AKT2, black diamonds). To compare currents with a similar instantaneous component, currents were normalized to the amplitudes measured at +60 mV. Current amplitudes measured in the presence of 10 mM Cs^+ are indicated (AKT2, dash-dotted line; AKT2-G186R, dashed line). (D) Relative conductance of AKT2 (black symbols) and AKT2-G186R (gray symbols) separated for gating mode#1 (circles) and #2 (triangles). Data are displayed as mean ± SD (n = 4–5). Solid lines represent nonlinear least-squares fittings of Eq. 4 to the data. To reduce the number of free parameters, fits were constrained by the following: (a) only one δ value was adjusted for all four datasets, and (b) the difference in the $V_{1/2}$ values between the two modes was kept identical in the wild type and in the mutant. The fit yielded $\delta = 0.71$, $V_{1/2}^{\text{AKT2-mode\#1}} = -152.3$ mV, $V_{1/2}^{\text{AKT2-mode\#2}} = +147.1$ mV, $V_{1/2}^{\text{AKT2-G186R-mode\#1}} = -65.9$ mV, $V_{1/2}^{\text{AKT2-G186R-mode\#2}} = +233.5$ mV.

AKT2 wild type, the mutant AKT2-G186R mediated both an instantaneous current component and a hyperpolarization-activated time-dependent current component (Fig. 6, A and B). However, the gating properties of the mutant channel were affected (Fig. 6 D): an analysis of the deactivation currents ("tail current" analysis as described in MATERIALS AND METHODS and in Dreyer et al., 2001) revealed a strong shift of the voltage dependence of channels of both gating modes. For the gating mode#1 (nonphosphorylated state; AKT2 wild-type channels function as inward rectifiers) the shift could be quantified to be ∼+85 mV (Fig. 6 D). Interestingly, the generation of an additional positive charge in the S4 segment of the K_{weak} channel AKT2 had a similar effect as previously shown for the K_{in} channel KAT1. In KAT1 the equivalent mutation, KAT1-S168R, changed the properties of voltage sensing by inducing a shift of the channel activation threshold by about +100 mV (Dreyer et al., 1997). The S4 segment may therefore be involved in the gating of AKT2 mode#1 channels as it has been shown for hyperpolarization-activated channels from plants (Latorre et al., 2003) and animals (Männikkö et al., 2002). In addition, the results indicated that the S4 segment was also involved in the unusual gating of AKT2 mode#2 (phosphorylated state) channels. Like in gating mode#1, also in gating mode#2 the mutant AKT2-G186R activated at more positive voltages than the wild type. The data were well described if we assumed that the mutation induced an identical shift in both gating modes (Fig. 6 D, gray lines).

A Lysine Residue in S4 Is Essential for the Instantaneous Current Component of AKT2

We identified nine channels closely related to AKT2 in publicly available databases, showing 60–75% identity with AKT2 and constituting a distinct channel subfamily (K_{weak} channels) (Pilot et al., 2003). These channels exhibit the conserved putative phosphorylation sites in the S4–S5 linker and downstream of the S6 segment, which were shown to be involved in setting the gating mode of AKT2 (Michard et al., 2005). The S4 segments of channels from the AKT2 subfamily were compared with those of K_{in} and K_{out} channels (Fig. 5). Among the different channel subfamilies, six positively charged residues (R or K) are highly conserved (Fig. 5, "+"). Positive residues in S4 are assumed to be essential for the task of voltage sensing (Bezanilla and Perozo, 2003; Swartz, 2004). In addition to these conserved charged residues, the S4 segment of AKT2 comprises two further positive charges: a lysine residue at AKT2-K197 (Fig. 5, arrow) and a histidine residue at AKT2-H198. Notably, the lysine residue is conserved in all members of the K_{weak} subfamily. K_{in} and K_{out} channels possess noncharged residues at the equivalent positions. The sequence comparison further revealed that the S4 segments of K_{weak}, K_{in}, and K_{out} channels show at the targeted positions the largest diversity.

Both, K197 and H198 were mutated to serines (Fig. 7), residues found at the equivalent positions in KAT1, the K_{in} model channel. The mutation H198S did not markedly affect AKT2 gating (Fig. 7 B). In contrast, the single mutant AKT2-K197S as well as the double mutant AKT2-K197S-H198S resembled plant K_{in} channels, i.e., they were purely inward rectifying (Fig. 7, A and C). Both mutants completely lacked the instantaneous current component and only exhibited time- and voltage-dependent currents upon voltage stimulation more negative than −80 mV. A similar result was obtained

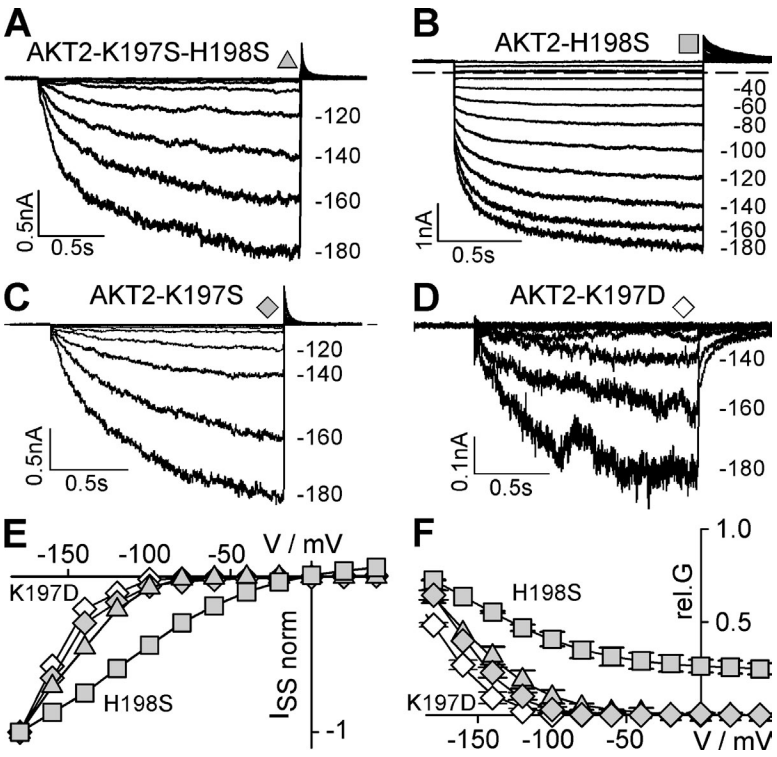

Figure 7. An exceptional lysine residue in the S4 segment is unique to K_{weak} channels and is essential for weak rectification. (A–D) Replacement of the histidine in S4 by serine does not change gating; replacement of the neighbored lysine abolishes "open leak" behavior. Representative K^+ currents obtained from COS cells expressing (A) AKT2-K197S-H198S, (B) AKT2-H198S, (C) AKT2-K197S, and (D) AKT2-K197D. Currents were elicited in voltage steps from +40 mV to voltages from +40 mV to −180 mV (20-mV decrements; dashed line, zero-current level). (E) Steady-state current–voltage characteristics measured at the end of the activation voltage steps shown in A–D (AKT2-K197S-H198S, gray triangles; AKT2-H198S, gray squares; AKT2-K197S, gray diamonds; AKT2-K197D, white diamonds). Currents were normalized to the current values measured at −180 mV ($I_{SS}[-180\ mV] = -1$). (F) Relative conductance of AKT2-K197S-H198S (gray triangles), AKT2-H198S (gray squares), AKT2-K197S (gray diamonds), and AKT2-K197D (white diamonds). Data are displayed as mean ± SD (n = 3–6). Solid lines represent nonlinear least-squares fittings of Eqs. 1 and 4 to the data yielding $\delta = 1.37$, $V_{1/2}^{AKT2\text{-}K197S} = -160.7$ mV, $V_{1/2}^{AKT2\text{-}K197D} = -175.5$ mV, $V_{1/2}^{AKT2\text{-}K197S\text{-}H198S} = -161.8$ mV, and $I_{max.mode\#2}^{AKT2\text{-}H198S} = 0.24$, $I_{max.mode\#1}^{AKT2\text{-}H198S} = 0.76$, $\delta_1^{AKT2\text{-}H198S} = 0.59$, $V_{1/2,1}^{AKT2\text{-}H198S} = -156.2$ mV.

when the lysine at position AKT2-K197 was replaced by aspartate, a negatively charged amino acid. Like AKT2-K197S, the mutant AKT2-K197D was also inward rectifying (Fig. 7, D–F). For AKT2-K197D K^+ currents were observed only at voltages more negative than −120 mV, indicating that this mutant channel activated more negative than AKT2-K197S. Thus, the lysine residue in the S4 segment of AKT2 is essential for the presence of the instantaneous K^+ current component. Moreover, the charge born by the residue at position 197 appeared to be important in determining channel properties. Its neutralization (via the K197 to S mutation) abolished instantaneous currents, and its replacement by a negative charge (via the K197 to D mutation) had an even stronger effect, by additionally shifting the activation threshold to more negative voltages.

The similarity between AKT2-K197S and K_{in} channels was further evidenced at the single channel level. When we employed the patch-clamp technique on AKT2-K197S expressing COS cells in the inside-out configuration, AKT2-K197S activity was lost in the time range of seconds (even with 2.5 mM MgATP in the bath solution; unpublished data). We therefore performed AKT2-K197S single channel recordings in the cell-attached configuration (Fig. 8). When a membrane patch containing a single ion channel was challenged with different membrane voltages, channel openings were only observed at membrane voltages more negative than −80 mV. Frequency of channel openings and lifetime of the open state increased upon further membrane hyperpolarization (Fig. 8 A). When the membrane voltage was stepped from −40 to −180 mV, channel activity was observed after a significant delay (Fig. 8 B, white arrow). After stepping back to −40 mV, the activated open channel remained open for a short time before it closed permanently (Fig. 8 B, gray arrow). The single channel conductance of the observed channel was ∼21 pS (Fig. 8 C), similar to that reported for the AKT2 wild type (25–30 pS) (Marten et al., 1999; Lacombe et al., 2000). Thus, the mutation K197S did not significantly alter the single channel conductance. Further evidence that the mutant AKT2-K197S underlies the investigated single channel activity was provided by analyzing the single channel open probability (Fig. 8 D). The single channel p_{open} values superimposed satisfyingly with the relative conductance values obtained for AKT2-K197S in whole-cell measurements (Fig. 8 D, solid line; Fig. 7 F). Thus, the gating features of the mutant AKT2-K197S resembled those of plant *Shaker*-like K_{in} channels (Hoshi, 1995; Mueller-Roeber et al., 1995; Zei and Aldrich, 1998).

The Response of AKT2-K197S to Phosphorylation Is Far Weaker than in the Wild Type

When expressed in COS cells or in *Xenopus* oocytes, the switch between the two gating modes of the AKT2 wild type is promoted by cell-intrinsic PKA-specific phosphorylation (Michard et al., 2005). The application of the PKA inhibitor H89 on AKT2-expressing oocytes induced an increase in time-dependent mode#1 currents

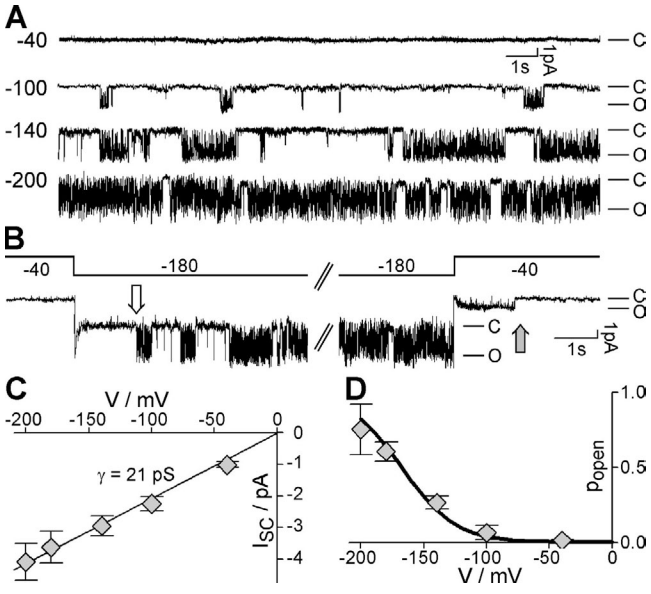

Figure 8. Single channel behavior of AKT2-K197S expressed in COS cells. (A) Representative single-channel currents (cell-attached) recorded at −40 mV, −100 mV, −140 mV, and −200 mV. C, closed state; O, open channel. (B) Delayed single channel activation and deactivation following voltage steps. Membrane voltage was stepped from −40 mV to −180 mV (left) and back to −40 mV (right). The voltage protocol is indicated. The white arrow illustrates the delayed activation at −180 mV; the gray arrow the delayed deactivation at −40 mV. (C) Current–voltage curve of the open K197S channel. Data are displayed as mean ± SD (n = 3–4). Linear regression ($R^2 \approx 0.99$) resulted in a single channel conductance of $\gamma \approx 21$ pS (solid line). (D) Voltage-dependent open probability of single K197S channels. Data are displayed as mean ± SD (n = 3–4). Solid line indicates the relative conductance of K197S deduced from macroscopic whole cell currents (from Fig. 7 F).

and a decrease in instantaneous mode#2 currents. The PKA activator Br-cAMP on the contrary increased mode#2 currents and decreased mode#1 currents. To investigate the role of phosphoregulation on the mutant AKT2-K197S we applied PKA inhibitors and activators to AKT2-K197S expressing *Xenopus* oocytes (Br-cAMP and H89) and COS cells (Br-cAMP), in parallel with experiments performed on the AKT2 wild type (Michard et al., 2005). However, whereas the effectors influenced the features of the wild type, the gating properties of AKT2-K197S were not significantly altered (unpublished data). Therefore we chose another approach to estimate the response of the K197S mutant to phosphorylation. As shown previously, the two double mutants AKT2-S210A-S329A (Fig. 9 B) and AKT2-S210N-S329N (Fig. 9 C) mimicked the dephosphorylated (mode#1) and the phosphorylated (mode#2) state of the AKT2 wild type, respectively (Fig. 9 G) (Michard et al., 2005). The AKT2-S210A-S329A mutant displayed inward-rectifying time-dependent currents, only, whereas the AKT2-S210N-S329N showed only instantaneous currents. Consequently, these double mutants were generated in the AKT2-K197S background (Fig. 9 D). Both triple mutants, AKT2-K197S-S210A-S329A (Fig. 9 E) and AKT2-K197S-S210N-S329N (Fig. 9 F), conducted inward-rectifying potassium currents when expressed in COS cells. Nevertheless, the two mutants differed in their activation threshold. Whereas AKT2-K197S-S210N-S329N was active at voltages more negative than −70 mV, AKT2-K197S-S210A-S329A activity was only observed at voltages more negative than −120 mV (Fig. 9 H).

The analysis of the gating properties of the triple mutants suggested that the AKT2-K197S mutant is still modulated by phosphorylation of the residues S210 and S329, but also that the phosphorylation of these two sites, instead of inducing a >200 mV shift of the activation potential (as observed for the AKT2 wild-type channel) only induced an ∼50 mV shift in the AKT2-K197S mutant channel.

Quantification of the Role of K197 in Phosphoregulation of AKT2

To quantify the gating parameters of gating modes#1 and #2 of the AKT2 wild type and the channel AKT2-K197S, the gating of each of the four mutants S210A-S329A, S210N-S329N, K197S-S210A-S329A, and K197S-S210N-S329N was approximated by a two-state model in which a channel can either be open, O, or closed, C (Fig. 10 A). In this model, the relative conductance of each channel can be described by a Boltzmann function (Eq. 4, rel.G = $(1 + \exp[\Delta G_{OC}/kT])^{-1}$; Fig. 9 G and H, circles and triangles, gray lines). The relative conductance of the AKT2 wild type and the mutant K197S were well described by weighted sums of the Boltzmann functions obtained for the matching double A and double N mutants (Fig. 9, G and H, diamonds, black lines).

From the obtained parameters we could estimate in as much phosphorylation influenced the activation energies of the channels AKT2 and AKT2-K197S, assuming that the double A and double N mutants represent the dephosphorylated (mode#1) and phosphorylated state (mode#2) (Fig. 10 B). It turned out that for the AKT2 wild type, phosphorylation (inducing a transition from gating mode#1 to mode#2) reduced the energy needed to activate the channel by about $\Delta(\Delta G) \approx 9\ kT$. As a consequence, the channel did not close and was locked in an open state in the entire physiological voltage range when phosphorylated. In contrast, the phosphorylation of the mutant AKT2-K197S resulted in a reduction of the activation energy of only $\Delta(\Delta G) \approx 2.3\ kT$; ∼6 kT smaller than in the wild type. As a consequence, changes of the phosphorylation status of the mutant do not dramatically affect channel gating, and the mutant AKT2-K197S appears to be similar to plant

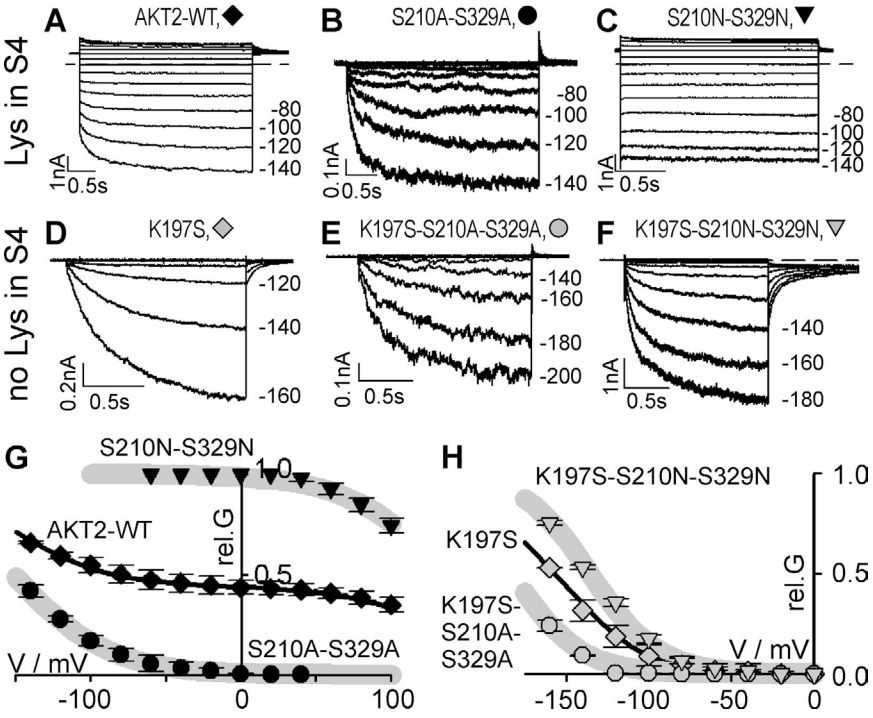

Figure 9. The two different gating modes of the AKT2 wild type and the mutant AKT2-K197S. (A–F) Representative K^+ currents obtained from COS cells expressing AKT2, AKT2-S210A-S329A, AKT2-S210N-S329N, AKT2-K197S, AKT2-K197S-S210A-S329A, and AKT2-K197S-S210N-S329N. Pulse protocols: currents elicited by voltage steps (duration T) from a holding potential of V_H to voltages from V_{min} to V_{max} (20-mV increments) followed by a further voltage step to V_T (pulse protocol indicated as [V_H; V_{min} . . . V_{max}, T; V_T] in the following). The dashed lines indicate the zero current level. (A) AKT2; (+40 mV; −140 mV . . . +140 mV, 3 s; +40 mV). (B) The mutant S210A-S329A mimics AKT2-mode#1 gating (+40 mV; −140 mV . . . +40 mV, 3 s; +40 mV). (C) The mutant S210N-S329N mimics AKT2-mode#2 gating (+40 mV; −140 mV . . . +140 mV, 2 s; +40 mV). (D) AKT2-K197S; (0 mV; −160 mV . . . +40 mV, 1.5 s; −80 mV). (E) The mutant K197S-S210A-S329A mimics AKT2-K197S-mode#1 gating (0 mV; −200 mV . . . +40 mV, 1.5 s; 0 mV). (F) The mutant K197S-S210N-S329N mimics AKT2-K197S-mode#2 gating (0 mV; −180 mV . . . +40 mV, 1.5 s; −80 mV). (G) Relative conductance of AKT2 (black diamonds), AKT2-S210A-S329A (black circles), and AKT2-S210N-S329N (black triangles). Data are displayed as mean ± SD (n = 3–6). Gray lines represent nonlinear least-squares fittings of Eq. 4 to the data for S210A-S329A and S210N-S329N ($R^2 > 0.95$). Fits were constrained by the adjustment of a common value δ for both datasets, yielding δ = 0.78, $V_{1/2}^{S210A\text{-}S329A} = -151.9$ mV, $V_{1/2}^{S210N\text{-}S329N} = +136.0$ mV. The solid line represents a weighted sum of the two gray lines: fit_rel.G_{AKT2} = 0.56 × fit_rel.$G_{S210A\text{-}S329A}$ + 0.44 × fit_rel.$G_{S210N\text{-}S329N}$. (H) Relative conductance of AKT2-K197S (gray diamonds), AKT2-K197S-S210A-S329A (gray circles), and AKT2-K197S-S210N-S329N (gray triangles). Data are displayed as mean ± SD (n = 3–6). Gray lines represent nonlinear least-squares fittings of Eq. 4 to the data for K197S-S210A-S329A and K197S-S210N-S329N ($R^2 > 0.95$). Fits were constrained by the adjustment of a common value δ for both datasets, yielding δ = 1.22, $V_{1/2}^{K197S\text{-}S210A\text{-}S329A} = -183.1$ mV, $V_{1/2}^{K197S\text{-}S210N\text{-}S329N} = -135.5$ mV. The solid line represents a weighted sum of the two gray lines: fit_rel.G_{K197S} = 0.46 × fit_rel.$G_{K197S\text{-}S210A\text{-}S329A}$ + 0.54 × fit_rel.$G_{K197S\text{-}S210N\text{-}S329N}$.

K_{in} channels, like e.g., KAT1. Similar to AKT2-K197S, the effects of phosphorylation on KAT1 channel gating are hardly observable (Tang and Hoshi, 1999). Thus, the presence of the lysine residue K197 in the putative voltage sensor of AKT2 sensitizes the K_{weak} channel to phosphoregulation.

DISCUSSION

The weak rectification of the channel AKT2 is unique among all *Shaker*-like K^+ channels of the model plant *Arabidopsis thaliana*. The ability to mediate both potassium uptake and release is the major characteristic of members of the K_{weak} channel subfamily and suggests that AKT2-like channels have enough functional flexibility to perform different tasks in the plant (Marten et al., 1999; Lacombe et al., 2000; Ache et al., 2001; Deeken et al., 2002). Besides these physiological aspects, the unique gating behavior of AKT2-like channels is also interesting from the biophysical/mechanistic point of view. Previous studies suggested that, despite their unique characteristics, K_{weak} channels share some functional similarities with K_{in} channels (e.g., their activation upon hyperpolarization). In this study we generated mutants of the K_{weak} channel AKT2 and created chimeras between AKT2 and the K_{in} channel KAT1 in order to get molecular insights into the mechanistic similarities and differences between K_{weak} and K_{in} channels.

Rectification Properties of K_{weak} Channels Do Not Depend on the Pore Region

The results presented here demonstrate that the weak rectification of AKT2 is not correlated with the structure of the pore, contrasting apparently a previous report by Hoth et al. (2001). Hoth and coworkers exchanged the pore region of the K_{weak} channel AKT3 (=AKT2-M1_D15del; nomenclature according to den Dunnen and Antonarakis, 2001) with that of the plant K_{in} channel KST1 (a channel homologous to KAT1 and 75% identical to KAT1 in the exchanged region). The resulting chimera was characterized as an inward-rectifying channel. The inverse chimera (i.e., KST1 bearing the pore region of AKT2) was characterized as a weak-rectifying channel. From their results, Hoth et al. concluded that essential elements for the rectifica-

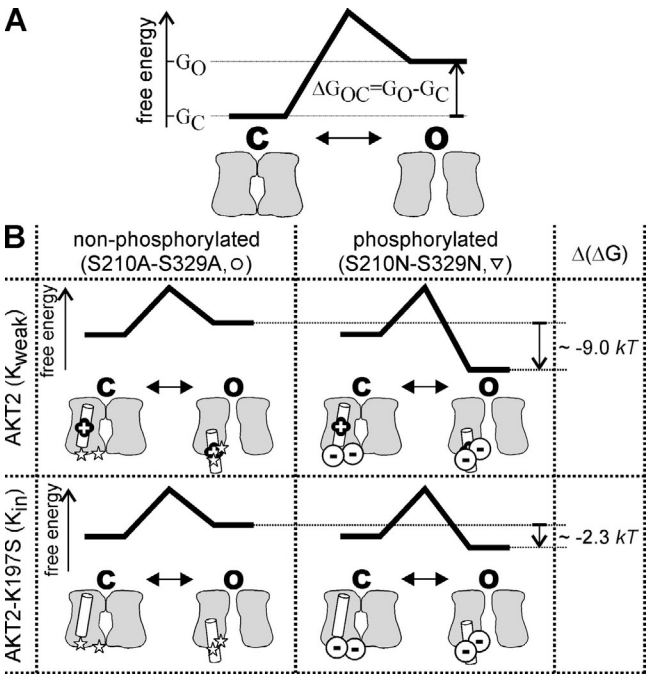

Figure 10. A model to illustrate the sensitization effect of the lysine residue. (A) A channel can exist in two conformations: open, O, and closed, C. The energy difference between open and closed conformation is $\Delta G_{OC} = G_O - G_C$. The probability to find the channel in the open conformation calculates as $p_O = (1 + \exp[\Delta G_{OC}/(kT)])^{-1}$ (Boltzmann function). From the fits to the data in Fig. 9 (G and H), the ΔG_{OC} values for the four channels S210A-S329A, S210N-S329N, K197S-S210A-S329A, and K197S-S210N-S329N are known: $\Delta G_{OC}^{S210A\text{-}S329A} = (0.78 \times F/[RT] \times [V + 151.9\ mV]) \times kT$, $\Delta G_{OC}^{S210N\text{-}S329N} = (0.78 \times F/[RT] \times [V - 136.0\ mV]) \times kT$, $\Delta G_{OC}^{K197S\text{-}S210A\text{-}S329A} = (1.22 \times F/[RT] \times [V + 183.1\ mV]) \times kT$, and $\Delta G_{OC}^{K197S\text{-}S210N\text{-}S329N} = (1.22 \times F/[RT] \times [V + 135.5\ mV]) \times kT$. (B) Consideration of four different situations: the channel can be phosphorylated (mimicked by the S210N-S329N mutation) or nonphosphorylated (mimicked by the S210A-S329A mutation), and the S4 region of the channel can contain the lysine residue (AKT2, K_{weak}, "+") or not (AKT2-K197S, K_{in}). The effect of channel phosphorylation, i.e., the energy difference, $\Delta(\Delta G) = \Delta G_{OC}^{P} - \Delta G_{OC}^{non\text{-}P}$, between the open conformations of a phosphorylated (mode#2) and a nonphosphorylated (mode#1) channel, can be approximated by calculating the difference in the ΔG_{OC} values between the mutants mimicking the phosphorylated and nonphosphorylated state: $\Delta(\Delta G^{AKT2}) = \Delta G_{OC}^{S210N\text{-}S329N} - \Delta G_{OC}^{S210A\text{-}S329A} \approx -9.0\ kT$, and $\Delta(\Delta G^{K197S}) = \Delta G_{OC}^{K197S\text{-}S210N\text{-}S329N} - \Delta G_{OC}^{K197S\text{-}S210A\text{-}S329A} \approx -2.3\ kT$. It should be noted that the value obtained for the AKT2 wild type is well in line with the energy difference $\Delta(\Delta G) = \Delta G_{OC}^{mode\#2} - \Delta G_{OC}^{mode\#1} \approx -8.5\ kT$ obtained from the data in Fig. 6 D.

tion are located within the channel pore (Hoth et al., 2001). The results of our study here do not support this conclusion: on the one hand, when the pore of AKT2 was exchanged with that of the K_{in} channel KAT1, the chimera was still weakly rectifying. On the other hand, the three purely inward-rectifying AKT2 mutants K197S, K197D, and S210A-S329A comprised the AKT2 pore.

Instead, the data here and a series of previous studies (Dreyer et al., 2001; Chérel et al., 2002; Michard et al., 2005) provide growing evidence for an alternative concept: (a) the weak rectification of AKT2 originates from the superimposition of channels gating in two distinct gating modes; (b) in both gating modes AKT2 channels are activated by hyperpolarization; (c) the main difference between channels of the two gating modes are their strongly distinct activation thresholds, so-called mode#2 channels activate >+200 mV more positive than so-called mode#1 channels; (d) the setting of the gating mode depends on the phosphorylation status of the channel; (e) the voltage sensor influences the response to phosphorylation.

Phosphorylation Feeds Back on Channel Gating

In AKT2 two putative phosphorylation sites (highly conserved among K_{weak} channels) have been pinpointed that are involved in setting the gating modes (Michard et al., 2005). One is located in the S4–S5 linker (AKT2-S210) and the other in the S6–COOH terminus linker (AKT2-S329). Interestingly, previous studies on animal depolarization-activated voltage-gated potassium channels and on hyperpolarization-activated cyclic nucleotide–gated pacemaker channels (HCN) identified these regions to be essential for coupling the voltage sensor to the intracellular activation gate (Chen et al., 2001; Lu et al., 2002). For both potassium channel classes (voltage-gated outward and inward rectifiers) it was shown that the S4–S5 linker and the S6–COOH terminus linker interact and modulate channel gating (Tristani-Firouzi et al., 2002; Decher et al., 2004). These reports suggest a conserved role of the S4–S5 and the S6–COOH terminus linkers in channel gating within the large superfamily of voltage-gated potassium channels. In this context the effect of phosphorylation of the two serine residues in AKT2 (S210 and S329) could be understood in terms of structural rearrangements within the S4–S5 and the S6–COOH terminus linkers, which in turn feed back on channel gating by affecting the activation threshold.

A Lysine Residue in S4 Amplifies the Feedback Process

Phosphorylation of the two serine residues in the S4–S5 linker and in the S6–COOH terminus linker of AKT2 shifts the activation threshold of the channel by >+200 mV positive along the voltage axis. Intriguingly, in this study we uncovered that a highly conserved lysine residue in the S4 segment of AKT2 plays an important role in this feedback process. If K197 was replaced by, e.g., a serine, the response to phosphorylation was so small that it could not be resolved by modulating the activity of endogenous kinases and phosphatases in COS cells and *Xenopus* oocytes. Only the mutation of the phos-

phorylation sites S210 and S329 suggested that AKT2-K197S was still modulated by phosphorylation, however, far weaker than the wild type. It can be concluded that the presence of the lysine residue sensitizes AKT2 to the structural rearrangements in the S4–S5 and S6–COOH terminus linkers induced by phosphorylation (or mimicked by mutations).

Reciprocal Effects of the Coupling between the Voltage Sensor and the Phosphorylated Regions

A previous study on AKT2 revealed that phosphorylation is voltage dependent (Michard et al., 2005), suggesting that the neighbored voltage sensor and the S4–S5 and S6–COOH terminus linkers (Lai et al., 2005) reciprocally affect each other. Recent structural analyses of a depolarization-activated potassium channel have revealed that the movement of the voltage sensor induces structural rearrangements in the S4–S5 and S6–COOH terminus linkers (Long et al., 2005b). We propose a similar mechanism also for AKT2. When AKT2 is in the closed state, the phosphorylation sites in the S4–S5 and S6–COOH terminus linkers (S210 and S329) are very likely shielded by other parts of the channel protein and therefore inaccessible to kinases. The movement of the voltage sensor upon hyperpolarization may induce structural rearrangements in the S4–S5 and S6–COOH terminus linkers, which then may lay the residues S210 and S329 bare to cytosolic kinases. Phosphorylation of these serines in turn may change further the structure of the two linkers and expose sites (either the phosphate groups themselves or other charged/polarized residues of the channel polypeptide), which then interact with the voltage sensor and lock the channel in the open state. The results presented in this study indicate that this interaction, i.e., the response to phosphorylation events, was strongly reduced in the AKT2-K197S mutant but not in the G186R mutant and therefore point to the importance of the lysine residue.

The Structure of the Entire Voltage-sensing Module Is Important for K_{weak} Properties

The lysine residue in S4 plays an essential role in determining the sensitivity of AKT2 toward phosphorylation events. However, the generation of a lysine residue in the S4 segment of the K_{in} channel KAT1 at the position equivalent to AKT2-K197 did not induce any significant change in channel gating (Fig. 11). At first glance this result is not surprising since neither the KAT1 wild type nor the KAT1-S179K mutant comprises any phosphorylation site in the S4–S5 or the S6–COOH terminus linker. At closer inspection, however, the comparison between the mutant KAT1-S179K and the chimera displayed in Fig. 3 A indicated that an additional lysine residue in an S4 segment of a K_{in} channel alone is not sufficient to generate a hypersensitive response to changes in the S4–S5 and S6–COOH terminus linkers. The hypersensitive response of the K_{weak} channel AKT2 to phosphorylation therefore depends on the overall structure of the entire voltage-sensing module (segments S1–S4).

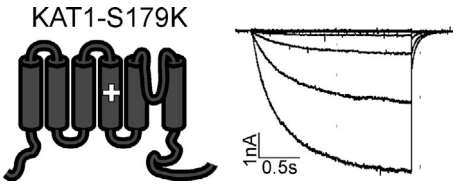

Figure 11. The lysine makes an impact in the AKT2 channel background but not in the KAT1 channel background. The mutant KAT1-S179K is an inward-rectifying K^+ channel. Representative K^+ currents measured in standard solution elicited by voltage steps from a holding potential of 0 mV by 2-s voltage steps to voltages from +60 mV to −180 mV (20-mV decrements) followed by a further voltage step to −80 mV. Data are representative for at least three repeats.

Physiological Implications of the Hypersensitive Response to Phosphorylation

Depending on its phosphorylation status an AKT2 channel gates in two distinct gating modes. Actually, current signatures of both AKT2 gating modes have been described in the plant (Bauer et al., 2000; Ivashikina et al., 2005), indicating that the hypersensitive response of K_{weak} channels to phosphorylation is a physiologically relevant mechanism. The bimodal gating behavior renders AKT2-like channels intriguingly versatile. Especially the observation that K_{weak} channel α subunits confer the weak rectification property even to heteromeric K^+ channels (Ache et al., 2001) indicates an important role of the hypersensitive response to phosphorylation at the cellular level. In gating mode#1 (nonphosphorylated) AKT2-like channels act as potassium uptake channels, allowing the cell (driven by plasma membrane H^+-ATPases) to accumulate larger amounts of K^+, e.g., during stomatal opening (Ivashikina et al., 2005). Phosphorylation switches K_{weak} channels from gating mode#1 to gating mode#2 and locks the channel open. This switch not only biases the membrane potential strongly to the equilibrium potential of K^+ and thus stabilizes the membrane voltage (Deeken et al., 2002), it also activates a physiologically important "potassium battery." In fact, "open leak" K^+ channels allow the use of the transmembrane potassium gradient (in addition to the transmembrane proton gradient) to energetically charge other electrogenic transport processes. Thus, by regulating the phosphorylation status of AKT2-like K^+ channel subunits the cell can control whether it charges the potassium battery or whether it makes use of it.

Conclusion

Together with a series of previous studies (Dreyer et al., 2001; Chérel et al., 2002; Michard et al., 2005) the data presented here allow us to reasonably explain the gating characteristics of K_{weak} channels. (a) Weakly rectifying plant K^+ channels (K_{weak} channels) are in fact specialized inwardly rectifying channels (K_{in} channels) in the sense that they activate upon hyperpolarization rather than upon depolarization. (b) The specialization of K_{weak} channels is their hypersensitive response to certain phosphorylation events that shift the activation threshold of the channels by $>+200$ mV positive along the voltage axis. (c) A lysine residue that is highly conserved among K_{weak} channels is essential for this hypersensitive response. Elimination of this lysine residue yielded channel mutants that gated like conventional K_{in} channels (e.g., AKT2-K197S, AKT2-K197D). (d) The lysine residue must be embedded in a proper structure of the voltage-sensing module to make an impact.

The understanding of the gating features of AKT2 suggests that this channel is very likely part (or target) of intra- and intercellular signaling cascades. Consequently, the future challenge will be to comprehend the integration of AKT2-like channels in these (currently unknown) signaling cascades.

We are grateful to Dr. R. O'Mahony for comments on the manuscript.

This work was supported in part by an EU Marie Curie Fellowship to I. Dreyer (contract no. ERBBIO4CT985058), by a Fellowship of the International Quality Network Program Potsdam to E. Michard, and by the GABI-Génoplante joint programs (GABI FKZ 0312852, GENOPLANTE contract no. AF2001093).

David C. Gadsby served as editor.

Submitted: 21 September 2005
Accepted: 10 November 2005

REFERENCES

Ache, P., D. Becker, R. Deeken, I. Dreyer, H. Weber, J. Fromm, and R. Hedrich. 2001. VFK1, a *Vicia faba* K^+ channel involved in phloem unloading. *Plant J.* 27:571–580.

Amtmann, A., P. Armengaud, and V. Volkov. 2004. Potassium nutrition and salt stress. *In* Membrane Transport in Plants. M.R. Blatt, editor. Blackwell, Oxford. 316–348.

Bauer, C.S., S. Hoth, K. Haga, K. Philippar, N. Aoki, and R. Hedrich. 2000. Differential expression and regulation of K^+ channels in the maize coleoptile: molecular and biophysical analysis of cells isolated from cortex and vasculature. *Plant J.* 24:139–145.

Becker, D., I. Dreyer, S. Hoth, J.D. Reid, H. Busch, M. Lehnen, K. Palme, and R. Hedrich. 1996. Changes in voltage activation, Cs^+ sensitivity, and ion permeability in H5 mutants of the plant K^+ channel KAT1. *Proc. Natl. Acad. Sci. USA.* 93:8123–8128.

Berkowitz, G., X. Zhang, R. Mercie, Q. Leng, and M. Lawton. 2000. Co-expression of calcium-dependent protein kinase with the inward rectified guard cell K^+ channel KAT1 alters current parameters in *Xenopus laevis* oocytes. *Plant Cell Physiol.* 41:785–790.

Bezanilla, F. 2000. The voltage sensor in voltage-dependent ion channels. *Physiol. Rev.* 80:555–592.

Bezanilla, F., and E. Perozo. 2003. The voltage sensor and the gate in ion channels. *Adv. Protein Chem.* 63:211–241.

Blatt, M.R. 2004. Membrane Transport in Plants. Blackwell Publishing, Oxford, UK. 372 pp.

Cao, Y., N.M. Crawford, and J.I. Schroeder. 1995a. Amino terminus and the first four membrane-spanning segments of the *Arabidopsis* K^+ channel KAT1 confer inward-rectification property of plant-animal chimeric channels. *J. Biol. Chem.* 270:17697–17701.

Cao, Y., J.M. Ward, W.B. Kelly, A.M. Ichida, R.F. Gaber, J.A. Anderson, N. Uozumi, J.I. Schroeder, and N.M. Crawford. 1995b. Multiple genes, tissue specificity, and expression-dependent modulation contribute to the functional diversity of potassium channels in *Arabidopsis thaliana*. *Plant Physiol.* 109:1093–1106.

Chen, J., J.S. Mitcheson, M. Tristani-Firouzi, M. Lin, and M.C. Sanguinetti. 2001. The S4-S5 linker couples voltage sensing and activation of pacemaker channels. *Proc. Natl. Acad. Sci. USA.* 98: 11277–11282.

Chérel, I., E. Michard, N. Platet, K. Mouline, C. Alcon, H. Sentenac, and J.B. Thibaud. 2002. Physical and functional interaction of the *Arabidopsis* K^+ channel AKT2 and phosphatase AtPP2CA. *Plant Cell.* 14:1133–1146.

Decher, N., J. Chen, and M.C. Sanguinetti. 2004. Voltage-dependent gating of hyperpolarization-activated, cyclic nucleotide-gated pacemaker channels—molecular coupling between the S4–S5 and c-Linkers. *J. Biol. Chem.* 279:13859–13865.

Deeken, R., D. Geiger, J. Fromm, O. Koroleva, P. Ache, R. Langenfeld-Heyser, N. Sauer, S.T. May, and R. Hedrich. 2002. Loss of the AKT2/3 potassium channel affects sugar loading into the phloem of *Arabidopsis*. *Planta.* 216:334–344.

den Dunnen, J.T., and S.E. Antonarakis. 2001. Nomenclature for the description of human sequence variations. *Hum. Genet.* 109: 121–124.

Dreyer, I., S. Antunes, T. Hoshi, B. Mueller-Roeber, K. Palme, O. Pongs, B. Reintanz, and R. Hedrich. 1997. Plant K^+ channel α-subunits assemble indiscriminately. *Biophys. J.* 72:2143–2150.

Dreyer, I., D. Becker, M. Bregante, F. Gambale, M. Lehnen, K. Palme, and R. Hedrich. 1998. Single mutations strongly alter the K^+-selective pore of the K_{in} channel KAT1. *FEBS Lett.* 430:370–376.

Dreyer, I., C. Horeau, G. Lemaillet, S. Zimmermann, D.R. Bush, A. Rodriguez-Navarro, D.P. Schachtman, E.P. Spalding, H. Sentenac, and R.F. Gaber. 1999. Identification and characterization of plant transporters using heterologous expression systems. *J. Exp. Bot.* 50:1073–1087.

Dreyer, I., E. Michard, B. Lacombe, and J.B. Thibaud. 2001. A plant Shaker-like K^+ channel switches between two distinct gating modes resulting in either inward-rectifying or "leak" current. *FEBS Lett.* 505:233–239.

Dreyer, I., B. Mueller-Roeber, and B. Köhler. 2004. Voltage-gated ion channels. *In* Membrane Transport in Plants. M.R. Blatt, editor. Blackwell Publishing, Oxford. 150–192.

Geiger, D., D. Becker, B. Lacombe, and R. Hedrich. 2002. Outer pore residues control the H^+ and K^+ sensitivity of the *Arabidopsis* potassium channel AKT3. *Plant Cell.* 14:1859–1868.

Hedrich, R., O. Moran, F. Conti, H. Busch, D. Becker, F. Gambale, I. Dreyer, A. Kuch, K. Neuwinger, and K. Palme. 1995. Inward rectifier potassium channels in plants differ from their animal counterparts in response to voltage and channel modulators. *Eur. Biophys. J.* 24:107–115.

Hoshi, T. 1995. Regulation of voltage dependence of the KAT1 channel by intracellular factors. *J. Gen. Physiol.* 105:309–328.

Hoth, S., I. Dreyer, P. Dietrich, D. Becker, B. Mueller-Roeber, and R. Hedrich. 1997. Molecular basis of plant-specific acid activation of K^+ uptake channels. *Proc. Natl. Acad. Sci. USA.* 94:4806–4810.

Hoth, S., D. Geiger, D. Becker, and R. Hedrich. 2001. The pore of

plant K^+ channels is involved in voltage and pH sensing: domain-swapping between different K^+ channel α-subunits. *Plant Cell.* 13: 943–952.

Ivashikina, N., R. Deeken, S. Fischer, P. Ache, and R. Hedrich. 2005. AKT2/3 subunits render guard cell K^+ channels Ca^{2+} sensitive. *J. Gen. Physiol.* 125:483–492.

Ketchum, K.A., and C.W. Slayman. 1996. Isolation of an ion channel gene from *Arabidopsis thaliana* using the H5 signature sequence from voltage-dependent K^+ channels. *FEBS Lett.* 378:19–26.

Lacombe, B., G. Pilot, E. Michard, F. Gaymard, H. Sentenac, and J.B. Thibaud. 2000. A shaker-like K^+ channel with weak rectification is expressed in both source and sink phloem tissues of *Arabidopsis*. *Plant Cell.* 12:837–851.

Lai, H.C., M. Grabe, Y.N. Jan, and L.Y. Jan. 2005. The S4 voltage sensor packs against the pore domain in the KAT1 voltage-gated potassium channel. *Neuron.* 47:395–406.

Latorre, R., R. Olcese, C. Basso, C. Gonzalez, F. Munoz, D. Cosmelli, and O. Alvarez. 2003. Molecular coupling between voltage sensor and pore opening in the *Arabidopsis* inward rectifier K^+ channel KAT1. *J. Gen. Physiol.* 122:459–469.

Li, J., Y.R. Lee, and S.M. Assmann. 1998. Guard cells possess a calcium-dependent protein kinase that phosphorylates the KAT1 potassium channel. *Plant Physiol.* 116:785–795.

Long, S.B., E.B. Campbell, and R. MacKinnon. 2005a. Crystal structure of a mammalian voltage-dependent *Shaker* family K^+-channel. *Science.* 309:897–903.

Long, S.B., E.B. Campbell, and R. MacKinnon. 2005b. Voltage sensor of Kv1.2: structural basis of electromechanical coupling. *Science.* 309:903–908.

Lu, Z., A.M. Klem, and Y. Ramu. 2002. Coupling between voltage sensors and activation gate in voltage-gated K^+ channels. *J. Gen. Physiol.* 120:663–676.

MacKinnon, R. 1991. Determination of the subunit stoichiometry of a voltage-activated potassium channel. *Nature.* 350:232–235.

Männikkö, R., F. Elinder, and H.P. Larsson. 2002. Voltage-sensing mechanism is conserved among ion channels gated by opposite voltages. *Nature.* 419:837–841.

Marquardt, D.W. 1963. An algorithm for least squares estimation of nonlinear parameters. *J. Soc. Ind. Appl. Math.* 11:431–441.

Marten, I., S. Hoth, R. Deeken, P. Ache, K.A. Ketchum, T. Hoshi, and R. Hedrich. 1999. AKT3, a phloem-localized K^+ channel, is blocked by protons. *Proc. Natl. Acad. Sci. USA.* 96:7581–7586.

Michard, E., I. Dreyer, B. Lacombe, H. Sentenac, and J.B. Thibaud. 2005. Inward rectification of the AKT2 channel abolished by voltage-dependent phosphorylation. *Plant J.* 10.1111/j.1365-313X.2005.02566.x

Mori, I.C., N. Uozumi, and S. Muto. 2000. Phosphorylation of the inward-rectifying potassium channel KAT1 by ABR kinase in *Vicia* guard cells. *Plant Cell Physiol.* 41:850–856.

Mueller-Roeber, B., J. Ellenberg, N. Provart, L. Willmitzer, H. Busch, D. Becker, P. Dietrich, S. Hoth, and R. Hedrich. 1995. Cloning and electrophysiological analysis of KST1, an inward rectifying K^+ channel expressed in potato guard cells. *EMBO J.* 14: 2409–2416.

Pilot, G., R. Pratelli, F. Gaymard, Y. Meyer, and H. Sentenac. 2003. Five-group distribution of the Shaker-like K^+ channel family in higher plants. *J. Mol. Evol.* 56:418–434.

Sakmann, B., and E. Neher, editors. 1995. Single-Channel Recording. Second edition. Plenum Press, New York. 700 pp.

Swartz, K.J. 2004. Towards a structural view of gating in potassium channels. *Nat. Rev. Neurosci.* 5:905–916.

Tang, X.D., and T. Hoshi. 1999. Rundown of the hyperpolarization-activated KAT1 channel involves slowing of the opening transitions regulated by phosphorylation. *Biophys. J.* 76:3089–3098.

Tristani-Firouzi, M., J. Chen, and M.C. Sanguinetti. 2002. Interactions between S4-S5 linker and S6 transmembrane domain modulate gating of HERG K^+ channels. *J. Biol. Chem.* 277:18994–19000.

Véry, A.A., F. Gaymard, C. Bosseux, H. Sentenac, and J.B. Thibaud. 1995. Expression of a cloned plant K^+ channel in *Xenopus* oocytes: analysis of macroscopic currents. *Plant J.* 7:321–332.

Véry, A.A., and H. Sentenac. 2003. Molecular mechanisms and regulation of K^+ transport in higher plants. *Annu. Rev. Plant Biol.* 54: 575–603.

Yellen, G. 2002. The voltage-gated potassium channels and their relatives. *Nature.* 419:35–42.

Zei, P.C., and R.W. Aldrich. 1998. Voltage-dependent gating of single wild-type and S4 mutant KAT1 inward rectifier potassium channels. *J. Gen. Physiol.* 112:679–713.

Online Supplemental Material for

Michard et al. **http://www.jgp.org/cgi/doi/10.1085/jgp.200509413**

Generation of Mutants and Chimeras

Mutants and chimeras were created by PCR-based techniques and with the pAlter mutagenesis system (Promega) using appropriate oligonucleotides to introduce the desired mutations.

AKT2 Mutations Generated with the pAlter System

The KpnI-XbaI fragment of the AKT2 coding region was cloned into the KpnI-XbaI sites of the vector pAlter-1. The mutagenesis reactions were performed according to the user manual of the pAlter mutagenesis system. To introduce the mutations the following oligonucleotides were used: AKT2-G186R: 5′-CACTTgTAATCTCTTgCgATTACTTAgATTTTggCgACTTCgACgCgTTAAACACCTCTTCACTAggC-3′, AKT2-K197S: 5′-gggATTACTTAgATTTTggCgACTTCgACgCgTTAgTCACCTCTTCACTAggCTCgAgAAgg-3′, AKT2-K197D: 5′-gggATTACTTAgATTTTggCgACTTCgACgCgTTgATCACCTCTTCACTAggCTCgAgAAgg-3′, AKT2-H198S: 5′-gggATTACTTAgATTTTggCgACTTCgACgCgTTAAAAgCCTCTTCACTAggCTCgAgAAgg-3′, AKT2-K197S-H198S: 5′-gggATTACTTAgATTTTggCgACTTCgACgCgTTAgTAgCCTCTTCACTAggCTCgAgAAgg-3′, AKT2-S210A: 5′-CgAgAAggACATAAgATATgCCTATTTCTggATCCgCTgCTTTCgACTTCTATC-3′ AKT2-S210N: 5′-CgAgAAggACATAAgATATAACTATTTCTggATCCgCTgCTTTCgACTTCTATC-3′, AKT2-S329A: 5′-ggACTCgTCgTACCATggAATTCAggAATgCCATTgAAgCAgCgTCAAACTTTgTTAACAg-3′, AKT2-S329N: 5′-ggACTCgTCgTACCATggAATTCAggAATAACATTgAAgCAgCgTCAAACTTTgTTAACAg-3′.

Subsequently, the KpnI-XbaI cassette of the pCI-AKT2 plasmid was replaced by the respective mutagenized cassette. All mutations were verified by sequencing the mutagenized cassette. To generate the double mutant S210A-S329A the 1.7-kb EcoRV-NotI fragment of pCI-AKT2-S210A was replaced by the corresponding fragment of pCI-AKT2-S329A. The double mutant S210N-S329N was created accordingly. For the triple mutants K197S-S210A-S329A and K197S-S210N-S329N the 1.8-kb XhoI-NotI fragment of pCI-AKT2-K197S was replaced by the corresponding fragments of pCI-S210A-S329A and pCI-S210N-S329N, respectively.

KAT1 Mutations Generated with the pAlter System

The entire KAT1 coding region was cloned as a SacI-BamHI fragment into the SacI-BamHI sites of the vector pAlter-1. The mutagenesis reactions were performed according to the user manual of the pAlter mutagenesis system. To introduce the mutations the following oligonucleotides were used: KAT1-XhoI: 5′-CgCTATTTgCAAggCTCgAgAAAgATATCCgTTTCAAC-3′ and KAT1-S179K: 5′-CgTCTCCggCgAgTTAAgTCgCTATTTgCAAggCTCgAgAAAgATATCCgTTTCAAC-3′ (XhoI site underlined in primer sequence and indicated in Fig. S1 B). Subsequently, the KpnI-XcmI cassette of the pCI-KAT1 plasmid was replaced by the mutagenized cassettes. The mutations were verified by sequencing the mutagenized cassette.

Generation of AKT2-KAT1 Chimeras

The exchange of the S5-P-S6 region from AKT2 by the corresponding region of KAT1 and vice versa was achieved by polymerase chain reactions using Pfu polymerase (Promega) in two-step protocols.

Replacing the S5-P-S6 Region of AKT2 by the S5-P-S6 Region of KAT1. Two PCRs were performed using for one PCR pCI-KAT1-XhoI as template and the primer KAT1-f: 5′-CCgCAAACACATAATCTCTCCTTTTAATCC-3′ together with the chimeric primer KAT1-AKT2-r: 5′-ggTACgACgAgTCCCTTCCACCACgAggTTggTCATATTTCCAATgAgg-3′, and for the other PCR pCI-AKT2 as template and the primer AKT2-r: 5′-CAATCTCAgCTCCATCTTCATTCgTCACC-3′ together with the chimeric primer KAT1-AKT2-f: 5′-CCTCATTggAAATATgACCAACCTCgTggTggAAgggACTCgTCgTACC-3′.

The PCR products were purified and used as templates for the second elongating step again by PCR using the KAT1-f and AKT2-r flanking primers. Subsequently, the XhoI-XbaI cassette of the pCI-AKT2 plasmid was replaced by the chimeric cassette. The chimera contained additionally a restriction site for BstXI (underlined in primer sequences and indicated in Fig. S1 A). The chimera was verified by sequencing the exchanged cassette.

Replacing the S5-P-S6 Region of KAT1 by the S5-P-S6 Region of AKT2. Two PCRs were performed using for one PCR pCI-AKT2 as template and the primer AKT2-f: 5′-CCAgAATCACATCAggTCTAgTggATgg-3′ together with the chimeric

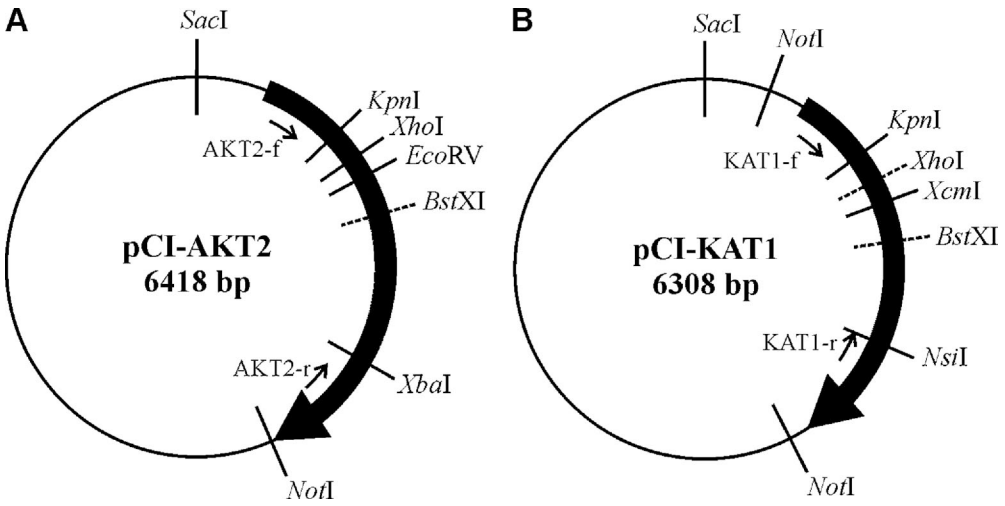

Figure S1. Vector maps. (A) Vector map of the plasmid pCI-AKT2. The coding sequence of AKT2 was cloned as SpeI-NotI fragment into the NheI-NotI sites of the pCI vector. The coding sequence of AKT2 is shown as black arrow. The restriction sites used in this study are displayed, the unique restriction sites for SacI, KpnI, XhoI, EcoRV, XbaI, and NotI. For the generation of chimeras the primers AKT2-f and AKT2-r were used. The restriction site for BstXI was introduced by silent base exchanges in chimeric plasmids (see below). (B) Vector map of the plasmid pCI-KAT1. The coding sequence of KAT1 was cloned as NotI fragment into the NotI site of a modified pCI vector. A large part of the MCS of pCI was removed by cleavage with the enzyme combination SalI/XhoI followed by religation. The coding sequence of KAT1 is shown as black arrow. The restriction sites used in this study are displayed: The unique restriction sites for SacI, KpnI, XcmI, and NsiI. The restriction site for XhoI was introduced by silent base exchanges (see below). For the generation of chimeras the primers KAT1-f and KAT1-r were used. The restriction site for BstXI was introduced by silent base exchanges in chimeric plasmids (see below).

primer AKT2-KAT1-r: 5′-ggTTCggCTAgTCCAATgAACCACgAggTTggTCATgTTACCAATAAgg-3′, and for the other PCR pCI-KAT1 as template and the primer KAT1-r: 5′-ATTgTTCATgATgACTCgTCCATCg-3′ together with the chimeric primer AKT2-KAT1-f: 5′-CCTTATTggTAACATgACCAACCTCgTggTTCATTggACTAgCCgAACC-3′.

The PCR products were purified and used as templates for the second elongating step again by PCR using the AKT2-f and KAT1-r flanking primers. Subsequently, the XhoI-NsiI cassette of the pCI-KAT1-XhoI plasmid was replaced by the chimeric cassette. The chimera contained additionally a restriction site for BstXI (underlined in primer sequences and indicated in Fig. S1 B). The chimera was verified by sequencing the exchanged cassette. All other chimeras were created by exchanging the corresponding SacI-XhoI fragments and/or the corresponding SacI-BstXI fragments.

⇒ zurück zur Übersicht

2005

Michard, **Dreyer**, Lacombe, Sentenac, Thibaud

Inward rectification of the AKT2 channel abolished by voltage-dependent phosphorylation.

Plant J. **44**:783-797.

The Plant Journal (2005) **44**, 783–797 doi: 10.1111/j.1365-313X.2005.02566.x

Inward rectification of the AKT2 channel abolished by voltage-dependent phosphorylation

Erwan Michard [†], Ingo Dreyer[‡], Benoît Lacombe, Hervé Sentenac and Jean-Baptiste Thibaud[*]
Biochimie et Physiologie Moléculaire des Plantes, UMR5004 Agro.M-CNRS-INRA-UM2, Montpellier, France

Received 29 June 2005; accepted 5 August 2005.
[*]For correspondence (fax +33 499 612 930; e-mail thibaud@ensam.inra.fr).
[†]Present address: Instituto Gulbenkian de Ciência, R. Quinta Grande 6, PT-2780-156 Oeiras, Portugal.
[‡]Present address: Universität Potsdam, Institut für Biochemie und Biologie, Abt. Molekularbiologie, Karl-Liebknecht-Str. 24/25, Haus 20, D-14476 Golm, Germany.

Summary

The Arabidopsis K^+ channel AKT2 possesses the remarkable property that its voltage threshold for activation can be either within the physiological range (gating mode 1), or shifted towards considerably more positive voltages (gating mode 2). Gating mode 1 AKT2 channels behave as delayed K^+-selective inward rectifiers; while gating mode 2 AKT2 channels are K^+-selective 'open leaks' in the physiological range of membrane potential. In the present study we have investigated modulation of AKT2 current by effectors of phosphatases/kinases in COS cells and *Xenopus* oocytes. These experiments show that (i) dephosphorylation can result in AKT2 channel silencing; and (ii) phosphorylation by protein kinase A (PKA) favors both recruitment of silenced AKT2 channels and transition from gating mode 1 to gating mode 2. Interestingly, phosphorylation of AKT2 by PKA in COS cells and *Xenopus* oocytes is favored by hyperpolarization. Two PKA phosphorylation sites (S210 and S329) were pinpointed in the region of the pore inner mouth. The role of these phosphorylation sites in the switch between the two gating modes was assessed by electrophysiological characterization of mutant channels. The molecular aspects of AKT2 regulation by phosphorylation, and the possible physiological meaning of such regulation in the plant context, are discussed.

Keywords: potassium, shaker, gating, post-translational regulation, protein kinase A, phosphatasein.

Introduction

Nine genes in the Arabidopsis genome encode K^+ channel subunits related to those of the superfamily of voltage-gated channels (Kv) expressed in animals. Four such so-called alpha-subunits must assemble as homomers (Daram *et al.*, 1997; Urbach *et al.*, 2000) or as heteromers (Baizabal-Aguirre *et al.*, 1999; Dreyer *et al.*, 1997; Obrdlik *et al.*, 2004; Pilot *et al.*, 2001; Reintanz *et al.*, 2002) to form a functional channel. The polypeptides encoded by these nine Arabidopsis genes can be sorted into three functional subtypes (Zimmermann and Sentenac, 1999). Six of them: AKT1 (Gaymard *et al.*, 1996); KAT1 (Schachtman *et al.*, 1992); KAT2 (Pilot *et al.*, 2001); AtKC1 (Reintanz *et al.*, 2002); SPIK (Mouline *et al.*, 2002); and AKT5 (not yet characterized, but 77% identity with SPIK) have been shown (or are assumed) to form inwardly rectifying Kv channels, functionally related to animal HCN channels (which open on membrane hyperpolarization). Two others, SKOR (Gaymard *et al.*, 1998; Lacombe *et al.*, 2000a) and GORK (Ache *et al.*, 2000; Hosy *et al.*, 2003), form outwardly rectifying Kv channels, functionally related to animal Shaker channels (which open on membrane depolarization). The third functional subtype corresponds to a single polypeptide (in Arabidopsis), AKT2 (Cao *et al.*, 1995), which forms so-called 'weakly rectifying' Kv channels as they can be found open within the whole physiological range of membrane potential. However, the whole-cell AKT2 current was originally shown to be the sum of an instantaneous component (flowing through channels open at all membrane potentials) and of a delayed one (appearing on hyperpolarization) (Lacombe *et al.*, 2000b; Marten *et al.*, 1999). It was subsequently demonstrated that these two current components are mediated by AKT2 channels gating in either of two different modes. So-called gating mode 1 channels mediate the delayed inwardly-rectifying current component, and gating mode 2 channels are responsible for the instantaneous one (Dreyer *et al.*, 2001). As transitions between the two gating modes have been

observed at the single-channel level (cell-attached patch-clamp recordings), it was proposed that these transitions could originate from some post-translational modifications of the AKT2 channel (Dreyer *et al.*, 2001). Subsequently it was shown that the instantaneous component of AKT2 current is more sensitive to *At*PP2CA phosphatase activity than the delayed AKT2 current, suggesting that gating mode 2 might require phosphorylation of AKT2 (Chérel *et al.*, 2002).

Here it is shown that AKT2 channels can populate a third 'silent' pool, in addition to the gating mode 1 and 2 pools. Specific effectors of protein kinase A (PKA) activity modified the distribution of AKT2 channels within these three pools, suggesting that transitions between these pools depend on the phosphorylation status of the AKT2 channels. In addition, PKA phosphorylation of AKT2 was found to be voltage-dependent. Finally, two PKA phosphorylation sites were pinpointed as being conserved in AKT2-related channels cloned from other plant species. AKT2 channels carrying point mutations at these sites were characterized, demonstrating that PKA phosphorylation of both sites is involved in switching AKT2 from one gating mode to the other.

Results

Transitions between gating modes 1 and 2 involve phosphorylation/dephosphorylation

Whole-cell recordings of AKT2 current were performed in COS cells 4.5 min after whole-cell break-in, so that pipette solution dialysis in the cell was completed. In control conditions, the presence of 2.5 mM Mg-ATP in the pipette solution made it possible to record fairly stable currents within the time of a standard experiment (see typical data in Figure 1a, gray squares). To assess stability of the current, cells were hold at a 0-mV membrane potential and currents were repeatedly (every 30 sec) stimulated by 1.6-sec-long pulses to −140 mV. The ratio between the current value sampled at the end of the −140-mV pulse 4.5 min after the patch-break ($I_{4.5min}$) and that sampled 20 min after the patch-break (I_{20min}) was calculated. The mean value of this I_{20min}:$I_{4.5min}$ ratio neighbored 100% in control conditions (Figure 1e, left graph bar). In these conditions the instantaneous component (mode 2 current, sampled at the beginning of the stimulation) and the delayed one (mode 1 current, obtained by subtracting the mode 2 current from the total one) were also stable (Figure 1a, white and black circles, respectively).

In contrast, in the absence of ATP (Mg-ATP-free pipette solution), the whole-cell AKT2 current ran down (50% of the current was lost within 24 ± 13 min, $n = 5$, Figure 1b and middle bar in Figure 1e) but with different time-courses for the instantaneous (mode 2) and delayed (mode 1) components (Figure 1b). Current records obtained at times indicated at bottom of Figure 1(b) are displayed in Figure 1(c), and the relative contributions to the total current of mode 1 and 2 components are shown in Figure 1(d).

Despite variability (Dreyer *et al.*, 2001), the time-course of current rundown could be separated systematically into three phases (Figure 1b). During the first phase, the decrease in total current was mainly due to a decrease in the instantaneous current component, with the delayed one remaining almost constant. Then, during the second phase, both delayed and instantaneous currents decreased. Finally, during the third phase, only the delayed current decreased, the instantaneous one having practically vanished. Regarding the first phase of rundown, it could be hypothesized either that mode 1 channels did not run down *per se*, or that loss of mode 1 channels (towards a silent pool) was roughly compensated by mode 2 to mode 1 conversion. The fact that, during the second and third phases, rundown of delayed current (mode 1) clearly occurred favors the second hypothesis. Thus absence of ATP favored the mode 2 to mode 1 conversion, well in line with the previously proposed hypothesis (Chérel *et al.*, 2002) that the switch from gating mode 1 to gating mode 2 would require phosphorylation of AKT2 channels. Here the absence of ATP presumably distorted the dynamic equilibrium between intracellular phosphorylation and dephosphorylation reactions, by depressing the former reactions.

Consequently, to address the features of AKT2 under controlled conditions (Figure 1a), rundown caused by ATP depletion was avoided by using a 2.5-mM ATP pipette solution in all subsequent experiments performed in COS cells. For example the effect of H89, a specific inhibitor of A-type protein kinases (PKA), was monitored under these experimental conditions. The presence of H89 in the pipette solution provoked a reduction of the AKT2 current (right bar graph, Figure 1e). This result demonstrated that AKT2 activity depends on the equilibrium between phosphorylations and dephosphorylations within the cell, and additionally suggested that PKA activity is involved in this control.

Modulation of AKT2 current by kinase/phosphatase effectors

The implications of PKA-dependent phosphorylation for the control of AKT2 channel activity were further investigated in *Xenopus* oocytes. It is worth noting that, in this expression system, no spontaneous rundown occurred when voltage clamping was obtained with two intracellular micro-electrodes. The effect of 8-bromo-cAMP (Br-cAMP), a membrane-permeant cAMP analogue that is able to activate oocyte endogenous PKA (Maurel *et al.*, 1995), was tested. Treatment of water-injected oocytes by Br-cAMP did not noticeably affect the endogenous currents (Figure 2a, upper traces). Likewise, none of the other treatments described in this study had any noticeable effect on oocyte-intrinsic currents (not shown, $n \geq 5$ for each treatment). In contrast,

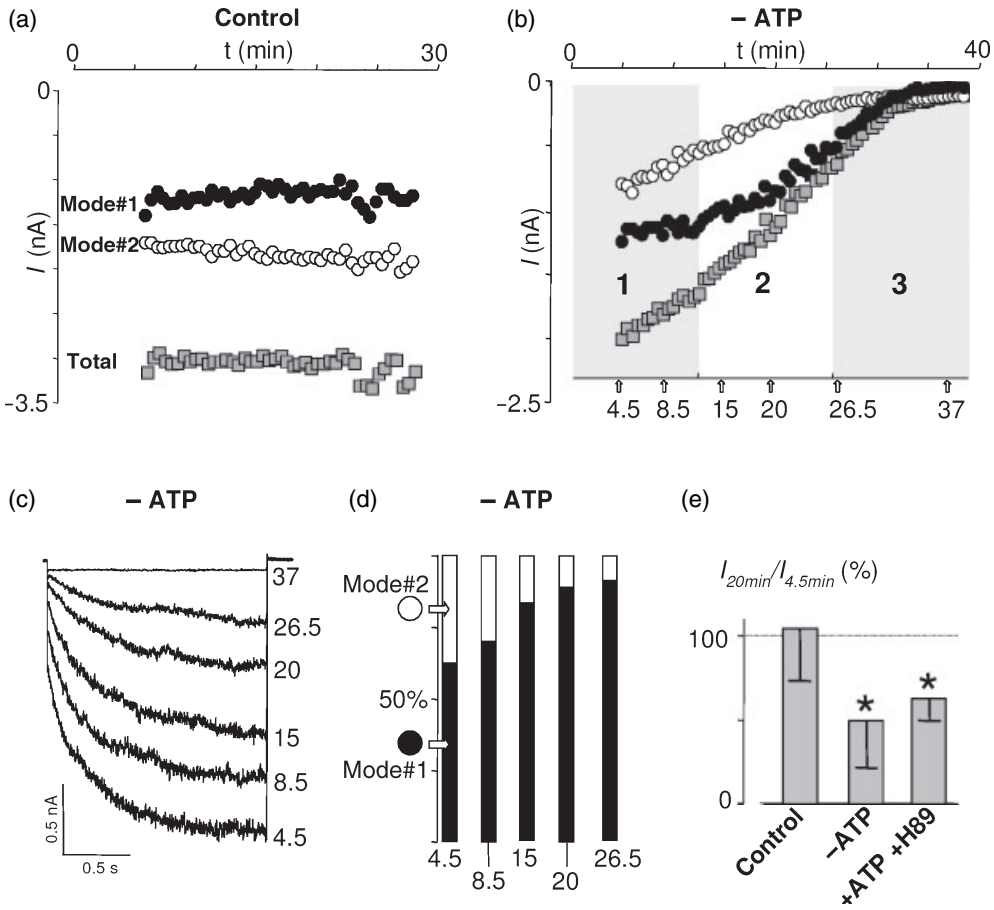

Figure 1. Sustained activity of AKT2 channels requires ATP-dependent phosphorylation.
COS cells expressing AKT2 were challenged every 30 sec with 1.6-sec pulses to −140 mV (from a holding potential of 0 mV).
(a) Virtually no rundown was observed when the pipette solution contained 2.5 mM MgATP (control condition). The total current (gray squares) and delayed (black circles, gating mode 1) and instantaneous (white circles, gating mode 2) components display flat kinetics when plotted against time.
(b) AKT2 current runs down in the absence of ATP (same conditions and symbols as in (a) except that the pipette solution did not contain ATP). Three phases could be distinguished in the rundown kinetics (see text) and are indicated by shading and labels 1–3. Time position of data displayed in (c) and (d) are indicated below the graph (arrows labeled with times in min).
(c) Sample records of currents elicited by the repeated pulses at −140 mV are shown for different times after rupturing the patch (labels in min at the right of records).
(d) Proportion (percentage scale) of the time-dependent (mode 1, black) and instantaneous (mode 2, white) current as a function of the time after whole-cell configuration. Data in (a–d) are from the same cell.
(e) Ratio of total currents recorded 4.5 and 20 min after patch break-in in COS cells, at −140 mV, with 2.5 mM Mg-ATP ($n = 4$, control), without Mg-ATP ($n = 4$, −ATP), and with 2.5 mM Mg-ATP and 1 μM H89 ($n = 3$, +H89) in the pipette solution. Data are given as means ± SD. Stars indicate values significantly different from 100% (Student's *t*-test, $P < 0.05$).

Br-cAMP was effective on AKT2-expressing oocytes: it increased the total AKT2 current by strongly increasing the instantaneous AKT2 current while decreasing the delayed one (Figure 2a, middle traces). Cs^+ application was efficient in inhibiting most of the recorded current before as well as after Br-cAMP application (currents recorded at −130 mV shown in Figure 2a, lower traces). This ruled out the hypothesis that the Br-cAMP-dependent increase in instantaneous current could have been due to an increase in some background, not K^+-selective, current. It is worth noting that such so-called 'cesium controls' were systematically performed before and after any pharmacological treatment throughout the whole study described in this paper (not systematically displayed in the figures). Regarding Br-cAMP, the data obtained indicated that it stimulates the net conversion of AKT2 channels from gating mode 1 to gating mode 2 (Figure 2b).

AKT2 (like all plant Shaker-related channels cloned so far) bears a putative cyclic nucleotide-binding site in its C-terminus (Cao *et al.*, 1995). Consequently, Br-cAMP could have modified AKT2 activity by a direct interaction rather than through an activation of PKA. The latter mode of action was, however, more likely because staurosporine, a protein kinase inhibitor which is active against PKA (Ohnishi *et al.*, 1998; Tamaoki, 1991), counteracted the effect of Br-cAMP and inhibited the AKT2 current, mainly at the level of the

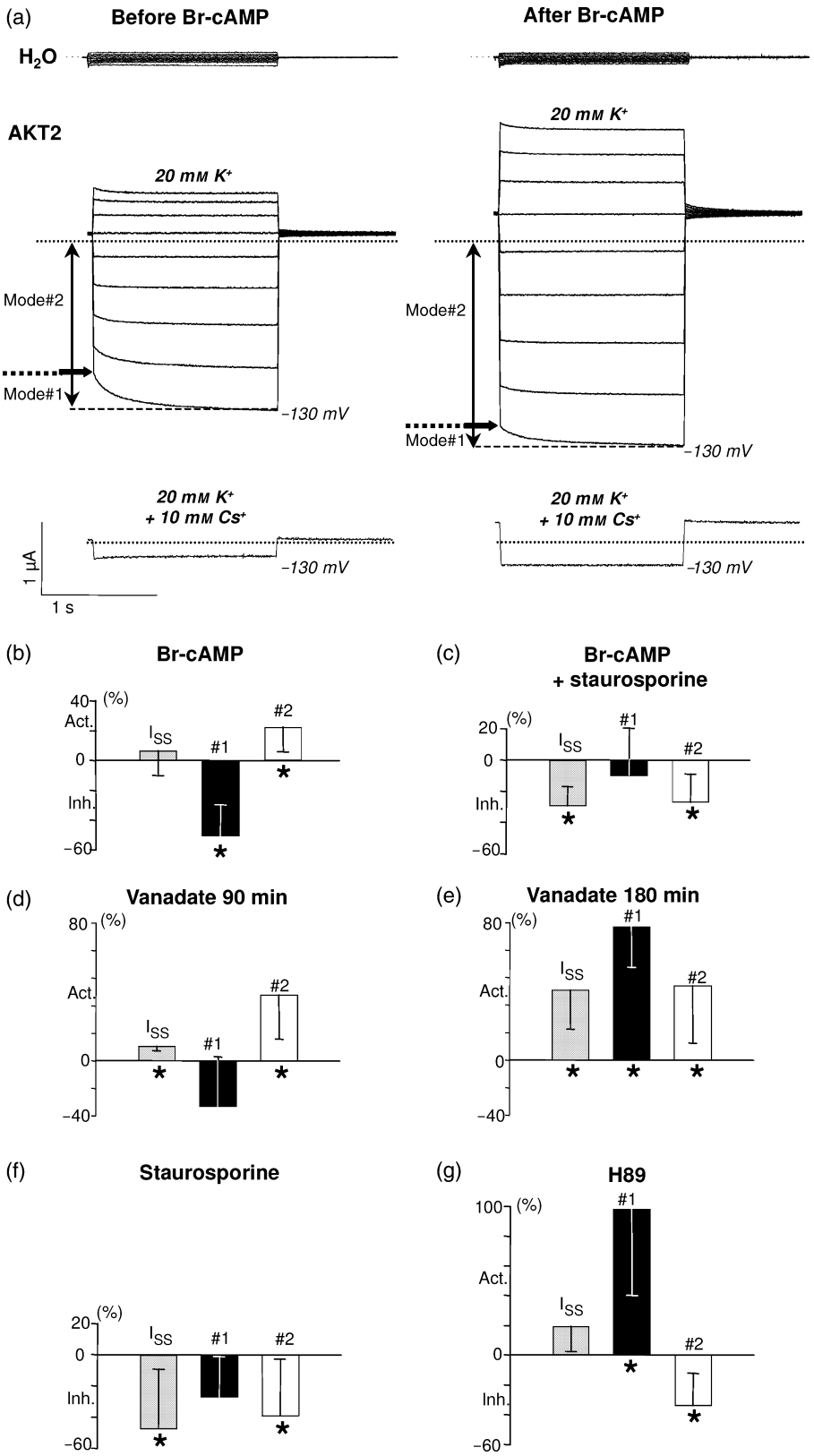

mode 2 component (Figure 2c). In accordance with a dependence of AKT2 activity on phosphorylation events, the application of vanadate, a non-specific phosphatase inhibitor, stimulated AKT2 currents. A 90-min treatment with vanadate stimulated mainly the mode 2 current (Figure 2d), while a 180-min treatment stimulated both current components (Figure 2e), suggesting that formerly silent AKT2 channels were recruited. While staurosporine had no effect on endogenous currents recorded under the same conditions in water-injected oocytes (data not shown, $n \geq 5$), when applied alone, it reduced AKT2 current without specificity for the gating mode (Figure 2f). Conversely, H89, which targeted the PKA activity more specifically than staurosporine, strongly affected the gating mode 1 versus gating mode 2 balance and poorly changed the bulk activity of AKT2 channels (Figure 2g). These data suggested that (i) PKA-mediated phosphorylation is mainly responsible for the difference between gating modes 1 and 2; and (ii) AKT2 activity also depends on some non-PKA-mediated phosphorylation.

PKA-dependent stimulation of AKT2 channels is voltage-dependent

Spontaneous conversions from gating mode 1 to gating mode 2 at hyperpolarized voltages have been reported previously for individual AKT2 channels in *Xenopus* oocytes (Dreyer *et al*., 2001). This was further observed for macroscopic whole-cell AKT2 currents in repeatedly hyperpolarized *Xenopus* oocytes. Figure 3(a,b) shows a typical example of data from three independent experiments: an AKT2-expressing oocyte was stimulated 50 times with a short time-interval between pulses (2-sec pulses at −140 mV from a 0-mV holding potential every 5 sec; the time interval between pulses was 30 sec in Figure 1). The first and last pulse are displayed in Figure 3(a). The total current for all pulses and both its mode 1 and mode 2 components (as in Figure 1a) are displayed in Figure 3(b). While the delayed (mode 1) fraction of the AKT2 current decreased (black circles), the instantaneous one (mode 2) increased more markedly (white circles), leading to a slight increase of the total AKT2 current (gray squares). Within the framework of the above-proposed hypothesis that PKA-dependent phosphorylation underlies mode 1 to mode 2 conversion, this could be understood assuming that the oocyte-endogenous PKA activity is more efficient in promoting conversion from gating mode 1 to mode 2 at hyperpolarized voltages (here −140 mV) than at the oocyte resting membrane potential.

The possibility of a combined effect of Br-cAMP and hyperpolarization was tested in AKT2-expressing COS cells using the following voltage-clamp protocol. From a +40-mV holding potential, the cell membrane was clamped to different test voltages between +60 and −160 mV (test pulse), then clamped back to +40 mV (tail pulse). The currents evoked by this protocol were recorded twice in the same cells: first under control conditions; and second in the presence of 200 μM Br-cAMP 2 min after addition of this compound to the bathing solution. Figure 3(c) shows typical current traces recorded with this voltage-clamp protocol. Only currents obtained for the −120, −80 and +40-mV test pulses are shown for easier viewing, the whole traces being displayed at a small scale above the enlarged corresponding tail currents. During the tail pulse, a fraction of the initial current deactivated. This transient fraction of the current corresponded to mode 1 channels, which opened during the test pulse and subsequently closed at +40 mV. The remaining fraction of the tail current with respect to the zero current (indicated by the dotted line) corresponded to the mode 2 channels, which have been shown to stay open at this voltage (Dreyer *et al*., 2001). Thus any conversion into gating mode 2 during the test pulse would appear at the end of the tail pulse as an increase in the steady-state (mode 2) current with respect to the previous record.

Before Br-cAMP was applied (left current traces, control), the voltage-clamp protocol left the level of mode 2 current essentially unchanged as one can judge from the tail current level. In particular, there was only a negligible increase in steady-state current following the −120-mV test pulse with respect to the steady-state current following the +40-mV test pulse (left tail currents in Figure 3c and statistics in Figure 3d, left bar indicating that so-called gained mode 2 was not significant). Conversely, in the presence of 200-μM Br-cAMP, stimulation of the same cell by hyperpolarized voltages markedly augmented the mode 2 current. Whereas the steady-state tail current following

Figure 2. Manipulating the endogenous phosphatase and (A-type) kinase activities in *Xenopus* oocytes affects AKT2 currents.
(a) Modification of AKT2 current by 8-bromo cAMP (Br-cAMP). Voltage protocol: from a holding potential of −30 mV, 1.6-sec pulses were applied to voltages between +30 and −130 mV (in −20-mV increments). Currents were recorded before (left) and after a 1.5-h incubation in 200 μM Br-cAMP (right), and in either water-injected oocytes (H_2O, upper traces) or AKT2-expressing oocytes (AKT2, middle and lower traces). All recordings were performed in a Ke_{20} bath solution (see Experimental procedures), except those displayed at the bottom, which were in the presence of additional 10 mM Cs^+ (only the record obtained at −130 mV is displayed). Dotted line, zero current level; thick arrow, mode 1 to mode 2 transition.
(b) Statistics of changes in AKT2 current after a 1.5-h exposure to 200 μM Br-cAMP. Bars represent stimulation or inhibition (percentage of value measured before treatment) of the delayed current (mode 1, black bar); instantaneous current (mode 2, white bar); and total (mode 1 + mode 2) current at steady state (I_{ss}, gray bar); data (from currents recorded at −130 mV) are given as mean ± SD (n = 5–6); *, values significantly different from zero (Student's t-test, $P < 0.05$).
(c–g) As (b), but after exposure to 200 μM Br-cAMP + 3 μM staurosporine (c); 1 mM vanadate (d, e) (see Experimental procedures); 3 μM staurosporine (f); and 50 μM H89 (g). All treatments lasted 1.5 h, except (e) 3 h.

the +40-mV test pulse was not different from that measured before Br-cAMP application (Figure 3c, cf. +40-mV traces in left and right panels), this current increased with increasing hyperpolarization during the test pulse (Figure 3c, right). The gain in mode 2 current is illustrated by the comparison of the steady-state current level following the +40-mV test pulse (i_{+40}; second out of 12 pulses in the pulse protocol) with the steady-state current level following the −120-mV test pulse (i_{-120}; 10th pulse). The normalized value describing the increase of mode 2 currents [gained mode 2 = $(i_{-120}-i_{+40})/i_{+40}$] averages in the 35–40% range (Figure 3d, right bar).

To further substantiate that the PKA-dependent mode 1 to mode 2 conversion is favored by hyperpolarization, a longer (5-min) exposure to 200-μM Br-cAMP was performed on COS cells voltage-clamped throughout at +40 or −40 or −80 mV (voltage value noted *X* in legend to Figure 3e). Before (control situation) and after this treatment, the total (mode 1 + mode 2) current and the two mode 1 and mode 2 components were sampled by recording the current elicited by a stimulation at −140 mV from a holding potential of +40 mV. Sample records obtained from the same cell are shown in Figure 3(e) (the cell was voltage-clamped at −80 mV during Br-cAMP application). As in Figure 3(c), the

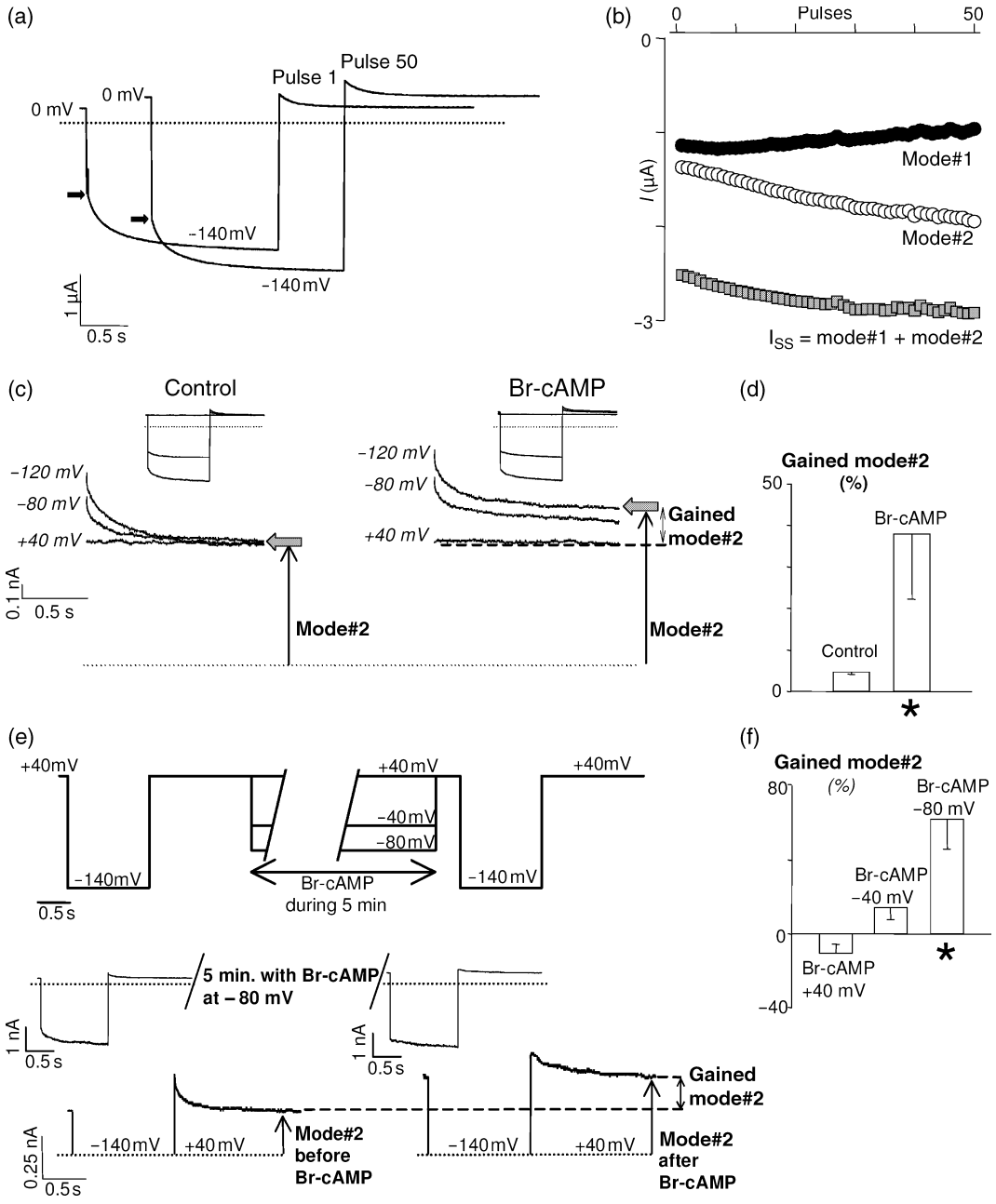

dotted line indicates the zero current level. The gained mode 2 current is determined, as indicated in Figure 3(c), by comparing the mode 2 current after the Br-cAMP treatment with the one before this treatment. In the example shown (Br-cAMP applied on a cell clamped at −80 mV), the gain in mode 2 current ranged around 75%. Figure 3(f) shows the changes in mode 2 current for the three voltages tested, expressed as a percentage. The 5-min Br-cAMP treatment resulted in a significant increase of the mode 2 current only when it was applied to cells being voltage-clamped at −80 mV. From the whole data set we conclude that open mode 1 channels (at −80 mV) were more sensitive to PKA-dependent conversion to mode 2 than closed mode 1 channels (at +40 or −40 mV).

Mapping residues possibly involved in AKT2 regulation by phosphorylation/dephosphorylation

When analyzing several AKT2-related plant channel subunits (Figure 4a, upper group of polypeptides) for PKA consensus phosphorylation sites (RxS/T), two phosphorylation sites were pinpointed which are strictly conserved within this channel subfamily. One was found in the S4–S5 linker (S210 in AKT2); the other in the S6–Cterminus linker (S329 in AKT2; Figure 4a). According to the assumed structure of Shaker channels (Jiang *et al.*, 2003; Sato *et al.*, 2002; Yellen, 2002), these regions are proximal to the inner mouth of the pore and are likely to undergo conformational changes on voltage-dependent S4 movements (Figure 4b, see Discussion).

The possible role of S210 and S329 in the control of AKT2 channel gating mode was studied by site-directed mutagenesis. Three mutant channels carrying double substitutions by alanine (S210A–S329A), glutamate (S210E–S329E) or asparagine (S210N–S329N) were compared with wild-type channels in COS cells.

Whole-cell currents in S210E–S329E mutant-expressing cells displayed both delayed and instantaneous current components (Figure 4c, left traces), the latter component being, however, larger than in wild-type AKT2-expressing cells (not shown, but see statistics in Figure 4e). In contrast, the S210A–S329A mutant produced delayed currents only (Figure 4c, middle traces), whereas almost no delayed currents were observed with the S210N–S329N mutant (Figure 4c, right traces).

As double substitutions of S by either A or N had the largest effects, single S-substitutions by A or N at the two pinpointed positions were studied. Representative traces for the two mutants S210A and S329N are displayed in Figure 4(d). The behavior of the single mutants suggested a synergistic contribution of each substitution to the dramatic effect of the corresponding double substitution. To quantify these observations, the relative amount of the instantaneous current in the total current recorded at −140 mV, denoted $r_{-140\ mV}$ (Dreyer *et al.*, 2001), was taken as an estimate of the proportion of mode 2 channels (white section of bar graphs, Figure 4e). COS cells expressing wild-type AKT2 channels typically displayed a mean $r_{-140\ mV}$ value in the 50% range (Figure 4e). In parallel experiments, COS cells expressing the S210E–S329E, S210A–S329A or S210N–S329N mutant AKT2 channels displayed $r_{-140\ mV}$ values of $70 \pm 6\%$, $5 \pm 5\%$ and $97 \pm 3\%$, respectively (Figure 4e). In addition to these effects on the gating modes, the double S-substitution by A considerably reduced the mean whole-cell AKT2 current when compared with wild type, while that by N did not (Figure 4f).

The S210A–S329A and S210N–S329N mutants were studied at the single channel level (cell-attached, Figure 4g,h). Gap-free records 20 sec long, obtained at +40, −40 and −80 mV on a patch apparently containing two S210A–S329A AKT2 channels (Figure 4g, top), showed transitions between open and long-lived closed states typical of mode 1 AKT2

Figure 3. PKA-dependent mode 1 to mode 2 conversion is favored by hyperpolarization in *Xenopus* oocytes and COS cells.
(a, b) Repeated hyperpolarization resulted in an increase of mode 2 current in *Xenopus* oocytes. Voltage-clamp protocol: from a holding potential of 0 mV, 50 2-sec pulses to −140 mV were applied every 5 sec to AKT2-expressing oocytes (Ke_{20} bathing solution). (a) The first and 50th records are displayed. Dotted line, zero current level. Arrows at left indicate mode 2–mode 1 demarcation. (b) Total AKT2 current (gray squares); delayed fraction (gating mode 1, black circles); and instantaneous fraction (gating mode 2, white circles) as a function of pulse number.
(c) Sampling of the mode 2 current fraction after the stimulation of a COS cell. Staircase voltage-clamp protocol: from a holding potential of +40 mV, steps to voltages between +40 and −160 mV, in −20-mV increments, were applied to AKT2-expressing COS cells. For better viewing, only the records obtained at +40, −80 and −120 mV are shown (top), with a magnification of the corresponding tail currents recorded at +40 mV, in the absence (control, bottom left) and presence of 200 μM Br-cAMP (Br-cAMP, bottom right). With respect to the zero current line (dotted line), the amplitude of mode 2 current at +40 mV after stimulation at −120 mV (I_{-120}) is marked by an arrow. With respect to mode 2 current after the +40 mV pulse (dashed line), the mode 2 current gained after the −120 mV pulse (I_{-120}–I_{+40}) is marked by a double-headed arrow.
(d) Statistics for the mode 2 current gained in conditions described in (c), expressed as a percentage of control, $(I_{-120}–I_{+40})/I_{+40}$ (mean ± SD, $n = 3$). *, Data significantly different from zero (Student's *t*-test, $P < 0.05$); as in (c) the mode 2 current gained is significant only in the presence of Br-cAMP.
(e) Voltage-dependence of the gain in mode 2 obtained in the presence of Br-cAMP. Two values of mode 2 current are sampled, as in (c), after a single stimulation at −140 mV, before and after Br-cAMP application on a COS cell being voltage-clamped at a fixed voltage, *X*, for 5 min. The mode 2 gained is the difference between the two values. Three values were tested for *X*: +40, −40 and −80 mV. In the example shown (top, full records; bottom, enlarged tail currents), the fixed voltage during Br-cAMP application was −80 mV.
(f) Statistics for mode 2 current gained in conditions described in (e). Data are expressed as percentage of the reference mode 2 current value, before Br-cAMP application [gain in mode 2 $= (I_{after}–I_{before})/I_{before}$; mean ± SD, $n = 10$ for $X = +40$ mV; $n = 4$ for $X = -40$ mV; $n = 7$ for $X = -80$ mV]. *, Data significantly different from zero (Student's *t*-test, $P < 0.05$).

channels, as described previously (Dreyer *et al.*, 2001). In similar conditions, at +40 and −100 mV, a single S210N–S329N AKT2 channel (Figure 4g, bottom) showed frequent incursions to a short-lived closed state from a long-lived open state. In fact, at negative voltages the S210N–S329N mutant seemed to reside in a quasi-continuous, although

(a)

	S4/S5-linker			S6/C-terminus	
AKT2	201	TRLEKDI**R**Y**S**YFWIRCFR	218	319	GTRRTMEF**R**N**S**IEAASNF 336
ZMK2	195	TRLEKDI**R**F**S**YFWIRSAR	212	314	GTRRTMEF**R**N**S**IRAASSF 331
VFK1	181	TRLEKDI**R**F**S**YFWVRCAR	198	300	GTRRTMEF**R**N**S**IEAASNF 317
SPICK1	206	TRLEKDI**R**F**S**YFWVRCAR	223	325	GTRRTMEF**R**N**S**IEAASSF 342
SPICK2	203	TRLEKDI**R**F**S**YFLIRCVR	220	322	GTCRTMEF**R**N**N**IEAATNF 339
SKT2	214	TRLEKDM**R**F**S**YFWIRCAR	231	333	GTSRTMEF**R**N**S**IQSASNF 350
NpKT1	194	TRLEKDM**R**F**S**YFWVRCAR	211	313	GTRRTMEF**R**N**S**IEAASNF 330
PKT2	188	TRLEKDI**R**F**S**YFWVRCAR	205	307	GTRRTMEF**R**N**S**IEAASNF 324
SKOR	203	HKMEKDIRINYLFTRIVK	220	330	G-SKTERFRDKMADIMRY 346
KAT1	183	ARLEKDIRFNYFWIRCTK	200	302	WTSRTRTF**R**D**S**VRAASEF 319
AKT1	176	ARLEKDRNFNYFWVRCAK	193	295	GTSRTRNF**R**D**T**IQAASNF 312

(b)

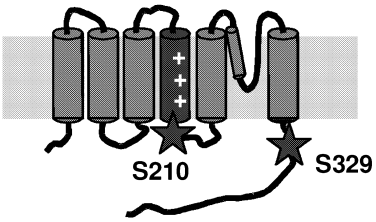

(c)

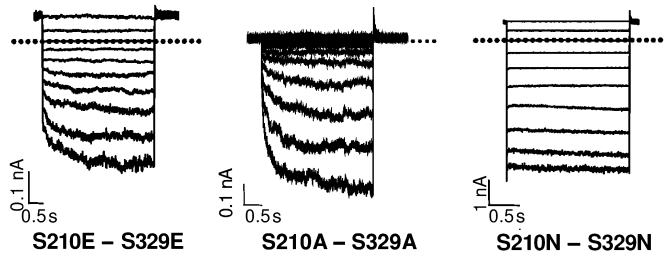

(d)

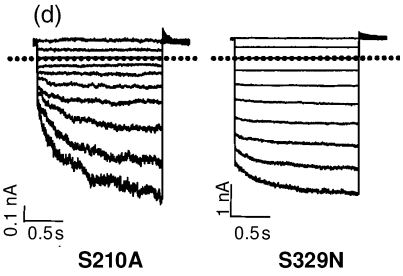

(e)

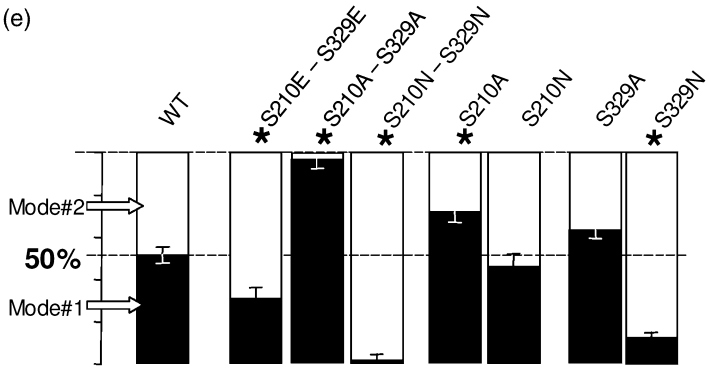

(f)

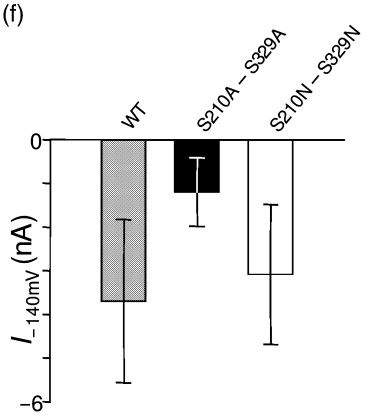

(g)

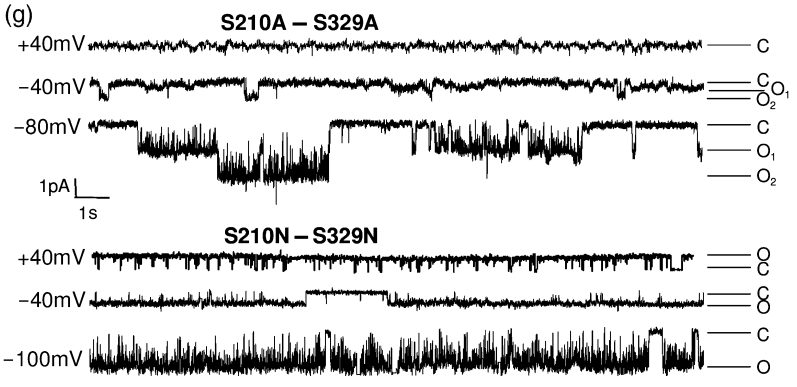

(h)

Voltage	nP_o S210A–S329A	nP_o S210N–S329N
+40 mV	0.00	0.88
−40 mV	0.07	0.86
−100 mV	0.78	0.84

flickering, open state, characteristic of mode 2 AKT2 channels (Dreyer *et al.*, 2001). Open-state probabilities (nP_o data, with n assumed to be 2 and 1, respectively for these S210A–S329A- and S210N–S329N-harboring patches) were calculated at +40, −40 and −100 mV (Figure 4h). The nP_o values (null at +40 mV for S210A–S329A and large at all tested voltages for S210N–S329N) were consistent, with a steady mode 1 behavior for S210A–S329A and steady mode 2 behavior for S210N–S329N channel(s).

Thus, taken together, the whole-cell as well as the single-channel data indicate that the double-mutant S210A–S329A mimicked AKT2-mode 1 channel behavior, and that the double-mutant S210N–S329N mimicked AKT2-mode 2 channel behavior. It was subsequently examined whether these mutants responded to treatments altering the phosporylation/dephosphorylation equilibrium in COS cells and *Xenopus* oocytes.

In both expression systems, the mutant S210A–S329A mediated small currents which could not be increased markedly by treatment with vanadate or Br-cAMP (not shown), suggesting that the increase in wild-type AKT2 channel activity by these treatments (Figure 2) would depend on the phosphorylation status of the serine residues at positions 210 and 329.

When the mutant S210N–S329N was expressed in *Xenopus* oocytes, the large instantaneously activating potassium-selective currents (Figure 5a,b) were not affected significantly by H89 (Figure 5c, left bar). In particular, there was no evidence for a PKA-mediated conversion between two active gating modes for the mutant S210N–S329N. Likewise, the inhibition of oocyte intrinsic phosphatases by the inhibitor vanadate (180-min treatment) did not induce any mode 1 currents; instead, formerly silent channels were directly recruited (Figure 5c, right bar) to gate in mode 2. Compared with the wild type (Figure 2g), however, the increase in total current was less pronounced. In summary, the S210N–S329N mutant was susceptible to changes in the phosporylation/dephosphorylation equilibrium of the context, albeit differently from the wild type. This became also

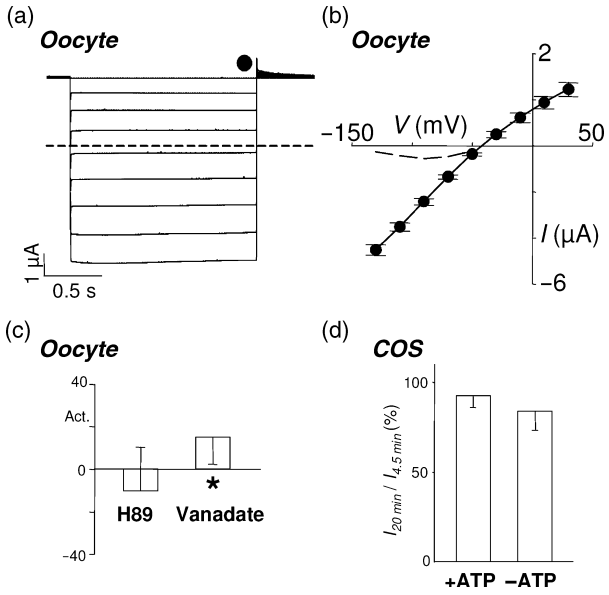

Figure 5. The mutant S210N–S329N exhibits an impaired phosphoregulation.

(a) Representative S210N–S329N currents measured in oocytes. Currents recorded in Ke_{20} and elicited in 1.6-sec voltage steps from +30 mV to voltages between +30 and −130 mV (20-mV decrements; dashed line indicates zero current level).

(b) Current-voltage characteristics of six independent experiments at the end of the activation pulses. Dashed line, current-voltage characteristic in the presence of 10 mM Cs^+ in the bath solution. Data are presented as means ± SD.

(c) Statistics of AKT2-S210N–S329N and wild-type current changes on exposition to 50 µM H89 (left, $n = 4$) and 1 mM vanadate for 180 min (right, $n = 5$).

(d) Current stability measured in the absence of ATP. Ratio of total currents recorded 4.5 and 20 min after patch break-in in COS cells ($I_{20min}/I_{4.5min}$; Figure 1e) at −140 mV without Mg-ATP in the pipette solution. Data are means ± SD (−ATP, $n = 5$; +ATP, $n = 4$).

evident when recording whole-cell currents in COS cells without ATP in the patch-pipette. Under these conditions, S210N–S329N-mediated currents ran down slightly (Figure 5d). Compared with the AKT2 wild type (Figure 1), however, the reduction in current was less pronounced:

Figure 4. Analysis of AKT2 mutants for PKA phosphorylation sites in COS cells.

(a) Two putative PKA phosphorylation sites pinpointed in AKT2 and related channels. Amino acid sequence alignments in the S4–S5 linker (left) and in the S6–Cterminus linker (right). Genebank accession numbers: AKT2, AAA97865; ZMK2, CAB54856; VFK1, CAA71598; SPICK1, AAD16278; SPICK2, AAD39492; SKT2, CAA70870; NpKT1, BAA84085; PTK2, CAC05489; SKOR, T52046; KAT1, AAA32824; AKT1, CAA44693.

(b) Schematic secondary structure of the AKT2 alpha-subunit showing the two putative PKA-phosphorylation sites (S210 and S329) that were mutagenized.

(c) Representative AKT2-S210E–S329E (left), AKT2-S210A–S329A (middle) and AKT2-S210N–S329N (right) macroscopic currents recorded in COS cells. Voltage protocol: from a holding potential of +40 mV, voltage steps were applied between +40 and −140 mV (−20-mV increments; dotted line is zero current level).

(d) Representative AKT2-S210A (left) and AKT2-S329N (right) macroscopic currents recorded in COS cells. Same voltage protocol as in (c).

(e) Proportion of delayed current (mode 1, black) and instantaneous (mode 2, white) recorded at −140 mV in COS cells expressing the wild-type channel, single or double mutants for S210 or/and S329. Bath and pipette solutions as in Figure 1(c) (2.5 mM Mg–ATP in the pipette solution). Data are given as mean ± SD with $n = 16$ for wild-type AKT2; $n = 6$, 4 and 6, respectively, for the S210A–S329A, S210E–S329E and S210N–S329N double mutants; and $n = 6$, 9, 9 and 11, respectively, for the S210A, S329A, S210N and S329N single mutants.

(f) Total (mode 1 + mode 2) current recorded at −140 mV for wild-type and mutant AKT2 channels [same COS cells as in (e), mean ± SD, *n*: see (e)].

(g) Typical cell-attached gap-free recordings from COS cells expressing S210A–S329A or S210N–S329N double-mutant AKT2 channels. Pipette and bath solution were the same as bath one in (c).

(h) nP_o data obtained for the cell-attached patches shown in (g) clamped at +40, −40 or −100 mV. Data were calculated over gap-free records longer than 50 sec; *n* was assumed to be 2 for S210A–S329A and 1 for S210N–S329N.

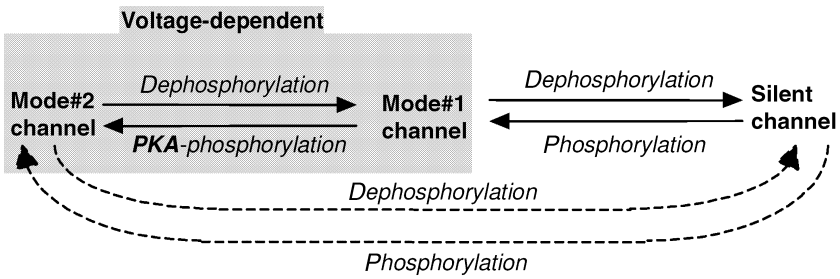

Figure 6. Model for the regulation of AKT2 channel activity and gating mode by (de)phosphorylation.

within the interval between 4.5 and 20 min after the patch-break, wild-type AKT2 currents reduced by $50 \pm 28\%$ ($n = 4$), and S210N–S329N currents only by $15 \pm 10\%$ ($n = 4$).

Discussion

The operation of AKT2 channel depends on their phosphorylation status

Phosphorylation/dephosphorylation have been shown to regulate the biophysical properties of animal Shaker potassium channels (Levitan, 1999). In plants, evidence that plant K^+ channels are regulated by signal cascades involving serine/threonine phosphorylation events has been obtained from the electrophysiological characterization of transgenic plants displaying an increased ABI1 phosphatase activity (Armstrong *et al.*, 1995; Pei *et al.*, 1997), and from analyses of the effects of kinase/phosphatase activators and inhibitors on currents recorded in intact cells (Li *et al.*, 1994a,b; Thiel and Blatt, 1994) and protoplasts (Moran, 1996; Spalding and Goldsmith, 1993). In heterologous systems, the activity (Berkowitz *et al.*, 2000) and gating (Tang and Hoshi, 1999) of the inward KAT1 channel are modulated by phosphorylation, and evidence for KAT1 phosphorylation *in planta* has been provided by biochemical approaches (Li *et al.*, 1998; Mori *et al.*, 2000). More generally, changes in membrane transporter activity by protein phosphorylation have been demonstrated for a wide range of plant transport proteins, including water channels (Johansson *et al.*, 1998; Maurel *et al.*, 1995); anion transporters and channels (Liu and Tsay, 2003); calcium (Köhler and Blatt, 2002; Stoelzle *et al.*, 2003); and potassium channels (Li *et al.*, 1994b; Luan *et al.*, 1993; Tang and Hoshi, 1999). Most of these studies have been performed *in planta* using pharmacological modification of protein phosphatase and/or kinase activities, and this did not allow us to discriminate between direct effects of (de-)phosphorylation on the transporter itself, or indirect effects through signal cascades. However, in some instances [e.g. aquaporin alpha-TIP, Maurel *et al.*, 1995; nitrate transporter NRT1.1 (CHL1), Liu and Tsay, 2003], studies of mutant transport proteins in heterologous expression systems have allowed the demonstration that phosphorylation of serine or threonine residues by endogenous cAMP-dependent protein kinase (PKA) activity does regulate transport activity.

As discussed in the following, a simple phosphorylation/dephosphorylation scheme can be proposed to interpret the present data regarding AKT2 channels (Figure 6). According to this model, AKT2 channels populate three pools (gating mode 2; gating mode 1; silent) that are characterized by a functional status related to a phosphorylation status. Moving from one pool to another depends on phosphorylation or dephosphorylation and, at steady state, the repartition between the three pools is in a state of dynamic equilibrium. In this scheme, the rightward transitions leading to the silent state (underlying the rundown of the current favored by the presence of a PKA inhibitor or the absence of ATP; Figure 1e) represent dephosphorylations. Among the reverse leftward transitions (representing phosphorylations), at least that from mode 1 to mode 2 is proposed to be stimulated by PKA-dependent phosphorylation. The dotted arrows at the bottom of Figure 6 indicate that direct transitions between the mode 2 pool and the silent pool could occur (see below). As stated above, one could wonder whether AKT2 channels themselves, or regulating factors, are phosphorylated. The mutant experiments (Figures 4 and 5) show that AKT2 channels bear phosphorylation sites that control the gating mode, thus supporting the former hypothesis. The voltage dependence of the Br-cAMP stimulation of the mode 1 to mode 2 transition also supports the hypothesis that AKT2 channels themselves are phosphorylated.

Four points are discussed below. First, the reversible silencing of AKT2 channels on dephosphorylation; second, the fact that PKA-dependent phosphorylation controls the repartition of active AKT2 channels between the mode 1 and mode 2 pools; third, the voltage dependence of AKT2 channel susceptibility to PKA; and fourth, the physiological meaning of the AKT2 dual gating mode.

Dephosphorylation silences AKT2 channels

COS cells as well as *Xenopus* oocytes are endowed with endogenous kinase and phosphatase activities, which prove capable of affecting heterologously expressed AKT2 channels. The two systems, however, provide different intracellular conditions to heterologously expressed ion channels. Cytoplasmic integrity is essentially preserved in oocytes that

are voltage-clamped by means of two intracellular microelectrodes; it is not in patch-clamped COS cells, of which the cytoplasm is diluted in the pipette solution after the whole-cell configuration is settled. This difference probably explains why the AKT2 current ran down in COS cells dialyzed by a 1-μM H89 pipette solution (Figure 1e), while only mode 2 to mode 1 conversion occurred (but no inhibition of total current) in oocytes bathed by a 50-μM H89 solution (Figure 2e). As proposed in Figure 6, AKT2 channels expressed in these contexts could populate three pools, including a silent one. Occupancy of these pools would depend on the balance of kinase/phosphatase activities that can target AKT2 channels. For example, inhibiting oocyte endogenous phosphatases with vanadate stimulated the AKT2 current (Figure 2f,g). It is worth noting that Arabidopsis *At*PP2CA phosphatase activity has been shown specifically to inhibit AKT2 (Chérel *et al.*, 2002), and that vanadate has been shown to reverse this effect.

In whole-cell recordings performed on COS cells, while removing ATP from the pipette solution provoked a rapid rundown (–ATP conditions in Figure 1b–d, middle bar in Figure 1e), the macroscopic AKT2 current was fairly stable under control conditions (Figure 1a, left bar in Figure 1e). This also suggests that phosphorylation would enable AKT2 channels to leave the silent state, or preserve them from falling into that state. Furthermore, the inhibitory effect of H89 (in the presence of ATP, right bar in Figure 1e) suggests that PKA activity could modify the distribution between silent and active (mode 1 + mode 2) pools, as H89 rather specifically blocks this kinase activity. It is also possible that AKT2 channels are less susceptible to the dephosphorylation that leads to silencing when they are in the conformational state corresponding to gating mode 2. This is suggested by the fact that the mode 2-mimicking S210N–S329N mutant displayed much less rundown in the absence of ATP (whole-cell recording in COS cells, Figure 5d) than wild-type AKT2 channels (Figure 1e). Conversely, mode 1 channels (or S210A–S329A double mutants) would be more susceptible to silencing, as suggested by the weak whole-cell current recorded in COS cells expressing the S210A–S329A mutant (Figure 4f).

In summary, silent AKT2 channels are mainly converted into mode 1 channels on phosphorylation (and the reciprocal), although the S210N–S329N double mutant behavior (recruitment of active mode 2 channels by vanadate in *Xenopus* oocytes, Figure 5c; and slight rundown provoked by ATP removal in COS cells, Figure 5d) suggests that some direct conversion between silent and mode 2 pools is possible (dotted arrows at the bottom of Figure 6).

Gating of AKT2 is regulated by PKA activity

Spontaneous transitions between gating modes 1 and 2 were observed during gap-free recordings of AKT2 channels in the cell-attached configuration (Dreyer *et al.*, 2001), suggesting that a cytoplasmic factor was involved in the control of AKT2 gating mode. In addition, the *At*PP2CA phosphatase activity had been shown to promote the transition from gating mode 2 to gating mode 1 (Chérel *et al.*, 2002). Here we obtain further evidence that (de)phosphorylation events are involved in AKT2 gating mode transitions: in *Xenopus* oocytes the non-specific kinase inhibitor staurosporine reduces total AKT2 currents by affecting mainly mode 2 currents (Figure 2d). The fact that Br-cAMP stimulates the transition from mode 1 to mode 2 in both *Xenopus* oocytes (Figure 2a,b) and COS cells (Figure 3c–f), and that this effect is reversed by staurosporine (Figure 2c), suggests the involvement of PKA in this process.

The role of PKA-dependent phosphorylation in mode 1 to mode 2 transition is further demonstrated by the electrophysiological characterization of mutations at the two pinpointed PKA phosphorylation consensus sites (S210, S329; Figure 4a). First, the double-A mutation, which mimics a non-phosphorylated state (Beck *et al.*, 1998; Wang *et al.*, 1998), resulted in a dramatic decrease of the mode 2:mode 1 ratio (Figure 4b). Second, the double-E mutation, expected to result in the opposite effect (Beck *et al.*, 1998; Wang *et al.*, 1998) did increase, although to a lesser extent, the mode 2:mode 1 ratio (Figure 4b). Third, the double-N mutation made the AKT2 channels gate in mode 2, so that asparagines seemed able to mimic phosphorylated serines (Figure 4). Asparagine (N) is uncharged, but is larger than S. Thus the mode 2 configuration might be favored by a steric effect at positions 210–329.

Voltage dependence of AKT2 phosphorylation by PKA

PKA-dependent stimulation of AKT2 channels is enhanced by membrane hyperpolarization (Figure 3). A similar voltage-dependent phenomenon, potentiation, has been described in animal cells for L-type Ca^{2+} channels, shown to be the target for PKA-dependent phosphorylation favored by a depolarizing pre-pulse (Sculptoreanu *et al.*, 1993a,b). A common feature of these PKA-dependent phosphorylations is that they appear to be enhanced after inactive channels have undergone a conformational change, resulting in opening (on depolarization for L-type Ca^{2+} channels and hyperpolarization for AKT2). In both cases, phosphorylation sites would be buried inside the protein structure and thus be inaccessible to PKA in the resting state, but not in the active state.

In the case of AKT2, the conformational changes on hyperpolarization would expose phosphorylation sites to PKA and favor both recovery from the silent state, and transition from gating mode 1 to gating mode 2 (Figure 6). The voltage-sensing of Shaker channels is ascribed notably to the fourth transmembrane segment, S4, which bears a net positive charge and moves within the membrane in

response to changes in the membrane electric field. The S4 movements, via an as yet unknown coupling mechanism, favor global conformational changes, which themselves result in channel opening or closing (Jiang *et al.*, 2003; Männikkö *et al.*, 2002). The two pinpointed S210 and S329 phosphorylation sites are in regions of the channel likely to undergo conformational changes on membrane potential variations (Figure 4a; Jiang *et al.*, 2003; Yellen, 2002). This particular location may explain why the phosphorylation of S210 and S329 would both help in recovery from the silent state (possibly hindering an interaction in the inner pore region that would otherwise result in channel silencing), and favor the transition towards gating mode 2 (the channel would somehow become locked in the open state with such a high energy barrier to cross that strong depolarizations would be required to close the channel). Phosphate groups at S210–S329 positions could, for instance, retain S4 in an internalized state, thereby locking the channel in a 'gated' conformation. Such mechanisms have been proposed to underlie the block of animal HCN channels in an open state when binding a thiol reagent to some cysteine-substituted positions in the S4s (Männikkö *et al.*, 2002), or the block of animal Shaker channels in an open state resulting from immobilization of the S6s by metal bridges (Holmgren *et al.*, 1998). The fact that the S to N mutations (AKT2-S210N–S329N) mimicked the phosphorylated state (Figure 4) suggests that a steric effect at positions 210–329 may be sufficient to raise the energy barrier that needs to be crossed for rightward AKT2 mode transitions to occur (Figure 6).

Physiological meaning of the AKT2 dual gating mode

AKT2 is mainly expressed in the mesophyll (Lacombe *et al.*, 2000b) and in the phloem tissues (Deeken *et al.*, 2000; Lacombe *et al.*, 2000b; Pilot *et al.*, 2003). The mesophyll is a symplasmic territory where most of the leaf photosynthetic activity takes place. The AKT2 channel has been proposed to ensure the K^+ transport needed for mesophyll growth (Dennison *et al.*, 2001), and subsequently for accompanying the photoassimilates, which must leave the mesophyll to be uploaded in the phloem (Deeken *et al.*, 2002; Lacombe *et al.*, 2000b; Marten *et al.*, 1999). The phloem is itself a reticulate symplasmic tissue, which ensures nutrient distribution in the whole plant from sources to sinks. K^+ and photoassimilates are loaded (in sources) and downloaded (in sinks) together. Depending on the cellular context, the average phosphorylation level of the AKT2 channels may change, enabling them to drive either inward or outward K^+ fluxes. Thus in both mesophyll and phloem tissues the post-translational regulation of AKT2 channels might play a role in the control of photoassimilate distribution within the plant.

Symplasmic territories in plants are occasionally the place of propagating action potentials (Wayne, 1994). This is documented for the phloem, which is believed to be the tissue conducting electrical signaling at the whole-plant level (Fromm and Bauer, 1994). The mesophyll could be the place for propagation of signals through the leaves, on localized mechanical or pathogen aggression (Herde *et al.*, 1996; Wildon *et al.*, 1992). AKT2 channels are expressed in both these symplasmic territories, where they might control membrane excitability. In their phosphorylated state, AKT2 channels (mainly gating mode 2) would behave as the so-called open-leak or background channels described in animal cells, which are believed to prevent or downregulate membrane potential oscillations (Lesage, 2003). In their dephosphorylated state, AKT2 channels (mainly gating mode 1 or silent) would no longer play such a role. Thus, like some pacemaker (Macri *et al.*, 2002; Proenza *et al.*, 2002) and background (Bockenhauer *et al.*, 2001) channels described in animal cells, AKT2 could be a modulator of membrane excitability in plant cells, with a possibility for fine tuning of this modulation through the phosphorylation status of the channel.

PKA-like protein kinase activity in plant cells is, as yet, poorly documented (Assmann, 1995). Which transduction chains involve plant 'PKA-like' kinases, and which messengers trigger their activity, are still open questions (Champion *et al.*, 2004). While the *At*PP2CA phosphatase has been demonstrated to produce the same effect on wild-type AKT2 channels (Chérel *et al.*, 2002) as the double-A mutation reported here (Figure 4), the kinase responsible, *in planta*, for AKT2 phosphorylation at S210 and S329 remains to be identified. Phosphorylation of PKA consensus sites such as those identified in AKT2 has been demonstrated *in planta* for NRT1.1 (Liu and Tsay, 2003). Interestingly, this nitrate transporter also displays a dual operating mode, switching the transport from low to high affinity on phosphorylation. If other enzymes are identified in the future, the activity of which would seem to be controlled by 'green' PKA activity, this should encourage and, hopefully, help in identifying the molecular support for such kinase activity in plants.

Experimental procedures

COS cells

Culture and transfection of COS-7 cells and subsequent patch-clamp experiments (cell-attached and whole-cell) were performed as described (Dreyer *et al.*, 2001). The bath solution contained 150 mM KCl, 1 mM $CaCl_2$, 1.5 mM $MgCl_2$, 10 mM HEPES/NaOH pH 7.4. Standard pipette solution contained 150 mM KCl, 1.5 mM $MgCl_2$, 3 mM EGTA, 10 mM HEPES/NaOH pH 7.2 and 2.5 mM MgATP (except in some experiments displayed in Figures 1 and 5d, where MgATP was removed to enable rundown). H89 *N*-(2-[bromocinnamylamino]-ethyl)-5-isoquinolinesulfonamide hydrochloride and staurosporine were purchased from Sigma (St Louis, MO, USA) and dissolved in

pure DMSO (10 mM). The resulting stock solutions were stored at −20°C and diluted to a final DMSO content of 0.01% (v/v, checked to have no effect by itself) in the pipette solution. The 8-Br-cAMP (200 μM dissolved in bath solution) was applied by perfusion.

Xenopus *oocytes*

Xenopus (CRBM, CNRS, Montpellier, France) oocytes were injected with 20 ng (0.02 μl) pCI-AKT2, or pCI-AKT2 mutant recombinant plasmids obtained as described (Lacombe *et al.*, 2000b). Control oocytes were injected with 0.02 μl deionized water. Two-electrode voltage-clamp experiments were performed as described (Lacombe and Thibaud, 1998; Véry *et al.*, 1995). The external standard solutions contained 20 or 100 mM KCl (denoted Ke_{20} and Ke_{100}, respectively), 80 mM NaCl for Ke_{20}, 1.5 mM $CaCl_2$, 3 mM $MgCl_2$, 10 mM HEPES/NaOH pH 7.5. When indicated, oocytes were treated (in multi-well plates at 18°C) for 1.5 or 3 h in external Ke_{20} standard solution supplemented with 200 μM Br-cAMP, or 200 μM Br-cAMP + 3 μM staurosporine, or 3 μM staurosporine, or 50 μM H89, or 1 mM vanadate. Vanadate (sodium orthovanadate, Na_3VO_4, Sigma) was dissolved on the day of the experiment in recording solution (strong magnetic stirring and boiling) and the pH was checked afterwards. When staurosporine or H89 was present in the bath solution, DMSO was 0.03 or 0.05% (v/v), respectively. These DMSO concentrations were checked to have no effect by themselves on either water-injected or AKT2-expressing oocytes.

Ascription of current to AKT2

Cesium controls (Chérel *et al.*, 2002; Dreyer *et al.*, 2001) were performed systematically before and after application of any drug (8-Br-cAMP, H89, staurosporine, vanadate) to ensure currents actually flowed through potassium-selective (Cs^+-blocked) channels. In both expression systems used, most of the current flowing at negative membrane potential was blocked by 10 mM extracellular Cs^+, and could then be ascribed to AKT2 channels. At −150 mV almost 100% of AKT2 current is blocked in these conditions, as reported previously (Lacombe *et al.*, 2000b; Marten *et al.*, 1999). In a few cases some control (water-injected) oocytes or (empty plasmid transfected) COS cells displayed significant endogenous inward currents. In such cases the whole oocyte or COS cell batches were discarded. Some treatments used here on COS cells (e.g. Figure 3) were expected to change the instantaneous component of the AKT2 current, an effect that could be mimicked by a change in the leak current. In all experiments Cs^+ and leak controls were combined on both control and AKT2-expressing cells/oocytes to assess ascription of current to AKT2. The two current components (instantaneous and delayed) were extracted from the total AKT2 current as described (Dreyer *et al.*, 2001) unless otherwise stated (Figure 3).

Recombinant DNA techniques

Standard methods of plasmid DNA preparation, restriction enzyme analysis, agarose gel electrophoresis and bacterial transformation were applied (Ausubel *et al.*, 1994). Mutants were generated using the pAlter mutagenesis system (Promega, Madison, WI, USA). The sequences of primers used were as follows (mutation: primer sequence):

S210A: 5′-cgagaaggacataagatatgcctatttctggatccgctgctttcgacttc-tatc-3′

S210E: 5′-cgagaaggacataagatatgagtatttctggatccgctgctttcgacttc-tatc-3′

S210N: 5′-cgagaaggacataagatataactatttctggatccgctgctttcgacttc-tatc-3′

S329A: 5′-ggactcgtcgtaccatggaattcaggaatgccattgaagcagcgtcaaa-ctttgttaacag-3′

S329E: 5′-ggactcgtcgtaccatggaattcaggaatgaaattgaagcagcgtcaaa-ctttgttaacag-3′

S329N: 5′-ggactcgtcgtaccatggaattcaggaataacattgaagcagcgtcaaa-ctttgttaacag-3′

Mutations and constructs were verified by DNA sequence analysis.

Acknowledgements

We are grateful to J. Boucherez for expert technical assistance. We thank Drs I.A. Lefevre and A.-A. Véry for helpful comments and critical reading of the manuscript. This work was partly supported by a Marie-Curie Fellowship of the European Union to I.D. (contract no. ERBBIO4CT985058, proposal no. 980115) and by GENOPLANTE (contract no. AF2001093).

References

Ache, P., Becker, D., Ivashikina, N., Dietrich, P., Roelfsema, M.R. and Hedrich, R. (2000) GORK, a delayed outward rectifier expressed in guard cells of *Arabidopsis thaliana*, is a K^+-selective, K^+-sensing ion channel. *FEBS Lett.* **486**, 93–98.

Armstrong, F., Leung, J., Grabov, A., Brearley, J., Giraudat, J. and Blatt, M.R. (1995) Sensitivity to abscisic acid of guard-cell K^+ channels is suppressed by *abi1-1*, a mutant Arabidopsis gene encoding a putative protein phosphatase. *Proc. Natl Acad. Sci. USA*, **92**, 9520–9524.

Assmann, S.M. (1995) Cyclic AMP as a second messenger in higher plants. *Plant Physiol.* **108**, 885–889.

Ausubel, F.M., Brent, R., Kingston, R.E., Moore, D.D., Seidman, J.G., Smith, J.A. and Struhl, K. (1994) *Current Protocols in Molecular Biology*. New York, USA: Wiley.

Baizabal-Aguirre, V.M., Clemens, S., Uozomi, N. and Schroeder, J.I. (1999) Suppression of inward-rectifying K^+ channels KAT1 and AKT2 by dominant negative point mutations in the KAT1 alpha-subunit. *J. Membr. Biol.* **167**, 119–125.

Beck, E.J., Sorensen, R.G., Slater, S.J. and Covarrubias, M. (1998) Interactions between multiple phosphorylation sites in the inactivation particle of a K^+ channel – insights into the molecular mechanism of protein kinase C action. *J. Gen. Physiol.* **112**, 71–84.

Berkowitz, G., Zhang, X., Mercie, R., Leng, Q. and Lawton, M. (2000) Co-expression of calcium-dependent protein kinase with the inward rectified guard cell K^+ channel KAT1 alters current parameters in *Xenopus laevis* oocytes. *Plant Cell Physiol.* **41**, 785–790.

Bockenhauer, D., Zilberberg, N. and Goldstein, S.A. (2001) KCNK2: reversible conversion of a hippocampal potassium leak into a voltage-dependent channel. *Nat. Neurosci.* **4**, 486–491.

Cao, Y., Ward, J.M., Kelly, W.B., Ichida, A.M., Gaber, R.F., Anderson, J.A., Uozumi, N., Schroeder, J.I. and Crawford, N.M. (1995) Multiple genes, tissue specificity, and expression-dependent modulation contribute to functional diversity of potassium channels in *Arabidopsis thaliana*. *Plant Physiol.* **109**, 1093–1106.

Champion, A., Kreis, M., Mockaitis, K., Picaud, A. and Henry, Y. (2004) Arabidopsis kinome: after the casting. *Funct. Integr. Genomics*, **4**, 163–187.

Chérel, I., Michard, E., Platet, N., Mouline, K., Alcon, C., Sentenac, H. and Thibaud, J.-B. (2002) Physical and functional interaction of

the *Arabidopsis* K^+ channel AKT2 and phosphatase *At*PP2CA. *Plant Cell*, **14**, 1133–1146.

Daram, P., Urbach, S., Gaymard, F., Sentenac, H. and Chérel, I. (1997) Tetramerization of the AKT1 plant potassium channel involves its C- terminal cytoplasmic domain. *EMBO J.* **16**, 3455–3463.

Deeken, R., Sanders, C., Ache, P. and Hedrich, R. (2000) Developmental and light-dependent regulation of a phloem-localised K^+ channel of *Arabidopsis thaliana*. *Plant J.* **23**, 285–290.

Deeken, R., Geiger, D., Fromm, J., Koroleva, O., Ache, P., Langenfeld-Heyser, R., Sauer, N., May, S.T. and Hedrich, R. (2002) Loss of the AKT2/3 potassium channel affects sugar loading into the phloem of Arabidopsis. *Planta*, **216**, 334–344.

Dennison, K.L., Robertson, W.R., Lewis, B.D., Hirsch, R.E., Sussman, M.R. and Spalding, E.P. (2001) Functions of AKT1 and AKT2 potassium channels determined by studies of single and double mutants of *Arabidopsis*. *Plant Physiol.* **127**, 1012–1019.

Dreyer, I., Antunes, S., Hoshi, T., Müller-Röber, B., Palme, K., Pongs, O., Reintanz, G. and Hedrich, R. (1997) Plant K^+ channel α-subunits assemble indiscriminately. *Biophys. J.* **72**, 2143–2150.

Dreyer, I., Michard, E., Lacombe, B. and Thibaud, J.-B. (2001) A plant Shaker-like K^+ channel switches between two distinct gating modes resulting in either inward-rectifying or 'leak' current. *FEBS Lett.* **505**, 233–239.

Fromm, J. and Bauer, T. (1994) Action potentials in maize sieve tubes change phloem translocation. *J. Exp. Bot.* **45**, 463–469.

Gaymard, F., Cerutti, M., Horeau, C., Lemaillet, G., Urbach, S., Ravallec, M., Devauchelle, G., Sentenac, H. and Thibaud, J.-B. (1996) The baculovirus/insect cell system as an alternative to *Xenopus* oocytes. First characterization of the AKT1 K^+ channel from *Arabidopsis thaliana*. *J. Biol. Chem.* **271**, 22863–22870.

Gaymard, F., Pilot, G., Lacombe, B., Bouchez, D., Bruneau, D., Boucherez, J., Michaux-Ferrière, N., Thibaud, J.-B. and Sentenac, H. (1998) Identification and disruption of a plant shaker-like outward channel involved in K^+ release into the xylem sap. *Cell*, **94**, 647–655.

Herde, O., Atzorn, R., Fisahn, J., Wasternack, C., Willmitzer, L. and Pena-Cortes, H. (1996) Localized wounding by heat initiates the accumulation of proteinase inhibitor II in abscisic acid-deficient plants by triggering jasmonic acid biosynthesis. *Plant Physiol.* **112**, 853–860.

Holmgren, M., Shin, K.S. and Yellen, G. (1998) The activation gate of a voltage-gated K^+ channel can be trapped in the open state by an intersubunit metal bridge. *Neuron*, **21**, 617–621.

Hosy, E., Vavasseur, A., Mouline, K. *et al.* (2003) The *Arabidopsis* outward K^+ channel GORK is involved in regulation of stomatal movements and plant transpiration. *Proc. Natl Acad. Sci. USA*, **100**, 5549–5554.

Jiang, Y., Lee, A., Chen, J., Ruta, V., Cadene, M., Chait, B.T. and MacKinnon, R. (2003) X-ray structure of a voltage-dependent K^+ channel. *Nature*, **423**, 33–41.

Johansson, I., Karlsson, M., Shukla, V.K., Chrispeels, M.J., Larsson, C. and Kjellbom, P. (1998) Water transport activity of the plasma membrane aquaporin PM28A is regulated by phosphorylation. *Plant Cell*, **10**, 451–459.

Köhler, B. and Blatt, M.R. (2002) Protein phosphorylation activates the guard cell Ca^{2+} channel and is a prerequisite for gating by abscisic acid. *Plant J.* **32**, 185–194.

Lacombe, B. and Thibaud, J.-B. (1998) Evidence for a multi-ion pore behavior in the plant potassium channel KAT1. *J. Membr. Biol.* **166**, 91–100.

Lacombe, B., Pilot, G., Gaymard, F., Sentenac, H. and Thibaud, J.-B. (2000a) pH control of the plant outwardly-rectifying potassium channel SKOR. *FEBS Lett.* **466**, 351–354.

Lacombe, B., Pilot, G., Michard, E., Gaymard, F., Sentenac, H. and Thibaud, J.-B. (2000b) A shaker-like K^+ channel with weak rectification is expressed in both source and sink phloem tissues of *Arabidopsis*. *Plant Cell*, **12**, 837–851.

Lesage, F. (2003) Pharmacology of neuronal background potassium channels. *Neuropharmacology*, **44**, 1–7.

Levitan, I.B. (1999) Modulation of ion channels by protein phosphorylation. How the brain works. *Adv. Second Messenger Phosphoprotein Res.* **33**, 3–22.

Li, W., Luan, S., Schreiber, S.L. and Assmann, S.M. (1994a) Cyclic AMP stimulates K^+ channel activity in mesophyll cells of *Vicia faba* L. *Plant Physiol.* **106**, 957–961.

Li, W., Luan, S., Schreiber, S.L. and Assmann, S.M. (1994b) Evidence for protein phosphatase 1 and 2A regulation of K^+ channels in two types of leaf cells. *Plant Physiol.* **106**, 963–970.

Li, J., Lee, Y.R. and Assmann, S.M. (1998) Guard cells possess a calcium-dependent protein kinase that phophorylates the KAT1 potassium channel. *Plant Physiol.* **116**, 785–795.

Liu, K.H. and Tsay, Y.F. (2003) Switching between the two action modes of the dual-affinity nitrate transporter CHL1 by phosphorylation. *EMBO J.* **22**, 1005–1013.

Luan, S., Li, W., Rusnak, F., Assmann, S.M. and Schreiber, S.L. (1993) Immunosuppressants implicate protein phosphatase regulation of K^+ channels in guard cells. *Proc. Natl Acad. Sci. USA*, **90**, 2202–2206.

Macri, V., Proenza, C., Agranovich, E., Angoli, D. and Accili, E.A. (2002) Separable gating mechanisms in a mammalian pacemaker channel. *J. Biol. Chem.* **277**, 35939–35946.

Männikkö, R., Elinder, F. and Larsson, H.P. (2002) Voltage-sensing mechanism is conserved among ion channels gated by opposite voltages. *Nature*, **419**, 837–841.

Marten, I., Hoth, S., Deeken, R., Ache, P., Ketchum, K.A., Hoshi, T. and Hedrich, R. (1999) AKT3, a phloem-localized K^+ channel, is blocked by protons. *Proc. Natl Acad. Sci. USA*, **96**, 7581–7586.

Maurel, C., Kado, R., Guern, J. and Chrispeels, M. (1995) Phosphorylation regulates the water channel activity of the seed-specific aquaporin alpha-TIP. *EMBO J.* **14**, 3028–3035.

Moran, N. (1996) Membrane-delimited phosphorylation enables the activation of the outward-rectifying K^+ channels in motor cell protoplasts of *Samanea saman*. *Plant Physiol.* **111**, 1281–1292.

Mori, I.C., Uozumi, N. and Muto, S. (2000) Phosphorylation of the inward-rectifying potassium channel KAT1 by ABR kinase in *Vicia* guard cells. *Plant Cell Physiol.* **41**, 850–856.

Mouline, K., Véry, A.-A., Gaymard, F., Boucherez, J., Pilot, G., Devic, M., Bouchez, D., Thibaud, J.-B. and Sentenac, H. (2002) Pollen tube development and competitive ability are impaired by disruption of a Shaker K^+ channel in *Arabidopsis*. *Genes Dev.* **16**, 339–350.

Obrdlik, P., El-Bakkoury, M., Hamacher, T. *et al.* (2004) K^+ channel interactions detected by a genetic system optimized for systematic studies of membrane protein interactions. *Proc. Natl Acad. Sci. USA*, **101**, 12242–12247.

Ohnishi, K., Wang, X., Takahashi, A., Matsumoto, H., Aoki, H. and Ohnishi, T. (1998) Effects of protein kinase inhibitors on heat-induced *hsp72* gene expression in a human glioblastoma cell line. *Cell. Signal.* **10**, 259–264.

Pei, Z.M., Kuchitsu, K., Ward, J.M., Schwarz, M. and Schroeder, J.I. (1997) Differential abscisic acid regulation of guard cell slow anion channels in *Arabidopsis* wild-type and *abi1* and *abi2* mutants. *Plant Cell*, **9**, 409–423.

Pilot, G., Lacombe, B., Gaymard, F., Chérel, I., Boucherez, J., Thibaud, J.-B. and Sentenac, H. (2001) Guard cell inward K^+ channel activity in *Arabidopsis* involves expression of the twin channel subunits KAT1 and KAT2. *J. Biol. Chem.* **276**, 3215–3221.

Pilot, G., Gaymard, F., Mouline, K., Chérel, I. and Sentenac, H. (2003) Regulated expression of *Arabidopsis* shaker K^+ channel genes involved in K^+ uptake and distribution in the plant. *Plant Mol. Biol.* **51**, 773–787.

Proenza, C., Angoli, D., Agranovich, E., Macri, V. and Accili, E.A. (2002) Pacemaker channels produce an instantaneous current. *J. Biol. Chem.* **277**, 5101–5109.

Reintanz, B., Szyroki, A., Ivashikina, N., Ache, P., Godde, M., Becker, D., Palme, K. and Hedrich, R. (2002) AtKC1, a silent *Arabidopsis* potassium channel alpha-subunit modulates root hair K^+ influx. *Proc. Natl Acad. Sci. USA*, **99**, 4079–4084.

Sato, Y., Sakaguchi, M., Goshima, S., Nakamura, T. and Uozumi, N. (2002) Integration of Shaker-type K^+ channel, KAT1, into the endoplasmic reticulum membrane: synergistic insertion of voltage-sensing segments, S3–S4, and independent insertion of pore-forming segments, S5-P-S6. *Proc. Natl Acad. Sci. USA*, **99**, 60–65.

Schachtman, D.P., Schroeder, J.I., Lucas, W.J., Anderson, J.A. and Gaber, R.F. (1992) Expression of an inward-rectifying potassium channel by the *Arabidopsis KAT1* cDNA. *Science*, **258**, 1654–1658.

Sculptoreanu, A., Rotman, E., Takahashi, M., Scheuer, T. and Catterall, W.A. (1993a) Voltage-dependent potentiation of the activity of cardiac L-type calcium channel alpha 1 subunits due to phosphorylation by cAMP-dependent protein kinase. *Proc. Natl Acad. Sci. USA*, **90**, 10135–10139.

Sculptoreanu, A., Scheuer, T. and Catterall, W.A. (1993b) Voltage-dependent potentiation of L-type Ca^{2+} channels due to phosphorylation by cAMP-dependent protein kinase. *Nature*, **364**, 240–243.

Spalding, E.P. and Goldsmith, M.H.M. (1993) Activation of K^+ channels in the plasma membrane of Arabidopsis by ATP produced photosynthetically. *Plant Cell*, **5**, 477–484.

Stoelzle, S., Kagawa, T., Wada, M., Hedrich, R. and Dietrich, P. (2003) Blue light activates calcium-permeable channels in Arabidopsis mesophyll cells via the phototropin signaling pathway. *Proc. Natl Acad. Sci. USA*, **100**, 1456–1461.

Tamaoki, T. (1991) Use and specificity of staurosporine, UCN-01, and Calphostin C as protein kinase inhibitors. *Methods Enzymol.* **201**, 340–347.

Tang, X.D. and Hoshi, T. (1999) Rundown of the hyperpolarization-activated KAT1 channel involves slowing of the opening transitions regulated by phosphorylation. *Biophys. J.* **76**, 3089–3098.

Thiel, G. and Blatt, M.R. (1994) Phosphatase antagonist okadaic acid inhibits steady-state K^+ currents in guard cells of *Vicia faba*. *Plant J.* **5**, 727–733.

Urbach, S., Chérel, I., Sentenac, H. and Gaymard, F. (2000) Biochemical characterization of the *Arabidopsis* K^+ channels KAT1 and AKT1 expressed or co-expressed in insect cells. *Plant J.* **23**, 527–538.

Véry, A.-A., Gaymard, F., Bosseux, C., Sentenac, H. and Thibaud, J.-B. (1995) Expression of a cloned plant K^+ channel in *Xenopus* oocytes: analysis of macroscopic currents. *Plant J.* **7**, 321–332.

Wang, Z.Y., Wang, F., Sellers, J.R., Korn, E.D. and Hammer, J.A., 3rd (1998) Analysis of the regulatory phosphorylation site in *Acanthamoeba* myosin IC by using site-directed mutagenesis. *Proc. Natl Acad. Sci. USA*, **95**, 15200–15205.

Wayne, R. (1994) The excitability of plant cells: with a special emphasis on characean internode cells. *Bot. Rev.* **60**, 265–367.

Wildon, D.C., Tahain, J.F., Minchin, P.E.H., Gubb, I.R., Reilly, A.J., Skipper, Y.D., Doherty, H.M., O'Donnell, P.J. and Bowles, D.J. (1992) Electrical signalling and systemic proteinase inhibitor induction in the wounded plant. *Nature*, **360**, 62–65.

Yellen, G. (2002) The voltage-gated potassium channels and their relatives. *Nature*, **419**, 35–42.

Zimmermann, S. and Sentenac, H. (1999) Plant ion channels: from molecular structures to physiological functions. *Curr. Opin. Plant Biol.* **2**, 477–482.

⇒ zurück zur Übersicht

2005

Porée, Wulfetange, Naso, Carpaneto, Roller, Natura, Bertl, Sentenac, Thibaud, **Dreyer**

Plant K_{in} and K_{out} channels: Approaching the trait of opposite rectification by analyzing more than 250 KAT1-SKOR chimeras.

Biochem. Biophys. Res. Commun. **332**:465-473.

Available online at www.sciencedirect.com
SCIENCE DIRECT®
Biochemical and Biophysical Research Communications 332 (2005) 465–473
BBRC
www.elsevier.com/locate/ybbrc

Plant K_{in} and K_{out} channels: Approaching the trait of opposite rectification by analyzing more than 250 KAT1–SKOR chimeras

Fabien Porée [a,b,c], Klaas Wulfetange [b], Alessia Naso [d], Armando Carpaneto [d], Anja Roller [e], Gabriel Natura [e], Adam Bertl [e], Hervé Sentenac [a], Jean-Baptiste Thibaud [a], Ingo Dreyer [a,b,c,*]

[a] *Biochimie et Physiologie Moléculaires des Plantes, UMR 5004, Agro.M-CNRS-INRA-UM2, Montpellier, France*
[b] *Universität Potsdam, Institut für Biochemie und Biologie, Molekularbiologie, Potsdam, Germany*
[c] *Max-Planck Institute of Molecular Plant Physiology, Cooperative Research Group, Potsdam, Germany*
[d] *Istituto di Biofisica, CNR, Sezione di Genova, Genoa, Italy*
[e] *Universität Karlsruhe, Botanisches Institut I, Karlsruhe, Germany*

Received 26 April 2005
Available online 5 May 2005

Abstract

Members of the Shaker-like plant K^+ channel family share a common structure, but are highly diverse in their function: they behave as either hyperpolarization-activated inward-rectifying (K_{in}) channels, or leak-like (K_{weak}) channels, or depolarization-activated outward-rectifying (K_{out}) channels. Here we created 256 chimeras between the K_{in} channel KAT1 and the K_{out} channel SKOR. The chimeras were screened in a potassium-uptake deficient yeast strain to identify those, which mediate potassium inward currents, i.e., which are functionally equivalent to KAT1. This strategy allowed us to identify three chimeras which differ from KAT1 in three parts of the polypeptide: the cytosolic N-terminus, the cytosolic C-terminus, and the putative voltage-sensor S4. Additionally, mutations in the K_{out} channel SKOR were generated in order to localize molecular entities underlying its depolarization activation. The triple mutant SKOR-D312N-M313L-I314G, carrying amino-acid changes in the S6 segment, was identified as a channel which did not display any rectification in the tested voltage-range.

Keywords: Potassium channel; Rectification; Yeast complementation; Chimera; Site-directed mutagenesis

Plant K^+ channels of the Shaker type are the best-characterized ion transporter family in plants. Several members have been identified at the molecular level since 1992 [1,2] and detailed structural analyses allowed Uozumi et al. [3] to determine their transmembrane topology. Like their animal counterparts plant Shaker-like K^+ channels are composed of four α-subunits [4], each of which is formed by a polypeptide with cytosolic N- and C-termini, six transmembrane regions (S1–S6), and a pore-forming linker (P) between S5 and S6.

The model plant *Arabidopsis thaliana* comprises nine genes coding for Shaker-like potassium channels, eight of which have been functionally characterized so far: AKT1 [1,5], KAT1 [2,6], KAT2 [7], and SPIK [8] belong to the subfamily of hyperpolarization-activated inward-rectifying K_{in} channels, SKOR [9] and GORK [10] belong to the subfamily of depolarization-activated outward-rectifying K_{out} channels, and AKT2 [11–15] to the subfamily of weakly rectifying K_{weak} channels. AtKC1 appears not to mediate currents when expressed alone, rather than modulating the K_{in} channels KAT1 and AKT1 [4,16].

* Corresponding author. Fax: +49 331 977 2512.
E-mail address: dreyer@rz.uni-potsdam.de (I. Dreyer).

0006-291X/$ - see front matter © 2005 Elsevier Inc. All rights reserved.
doi:10.1016/j.bbrc.2005.04.150

The diversity in function of Shaker-like plant K^+ channels, despite their common structure, emphasized the question on the molecular reasons underlying the differences. In this context, the K_{in} channel KAT1 became a model system for structure–function analyses. Several studies indicated that the S4 segment together with the cytosolic N- and C-termini is fundamentally involved in the gating process of this channel [4,17–22]. However, up to now, no report has addressed the question on the different gating properties of K_{in} and K_{out} channels.

In this study, we created 256 chimeras between the K_{in} channel KAT1 and the K_{out} channel SKOR, and tested them for their functionality. Additionally, we generated mutations in the SKOR channel in order to localize regions within the polypeptide which could be involved in the gating process.

Materials and methods

Recombinant DNA techniques. Standard methods of recombinant DNA manipulation were applied [23]. Cutting sites used for the creation of chimeras were introduced into the coding regions of KAT1 and SKOR with the pAlter mutagenesis system (Promega, Charbonnières, France). For experiments on yeast, the coding sequences of KAT1 and SKOR as well as their derivatives were cloned into the NotI sites of the vectors pFL61 [24] and pFL38His-PGK [25]. For experiments on oocytes, the coding sequences were cloned into the *Bam*HI site of the vector pGEMHE [26]. Further details concerning the more than 250 constructs tested in this study will be outlined in the text. Restriction endonucleases were purchased from New England Biolabs (Beverly, MA).

Electrophysiology. Two-electrode voltage-clamp experiments on *Xenopus* oocytes were carried out as previously described [27]. All external solutions were composed of 1 mM $CaCl_2$, 2 mM $MgCl_2$, 10 mM Tris/Mes, pH 7.4. Additionally, the different solutions contained (in mM): K3—3 KCl, 97 NaCl; K10—10 KCl, 90 NaCl; K30—30 KCl, 70 NaCl; K100—100 KCl; K3 + Cs—3 KCl, 97 CsCl. Patch-clamp experiments on yeast protoplasts were carried out as recently described [28]. Standard pipette solution contained 175 mM KCl, 4 mM $MgCl_2$, 4 mM K-ATP, 1 mM EGTA, and 152 μM $CaCl_2$, adjusted to pH 7.0 with KOH. Extracellular solution contained 150 mM KCl, 10 mM $CaCl_2$, and 5 mM $MgCl_2$, buffered to pH 6.5 with Mes/Tris.

Yeast complementation. Experiments with the yeast strain Wagf2 (*Δtrk1,2*-mutant) were carried out as previously described [29]. Yeast growth was described by the equation

$$OD_{600}(t) = (OD_\infty \times OD_0)/[OD_0 + (OD_\infty - OD_0) \times \exp(-t/\tau)], \quad (1)$$

OD_0 and OD_∞ denote the optical densities at $t = 0$ and infinity, respectively [29].

Results and discussion

KAT1 and SKOR, same structure–different function

Despite their common structure, the plant Shaker-like K^+ channels KAT1 and SKOR showed significant differences in their functional behavior after expression in animal or yeast cells. When expressed in oocytes and in COS cells, SKOR mediated outwardly rectifying currents activating at voltages more positive than −40 mV (Figs. 1A and B). KAT1 mediated inwardly rectifying currents activating at voltages more negative than −80 mV (Figs. 1C and D). When expressed in yeast, this functional difference is responsible for an altered growth phenotype. Whereas KAT1 was able to complement the potassium-uptake deficient yeast strain Wagf2 (*Δtrk1,2*-mutant), SKOR was not. In high potassium concentrations (50 mM K^+), yeast cells transformed with the empty pFL61 vector, the pFL61-KAT1 and pFL61-SKOR plasmids showed significant growth (Fig. 1E, left panel). Lowering the potassium concentration of the medium to 2 mM K^+ allowed only those cells to grow which expressed the KAT1 channel (Fig. 1E, right panel). Thus, in contrast to SKOR, KAT1 complemented the K^+-uptake deficiency of the yeast Wagf2 enabling growth in low potassium concentrations.

An alignment between KAT1 and SKOR revealed that both channels show an overall identity of about 20%. The largest differences were found in the cytoplasmic N- and C-termini. More similarities were observed within the hydrophobic core regions and here mainly in the transmembrane segments (47% identity) whereas the extracellular and cytoplasmic linkers between them were less conserved (25% identity). These observations proposed the generation of KAT1–SKOR chimeras to obtain information on the structural necessities for a channel to be able to complement the K^+-uptake deficient yeast strain.

Generation of 256 KAT1–SKOR chimeras

In order to generate KAT1–SKOR chimeras, the coding sequences of both channels were slightly modified. Using site-directed mutagenesis, seven new unique endonuclease recognition sites were introduced in the DNA coding sequence of each channel at the same position (Fig. 2A, a–g). A *Rsr*II restriction site was created in the sequence coding for the first transmembrane segment S1, a *Sal*I site in S2, a *Bsu*36I site in S3, a *Bss*HII site in S4, a *Sac*II site in S5, a *Mlu*I site in the outer pore P, and a *Bst*XI site in the sequence coding for S6 were created. Some of these restriction sites could be introduced by silent mutations (in KAT1, *Bss*HII and *Bst*XI; in SKOR, *Sal*I, *Sac*II, and *Mlu*I). The introduction of the others caused moderate exchanges at the amino-acid level (Fig. 2C) without affecting the general features of the channels. Neither their rectification behavior was altered nor the physiological yeast-expression phenotype. The modified KAT1* was still able to complement the yeast Wagf2 whereas SKOR* was not (Fig. 1F). The seven restriction sites subdivided the channels in eight parts (Fig. 2A, 1–8). Therefore, KAT1* and SKOR* were represented by the eight letter strings

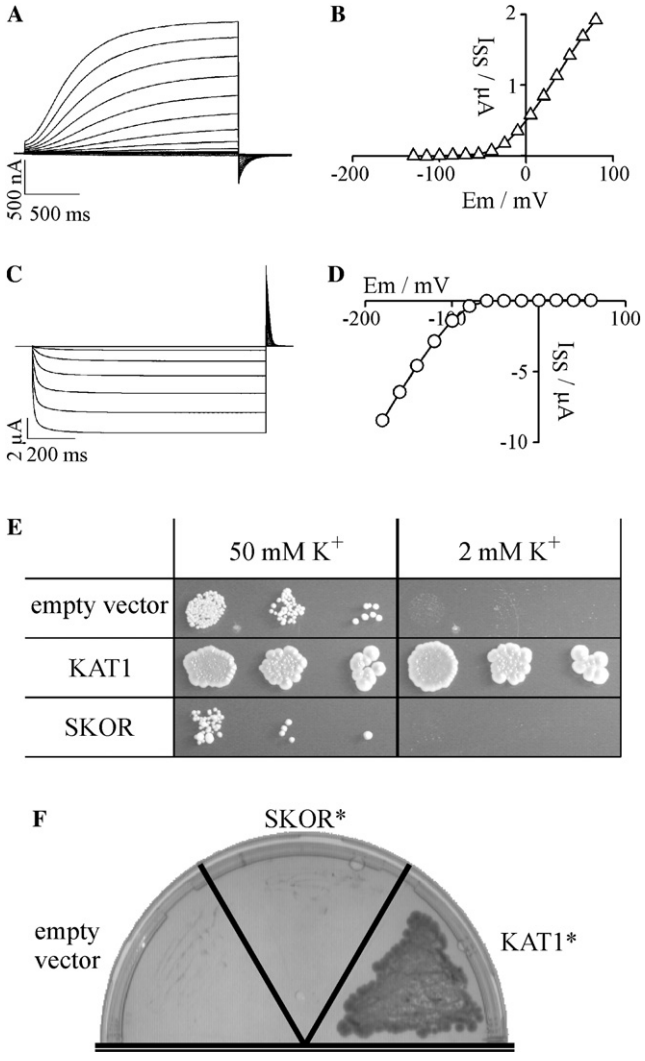

Fig. 1. SKOR promotes potassium release, KAT1 potassium influx. (A) Representative outward K^+ currents in solution K10 obtained from an oocyte injected with *SKOR* cRNA. From a holding potential of −100 mV currents were evoked by 2-s activating voltage-pulses from −130 to +80 mV (15-mV steps). (B) Steady-state current–voltage characteristic for the oocyte shown in (A). (C) Representative inward K^+ currents in solution K10 obtained from an oocyte injected with *KAT1* cRNA. From a holding potential of 0 mV currents were evoked by 1-s activating voltage-pulses from −180 to +60 mV (20-mV steps). (D) Steady-state current–voltage characteristic for the oocyte shown in (C). (E) Expression of KAT1 and SKOR in the K^+-uptake deficient yeast strain Wagf2. Drop test on solid medium. Isolated yeast colonies transformed either with the empty vector pFL61, the pFL61-KAT1 or the pFL61-SKOR plasmid were pre-incubated in overnight liquid culture containing 50 mM K^+. After two washing steps, the optical density of the cell suspension at 600 nm was adjusted to 0.1, 0.05, and 0.01, respectively. Ten microliters of these suspensions were dropped on plates ($OD_{600} = 0.1$, left spot in each part of the figure; $OD_{600} = 0.05$, middle spot; $OD_{600} = 0.01$, right spot) containing 50 mM (left panel) and 2 mM K^+ (right panel). Plates were incubated for 5 days at 30 °C. Data are representative for at least five independent repeats. (F) Expression of KAT1* and SKOR* in yeast. Colonies transformed with KAT1* (=KKKKKKKK), SKOR* (=SSSSSSSS), and the empty vector were plated on selection medium containing 2 mM K^+. Plates were incubated for 4 days at 30 °C. The presented result is representative for at least four repeats.

KKKKKKKK and SSSSSSSS, respectively (Fig. 2B). This code was also used in the following to facilitate the depiction of the chimeric channels. A "K" ("S") at the *x*th position indicates that in this chimera the *x*th region was of KAT1 (SKOR) origin.

Based on the KAT1* (=KKKKKKKK) and SKOR* (=SSSSSSSS) constructs, in a first step the 16 different chimeras displayed in Fig. 3A were created in the yeast-expression vector pFL61. Only the first (a), second (b), fourth (d), fifth (e), and sixth (f) restriction sites were used in this step. The third (c) and seventh (g) sites were exploited in a second step (Fig. 3B): the 16 chimeric plasmids were digested with the enzyme combination *Bsu*36I(c)/*Bst*XI(g) generating a smaller fragment and a larger fragment for each construct (Fig. 3C). Each of the resulting 16 larger fragments represents one of the possible 16 K/S combinations for the regions 1, 2, 3, and 8, and each of the resulting 16 smaller fragments one of the possible 16 K/S combinations for the regions 4, 5, 6, and 7 (Fig. 3A). The cohesive ends produced by the *Bsu*36I/*Bst*XI digestion were not self-compatible. The smaller fragments showed 5′-TTA and 3′-GTTT overhangs and the larger fragments 5′-TAA and 3′-AAAC overhangs. Thus, in subsequent ligation steps only one smaller fragment can combine with only one larger fragment to reconstitute a chimeric plasmid.

Screening for chimeras complementing the Wagf2 yeast strain

For a first screening approach, the 16 smaller fragments were pooled and randomly ligated into one of the larger fragments. This procedure allowed us to create 16 pools comprising each 16 possible chimeras (=256 chimeric plasmids). Reconstituted plasmids were amplified in *Escherichia coli* in liquid culture. An aliquot of the transformed *E. coli* cells was plated on solid medium to calculate the transformation efficiency. Assuming that all constructs were created and transformed with the same probability, the probability to miss one of the 16 possible constructs calculates to $(15/16)^n$ where n is the number of transformants. An $n > 150$ indicated that the probability to miss one of the 16 possible constructs per pool was $<10^{-4}$. Plasmid DNA was extracted from each of the 16 pools and used to transform the yeast Wagf2. An aliquot of the transformed cells was plated on medium containing 50 mM K^+, selecting only for uracil auxotrophy to verify the transformation efficiency ($n > 150$, see above). The rest was plated on minimal medium (without uracil) containing 2 mM K^+. Plates were incubated for up to 10 days at 30 °C.

For three of the 16 pools, yeast colony growth could be observed on low K^+ medium after 2–3 days indicating that these yeast cells were expressing chimeric channels mediating K^+ uptake. The compositions of the

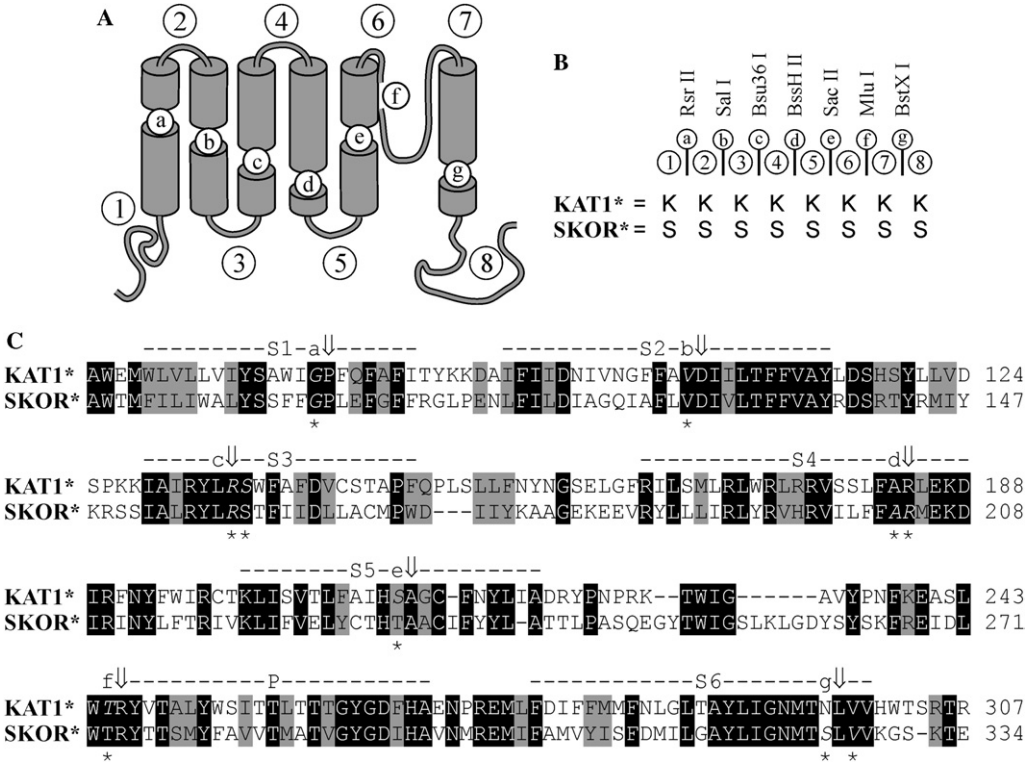

Fig. 2. Seven new, unique cutting sites introduced into *KAT1* and *SKOR*. (A) Seven newly introduced cutting sites (a–g) subdivide SKOR and KAT1 in eight parts (1–8) each. (B) The introduced cutting sites are *Rsr*II (a, base recognition sequence on the non-matrix strand: CG′GTCCG), *Sal*I (b, G′TCGAC), *Bsu*36I (c, CC′TTAGG), *Bss*HII (d, G′CGCGC), *Sac*II (e, CCGC′GG), *Mlu*I (f, A′CGCGT), and *Bst*XI (g, CCAXTTTG′GTGG, X = G for SKOR* and A for KAT1*). The modified KAT1 and SKOR polypeptides are named KAT1* and SKOR*, and are represented by the eight letter strings KKKKKKKK and SSSSSSSS, respectively. (C) Comparison of the amino-acid sequences of the hydrophobic cores of KAT1* and SKOR*. The six transmembrane segments S1–S6, the pore-forming region P as well as the position of the cutting sites (a–g, present in the underlying cDNAs) are marked. Asterisks point to the positions where the introduction of a cutting site resulted in a change of the amino-acid sequence. Namely these changes are (italic letters) in KAT1: C77G, I104V, S135R, T136S, C211S, N245T, and in SKOR: T100G, K158R, H203A, K204R, A325S, and I327V.

sequences of these chimeras were determined by applying a PCR-based macro-sequencing method. This method made it possible to resolve the chimeric structure of the channel-coding plasmid with 16 polymerase chain reactions (Fig. 4). Sequencing of about 30 yeast colonies allowed the identification of four different KAT1–SKOR chimeras: KKKKKKKK (the trivial construct), KKKKKKKS, SKKSSKKS, and KKKSKKKK.

In order to test whether some functional K^+-uptake mediating chimeras were missed by the first screening approach, in a second round all 256 chimeric plasmids were at first created one by one. The plasmid DNA was then pooled into 16 pools whereby those chimeras were not included in the pools which were identified in the first screening. The yeast strain Wagf2 was transformed with the DNA pools and transformed cells plated on K^+-rich (50 mM) and low K^+ (2 mM) media. Although the transformation efficiency was high, no further colony could be observed to grow on low K^+ medium. Thus, very likely no further chimera among the remaining 252 was able to complement the potassium-uptake deficient yeast strain.

KAT1–SKOR chimeras complement Wagf2

To prove independently the results obtained with the four identified channels, the chimerical plasmids pFL61-KKKKKKKS, pFL61-KKKSKKKK, and pFL61-SKKSSKKS were created one by one on the basis of pFL61-KAT* and pFL61-SKOR*. Plasmids were sequenced (this time determination of the exact base composition) and used to transform Wagf2 yeast cells. Yeast growth was analyzed in drop test experiments on solid medium (Fig. 5A) and growth kinetics was monitored in liquid culture (Fig. 5B). These experiments confirmed the results of the first screening approach. In contrast to the empty vector, all three chimeras (like the KAT1* channel = KKKKKKKK) enabled Wagf2 to grow on solid low K^+ medium. However, the complementation efficiency of the four channels differed. Whereas in drop tests cells expressing the chimeras KKKKKKKS and SKKSSKKS grew similarly well as cells expressing KKKKKKKK (=KAT1*), growth of yeast cells was weaker when transformed with KKKSKKKK. Subsequently, the channels were tested in liquid culture. By fitting the time course of yeast

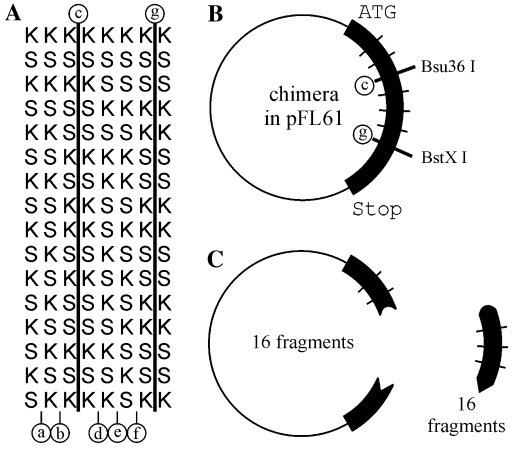

Fig. 3. Creation of 256 KAT1–SKOR chimeras. All possible 256 KAT1–SKOR chimeras were generated in a two-step strategy. (A) In a first step, using the cutting sites a, b, d, e, and f (compare with Fig. 2), 16 different, pre-selected KAT1–SKOR chimeras were generated on the basis of the pFL61-KAT1* and pFL61-SKOR* plasmids. The cutting sites c (*Bsu*36I) and g (*Bst*XI) (solid lines) have not been used in this step. Each chimera is represented by an eight-letter string (compare with Fig. 2B). (B) In the second step, restriction with *Bsu*36I (c) and *Bst*XI (g) produces a larger fragment with a 5′-TAA and a 3′-AAAC overhang, and a smaller fragment with a 5′-TTA and a 3′-GTTT overhang. Note that these ends are not self-compatible. (C) Restriction of the 16 different KAT1–SKOR chimeras shown in (A) with *Bsu*36I (c) and *Bst*XI (g) results in 16 different larger fragments comprising the coding sequences for the regions 1, 2, 3, and 8 (compare with Fig. 2A) and 16 different smaller fragments comprising the coding sequences for the regions 4, 5, 6, and 7. The combination of the 32 fragments allows us to generate $16 \times 16 = 256$ chimeras in a single random ligation step.

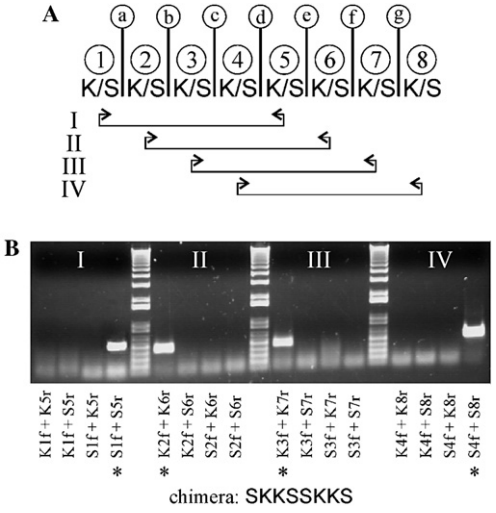

Fig. 4. PCR-based macro-sequencing strategy to identify the composition of unknown chimeras. (A) Each of the eight regions of an unknown chimera is either of KAT1- (K) or of SKOR- (S) origin. Using KAT1- and SKOR-specific primers the composition of the plasmid coding for the unknown chimera can be identified in four sets of four polymerase chain reactions. In the first set, (I) KAT1- and SKOR-specific forward primers for the region 1 (K1f and S1f) are combined with KAT1- and SKOR-specific reverse primers for the region 5 (K5r and S5r). In the second set, (II) primer pairs for the regions 2 and 6 are combined (K2f, S2f, K6r, and S6r), in the third set (III) pairs for the regions 3 and 7 (K3f, S3f, K7r, and S7r), and in the fourth set (IV) pairs for the regions 4 and 8 (K4f, S4f, K8r, and S8r) are used. (B) Example for the PCR-based macro-sequencing strategy. The asterisks indicate the primer pairs resulting in DNA amplification: S1f and S5r, K2f and K6r, K3f and K7r, and S4f and S8r. The yeast colony which served as target for the 16 polymerase chain reactions comprises a plasmid coding for the chimera SKKSSKKS.

growth with a mathematical function describing growth under limiting conditions (Fig. 5B, solid lines), differences between the distinct cell lines could be quantified. The growth kinetics of KAT1* expressing cells saturated at $OD_{\infty} = 1.87$ while that of the cells expressing KKKKKKKS did so at $OD_{\infty} = 1.81$, and that of cells expressing SKKSSKKS at $OD_{\infty} = 1.70$, indicating a slightly less efficient exploitation of the limiting resources (potassium) [29] by the latter two chimeras than by the KAT1* channel. This exploitation efficiency was even more reduced in cells expressing KKKSKKKK ($OD_{\infty} = 1.41$). Moreover, these cells showed an apparent proliferation time constant (τ value) about 2.5 times larger than cells expressing the KKKKKKKK, KKKKKKKS, and SKKSSKKS chimeras. This is equivalent to a 60% reduction in the proliferation rate constant [29], which could be the consequence of reduced potassium-uptake rates in these cells.

In an independent approach, the dependency of yeast growth on the expression level of functional channels was tested. We performed co-expression experiments with the N-terminally truncated SKOR polypeptide SKOR-ΔNt (spanning from the fourth transmembrane region to the C-terminus, Fig. 6A). In a previous study, it was demonstrated that SKOR-ΔNt depresses the formation of functional SKOR channels after co-expression via interactions between the assembly domains in the cytosolic C-terminus [29]. Analogous to these experiments we cloned the coding regions of the KKKKKKKK, KKKKKKKS, and SKKSSKKS channels into the low-copy (centromeric) plasmid pFL38His-PGK, and cotransformed yeast cells with these constructs in combinations with pFL61-SKOR-ΔNt (Fig. 6A). The presence of the SKOR-ΔNt polypeptide did not affect yeast complementation by the KKKKKKKK channel (Fig. 6B, black and gray circles) since the assembly domains of KAT1 and SKOR are not compatible [29]. In contrast, yeast growth was inhibited upon co-expressing KKKKKKKS + SKOR-ΔNt (Fig. 6C, white and gray triangles) and SKKSSKKS + SKOR-ΔNt (Fig. 6D, white and gray squares) indicating: (i) the interaction between SKOR-ΔNt and KKKKKKKS and SKKSSKKS, and (ii) the dependency of yeast growth on the expression level of functional KKKKKKKS and SKKSSKKS channels. The latter became also evident by analyzing the saturation level of the growth kinetics in the control condition, i.e., cotransformation of the pFL38His-PGK constructs with the empty pFL61 vector.

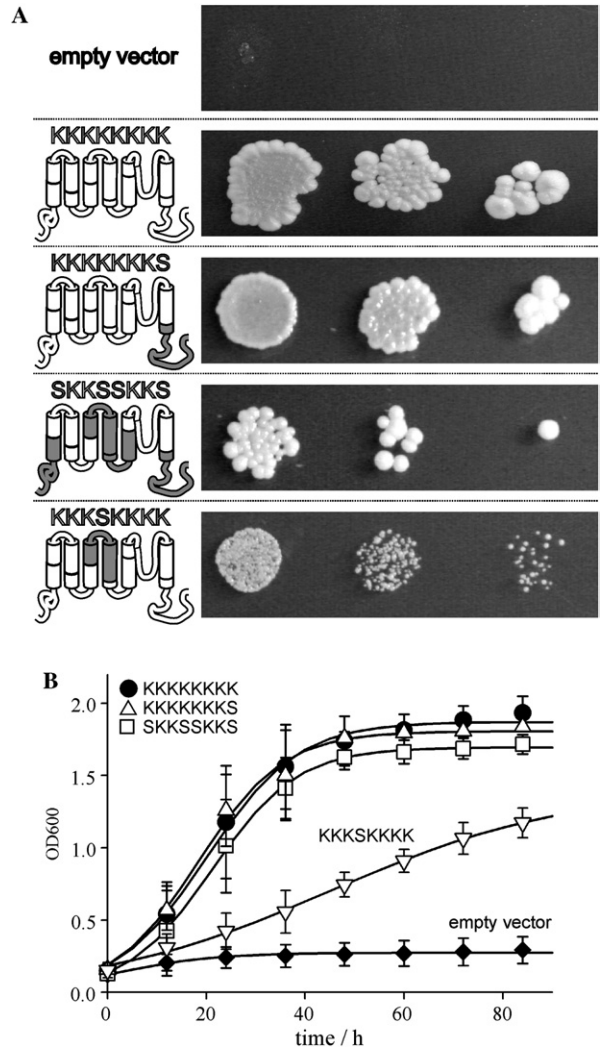

Fig. 5. KAT1–SKOR chimeras complementing the potassium-uptake deficient yeast strain Wagf2. (A) The empty vector, the KAT1* channel (KKKKKKKK chimera) and the three chimeras KKKKKKKS, SKKSSKKS, and KKKSKKKK, identified in a screening strategy, are tested in drop tests for their ability to complement the yeast strain Wagf2. Isolated yeast colonies were pre-incubated overnight in liquid culture containing 50 mM K^+. After two washing steps, the optical density of the cell suspension at 600 nm was adjusted to 0.1, 0.05, and 0.01, respectively. Ten microliters of these suspensions were dropped on plates containing 2 mM K^+ ($OD_{600} = 0.1$, left spot in each part of the figure; $OD_{600} = 0.05$, middle spot; $OD_{600} = 0.01$, right spot). Plates were incubated for 5 days at 30 °C. (B) Growth test in liquid medium. Liquid minimal medium containing 2 mM K^+ was inoculated with different yeast transformants pre-treated as described in (A) so that the optical density was about 0.15. Cultures were incubated at 30 °C on a shaker (190 rpm). At the time points indicated the OD_{600} was determined. Symbols: empty vector (filled diamonds), KKKKKKKK (filled circles), KKKKKKKS (triangles up), SKKSSKKS (squares), and KKKSKKKK (triangles down). Lines represent best fits with the Eq. (1) describing growth under limited conditions yielding $OD_0 = 0.12 \pm 0.01$, $OD_\infty = 0.27 \pm 0.01$ for the empty vector, $OD_0 = 0.19 \pm 0.04$, $OD_\infty = 1.87 \pm 0.03$, $\tau = 9.2 \pm 0.7$ for KKKKKKKK, $OD_0 = 0.20 \pm 0.05$, $OD_\infty = 1.81 \pm 0.03$, $\tau = 8.6 \pm 0.8$ for KKKKKKKS, $OD_0 = 0.14 \pm 0.02$, $OD_\infty = 1.70 \pm 0.01$, $\tau = 8.6 \pm 0.3$ for SKKSSKKS, and $OD_0 = 0.19 \pm 0.02$, $OD_\infty = 1.41 \pm 0.07$, $\tau = 24.0 \pm 1.6$ for KKKSKKKK. Data are shown as means ± SD of four to six independent samples.

Whereas KKKKKKKK expressing cells saturated at $OD_\infty = 1.86$, KKKK KKKS expressing cells did so at $OD_\infty = 1.49$ and SKKSSKKS expressing cells at $OD_\infty = 0.97$. The reduced expression (compare results with the two vectors pFL61/Fig. 5 and pFL38His-PGK/Fig. 6) increased the visibility of the differences in the potassium-uptake efficiency of the three chimeras. Thus, yeast growth correlates with the expression level of functional chimeric channels.

Chimeras tested in electrophysiological experiments

The results presented here indicate that the three chimeric channels KKKKKKKS, KKKSKKKK, and SKKSSKKS (like the trivial construct KKKKKKKK) are functional potassium-uptake systems. With the aim to obtain more insights into the nature of the transport characteristics of the chimeras, electrophysiological experiments were carried out. In a first approach, the four chimeras were expressed in *Xenopus* oocytes and analyzed with the two-electrode voltage-clamp technique. However, the chimeras KKKKKKKS, KKKSKKKK, and SKKSSKKS were electrically silent. No currents different from those measured in water-injected oocytes could be registered. Only the trivial construct KKKKKKKK mediated inward-rectifying potassium currents which were not significantly different from those mediated by the KAT1 wild-type (not shown). Also patch-clamp experiments on yeast did not provide much further information about the SKKSSKKS chimera. No significant currents could be monitored in the experimentally accessible voltage-interval (less negative than −200 mV; for a characterization of a KKKKKKKS-type chimera see [29]). Thus, we may speculate that the SKKSSKKS chimera activates at very negative voltages. Similar results were obtained by expressing several other KAT1–SKOR chimeras in oocytes. No ionic transport by the chimeric proteins KKKSSKKK, KKKKKKSS, KKKKKKSK, KKKKKSSK, KKKKKSKK, KKKSKSKK, KKKSSSKK, KSKKKKKK, KSKSKKKK, KSKSKSKK, KSKSKSSK, KSSSKKKK, KSSSSSSS, SKKKKKKS, and SSSSSSSK was detectable.

Thus, the conclusive proof that the chimera SKKSSKKS is a hyperpolarization-activated potassium channel like the KKKKKKKK channel (=KAT1*) could not be provided. Nevertheless, the fact that this chimera, just as KKKKKKKS [29], mediated K^+ uptake, evidenced by reproducible complementation of the Wagf2 yeast strain, may justify a closer look at its structure. Intriguingly, the SKKSSKKS channel comprises the N-terminus, the C-terminus, and the voltage-sensor (S4 segment) of the outward-rectifying SKOR channel. Earlier structure–function studies on KAT1 have identified exactly these parts to be involved in the gating of this hyper-

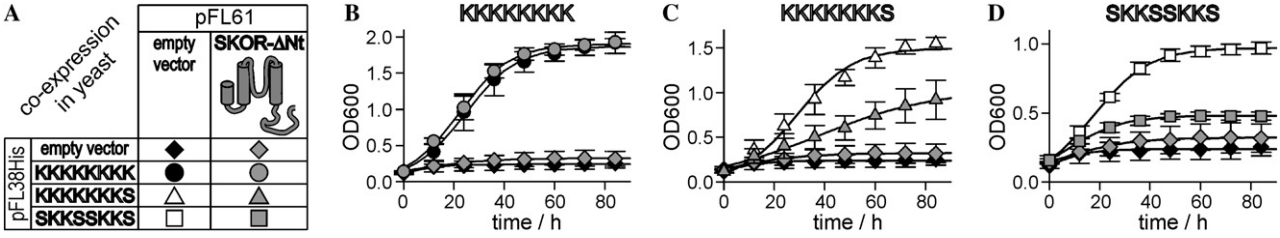

Fig. 6. Yeast growth depends on the expression level of the chimeras. Co-expression of KKKKKKKK, KKKKKKKS, and SKKSSKKS with the N-terminally truncated protein SKOR-ΔNt in the K^+-uptake deficient yeast strain Wagf2. (A) Overview of the tested combinations. Symbols cross-referenced with (B–D). (B–D) Growth test in liquid medium performed as described in Fig. 5. (B) Co-expression with KKKKKKKK. (C) Co-expression with KKKKKKKS. (D) Co-expression with SKKSSKKS. Lines represent best fits with the Eq. (1) yielding $OD_0 = 0.12 \pm 0.01$, $OD_\infty = 0.24 \pm 0.01$ (EV + EV), $OD_0 = 0.14 \pm 0.01$, $OD_\infty = 0.32 \pm 0.01$ (EV + SKOR-ΔNt), $OD_0 = 0.16 \pm 0.02$, $OD_\infty = 1.86 \pm 0.03$, $\tau = 10.4 \pm 0.7$ (KKKKKKKK + EV), $OD_0 = 0.19 \pm 0.02$, $OD_\infty = 1.90 \pm 0.02$, $\tau = 10.1 \pm 0.6$ (KKKKKKKK + SKOR-ΔNt), $OD_0 = 0.10 \pm 0.01$, $OD_\infty = 1.49 \pm 0.04$, $\tau = 11.0 \pm 0.7$ (KKKKKKKS + EV), $OD_0 = 0.17 \pm 0.02$, $OD_\infty = 1.04 \pm 0.08$, $\tau = 23.4 \pm 3.3$ (KKKKKKKS + SKOR-ΔNt), $OD_0 = 0.16 \pm 0.01$, $OD_\infty = 0.97 \pm 0.01$, $\tau = 10.9 \pm 0.2$ (SKKSSKKS + EV), and $OD_0 = 0.16 \pm 0.01$, $OD_\infty = 0.48 \pm 0.01$ (SKKSSKKS + SKOR-ΔNt). Data are shown as means ± SD of three to four independent samples.

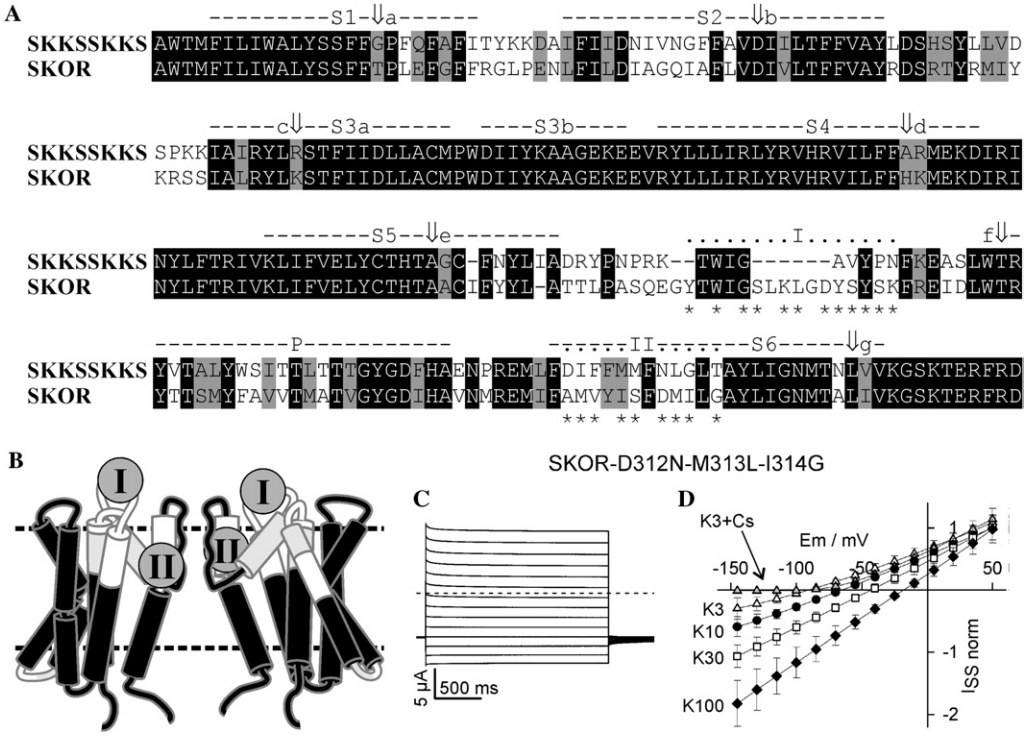

Fig. 7. The differences between SKOR and SKKSSKKS. (A) Comparison of the amino-acid sequences of the hydrophobic cores of the outward-rectifying SKOR wild-type and the chimera SKKSSKKS. Note that the cytoplasmic N-termini and C-termini are identical. The six transmembrane segments S1–S6, the pore-forming region P as well as the position of the cutting sites in the chimera (a–g, present in the underlying cDNA) are marked. Furthermore, two regions (I and II) were identified for further mutagenesis approaches. Asterisks point to the positions which have been mutated in the SKOR channel in order to localize molecular determinants for rectification. The tested mutants were Y250S, W252C, G254T-S255C, K257T-L258C, D260T-Y261C, Y261H, Y261A, S262A, S262T-Y263C, S264T-K265C, A305D, M306I, V307F, I309M, S310L, D312N, M313L, I314G, G316T, and D312N-M313L-I314G. Additionally the regions TWIGSLKLGDYSYSKFREID and TWIGAVYPNFKEAS were swapped between SKOR and KAT1. (B) Structural model for a plant K^+ channel developed on the basis of the modified crystal structure of the voltage-gated K^+ channel KvAP [30,31]. Based on the comparison between SKOR and SKKSSKKS shown in (A), differences and similarities were color-coded: identical regions (black), divergent regions (white), and regions showing stronger similarities (gray). The marking of the regions I and II corresponds to that in (A). (C,D) The mutant SKOR-D312N-M313L-I314G appears to be a K^+-selective leak. (C) Representative K^+ currents obtained from an oocyte injected with *SKOR-D312N-M313L-I314G* cRNA. From a holding potential of −100 mV currents were evoked by 4-s activating voltage-pulses from −145 to +50 mV (15-mV steps). The zero current-level is indicated as dotted line. (D) Steady-state current–voltage characteristics measured in the solutions K3 (open triangles), K10 (closed circles), K30 (open squares), K100 (closed diamonds), and K3 + Cs (gray triangles). Note that inward currents are completely blocked in the presence of cesium. Data were normalized for each cell to $I(\mathrm{K10}, 50\ \mathrm{mV}) = 1$. Data are shown as means ± SD of four different cells.

polarization-activated channel [17,18,21]. It might thus be speculated that these parts are implicated in gating but that they are possibly not essential for the determination of rectification.

Mutations in S6 convert SKOR into a non-rectifying channel

The experiments presented so far were designed to answer the question: 'Which regions in KAT1 can be replaced by regions of SKOR origin without eliminating its function as a hyperpolarization-activated potassium-uptake channel?' Nevertheless, the obtained results may also provide hints for the inverse question on: 'which parts of the SKOR channel were essential for its function as an outward rectifier?' Therefore, in a first step we compared the amino-acid sequence of the chimera SKKSSKKS with that of the outward-rectifying SKOR channel (Fig. 7A). The two proteins share an identity of about 90% (identity in 741 amino-acids). The major differences between them are localized in the S1–S2 linker, the first part of the S2 segment, the S5–P linker, and in the first part of the S6 segment (Fig. 7A). When modeling and comparing the 3D-structures of SKKSSKKS and SKOR on the basis of the X-ray structure of the voltage-dependent K^+ channel KvAP [30] and its modification according to Cuello et al. [31], it became evident that the lesser conserved parts of the channel proteins (Fig. 7B, white parts) cluster in a region different from the postulated voltage-sensor S4. This may suggest that plant K_{in} (e.g., KAT1) and K_{out} (e.g., SKOR) channels use an identical mechanism for voltage perception, but differently transform the voltage signal into conformational changes of the protein. Similar conclusions have been suggested for animal depolarization-activated Kv channels and hyperpolarization-activated HCN channels [32].

In a second step, we carried out further mutagenesis experiments. Based on the structural similarity model (Fig. 7B), we focused on the two regions I (S5–P linker) and II (first part of S6) as displayed in Figs. 7A and B. The remarkable characteristic of region I is that it comprises eight additional amino-acid residues in K_{out} channels compared to K_{in} channels (Fig. 7A). Swapping the region I (Figs. 7A and B) from KAT1 to SKOR and vice versa resulted in channels which were electrically silent in oocytes. Additionally, upon co-expression with the KAT1 and SKOR wild-types these chimeras showed no significant effect on the rectification behavior of the channels. Likewise, single mutations in the region I of SKOR (mutated positions marked with asterisks in Fig. 7A) resulted either in non-functional channels or in channels with gating properties not significantly different from those of the SKOR wild-type (not shown). Among the mutations generated in the S6 segment (Fig. 7A, II, mutated positions marked with asterisks) the triple mutant SKOR-D312N-M313L-I314G substantially changed the rectification behavior of SKOR. These three residues in S6 appear to encode a fingerprint for K_{out} and K_{in} channels. In K_{out} channels, a DM[*V/I*] motif is found whereas K_{in} channels have a NLG motif instead. The swapping of this motif resulted in a channel (SKOR-D312N-M313L-I314G) which showed no rectification anymore in the voltage-interval tolerated by oocytes (Fig. 7C). It behaved like an open K^+-selective pore (Fig. 7D), indicating that in Shaker-like plant K^+ channels part of the S6 segment plays an important role in determining voltage-dependent rectification.

Conclusion

This study indicates that the plant K_{in} channel KAT1 still mediates potassium uptake even when the cytoplasmic N-terminus, the cytoplasmic C-terminus, and the voltage-sensing S4 segment were exchanged by the corresponding parts of the plant K_{out} channel SKOR. In previous studies, these three parts of the KAT1 channel were correlated with voltage-dependent gating. It might be speculated that the molecular machinery responsible for voltage-sensing is similar in plant K_{out} and K_{in} channels. The molecular entities defining the link between V-sensing and gating, i.e., the character of rectification, hyperpolarization-activated or depolarization-activated, are very likely located in different positions of the polypeptides. One possible candidate is the NLG (K_{in}) and DM[*V/I*] (K_{out}) motif in the last transmembrane domain S6. However, since the exchange of this motif in a K_{out} channel only eliminated depolarization-activated gating but did not convert it into hyperpolarization-activated gating, we have to conclude that also other, so far unknown, motifs strongly contribute to the setting of the gating properties. The identification of these additional motifs will be the challenge of future studies.

Acknowledgments

This work was partly supported by a Marie Curie Fellowship of the European Union to I.D. (Contract No. ERBBIO4CT985058, Proposal No. 980115) and by the GABI-Génoplante joint programs (GABI FKZ 0312852, GENOPLANTE contract Nr. AF2001093). I.D. is grateful to Frédéric Gaymard, Jossia Boucherez, and Isabelle Chérel (Montpellier) for initial help in setting up the project, and to Bernd Mueller-Roeber (Potsdam-Golm) for lab space and support in the final phase of the project.

References

[1] H. Sentenac, N. Bonneaud, M. Minet, F. Lacroute, J.M. Salmon, F. Gaymard, C. Grignon, Cloning and expression in yeast of a plant potassium ion transport system, Science 256 (1992) 663–665.

[2] J.A. Anderson, S.S. Huprikar, L.V. Kochian, W.J. Lucas, R.F. Gaber, Functional expression of a probable *Arabidopsis thaliana* potassium channel in *Saccharomyces cerevisiae*, Proc. Natl. Acad. Sci. USA 89 (1992) 3736–3740.

[3] N. Uozumi, T. Nakamura, J.I. Schroeder, S. Muto, Determination of transmembrane topology of an inward-rectifying potassium channel from *Arabidopsis thaliana* based on functional expression in *Escherichia coli*, Proc. Natl. Acad. Sci. USA 95 (1998) 9773–9778.

[4] I. Dreyer, S. Antunes, T. Hoshi, B. Mueller-Roeber, K. Palme, O. Pongs, B. Reintanz, R. Hedrich, Plant K^+ channel alpha-subunits assemble indiscriminately, Biophys. J. 72 (1997) 2143–2150.

[5] F. Gaymard, M. Cerutti, C. Horeau, G. Lemaillet, S. Urbach, M. Ravallec, G. Devauchelle, H. Sentenac, J.B. Thibaud, The baculovirus/insect cell system as an alternative to *Xenopus* oocytes. First characterization of the AKT1 K^+ channel from *Arabidopsis thaliana*, J. Biol. Chem. 271 (1996) 22863–22870.

[6] D.P. Schachtman, J.I. Schroeder, W.J. Lucas, J.A. Anderson, R.F. Gaber, Expression of an inward-rectifying potassium channel by the *Arabidopsis* KAT1 cDNA, Science 258 (1992) 1654–1658.

[7] G. Pilot, B. Lacombe, F. Gaymard, I. Cherel, J. Boucherez, J.B. Thibaud, H. Sentenac, Guard cell inward K^+ channel activity in *Arabidopsis* involves expression of the twin channel subunits KAT1 and KAT2, J. Biol. Chem. 276 (2001) 3215–3221.

[8] K. Mouline, A.A. Very, F. Gaymard, J. Boucherez, G. Pilot, M. Devic, D. Bouchez, J.B. Thibaud, H. Sentenac, Pollen tube development and competitive ability are impaired by disruption of a Shaker K^+ channel in *Arabidopsis*, Genes Dev. 16 (2002) 339–350.

[9] F. Gaymard, G. Pilot, B. Lacombe, D. Bouchez, D. Bruneau, J. Boucherez, N. Michaux-Ferriere, J.B. Thibaud, H. Sentenac, Identification and disruption of a plant shaker-like outward channel involved in K^+ release into the xylem sap, Cell 94 (1998) 647–655.

[10] P. Ache, D. Becker, N. Ivashikina, P. Dietrich, M.R. Roelfsema, R. Hedrich, GORK, a delayed outward rectifier expressed in guard cells of *Arabidopsis thaliana*, is a K^+-selective, K^+-sensing ion channel, FEBS Lett. 486 (2000) 93–98.

[11] Y. Cao, J.M. Ward, W.B. Kelly, A.M. Ichida, R.F. Gaber, J.A. Anderson, N. Uozumi, J.I. Schroeder, N.M. Crawford, Multiple genes, tissue specificity, and expression-dependent modulation contribute to the functional diversity of potassium channels in *Arabidopsis thaliana*, Plant Physiol. 109 (1995) 1093–1106.

[12] K.A. Ketchum, C.W. Slayman, Isolation of an ion channel gene from *Arabidopsis thaliana* using the H5 signature sequence from voltage-dependent K^+ channels, FEBS Lett. 378 (1996) 19–26.

[13] I. Marten, S. Hoth, R. Deeken, P. Ache, K.A. Ketchum, T. Hoshi, R. Hedrich, AKT3, a phloem-localized K^+ channel, is blocked by protons, Proc. Natl. Acad. Sci. USA 96 (1999) 7581–7586.

[14] B. Lacombe, G. Pilot, E. Michard, F. Gaymard, H. Sentenac, J.B. Thibaud, A shaker-like K^+ channel with weak rectification is expressed in both source and sink phloem tissues of *Arabidopsis*, Plant Cell 12 (2000) 837–851.

[15] I. Dreyer, E. Michard, B. Lacombe, J.B. Thibaud, A plant Shaker-like K^+ channel switches between two distinct gating modes resulting in either inward-rectifying or leak current, FEBS Lett. 505 (2001) 233–239.

[16] B. Reintanz, A. Szyroki, N. Ivashikina, P. Ache, M. Godde, D. Becker, K. Palme, R. Hedrich, AtKC1, a silent *Arabidopsis* potassium channel alpha -subunit modulates root hair K^+ influx, Proc. Natl. Acad. Sci. USA 99 (2002) 4079–4084.

[17] I. Marten, T. Hoshi, Voltage-dependent gating characteristics of the K^+ channel KAT1 depend on the N and C termini, Proc. Natl. Acad. Sci. USA 94 (1997) 3448–3453.

[18] I. Marten, T. Hoshi, The N-terminus of the K channel KAT1 controls its voltage-dependent gating by altering the membrane electric field, Biophys. J. 74 (1998) 2953–2962.

[19] Y. Cao, N.M. Crawford, J.I. Schroeder, Amino terminus and the first four membrane-spanning segments of the *Arabidopsis* K^+ channel KAT1 confer inward-rectification property of plant–animal chimeric channels, J. Biol. Chem. 270 (1995) 17697–17701.

[20] P.C. Zei, R.W. Aldrich, Voltage-dependent gating of single wild-type and S4 mutant KAT1 inward rectifier potassium channels, J. Gen. Physiol. 112 (1998) 679–713.

[21] R. Latorre, R. Olcese, C. Basso, C. Gonzalez, F. Munoz, D. Cosmelli, O. Alvarez, Molecular coupling between voltage sensor and pore opening in the *Arabidopsis* inward rectifier K^+ channel KAT1, J. Gen. Physiol. 122 (2003) 459–469.

[22] R. Latorre, F. Munoz, C. Gozalez, D. Cosmelli, Structure and function of potassium channels in plants: some inferences about the molecular origin of inward rectification in KAT1 channels, Mol. Membr. Biol. 20 (2003) 19–25.

[23] F.M. Ausubel, R. Brent, R.E. Kingston, D.D. Moore, J.G. Seidam, J.A. Smith, K. Struhl, Current Protocols in Molecular Biology, Green Publishing Associates, John Wiley & Sons, USA, 1993.

[24] M. Minet, M.E. Dufour, F. Lacroute, Complementation of *Saccharomyces cerevisiae* auxotrophic mutants by *Arabidopsis thaliana* cDNAs, Plant J. 2 (1992) 417–422.

[25] R. Ros, G. Lemaillet, A.G. Fonrouge-Desbrosses, P. Daram, M. Enjuto, J.M. Salmon, J.B. Thibaud, H. Sentenac, Molecular determinants of the *Arabidopsis* AKT1 K^+ channel ionic selectivity investigated by expression in yeast of randomly mutated channels, Physiol. Plantarum 105 (1999) 459–468.

[26] E.R. Liman, J. Tytgat, P. Hess, Subunit stoichiometry of a mammalian K^+ channel determined by construction of multimeric cDNAs, Neuron 9 (1992) 861–871.

[27] D. Becker, I. Dreyer, S. Hoth, J.D. Reid, H. Busch, M. Lehnen, K. Palme, R. Hedrich, Changes in voltage activation, Cs^+ sensitivity, and ion permeability in H5 mutants of the plant K^+ channel KAT1, Proc. Natl. Acad. Sci. USA 93 (1996) 8123–8128.

[28] A. Bertl, H. Bihler, C. Kettner, C.L. Slayman, Electrophysiology in the eukaryotic model cell *Saccharomyces cerevisiae*, Pflugers Arch. 436 (1998) 999–1013.

[29] I. Dreyer, F. Poree, A. Schneider, J. Mittelstädt, A. Bertl, H. Sentenac, J.B. Thibaud, B. Mueller-Roeber, Assembly of plant *Shaker*-like K_{out} channels requires two distinct sites of the channel alpha-subunit, Biophys. J. 87 (2004) 858–872.

[30] Y. Jiang, A. Lee, J. Chen, V. Ruta, M. Cadene, B.T. Chait, R. MacKinnon, X-ray structure of a voltage-dependent K^+ channel, Nature 423 (2003) 33–41.

[31] L.G. Cuello, D.M. Cortes, E. Perozo, Molecular architecture of the KvAP voltage-dependent K^+ channel in a lipid bilayer, Science 306 (2004) 491–495.

[32] R. Mannikko, F. Elinder, H.P. Larsson, Voltage-sensing mechanism is conserved among ion channels gated by opposite voltages, Nature 419 (2002) 837–841.

⇒ zurück zur Übersicht

2005

Riaño-Pachón, **Dreyer**, Mueller-Roeber

Orphan transcripts in *Arabidopsis thaliana*: identification of several hundred previously unrecognised genes.

Plant J. **43**:205-212.

The Plant Journal (2005) **43**, 205–212 doi: 10.1111/j.1365-313X.2005.02438.x

Orphan transcripts in *Arabidopsis thaliana*: identification of several hundred previously unrecognized genes

Diego Mauricio Riaño-Pachón[1,2], Ingo Dreyer[1,2] and Bernd Mueller-Roeber[1,2,*]

[1]*Department of Molecular Biology, Institute for Biochemistry and Biology, University of Potsdam, Karl-Liebknecht-Str. 25, Haus 20, D-14476 Golm/Potsdam, Germany, and*

[2]*Cooperative Research Group, Max-Planck Institute of Molecular Plant Physiology, Am Mühlenberg 1, D-14476 Golm/Potsdam, Germany*

Received 11 January 2005; revised 15 April 2005; accepted 21 April 2005.
*For correspondence (fax +49 331 977 2512; e-mail: bmr@rz.uni-potsdam.de).

Summary

Expressed sequence tags (ESTs) represent a huge resource for the discovery of previously unknown genetic information and functional genome assignment. In this study we screened a collection of 178 292 ESTs from *Arabidopsis thaliana* by testing them against previously annotated genes of the Arabidopsis genome. We identified several hundreds of new transcripts that match the Arabidopsis genome at so far unassigned loci. The transcriptional activity of these loci was independently confirmed by comparison with the Salk Whole Genome Array Data. To a large extent, the newly identified transcriptionally active genomic regions do not encode 'classic' proteins, but instead generate non-coding RNAs and/or small peptide-coding RNAs of presently unknown biological function. More than 560 transcripts identified in this study are not represented by the Affymetrix GeneChip arrays currently widely used for expression profiling in *A. thaliana*. Our data strongly support the hypothesis that numerous previously unknown genes exist in the Arabidopsis genome.

Keywords: Arabidopsis, expressed sequence tags, genome annotation, ncRNAs, peptides.

Introduction

Life relies on the activity of thousands of genes and their gene products (proteins, rRNAs, tRNAs, microRNAs and other non-coding RNAs) that coordinately and dynamically interact at the cellular and whole-organism level to establish developmental and physiological processes. Today, the genome composition of an appreciable number of organisms is known, including more than 150 bacteria and archaea, as well as several uni- and multicellular eukaryotes. A full understanding of the genome's complexity and activity requires that all gene products of a genome are identified and assigned with respect to their biological function. Therefore, the large-scale identification of expressed genes has been a major task for researchers over the last years. For more than a decade (Adams *et al.*, 1991) expressed sequence tags (ESTs) were obtained from a large number of organisms and tissues, stored in public and private databases, and often employed as a source for gene identification. Because ESTs are derived from cDNA (and hence mRNA) populations, the vast majority of them code for proteins. In addition, it is now also evident that mRNA species exist that encode relatively short peptides, that may exert important biological functions (Cock and McCormick, 2001; Olsen *et al.*, 2002; Wen *et al.*, 2004). Thus, one can therefore expect that a certain fraction of available ESTs code for such small peptides. Because of experimental design, cDNA collections may also contain molecules that are not derived from mRNAs, but rather from non-coding RNAs, including rRNAs, tRNAs and others.

Recently, a DNA microarray-based technology has allowed to measure the transcriptional activity of a plant's complete genome (Whole Genome Array, Yamada *et al.*, 2003). The data obtained with such a genome tiling array provide an unbiased measurement of the transcriptional activity of each individual genomic region, even if not annotated yet as a functional gene. However, whole-genome tiling arrays are currently not commercially available, excluding their broad exploitation in most research laboratories. Besides whole-genome tiling arrays, the analysis of existing EST data may assist in the identification of previously unrecognized transcribed genomic regions.

Because genome annotation often relies on the presence of relatively long open reading frames (and hence protein-coding sequences) derived from cDNA/EST sequences, non-coding gene products and peptide-coding genes are often overlooked. Here, we specifically screened for ESTs that could be assigned to their genomic counterparts but for which no underlying genes have been described before. Previous to this study, different groups have employed EST data to refine the annotation of the *Arabidopsis thaliana* genome (Wortman *et al.*, 2003; Zhu *et al.*, 2003). These groups had concentrated their efforts on the annotation of protein-coding genes, and did not analyse non-annotated transcribed regions to a large extent. Here, we describe a systematic search for transcribed regions of the Arabidopsis genome which have not been annotated before. Information on these 'orphan' transcripts is provided in an easily browsable database.

Results and discussion

Transcriptional activity of new locations of the Arabidopsis genome

Expressed sequence tags are generally derived from transcribed mRNA and, hence, represent the fraction of the genome that is transcriptionally active. To extract and analyse ESTs for which no annotation in the Arabidopsis genome has been reported before we employed the following step-wise screening protocol (Figure 1).

The complete *A. thaliana* EST collection was downloaded from The Arabidopsis Information Resource (TAIR, http://www.arabidopsis.org, accessed on: 15 February 2003. 178 292 sequences). A first inspection revealed that 195 of these sequences were duplicated entries; consequently they were removed from the data set (Figure 1(i)). The remaining sequences (178 097 ESTs) were clustered by means of the stackPACK™ system (Miller *et al.*, 1999). The clustering allowed to group and align overlapping ESTs into contigs that are represented as consensus sequences. At the end of this step 148 666 ESTs were clustered in 20 717 contigs, while 29 431 ESTs remained as single sequences (Figure 1(ii)). To identify among these 50 148 sequences those ESTs and contigs that are represented by known and already annotated genes, a series of BLAST searches was performed against several databases using various search criteria (Table 1). These combined approaches allowed to link 46 205 of the 50 148 sequences to known annotated genes (Figure 1(iii)). These sequences were discarded from the data set. The remaining 3943 sequences were analysed further in a two-step process in order to find the chromosomal locations within the Arabidopsis genome. First, the preliminary chromosomal coordinates of each sequence was determined by performing a BLAST search against chromosomal sequences downloaded from The Institute for Genomic Research website (TIGR, http://www.tigr.org, release: January 2004). An alignment of at least 50% of the length of the query sequence against a chromosomal region with an *e*-value smaller than 10^{-4} was arbitrarily chosen as the cut-off criterion for locating a sequence on the chromosome. Subsequently, for positive hits, the genomic region reported by BLAST was extended by 2000 bases on each side. The expanded region was extracted from the chromosome-sequence database using the program 'extractseq' from the EMBOSS package (Rice *et al.*, 2000), and the extracted

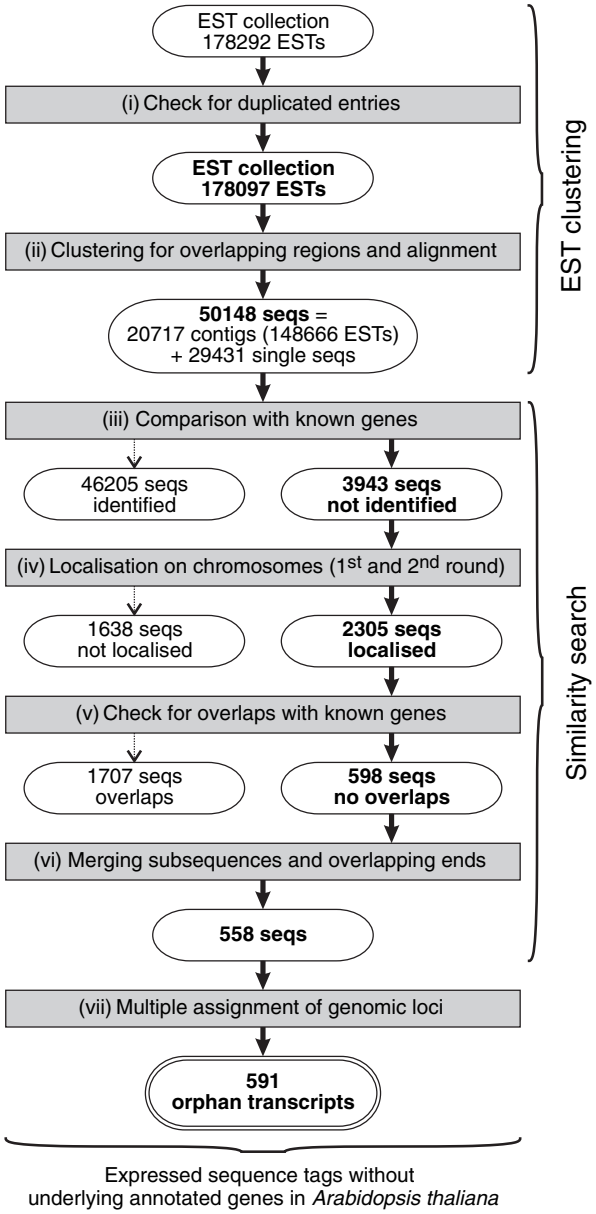

Figure 1. Flow scheme to illustrate the identification of orphan expressed sequence tags (ESTs). Computational processes are represented by shadowed rectangles, sequences by round boxes. Details are given in the text.

Table 1 Databases and criteria used to perform BLAST searches. The first and second series of searches were performed as described by the Schroeder lab (http://www-biology.ucsd.edu/labs/schroeder/howandwhy.html), initially used to match Affymetrix probes to the *Arabidopsis thaliana* genome. Search criteria for series 3–7 were established in-house and employed softer, but still reliable, criteria to identify remaining sequences. The sixth and seventh searches differ in that the former needs an alignment with more than 70% of amino acid identity, while the last requires at least 70% conserved amino acids; conservation is evaluated using the substitution matrix BLOSUM62

Series	Databases searched against	Criteria to consider a hit as identified	Identified	Remaining, not identified
1	Predicted coding sequences from TIGR[a] cDNA Salk Collection Gene sequences, including introns and UTRs[a]	Bases aligned ≥100 Identity >98%	37258	12890
2	Predicted coding sequences from TIGR Gene sequences, including introns and UTRs	Bases aligned ≥50 Identity = 100%	1122	11768
3	Same as in 1	Bases aligned ≥300 Identity >96%	1992	9776
4	Same as in 1	Aligned ≥50% of sequence Identity >70% *e*-value <0.001	5267	4509
5	Predicted coding sequences from chloroplasts Predicted coding sequences from mitochondria	Same as in 4	70	4439
6	UniProt[b]	Same as in 4	362	4077
7	Same as in 6	Aligned ≥50% of sequence Conservation >70% *e*-value <0.001	134	3943
Total			46205	

[a]The Institute for Genomic Research, January 2004 (http://www.tigr.org).
[b]UniProt, release 1.2, Feb 2004 (http://www.expasy.uniprot.org).

region was then aligned to the corresponding EST using the program 'est2genome'. This program aligns spliced DNA (e.g. EST) to non-spliced DNA allowing the recognition of introns of arbitrary length and the detection of splicing sites (Mott, 1997). This strategy, however, failed to locate all sequences on the five Arabidopsis chromosomes. Therefore, to pinpoint the location of the remaining sequences on the chromosomes an alternative strategy was applied. In the first step a modified BLAST search against the chromosomal sequences was conducted, collecting all hits with an *e*-value smaller than 10^{-3}. In the second step, all those hits for a given sequence that were located on both, the same chromosome and the same DNA strand, were joined, and the maximum and minimum chromosome locations reported by BLAST were extracted. In step 3 the entire region flanked by these coordinates, expanded by 2000 bases on each side, was extracted from the chromosome and used for an alignment with the expressed sequences employing 'est2genome' (Figure 1(iv)). Collectively, 2305 previously unmatched sequences were precisely located on the chromosomes. The remaining 1638 sequences that could not be localized accurately were excluded from further analyses.

The genomic counterparts of the 2305 sequences were extracted, and used for further studies. The coordinates of each sequence were compared against chromosome tables obtained from XML files from TIGR website (http://www.tigr.org, release: January 2004), which contain the chromosomal coordinates of each annotated gene. This comparison allowed to identify regions with more than 10% overlap between expressed sequences and known genes in 1707 of the 2305 cases (Figure 1(v)). These sequences were considered as identified transcripts of known genes and consequently excluded from further analysis. The set of the remaining 598 sequences is redundant in the sense that some sequences are subsequences of others, and that there are overlapping pairs which represent the 3′ and 5′ end of one single transcript. After merging (Figure 1(vi)), 558 transcripts remained. Considering that some of these sequences represent more than one EST (because some ESTs were joined into clusters by the stackPACK™ system), 879 original ESTs remained, representing 0.49% of the original set of EST sequences (178 292).

Thirty of the 558 sequences were mapped to more than one location of the Arabidopsis genome: 28 sequences were assigned to two genomic loci, one sequence was assigned to three loci, and one sequence was assigned to four loci. With one of these locations the similarity was always close to 100%, while it was more divergent (78 ± 12% identity) when compared with the other loci, strongly suggesting that these secondary assignments correspond to duplicated genes (for an example see Figure 2). In total, 591 loci were discovered (Figure 1(vii)), matching 558 previously unassigned transcripts. In the following, we concentrated our analysis on this set of genomic regions, and called them orphan transcripts, abbreviated as At_oRNA_xxx (with xxx representing any number between 001 and 591. We established a database, AtoRNADB, available via the World Wide Web at http://atornadb.bio.uni-potsdam.de/, to display sequences

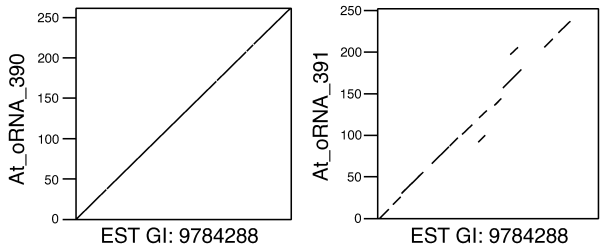

Figure 2. The sequence GI: 9784288 was assigned to two different genomic loci. Polydotplot of EST GI:9784288 and its corresponding genomic loci (At_oRNA_390, and At_oRNA_391). A line represents the region of similarity between the two compared sequences.

and sequence features of the orphan transcripts, alignments of original ESTs with their genomic source counterparts and chromosomal positions of the orphan transcripts. Additional information describing features of the orphan transcripts is provided in the Supplementary Material S1–S10 which are available in the online version of the journal.

The percentage of orphan transcripts represented by a single EST was 69.5% of the whole pool. Orphan transcripts detected by two, three, four and five ESTs accounted for 18.1, 6.8, 2.2 and 0.8% of the pool, respectively. The remaining orphan transcripts (2.6%) were represented by more than five (up to 27) ESTs. Therefore, most of the identified transcripts arose from loci that are expressed at a relatively weak to moderate level. Evidence for transcription was also obtained by comparison with the data generated by the Arabidopsis Massively Parallel Signature Sequencing (MPSS) program (http://mpss.udel.edu/at; download November 2004). MPSS generates short sequence signatures for a defined position within an mRNA. The abundance of these signatures in a given cDNA library indicates the expression level of that gene. Only 35 orphan transcripts produced hits against the collection of 17-bp long MPSS tags, consistent with a relatively low expression level of the identified loci, or their cell-specific expression patterns. However, it cannot be excluded that some of the orphan transcripts represent only a fragment of the transcriptional unit they originated from. Therefore, we extended the sequence of each orphan transcript over 500 bp at its 3′-end, and compared this enlarged unit with the MPSS signatures. This approach allowed us to assign an MPSS signature to 341 orphan transcripts. Among these 341 MPSS signatures 164 (48.1%) have not been assigned to any known gene in *A. thaliana*. In 130 additional cases the orphan transcript and the associated annotated gene carrying the MPSS signature were on opposite strands suggesting that the nearest MPSS signature did not belong to the orphan transcript. In 10 cases the MPSS signatures found were assigned to an annotated gene on a different chromosome. In this context it should be noted that in a related recent study MPSS data were used to identify unknown genes in Arabidopsis (Meyers *et al.*, 2004). The analyses by Meyers *et al.* (2004) and the data presented in our study clearly indicate the presence of orphan transcripts and therefore the existence of several overlooked genes in the Arabidopsis genome. The lack of a complete overlap of the orphan transcripts detected in the present study with the MPSS data set illustrates the complementary character of the two different approaches (using EST and MPSS data).

The 591 sequences are evenly distributed along the five Arabidopsis chromosomes, with the exception of the centromeric regions and a high peak on chromosome 2, at the short arm close to the centromere. The alignment of 121 of the 591 sequences required the prediction of an intron to obtain a reliable alignment with the genome, showing that these transcripts were processed after transcription. Additionally, only nine orphan transcripts are highly conserved between *A. thaliana* and *Oryza sativa* (rice), including At_oRNA_141 (see below). Thirty-two additional transcripts are weakly conserved between the two species (Supplementary Material S10).

Experimental confirmation of transcriptional activity

Inspection of the Salk Whole Genome Array data (WGA; Yamada *et al.*, 2003) allowed us to independently verify the transcriptional activity of 587 of the 591 identified genomic locations. The WGA repository contains information about the transcriptional activity of the whole Arabidopsis genome in five different experimental conditions: (i) light-grown seedlings, (ii) anthers, (iii) flowers (mixed stages), (iv) roots and (v) suspension cell culture. Some of the orphan transcripts (e.g. At_oRNA_115 and At_oRNA_534) showed a relatively high expression level in several experiments assayed with the WGA. Some others were preferentially expressed only in some ‘experiments’ (i.e. tissues): At_oRNA_311, for example, showed a higher hybridization signal in light-grown seedlings and roots, than in suspension cell culture, anthers and flowers (mixed stages). Four orphan transcripts lacked any hybridization signal in the WGA data. However, for two of them (At_oRNA_466 and At_oRNA_565) other supporting evidence for transcriptional activity (cDNA or MPSS data) was obtained. Of the remaining two orphan transcripts one (At_oRNA_467) is a predicted protein-coding RNA (see below), and the other (At_oRNA_566) corresponds to a known bacterial vector sequence. Surprisingly, our analysis also identified two further vector sequences in the Arabidopsis genome (At_oRNA_141 and At_oRNA_413), which, according to WGA data, are transcribed.

Thus, for at least 99.6% of the 591 unassigned genomic loci further independent experimental evidence for transcriptional activity was obtained.

A subset of sequences represents known ncRNAs

To further characterize the orphan transcripts, a series of BLAST searches against different databases was conducted. Details of the results are provided in Supplementary Material S1. In the following we present a short summary of the main results (Tables 2 and 3): (i) As mentioned above, three sequences had perfect matches with bacterial vector sequences which might be regarded as an error in the assembled Arabidopsis genomic sequence. (ii) Seven sequences were assigned to ribosomal RNAs in *A. thaliana*. (iii) One sequence was found to represent a tRNA, and (iv) 21 sequences were correlated with other known non-coding RNAs (ncRNAs). Among them were sequences which were similar to known small nucleolar RNAs (snoRNAs; Brown *et al.*, 2003b); and some of these carried more than one snoRNA (Figure 3; Supplementary Material S2) reflecting the fact that some snoRNAs are processed from polycistronic pre-snoRNAs (Brown *et al.*, 2003a; Leader *et al.*, 1997).

Besides sequence similarities, the secondary structure of the RNA may also provide useful information to assign orphan transcripts to existing RNA families. Therefore, we compared our data set with structural models for RNA families (Griffiths-Jones *et al.*, 2003), deposited in the Rfam database (Table 3). Rfam confirmed the results obtained by BLAST searches for 12 of the orphan transcripts. Additionally, one orphan transcript was assigned to an RNA family that had not been assigned before with BLAST searches. Conversely, some ncRNAs that were identified through BLAST were not identified by Rfam. Therefore, BLAST and Rfam searches complemented each other.

The Arabidopsis Small RNA Project (http://cgrb.orst.edu/smallRNA/db/) collects experimental information about small RNAs in *A. thaliana*. Eleven of the orphan transcripts identified in this work were similar to small RNAs (Supplementary Material S1), indicating that either they are themselves small RNAs, or alternatively that they are targeted by small RNAs. Experimental evidence for small RNAs is increasing rapidly. Therefore, we expect that the number of orphan transcripts matching small RNAs will rise in the near feature.

Table 3 Orphan transcripts identified as ncRNAs through Rfam searches. The data set of orphan transcripts was searched against a collection of covariance models (Rfam; http://www.sanger.ac.uk/Software/Rfam/). The cut-off parameters used to decide a significant match were those employed to build the corresponding RNA family, as reported for each model in Rfam

Sequence	Model name	Model number	Rfam 6.0 score
At_oRNA_119	U14	RF00016	66.08
At_oRNA_290[a]	Intron_gpII	RF00029	45.34
At_oRNA_401	U25	RF00054	49.76
At_oRNA_422	SSU_rRNA_5	RF00177	447.29
At_oRNA_423	SSU_rRNA_5	RF00177	448.15
At_oRNA_426	tRNA	RF00005	57.32
At_oRNA_439	U14	RF00016	62.67
At_oRNA_500	snoR37	RF00213	41.97
At_oRNA_513	snoZ7	RF00268	37.61
At_oRNA_548	snoZ223	RF00135	59.85
At_oRNA_549	snoZ223	RF00135	59.85
At_oRNA_557	snoZ105	RF00145	34.41
	U15	RF00067	39.42
At_oRNA_587	snoZ195	RF00133	9.98

Rfam searches missed the sequences representing the 28S rRNA, and most of the snoRNAs.
[a]The sequence At_oRNA_290 was not found with a BLAST search.

Search for known protein motifs in orphan transcript-encoded polypeptides

In the final step we tested whether any of the orphan transcripts identified in our screen would encode a protein with known protein motifs. Therefore, sequences of orphan

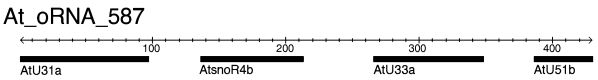

Figure 3. The transcript At_oRNA_587 is a polycistronic pre-snoRNA. It carries four different snoRNAs, all belonging to the class Box C/D according to Brown *et al.* (2003b).

Table 2 Orphan transcripts identified as ncRNAs through BLAST searches. Summary of the results obtained with BLAST searches; number of sequences per category and identifiers in At oRNA DB. For details see Supplementary Material S1 and http://atornadb.bio.uni-potsdam.de

Category	Number of seqs	Identifier
Vectors	3	At_oRNA_141, At_oRNA_413, At_oRNA_566
rRNA	7	At_oRNA_092, At_oRNA_093, At_oRNA_372, At_oRNA_422, At_oRNA_423, At_oRNA_567, At_oRNA_568
tRNA	1(1)[a]	At_oRNA_426, (At_oRNA_425)[a]
Other ncRNAs	21	At_oRNA_017, At_oRNA_119, At_oRNA_125, At_oRNA_134, At_oRNA_139, At_oRNA_140, At_oRNA_290, At_oRNA_401, At_oRNA_439, At_oRNA_485, At_oRNA_486, At_oRNA_500, At_oRNA_510, At_oRNA_513, At_oRNA_522, At_oRNA_542, At_oRNA_548, At_oRNA_549, At_oRNA_555, At_oRNA_557, At_oRNA_587

[a]The sequence At_oRNA_425 matched to a tRNA using a BLAST search, but the result could not be confirmed by the program tRNAscan-SE (Lowe and Eddy, 1997). Both, At_oRNA_425 and At_oRNA_426 are two genomic assignments for the same transcript. Therefore, it is possible that At_oRNA_425 is a non-functional version of the gene represented by At_oRNA_426.

transcripts were translated into all six reading frames and the deduced peptides/proteins were scanned by means of the InterProScan program (Zdobnov and Apweiler, 2001) against several pattern and profile databases (see Experimental procedures). Only 42 sequences matched to known protein motifs (Supplementary Material S3). We therefore applied the three gene prediction programs Unveil (Majoros *et al.*, 2003), Genscan (Burge and Karlin, 1997) and GlimmerM (Majoros *et al.*, 2003) to analyse the 591-sequence data set for transcripts exhibiting a sequence bias characteristic of protein-coding genes. We found that 192 of 591 sequences had exons predicted by at least two of the programs. When comparing the results obtained from the protein motif search and the gene prediction programs, all sequences with predicted motifs/domains were found to be present in the set of predicted exons. Additionally, two sequences, for which exons were predicted, were similar to snoRNAs. In one case (At_oRNA_125) the snoRNA appeared to match a sequence predicted to be an intron by the gene prediction programs. In the other case (At_oRNA_513) the snoRNA overlapped with one predicted exon. Both cases are rare in *A. thaliana* because intronic snoRNAs are not common in this genome (Brown *et al.*, 2003a).

Representation of orphan sequences on the Affymetrix chip array

Transcript profiling is often used to study simultaneously the activity status of thousands of genes. A prominent method employs Affymetrix GeneChip arrays. The Arabidopsis AtGenome1 Array was the first-generation Arabidopsis array which measured the relative transcript levels of approximately 8300 genes. The more recent ATH1 Arabidopsis Genome Array contains more than 22 500 so-called probe sets representing approximately 24 000 Arabidopsis genes (Liu *et al.*, 2003). We were interested to know how many of the orphan transcripts identified here are represented by the arrays. Our analysis found that only 18 of 591 sequences (3%) are represented by chip AtGenome1, 10 of them matching five or more probes (Supplementary Material S4), and only five of the 591 sequences (<1%) are represented by the ATH1 Genome Array; none by more than three probes. Thus, more than 580 transcribed genomic regions are not yet served by the Affymetrix ATH1 Genome Array.

Conclusions

The Arabidopsis genome contains expressed loci which have been almost totally overlooked so far. In this study, 591 expressed, unrecognized genomic loci were identified. Twenty-nine of these produce non-coding RNAs of different classes, 192 transcripts have characteristics typical of protein-coding genes. The remaining 369 transcripts do not have matches to any known gene, neither protein-coding nor non-coding. The many overlooked Arabidopsis genes that we discovered here may provide a fertile ground for further experimental analyses. In this context, the set of Arabidopsis non-coding RNAs may be of particular interest. Our data analysis provides independent proof for the presence of a large number of transcribed regions of the Arabidopsis genome and confirms recent experimental results obtained by testing the Arabidopsis transcriptional activity on a genome-wide scale, using whole-genome tiling arrays (Yamada *et al.*, 2003). In addition, they provide information about the minimal length of the transcribed regions which apparently is more difficult to extract from tiling arrays alone. They also deliver information about exon–intron structures and the precise fusion of exons in the mature transcripts. Importantly, the vast majority of transcriptionally active genes discovered here on the basis of EST data does not overlap with the transcriptionally active genomic loci identified using MPSS (Meyers *et al.*, 2004), and also does most likely not include micro-RNA genes. Hence, the sofar discovered transcriptionally active regions of the Arabidopsis genome almost certainly do not cover the complete set of active genes in the plant. Future work has to include (i) the analysis of the transcriptional activity in highly differentiated (but often under-represented) cell types, and (ii) the search for transcripts that typically do not harbour poly-(A)-tails at their 3′-ends to include those originating from atypical transcriptional activities.

Recent data indicate that large portions of human chromosomes 21 and 22 are transcribed into non-coding RNAs (Kampa *et al.*, 2004; Kapranov *et al.*, 2002), and Sémon and Duret (2004) provided evidence that functional transcription units cover at least half of the human genome. Also, analysis of the mouse transcriptome, based on the functional annotation of more than 60 770 cDNAs, revealed a large number of non-coding messages (Okazaki *et al.*, 2002). The functional role of the vast majority of the transcripts remains almost totally unexplored at the current stage, but interestingly, non-coding RNAs are emerging as a rapidly growing class of regulatory transcripts important for a number of biological processes, including translational control, abiotic and biotic signalling, differentiation and others (Erdmann *et al.*, 2001; Hüttenhofer *et al.*, 2002).

Experimental procedures

All procedures were run on an Intel Pentium 4 computer powered by SuSe Linux 8.1. The stackPACK^{TM} system (Miller *et al.*, 1999) was employed to cluster sequences based on overlapping regions and to obtain consensus sequences (for a description of the clustering procedure see the stackPACK^{TM} Manual). BLAST databases were created and formatted locally, and standalone BLAST programs were run. Results were filtered by means of PERL scripts specially written for this purpose, using BioPerl modules (http://www.bioperl.org). Rfam database files (Griffiths-

Jones *et al.*, 2003), release 6.0, were downloaded from http://www.sanger.ac.uk/Software/Rfam/ftp.shtml. Rfam is a collection of Stochastic Context Free Grammars (SCFG) of RNA families. Before the SCFG search, a BLAST search for each orphan transcript against the sequences belonging to each SCFG was carried out. This allowed us to perform the SCFG search only with those models which had hits with orphan transcripts. The SCFG search was performed employing the program INFERNAL (Eddy, 2002), using as thresholds the values found in the threshold file from the Rfam database. InterProScan (Zdobnov and Apweiler, 2001) was employed to find known protein motifs in orphan transcripts computationally translated in all possible reading frames. Six-frame translated orphan transcripts were scanned against all InterPro member databases (http://www.ebi.ac.uk/InterProScan). Orphan transcripts were analysed with three different gene prediction programs, Unveil (Majoros *et al.*, 2003), Genscan (Burge and Karlin, 1997) and GlimmerM (Majoros *et al.*, 2003). All three programs were prepared to detect Arabidopsis genes, with the training sets provided by the authors of the programs.

Acknowledgements

Financial support was provided by the 'Ministerium für Wissenschaft, Forschung und Kultur' (MWFK) of the State Brandenburg, Germany, and the Interdisciplinary Research Centre 'Advanced Protein Technologies' (IZ-APT) of the University of Potsdam. Bernd Mueller-Roeber thanks the Fonds der Chemischen Industrie for financial support (no. 0164389). The authors are grateful to Dr Roy O'Mahony for comments on the manuscript and to three anonymous reviewers for helpful comments.

Supplementary Material

The following supplementary material is available for this article online:

Text S1. Results from BLAST searches against several ncRNA databases

Figure S2. Some orphan transcripts carry snoRNAs.

Table S3. Protein motifs found in orphan transcripts

Table S4. Representation of orphan sequences on the Affymetrix chip arrays

Table S5. Summary information for orphan transcripts in At oRNA DB

Table S6. ESTs per orphan transcript

Table S7. Interesting cases about some orphan transcripts that overlap annotated genes

Table S8. List of orphan transcripts overlapping with known transcriptional units

Table S9. Annotated genes closest to orphan transcripts

Table S10. Conserved orphan transcripts in rice (*Oryza sativa*)

The *Arabidopsis thaliana* orphan RNA database is accessible via http://atornadb.bio.uni-potsdam.de.

References

Adams, M.D., Kelley, J.M., Gocayne, J.D., Dubnick, M., Polymeropoulos, M.H., Xiao, H., Merril, C.R., Wu, A., Olde, B. and Moreno, R.F. (1991) Complementary DNA sequencing: Expressed Sequence Tags and Human Genome Project. *Science*, **252**, 1651–1656.

Brown, J.S.W., Echeverria, M. and Qu, L.H. (2003a) Plant snoRNAs: functional evolution and new modes of gene expression. *Trends Plant Sci.* **8**, 42–49.

Brown, J.S.W., Echeverria, M., Qu, L.H., Lowe, T.M., Bachellerie, J.P., Huttenhofer, A., Kastenmayer, J.P., Green, P.J., Shaw, P. and Marshall, D.F. (2003b) Plant snoRNA database. *Nucleic Acids Res.* **31**, 432–435.

Burge, C. and Karlin, S. (1997) Prediction of complete gene structures in human genomic DNA. *J. Mol. Biol.* **268**, 78–94.

Cock, J.M. and McCormick, S. (2001) A large family of genes that share homology with CLAVATA3. *Plant Physiol.* **126**, 939–942.

Eddy, S.R. (2002) A memory efficient dynamic programming algorithm for optimal structural alignment of a sequence to an RNA secondary structure. *BMC Bioinformatics*, **3**, 18.

Erdmann, V.A., Barciszewska, M.Z., Hochberg, A., de Groot, N. and Barciszewski, J. (2001) Regulatory RNAs. *Cell. Mol. Life Sci.* **58**, 960–977.

Griffiths-Jones, S., Bateman, A., Marshall, M., Khanna, A. and Eddy, S.R. (2003) Rfam: an RNA family database. *Nucleic Acids Res.* **31**, 439–441.

Hüttenhofer, A., Brosius, J. and Bachellerie, J.P. (2002) RNomics: identification and function of small, non-messenger RNAs. *Curr. Opin. Chem. Biol.* **6**, 835–843.

Kampa, D., Cheng, J., Kapranov, P. *et al.* (2004) Novel RNAs identified from an in-depth analysis of the transcriptome of human chromosomes 21 and 22. *Genome Res.* **14**, 331–342.

Kapranov, P., Cawley, S.E., Drenkow, J., Bekiranov, S., Strausberg, R.L., Fodor, S.P. and Gingeras, T.R. (2002) Large-scale transcriptional activity in chromosomes 21 and 22. *Science*, **296**, 916–919.

Leader, D.J., Clark, G.P., Watters, J., Beven, A.F., Shaw, P.J. and Brown, J.W.S. (1997) Clusters of multiple different nucleolar RNA genes in plants are expressed as and processed from polycistronic pre-snoRNAs. *EMBO J.* **16**, 5742–5751.

Liu, G., Loraine, A.E., Shigeta, R., Cline, M., Cheng, J., Valmeekam, V., Sun, S., Kulp, D. and Siani-Rose, M.A. (2003) NetAffx: Affymetrix probesets and annotations. *Nucleic Acids Res.* **31**, 82–86.

Lowe, T.M. and Eddy, S.R. (1997) tRNAscan-SE: a program for improved detection of transfer RNA genes in genomic sequence. *Nucleic Acids Res.* **25**, 955–964.

Majoros, W.H., Pertea, M., Antonescu, C. and Salzberg, S.L. (2003) GlimmerM, Exonomy and Unveil: three *ab initio* eukaryotic genefinders. *Nucleic Acids Res.* **31**, 3601–3604.

Meyers, B.C., Vu, T.H., Singh Tej, S., Ghazal, H., Matvienko, M., Agrawal, V., Ning, J. and Haudenschild, C.D. (2004) Analysis of the transcriptional complexity of *Arabidopsis thaliana* by massively parallel signature sequencing. *Nat. Biotechnol.* **22**, 1006–1011.

Miller, R.T., Christoffels, A.G., Gopalakrishnan, C., Burke, J., Ptitsyn, A.A., Broveak, T.R. and Hide, W.A. (1999) A comprehensive approach to clustering of expressed human gene sequence: The Sequence Tag Alignment and Consensus Knowledgebase. *Genome Res.* **9**, 1143–1155.

Mott, R. (1997) EST_GENOME: a program to align spliced DNA sequences to unspliced genomic DNA. *Comput. Appl. Biosci.* **13**, 477–478.

Okazaki, Y., Furuno, M., Kasukawa, T. *et al.* (2002) Analysis of the mouse transcriptome based on functional annotation of 60 770 full-length cDNAs. *Nature*, **420**, 563–573.

Olsen, A.N., Mundy, J. and Skriver, K. (2002) Peptomics, identification of novel cationic *Arabidopsis* peptides with conserved sequence motif. *In silico Biol.* **2**, 441–451.

Rice, P., Longden, I. and Bleasby, A. (2000) EMBOSS: The European Molecular Biology Open Software Suite. *Trends Genet.* **16**, 276–277.

Sémon, M. and Duret, L. (2004) Evidence that functional transcription units cover at least half of the human genome. *Trends Genet.* **20**, 229–232.

Wen, J., Lease, K.A. and Walker, J.C. (2004) DVL, a novel class of small polypeptides: overexpression alters *Arabidopsis* development. *Plant J.* **37**, 668–677.

Wortman, J.R., Haas, B.J., Hannick, L.I. *et al.* (2003) Annotation of the Arabidopsis genome. *Plant Physiol.* **132**, 461–468.

Yamada, K., Lim, J., Dale, J.M. *et al.* (2003) Empirical analysis of transcriptional activity in the *Arabidopsis* genome. *Science*, **302**, 842–846.

Zdobnov, E.M. and Apweiler, R. (2001) InterProScan – an integration platform for the signature-recognition methods in InterPro. *Bioinformatics*, **17**, 847–848.

Zhu, W., Schlueter, S.D. and Brendel, V. (2003) Refined annotation of the Arabidopsis genome by complete expressed sequence tag mapping. *Plant Physiol.* **132**, 469–484.

⇒ zurück zur Übersicht

2004

Dreyer, Porée, Schneider, Mittelstädt, Bertl, Sentenac, Thibaud, Mueller-Roeber

Assembly of plant *Shaker*-like K_{out} channels requires two distinct sites of the channel alpha-subunit.

Biophys. J. **87**:858-872.

Assembly of Plant *Shaker*-Like K_{out} Channels Requires Two Distinct Sites of the Channel α-Subunit

Ingo Dreyer,*†‡ Fabien Porée,*†‡ Antje Schneider,†‡ Jessica Mittelstädt,† Adam Bertl,§ Hervé Sentenac,* Jean-Baptiste Thibaud,* and Bernd Mueller-Roeber†‡

*Biochimie et Physiologie Moléculaires des Plantes, UMR 5004, Agro-M/CNRS/INRA/UM2, F-34060 Montpellier Cedex 1, France; †Universität Potsdam, Institut für Biochemie und Biologie, Abteilung Molekularbiologie, D-14476 Golm/Potsdam, Germany; ‡Max-Planck Institute of Molecular Plant Physiology, Cooperative Research Group, D-14476 Golm/Potsdam, Gemany; and §Botanisches Institut I, Universität Karlsruhe, 76128 Karlsruhe, Germany

ABSTRACT SKOR and GORK are outward-rectifying plant potassium channels from *Arabidopsis thaliana*. They belong to the *Shaker* superfamily of voltage-dependent K^+ channels. Channels of this class are composed of four α-subunits and subunit assembly is a prerequisite for channel function. In this study the assembly mechanism of SKOR was investigated using the yeast two-hybrid system and functional assays in *Xenopus* oocytes and in yeast. We demonstrate that SKOR and GORK physically interact and assemble into heteromeric K_{out} channels. Deletion mutants and chimeric proteins generated from SKOR and the K_{in} channel α-subunit KAT1 revealed that the cytoplasmic C-terminus of SKOR determines channel assembly. Two domains that are crucial for channel assembly were identified: i), a proximal interacting region comprising a putative cyclic nucleotide-binding domain together with 33 amino acids just upstream of this domain, and ii), a distal interacting region showing some resemblance to the K_T domain of KAT1. Both regions contributed differently to channel assembly. Whereas the proximal interacting region was found to be active on its own, the distal interacting region required an intact proximal interacting region to be active. K_{out} α-subunits did not assemble with K_{in} α-subunits because of the absence of interaction between their assembly sites.

INTRODUCTION

Potassium (K^+) is the most abundant cation in plants and is involved in many cellular processes. The uptake of K^+ and its redistribution throughout the plant is accomplished by a variety of membrane transport systems (for reviews see Dreyer et al., 1999, 2002; Maser et al., 2001; Very and Sentenac, 2002, 2003). Most of the present knowledge in this field concerns K^+ channels of the *Shaker* type, which have been shown to form the major (voltage-gated) K^+ conductance in several cell types and to play physiologically important roles in various K^+ transport processes (Pilot et al., 2003a).

Like their animal relatives, plant *Shaker*-like K^+ channels are composed of four α-subunits. Each subunit displays a hydrophobic core comprising six transmembrane segments, named S1–S6, and a pore forming loop, named P, between S5 and S6. A putative cyclic nucleotide-binding domain (cNBD) is present downstream of the hydrophobic core. Based on phylogenetic analyses it has been shown that the family of plant *Shaker*-like K^+ channels can be subdivided into five subfamilies (Pilot et al., 2003b). However, at the functional level this segregation simplifies to three subfamilies: inwardly rectifying K_{in} channels mediating potassium uptake, outwardly rectifying K_{out} channels mediating potassium release, and weakly rectifying K_{weak} channels thought to be able to mediate both K^+ uptake or release depending on the local K^+ electrochemical gradients. In the model plant *Arabidopsis thaliana*, the nuclear genome comprises a total of nine genes coding for *Shaker*-like K^+ channels. Among those, seven have functionally been characterized: four K_{in}, i.e., KAT1, KAT2, AKT1, and SPIK; one K_{weak}, i.e., AKT2; and two K_{out} channels, i.e., SKOR and GORK (Very and Sentenac, 2002, 2003).

In the case of *Shaker*-type K^+ channels, tetramerization of α-subunits is a prerequisite for pore formation and electric activity (Dreyer et al., 1997). The availability of α-subunits, and the amount of α-subunits assembled into a functional tetrameric complex, is of central cellular importance. The assembly process itself may be regulated according to the physiological needs of the cell. Identifying the protein domains in K^+ channel α-subunits that trigger and contribute to channel assembly is therefore an important task. Previously, various research groups have investigated the assembly of plant K_{in} channels, but not of K_{out} channels. Initial information in this field was provided by three studies in 1997. Using KAT1 as a model, Marten and Hoshi (1997) showed through deletion experiments that the far C-terminus of the α-subunit is not essential for functional channel assembly. KAT1 was still functional when its C-terminal part downstream of the putative cyclic nucleotide-binding domain was deleted. Further deletions toward the N-terminus of the protein resulted in nonfunctional channels (Marten and Hoshi, 1997). In a second study, using a biochemical approach, Daram et al. showed that the C-terminus of AKT1 has the capability to form a homotetrameric

Submitted November 25, 2003, and accepted for publication May 5, 2004.

Address reprint requests to Ingo Dreyer, Universität Potsdam, Institut für Biochemie und Biologie, Abteilung Molekularbiologie, Karl-Liebknecht-Strasse 24-25, Haus 20, D-14476 Golm/Potsdam, Germany. Fax: 49-331-977-2512; E-mail: dreyer@rz.uni-potsdam.de.

0006-3495/04/08/858/15 $2.00

doi: 10.1529/biophysj.103.037671

complex (Daram et al., 1997). Subsequent yeast two-hybrid interaction tests using eight different constructs generated from the AKT1 C-terminus provided more detailed information about protein regions involved in the aggregation process. An internal fragment of 145 amino acid residues, comprising the putative cyclic nucleotide-binding domain, was shown to display self-interaction, suggesting a role in subunit assembly. However, evidence was provided that this region was not the only determinant of C-terminus interaction because C-terminal fragments lacking it still aggregated with others. An additional type of interaction between a domain at the far end of the C-terminus and a region located between transmembrane segment S6 and the putative cyclic nucleotide-binding domain was proposed. In addition to these results, a third type of interaction has been reported. Whereas the far end of the C-terminus (the so called K_{HA} domain) failed to self-interact in the case of AKT1 (Daram et al., 1997), Erhardt et al. observed self- and cross-interactions between the K_{HA} domains of three different K_{in} channels from potato (Ehrhardt et al., 1997).

Plant *Shaker*-type K_{in} α-subunits have not only the capability to homotetramerize. Importantly, different types of K_{in} α-subunits assemble, in different combinations, into heteromeric, electrically fully active K_{in} channels when expressed in heterologous systems (Dreyer et al., 1997), adding a further potential level of regulation, that in part may rely on the interaction domains present in these proteins. Recently, an electrophysiological study on the potato K_{in} channels SKT1 and KST1 related another domain, named K_T, and located directly upstream of the K_{HA} domain, with channel heterotetramerization (Zimmermann et al., 2001).

The above reports provide some aspects about the assembly of plant *Shaker* K_{in} channels. However, the picture is still vague and in part contradictory. Furthermore, none of these studies correlated physical interactions between protein regions with their functional consequences for channel assembly.

This report investigates the assembly behavior of the plant K_{out} channels SKOR and GORK (Gaymard et al., 1998; Ache et al., 2000). Using the yeast two-hybrid system and two different heterologous expression systems (*Xenopus* oocytes and yeast) suitable for functional analyses, we studied intersubunit physical interactions and analyzed their importance for functional channel assembly. We demonstrate that in plant K_{out} channels two distinct domains located in the cytoplasmic C-terminal part of the protein are essential for channel assembly.

MATERIALS AND METHODS

Recombinant DNA techniques

Standard methods of plasmid DNA preparation, PCR, restriction enzyme analysis, agarose gel electrophoresis, and bacterial transformation were applied (Ausubel et al., 1993). Chimeras and mutants were created by PCR-based techniques and with the pAlter mutagenesis system (Promega, Charbonnières, France). Further detailed information concerning the 77 constructs tested in this study will be provided upon request.

Electrophysiology

Xenopus oocytes were injected with a volume of 40 nl of cRNA mixtures. Mixtures indicated in the figure legends were prepared from 1 μg/μl cRNA stock solutions. Control oocytes were injected with 40 nl of deionized water. Two-electrode voltage-clamp experiments were carried out as previously described (in France according to Lacombe and Thibaud, 1998; in Germany according to Becker et al., 1996). External standard solution was composed of 10 mM KCl, 90 mM NaCl, 1 mM $CaCl_2$, 2 mM $MgCl_2$, 10 mM Tris/MES pH 7.0. Patch-clamp experiments on yeast protoplasts were carried out as recently described by Bertl et al. (1998). Standard pipette solution contained 175 mM KCl, 4 mM $MgCl_2$, 4 mM K-ATP, 1 mM EGTA, 152 μM $CaCl_2$, adjusted to pH 7.0 with KOH. Extracellular solution contained 150 mM KCl, 10 mM $CaCl_2$, 5 mM $MgCl_2$, buffered to pH 6.5 with MES/Tris. Measurements were carried out from a holding potential of -40 mV. Currents were evoked by 2.5-s activating voltage pulses from $+100$ mV to -200 mV (20-mV steps).

Yeast complementation

The yeast strain Wagf2 (*ade2-101*; *his3-11,15*; *leu2-3,112*; *trp1-1*; *ura3-1*; *trk1*Δ*::LEU2*; *trk2*Δ*::TRP1*; *can*^{r}) (Ros et al., 1999) is deficient for K^+ uptake and displays reduced growth in physiological conditions, when the external concentration of K^+ is low ($\sim$5 mM). It was used for complementation tests together with two yeast expression plasmids: the multicopy plasmid pFL61 (*URA3* as a selection marker) (Minet et al., 1992), and the centromeric plasmid pFL38His-PGK (*HIS3* as a selection marker) (Ros et al., 1999). Selection minimal medium was based on a synthetic arginine/phosphate medium (Rodriguez-Navarro and Ramos, 1984) containing 2% glucose, 10 mM L-arginine, 150 μM adenine, 2 mM $MgSO_4$, 200 μM $CaCl_2$, 13 μM FeNa-EDTA, 8 μM H_3BO_3, 0.25 μM $CuSO_4$, 0.6 μM KI, 2.7 μM $MnSO_4$, 1 μM Na_2MoO_4, 2.5 μM $ZnSO_4$, 0.5 μM $CoCl_2$, 0.5 μM $NiCl_2$, 1% BME vitamins solution (Sigma, Taufkirchen, Germany, No. B6891), the pH being adjusted to 6.5 using orthophosphoric acid. Solid minimal medium contained additionally 2% (w/v) Agar (Sigma, No. A7921). Yeast transformation was performed according to Gietz et al. (1992). Transformed yeast cells were selected on minimal medium added with 50 mM K^+ (introduced as chloride salt). Complementation growth tests were performed with solid and liquid minimal medium added with 2 mM KCl, a condition not allowing growth of the noncomplemented Wagf2 strain. For the drop tests on solid medium, isolated yeast colonies were preincubated for 12 h in liquid culture containing 50 mM K^+. They were then diluted in fresh culture medium (final absorption at 600 nm of $\sim$0.25) and grown again until the absorption at 600 nm reached 0.6. The cells were collected, washed twice with sterile water, and resuspended in water (the absorption at 600 nm being adjusted to the desired value; see the figure legends).

Yeast two-hybrid interaction tests

The two-hybrid technique was used to identify domains responsible for the assembly of SKOR. Constructs specified in the figures were cloned into the pLexPD vector (van der Ven et al., 2000) in fusion with the LexA DNA-binding domain, and into the pAD-GAL4 vector (Stratagene, Amsterdam, The Netherlands) in fusion with the GAL4 activator domain. Combinations of these constructs were used to cotransform the L40 yeast strain, which has two independent reporter genes, *lacZ* and *HIS3*, under the control of the minimal GAL1 promoter fused to multimerized LexA binding sites. Double transformants were tested for both, growth in the absence of histidine in the medium and for β-galactosidase activity. β-galactosidase activity in liquid culture was determined using ONPG (o-nitrophenyl β-D-galactopyranoside;

Sigma, No. N1127) as substrate according to the Yeast Protocol Handbook (www.clontech.com).

In vivo radioactive protein labeling

Six injected oocytes per construct were kept in 990 μl ND96 (96 mM NaCl, 2 mM KCl, 1 mM $CaCl_2$, 1 mM $MgCl_2$, 10 mM HEPES/NaOH pH 7.4) added with 10 μl of Met-[^{35}S]-label ([^{35}S]-L-methionine, [^{35}S]-L-cysteine, *Escherichia coli* ^{35}S hydrolysate; Hartmann Analytic, Braunschweig, Germany). Oocytes were incubated for 3 days at 18°C. To isolate protein, oocytes were chilled on ice for 10 min, washed twice with ND96, and homogenized in 1 ml 10 mM K-phosphate, pH 7.4, 5 mM EDTA, 5 mM EGTA, 1 mM AEBSF, 2 μg/ml leupeptin, and 1 μg/ml aprotinin. The suspensions were centrifuged for 5 min at 100 $\times$ g. The supernatant was collected and centrifuged again for 30 min at 16,000 $\times$ g. After a washing step with the homogenization medium, the pellet was resuspended in 60 μl gel loading buffer, and incubated for 6 min at 55°C. The amount of radioactivity present in the sample was determined with a liquid scintillation (LS) counter (Beckman Coulter LS6500, Unterschleissheim, Germany). Aliquots corresponding to 10^5 cpm were loaded onto 10% SDS-PAGE gels. After electrophoresis, the gels were dried and exposed to x-ray films overnight at room temperature.

Protein expression in tobacco BY2 protoplasts and targeting of GFP-fusion constructs

Suspension cultures of tobacco BY2 cells (*Nicotiana tabaccum* L. cv. Bright Yellow 2) were maintained in LS medium containing 0.2 mg/l 2,4-dichlorophenoxyacetic acid (2,4-D) in the dark at 26°C. For transformation 10-day-old cultures were harvested by vacuum filtration on a nylon membrane, resuspended (1g/10 ml) in enzyme solution (0.1% pectolyase Y-23, 0.2% driselase, 1% cellulase, 25 mM MES/KOH, 0.6 M mannitol, pH 5.5), and incubated in the dark (shaker, 50 rpm; 35°C; 3 h). Protoplasts were recovered by centrifugation (1200 $\times$ g), washed with HEPES buffer (25 mM HEPES, 0.6 M sorbitol, pH 6.7) and purified by gradient centrifugation (HEPES buffer with 0%, 10%, and 20% Ficoll, 30 min. at 1200 $\times$ g). Protoplasts collected from the interfaces were washed twice with W5 solution (154 mM NaCl, 125 mM $CaCl_2$, 5 mM KCl, 5 mM glucose, 100 mM mannitol, 0.1% MES, pH 5.8) and resuspended to a concentration of 3 $\times$ 10^6 cells/ml in MaMg solution (0.55 M mannitol, 15 mM $MgCl_2$, 0.1% MES, pH 5.8). For the transformation ($\sim$1 $\times$ 10^6 cells per transformation) a heat shock of 45°C was applied for 5 min followed by the immediate cooling on ice for 5 min. Subsequently, the plasmid DNA (containing the coding region of the fusion protein under the control of the CaMV 35S Promoter, 30 μg) and 50 μg of carrier herring sperm DNA were added. After 5-min incubation at room temperature an equal volume of PEG solution (0.1 M $Ca(NO_3)_2$, 0.5 M mannitol, 0.1% MES, pH 6.5, 40% PEG 3350) was added. After an additional 20 min at room temperature the transformation mix was supplemented with 4 ml of culture medium (LS medium + 0.4 M mannitol) and transferred to small Petri dishes. These were incubated at 26°C without shaking in the dark for 2 days. For the analysis of GFP fluorescence, protoplasts were collected by centrifugation (1200 $\times$ g, 5 min) and resuspended in 1.5 ml W5 solution. GFP fluorescence was analyzed by confocal laser scanning microscopy (Leica DM IRBE inverse microscope with Leica TCS SP laser scanning unit).

Mathematical description of yeast growth rate under limiting conditions

Yeast growth was described as follows. Yeast cells, number n, proliferate with a rate $dn/dt = \beta \times n(t) \times r(t)$. Under optimal conditions, i.e., in an infinite volume of liquid culture and with a constant level of ''resources'' needed for growth, e.g., a high concentration of K^+, the resource function $r(t)$ would be set to the constant value of 1. Cells would proliferate with the rate $\beta \times n(t)$ resulting in exponential growth. Under experimental conditions, however, i.e., in a finite volume and with consumption of resources (K^+), the resource function decreases below 1 with cell proliferation. The decrease is defined proportional to the increase in cell number as $dr = -\gamma \times dn$. At the saturation level the resource function is $r(t \rightarrow \infty) = 0$ and therefore $dn/dt = 0$, and $n(t \rightarrow \infty) = n_\infty$. Because the cell number is proportional to the optical density measured at $\lambda = 600$ nm, the n values can be replaced by $OD600$ values without changing the structure of the equations. An analytical solution of the two coupled differential equations is $OD600(t) = (OD_\infty \times OD_0)/[OD_0 + (OD_\infty - OD_0) \times \exp(-t/\tau)]$. OD_0 and OD_∞ denote the optical densities at $t = 0$ and infinity, respectively. The apparent proliferation time constant, τ, is a function of the constants β and γ.

RESULTS

SKOR assembles with GORK but not with KAT1

On the basis of K_{in} and K_{weak} channels it has been proven that *Shaker*-like plant K^+ channel α-subunits can form heteromeric channels (Dreyer et al., 1997; Baizabal-Aguirre et al., 1999; Ache et al., 2001; Pilot et al., 2001; Zimmermann et al., 2001). In this study, a first set of experiments was performed to address the question of whether plant K_{out} channel subunits also contribute to the formation of heteromeric channels. After coexpression of the K_{in} channel α-subunit KAT1 and the K_{out} channel α-subunit SKOR in *Xenopus* oocytes, inward currents activating more negative than -80 mV were observed along with outward currents activating more positive than -20 mV (Fig. 1 *A*). From the analyses of the steady-state current-voltage characteristics, the simplest hypothesis was that the two current components originated from two distinct homomeric entities comprising either KAT1 or SKOR subunits (Fig. 1 *B*; cf. Ache et al., 2000, for KAT1 and GORK expressing oocytes). This interpretation was fully confirmed by coexpressing KAT1 with a dominant-negative mutant of SKOR, dnSKOR (= SKOR-G292R-D293N-A296V). When this mutant was coexpressed with the SKOR wild-type, outward-rectifying K^+ currents were efficiently suppressed. When coexpressed with KAT1, dnSKOR did not affect the current amplitude compared to the control experiment (KAT1/H_2O control: same volume of *KAT1* cRNA and same volume of water injected; not shown). In contrast, the two *Arabidopsis* K_{out} channel α-subunits SKOR and GORK were able to form heteromeric channels. When SKOR was coexpressed with a dominant-negative mutant of GORK, dnGORK (= GORK-G273R-Y274R; Hosy et al., 2003), the level of functional channels, reflected by the observed current amplitude, was significantly reduced compared to the control (SKOR/H_2O; Student's t-test, $P < 10^{-7}$). Similar findings were obtained by testing the combinations SKOR/dnSKOR, GORK/dnSKOR, and GORK/dnGORK (Fig. 1, *C* and *D*). It should be emphasized that the same amount of wild-type *SKOR*-cRNA and *GORK*-cRNA, respectively, was injected in all the oocytes, and that compared experiments were carried out at the same time interval after injection.

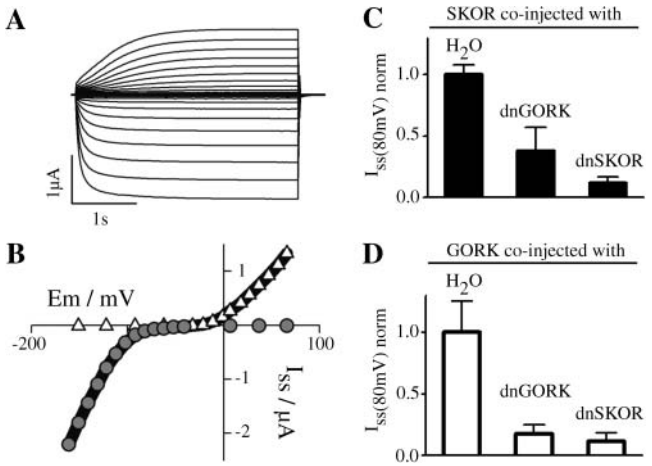

FIGURE 1 SKOR assembles with plant K_{out} but not with plant K_{in} channel α-subunits after coexpression in *Xenopus* oocytes. (*A*) Representative inward and outward K^+ currents obtained from oocytes injected with a *SKOR*/*KAT1* cRNA mixture (1:1 ratio). From a holding potential of −100 mV currents were evoked by 3.5-s activating voltage pulses from −160 mV to +70 mV (10-mV steps). (*B*) Steady-state current-voltage characteristic (*solid line*) for the oocyte shown in *A*, superimposed with the respective current-voltage relationship for homomeric KAT1 (*shaded circles*) and SKOR (*open triangles*). (*C* and *D*) Steady-state K^+ current amplitudes after coexpression (1/1 cRNA mixtures) of SKOR (*C*) and GORK (*D*) with dominant-negative mutants of SKOR (dnSKOR = SKOR-G292R-D293N-A296V) and GORK (dnGORK = GORK-G273R-Y274R). Current amplitudes were measured at the end of 3-s voltage pulses to +80 mV. To compare results obtained from different oocyte batches, the data were normalized to the mean value (I_{ss}) of the respective controls SKOR/H_2O and GORK/H_2O. Data are shown as means ± SD (n = 6–17, two different oocyte batches).

Furthermore, coexpression of a dominant-negative mutant of KAT1 (KAT1-G262R-Y263R) with SKOR and GORK affected neither the current amplitude of SKOR nor that of GORK (not shown). Therefore it could be excluded that reduced current amplitudes in coexpression experiments involving SKOR/dnSKOR, GORK/dnGORK, SKOR/dnGORK, and GORK/dnSKOR resulted from a saturation of the translation machinery of the oocyte due to an increased amount of injected cRNA. Thus, the above data clearly demonstrated that K_{out} channel α-subunits encoded by different genes form heteromeric K_{out} channels, whereas they do not coassemble with the K_{in} channel subunit KAT1.

The cytoplasmic C-terminal part of SKOR comprises the assembly domain

The region responsible for assembly of SKOR channels was narrowed down by coexpressing the entire SKOR α-subunit with N- and C-terminal truncations of itself (Fig. 2 *A*). The C-terminal deletion, SKOR-ΔCt, corresponds to the SKOR polypeptide extending from the N-terminus to the fourth transmembrane segment (S4), whereas the N-terminal deletion, SKOR-ΔNt, represents the SKOR polypeptide spanning from the fourth transmembrane region to the C-terminus. The two truncated α-subunits had different effects on the functional expression of SKOR channels. The amplitudes of the K^+ currents measured in oocytes injected with mixtures of *SKOR*/H_2O (Fig. 2 *A*, *left traces*) and *SKOR*/*SKOR*-Δ*Ct* (Fig. 2 *A*, *middle traces*) did not differ markedly from each other. The steady-state current amplitudes at +40 mV were $I_{40mV} = 1.76 \pm 0.12$ μA and 1.58 ± 0.19 μA, respectively (Fig. 2 *B*). In contrast, in oocytes injected with *SKOR*/*SKOR*-Δ*Nt* the formation of functional channels was reduced to ~20% (Fig. 2, *A* (*right traces*) and *B*). Oocytes expressing SKOR-ΔNt, SKOR-ΔCt, or SKOR-ΔNt/SKOR-ΔCt did not display any currents significantly different from the baseline in control oocytes injected with water only (not shown). Collectively, these results suggested that the assembly domain of SKOR is located in the channel region downstream of S4. Hence, the formation of functional tetrameric structures in the case of plant K_{out} channels appears not to involve an assembly domain at the N-terminus, which contrasts with the situation known from animal *Shaker* channels. Instead, assembly of plant K_{out} channels appears to be triggered via a domain(s) located at the C-terminus, like in plant K_{in} channels or animal EAG channels. To test this hypothesis further, the C-terminal part of KAT1, which is supposed to comprise the assembly domain of the channel (Marten and Hoshi, 1997), was replaced by the C-terminus of SKOR. Unfortunately, the chimera KAT1-Ct_{SKOR} appeared to be nonfunctional in oocytes: under different experimental conditions (different bath pH and K^+ concentrations), no currents different from the baseline could be elicited in the voltage interval from −170 mV to +80 mV (not shown). On the other hand, the chimera complemented the Wagf2 (Δ*trk1,2*) yeast strain (Ros et al., 1999), which is deficient in potassium uptake (Fig. 2, *C* (*left bottom*) and *D* (*open circles*)). This yeast strain, which does not display significant growth on media containing <5 mM K^+, is auxotroph for two selection markers, histidine and uracil, enabling coexpression experiments. Taking advantage of these properties in a subsequent set of experiments, the cDNAs encoding two channel α-subunits, namely KAT1 and the KAT1-Ct_{SKOR} chimera, were cloned into the low-copy (centromeric) plasmid pFL38His-PGK containing the *HIS3* marker, and those of three potential effectors, dnSKOR, SKOR-ΔCt, and SKOR-ΔNt, were cloned into the multicopy plasmid pFL61 carrying *URA3* as a marker. Yeast cells were cotransformed with pairwise combinations of these constructs and the empty vectors, and selected for the simultaneous presence of the two marker genes on K^+-rich (50 mM) medium. Positive colonies were subsequently tested for their ability to grow in low K^+ (2 mM) medium. Independent of the absence or presence of dnSKOR, SKOR-ΔCt, and SKOR-ΔNt, the empty pFL38His-PGK plasmid did not allow the mutant yeast to grow in this medium (Fig. 2, *C* (*top*) and *D* (*dashed-dotted line*)). The positive control experiment showed that yeast growth supported by KAT1 was not affected by any of

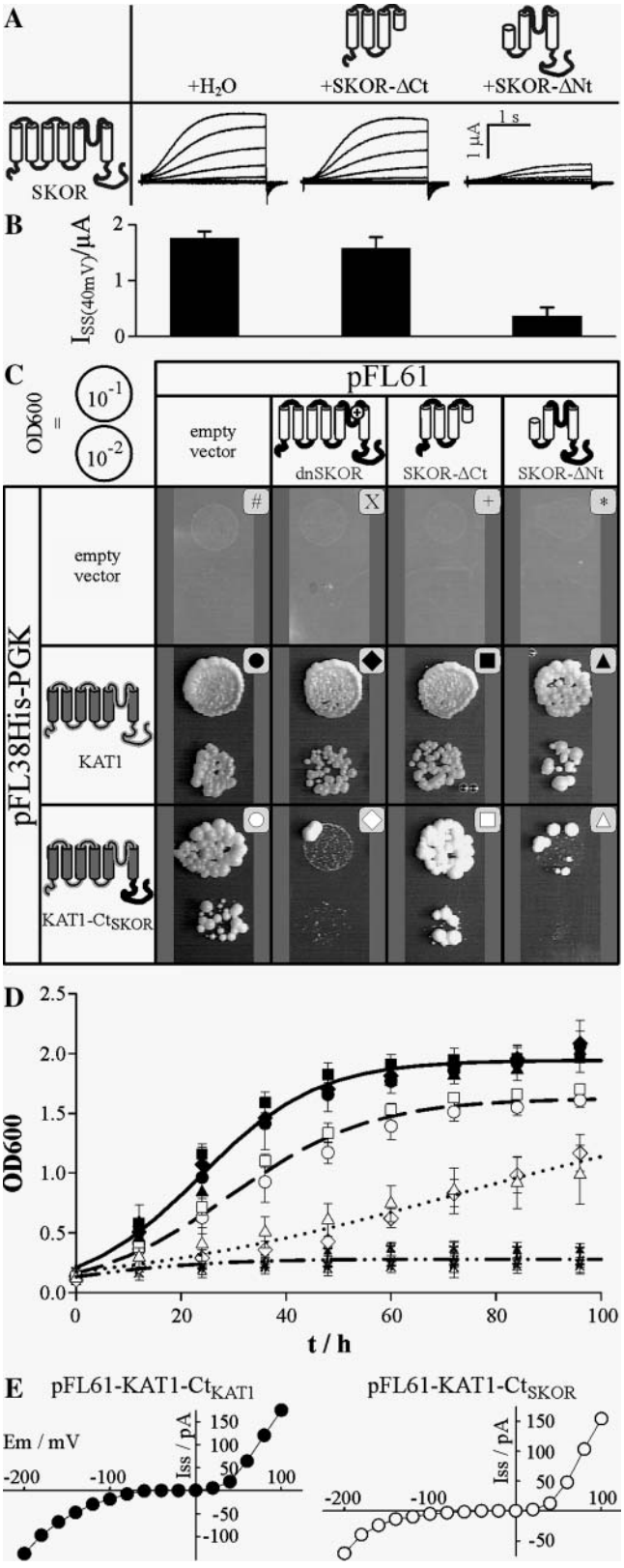

FIGURE 2 The assembly domain of SKOR is located in the cytoplasmic C-terminal part. (*A* and *B*) Coexpression of SKOR with N-terminally (SKOR-ΔNt = SKOR-M1_D172del-I173M-I174V, nomenclature according to den Dunnen and Antonarakis, 2001) and C-terminally (SKOR-ΔCt = SKOR-I211X-N212_T828del; X, stop codon) truncated SKOR proteins in *Xenopus* oocytes. (*A*) Representative K^+ currents obtained from oocytes injected with *SKOR*/*SKOR-ΔNt* (*right traces*), *SKOR*/*SKOR-ΔCt* (*middle traces*), and *SKOR*/H_2O (*left traces*) cRNA (1:1) mixtures. From a holding potential of −100 mV currents were evoked by 3-s activating voltage pulses from −120 mV to +60 mV (20-mV steps). (*B*) Mean ± SD of current amplitudes (I_{SS}) measured at the end of 3-s voltage pulses to +40 mV (n = 5–13). The data correspond to the tested combinations shown in panel *A*. (*C* and *D*) Coexpression of KAT1 and the chimera KAT1-Ct_{SKOR} (= KAT1-M1_R305-SKOR-T333_T828) with the N- and C-terminally truncated SKOR proteins SKOR-ΔNt and SKOR-ΔCt, and the dominant-negative mutant dnSKOR in the K^+ uptake deficient yeast strain Wagf2. (*C*) Drop test on solid medium. Isolated yeast colonies were preincubated overnight in liquid culture containing 50 mM K^+. After two washing steps the optical density of the cell suspension at 600 nm was adjusted to 0.1 and 0.01, respectively. These suspensions (10 μl) were dropped on plates containing 2 mM K^+ ($OD600 = 0.1$, *upper spot* in each part of the figure; $OD600 = 0.01$, *lower spot*). Plates were incubated for 5 days at 30°C. (*D*) Growth test in liquid medium. Liquid minimal medium containing 2 mM K^+ was inoculated with different yeast transformants pretreated as described in *C* so that the optical density was ~0.15. Cultures were incubated at 30°C on a shaker (190 rpm). At the time points indicated the OD600 was determined. For an explanation of the symbols, see panel *C*. Lines represent best fits with the equation $OD600(t) = (OD_\infty \times OD_0)/[OD_0 + (OD_\infty - OD_0) \times \exp(-t/\tau)]$ describing growth under limited conditions. Here, OD_0 and OD_∞ denote the optical densities at $t = 0$ and infinity, respectively. The apparent proliferation time constant is τ. Because the 12 data sets cluster into four groups, within which they do not differ significantly from each other, only one representative fit is displayed for each group. One group comprises the data obtained with KAT1 as target (*solid symbols*, *solid line*): $OD_0 = 0.21$, $OD_\infty = 1.94$, $\tau = 11.2$ h. A second group includes the control data from the empty pFL38H-PGK vector (#, X, +, *, *dashed-dotted line*): $OD_0 = 0.20$, $OD_\infty = 0.28$. A third group contains the data obtained with the chimera KAT1-Ct_{SKOR} alone and in coexpression with SKOR-ΔCt (*open circles* and *open squares*, *dashed line*): $OD_0 = 0.16$, $OD_\infty = 1.62$, $\tau = 13.4$ h. The fourth group consists of data gained with the chimera KAT1-Ct_{SKOR} as target in coexpression with dnSKOR and SKOR-ΔNt (*open diamonds* and *open triangles*, *dotted line*): $OD_0 = 0.17$, $OD_\infty = 1.64$, $\tau = 33.9$ h. The data represent the means ± SD of three to four independent samples. (*E*) Representative steady-state current-voltage characteristics obtained from patch-clamped Wagf2 yeast cells expressing a pFL61-KAT1-Ct_{KAT1} construct (*left*) and a pFL61-KAT1-Ct_{SKOR} construct (*right*). Note that outward currents at positive potentials are flowing through the depolarization-activated endogenous TOK1 channel. Data are representative for four repeats.

the SKOR-based constructs (Fig. 2, *C* (*middle*) and *D* (*solid symbols*)). This observation confirmed the result obtained in oocytes, where KAT1 did not functionally interact with SKOR. In contrast, yeast growth mediated by the chimera KAT1-Ct_{SKOR} (Fig. 2 *C*, *bottom*) was selectively inhibited by dnSKOR and SKOR-ΔNt (Fig. 2 *D*, *open diamonds* and *open triangles*), whereas the presence of SKOR-ΔCt had no inhibiting effect (Fig. 2 *D*, *open squares*). By fitting the time course of yeast growth with a mathematical function that describes growth under limiting nutrient (K^+) conditions (Fig. 2 *D*, *lines*), we were able to quantify and interpret the differences between the distinct genotypes in the following way. The growth of KAT1 expressing cells saturated at an optical density of $OD_\infty = 1.9$, whereas growth of the cells expressing KAT1-Ct_{SKOR} did at $OD_\infty = 1.6$, indicating a less

efficient exploitation of the limiting K^+ resource by the chimera in comparison with the wild-type KAT1. Additionally, yeast cells coexpressing KAT1-Ct_{SKOR} and dnSKOR, or SKOR-ΔNt, showed a τ-value 2.5 times larger than the control (KAT1-Ct_{SKOR}/empty pFL61). This is equivalent to a 40% reduction in the proliferation rate constant β (see Materials and Methods), likely to be the consequence of a reduced potassium uptake rate in these cells. The whole set of data therefore indicated that the chimera KAT1-Ct_{SKOR}, by interacting with dnSKOR and SKOR-ΔNt in yeast, exhibited the same behavior as SKOR in *Xenopus* oocytes. Thus, KAT1-Ct_{SKOR} combined characteristic functional features of the parental channels KAT1 and SKOR: from KAT1 it inherited the ability to complement a potassium uptake-deficient yeast strain, and from SKOR it inherited its assembly domain located at the C-terminus. This conclusion was further substantiated by electrophysiological studies of yeast cells transformed with a pFL61-KAT1-Ct_{SKOR} construct. Patch-clamp analyses and comparisons with yeast cells transformed with a pFL61-KAT1-Ct_{KAT1} construct indicated that this chimera mediated potassium inward currents (Fig. 2 *E*).

The role of the putative cyclic-nucleotide binding domain in SKOR channel assembly

To gain further clues on the molecular basis of SKOR channel assembly, its cytoplasmic C-terminus was analyzed for the presence of functional domains. Sequence comparisons with motifs in protein databases and in other plant K^+ channels identified three domains (Fig. 3 *A*). The region from L419 to H511 shows high homology (40% identity) to the motif pfam00027 (http://www.sanger.ac.uk/Software/Pfam/index.shtml) representing a cyclic-nucleotide binding domain (cNBD). The region from D580 to R709 contains six ankyrin motif repeats (forming the so-called ankyrin domain; Sentenac et al., 1992; Gaymard et al., 1998). The region from G774 to T828 (K_{HA}) is rich in acidic amino acid residues similar to the K_{HA}-domain previously characterized in the potato K_{in} channel KST1 (Ehrhardt et al., 1997). To uncover the role of the different domains, deletions in both, the SKOR wild-type polypeptide and the dominant-negative mutant dnSKOR were generated. The deleted polypeptide SKOR-ΔcNBD (= SKOR-D438_L506del; nomenclature according to den Dunnen and Antonarakis, 2001) lacks 69 amino acid residues within the putative cNBD, and SKOR-Δ746 (= SKOR-K746X-E747_T828del; X, stop codon) lacks the last 83 residues of the polypeptide including the K_{HA} domain (last 55 amino acids). After expression in oocytes, SKOR-Δ746 mediated potassium currents reminiscent of the wild-type SKOR channel (not specifically illustrated, but see Fig. 3 *B*, *shaded columns*), whereas SKOR-ΔcNBD remained electrically silent (not shown). In coexpression experiments only dnSKOR-Δ746 was found to affect the expression level of functional SKOR channels

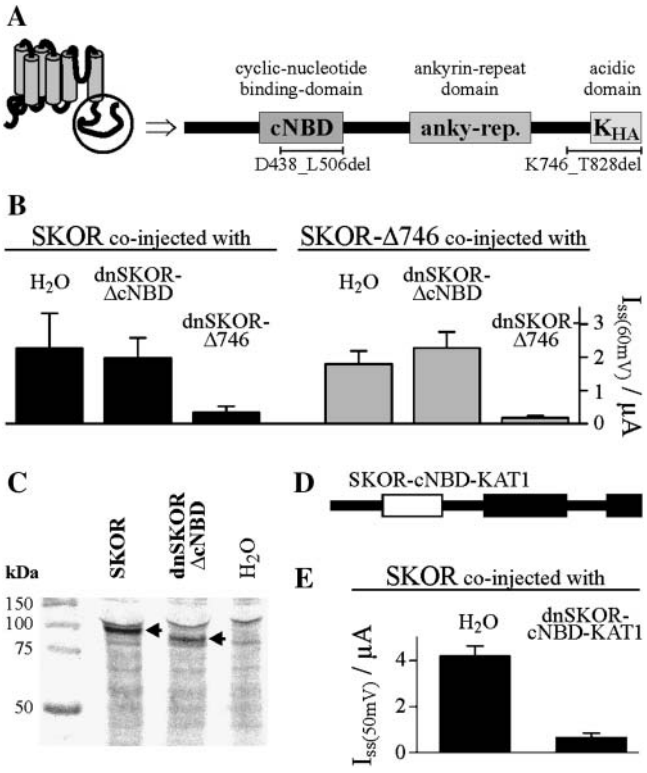

FIGURE 3 The putative cyclic-nucleotide binding domain, but not the acidic domain, is essential for SKOR assembly. (*A*) Schematic representation of the cytoplasmic SKOR C-terminus. The C-terminus contains three regions showing strong homology to previously characterized functional domains: a cyclic-nucleotide binding domain (*cNBD*), an ankyrin domain (*anky-rep.*), and an acidic domain (K_{HA}). (*B*) K^+ current amplitudes (I_{SS}) measured in oocytes after coexpression (injection of 1:1 cRNA mixtures) of SKOR (*solid columns*) and SKOR-Δ746 (= SKOR-K746X-E747_T828del, *shaded columns*), respectively, with dominant-negative mutants of SKOR-Δ746 (dnSKOR-Δ746 = SKOR-G292R-D293N-A296V-K746X-E747_T828del, *right columns*) and SKOR-ΔcNBD (dnSKOR-ΔcNBD = SKOR-G292R-D293N-A296V-D438_L506del, *middle columns*), and H_2O (*left columns*). Current amplitudes were measured at the end of 3-s voltage pulses to +60 mV. Data are shown as means ± SD (n = 3–6). (*C*) The protein dnSKOR-ΔcNBD is expressed in *Xenopus* oocytes. ^{35}S-labeled proteins obtained from water-injected control oocytes (*right lane*) and oocytes injected with *SKOR* or *dnSKOR-ΔcNBD* cRNA, respectively (*left* and *middle lanes*). Proteins were analyzed by SDS-PAGE followed by autoradiography. Molecular weight markers are on the left. Calculated molecular weights are 93.9 kDa for SKOR, and 86.1 kDa for dnSKOR-ΔcNBD. Arrows indicate the heterologously expressed proteins. (*D*) C-terminus of the chimera dnSKOR-cNBD-KAT1. The cNBD of SKOR (fragment SKOR-E410_L530) was replaced by the cNBD of KAT1 (fragment KAT1-N384_L493, *white rectangle*). (*E*) K^+ current amplitudes (I_{SS}) measured in oocytes after coexpression (injection of 1:1 cRNA mixtures) of SKOR with the dominant-negative mutant dnSKOR-cNBD-KAT1 (*right column*) or H_2O (*left column*). Current amplitudes were measured at the end of 3-s voltage pulses to +50 mV. Data are shown as means ± SD (n = 5–6).

(estimated from the amplitude of the exogenous currents): as shown in Fig. 3 *B* (*solid columns*), the presence of the dnSKOR-Δ746 α-subunit resulted in an ~85% decrease in current amplitude, whereas the presence of dnSKOR-

ΔcNBD did not significantly affect the current of SKOR. Similar results were obtained using SKOR-Δ746 as target α-subunit (Fig. 3 *B*, *shaded columns*). When compared with SKOR-Δ746 expressing oocytes, current amplitudes were strongly reduced in oocytes coexpressing SKOR-Δ746 and dnSKOR-Δ746. In contrast, a reduction of functionally active channels was not observed after coinjection of *SKOR-Δ746/dnSKOR-ΔcNBD* cRNA mixtures. The lack of currents in oocytes injected with *SKOR-ΔcNBD* cRNA, and the absence of any effect of dnSKOR-ΔcNBD in coexpression studies could be caused by some disruption of an essential assembly domain due to the deletion in the cNBD. Alternatively, it is possible that the protein encoded by the modified *(dn)SKOR-ΔcNBD* cRNAs or even the cRNA itself is rapidly degraded in oocytes. If this were the case, dnSKOR-ΔcNBD polypeptides would not be able to interact with SKOR α-subunits. To check for this possibility, three batches of oocytes injected with *SKOR*-cRNA, *dnSKOR-ΔcNBD*-cRNA, or H_2O, respectively, were incubated with ^{35}S-labeled methionine and cysteine. After 3 days of incubation, proteins were extracted from the oocytes, separated by SDS-PAGE, and visualized by autoradiography (Fig. 3 *C*). The lane corresponding to SKOR-injected oocytes specifically displayed a band close to the 100-kDa marker (*left lane*). The deletion of 69 amino acids in dnSKOR-ΔcNBD resulted in a band with a slightly smaller apparent molecular weight (*middle lane*). Both bands were absent from H_2O-injected control oocytes (Fig. 3 *C*, *right lane*). The position of the two polypeptide bands corresponded quite well with the theoretical calculations of 93.9 kDa and 86.1 kDa for the molecular weight of monomeric SKOR and dnSKOR-ΔcNBD, respectively. Thus, the polypeptide dnSKOR-ΔcNBD was expressed in oocytes. However, an investigation of the subcellular localization of a GFP-dnSKOR-ΔcNBD fusion protein in tobacco BY2 cells using a confocal laser scanning microscope revealed that it was not targeted to the plasmamembrane. Instead it accumulated in the ER (not shown), a result well known for mutants of animal channel proteins that exhibit a distorted or disrupted assembly behavior (Ma and Jan, 2002; Jenke et al., 2003).

To unravel the role of the cNBD in SKOR channel assembly the entire cyclic nucleotide-binding domain of the mutant dnSKOR (dnSKOR-E410_L520) was replaced by the corresponding domain of KAT1 (KAT1-N384_L493, Fig. 3 *D*). The two cNBDs are supposed to have a similar structure but share an identity of only 30% (for comparison: the cNBDs of SKOR and GORK are 70% identical). Upon coexpression with the SKOR wild type the dnSKOR-cNBD-KAT1 chimeric protein displayed a dominant-negative behavior (Fig. 3 *E*) identical to the mutant dnSKOR-cNBD-SKOR (= dnSKOR; Fig. 1 *C*). We concluded that in the deletion mutants (dn)SKOR-ΔcNBD misfolding of the polypeptide likely disrupted functional channel assembly and affected its targeting. This defect could be compensated by the presence of the KAT1-cNBD. Therefore it appears that the cNBD is essential for SKOR assembly by maintaining the structural integrity of the protein. The cNBD, itself, however, does not determine the specificity of the assembly.

Two-hybrid analyses to map physical interactions within the C-terminal region

To gain further insights into the assembly behavior of SKOR physical protein-protein interactions were tested employing the yeast two-hybrid system. In a first set of experiments, the cytoplasmic C-termini downstream of the membrane-spanning domains of SKOR and GORK were fused to the LexA DNA binding domain and to the GAL4 activator domain. After pairwise coexpression in yeast, growth on histidine-free medium and expression of β-galactosidase activity were detected in all possible combinations (Fig. 4 *A*). These results indicated that the C-terminus of SKOR, which comprises the domain(s) required for channel assembly (compare Figs. 2 and 3), does physically self-interact. The fact that identical results were obtained for both, the C-terminus of SKOR and GORK, suggests a similar assembly mechanism for the two plant K_{out} channels. Finally, the physical interaction between Ct-SKOR and Ct-GORK revealed by the two hybrid tests (Fig. 4) is very likely a major reason for the formation of heteromeric channels in *Xenopus* oocytes (Fig. 1, *C* and *D*).

In a following set of experiments, seven regions of the C-terminus of SKOR were defined and named A–G (Fig. 4 *B*). Nine deletions were generated as shown in Fig. 4 *B*. The construct ABCDEF- is identical to the C-terminus of the mutant SKOR-Δ746, and AB-DEFG to the C-terminus of dnSKOR-ΔcNBD. Unfortunately, six of the nine constructs fused to the LexA DNA binding domain in pLexPD showed autoactivity when cotransformed with the empty plasmid pAD-GAL4 and tested for growth on histidine-free medium. Two-hybrid combinations involving these six constructs were consequently not further considered for analyses of β-galactosidase activities. Twenty-five construct pairs were tested for protein-protein interactions in both reporter assays (Fig. 4 *C*). The following results were obtained: When the cNBD was deleted (AB-DEFG) no positive signal could be observed in any of the combinations tested, indicating that the presence of the cNBD, maintaining the structural integrity of the polypeptide, is essential not only for channel assembly but also for the physical interaction of the C-termini of both, SKOR and GORK. The cNBD alone apparently was not actively involved in establishing the interaction because the two-hybrid tests were negative when any one of the tested constructs was restricted to the cNBD alone (--C----), or to a region starting with this domain and ending at the channel C-terminus (--CDEFG). The fact that the constructs ABC---- and -BCDEFG interacted with Ct-SKOR (whereas --CDEFG did not), suggested that region B (representing a 33 amino acid stretch just upstream of the

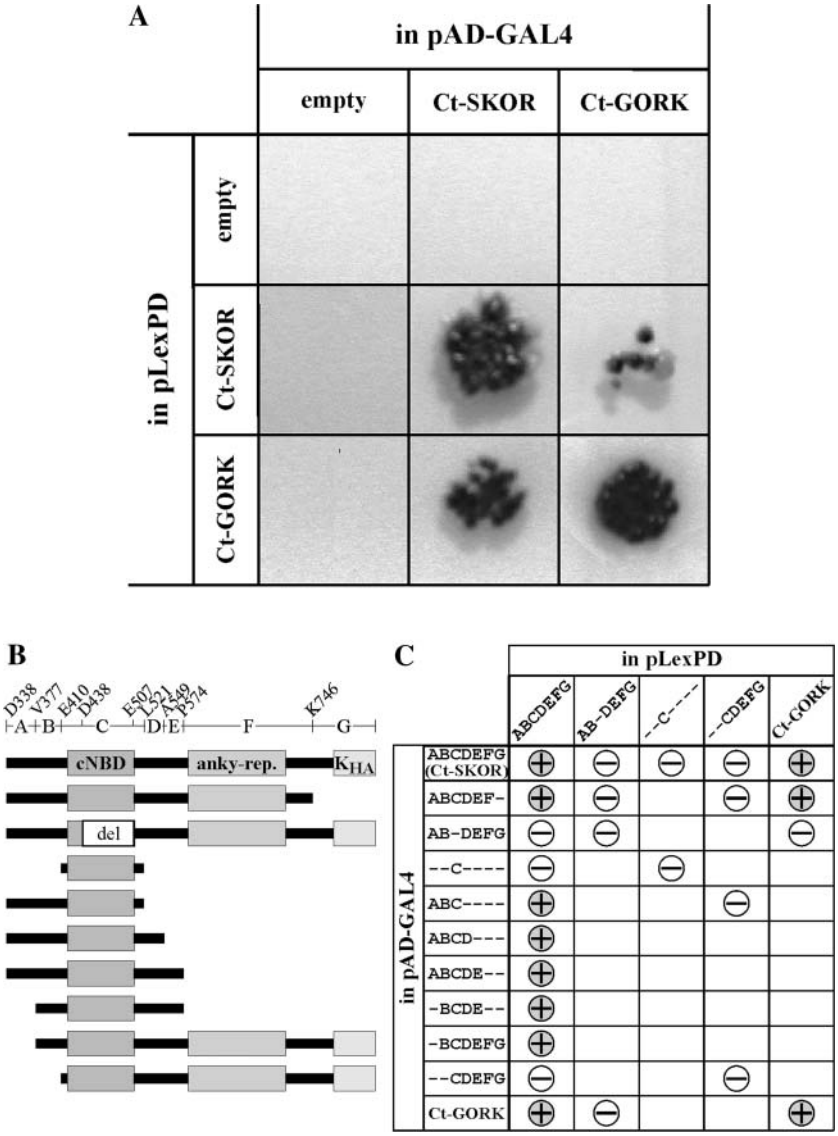

FIGURE 4 Intermolecular interaction of SKOR and GORK, and different SKOR C-terminal fragments tested in the yeast two-hybrid system. (*A*) Reciprocal interactions between SKOR and GORK C-termini. C-termini (SKOR-D338_T828, GORK-N324_T820) were fused to the LexA DNA binding domain of the vector pLexPD and to the GAL4 activator domain of the vector pAD-GAL4. Interactions were monitored in a drop test (10 μl, OD600 adjusted to 0.1) on Leu^--Trp^--His^- medium containing 5-bromo-4-chloro-3-indolyl-beta-D-galactopyranoside. Growth and blue dye formation report the physical association of the coexpressed fusion proteins. (*B*) Generation of fragments of the cytoplasmic SKOR C-terminus. The SKOR C-terminus was subdivided into seven regions (*A–G*). The position of the first amino acid of each region is indicated. Additionally, the positions D438 and E507 within region C are specified. Ten constructs were created and fused to the LexA DNA binding domain and the GAL4 activator domain, respectively. (*C*) Detection of protein associations in growth tests on Leu^--Trp^--His^- medium, and by analyzing β-galactosidase activities. A positive answer in both tests is denoted by a ''(+)'', a negative answer by a ''(−)''. Combinations indicated by empty fields have not been tested. The fragments ABCDEF-, ABC----, ABCD---, ABCDE--, -BCDE--, and -BCDEFG fused to the LexA DNA binding domain showed autoactivity (not shown). Results obtained with these constructs are not presented and are not taken into account for the interpretation of the data. The presented results are representatives of three to seven independent experiments each.

cNBD) plays an important role in triggering the physical interactions of the K_{out} channel C-termini.

Mapping C-terminal assembly domains by functional tests

To investigate which domains of the SKOR C-terminal region play a role in the formation of active channels, functional approaches were developed in both, yeast and *Xenopus* oocytes. In yeast, we tested the ability of different new chimeric constructs to complement a strain defective for K^+ uptake. These constructs were obtained by concatenating the KAT1 transmembrane channel core (KAT1-M1_R305) with C-terminal chimeras, which themselves consisted of parts of the KAT1 and SKOR C-terminal regions. Generation of the C-terminal chimeras was based on sequence comparisons of the C-terminal regions of SKOR and KAT1. Both segments display a similar structural organization except that an ankyrin domain is present in the C-terminal part of SKOR, downstream of the cNBD, but is absent from the C-terminal region of KAT1 (Figs. 4 *B* and 5 *A*). The C-termini of both channel α-subunits were subdivided into six regions. The first five parts coincided with the fragments A–E previously defined, and the sixth region corresponded to the combined fragments F and G (compare Fig. 4 *B* with Fig. 5 *A*). In all C-terminal chimeras, the region C (the cNBD) was fixed to originate from SKOR. The other regions were successively transferred from KAT1 to SKOR. In total, 12 chimeric constructs were created (Fig. 5, *A* and *B*). Each construct was defined by a stretch of six letters, either s or k, corresponding to the six successive regions from A to F/G, an s indicating that the referred region was from SKOR, and a k that the region was from KAT1. The C-terminal chimeras were fused to the hydrophobic core of KAT1 and expressed

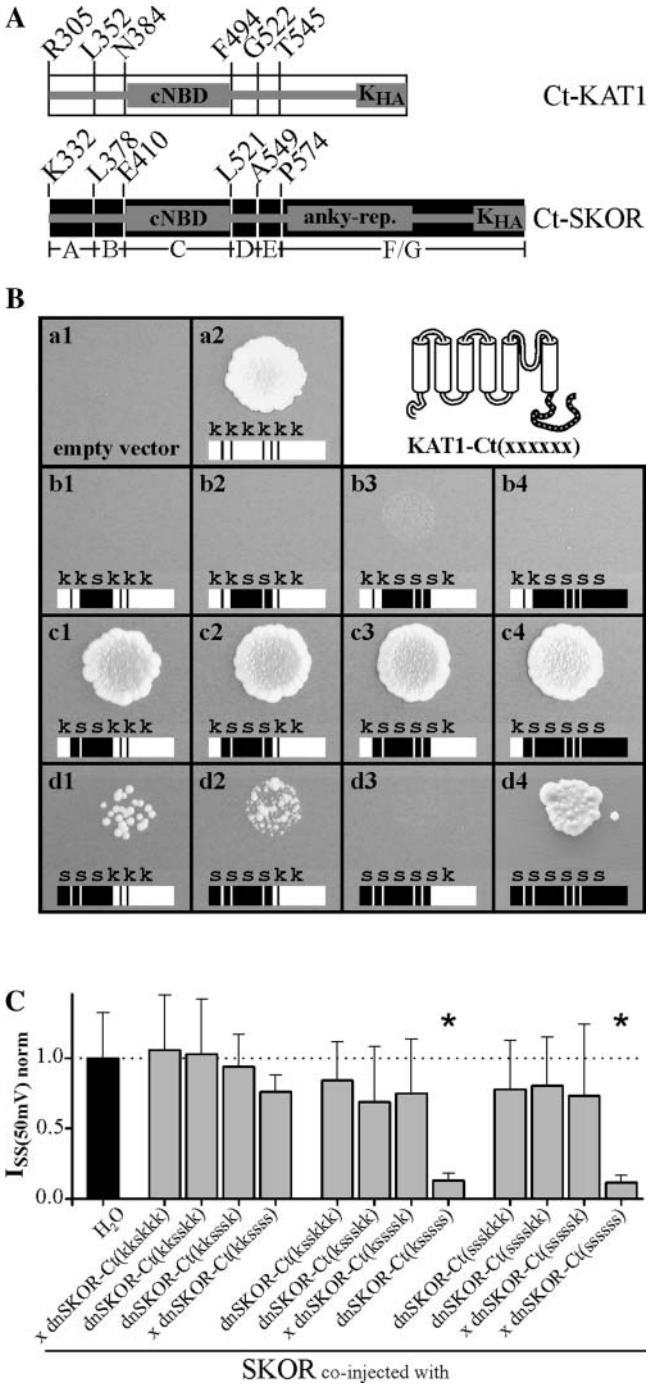

FIGURE 5 Refined SKOR/KAT1 chimeras analyzed in yeast growth tests and by coexpression with SKOR in oocytes. In the KAT1 channel several parts of the C-terminus were replaced by equivalent parts from SKOR. (*A*) The division of each C-terminus into six regions is represented schematically. The position of the first amino acid of each region is indicated. The separation (*A–G*) illustrates the division made in Fig. 4. (*B*) In the chimeras containing the KAT1 core and the chimeric C-termini, C-terminal parts originating from KAT1 are illustrated by white rectangles, and parts from SKOR by black rectangles. Additionally, the origin of the different C-terminal parts is indicated by a six-letters patch, ''xxxxxx'', where ''x'' can be ''k'' (of KAT1 origin) or ''s'' (of SKOR origin). The six white rectangles and kkkkkk (*B*, *a2*) represent the KAT1 channel, the six black rectangles and ssssss (*B*, *d4*) the chimera KAT1-Ct_{SKOR} (cf. Fig. 2 *C*). in the yeast strain Wagf2. Positive colonies were tested for their ability to grow in low K^+ conditions. As already shown in Fig. 2 *C*, KAT1 (i.e., KAT1-Ct(kkkkkk), according to the above-defined nomenclature, Fig. 5 *B*, *a2*) as well as the chimera KAT1-Ct_{SKOR} (KAT1-Ct(ssssss), Fig. 5 *B*, *d4*) complemented the mutant yeast strain. When region C (i.e., cNBD) in KAT1 was replaced by the corresponding region of SKOR, the construct (i.e., the kkskkk chimera) was found to no longer complement the yeast cells (Fig. 5 *B*, *b1*). Further k-to-s substitutions toward the C-terminus (chimeras kksskk, kksssk, and kkssss) did not restore the ability of the chimeric proteins to complement the yeast mutant. Importantly, however, this ability was restored by introducing k-to-s substitutions toward the N-terminus: When the second region (region B) was of SKOR origin, the resulting chimeras (ksskkk, kssskk, kssssk, and ksssss) appeared to be as efficient in complementing the yeast mutant cells (Fig. 5 *B*, *c1*, *c2*, *c3*, and *c4*) as the wild-type KAT1 control. Finally, substituting the KAT1-derived A region for the corresponding region of SKOR origin gave surprising results: the resulting chimeras were less efficient (chimeras sssskk and sssssk; Fig. 5 *B*, *d1* and *d2*) or not at all able (chimera ssssssk, Fig. 5 *B*, *d3*) in complementing the yeast mutant.

Taken together, the yeast complementation experiments revealed that at least seven of the twelve chimeric α-subunits were able to assemble into functional channels. In all functional chimeric proteins fragments B and C were of SKOR origin, indicating a dominant role of the region located upstream of the cNBD not only for physical C-terminal interactions, but also for the formation of functional channels.

Evidence for a further site involved in SKOR channel formation

The yeast experiments above provided some useful but still incomplete information: On the one hand, the functionality of a chimera indicates that its assembly mechanism is intact.

Only chimeras containing the cNBD from SKOR (xxsxxx) were tested. Note that the C-terminus of KAT1 is shorter than that of SKOR because it does not contain an ankyrin domain. The chimeras were expressed in the potassium uptake deficient yeast strain Wagf2 and analyzed in drop tests (10 μl, OD600 adjusted to 0.1) on minimal medium supplemented with 2 mM K^+. The presented results are representative for at least three repeats. (*C*) Coexpression (1:1 cRNA mixtures) of SKOR with chimeric mutants in *Xenopus* oocytes. The chimeric mutants are built of the core (Nterm-S6) of dnSKOR (= SKOR-G292R-D293N-A296V) and the chimeric C-termini as displayed in panel *B*. Current amplitudes (I_{SS}) were measured at the end of 2-s voltage pulses to +50 mV. To compare results obtained from different oocyte batches, the data were normalized to the mean value of the control SKOR/H_2O (*solid column*). Data are shown as means ± SD ($n = 5$–18, six different oocyte batches). The asterisks indicate combinations where the mutant showed a strong dominant-negative effect, i.e., ≈80% reduction in the K^+ current amplitude (Student's *t*-test, $P < 10^{-7}$). The expression of five constructs (marked with *x*) was verified in ^{35}S-protein-labeling experiments.

However, the assembly mechanism of a functional chimera is not necessarily identical to that of SKOR. On the other hand, the lack of demonstration of function for a chimera is not automatically an indication for a distorted assembly mechanism. Therefore, the C-terminal chimeras, tested in the preceding experiment, were fused to the hydrophobic core of the dominant-negative mutant channel dnSKOR. The resulting constructs were coexpressed with the wild-type SKOR channel in *Xenopus* oocytes. Using ^{35}S-labeled methionine and cysteine, chimerical protein expression was checked exemplarily for the constructs dnSKOR-Ct(kkskkk), dnSKOR-Ct(kkssss), dnSKOR-Ct(kssssk), dnSKOR-Ct(sssssk), and dnSKOR-Ct(ssssss) (marked *x* in Fig. 5 *C*, cf. Fig. 3 *C*). Nevertheless, coexpression of SKOR with chimeras in which region B was of KAT1 origin, i.e., chimeras of the type dnSKOR-Ct(kksxxx) (cf. Fig. 5 *B*, *b1–b4*), did not significantly influence the measured K^+ currents in comparison to SKOR/H_2O (Fig. 5 *C*). This result supported the above-made conclusion that region B (together with the cNBD, region C) plays an essential role in SKOR channel formation. Whereas region C appeared to be essential for assembly by maintaining the structural integrity of the protein, region B seemed to be involved in determining the specificity of the assembly. Interestingly, however, some chimeras in which both regions, B and C, were of SKOR origin were also not able to strongly reduce SKOR currents. Only two constructs with F/G segments of SKOR origin, i.e., the dnSKOR-Ct(kksssss) chimera and the SKOR dominant-negative mutant itself (''dnSKOR-Ct(ssssss) chimera''), were endowed with a strong dominant-negative behavior (Fig. 5 *C*). These data suggested the presence of another domain in the far C-terminus (in region F/G) involved in the formation of tetrameric channels. This hypothesis was also supported by the fact that the functional chimeras KAT1-Ct(ssskkk), KAT1-Ct(sssskk), and KAT1-Ct(ssssss) (Fig. 5 *B*, *d1*, *d2*, and *d4*) lost their ability to complement yeast when the last three segments of the constructs were deleted (resulting in the chimeric polypeptide KAT1-Ct(sss---); data not shown).

A K_T-like domain involved in SKOR channel assembly

To further analyze the role of the F/G region in channel assembly, additional chimeras, and deletions at the very C-terminus were generated in the dnSKOR mutant background (Fig. 6 *A*). When the K_{HA} domain of dnSKOR (G774_T828) was replaced by the K_{HA} domain of KAT1 (G624_N677; Fig. 6 *A*, *i*) the resulting channel exhibited dominant-negative behavior upon coexpression with wild-type SKOR (Fig. 6 *B*, *i*). However, when a slightly larger region was exchanged (KAT1-R608_N677 replacing SKOR-V752_T828; Fig. 6 *A*, *ii*), dominant-negative behavior was no longer observed. In coexpression experiments with

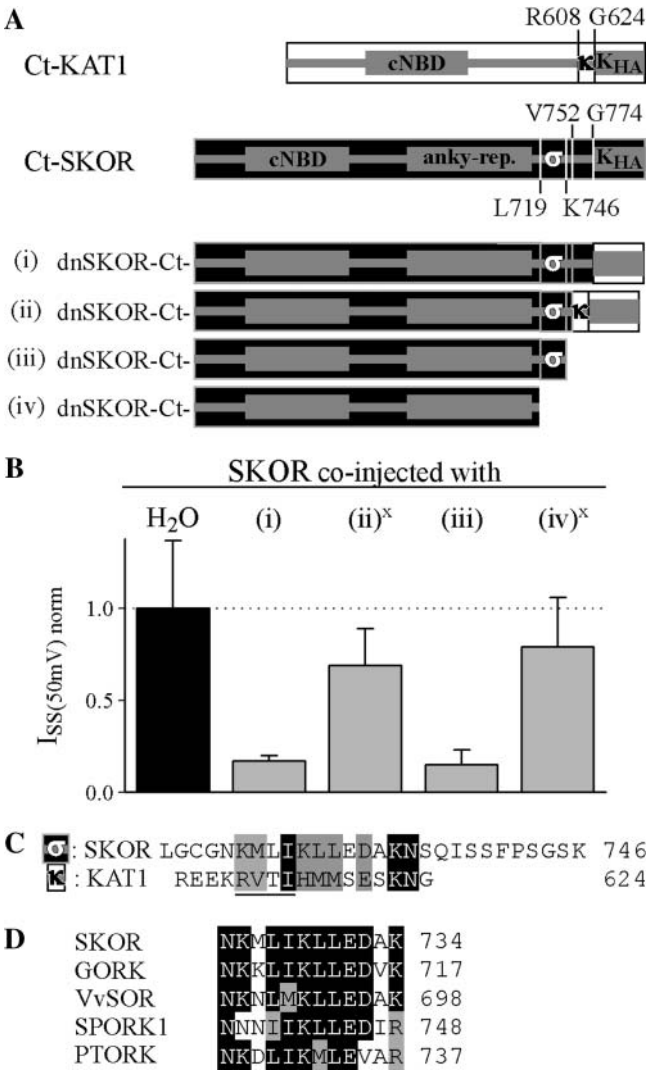

FIGURE 6 A second domain at the C-terminus is involved in SKOR channel assembly. (*A*) Generation of chimeric/truncation mutants on the basis of dnSKOR. In dnSKOR, regions at the end of the C-terminus were either deleted or replaced by equivalent parts of KAT1. The individual C-termini are represented schematically (*i–iv*). The position of the first amino acid of each region is indicated. Parts originating from KAT1 are illustrated by white rectangles, and parts from SKOR are shown as black rectangles. (*B*) Coexpression experiments (1:1 cRNA mixtures) with SKOR and the constructs shown in panel *A* in *Xenopus* oocytes. Current amplitudes (I_{SS}) were measured at the end of 2-s voltage pulses to +50 mV. To compare results obtained from different oocyte batches, the data were normalized to the mean value of the control SKOR/H_2O (*solid column*). Data are shown as means ± SD ($n = 6–12$, two different oocyte batches). The expression of the constructs (*ii*) and (*iv*) (marked with *x*) was verified in ^{35}S-protein-labeling experiments. (*C*) Sequence comparison of the regions ''σ'' (SKOR-L719_K746) and ''κ'' (KAT1-R608_G624) marked in *A*. The conserved tetra-peptide of the K_T domain ([R-V-T-I] in KAT1) is underlined. (*D*) Sequence comparison of the ''σ'' domains of the plant K_{out} channels SKOR (GenBank protein accession number CAA11280), GORK (CAC17380), *Vitis vinifera* VvSOR (CAD35400), *Samaea saman* SPORK1 (CAC10514), and *Populus tremula x tremuloides* PTORK (CAC05488).

SKOR, this mutant caused only a small decrease (30%) in the K^+ current level (Fig. 6 *B*, *ii*). When in this mutated chimera, the 70 residues of KAT1 origin as well as seven more residues of SKOR were deleted (Fig. 6 *A*, *iii* (= dnSKOR-Δ746)), the dominant-negative behavior was restored (Fig. 6 *B*, *iii*). As already shown (Fig. 3), the truncation of the terminal 83 amino acid residues of the SKOR α-subunit (SKOR-Δ746) affected neither the ability of the polypeptide to form functional channels nor its capacity to assemble with SKOR. However, the removal of 27 more residues (marked ''σ'' in Fig. 6 *A*) did. The deletion mutant SKOR-Δ719 (=SKOR-L719X-G720_T828del) did not mediate currents when expressed in *Xenopus* oocytes (not shown). Similarly, the mutant dnSKOR-Δ719 (Fig. 6 *A*, *iv*) only slightly (20%) reduced the K^+ current levels in coexpression experiments with the wild-type SKOR α-subunit (Fig. 6 *B*, *iv*). These results indicated that the two segments ''σ'' (SKOR-L719_K746) and ''κ'' (KAT1-R608_G624) are involved in determining the assembly specificity of the channel proteins. Sequence comparisons between the segments ''σ''and ''κ'' revealed some resemblance (17% identity, 67% similarity) in a 12 amino-acid-residue-long fragment (Fig. 6 *C*). In K_{in} channels, a previous study proposed that this domain, called K_T, is involved in heteromerization of K_{in} channel α-subunits encoded by different genes (Zimmermann et al., 2001). The characteristic feature of the K_T domain is a conserved tetrapeptide [R-(V/I)-(T/S/I)-(I/V)], which is at positions R612–I615 in KAT1 (*underlined* in Fig. 6 *C*), and which harbors a putative phosphorylation site. A similar motif, however, is absent in K_{out} channels. Instead, by comparing the sequences of five different K_{out} channels available from diverse plant species (Gaymard et al., 1998; Ache et al., 2000; Langer et al., 2002; Moshelion et al., 2002) a dodecapeptide consensus pattern [N-(K/N)-x-(I/L)-(I/M)-K-(L/M)-L-E-(D/N)-x-(K/R)] could be deduced (Fig. 6 *D*). In contrast to the K_T domain, this motif does not comprise any putative phosphorylation site.

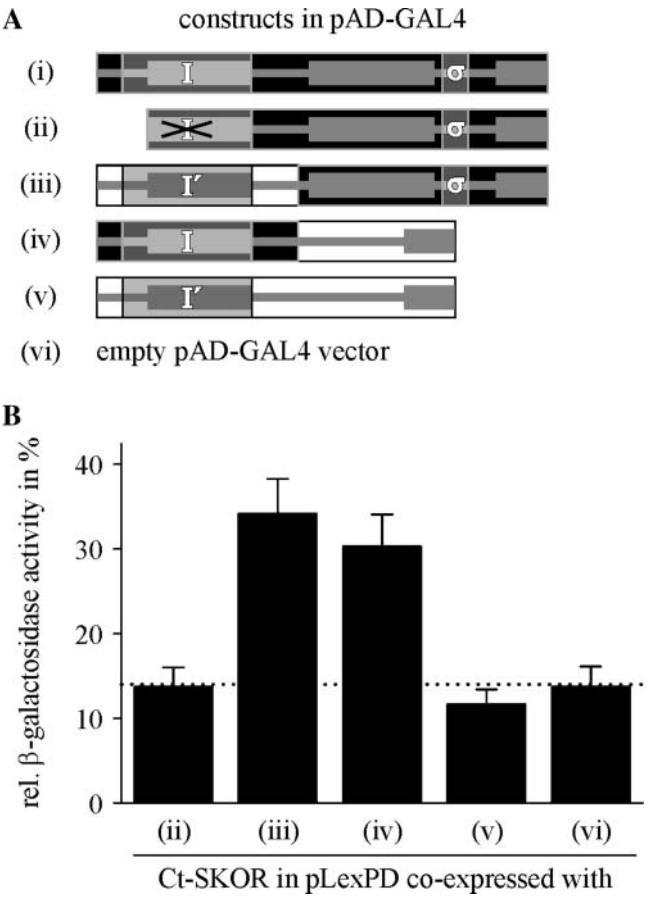

FIGURE 7 Identification of weak intermolecular interactions between Ct-SKOR and different C-terminus constructs in the yeast two-hybrid system. (*A*) Generation of chimeric/truncation mutants on the basis of the SKOR (*i*) and the KAT1 (*v*) C-terminus. The individual C-termini are represented schematically (*i–vi*). Parts originating from KAT1 are illustrated by white rectangles, and parts from SKOR are shown as black rectangles. The label ''I'' indicates the proximal interacting region of SKOR, the label ''I′'' its counterpart found in KAT1, and the label ''σ'' the distal interacting region. Note that in construct (*ii*) the proximal interacting region was partly deleted. The constructs were fused to the GAL4 activator domain. (*B*) Identification of protein interactions between Ct-SKOR (fused to the LexA binding domain) and the constructs shown in *A* by analyzing β-galactosidase activities. Data are shown as means ± SD (n = 4–8). To facilitate the comparison all values were normalized to the mean value measured for the positive control (self-interaction of Ct-SKOR = 100%, *i* in panel *A*). The dotted line indicates the background level of β-galactosidase activity measured with Ct-SKOR in combination with the empty pAD-GAL4 vector (*vi*).

The two distinct assembly regions contribute separately to the interaction of SKOR C-terminal regions

The results presented so far indicated that the specificity of SKOR channel assembly was determined by two distinct regions: segment B (Fig. 4 *B*, together with the cNBD named ''proximal interacting region'' in the following) and segment ''σ'' (Fig. 6 *A*, named ''distal interacting region'' in the following). Whereas the upstream region (labeled *I* in Fig. 7 *A*) could be correlated with direct physical interactions of the SKOR C terminus (Fig. 4), the contribution of the downstream region to channel assembly was less clear. Therefore, physical interactions of C-termini were further analyzed in yeast, using a more sensitive two-hybrid assay. Cells grown in liquid culture were tested for β-galactosidase activity using ONPG (o-nitrophenyl β-D-galactopyranoside) as substrate. The SKOR C-terminus, fused to the LexA binding domain, served as a potential target for six different constructs fused to the GAL4 DNA-binding domain (Fig. 7 *A*). When the functionality of the proximal interacting region was disrupted by deleting the essential part *B* (Fig. 7, *ii*; Fig. 4 *B* (construct --CDEFG)); reporter (β-galactosidase) activity was close to the background level (Ct-SKOR +

empty vector, Fig. 7, *vi*, and Ct-SKOR + Ct-KAT1, Fig. 7, *v*). When the proximal assembly domain was not deleted, but instead was replaced by the corresponding region of KAT1 (labeled *I′* in Fig. 7 *A*), a physical interaction with the SKOR C-terminus could be monitored (Fig. 7, *iii*). Similarly, when the downstream part of the SKOR C-terminus (comprising the distal interacting region "σ") was replaced by the distal region of the KAT1 protein, significant β-galactosidase activity was detected (Fig. 7, *iv*). Because the SKOR C-terminus did not interact with any segment of the KAT1 C-terminus (Fig. 7, *v*), these results suggested a joint contribution of the proximal and the distal assembly regions of SKOR to physical C-terminus interaction. Hereby, the contribution of the distal interacting region depends on the presence of an intact proximal assembly region.

DISCUSSION

In this report we investigated the assembly of plant *Shaker*-like K_{out} channels by combining two-hybrid assays with functional analyses, i.e., electrophysiological recordings of exogenous currents in *Xenopus* oocytes and tests of restoration of K^+ transport activity in a yeast strain deficient for K^+ uptake.

Our data demonstrate that plant K_{out} channels, like the plant K_{in} channel AKT1 (Daram et al., 1997), assemble through interaction sites located at the cytoplasmic C-terminus of the protein rather than by an N-terminal tetramerization domain. Hence, the assembly process of plant K_{out} channels, seen in the light of the present knowledge about the assembly of animal potassium channels, is more related to that of members of the EAG or KCNQ families (Ludwig et al., 1997; Schmitt et al., 2000) than to that of typical voltage-gated *Shaker* (Kv) channels (Li et al., 1992). Recent analyses revealed that channels of the EAG superfamily assemble via a tetramerizing coiled coil, a domain in which the probability for the formation of a coiled coil peaks (Jenke et al., 2003). For K_{out} and K_{in} channels, the existence of a similar domain does not seem likely. The SKOR polypeptide, for example, has been analyzed with the program Coils, Version 2.2 (Lupas et al., 1991; http://www.ch.embnet.org) to determine the local probability for coiled-coil formations. Although coiled regions were predicted with a probability of 0.77 for the section K524_I537 (fragment D in Fig. 4 *B*), and with a probability of 0.83 for the section R781_V796 (within the K_{HA} domain), the experimental data presented in this study do not provide evidence for a role of these regions in channel tetramerization. Our results rather suggest that other interaction sites drive multimerization of plant K_{out} channels: a proximal interacting region (regions B and C in Fig. 4 *B*; region I in Fig. 7 *A*), and a distal interacting region downstream of the ankyrin domain (segment "σ" in Fig. 6 *A* and in Fig. 7 *A*).

The two distinct assembly regions contribute differently to interaction of SKOR C-terminal regions

In yeast two-hybrid assays the proximal interacting region is active on its own in promoting protein-protein interactions. In contrast, the detection of interactions mediated by the distal interacting region was coupled to the presence of a functional proximal interacting region. This result may indicate that either a proximal interacting region is necessary to maintain the structural integrity of the protein, and/or that the interaction mediated by the proximal interacting region is needed as a prerequisite for the activity of the distal interacting region. In the latter case the assembly of SKOR polypeptides would involve at least two consecutive steps. In this model, the proximal interacting region would play an essential role in a first interaction process, e.g., in the dimerization of two SKOR α-subunits, causing conformational changes that then allow formerly inactive interacting regions to contribute to the subsequent steps. In other words, these newly recruited interacting sites would not belong to the α-subunit itself but to the dimer. The assembly behavior of SKOR would then be comparable to that of Kv channels that have been proposed to form tetramers from preassembled dimers (Tu and Deutsch, 1999).

Despite the apparent involvement of the distal interacting region in channel assembly it cannot, however, be excluded that it might additionally play a role in channel trafficking. Future cell-biological studies addressing channel maturation and processing will allow further conclusions in this context.

Distinct protein interactions contribute jointly to functional SKOR channel formation

It should be emphasized that the interactions identified in yeast two-hybrid experiments (Figs. 4 and 7) appeared to be contradictory to the results obtained from analyzing channel function. Positive protein-protein interaction of the construct *iv* (Fig. 7 *A*) with Ct-SKOR (Fig. 7 *B*, *iv*), for example, apparently did not fit with the negative results obtained after coexpressing dnSKOR-Ct(ssssk) and SKOR (Fig. 5 *C*). Additionally, in two-hybrid experiments Ct-SKOR was interacting with the constructs ABC----, ABCD---, ABCDE--, and -BCDE-- (Fig. 4), all of them lacking the region "σ." However, when the "σ" region was absent, no evidence for functional channel assembly could be gained in different approaches with different experimental systems: a), construct dnSKOR-Ct(sssss-) had no dominant negative effect on functional SKOR channel formation (Fig. 6 *B*, *iv*); b), the channel SKOR-Ct(sssss-) did not mediate currents (not shown); c), the chimera KAT1-Ct(sss---) did not complement yeast (not shown). These apparent discrepancies in the experimental findings may be explained by taking into account the different stringencies of the chosen assays. Whereas the low-stringent yeast two-hybrid assays

reported protein-protein interactions, the highly stringent functional assays tested for the presence of fully assembled, intact channels in the membrane. Thus, successful interaction detected in two-hybrid experiments will not necessarily translate into successful channel assembly. From the presented results we rather have to conclude that the contribution of both interacting regions, proximal and distal, is required for functional channel formation.

Assembly of SKOR in comparison to other channels

The two-hybrid tests (Fig. 4), in combination with functional assays in *Xenopus* oocytes (Fig. 1, *C* and *D*), demonstrated that the two K_{out} subunits SKOR and GORK interact and form heteromeric channels under suitable experimental conditions. Whether such interactions actually occur in planta, allowed by overlapping expression patterns of K_{out} channel genes, has to be investigated in subsequent studies. On the other hand, functional data obtained in oocytes and yeast (e.g., Fig. 1, *A* and *B*, and Fig. 2 *C*) point to the absence of heteromerization between the K_{in} channel subunit KAT1 and the K_{out} channel subunits SKOR or GORK. Nevertheless, KAT1 contains segments at its C-terminus that are functionally equivalent to the interacting regions of SKOR. In substitution experiments, the KAT1 regions compensated for the loss of the SKOR domains (Figs. 3, 5, 6, and 7). Despite these functional similarities, however, the KAT1 and SKOR regions appear not to be compatible. In yeast two-hybrid assays no interaction between the C-termini of KAT1 and SKOR could be detected. Furthermore, functional dnSKOR chimera, carrying one of the two interaction regions of KAT1, were not endowed with a strong dominant-negative behavior. Thus, the incompatibility of the C-terminal regions is very likely the molecular reason why K_{in} and K_{out} channel α-subunits do not coassemble. Additionally, the assembly of SKOR and KAT1 appeared to be different. Whereas SKOR assembles properly only in the presence of both, the proximal and the distal interacting regions (Figs. 5 and 6), KAT1 does not need a distal region for tetramerization. This channel remains functional when its complete C-terminal part downstream of the putative cyclic nucleotide-binding domain (therefore downstream of the proximal interaction region) is deleted (Marten and Hoshi, 1997). With this feature KAT1 fits well into a picture that was recently developed on the basis of the crystal structure of the C-terminus of the mouse hypolarization-activated, cyclic nucleotide-modulated channel HCN2 (Zagotta et al., 2003). In the tetrameric C-terminus of this channel a domain linking the last transmembrane segment with the cyclic nucleotide-binding domain (called ''C-linker domain,'' equivalent to the joint regions A and B in Fig. 4 *B*) mediates most of the subunit-subunit contacts. The C-linker domain consists of six α-helices, which are separated by short loops. The first two helices of each subunit (equivalent to region A in Fig. 4 *B*) form an antiparallel helix-turn-helix motif that interacts with the third and fourth helices (fourth helix is equivalent to region B in Fig. 4 *B*) of the neighboring subunit. It was suggested that KAT1-related potassium channels are related to animal HCN channels in structure and mechanism (Zagotta et al., 2003). The data available for KAT1 are in good agreement with this model. However, for SKOR the structural data of HCN2 can only partially explain the C-terminal interactions underlying channel assembly. We found that the region upstream of the cNBD has an important role in SKOR C-terminus interaction. However, this interaction is insensitive to the removal of the first 39 amino acid residues (region A; Fig. 4, *B* and *C*) that correspond to the first three interacting helices in HCN2. Furthermore, in contrast to SKOR and KAT1 (Marten and Hoshi, 1997) the assembly of HCN2 is apparently not disrupted when the cNBD is deleted. HCN2 still functions as a channel after removal of the cNBD (Wainger et al., 2001). Finally, as outlined before, subunit-subunit interactions in SKOR strongly depend on another distal region for which no equivalent part could be identified in the crystal structure of HCN2. Thus, to explain SKOR channel assembly the crystal structure data of HCN2 do not serve as a fully applicable model. However, other observations and suggestions based on the HCN2 data are very intriguing. Because the cNBD of SKOR lacks many of the key residues that were identified by Zagotta et al. (2003) in HCN2 to interact with cyclic nucleotides, it is very likely that the putative cNBD of SKOR does actually not interact with cyclic nucleotides but rather with other small (so far unknown) molecules. Future studies will clarify to what extend cyclic nucleotides modify the activity of SKOR and/or its assembly behavior.

CONCLUSION

In summary, this study provides evidence that plant K_{out} channel α-subunits, like plant K_{in} channel α-subunits, assemble via interaction domains located in the cytoplasmic C-terminal parts of the polypeptides. The data indicate that the assembly of plant K_{out} channels is a complex process involving different regions of the α-subunit: i), a proximal interacting region, consisting of two functionally distinct parts, and ii), a distal interacting region. The contribution of both regions to channel assembly appears to be different. Whereas the proximal interacting region is active on its own in promoting protein-protein interactions, the distal interacting region needs an intact proximal interacting region to be active. The contribution of both interactions is required for functional channel formation. Similar to K_{in}, K_{out} α-subunits have the potential to form heteromeric channels. However, the formation of heteromeric channels consisting of K_{in} and K_{out} α-subunits was not observed in our experiments. We rather provide evidence for the existence of barriers preventing K_{in}-K_{out} heteromerization. This result is not totally unexpected. In a physiological constellation such an

interaction would seem rather inappropriate, if not deleterious, as it would drive K^+ transport out of efficient cellular control. It appears that evolution has not only created plant K^+ channels with different rectification properties, but also mechanisms that help to avoid interactions between K_{in} and K_{out} α-subunits.

We thank Dr. Ingela Johansson, Glasgow, for the ^{35}S-labeling protocol, and Dr. Isabelle Chérel for initial help with the yeast expression system. B.M.R. thanks the Max-Planck Institute of Molecular Plant Physiology for providing lab space and electrophysiology equipment. We are grateful to two anonymous reviewers for valuable constructive criticisms that helped to improve the manuscript.

This work was partly supported by a Marie Curie Fellowship of the European Union to I.D. (contract no. ERBBIO4CT985058, proposal no. 980115), and by the GABI-Génoplante joint programs (GABI FKZ 0312852, GENOPLANTE contract no. AF2001093).

REFERENCES

Ache, P., D. Becker, R. Deeken, I. Dreyer, H. Weber, J. Fromm, and R. Hedrich. 2001. VFK1, a *Vicia faba* K^+ channel involved in phloem unloading. *Plant J.* 27:571–580.

Ache, P., D. Becker, N. Ivashikina, P. Dietrich, M. R. Roelfsema, and R. Hedrich. 2000. GORK, a delayed outward rectifier expressed in guard cells of *Arabidopsis thaliana*, is a K^+-selective, K^+-sensing ion channel. *FEBS Lett.* 486:93–98.

Ausubel, F. M., R. Brent, R. E. Kingston, D. D. Moore, J. G. Seidam, J. A. Smith, and K. Struhl. 1993. Current Protocols in Molecular Biology. Green Publishing Associates, John Wiley & Sons, New York.

Baizabal-Aguirre, V. M., S. Clemens, N. Uozumi, and J. I. Schroeder. 1999. Suppression of inward-rectifying K^+ channels KAT1 and AKT2 by dominant negative point mutations in the KAT1 alpha-subunit. *J. Membr. Biol.* 167:119–125.

Becker, D., I. Dreyer, S. Hoth, J. D. Reid, H. Busch, M. Lehnen, K. Palme, and R. Hedrich. 1996. Changes in voltage activation, Cs^+ sensitivity, and ion permeability in H5 mutants of the plant K^+ channel KAT1. *Proc. Natl. Acad. Sci. USA.* 93:8123–8128.

Bertl, A., H. Bihler, C. Kettner, and C. L. Slayman. 1998. Electrophysiology in the eukaryotic model cell Saccharomyces cerevisiae. *Pflugers Arch.* 436:999–1013.

Daram, P., S. Urbach, F. Gaymard, H. Sentenac, and I. Cherel. 1997. Tetramerization of the AKT1 plant potassium channel involves its C-terminal cytoplasmic domain. *EMBO J.* 16:3455–3463.

den Dunnen, J. T., and S. E. Antonarakis. 2001. Nomenclature for the description of human sequence variations. *Hum. Genet.* 109:121–124.

Dreyer, I., S. Antunes, T. Hoshi, B. Mueller-Roeber, K. Palme, O. Pongs, B. Reintanz, and R. Hedrich. 1997. Plant K^+ channel alpha-subunits assemble indiscriminately. *Biophys. J.* 72:2143–2150.

Dreyer, I., C. Horeau, G. Lemaillet, S. Zimmermann, D. R. Bush, A. Rodriguez-Navarro, D. P. Schachtman, E. P. Spalding, H. Sentenac, and R. F. Gaber. 1999. Identification and characterization of plant transporters using heterologous expression systems. *J. Exp. Bot.* 50:1073–1087.

Dreyer, I., B. Mueller-Roeber, and B. Köhler. 2002. New challenges in plant ion transport research: from molecules to phenomena. *In* Recent Research Developments in Molecular & Cellular Biology, Vol. 3, Part II. Research Signpost, Kerala, India. 379–95.

Ehrhardt, T., S. Zimmermann, and B. Mueller-Roeber. 1997. Association of plant K^+_{in} channels is mediated by conserved C-termini and does not affect subunit assembly. *FEBS Lett.* 409:166–170.

Gaymard, F., G. Pilot, B. Lacombe, D. Bouchez, D. Bruneau, J. Boucherez, N. Michaux-Ferriere, J. B. Thibaud, and H. Sentenac. 1998. Identification and disruption of a plant shaker-like outward channel involved in K^+ release into the xylem sap. *Cell.* 94:647–655.

Gietz, D., A. St Jean, R. A. Woods, and R. H. Schiestl. 1992. Improved method for high efficiency transformation of intact yeast cells. *Nucleic Acids Res.* 20:1425.

Hosy, E., A. Vavasseur, K. Mouline, I. Dreyer, F. Gaymard, F. Poree, J. Boucherez, A. Lebaudy, D. Bouchez, A. A. Very, T. Simonneau, J. B. Thibaud, and H. Sentenac. 2003. The *Arabidopsis* outward K^+ channel GORK is involved in regulation of stomatal movements and plant transpiration. *Proc. Natl. Acad. Sci. USA.* 100:5549–5554.

Jenke, M., A. Sanchez, F. Monje, W. Stuhmer, R. M. Weseloh, and L. A. Pardo. 2003. C-terminal domains implicated in the functional surface expression of potassium channels. *EMBO J.* 22:395–403.

Lacombe, B., and J. B. Thibaud. 1998. Evidence for a multi-ion pore behavior in the plant potassium channel KAT1. *J. Membr. Biol.* 166: 91–100.

Langer, K., P. Ache, D. Geiger, A. Stinzing, M. Arend, C. Wind, S. Regan, J. Fromm, and R. Hedrich. 2002. Poplar potassium transporters capable of controlling K^+ homeostasis and K^+-dependent xylogenesis. *Plant J.* 32:997–1009.

Li, M., Y. N. Jan, and L. Y. Jan. 1992. Specification of subunit assembly by the hydrophilic amino-terminal domain of the Shaker potassium channel. *Science.* 257:1225–1230.

Ludwig, J., D. Owen, and O. Pongs. 1997. Carboxy-terminal domain mediates assembly of the voltage-gated rat ether-a-go-go potassium channel. *EMBO J.* 16:6337–6345.

Lupas, A., M. Van Dyke, and J. Stock. 1991. Predicting coiled coils from protein sequences. *Science.* 252:1162–1164.

Ma, D., and L. Y. Jan. 2002. ER transport signals and trafficking of potassium channels and receptors. *Curr. Opin. Neurobiol.* 12:287–292.

Marten, I., and T. Hoshi. 1997. Voltage-dependent gating characteristics of the K^+ channel KAT1 depend on the N and C termini. *Proc. Natl. Acad. Sci. USA.* 94:3448–3453.

Maser, P., S. Thomine, J. I. Schroeder, J. M. Ward, K. Hirschi, H. Sze, I. N. Talke, A. Amtmann, F. J. Maathuis, D. Sanders, J. F. Harper, J. Tchieu, M. Gribskov, M. W. Persans, D. E. Salt, S. A. Kim, and M. L. Guerinot. 2001. Phylogenetic relationships within cation transporter families of *Arabidopsis*. *Plant Physiol.* 126:1646–1667.

Minet, M., M. E. Dufour, and F. Lacroute. 1992. Complementation of *Saccharomyces cerevisiae* auxotrophic mutants by Arabidopsis thaliana cDNAs. *Plant J.* 2:417–422.

Moshelion, M., D. Becker, K. Czempinski, B. Mueller-Roeber, B. Attali, R. Hedrich, and N. Moran. 2002. Diurnal and circadian regulation of putative potassium channels in a leaf moving organ. *Plant Physiol.* 128:634–642.

Pilot, G., F. Gaymard, K. Mouline, I. Cherel, and H. Sentenac. 2003a. Regulated expression of *Arabidopsis* shaker K^+ channel genes involved in K^+ uptake and distribution in the plant. *Plant Mol. Biol.* 51: 773–787.

Pilot, G., B. Lacombe, F. Gaymard, I. Cherel, J. Boucherez, J. B. Thibaud, and H. Sentenac. 2001. Guard cell inward K^+ channel activity in *Arabidopsis* involves expression of the twin channel subunits KAT1 and KAT2. *J. Biol. Chem.* 276:3215–3221.

Pilot, G., R. Pratelli, F. Gaymard, Y. Meyer, and H. Sentenac. 2003b. Five-group distribution of the Shaker-like K^+ channel family in higher plants. *J. Mol. Evol.* 56:418–434.

Rodriguez-Navarro, A., and J. Ramos. 1984. Dual system for potassium transport in Saccharomyces cerevisiae. *J. Bacteriol.* 159:940–945.

Ros, R., G. Lemaillet, A. G. Fonrouge-Desbrosses, P. Daram, M. Enjuto, J. M. Salmon, J. B. Thibaud, and H. Sentenac. 1999. Molecular determinants of the *Arabidopsis* AKT1 K^+ channel ionic selectivity investigated by expression in yeast of randomly mutated channels. *Physiol. Plant.* 105:459–468.

Schmitt, N., M. Schwarz, A. Peretz, I. Abitbol, B. Attali, and O. Pongs. 2000. A recessive C-terminal Jervell and Lange-Nielsen mutation of the KCNQ1 channel impairs subunit assembly. *EMBO J.* 19:332–340.

Sentenac, H., N. Bonneaud, M. Minet, F. Lacroute, J. M. Salmon, F. Gaymard, and C. Grignon. 1992. Cloning and expression in yeast of a plant potassium ion transport system. *Science*. 256:663–665.

Tu, L., and C. Deutsch. 1999. Evidence for dimerization of dimers in K^+ channel assembly. *Biophys. J*. 76:2004–2017.

van der Ven, P. F., S. Wiesner, P. Salmikangas, D. Auerbach, M. Himmel, S. Kempa, K. Hayess, D. Pacholsky, A. Taivainen, R. Schroder, O. Carpen, and D. O. Furst. 2000. Indications for a novel muscular dystrophy pathway. Gamma-filamin, the muscle-specific filamin isoform, interacts with myotilin. *J. Cell Biol*. 151:235–248.

Very, A. A., and H. Sentenac. 2002. Cation channels in the *Arabidopsis* plasma membrane. *Trends Plant Sci*. 7:168–175.

Very, A. A., and H. Sentenac. 2003. Molecular mechanisms and regulation of K^+ transport in higher plants. *Annu. Rev. Plant Physiol. Plant Mol. Biol*. 54:575–603.

Wainger, B. J., M. DeGennaro, B. Santoro, S. A. Siegelbaum, and G. R. Tibbs. 2001. Molecular mechanism of cAMP modulation of HCN pacemaker channels. *Nature*. 411:805–810.

Zagotta, W. N., N. B. Olivier, K. D. Black, E. C. Young, R. Olson, and E. Gouaux. 2003. Structural basis for modulation and agonist specificity of HCN pacemaker channels. *Nature*. 425:200–205.

Zimmermann, S., S. Hartje, T. Ehrhardt, G. Plesch, and B. Mueller-Roeber. 2001. The K^+ channel SKT1 is co-expressed with KST1 in potato guard cells–both channels can co-assemble via their conserved K_T domains. *Plant J*. 28:517–527.

⇒ zurück zur Übersicht

2003

Hosy, Mouline, Vavasseur, **Dreyer**, Gaymard, Poree, Boucherez, Bouchez, Very, Simmonneau, Thibaud, Sentenac

The Arabidopsis outward K^+ channel GORK is involved in regulation of stomatal movements and plant transpiration.

Proc. Natl. Acad. Sci. USA **100**:5549-5554.

The *Arabidopsis* outward K^+ channel *GORK* is involved in regulation of stomatal movements and plant transpiration

Eric Hosy*, Alain Vavasseur†, Karine Mouline*, Ingo Dreyer*‡, Frédéric Gaymard*, Fabien Porée*‡, Jossia Boucherez*, Anne Lebaudy*, David Bouchez§, Anne-Aliénor Véry*, Thierry Simonneau¶, Jean-Baptiste Thibaud*, and Hervé Sentenac*‖

*Biochimie et Physiologie Moléculaires des Plantes, Unité Mixte de Recherche 5004, Agro-M/Centre National de la Recherche Scientifique/Institut National de la Recherche Agronomique/UM2, F-34060 Montpellier Cedex 1, France; †Commissariat à l'Energie Atomique Cadarache, Direction des Sciences du Vivant, Département d'Ecophysiologie Végétale et Microbiologie, Laboratoire des Echanges Membranaires et Signalisations, Unité Mixte de Recherche 163, Centre National de la Recherche Scientifique/Commissariat à l'Energie Atomique/Univ-Méditerranée, F13108, St. Paul-Lez-Durance Cedex, France; and §Station de Génétique et Amélioration des Plantes, Institut National de la Recherche Agronomique Centre de Versailles, F-78026 Versailles Cedex, France; and ¶Laboratoire d'Ecophysiologie des Plantes sous Stress Environnementaux, Unité Mixte de Recherche 759, Institut National de la Recherche Agronomique/Ecole Nationale Supérieure d'Agronomie de Montpellier, 2 Place Viala, F-34060 Montpellier Cedex 1, France

Edited by Enid MacRobbie, University of Cambridge, Cambridge, United Kingdom, and approved February 5, 2003 (received for review July 4, 2002)

Microscopic pores present in the epidermis of plant aerial organs, called stomata, allow gas exchanges between the inner photosynthetic tissue and the atmosphere. Regulation of stomatal aperture, preventing excess transpirational vapor loss, relies on turgor changes of two highly differentiated epidermal cells surrounding the pore, the guard cells. Increased guard cell turgor due to increased solute accumulation results in stomatal opening, whereas decreased guard cell turgor due to decreased solute accumulation results in stomatal closing. Here we provide direct evidence, based on reverse genetics approaches, that the *Arabidopsis GORK Shaker* gene encodes the major voltage-gated outwardly rectifying K^+ channel of the guard cell membrane. Expression of GORK dominant negative mutant polypeptides in transgenic *Arabidopsis* was found to strongly reduce outwardly rectifying K^+ channel activity in the guard cell membrane, and disruption of the *GORK* gene (T-DNA insertion knockout mutant) fully suppressed this activity. Bioassays on epidermal peels revealed that disruption of GORK activity resulted in impaired stomatal closure in response to darkness or the stress hormone azobenzenearsonate. Transpiration measurements on excised rosettes and intact plants (grown in hydroponic conditions or submitted to water stress) revealed that absence of GORK activity resulted in increased water consumption. The whole set of data indicates that *GORK* is likely to play a crucial role in adaptation to drought in fluctuating environments.

The epidermis of the aerial organs of terrestrial plants presents a waxy cuticle that prevents water loss and desiccation but impedes diffusion of atmospheric CO_2 toward the inner tissues. Gas exchanges mainly take place through microscopic pores, the stomata. Two highly differentiated epidermal cells surrounding the pore, named guard cells, control stomatal aperture, allowing the plant to cope, under diverse environmental conditions, with the conflicting needs of maintaining a sufficient internal CO_2 concentration for photosynthesis and of preventing excessive transpirational water loss (1, 2).

Regulation of stomatal aperture relies on turgor changes of the two guard cells; an increase in turgor, caused by increased solute accumulation, promotes pore opening, whereas a decrease in turgor, caused by solute efflux, leads to stomatal closure (1, 2). The available information indicates that the main solutes involved in the osmoregulation process are sucrose, K^+, and accompanying anions (malate and chloride), depending on the environmental conditions. In the normal diurnal cycle, stomatal opening in the morning would mainly result from K^+ salt accumulation. In the afternoon, it would mainly rely on sucrose accumulation (3, 4).

The changes in guard cell K^+ contents contributing to stomatal opening/closure have been shown to involve various channels working in a coordinated way in the plasma membrane and tonoplast. Two types of K^+-permeable voltage-gated channels, either inwardly or outwardly rectifying, have been extensively characterized in the plasma membrane. The inwardly rectifying K^+ channels activate on membrane hyperpolarization and are therefore mainly involved in K^+ entry into the cell. The outwardly rectifying channels activate on membrane depolarization, at membrane potentials more positive than the K^+-equilibrium potential, and thus allow K^+ release (5, 6). Molecular and electrophysiological analyses support the hypothesis that these channels are encoded by genes of the *Shaker* family. This family comprises nine members in *Arabidopsis* (7). Three of them, *KAT1* and *KAT2*, which encode inwardly rectifying channels, and *GORK*, which encodes an outwardly rectifying channel, display high expression levels in guard cells as suggested by *GUS* reporter gene approaches (8) and/or quantitative RT-PCR analyses (9, 10). Reverse genetics approaches have been developed to investigate the role of *KAT1* in stomatal opening, using an *Arabidopsis* mutant carrying a knockout mutation in this gene (10) or transgenic *Arabidopsis* lines expressing dominant negative KAT1 polypeptides (11). The knockout mutation and the expression of dominant negative polypeptides affected inward K^+ channel activity in the guard cell membrane but did not result in total suppression of the inward K^+ current, probably because of inwardly rectifying K^+ channel redundancy. Although the plants expressing dominant negative mutant KAT1 polypeptides displayed reduced light-induced stomatal opening (11), the relative contribution of the different guard cell inward K^+ channels in stomatal movements remains unclear.

In the present study, we provide evidence that the *Arabidopsis GORK* gene encodes the major voltage-gated outwardly rectifying K^+ channel of the guard cell membrane. We also demonstrate that *GORK* plays a role in the control of stomatal movements and allows the plant to significantly reduce transpirational water loss.

Materials and Methods

Isolation of the T-DNA-Tagged Mutant *gork-1* Disrupted in the *GORK* Gene. The *gork-1* knockout line was obtained by PCR screening of ≈40,000 *Arabidopsis thaliana* T-DNA insertion mutants (Was-

This paper was submitted directly (Track II) to the PNAS office.

See commentary on page 4976.

‡Present address: Universität Postdam, Institut für Biochemie und Biologie, Department of Molekularbiologie, D-14476 Golm, Germany.

‖To whom correspondence should be addressed. E-mail: sentenac@ensam.inra.fr.

silevskija ecotype; library constructed by the Station de Génétique et Amélioration des Plantes, Versailles, France; ref. 12), with primers corresponding to the *GORK* gene and to the T-DNA left and right borders. Selection on kanamycin revealed a single insertion locus. The exact position of the T-DNA insertion was determined by sequencing the T-DNA flanking sequences. Plants homozygous for the disruption were selected by PCR in the F_3 progeny of the positive line.

Obtention of the *gork-dn* Dominant Negative Transgenic Lines. The sequence encoding the hallmark GlyTyrGlyAsp motif in the GORK pore domain (typical of K^+-selective channels) was replaced by ArgArgGlyAsp (by site-directed mutagenesis) in the *GORK* gene. The mutated gene, named *gork-dn* (8.78 kb in total, with 2.714 kb upstream from the initiation codon) was cloned into the *Kpn*I–*Sst*I sites of the binary vector pBIB-HYGRO (13). The resulting plasmid was introduced into *Agrobacterium tumefaciens* GV3010 (pMP90) strain (14). *A. thaliana* (Wassilevskija ecotype) was transformed by using the floral dip method (15). Selection on hygromycin allowed us to identify transformed lines displaying a single insertion locus.

Intact Plant Transpiration Measurements. *Arabidopsis* plants were hydroponically grown in a growth chamber (22°C, 65% relative humidity, 8 h/16 h light/dark, 300 μmol·m^{-2}·s^{-1}) for 4 weeks before being transferred (a single plant per experiment) to an experimental chamber allowing gas exchange measurements (dew-point hygrometers and infrared gas analyzer) as described (16). The root compartment (500 ml, 21°C) contained an aerated half-strength Hoagland solution. The shoot compartment (23°C, 8 h/16 h light/dark, 400 μmol·m^{-2}·s^{-1}; HQI-TS NDL, Osram, Berlin) was attached to an open-flow gas circuit (air flow: 160 liters/h). At the inlet, the water-vapor pressure was held constant (1.5 kPa) and controlled with a dew-point hygrometer (Hygro, General Eastern Instruments, Woburn, MA). Humidity at the outlet was measured with a second dew-point hygrometer. The water-vapor pressure deficit in the leaf chamber was 0.9 ± 0.1 kPa (leaf and air temperatures measured with thermistors). Transpiration and photosynthesis were monitored for at least 8 days, including a 3-day adaptation period (the data corresponding to the adaptation period were not taken into account in the analyses). Photosynthesis was proportional to the leaf fresh weight and leaf area (data not shown).

Stomatal Aperture Measurements. Leaves from 4- to 6-week-old *Arabidopsis* plants were excised at the end of the night period, and epidermal strips were prepared as described (17). After peeling, epidermal strips were placed in Petri dishes containing 5 ml of the incubation solution (usual buffer unless otherwise noted: 30 mM KCl/10 mM Mes-iminodiacetic acid, pH 6.5). To standardize the initial state, epidermal strips were kept in the incubation solution for 30 min in darkness. Then, they were submitted to different treatments at 20°C in darkness or light (300 μmol·m^{-2}·s^{-1}). Stomatal apertures were measured (pore width; at least 60 measurements per experiment in <5 min) with an optical microscope (Optiphot, Nikon) fitted with a camera lucida and a digitizing table (Houston Instruments) linked to a personal computer. Each experiment was performed at least in triplicate.

Electrophysiological Recordings. Plants were grown for ≈5 weeks in compost (individual containers) in a growth chamber (21°C, 70% relative humidity, 8 h/16 h light/dark, 300 μmol·m^{-2}·s^{-1}). Guard cell protoplasts were isolated by digestion of leaf epidermal peels. The digestion solution contained 1 mM $CaCl_2$, 2 mM ascorbic acid, Onozuka RS cellulase (1% wt/vol, Yakult Pharmaceutical, Tokyo), Y-23 pectolyase (0.1% wt/vol, Seishin Pharmaceutical, Tokyo), and 1 mM Mes-KOH (pH 5.5). The osmolarity was adjusted to 420 mosM with D-mannitol. The epidermal peels were digested for 40 min at 27°C. Filtration through 50-μm mesh allowed recovery of protoplasts. The filtrate was mixed with three volumes of conservation buffer (10 mM potassium glutamate/1 mM $CaCl_2$/2 mM $MgCl_2$/10 mM Mes-HCl, pH 5.5, with osmolarity adjusted to 500 mosM with D-mannitol). The protoplast suspension (≈10% of guard cell protoplasts, based on microscopic observations) was kept on ice. Patch-clamp pipettes were pulled (P97, Sutter Instruments, Novato, CA) from borosilicate capillaries (Kimax-51, Kimble, Toledo, OH) and fire polished (L/M CPZ 101, List Medical, Darmstadt, Germany). The pipette solution contained 1 mM $CaCl_2$, 5 mM EGTA, 2 mM $MgCl_2$, 100 mM potassium glutamate, 2 mM MgATP, 10 mM Hepes-NaOH, pH 7.5, with osmolarity adjusted to 520 mosM with D-mannitol. The bath solution contained 20 mM $CaCl_2$, 2 mM $MgCl_2$, 100 mM potassium glutamate, 10 mM Mes-HCl, pH 5.5, with osmolarity adjusted to 500 mosM with mannitol. In these conditions, the pipette resistance was ≈10 MΩ. Seals with resistance >5 GΩ were used for electrophysiological analyses. Whole-cell recordings were obtained by using an Axon Instruments Axopatch 200A amplifier. PCLAMP 6.0.3 software (Axon Instruments, Foster City, CA) was used for voltage pulse stimulation, online data acquisition, and data analysis. The voltage protocol consisted in stepping the membrane potential to voltages from −200 to +80 mV in 20-mV increments from a holding potential of −60 mV.

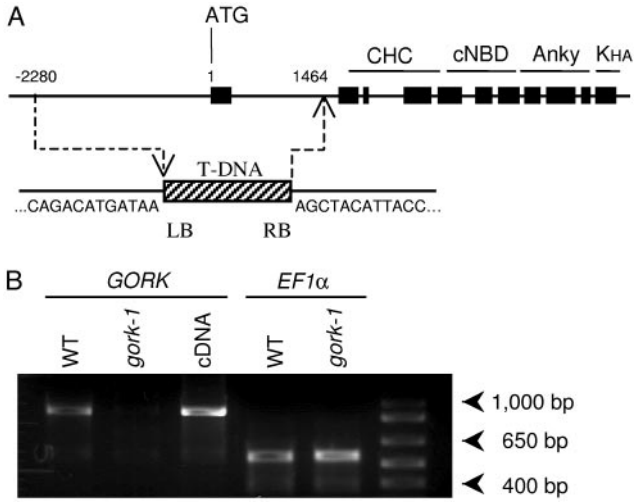

Fig. 1. Identification of a T-DNA insertion mutant. (*A*) Schematic diagram of the *GORK* gene indicating the site of insertion of the disrupting T-DNA in the *gork-1* mutant line. Black boxes represent exons. Typical domains of plant Shaker channels (30) are indicated as follows: CHC, channel hydrophobic core; cNBD, putative cyclic-nucleotide binding domain; Anky, ankyrin domain; KHA, KHA domain. The hatched box represents T-DNA. The nucleotide sequence flanking the T-DNA left (LB) and right (RB) borders in the disrupted gene are given. The T-DNA insertion resulted in a 3.7-kb deletion in the 5′ region of the gene, from nucleotide −2,280 (upstream from the initiation codon) to nucleotide 1,464 (downstream from this codon). (*B*) Absence of *GORK* transcripts in the *gork-1* mutant. RT-PCR analyses were performed on total RNA extracted from aerial parts of either wild-type or *gork-1* plants (WT and *gork-1* lanes) by using primers (sequences available on request) specific for *GORK* or for the *Arabidopsis EF1α* elongation factor gene (used as a control). The cDNA lane shows PCR-amplified DNA fragment using the same *GORK* primers on the *GORK* cDNA (control).

Results

Obtention of *Arabidopsis* Mutants Affected in GORK Activity. An *Arabidopsis* mutant line, named *gork-1*, was identified by PCR screening of a collection of T-DNA-transformed plants (Fig. 1*A*; T-DNA insertion flanking sequences indicated in the figure).

Growth tests on selection medium revealed a single insertion locus (data not shown). The T-DNA insertion was shown to result in a 3.7-kb deletion in the 5′ region of the gene (Fig. 1). RT-PCR experiments performed on total RNA extracted from aerial parts of 4-week-old plants grown in a greenhouse indicated that *GORK* transcripts were not accumulated in homozygous *gork-1* plants (Fig. 1*B*).

Shaker channels are tetrameric proteins (18–20). This structural feature allows us to develop reverse genetics approaches by using dominant negative mutant subunits (obtained by site-directed mutagenesis) able to coassemble with wild-type subunits and to lead to formation of nonfunctional channels (11, 21). Mutations were introduced in the *GORK* coding sequence to replace the hallmark motif GlyTyrGlyAsp, expected to play a crucial role in the formation of the channel-conducting pathway (22), by ArgArgGlyAsp. Experiments in *Xenopus* oocytes revealed that the polypeptide encoded by the mutated sequence was electrically silent (not shown) and indeed endowed with dominant negative behavior; for instance, coinjection of mutant cRNA with wild-type cRNA (*in vitro* transcription) with a mutant/wild-type stoichiometry of 1:1 resulted in 82 ± 6% (n = 10) inhibition of the GORK current. The corresponding mutation was introduced in the *GORK* gene (8.7 kb in total, with a 2.7-kb promoter region), and the mutated gene was introduced into *Arabidopsis* plants. Single locus transformed lines (checked on hygromycin selection medium) were obtained. Patch-clamp experiments were performed on homozygous transgenic plants from the progeny (F_4 generation) of two of them, named *gork-dn1* and *gork-dn2* in this article.

Homozygous *gork-1*, *gork-dn1*, or *gork-dn2* plants were grown in a greenhouse or growth chamber (20°C, 50% relative humidity, 8 h/16 h light/dark, 300 μmol·m^{-2}·s^{-1}). Comparison with control wild-type plants grown in parallel in these conditions did not reveal any obvious phenotype. Because previous RT-PCR experiments had shown that *GORK* transcripts are also present in root hairs (23), root systems from plants grown *in vitro* on agar plates were examined under microscope. No obvious effect of the *gork-1* mutation on root hair density or development could be detected (data not shown).

The *gork-1* Mutation Prevents Expression of the Major Voltage-Gated Outwardly Rectifying K^+ Channel of the Guard Cell. Patch-clamp experiments on guard cell protoplasts prepared from wild-type plants revealed both inward and outward currents (Fig. 2*A*), in agreement with previous analyses (6). The outward current was dominated by a slowly activating sigmoidal component, appearing beyond a threshold potential of ≈0 mV (with 100 mM K^+ in both the bath and pipette solutions) and strongly reminiscent of that recorded in *Xenopus* oocytes expressing *GORK* cRNA (10). Similar experiments were performed on guard cell protoplasts prepared from homozygous *gork-1* plants (Fig. 2*B*) or from *gork-dn1* or *gork-dn2* plants (Fig. 2*C*). They revealed inward K^+ currents quite similar to those recorded in wild-type protoplasts but strongly reduced outward currents. The time course of the remaining outward K^+ current observed in *gork-dn1* (see the current trace at +80 mV magnified ×10 in Fig. 2*C*) and *gork-dn2* (data not shown) protoplasts suggested some residual GORK activity. No GORK activity could be detected in *gork-1* guard cells, as shown by the flat kinetics of the residual outward current (current trace at +80 mV magnified ×10 in Fig. 2*B*). It can therefore be concluded that *gork-1* is actually a knockout mutation.

Bioassays on Epidermal Peels Indicate That Disruption of GORK Activity Affects Stomatal Functioning. The role of *GORK* in stomatal movements was investigated *in vitro* by submitting epidermal peels from wild-type, *gork-1*, or *gork-dn1* plants to treatments inducing either stomatal closure (azobenzenearsonate or darkness; Fig. 3 *A* and *B*, respectively) or opening (light; Fig. 3*C*).

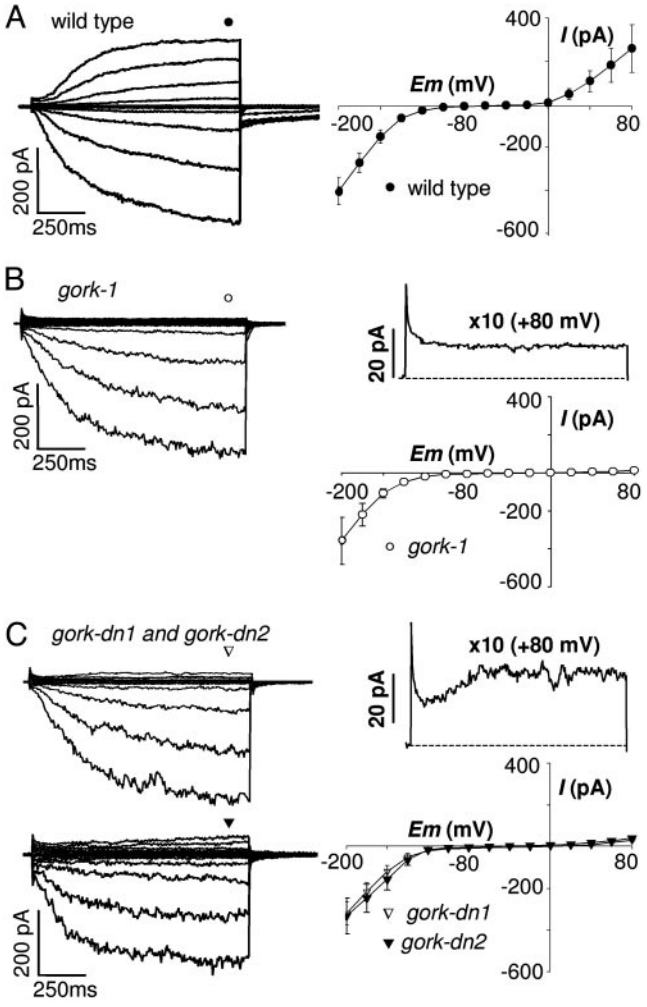

Fig. 2. *GORK* encodes the major voltage-gated outwardly rectifying K^+ channel of the guard cell membrane. Patch-clamp experiments were performed on guard cell protoplasts prepared from wild-type plants (*A*), homozygous *gork-1* mutant plants (*B*), or homozygous *gork-dn1* or *gork-dn2* plants, which both express a GORK dominant negative mutant polypeptide (*C*). (*A–C Left*) Typical examples of inward and outward currents recorded in whole protoplasts. The current traces obtained at +80 mV in the *gork-1* and the *gork-dn1* protoplasts are shown at ×10 scale for easier visualization of kinetics in *B* and *C Right* (dotted line, zero current level). Current–voltage relationships at steady state (means ± SE; n = 9 for wild type, 8 for *gork-1*, 5 for *gork-dn1*, and 5 for *gork-dn2*) are shown (*Right*). The bath and pipette solutions contained 100 mM potassium glutamate. The voltage steps ranged between −200 and +80 mV in 20-mV increments from a holding potential of −60 mV.

Stomatal closure was strongly altered in the *gork-1* and, to a lesser extent, in the *gork-dn1* plants (Fig. 3 *A* and *B*), indicating that GORK activity was required for efficient stomatal closure. On the other hand, the *gork-1* mutation weakly increased light-induced stomatal opening (Fig. 3*C*). It is worth noting, however, that *gork-1* peels consistently displayed slightly larger apertures, e.g., by 10–15% at the end of the 3-h light pretreatment in Fig. 3 *A* and *B* (t = 0).

Excised Rosettes from *gork-1* Plants Display Increased Transpirational Water Loss. As a first step in investigating the role of *GORK* in the control of leaf transpiration, we measured water loss (decrease in weight) of rosettes excised from wild-type, *gork-1*, or *gork-dn1* plants. The *gork-1* rosettes displayed greater water loss than the wild-type ones, by ≈35% during the first hour after the excision (Fig. 4). The *gork-dn1* rosettes displayed an intermediate phe-

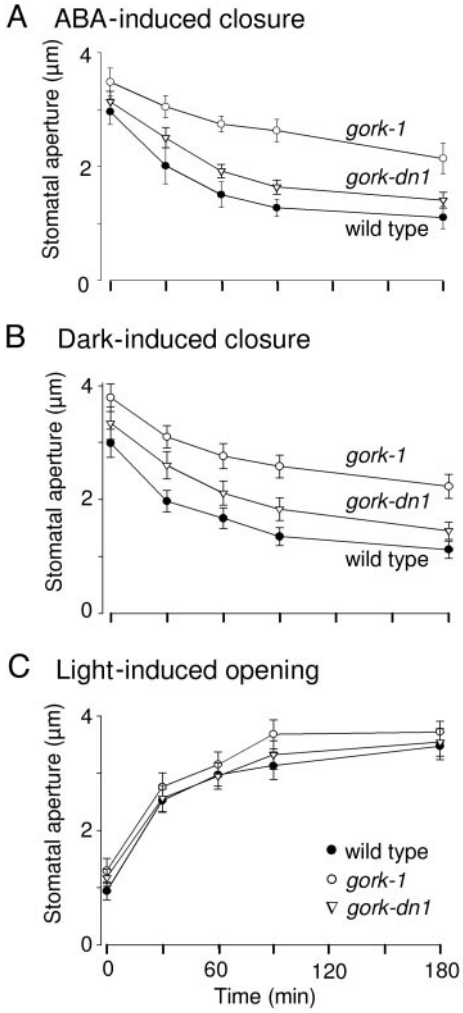

Fig. 3. Disruption of GORK activity affects stomatal movements. Epidermal strips were peeled from wild-type (●), homozygous *gork-1* (○), or *gork-dn1* (▽) plants at the end of dark period and transferred to 30 mM KCl and 10 mM Mes-KOH (pH 6.5). (*A* and *B*) Epidermal strips were placed under light for 3 h (stomatal opening pretreatment) before stomatal closure was induced ($t = 0$) by adding 20 μM azobenzenearsonate in the bath solution (*A*) or switching the light off (*B*). (*C*) Epidermal peels were kept in darkness for 3 h. Then, the light was switched on to induce stomatal opening. Measurements of stomatal apertures were performed at various times on the same strips during 3 h. Means ± SE from four independent experiments, 60 measurements per experiment, are shown).

notype. This provided the first experimental evidence that GORK activity participates in leaf transpiration control.

Intact Plant Transpirational Water Loss Is Increased by the *gork-1* Mutation. In a second set of experiments, the effect of the *gork-1* mutation on intact plant transpiration was investigated by using an experimental setup that allowed us to control the water-vapor pressure deficit (0.9 kPa) and to continuously record the plant transpiration and CO_2 fixation rates (open-flow gas circuit). Switching light on and off induced an increase and decrease, respectively, in transpiration rate, leading to a new steady state (Fig. 5*A*). Analysis of the steady-state data (Fig. 5*B*) revealed that the *gork-1* plants displayed higher transpiration rates than the wild-type controls, by ≈25% in darkness and ≈7% in light (the latter difference, however, being not statistically significant). The kinetics of the transitions between the successive steady states were fitted (least-squares adjustment) with first

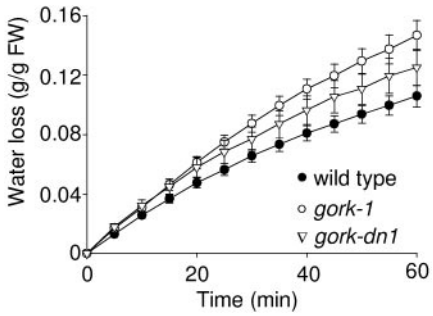

Fig. 4. Disruption of GORK activity results in increased water loss from excised rosettes. Rosettes from wild-type (●), *gork-1* (○), and *gork-dn1* (▽) plants grown on compost in growth chamber (21°C, 70% relative humidity, 8 h/16 h light/dark, 300 μmol·m^{-2}·s^{-1}) were excised just before the end of the light period and transferred to darkness. Water loss was determined by monitoring the decrease in fresh weight of the excised rosettes. Means ±SE of six independent measurements are shown. The difference in transpiration between the wild-type and *gork-1* genotypes is statistically significant (paired values, Student's *t* test $P \ll 0.01$).

order exponential functions to derive the time constants, τ (Fig. 5*C*), assumed to reflect the rate of stomatal movements. The *gork-1* mutation was without any significant effect on the rate of stomatal opening but resulted in a strong decrease in the rate of stomatal closure, the mean τ value being shifted from ≈12 to 19 min. The former value is consistent with previous analyses of dark-induced stomatal closing in *Arabidopsis* (24) and of dark-induced Rb^+ efflux kinetics in *Commelina* (25).

In another experiment, 6-week-old wild-type and *gork-1* plants grown on compost were submitted to a progressive drought stress over 7 days, leading to loss of leaf turgor. The *gork-1* plants displayed higher transpirational water loss (weight loss) than the wild-type plants, during both the night and the light periods (Fig. 6). The relative difference was clearly more important at the end than at the beginning of the stress treatment (≈30–50% and 5–15%, respectively), suggesting that the relative contribution of GORK to transpiration control is more important in conditions of water shortage.

Discussion

***GORK* Encodes the Major Outwardly Rectifying K^+ Channel Active in the Guard Cell Membrane.** *In planta* (electro)physiological analyses have led to the conclusion that K^+ release from the guard cell, leading to stomatal closure, involves the activity of K^+-selective slowly activating voltage-gated outwardly rectifying channels (6, 26). The functional features of these channels characterized *in vivo* in guard cells of *Arabidopsis* and of a number of other species are very similar to those displayed by the *Arabidopsis* SKOR and GORK channels expressed in heterologous systems (10, 27). These two channels belong to the so-called Shaker family, which comprises nine members in *Arabidopsis* (7). SKOR is expressed in root stelar tissues, where it plays a role in K^+ secretion into the xylem sap (27). RT-PCR experiments have revealed *GORK* transcripts in guard cells and in root hairs (9, 23). This information supported the hypothesis that the outward K^+ channel active in guard cells was encoded by the *GORK* gene (in *Arabidopsis*; ref. 10). Here, we show that expressing a dominant negative mutant allele of the *GORK* gene in *Arabidopsis* leads to a strong decrease in the outward K^+ conductance of the guard cell membrane and that disruption of the *GORK* gene results in full suppression of this conductance (Fig. 2). Thus, the present data demonstrate that *GORK* and *SKOR* are not redundantly expressed in guard cells and that functional expression of the *GORK* gene is required for voltage-gated outwardly rectifying K^+ channel activity in the guard cell plasma membrane. The

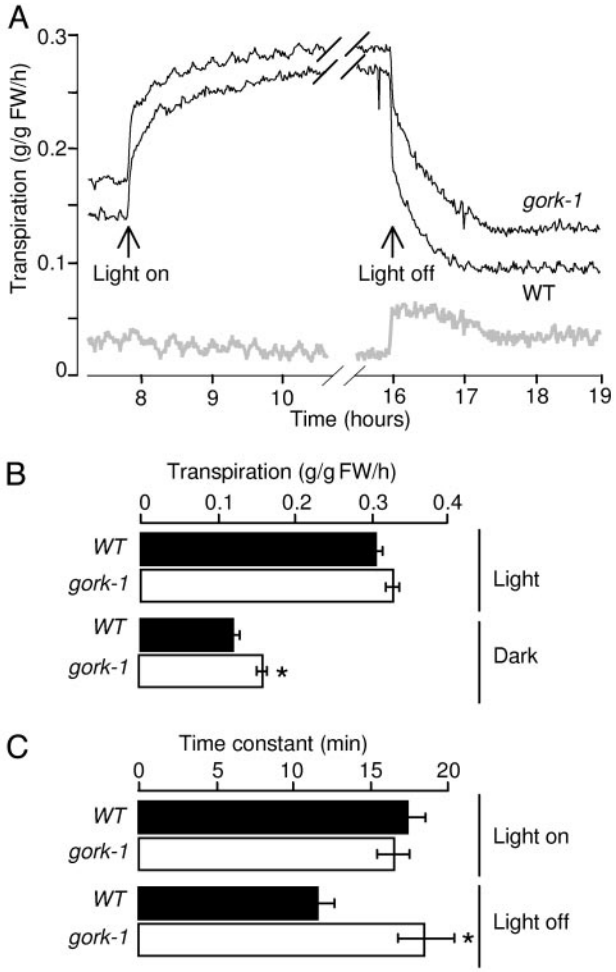

Fig. 5. Effect of the *gork-1* mutation on intact plant transpiration in hydroponic conditions. (*A*) Typical examples of transpiration recordings. A single hydroponically grown wild-type or *gork-1* plant was present in the experimental chamber. The gray curve shows the difference in transpiration between the two plants. (*B*) Transpiration rates measured as described in *A* at the end of the light and dark periods (means ± SE, four plants per genotype, five successive photoperiods taken into account for each plant). (*C*) Time constants describing the changes in transpiration rates induced by light or darkness. To derive time constants reflecting the rate of stomatal opening and closure, experimental kinetics (as those shown in *A*) describing the changes in transpiration rates observed when light was switched on or off were fitted by exponential equations (dashed lines; least-squares fitting, Levenberg–Marquardt algorithm), respectively (means ± SE, four plants, five photoperiods per plant). Asterisks indicate that the corresponding differences in dark-induced stomatal closure (lower bars in *B* and *C*) are statistically significant (Student's *t* test, $P < 0.01$).

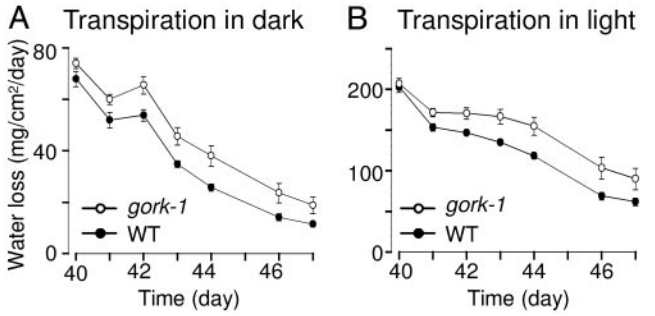

Fig. 6. Increased contribution of GORK to water saving during water stress. Wild-type or *gork-1* plants were grown in parallel for 6 weeks on compost in a growth chamber (20°C, 50% relative humidity, 8 h/16 h light/dark, 300 μmol·m^{-2}·s^{-1}). The experimental procedure ensured that water loss (decrease in weight) resulted from leaf transpiration (mean total leaf area of ≈90 cm^2 per plant at this stage). Periodic weighing and watering allowed us to maintain the water content of the compost at ≈70% (wt/wt) during this period. Then, watering of the plants was stopped ($t = 0$; beginning of the water stress period). Only small amounts of water were daily added to the *gork-1* plant containers, after weighing the devices, to strictly compensate for the difference in transpiration rates between the two genotypes. The compost water content of every container decreased in a similar (and almost linear) way, whatever the plant genotype. The devices were weighed twice a day, at the end of the dark and light periods. The transpirational water loss (mean ± SE; $n = 9$ for the wild-type genotype and 7 for the *gork-1* genotype) during the dark (*A*) and light (*B*) periods was expressed on a leaf area basis, the plants being photographed daily (leaf area determined by using OPTIMAS 6.1 software). Plants conspicuously began to suffer from water stress (loss of leaf turgor) 4 days after watering was stopped. The differences between the two genotypes in *A* and *B* are statistically significant (paired values, Student's *t* test, $P \ll 0.01$).

simplest hypothesis is that a single gene, *GORK*, encodes the major voltage-gated outwardly rectifying K^+ channel characterized in this membrane (6).

GORK Activity Is Involved in the Control of Stomatal Movements. Circumstantial evidence supported the hypothesis that, by mediating K^+ release, the outward rectifier of the guard cell membrane could play a major role in stomatal closure and thereby in transpiration control. The reverse genetics approach developed in our study provides direct support to this hypothesis. The whole set of data indicates that transpiration is more important in *gork-1* than in wild-type plants, from 10% (Fig. 5) up to ≈50% (Fig. 6), depending on the environmental conditions (water availability in these experiments). Thus, whereas disruption of the guard cell inward K^+ channel gene *KAT1* has been found to be without any effect on the regulation of stomatal aperture (9), that of the outward channel GORK results in both impaired stomatal movements and impaired transpiration control. This difference is likely to result from the fact that expression of inward K^+ channel activity in guard cells would involve at least two different genes, *KAT1* and *KAT2* (8), whereas the outwardly rectifying K^+ channel activity relies mainly on a single gene, *GORK*.

In vitro analyses using epidermal peels are likely to give a distorted view of *in planta* stomatal control because of the lack of functional interactions with the surrounding epidermal cells. The bioassays shown in Fig. 3 would suggest larger differences in transpiration between wild-type and *gork-1* plants than those observed in Fig. 5. However, this discrepancy could result, at least in part, from the fact that hydroponic conditions (Fig. 5) lessen the importance of stomata, and thus of GORK activity, in the control of transpiration. Indeed, larger differences in transpirational water loss between the wild-type and *gork-1* genotypes were observed when the plants were grown in compost and submitted to water shortage (Fig. 6).

Larger steady-state stomatal apertures were found in *gork-1* than in wild-type epidermal peels not only at the end of closure-inducing treatments (azobenzenearsonate, darkness; Fig. 3 *A* and *B*) but also at the end of 3-h light-induced opening pretreatments/treatments (experimental points corresponding to time 0 in Fig. 3). Consistent with these observations, *in planta* analyses revealed that *gork-1* plants displayed higher transpiration rates than wild-type plants not only in darkness but also in light (Figs. 5 and 6). These results suggest that GORK could act as a negative regulator of stomatal opening in light, in addition to playing a role in stomatal closure. It has been shown that the membrane voltage in guard cells can undergo large (>100 mV) and rapid (≈10-s period) oscillations between hyperpolarized

values allowing K^+ uptake and depolarized values allowing K^+ release (28). This has led to the hypothesis that control of stomatal movements and steady-state aperture depends on variations in the pattern of these oscillations, enabling the net guard cell K^+ content to increase or to decrease as a result of changes in the balance of K^+ uptake through hyperpolarization-activated channels and K^+ release through depolarization-activated channels (28). The proposal that GORK might act as a negative regulator of stomatal opening stands coherently within the framework of this hypothesis.

Physiological Significance and Role in Natural Conditions. The available information indicates that the dominant solutes involved in guard cell osmoregulation and control of stomatal aperture are K^+ salts and sugars (mainly sucrose), depending on the environmental conditions and the time of the day (4, 29). Genetic tools allowing the assessment of the relative contribution of these solutes and of the mechanisms responsible for their transport and accumulation are highly needed. The present data provide direct genetic evidence that *GORK* encodes the major voltage-gated outwardly rectifying K^+ channel expressed in the guard cell plasma membrane, its disruption resulting in a dramatic decrease in the membrane outward K^+ conductance. However, when grown in standard controlled conditions or even in the greenhouse, *gork-1* plants do not display any obvious phenotype. Furthermore, the *gork-1* stomata can undergo large movements (Fig. 3). This indicates that, in the absence of the GORK channel, different processes, likely to involve activity of other K^+ efflux systems, can efficiently contribute to the decrease in turgor pressure leading to stomatal closure. Based on the present data, it cannot be said whether these processes/systems significantly contribute to stomatal closure also in the presence of GORK activity or whether they correspond to compensation mechanisms resulting from the loss of GORK activity. It is worthy to note that the very low level of GORK current remaining in the plants expressing the dominant negative mutant channel resulted in a stomatal phenotype closer to that of the wild-type plants than to that of the *gork-1* plants (Fig. 3). The dominant negative mutant lines could be valuable genetic tools to further investigate why stomatal physiology requires the guard cell membrane to be fitted with a large voltage-gated outwardly rectifying K^+ conductance.

In hydroponic conditions, the absence of GORK activity resulted in an increase in steady-state transpiration, by ≈7% in light and 25% in darkness (Fig. 5*B*). During the light-to-dark transition, the increase in water loss reached higher percentages (up to 40–50%; see the peak displayed by the gray curve in Fig. 5*A*) because of the slower closure kinetics during the transition from the open to the closed steady state once light was turned off. Thus, the contribution of GORK to water saving would be more important in natural conditions with fluctuating environmental conditions requiring rapid adaptation of stomatal opening (e.g., sudden changes in water-vapor pressure deficit and/or light intensity). Also, the data shown in Fig. 6 highlight that drought conditions amplify the relative contribution of GORK to water saving. Reduced water consumption by ≈10–20% can allow the plant to postpone dehydration by several days. Thus, the *GORK* gene is likely to play an important role in drought adaptation and to be under high selection pressure in natural fluctuating environments.

We are grateful to I. A. Lefevre and S. Zimmermann for helpful discussions and comments on the manuscript. This work was partly supported by a Marie Curie Fellowship of the European Union (to I.D.) and an Indo-French Center for the Promotion of Advanced Research grant (to A.V.).

1. Assmann, S. M. (1993) *Annu. Rev. Cell Biol.* **9,** 345–375.
2. MacRobbie, E. A. C. (1981) *J. Exp. Bot.* **32,** 563–572.
3. Talbott, L. D. & Zeiger, E. (1993) *Plant Physiol.* **102,** 1163–1169.
4. Tallman, G. & Zeiger, E. (1988) *Plant Physiol.* **88,** 887–895.
5. Schroeder, J. I., Raschke, K. & Neher, E. (1987) *Proc. Natl. Acad. Sci. USA* **84,** 4108–4112.
6. Roelfsema, M. R. G. & Prins, H. B. A. (1997) *Planta* **202,** 18–27.
7. Véry, A.-A. & Sentenac, H. (2002) *Trends Plant Sci.* **7,** 168–175.
8. Pilot, G., Lacombe, B., Gaymard, F., Chérel, I., Boucherez, J., Thibaud, J. B. & Sentenac, H. (2001) *J. Biol. Chem.* **276,** 3215–3221.
9. Szyroki, A., Ivashikina, N., Dietrich, P., Roelfsema, M. R. G., Ache, P., Reintanz, B., Deeken, R., Godde, M., Felle, H., Steinmeyer, R., *et al.* (2001) *Proc. Natl. Acad. Sci. USA* **98,** 2917–2921.
10. Ache, P., Becker, D., Ivashikina, N., Dietrich, P., Roelfsema, M. R. G. & Hedrich, R. (2000) *FEBS Lett.* **486,** 93–98.
11. Kwak, J. M., Murata, Y., Baizabal-Aguirre, V. M., Merrill, J., Wang, M., Kemper, A., Hawke, S. D., Tallman, G. & Schroeder, J. I. (2001) *Plant Physiol.* **127,** 473–485.
12. Bechtold, N., Ellis, J. & Pelletier, G. (1993) *C. R. Acad. Sci.* **316,** 1194–1199.
13. Becker, D. (1990) *Nucleic Acids Res.* **18,** 203.
14. Koncz, C. & Schell, J. (1996) *Mol. Gen. Genet.* **204,** 383–396.
15. Clough, S. J. & Bent, A. F. (1998) *Plant J.* **16,** 735–743.
16. Vavasseur, A., Lascève, G. & Couchat, P. (1988) *Physiol. Plant* **73,** 547–552.
17. Leonhardt, N., Marin, E., Vavasseur, A. & Forestier, C. (1997) *Proc. Natl. Acad. Sci. USA* **94,** 14156–14161.
18. Dreyer, I., Antunes, S., Hoshi, T., Müller-Röber, B., Palme, K., Pongs, O., Reintanz, G. & Hedrich, R. (1997) *Biophys. J.* **72,** 2143–2150.
19. Daram, P., Urbach, S., Gaymard, F., Sentenac, H. & Chérel, I. (1997) *EMBO J.* **16,** 3455–3463.
20. Urbach, S., Chérel, I., Sentenac, H. & Gaymard, F. (2000) *Plant J.* **23,** 527–538.
21. Baizabal-Aguirre, V. M., Clemens, S., Uozumi, N. & Schroeder, J. I. (1999) *J. Membr. Biol.* **167,** 119–125.
22. Nakamura, R. L., Anderson, J. A. & Gaber, R. F. (1997) *J. Biol. Chem.* **272,** 1011–1018.
23. Ivashikina, N., Becker, D., Ache, P., Meyerhoff, O., Felle, H. H. & Hedrich, R. (2001) *FEBS Lett.* **508,** 463–469.
24. Felle, H. H., Hanstein, S., Steinmeyer, R. & Hedrich, R. (2000) *Plant J.* **24,** 297–304.
25. MacRobbie, E. A. C. (1983) *J. Exp. Bot.* **34,** 1695–1710.
26. Thiel, G. & Wolf, A. H. (1997) *Trends Plant Sci.* **2,** 339–345.
27. Gaymard, F., Pilot, G., Lacombe, B., Bouchez, D., Bruneau, D., Boucherez, J., Michaux-Ferriere, N., Thibaud, J. B. & Sentenac, H. (1998) *Cell* **94,** 647–655.
28. Gradmann, D. & Hoffstadt, J. (1998) *J. Membr. Biol.* **166,** 51–59.
29. Talbott, L. D. & Zeiger, E. (1998) *J. Exp. Bot.* **49,** 329–337.
30. Zimmermann, S. & Sentenac, H. (1999) *Curr. Opin. Plant Biol.* **2,** 477–482.

Corrections

BIOPHYSICS, CHEMISTRY. For the article "Watching proteins fold one molecule at a time," by Elizabeth Rhoades, Eugene Gussakovsky, and Gilad Haran, which appeared in issue 6, March 18, 2003, of *Proc. Natl. Acad. Sci. USA* (**100,** 3197–3202; First Published February 28, 2003; 10.1073/pnas.2628068100), the locants for Fig. 6 on page 3201 were incorrect. Locant *C* should have appeared as *B*, *E* should have appeared as *C*, *B* should have appeared as *D*, and *D* should have appeared as *E*. The corrected figure and its legend appear below.

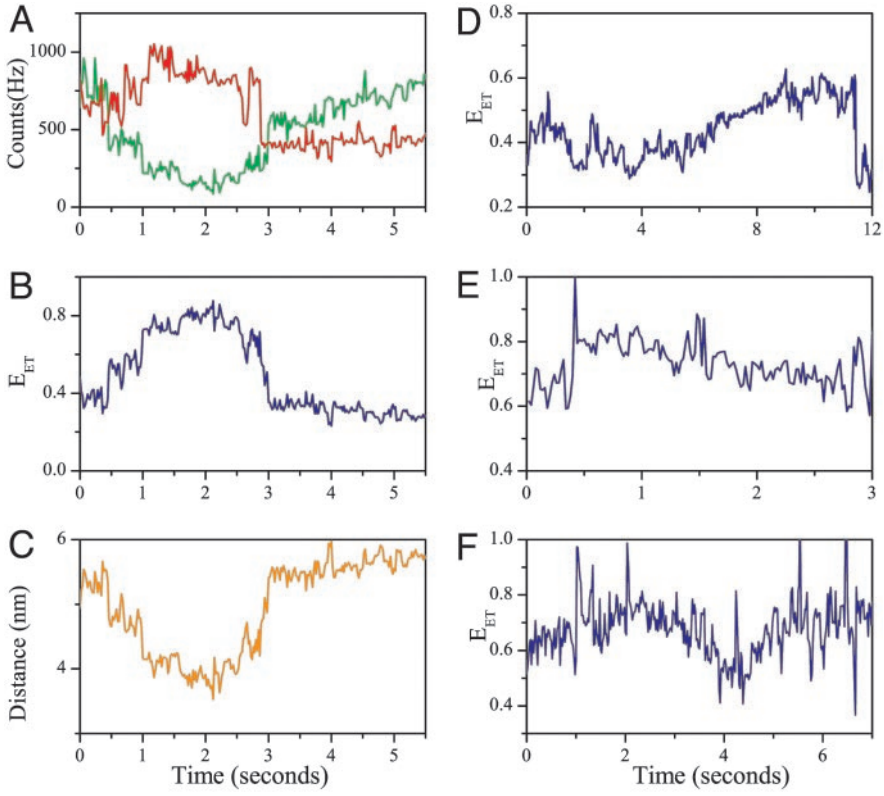

Fig. 6. Time-dependent signals from single molecules showing slow folding or unfolding transitions. (*A*) Signals showing a slow folding transition starting at ≈0.5 sec and ending at ≈2 sec. The same signals display a fast unfolding transition as well (at ≈3 sec). The acceptor signal is shown in red, and the donor is shown in green. (*B*) E_{ET} trajectory calculated from the signals in *A*. (*C*) The interprobe distance trajectory showing that the slow transition involves a chain compaction by only 20%. The distance was computed from the curve in *B* (32) by using a Förster distance (R_0) of 49 Å. This Förster distance was calculated by assuming an orientational factor (κ^2) of 2/3. However, the point discussed here (and in the text) does not depend on the exact value of κ^2 or R_0. (*D–F*) Additional E_{ET} trajectories demonstrating slow transitions. These transitions were identified, as already noted, by anticorrelated donor-acceptor intensity changes.

www.pnas.org/cgi/doi/10.1073/pnas.1232163100

PLANT BIOLOGY. For the article "The *Arabidopsis* outward K^+ channel *GORK* is involved in regulation of stomatal movements and plant transpiration," by Eric Hosy, Alain Vavasseur, Karine Mouline, Ingo Dreyer, Frédéric Gaymard, Fabien Porée, Jossia Boucherez, Anne Lebaudy, David Bouchez, Anne-Aliénor Véry, Thierry Simonneau, Jean-Baptiste Thibaud, and Hervé Sentenac, which appeared in issue 9, April 29, 2003, of *Proc. Natl. Acad. Sci. USA* (**100,** 5549–5554; First Published April 1, 2003; 10.1073/pnas.0733970100), the authors note that the word "azobenzenearsonate" should have read "abscisic acid" throughout the article. This error occurred in line 20 of the abstract; on page 5551, left column, second line from the bottom; on line 6 of the Fig. 3 legend; and on page 5553, right column, 11 lines from the bottom. The conclusions presented are unaffected by this change.

www.pnas.org/cgi/doi/10.1073/pnas.1332514100

Knockout of the guard cell K^+out channel and stomatal movements

Julian I. Schroeder*

Cell and Developmental Biology Section, Division of Biological Sciences, University of California at San Diego, La Jolla, CA 92093-0116

The central roles of potassium channels in regulating membrane potential and controlling action potential repolarization are well documented (1). In plants an additional important function of potassium channels in mediating long-term potassium transport during cell movements, turgor changes, and tropisms has been proposed. Two guard cells surround each stomatal pore in leaves and control the opening and closing of their central pore via increases in their solute content during stomatal opening (2) and decreases in solute content during stomatal closing (3). In this issue of PNAS, Hosy *et al.* (4) provide direct genetic evidence that outward rectifying potassium (K^+out) channels in guard cells contribute to stomatal closing in leaves. Guard cells accumulate potassium (K^+), which results in stomatal opening (2) and release K^+, which results in stomatal closing (3). Ion channel characterizations in guard cells, and motor cells that control turgor-driven leaf movements, led to the model that K^+ channels can contribute to the underlying long-term K^+ influx (5, 6) and K^+ efflux (5–7). Biophysical, cell biological, and second messenger regulation analyses by several groups have supported this model.

Hosy *et al.* identified an insertional T-DNA disruption mutant in the *Arabidopsis* guard cell-expressed outward-rectifying K^+out channel gene, *GORK*. Heterologous expression in *Xenopus* oocytes has previously shown that the *GORK* cDNA encodes an outward rectifying K^+ channel activity with properties similar to those described in guard cells and *GORK* is expressed in guard cells (8). Hosy *et al.* further generated a dominant negative GORK mutant by inserting the positively charged amino acid arginine into the K^+ selectivity filter domain of the GORK channel. The T-DNA disruption mutant, *gork-1*, showed no measurable K^+out channel activity in guard cells and dominant negative mutant lines showed <10% of native K^+ channel activity (4).

Stomatal movement analyses in response to abscisic acid and darkness showed that the *gork-1* disruption mutant caused a reduced stomatal closing response, providing genetic evidence for the function of K^+out channels (4). Furthermore, *gork* dominant negative mutants showed slight slowing of stomatal closure compared with WT responses. K^+ channel current activities in guard cells are approximately an order of magnitude larger than physiological K^+ fluxes during stomatal movements (6), which may account for the relatively limited effect of partial dominant negative *gork* repression. Gas exchange and plant water loss analyses also show that *gork-1* disruption reduces the rate of stomatal closing and increases water loss of leaves and whole plants. The *gork-1* mutant also shows slightly enhanced light-induced stomatal opening, which can be explained by the functions of K^+ channels in balancing K^+ efflux and K^+ influx in guard cells (4).

Genetic evidence shows that outward rectifying potassium channels in guard cells contribute to stomatal closing in leaves.

The *gork-1* mutant clearly shows a role for the GORK K^+ channel in stomatal closing. However, a residual abscisic acid (ABA)- and darkness-induced stomatal closing response in *gork-1* further points to redundant parallel turgor reduction mechanisms. Potassium salts and sucrose both have been proposed to function as major intracellular solutes that mediate stomatal opening (9). The *gork-1* mutant provides a model system in which the contribution of sucrose removal to stomatal closing by physiological stimuli such as ABA, CO_2, or darkness could be analyzed.

It is further likely that the *gork-1* mutant shows residual K^+ efflux via mechanisms other than GORK. In *Commelina communis* guard cells radiolabeled Rb^+ flux measurements allow quantification of time-dependent K^+ (Rb^+) transport in guard cells (3). This method has not been established in the smaller *Arabidopsis* guard cells, but if feasible, would be an important tool to compare K^+ efflux rates in *gork* mutants and WT. Analyses of inward-rectifying K^+ (K^+in) channel mutants have shown roles for these K^+in channels in long-term K^+ uptake (10, 11). For example, sodium hexanitrocobaltate (III) K^+ staining has been used to measure changes in *Arabidopsis* guard cell K^+ content during light-induced stomatal opening in these inward-rectifying K^+ uptake channel mutant lines (11) and could be used to analyze *gork* mutants. Elemental x-ray microanalysis can also be used to compare K^+ content in *Vicia faba* and WT and mutant *Arabidopsis* guard cells (2, 11). The characterization of the *gork-1* mutant will allow future analysis of the relative contributions of additional K^+, sucrose, and other possible solute transport and metabolic mechanisms to stimulus-induced stomatal closing.

Hosy *et al.* pose an interesting question of whether redundant solute release mechanisms function directly in parallel to K^+out channels or whether their roles become more prominent in the *gork-1* mutant background. Identification and mutation of other K^+ and solute efflux mechanisms will be needed to answer this question.

Although ABA enhances K^+out current activity (12), and K^+out channels are the predominant K^+ efflux current activity in guard cells (6, 13), other possible K^+ efflux mechanisms have been reported in these cells. In halophyte guard cells a cation-permeable conductance that mainly mediates Na^+ sodium influx has been characterized (14). This conductance is inhibited at elevated Ca^{2+} levels. Furthermore a transiently activated outward-rectifying K^+ current, named I_{AP}, was characterized in *Arabidopsis* guard cells and was predicted to contribute to K^+ efflux (15). Both of these conductances are down-regulated by Ca^{2+} elevations (14, 15). Because the present characterization of K^+ currents in *gork-1* mutants was performed at 20 mM extracellular $CaCl_2$ (4), reducing extracellular Ca^{2+} concentrations may unmask additional K^+ efflux activities.

The finding that the K^+out channel currents do not inactivate even when guard cells are depolarized for long con-

See companion article on page 5549.

*E-mail: julian@biomail.ucsd.edu.

tinuous periods of 20 min (16) suggests that these channels can mediate K^+ efflux during long-term depolarizations that occur in response ABA (17). However, some guard cells have also been shown to undergo repetitive transient depolarizations (18). Furthermore, ABA is known to cause repetitive cytoplasmic calcium increases (19, 20). Repetitive cytosolic Ca^{2+} elevations have been linked to transient plasma membrane voltage changes (21). The transiently activated outward rectifying K^+ conductance I_{AP} (15) could conceivably contribute to transient K^+ efflux in response to repetitive depolarizations.

Even the nontransient GORK-type K^+out channel would be activated during short-term depolarizations, which in turn would favor repolarization to negative membrane voltages. Therefore, it would also be interesting to determine whether *gork-1* knockout enhances guard cell depolarizations and affects membrane potential and cytoplasmic Ca^{2+} oscillations.

Upon water withdrawal *gork-1* plants showed increased water loss both in leaves and whole plants (4). These findings are consistent with the enhanced stomatal apertures and reduced ABA response in the *gork-1* mutant. Presently only two *Arabidopsis* genes, *SKOR* and *GORK*, have been unequivocally characterized as plant plasma membrane K^+out channel genes (4, 8, 22). A different type of plant K^+ channel gene, the *KCO* class, has been proposed to also contribute to plasma membrane K^+out channel activities (23). It is interesting that the *gork-1* knockout line did not show any further pleiotropic growth or morphological or developmental defects (4). Despite RT-PCR analysis showing expression of *GORK* in root hair cells (24), no root hair phenotype was found for the *gork-1* mutant (4). Further studies may reveal conditional phenotypes and redundancies.

In conclusion, the *gork-1* knockout analysis of Hosy *et al.* provides molecular genetic evidence for the model that K^+out channels function in mediating stomatal closing and turgor reduction in plant cells (6, 7). Furthermore, the availability of a K^+out channel knockout mutant will allow researchers to address important new future questions in stomatal physiology and plant K^+ transport.

1. Hille, B. (2001) *Ionic Channels of Excitable Membranes* (Sinauer, Sunderland, MA).
2. Humble, G. D. & Raschke, K. (1971) *Plant Physiol.* **48,** 447–453.
3. MacRobbie, E. A. C. (1981) *J. Exp. Bot.* **32,** 563–572.
4. Hosy, E., Vavasseur, A., Mouline, K., Dreyer, I., Gaymard, F., Porée, F., Boucherez, J., Lebaudy, A., Bouchez, D., Véry, A.-A., *et al*. (2003) *Proc. Natl. Acad. Sci. USA* **100,** 5549–5554.
5. Schroeder, J. I., Hedrich, R. & Fernandez, J. M. (1984) *Nature* **312,** 361–362.
6. Schroeder, J. I., Raschke, K. & Neher, E. (1987) *Proc. Natl. Acad. Sci. USA* **84,** 4108–4112.
7. Moran, N., Ehrenstein, G., Iwasa, K., Mischke, C., Bare, C. & Satter, R. L. (1988) *Plant Physiol.* **88,** 643–648.
8. Ache, P., Becker, D., Ivashikina, N., Dietrich, P., Roelfsema, M. & Hedrich, R. (2000) *FEBS Lett.* **486,** 93–98.
9. Talbott, L. D. & Zeiger, E. (1998) *J. Exp. Bot.* **49,** 329–337.
10. Hirsch, R. E., Lewis, B. D., Spalding, E. P. & Sussman, M. R. (1998) *Science* **280,** 918–921.
11. Kwak, J. M., Murata, Y., Baizabal-Aguirre, V. M., Merrill, J., Wang, J., Kemper, A., Hawke, D., Tallman, G. & Schroeder, J. I. (2001) *Plant Physiol.* **127,** 1–13.
12. Blatt, M. R. (1992) *J. Gen. Physiol.* **99,** 615–644.
13. Roelfsema, M. R. G. & Prins, H. B. A. (1997) *Planta* **202,** 18–27.
14. Véry, A.-A., Robinson, M. F., Mansfield, T. A. & Sanders, D. (1998) *Plant J.* **14,** 509–521.
15. Pei, Z.-M., Baizabal-Aguirre, V. M., Allen, G. A. & Schroeder, J. I. (1998) *Proc. Natl. Acad. Sci. USA* **95,** 6548–6553.
16. Schroeder, J. I. (1988) *J. Gen. Physiol.* **92,** 667–683.
17. Thiel, G., MacRobbie, E. A. C. & Blatt, M. R. (1992) *J. Membr. Biol.* **126,** 1–18.
18. Gradmann, D., Blatt, M. R. & Thiel, G. (1993) *J. Membr. Biol.* **136,** 327–332.
19. Staxen, I., Pical, C., Montgomery, L. T., Gray, J. E., Hetherington, A. M. & McAinsh, M. R. (1999) *Proc. Natl. Acad. Sci. USA* **96,** 1779–1784.
20. Allen, G. J., Chu, S. P., Harrington, C. L., Schumacher, K., Hoffmann, T., Tang, Y. Y., Grill, E. & Schroeder, J. I. (2001) *Nature* **411,** 1053–1057.
21. Grabov, A. & Blatt, M. R. (1998) *Proc. Natl. Acad. Sci. USA* **95,** 4778–4783.
22. Gaymard, F., Pilot, G., Lacombe, B., Bouchez, D., Bruneau, D., Boucherez, J., Michaux-Ferriere, N., Thibaud, J. B. & Sentenac, H. (1998) *Cell* **945,** 647–655.
23. Czempinski, K., Zimmermann, S., Ehrhardt, T. & Müller-Röber, B. (1997) *EMBO J.* **16,** 2565–2575.
24. Ivashikina, N., Becker, D., Ache, P., Meyerhoff, O., Felle, H. H. & Hedrichh, R. (2001) *FEBS Lett.* **508,** 463–469.

⇒ zurück zur Übersicht

2001

Dreyer, Michard, Lacombe, Thibaud

A plant *Shaker*-like K^+ channel switches between two distinct gating modes resulting in either inward-rectifying or 'leak' current.

FEBS Lett. **505**:233-239.

A plant Shaker-like K^+ channel switches between two distinct gating modes resulting in either inward-rectifying or 'leak' current

Ingo Dreyer[1,2], Erwan Michard[2], Benoît Lacombe[3], Jean-Baptiste Thibaud*

Laboratoire de Biochimie et Physiologie Moléculaire des Plantes, UMR 5004, Agro-M/CNRS/INRA/UM2, Place Viala, 34060 Montpellier, Cedex 1, France

Received 12 July 2001; revised 31 July 2001; accepted 31 July 2001

First published online 27 August 2001

Edited by Maurice Montal

Abstract Among the Shaker-like plant potassium channels, AKT2 is remarkable because it mediates both instantaneous 'leak-like' and time-dependent hyperpolarisation-activated currents. This unique gating behaviour has been analysed in *Xenopus* oocytes and in COS and Chinese hamster ovary cells. Whole-cell and single-channel data show that (i) AKT2 channels display two distinct gating modes, (ii) the gating of a given AKT2 channel can change from one mode to the other and (iii) this conversion is under the control of post-translational factor(s). This behaviour is strongly reminiscent of that of the KCNK2 channel, recently reported to be controlled by its phosphorylation state. © 2001 Published by Elsevier Science B.V. on behalf of the Federation of European Biochemical Societies.

Key words: Potassium channel; Voltage-gating; Post-translational modification; Patch-clamp

1. Introduction

All Shaker-like plant K^+ channel α-subunits are characterised by a common structure, a hydrophobic core displaying six transmembrane segments (S1–S6) and a pore forming motif P between S5 and S6. The tetrameric channels they form, however, segregate into two channel sub-families according to the direction in which they transport K^+ ions. Inwardly-rectifying K^+ (K^+_{in}) Shaker channels like KAT1 [1–5], KAT2 [6], KST1 [7], AKT1 [8,9], SKT1 [10], ZMK1 [11] and LKT1 [12] are closed at membrane voltages less negative than about −80 mV. They open upon hyperpolarisation and thus mediate potassium uptake under physiological conditions. In contrast, outwardly-rectifying (K^+_{out}) Shaker channels like SKOR [13] and GORK [14] mediate K^+ efflux by closing upon hyperpolarisation and opening upon depolarisation.

In this context, the potassium channels AKT2 from *Arabidopsis thaliana* and ZMK2 cloned from *Zea mays* display a particular behaviour because they mediate both potassium influx and potassium efflux [15–20]. These channels, which share about 40% identity with K^+_{in} channels such as KAT1 and 27% with K^+_{out} channels such as SKOR, are characterised by an instantaneous, 'leak-like' potassium conductance which superimposes with a time-dependent component increasing in magnitude upon hyperpolarisation. This unique gating behaviour and its modulation are poorly understood, and therefore, their roles in the physiological activity of AKT2 and its homologues remain speculative.

2. Materials and methods

2.1. Expression of AKT2 in COS and Chinese hamster ovary (CHO) cells and in Xenopus oocytes

AKT2 cDNA was cloned in pCI (Promega, Madison, WI, USA) or pIRES [21], which allowed co-expression of AKT2 and the membrane protein CD8 [22].

COS-7 cells were cultured in Dulbecco's modified Eagle's medium (DMEM) (Gibco-BRL) complemented with 10% foetal bovine serum (Gibco-BRL) at 37°C in 5% CO_2. One day before transfection, cells were detached with trypsin–EDTA (Gibco-BRL) and transferred to 35-mm dishes (20 000 cells per dish). Per dish, 80 μl HBS 2× (NaCl 280 mM, HEPES 50 mM, Na_2HPO_4 15 mM, pH 7.15) were gently mixed with 80 μl TE–$CaCl_2$ (1 mM Tris–HCl, pH 8, EDTA 1 mM; $CaCl_2$ 250 mM) containing 1.5 μg pIRES-AKT2. The DNA precipitate was added to cells in their culture media. After 8 h, cells were rinsed twice with DMEM. Electrophysiological analysis was performed 3 or 4 days later.

CHO cells were cultured in the same conditions as COS cells (HT media supplement (Sigma) was added to culture media). The day before transfection, cells were detached with trypsin–EDTA and transferred to 35-mm dishes (160 000 cells per dish). Cells were then transfected with 1.5 μg pIRES-AKT2 DNA per plate using Fugene 6 reagent (Boehringer Mannheim) as described by the manufacturer. Electrophysiological analysis was performed 2 or 3 days later. Control experiments were performed on cells transfected with pIRES alone.

Xenopus oocytes (CRBM, CNRS, Montpellier, France) were injected with 20 ng (0.02 μl) of pCI-AKT2. Control oocytes were injected with 0.02 μl deionised water.

2.2. Electrophysiological recordings

Two-electrode voltage-clamp experiments on oocytes were carried out as previously described [23]. Patch-clamp experiments on oocytes (single-channel) and on COS and CHO cells (whole-cell) expressing AKT2 were carried out as previously described [17].

2.3. Tail-current analysis

In whole-cell experiments tail currents were recorded after the test pulse. They displayed a single-exponential time course as routinely checked with the fitting procedure featured by Clampfit software (version 6.4, Axon Instruments Inc., USA). All subsequent analyses were made on the initial value of the tail current sampled on the exponential fit and denoted i_0. The dependence of i_0 on the test-pulse voltage (E) was fitted by the following equation, which is a modified form of the classically used Boltzmann law:

$$i_0(E) = i_{0,\min} + (i_{0,\max} - i_{0,\min}) * [1/(1 + \exp[z * F/(R * T) * (E - E_{1/2})])]$$

*Corresponding author. Fax: (33)-499-612 930.
E-mail address: thibaud@ensam.inra.fr (J.-B. Thibaud).

[1] Present address: Universität Potsdam, Institut für Biochemie und Biologie, Abt. Molekularbiologie, Karl-Liebknecht-Str. 24/25, Haus 20, D-14476 Golm, Germany.
[2] These authors contributed equally to this work.
[3] Present address: Julius-von-Sachs-Institut für Biowissenschaften, Lehrstuhl Botanik I, Molekulare Pflanzenphysiologie und Biophysik, Julius-von-Sachs-Platz 2, D-97082 Würzburg, Germany.

0014-5793/01/$20.00 © 2001 Published by Elsevier Science B.V. on behalf of the Federation of European Biochemical Societies.
PII: S0014-5793(01)02832-0

where there are four adjustable parameters: $i_{0,max}$ and $i_{0,min}$, the values of maximum and minimum i_0, z, the apparent gating charge, and $E_{1/2}$, the half-activation potential. In the example of Fig. 2, data from five cells were pooled to yield the common z and $E_{1/2}$ values used for curves shown in Fig. 2C,D.

3. Results and discussion

3.1. AKT2 macroscopic current diversity

AKT2 macroscopic current was recorded (whole-cell configuration) in COS and CHO cells. Pulses of 1.6 s were applied from a holding potential of +40 mV to a voltage ranging from +60 mV (CHO) or +80 mV (COS) to −140 mV (steps of −20 mV). In the two systems, AKT2 currents displayed similar properties to those previously reported [17]: these currents showed a time- and voltage-dependent component in addition to an instantaneous (i.e. both time- and voltage-independent) component. Both components were routinely identified as K^+ currents, displaying reversal at E_K and block by Cs^+ ions (not shown, see ref. [17]) and were never observed in control cells (see Section 2). Intriguingly, the relative importance of the so-called leak current with respect to the total AKT2 current (this was arbitrarily calculated at −140 mV, expressed in % and hereafter denoted $r_{-140\,mV}$) was extremely variable. In 22 tested CHO cells (2 or 3 days after transfection) $r_{-140\,mV}$ varied from 0.68 to 73%. The $r_{-140\,mV}$ variation range extended from 22 to 94% in 56 tested COS cells (3 or 4 days after transfection). Sample records shown in Fig. 1A exemplify this fact: from left to right the $r_{-140\,mV}$ value (figured as the white portion of the bar aside current records, Fig. 1A) varied from 11 up to 84%. As a consequence of such a variation, the whole-cell current/voltage relationship at steady-state could vary from a strongly inward-rectifying pattern to an essentially leaky one: Fig. 1B shows AKT2 current from two COS cells of the same batch; for a similar current intensity, the $r_{-140\,mV}$ value is 22% in one cell, 94% in the other. In both COS- and CHO-expression systems, it was noticed that $r_{-140\,mV}$ increased with time 'post-transfection' (Fig. 1C), while the total AKT2 current tended to increase. For example, in CHO cells, total AKT2 current and $r_{-140\,mV}$ were -1.33 ± 0.21 nA and $22.9 \pm 6.0\%$ ($n = 12$) after 2 days and -3.08 ± 0.62 nA and $48.9 \pm 5.3\%$ ($n = 11$) after 3 days. In

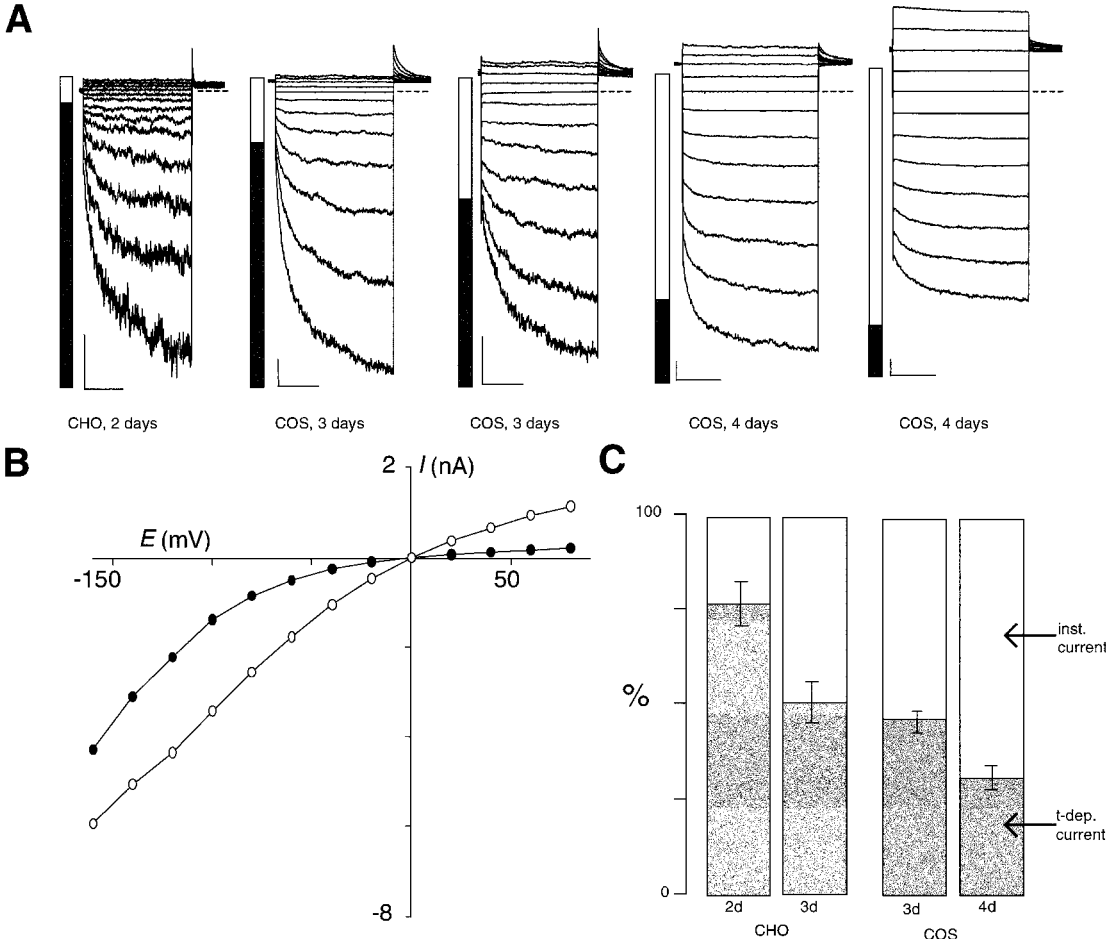

Fig. 1. Broad pattern of whole-cell currents recorded in COS or CHO cells expressing AKT2. A: Sample current records obtained in CHO or COS cells. Horizontal scale bar is 0.5 s and vertical one is 0.5 nA. Bar graphs at left of traces display the relative importance, at −140 mV, of time-dependent current (grey) and instantaneous current (white). B: Current/voltage (*I*/*E*) relationship at steady-state in two AKT2-expressing COS cells. These cells are from the same batch (3 days after transfection) and exemplify the variability of membrane rectification resulting from AKT2 expression. C: Increase of the relative importance at −140 mV (shown by the white section of bar graphs) of the instantaneous current with time after cell transfection. Data are shown as mean ± S.D. ($n = 5$). Bath solution contained (mM): KCl (150), $CaCl_2$ (1), $MgCl_2$ (1.5), HEPES/NaOH (10, pH 7.4); pipette solution contained (mM): KCl (150), $MgCl_2$ (1.5), EGTA (3), HEPES/NaOH (10, pH 7.2). Potassium equilibrium potential (E_K) is at 0 mV. From a holding potential of +40 mV, 1.6-s-long pulses were applied at voltages ranging from +60 mV (CHO) or +80 mV (COS) to −140 mV (20 mV steps).

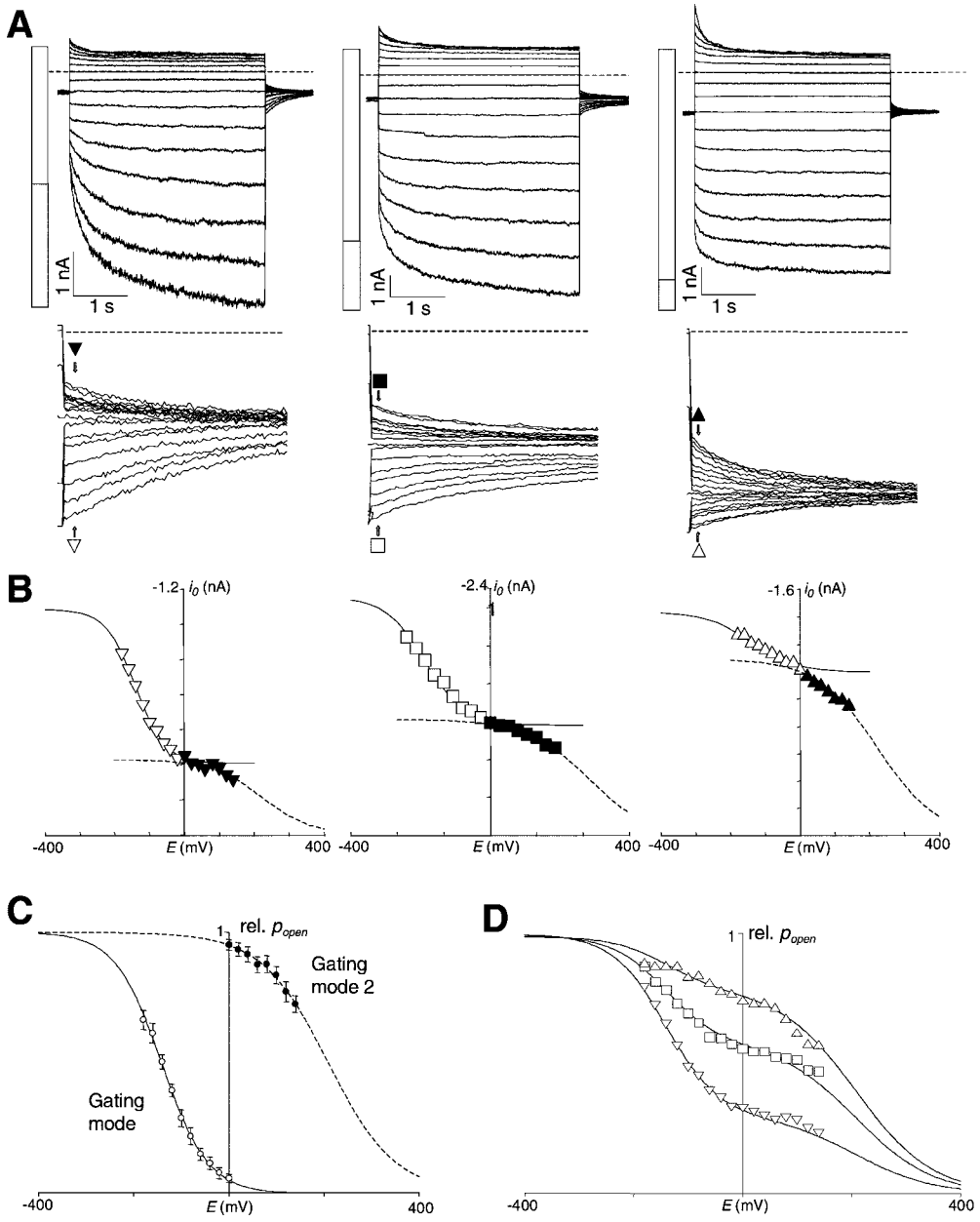

Fig. 2. Tail-currents analysis suggesting dual voltage-gating of AKT2 channels. A: Pulse and tail whole-cell AKT2 currents elicited by stimulation in the −180 to +140 mV range (example of three COS cells). Top: Horizontal scale bar is 1 s and vertical one is 1 nA. Bar graphs have the same meaning as in Fig. 1 (white area shows $r_{-140\,mV}$). Bottom: Tail currents are shown at larger scale below the whole records. Symbols (black or white, respectively, for i_0 resulting from pulses at positive or negative voltages) indicate the sampling-time of data (i_0) analysed in (B). Horizontal dashed lines in top and bottom graphs indicate the zero current level. B: Dependence of i_0 on test-pulse voltage. Data are from (A) with cross-referenced symbols. Parameters of two Boltzmann equations were adjusted (Marquardt–Levenberg algorithm, see Section 2) to fit separately the white and black point sets. The resulting curves are shown with plain and dashed lines respectively. C: Averaged dual Boltzmann curves obtained for five cells, as in (B). Data are shown as rel. p_{open} (mean ± S.D., $n = 5$) after normalisation of i_0 data. Left-hand/right-hand curve show, respectively, voltage-gating of type-1/type-2 AKT2 channels. D: Rel. p_{open} (E) curves resulting from combination of $(1-r_{abs.})$% type-1 and $r_{abs.}$% type-2 channels (see text). Parameters of the two Boltzmann components were from (C) and the value of $r_{abs.}$ was adjusted to fit normalised data from (B) (cross-referenced symbols). See Fig. 1 for bath and pipette solutions.

COS cells, between 3 and 4 days after transfection, the total AKT2 current increase (from −3.34 ± 0.99 nA to −5.01 ± 0.92 nA, $n = 11$) was, however, less than the increase of $r_{-140\,mV}$ (from 53.9 ± 2.9% to 68.7 ± 3.3%, $n = 17$).

3.2. May the AKT2 channel have two gating modes?

Neither the fact that a Shaker-like channel can enable some leak current to flow in addition to a time- and voltage-dependent one, nor the fact that the relative importance of this leak current (i.e. $r_{-140\,mV}$) can greatly vary are as yet understood. One hypothesis would be that two types of AKT2 channels were operating. The so-called type-1 AKT2 channels would behave as voltage-gated channels, while the so-called type-2 AKT2 channels would behave as open-leak channels. Among the three expression systems (CHO and COS cells, and *Xenopus* oocytes) in which this unexplained AKT2 behaviour was observed, the COS cell line we used was the one which withstood the more extended voltage range, with less endogenous

current. Exploring strongly positive values of membrane potential (up to +140 mV) revealed a slow current component ($\tau_{100\,mV} = 450$ ms) in AKT2-expressing COS cells, which was never observed in control cells. For example, upon a voltage step from −40 mV to +140 mV, the evoked current not only responded instantaneously to the altered electrochemical gradient but deactivated in a time- and voltage-dependent manner and, accordingly, the tail current recorded subsequently (i.e. upon a step back to −40 mV, see dashes and symbols in Fig. 2A) showed re-activation ($\tau = 280$ ms).

Currents recorded from three cells displaying $r_{-140\,mV}$ values of 53, 74 and 88% are shown in Fig. 2A. The amplitude of the time-dependent (deactivating) current recorded at strongly positive potential values increased with the relative importance of the leak current at −140 mV (i.e. the $r_{-140\,mV}$ value). In the framework of the hypothesis proposed above, this de-

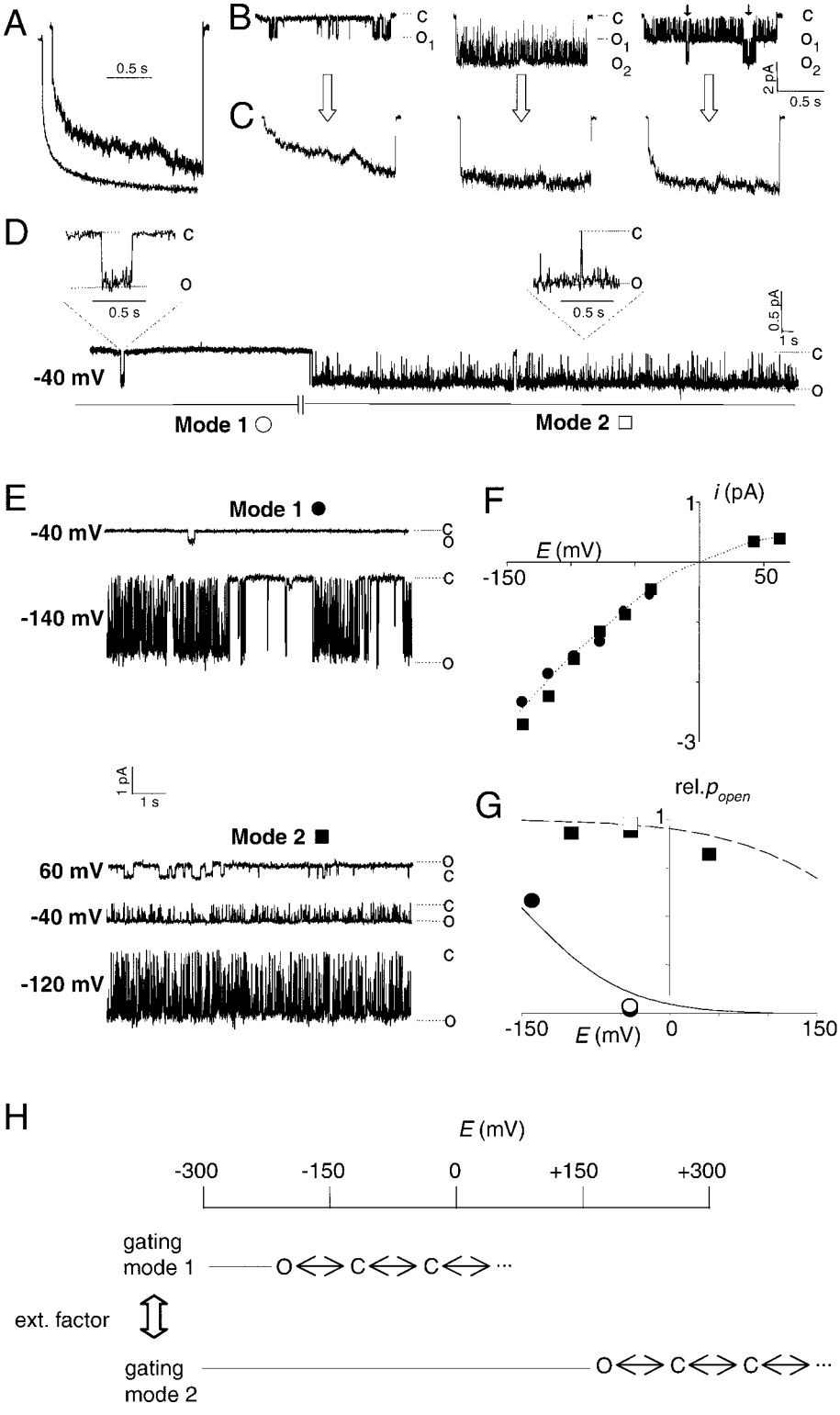

activating current could be ascribed to type-2 channels. By the same token, the current re-activating at −40 mV following pulses to positive potential values could be ascribed to type-2 channels (see enlargement of the tail currents in Fig. 2A). The initial value of tail current (i_0) was plotted against the pulse potential (Fig. 2B). From extreme negative to extreme positive potentials, the curve displayed two phases, i_0 tending sigmoidally to a 'plateau' value (reached at about 0 mV) within the first phase, and then varying further towards zero within the second (Fig. 2B). Each of these two phases could reflect the voltage dependence of relative open probability (rel. p_{open}) of each of the two AKT2 channel populations. Namely, type-1 AKT2 channels would be fully activated at very negative potentials and fully deactivated at positive potentials, while type-2 channels would show partial deactivation only at potential values positive to +50 mV and would probably be fully deactivated at strongly positive potentials. This logical deduction from the initial hypothesis is further illustrated in Fig. 2C, where data were gathered from five cells displaying $r_{-140\,mV}$ values ranging from 53 to 88%. i_0 data obtained for a stimulation in the −180 mV to 0 mV range and those obtained for a stimulation in the 0 mV to +140 mV range were analysed separately. Whatever the $r_{-140\,mV}$ value, a single pair of Boltzmann curves, with apparent gating charges of 0.46 and 0.33 and midpoint found at −143 mV and +222 mV for type-1 and type-2, respectively, acceptably fitted rel. p_{open} data (see Section 2). The two rel. $p_{open}(E)$ terms obeying Boltzmann's law and being denoted *B1* and *B2*, it was checked that the biphasic curves shown in Fig. 2B could be fitted by $(1-r_{abs.})*B1+r_{abs.}*B2$, with $r_{abs.}$ representing the absolute (i.e. at any voltage) proportion of type-2 channels in the AKT2 channel population (Fig. 2D): this yielded $r_{abs.}$ values of 30, 59 and 80%. The $r_{-140\,mV}$ parameter introduced above was an underestimation of $r_{abs.}$ because type-1 channels are only partially activated at −140 mV. In turn, the $r_{abs.}$ and the Boltzmann parameters obtained in Fig. 2C,D respectively allowed to estimate the $r_{-140\,mV}$ parameter values for the three cells shown in Fig. 2A. This yielded 52, 78 and 91%, $r_{-140\,mV}$ values very similar to those obtained graphically from the raw data of Fig. 2A.

3.3. Two types of gating at the single-channel level

If the population of AKT2 channels actually sub-divides into two sub-populations, this should be observed at the single-channel level. In order to check the relevance of the ad hoc hypothesis stated above, further experiments were performed in conditions allowing recording of AKT2 unitary currents. Patch-clamp experiments on oocytes were performed in the cell-attached configuration because channel activity was invariably lost upon patch excision. Multi-channel patches (Fig. 3A–C) as well as single-channel patches (Fig. 3D–G) could be obtained. Histogram amplitudes (not shown) yielded a single value of unitary current, ≈2.3 pA at −100 mV, well in line with the unitary conductance of 22–25 pS reported previously for AKT2 [16,17]. Repeated 1.6 s pulses from a 0 mV holding potential to −100 mV were applied to multi-channel patches and subsequently averaged to yield pseudo-macroscopic current traces. A typical result is shown in Fig. 3A (201 records averaged) and compared to a macroscopic current trace obtained in a two-electrode voltage-clamp experiment. Similar time courses of both traces further support that the ≈2.3 pA unitary current denoted AKT2 activity. Analysing the pulses in deeper detail revealed an interesting feature. Although the unitary current amplitude was always the same, two different kinds of openings were observed: short openings with a mean open time of about 40 ms (Fig. 3B, left) and long openings of a duration apparently longer than 1.6 s, which were frequently interrupted by very short (< 3 ms) flickering closing events (Fig. 3B, middle). The 201 pulses were then sub-grouped in three categories: (I) 112 traces with only short openings (Fig. 3B, left), (II) 24 traces with only long openings (Fig. 3B, middle) and (III) 65 traces where the two types of openings were observed in the same pulse interval (Fig. 3B, right). The average of category I pulses displayed time-dependent activation kinetics but lacked any instantaneous component (Fig. 3C, left). The average of category II pulses displayed the instantaneous component but lacked any time-dependent activation kinetics (Fig. 3C, middle). The average of category III pulses displayed both an instantaneous and a time-dependent component (Fig. 3C, right). As suggested by macroscopic current analyses (Fig. 2), the two kinetic components of the AKT2 current would therefore correspond, at the single-channel level, to two different gating modes: a 'mode 1' resulting in short openings at −100 mV (Fig. 3C, left) and a 'mode 2' resulting in long openings at −100 mV (Fig. 3C, middle). Thus, two sub-populations of AKT2 channels would actually co-exist in the membrane.

In the following, two alternatives are considered, which

←

Fig. 3. Separation of two gating components of AKT2 at the single-channel level. A: Average of 201 current traces recorded on a multi-channel patch (cell-attached configuration, upper trace) compared to a macroscopic current trace obtained by two-electrode voltage-clamp experiments on an AKT2-expressing *Xenopus* oocyte (lower trace). In both cases, currents were evoked by 1.6-s-long voltage steps to −100 mV from a holding potential of 0 mV. External standard solution was composed of 100 mM KCl, 1 mM $CaCl_2$, 1.5 mM $MgCl_2$, 10 mM HEPES, pH 7.4 (NaOH). Pipettes were filled with 3 M KCl (two-electrode voltage-clamp) or with 100 mM KCl, 1 mM $CaCl_2$, 1.5 mM $MgCl_2$, 10 mM HEPES, pH 7.4 (NaOH) (cell-attached). B: Representative examples of the three categories of current traces obtained within the whole set of 201 traces. Left: One of the 112 traces showing short openings only; middle: one of the 24 traces showing long openings only; right: one of the 65 traces showing both types of opening (small arrows indicate short openings). C: Average of each category of traces shown in (B). D: 60-s-long segment of a gap-free record obtained at −40 mV on a single-channel patch showing a transition from gating mode 1 to gating mode 2. White symbols cross-refer to rel. p_{open} values plotted in (G). E: 10-s-long segments of a gap-free record obtained at different potential values on a single-channel patch gating either in mode 1 (two traces at top) or in mode 2 (three traces at bottom). Black symbols cross-refer to rel. p_{open} values plotted in (G). F: Values of unitary current obtained in same conditions as (D) and (E) plotted against potential. Circles and squares indicate, respectively, data from gating mode 1 and from gating mode 2. G: Rel. p_{open} in the patches shown in (D) (white) and (E) (black) plotted against voltage. The lines represent the rel. p_{open} (E) curves obtained in Fig. 2D. H: Proposed gating scheme for AKT2. The AKT2 channel population divides into two different fractions characterised by different gating modes. In mode 1, the gating is described by voltage-dependent transitions between several closed states (C) and the open state (O). In mode 2, the activation threshold is shifted to more positive values. In our experimental conditions with moderate voltages tolerated by the oocytes (−160 mV to +50 mV), a channel in mode 2 seems to be open all the time. The conversion of one channel from one mode into the other (figured by a ⇕) is under the control of – yet unknown – channel extrinsic factors.

have clearly different biophysical meanings: (i) a given channel belongs definitely to either type-1 or type-2 and (ii) any given channel can switch between the two gating modes. In the former situation, the above defined $r_{abs.}$ parameter represents the proportion of type-2 channels in the whole population, e.g. after irreversible post-transcriptional events resulting in expression of AKT2 channels of two types. In the latter situation, the $r_{abs.}$ value at steady-state has the meaning of a probability, namely the probability for any channel to gate in mode 2, i.e. to be of type-2; this may result from late and reversible post-translational events such as interaction with a cytosolic regulatory factor that could change the gating mode of the AKT2 channel. It is worth noting that the two gating modes were always observed in all studied patches. For instance, in the experiment displayed in Fig. 3A–C, the patch harboured channels showing the two gating modes. Up to three channels gating in mode 2 and up to two channels gating in mode 1 were observed simultaneously in some pulses. However in all the 201 pulses, never more than three channels were active at the same time. With respect to these data, the first of the two above alternatives would imply (i) that at least five channels co-existed in this patch (two of mode 1 and three of mode 2), (ii) that they never opened all at the same time (none of the 65 category-III records showed more than three channels open), (iii) that the mode 1 channels remained silent in all the 24 category-II records and (iv) that the mode 2 channels remained silent in all the 112 category-I records.

To obtain further lines of evidence for the ability of a given channel to switch between the two gating modes, gap-free records obtained on single-channel patches were analysed (Fig. 3D–G). In such records, transitions from one gating mode to the other were often observed. An example of transition from mode 1 to mode 2 at −40 mV is shown in panel D. During the phase in mode 1 (more than 49 s long), the rel. p_{open} was 0.014 at −40 mV. During the phase in mode 2 (more than 60 s long), rel. p_{open} was 0.96 at −40 mV. The white circle and the white square in panel G show that these rel. p_{open} values are in good agreement with the curves derived from macroscopic currents. 10-s-long segments of a gap-free record made on another patch are shown in panel E. These segments of record were selected before (Fig. 3E, top) and after (Fig. 3E, bottom) a clear transition from mode 1 and mode 2, such as the one shown in panel D. The effect of voltage on the channel is shown in both gating modes in panel E. At any studied potential, open time was much longer in mode 2 than in mode 1 (see above text relative to Fig. 3B). For instance, at +60 mV the channel never opened in mode 1 (not shown), while it showed long open and short closed times in mode 2 (Fig. 3E). Unitary current (i) and rel. p_{open} corresponding to sample records obtained in the −140 to +60 mV range are plotted against voltage in panels F and G, respectively (black circles: mode 1; black squares: mode 2). Analysis of mode 1 and mode 2 records yielded the same value for unitary current (at potential values negative to −40 mV; Fig. 3F). By contrast, rel. p_{open} values determined in each case were clearly different for mode 1 and mode 2 records and agreed well with the Boltzmann curves derived from the analyses of macroscopic currents recorded in COS cells (Fig. 3G).

3.4. Dual-gating mode of AKT2 channel: control by some unidentified post-translational event

Based on the whole set of observations, a model can be proposed accounting for the complex behaviour of AKT2. At a given time, the AKT2 channel population divides into two sub-populations. Some AKT2 channels gate in mode 1, the others in mode 2. The former channels display a voltage-gating behaviour within the commonly studied voltage range (half-activation potential in the −140 mV range), like the well-described KAT1 channel [24]. The gating of this fraction could be described by a multi-state scheme (Fig. 3H, mode 1). Mode 2 channels are also voltage-gated (rel. p_{open} at −40 mV > rel. p_{open} at +60 mV, see Fig. 3G), the half-activation potential being, however, far more positive (> +200 mV, see also Fig. 2), similar to that of the S4-mutant KAT1-S168R [25]. The gating of mode 2 channels might also be described by a multi-state scheme (Fig. 3H, mode 2). There must be, as suggested in the preceding section, some late and reversible post-translational events (figured by the vertical ⇔ in Fig. 3H) that affect the gating mode of AKT2 channels. Whether this may be an interaction with some cytoplasmic factor, which would result either in the binding of a cyclic nucleotide, a regulatory peptide, etc., or in a protonation, an oxidation, a phosphorylation event remains to be elucidated. Interestingly, Bockenhauer and coworkers recently reported an analogous change in gating mode of the animal KCNK2 channel: this TWIK-like (2-pore and K^+-selective) channel behaves as a leak channel when dephosphorylated and as a depolarisation-activated outward rectifier upon phosphorylation [26]. We are currently investigating a possible phosphorylation dependency of AKT2 channel operation.

Acknowledgements: We are grateful to Jossia Boucherez for expert technical assistance. Furthermore, we thank Isabel Lefevre for helpful comments and critical reading of the manuscript. This work was partly supported by the European Communities' BIOTECH Program (BIO4-CT96), by Rhône-Poulenc, and by a Marie-Curie Fellowship of the European Union to I.D. (Contract No. ERBBIO4CT985058, Proposal No. 980115).

References

[1] Anderson, J.A., Huprikar, S.S., Kochian, L.V., Lucas, W.J. and Gaber, R.F. (1992) Proc. Natl. Acad. Sci. USA 89, 3736–3740.
[2] Schachtman, D.P., Schroeder, J.I., Lucas, W.J., Anderson, J.A. and Gaber, R.F. (1992) Science 258, 1654–1658.
[3] Hedrich, R., Moran, O., Conti, F., Busch, H., Becker, D., Gambale, F., Dreyer, I., Küch, A., Neuwinger, K. and Palme, K. (1995) Eur. Biophys. J. 24, 107–115.
[4] Hoshi, T. (1995) J. Gen. Physiol. 105, 309–328.
[5] Véry, A.-A., Gaymard, F., Bosseux, C., Sentenac, H. and Thibaud, J.-B. (1995) Plant J. 7, 321–332.
[6] Pilot, G., Lacombe, B., Gaymard, F., Cherel, I., Boucherez, J., Thibaud, J.-B. and Sentenac, H. (2001) J. Biol. Chem. 276, 3215–3221.
[7] Müller-Röber, B., Ellenberg, J., Provart, N., Willmitzer, L., Busch, H., Becker, D., Dietrich, P., Hoth, S. and Hedrich, R. (1995) EMBO J. 14, 2409–2416.
[8] Sentenac, H., Bonneaud, N., Minet, M., Lacroute, F., Salmon, J.-M., Gaymard, F. and Grignon, C. (1992) Science 256, 663–665.
[9] Gaymard, F., Cerutti, M., Horeau, C., Lemaillet, G., Urbach, S., Ravallec, M., Devauchelle, G., Sentenac, H. and Thibaud, J.-B. (1996) J. Biol. Chem. 271, 22863–22870.
[10] Zimmermann, S., Talke, I., Ehrhardt, T., Nast, G. and Müller-Röber, B. (1998) Plant Physiol. 116, 879–890.
[11] Philippar, K., Fuchs, I., Lüthen, H., Hoth, S., Bauer, C.S., Haga, K., Thiel, G., Ljung, K., Sandberg, G., Böttger, M., Becker, D. and Hedrich, R. (1999) Proc. Natl. Acad. Sci. USA 96, 12186–12191.
[12] Hartje, S., Zimmermann, S., Klonus, D. and Müller-Röber, B. (2000) Planta 210, 723–731.

[13] Gaymard, F., Pilot, G., Lacombe, B., Bouchez, D., Bruneau, D., Boucherez, J., Michaux-Ferriere, N., Thibaud, J.-B. and Sentenac, H. (1998) Cell 94, 647–655.
[14] Ache, P., Becker, D., Ivashikina, N., Dietrich, P., Roelfsema, M.R. and Hedrich, R. (2000) FEBS Lett. 486, 93–98.
[15] Philippar, K., Fuchs, I., Lüthen, H., Hoth, S., Bauer, C.S., Haga, K., Thiel, G., Ljung, K., Sandberg, G., Böttger, M., Becker, D. and Hedrich, R. (1999) Proc. Natl. Acad. Sci. USA 96, 12186–12191.
[16] Marten, I., Hoth, S., Deeken, R., Ache, P., Ketchum, K.A., Hoshi, T. and Hedrich, R. (1999) Proc. Natl. Acad. Sci. USA 96, 7581–7586.
[17] Lacombe, B., Pilot, G., Michard, E., Gaymard, F., Sentenac, H. and Thibaud, J.B. (2000) Plant Cell 12, 837–851.
[18] Cao, Y., Ward, J.M., Kelly, W.B., Ichida, A.M., Gaber, R.F., Anderson, J.A., Uozumi, N., Schroeder, J.I. and Crawford, N.M. (1995) Plant Physiol. 109, 1093–1106.
[19] Ketchum, K.A. and Slayman, C.W. (1996) FEBS Lett. 378, 19–26.
[20] Uozumi, N., Nakamura, T., Schroeder, J.I. and Muto, S. (1998) Proc. Natl. Acad. Sci. USA 95, 9773–9778.
[21] Reyes, R., Duprat, F., Lesage, F., Fink, M., Salinas, M., Farman, N. and Lazdunski, M. (1998) J. Biol. Chem. 273, 30863–30869.
[22] Jurman, M.E., Boland, L.M., Liu, Y. and Yellen, G. (1994) BioTechniques 17, 876–881.
[23] Lacombe, B. and Thibaud, J.-B. (1998) J. Membr. Biol. 166, 91–100.
[24] Zei, P.C. and Aldrich, R.W. (1998) J. Gen. Physiol. 112, 679–713.
[25] Dreyer, I., Antunes, S., Hoshi, T., Müller-Röber, B., Palme, K., Pongs, O., Reintanz, B. and Hedrich, R. (1997) Biophys. J. 72, 2143–2150.
[26] Bockenhauer, D., Zilberberg, N. and Goldstein, S.A.N. (2001) Nat. Neurosci. 4, 1–6.

⇒ zurück zur Übersicht

2001

Ache, Becker, Deeken, **Dreyer**, Weber, Fromm, Hedrich

VFK1, a *Vicia faba* K^+ channel involved in phloem unloading.

Plant J. **27**:571-580.

The Plant Journal (2001) **27**(6), 571–580

VFK1, a *Vicia faba* K^+ channel involved in phloem unloading

Peter Ache[1], Dirk Becker[1], Rosalia Deeken[1], Ingo Dreyer[1,†], Hans Weber[2], Jörg Fromm[3] and Rainer Hedrich[1,*]
[1]*Julius-von-Sachs-Institut, Molekulare Pflanzenphysiologie und Biophysik, Lehrstuhl Botanik I, Universität Würzburg, D-97082 Würzburg, Germany,*
[2]*Institut für Pflanzengenetik und Kulturpflanzenforschung (IPK), D-06466 Gatersleben, Germany, and*
[3]*Institut für Holzforschung, Universität München, D-80797 München, Germany*

Received 28 February 2001; revised 1 June 2001; accepted 25 June 2001.
[*]For correspondence (fax +49-(0)931–888–6158; e-mail hedrich@botanik.uni-wuerzburg.de).
[†]Present address: Max-Planck-Institut für Molekulare Pflanzenphysiologie, D-14476 Golm, Germany.

Summary

In search of a K^+ channel involved in phloem transport we screened a *Vicia faba* cotyledon cDNA library taking advantage of a set of degenerated primers, flanking regions conserved among K^+ uptake channels. We cloned VFK1 (for *Vicia faba* K^+ channel 1) characterised by a structure known from the *Shaker* family of plant K^+ channels. When co-expressed with a KAT1 mutant in *Xenopus* oocytes, heteromers revealed the biophysical properties of a K^+ selective, proton-blocked channel. Northern blot analyses showed high levels of expression in cotyledons, flowers, stem and leaves. Using *in situ* PCR techniques we could localise the K^+ channel mRNA in the phloem. In the stem *VFK1* expression levels were higher in the lower internodes. There channel transcripts increased in the light and thus under conditions of increased photosynthate allocation. *VFK1* transcripts are elevated in sink leaves, and rise in source leaves during the experimental transition into sinks. Fructose- rather than sucrose- or glucose-feeding via the petiole induced *VFK1* gene activity. We therefore monitored the fructose sensitivity of the sieve tube potential through cut aphid stylets. In response to an 1 h fructose treatment the sieve tube potential shift increased from 19 mV to 53 mV per 10-fold change in K^+ concentration. Under these conditions K^+ channels dominated the electrical properties of the plasma membrane. Based on the phloem localisation and expression patterns of VFK1 we conclude that this K^+ channel is involved in sugar unloading and K^+ retrieval.

Keywords: K^+ channel, phloem, *Vicia faba*, sink-source relation, aphid technique, *in situ*-RT–PCR.

Introduction

Potassium plays an important role in many physiological processes in plants. Since the introduction of the patch-clamp technique to study the role of ion channels in plant physiology, K^+ channels have been identified in all plant cells investigated (Hedrich and Dietrich, 1996; Hedrich and Roelfsema, 1999; Schroeder *et al.*, 1994; and references therein). K^+ channels such as KAT1, KAT2, AKT1, AKT2/3 and GORK, for example, provide the basis for volume changes in guard cells (Anderson *et al.*, 1992; Pilot *et al.*, 2001;Szyroki *et al.*, 2001; Ache *et al.*, 2000). Furthermore, it has been shown that the AKT1 channel mediates high and low affinity K^+ uptake into the root (Hirsch *et al.*, 1998; Sentenac *et al.*, 1992) and SKOR, the secretion of this cation from xylem parenchyma cells into the xylem vessels (Gaymard *et al.*, 1998). Following long distance transport along the xylem K^+ is taken up by growing cells of the developing shoot (Marschner *et al.*, 1997). Among them growing coleoptile cells are characterised by the auxin-dependent K^+ channel ZMK1 (Philippar *et al.*, 1999). From mature (source) leaves photosynthates and K^+ are allocated via the phloem to sink tissues (Jeschke and Pate, 1991) represented by growing leaves, developing flowers, ripening fruits and seeds (Marschner *et al.*, 1996). In this context mild K^+ deficiency has been shown to suppress assimilate translocation (Vreugdenhil, 1985). This led to the suggestion that K^+ is involved in phloem transport, too. It is, however, still a matter of debate whether K^+ exerts an effect on phloem loading, transport and retrieval or unloading. In order to elucidate the role of potassium in phloem physiology we screened for K^+ channels

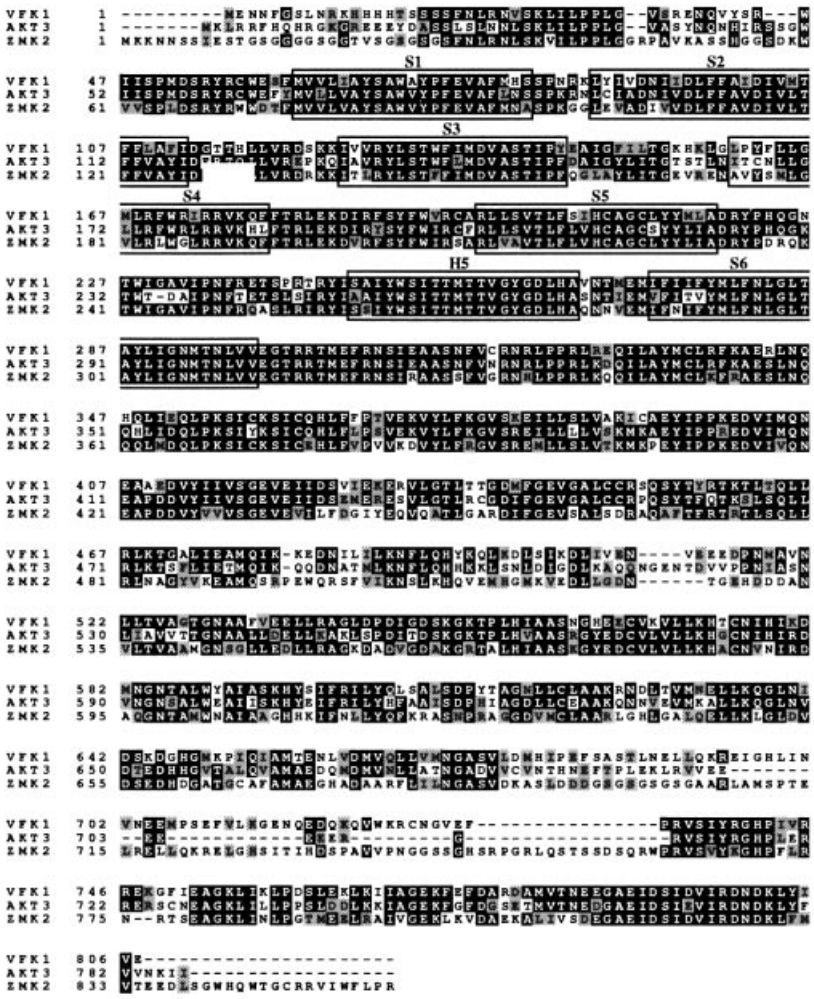

Figure 1. VFK1 belongs to the AKT2/3 family of plant potassium channels.
Alignment of the deduced amino-acid sequence of VFK1 with known plant K^+ channels revealed 64% and 55% identity to AKT3 and ZMK2, respectively. Given an identity of 37% to AKT1 and 32% to KAT1 only (not shown), the VFK1 channel can be grouped into the AKT2/3 subfamily. Boxed blocks denote predicted transmembrane regions (S1 to S6) and the pore region (H5). The alignment was performed using Vector NTI Suite (Informax, North Bethesda, USA).

expressed in the phloem of *Vicia faba*. Thereby we identified VFK1, an AKT2/3-like K^+ channel predominantly expressed in sink tissues and the stem. *In situ* analysis of the petioles allowed us to localise *VFK1* transcripts mainly to the phloem. Thus VFK1 represents a member of a K^+ channel family likely to be involved in phloem physiology.

Results

Cloning of VFK1

Within the increasing number of plant K^+ uptake channels cloned so far, amino acid sequences within the second (S2) and sixth (S6) putative transmembrane domain and the amphiphilic linker between S5 and S6 (H5) are highly conserved (Hedrich and Roelfsema, 1999). Taking advantage of two sets of degenerated oligonucleotides we cloned a 212-bp (H5 – S6) and a 597-bp (S2 – S6) fragment of the *VFK1* cDNA. Using the larger fragment as a homologous probe we cloned the full-length *VFK1* cDNA from a cotyledon library. This cDNA of 2818 bp with an open reading frame from nucleotide 151–2571 translates into a protein of 807 amino acids (GenBank accession number Y10579). When we aligned the amino acid sequence to those of other known K^+ channels, VFK1 exhibited all structural features of members belonging to the 'green' *Shaker* channel family (Hedrich and Becker, 1994). Based on amino acid alignments with known plant K^+ channels VFK1 showed highest homologies to the AKT3 and ZMK2 members of the AKT2/3 family (Figure 1).

Functional expression in Xenopus oocytes

To probe for K^+ channel activity we expressed VFK1 in *Xenopus* oocytes (Figure 2). As with AKT1, the injection of *VFK1* cRNA alone did not result in active K^+ channels (Dreyer *et al.*, 1997; Gaymard *et al.*, 1996). To still obtain basic information about the functional features of VFK1 we co-expressed this channel with the KAT1 mutant T256G. The replacement of threonine by glycine in KAT1-T256G

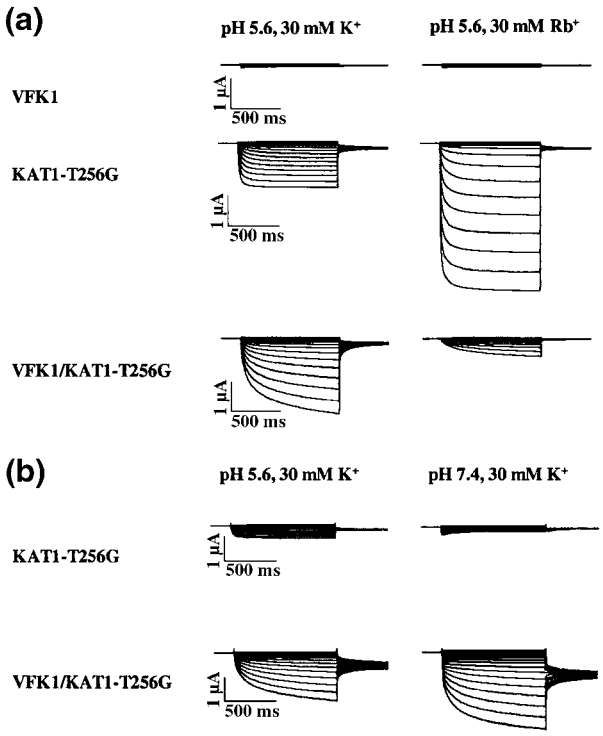

Figure 2. VFK1 constitutes a potassium-selective, proton-blocked channel.
(a) K^+ current through VFK1, KAT1-T256G and after co-expression of both cRNAs in *Xenopus* oocytes. *VFK1* cRNA alone failed to elicit currents (upper panel); the KAT1 mutant T256G is characterised by a higher permeability for Rb^+ over K^+ (middle panel). Co-expression of both cRNAs resulted in hyperpolarisation activated, inwardly rectifying currents showing an inverted Rb^+: K^+-permeability ratio compared with KAT1-T256G (lower panel). This indicates the formation of functional heteromeric channels, with VFK1 significantly contributing to the ion permeation pathway.
(b) Changing the extracellular H^+ concentration from pH 5.6 to pH 7.4 increased the steady-state current amplitude of co-expressed channels in external K^+. While the KAT1 mutant T256G, when solely expressed in *Xenopus* oocytes, is proton activated like KAT1 (upper panel), coexpression experiments resulted in a dominant, VFK1-mediated proton-block (lower panel), reminiscent of members of the AKT2/3 subfamily (cf. Marten *et al.*, 1999; Hoth *et al.*, 2001). From a holding potential of –20 mV currents were elicited by voltage steps from +20 mV to –170 mV (10 mV increments) followed by a voltage step to –70 mV.

creates a K^+ channel with a higher permeability to Rb^+ compared with K^+ (Uozumi *et al.*, 1995). These characteristics fundamentally changed following co-injection of VFK1 and the KAT1 mutant T256G (Figure 2a). In the presence of VFK1 subunits voltage-dependent currents were higher in K^+ compared with Rb^+, indicating the formation of heteromeric VFK1/KAT1-T256G channels (Dreyer *et al.*, 1997) with a higher K^+ selectivity than mutant K^+ channel homomers. Recent measurements on the corresponding members of the AKT2/3-subfamily in *Arabidopsis* (Lacombe *et al.*, 2000; Marten *et al.*, 1999; Philippar *et al.*, 1999), *Zea mays* (Bauer *et al.*, 2000) and *Populus* (K. Langer *et al.* unpublished), identified a slow

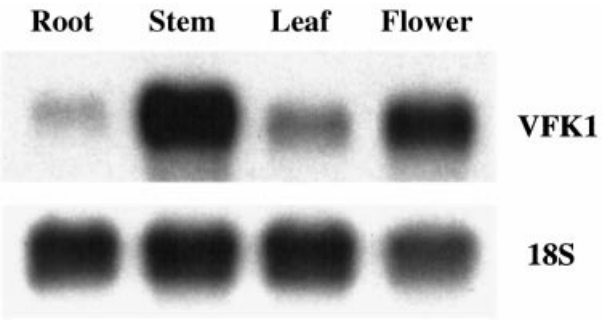

Figure 3. *VFK1* is dominantly expressed in the shoot.
Northern blot analysis of roots, stems, leaves and flowers (2 µg mRNA each lane) probed against *VFK1* full-length cDNA. Highest abundance was detected in stem- and floral-tissue (upper panel). Blots were stripped and re-probed with 18S DNA to prove equal loading (lower panel).

and an instantaneous current component in this channel type. Whereas KAT1 and also the Rb^+-selective mutant KAT-T256G show fast kinetics, in co-expression experiments the slow component of VFK1 superimposes the KAT1 activation kinetics (Figure 2a). In addition the interaction with external protons was altered (Figure 2b). While KAT1-T256G like the KAT1 wild-type was activated by protons (cf. Brüggemann *et al.*, 1999; Hoth *et al.*, 1997), channels containing VFK1 subunits were blocked. Reminiscent of AKT2/3-like potassium channels, the presence of VFK1 subunits resulted in an instantaneous current component, which was more pronounced at pH 7.4 than at pH 5.6. To estimate the significance of these results we further tested the coexpression of the mutant KAT1-T256G with AKT3. Heteromeric AKT3/KAT1-T256G channels exhibited similar features in response to Rb^+ and H^+ when compared with VFK1/KAT1-T256G (not shown; but cf. AKT3/KAT-T256G in Baizabal-Aguirre *et al.*, 1999). This might suggest that VFK1, ZMK2 and AKT3 are structurally and functionally related K^+ channels.

Localisation

To localise the site of *VFK1* expression, we isolated mRNA from roots, stem, leaves, flowers and cotyledons for Northern blot analyses (Figure 3). Highest amounts of *VFK1* transcripts were detected in flowers, stem and leaves and at low levels in roots. In the petiole and major veins of the leaf *VFK1* mRNA was as abundant as in the stem, while in mesophyll protoplasts K^+ channel transcripts were almost not detectable (not shown, but cf. AKT3 in Marten *et al.*, 1999). The cellular localisation of *VFK1* mRNA was determined using cross sections through the stem for *in situ* RT–PCR (Figure 4a,b) and petioles for *in situ* hybridisation experiments (Figure 4c,d). In response to both techniques, the label appeared exclusively in the phloem, whereas only background staining was detected in parenchyma and epidermal cells. Within the phloem the

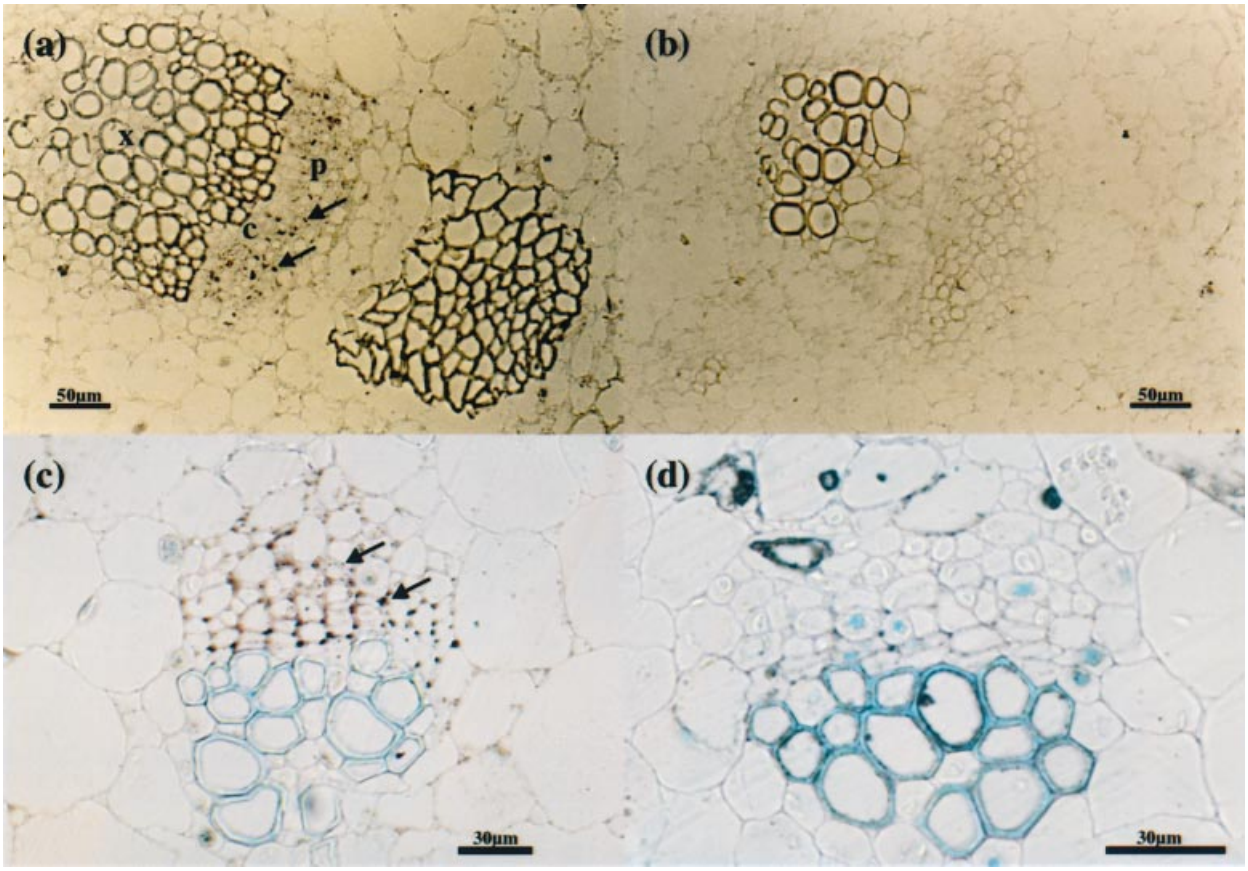

Figure 4. *VFK1* is expressed in the sieve-element-companion-cell-complex (SECC).
Following *in situ* PCR on 8 µm thin sections (a, b) and *in situ* hybridisation (c, d), the *VFK1* mRNA could be localised to the SECC.
(a) *In situ* PCR: Positive reaction. Stem sections were subjected to reverse transcription followed by PCR amplification using *VFK1*-specific oligonucleotides.
(b) *In situ* PCR: Negative control reaction. Stem sections were directly subjected to PCR amplification without previous reverse transcription reaction.
(c) *In situ* hybridisation: Positive reaction. Hybridisation of petiole sections with *Dig*-labelled *VFK1* antisense probes.
(d) *In situ* hybridisation: Negative control reaction. Hybridisation of petiole sections with *Dig*-labelled *VFK1* sense probes. Arrows mark distinct signals in (a) and (c); *x* = xylem; c = cambium; p = phloem.

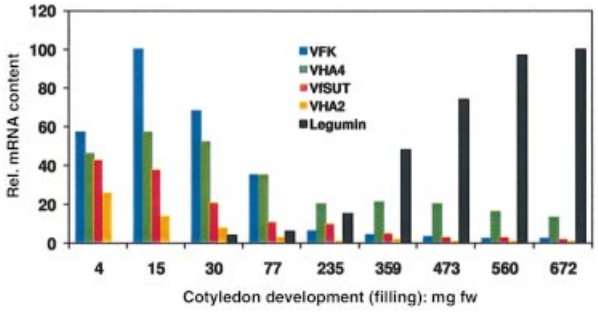

Figure 6. Temporal expression patterns in cotyledons indicate a role of *VFK1* in phloem unloading.
Quantitative Northern-blot analysis of transcripts in cotyledons of developing *Vicia faba* seeds. In early states of seed development, at the beginning of the storage phase, when import rates of sugars and amino acids are maximal, the expression of the K^+ channel *VFK1,* the sucrose transporter *VfSUT1 and* the H^+-pump *VHA4* (AccNo. AJ310523) in the cotyledons is highest. These transcript levels, like those of the H^+-pump *VHA2* (AccNo. AB022442) gradually decreased to almost background levels until seed maturation and declining import rates. In contrast LeguminB expression increased continuously with the onset of seed maturation. Representative plots of at least three independent experiments are shown.

sieve-element-companion-cell-complex (SECC) was identified as the site of strongest *VFK1* expression (Figure 4a,c, arrows).

Transcriptional regulation

Following the identification of *VFK1* in the phloem we tested whether the expression of this K^+ channel is sensitive to changes in the sink strength. When we compared the *VFK1* mRNA abundance between mature (source) leaves and young, developing (sink) leaves, Northern analysis in all experiments revealed two-fold higher levels in the latter (Figure 5). To further study the sink-specific transcriptional regulation of *VFK1*, source leaves of the same age and position were forced to become sink leaves. For this purpose source leaves were kept in the dark with CO_2 removed from the atmosphere (Eschrich and Eschrich, 1987). In agreement with a sink-

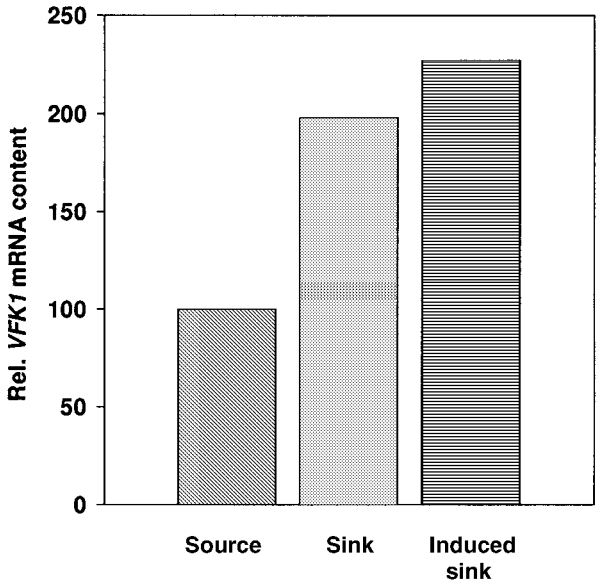

Figure 5. *VFK1* is expressed in sink leaves.
Northern blot analysis from source and sink leaves of 2-week-old *Vicia faba* plants. Note a two-fold higher *VFK1* mRNA abundance in the sink leave. A two-fold induction of *VFK1* transcript levels was detected following experimental transition from source to sink leaves, indicating that *VFK1* expression is regulated by sink strength. Representative plots of at least three independent experiments are shown.

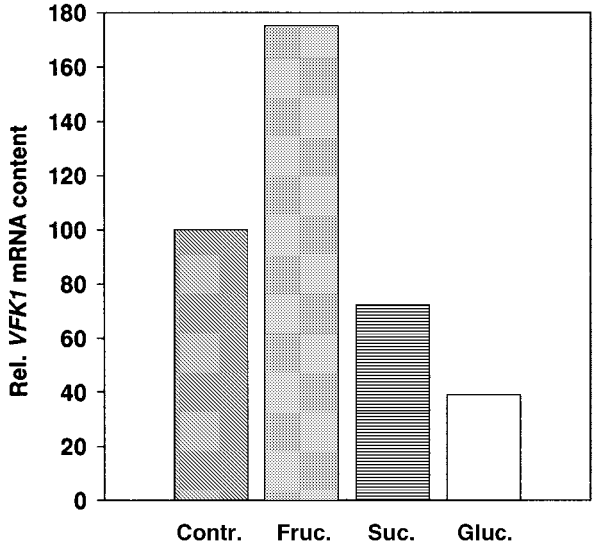

Figure 7. Fructose controls *VFK1* expression.
VFK1 transcript levels after 1 h sugar feeding of leaves via the petiole. Fructose rather than glucose or sucrose itself significantly induced *VFK1* transcription.

dependent expression of *VFK1*, within 3 hours of experimental source-sink transition, channel mRNA increased at least two-fold (Figure 5).

These findings led us to the conclusion that the phloem K^+ channel is involved in phloem unloading. To test this hypothesis and since VFK1 was cloned from a cotyledon library, we followed the expression of this K^+ channel during the sugar and amino acid unloading into cotyledons. From stage V to VI during seed development this strong sink tissue imports sugars and amino acids from the phloem and thereby increase its FW by about 20-fold (Borisjuk *et al.*, 1995). This process can be followed by the temporal and spatial expression patterns of the *Vicia faba* sucrose transporter VfSUT1 that we used as a molecular marker (Figure 6 and Weber *et al.*, 1997). The expression of *VfSUT1* was highest at the beginning of the storage phase and decreased until maturation. An inverse kinetics, however, characterised LeguminB mRNA levels (Figure 6, black columns). In line with its proposed role in phloem unloading, the initially high levels of *VFK1* transcripts at the beginning of the storage phase dropped with the termination of sugar loading into the cotyledons. The superimposing expression kinetics of the phloem K^+ channel on one side and the sucrose transporter VfSUT1 as well as the H^+-ATPases VHA2 and 4 indicate a tight correlation between sucrose and K^+ unloading from the phloem and hexose uptake into this sink tissue. Since glucose and fructose represent the products of invertase activity common to all sinks, we fed 100 mM sucrose, glucose or fructose into the transpiration stream of source leaves. To our surprise, fructose rather than sucrose or glucose doubled *VFK1* expression within 1–2 h (Figure 7).

Membrane potential and K^+ conductance in the phloem

The stem is the site of the transport phloem (van Bel, 1996) involved in long distance transport from source leaves to roots on one side and flower and sink leaves on the other. In line with the high phloem density in the stem, large amounts of *VFK1* transcripts were found in the internodes (cf. Figure 3). Using 2-week old plants with three to four internodes, we found increasing concentrations of phloem channel transcripts in the basipetal stem segments (Figure 8). This *VFK1* gradient correlates with the redistribution patterns of K^+ via the phloem (Jeschke and Pate, 1991). Although phloem transport is maintained during the night, the majority of the photosynthates are allocated in the light. Upon illumination *VFK1* mRNA in the stem (transport phloem) increased by about 40%, indicating that the flux control and retrieval of K^+ seem to depend on K^+ channel density. Microelectrodes brought into contact with the droplet of sieve tube exudates, appearing at the cut end of an aphid stylet (Fromm and Eschrich, 1988; Wright and Fisher, 1981) enabled us to monitor the sieve tube potential. When the petiole of a leaflet from a 3-week old *Vicia faba* source leaf was incubated in 1 mM K^+, membrane potentials around –150 mV were recorded (Table 1), well

in line with values found in other systems and by other methods (Eschrich *et al.*, 1988; Sibaoka, 1982; van Bel and van Rijen, 1994). Increasing the K^+ concentration in the transpiration stream by switching to a 100-mM K^+ perfusion buffer depolarised the membrane by 39 mV (19.5 mV per 10-fold change in K^+). This indicates that K^+ transporters provide a major but not the sole ionic conductance of the sieve tube plasma membrane. As predicted from an increase in the number of K^+ channels in the phloem, after a 1-hour incubation with 100 mM fructose the potassium dependent depolarisation increased to 53 mV per 10-fold increase in K^+ concentration (Table 1). This almost Nernstian behaviour in response to fructose allows the sieve tube membrane potential to respond almost like a K^+ selective electrode. Although we cannot exclude the possibility that fructose additionally altered the channel activity itself, these results and the kinetics of VFK1 expression in Figure 7 are in agreement with the increased number of active K^+ channels in the phloem. In this context it should be mentioned that very recently evidence for the role of fructose in the regulation of members from the phloem K^+ channel family has been provided. These experiments showed a fructose-induced developmental retardation of *Arabidopsis* mutants lacking the VFK1 homologue AKT2/3 (R. Deeken *et al.*, unpublished). *Arabidopsis akt2/3–1* plants, when grown on MS-medium supplemented with 2% fructose were characterised by reduced growth rates and delayed flowering compared with wildtype (not shown).

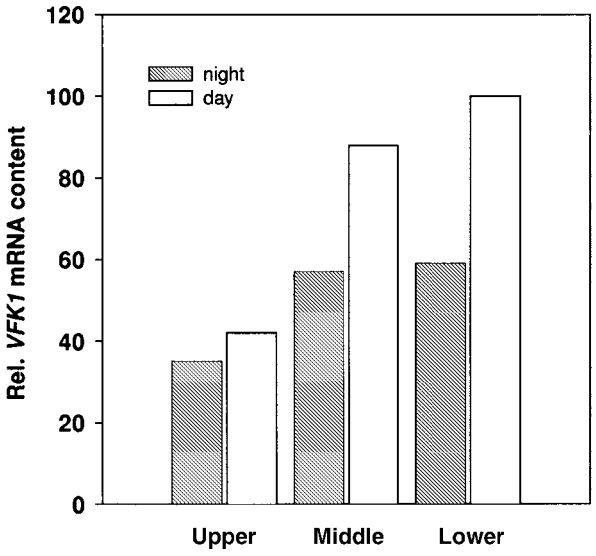

Figure 8. *VFK1* expression increases basipetaly.
Northern-blot analysis of stem segments demonstrating the spatial and temporal distribution of *VFK1* transcripts. In line with the redistribution profile of potassium ions, *VFK1* expression is increasing basipetaly. Higher transcript abundance at day compared with at night correlates with enhanced photosynthate allocation rates in the light. Representative plots of at least three independent experiments are shown.

Discussion

In this report we have described the cloning of VFK1, a K^+ selective channel expressed in phloem cells. Since the numerous plasmodesmata metabolically and electrically couple the sieve-tube companion cell-complex (Kempers *et al.*, 1998; Knoblauch and van Bel, 1998; Kühn *et al.*, 1997; Lucas, 1993; Stadler *et al.*, 1995), electrical recordings through cut stylets of aphids monitor the ensemble activity of all electrogenic transport processes within the plasma membrane of both cell types. These 'bio-electrodes', which accessed the sieve tubes, allowed us to record the phloem potential. Depolarisation in response to 10-fold changes in the apoplastic K^+ concentration indicated that K^+ transporters represent a major ionic conductance in the sieve tube companion cell complex. Under *VFK1*-inducing conditions, mimicking unloading by the presence of fructose, however, K^+ channels even develop to the predominant membrane conductance. A fructose-dependent doubling of VFK1 density seems to account for the observed membrane potential changes in the phloem. In line with its predicted function, VFK1 when characterised in oocytes exhibits the basic properties of a K^+ selective ion channel sensitive to pH changes. Similar features have been recently observed with other members of the AKT2/3 family from *Arabidopsis thaliana*, *Zea mays* and *Populus tremula* (Bauer *et al.*, 2000; Lacombe *et al.*, 2000; Marten *et al.*, 1999; Philippar *et al.*, 1999; K. Langer *et al.*, unpublished).

Table 1. Fructose controls the K^+ dependence of the phloem membrane potential. Phloem membrane potential measurements in response to changing potassium concentrations in APW were performed through the cut stylet of aphids. Fructose, which induces *VFK1* transcription, evoked a pronounced potassium permeability in sieve tube elements, when compared to control conditions. By changing the potassium concentration 10fold in the presence of fructose the sieve tube membrane responded almost like a K^+ electrode. Data represent the mean values ± secD, $n = 3$. (MP = membrane potential; APW = artificial pond water)

	MP 1 mM K^+	MP 100 mM K^+	ΔV	ΔV/10-fold [K^+]
APW	– 145 mV (5.5)	– 106 mV (5.5)	39 mV	19.5 mV
APW + 100 mM fructose	– 136 mV (6.6)	– 30 mV (6.6)	106 mV	53.0 mV

At the site of phloem loading in *Vicia faba* the apoplastic K^+ concentration is around 10 mM (Figure 9, Mühling and Sattelmacher, 1997) and the equilibrium potential for potassium (E_K) close to –60 mV. Since the membrane potential (E_m) of the SECC is between –130 and –200 mV (Table 1 and cf. van Bel, 1993) and thus more negative than E_K, VFK1 loads K^+ into the phloem.

In sinks at the sites of phloem unloading, sucrose is released. There an apoplastic invertase converts the disaccharide into glucose and fructose, which are the substrates of the monosaccharide transporters in, e.g. cotyledons (Figure 9). Glucose or fructose uptake into the sink cell will lower the H^+ concentration in the apoplast and activate the phloem K^+ channel. The presence of fructose may guarantee that the K^+ channel density is higher in the sink compared with the source. This will clamp the membrane potential close to E_K (around –120 mV). Due to increased channel- or carrier-mediated K^+ uptake into the growing or storing sink cells surrounding the unloading site, the apoplastic K^+ concentration is in the low-millimolar range (Walker *et al.*, 2000). Thus, whenever the membrane potential is more positive than E_K (E_m = – 95 to – 70 mV; Walker *et al.*, 2000), potassium is released from the phloem. A predicted but neither on the molecular level identified nor mechanistically understood proton/sucrose anti-porter or facilitator would further depolarise the membrane potential and increase K^+ unloading (Figure 9).

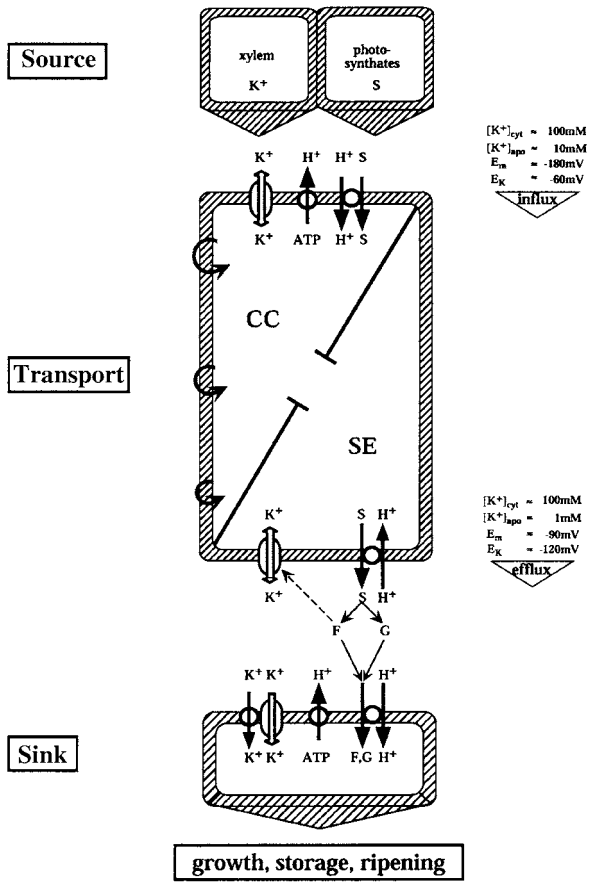

Figure 9. Model: Contribution of K^+ channels to phloem transport processes.

The source site is characterised by K^+ concentrations of about 100 mM within the cytoplasm of phloem cells ($[K^+]_{cyt}$) and 10 mM in the apoplast ($[K^+]_{apo}$), resulting in an equilibrium potential for potassium ions (E_K) of around –60 mV. The resting potential (E_m) of phloem cells at the source site is negative to E_K (see Results). For simplicity of comparing E_m with E_K and thus the direction of K^+ flux we had chosen –180 mV, which is three times E_K. Note that any value for E_m negative to E_K fits the model. At the sink site, however, the K^+ gradient is two orders of magnitude and E_K consequently at around –120 mV. E_m at the sink site is around –90 mV. The dotted line indicates that the number of K^+ channels is increased via fructose-dependent *VFK1* expression. Abbreviations: CC = Companion Cell, SE = Sieve Element, F = Fructose, G = Glucose, S = Sucrose. Symbols: ⇳ = VFK1 channel, ⏚ = transporter, ⏃ = pump, ↓○↓ = symporter.

In conclusion the studies presented provide evidence for K^+ channels involved in the control of the membrane potential as well as sugar and potassium translocation from source to sink via the phloem. This is accomplished by changes in the number and activity of K^+ channels in response to changes in the sink/source relation, fructose concentration and pH. In line with the predicted role of VFK1, the akt 2/3–1 mutant in *Arabidopsis thaliana* is impaired in sugar allocation (R. Deeken *et al.*, unpublished).

Experimental procedures

Plant growth conditions

Vicia faba L. cv. Grünkernige Hangdown plants were grown in a growth chamber in soil with 14 h light (20°C) at a photon-flux density of 300 μmol m^{-2} sec^{-1} (HQI-TS 250 W D^{-1}, Osram, München, Germany) and 10 h dark (14°C) periods.

Cloning of VFK1 cDNA

Degenerated oligonucleotide primers, directed towards homologous regions of known plant inwardly rectifying K^+ channels, were used to amplify corresponding regions from reverse transcribed RNA derived from major veins of *Vicia faba* (RT–PCR). First strand synthesis was performed with S6rev primer (5′-ACIAGRTTIGTCATRTTICC-3′) in a standard RT reaction (GIBCO BRL, Eggenstein, Germany). The resulting cDNA was used as a template for PCR amplification with S2fwd (5′-TTYTTYGCIA-THGAYAT-3′) and H5fwd (5′-AARACITGGATHGGIGC-3′) as forward primers, respectively, and S6rev as reverse primer at 150 pmol each in a 50 μl standard PCR reaction (Promega, Heidelberg, Germany). The following temperature profile was used for amplification: (five cycles) denaturation: 94°C, 60 sec; primer annealing, 37°C, 60 sec, followed by a 120 s ramp up to 72°C; primer extension, 72°C, 30 sec (35 cycles) 94°C, 60 sec; 48°C, 60 sec; 72°C, 90 sec. The resulting PCR fragments H5 – S6 (212 bp, GenBank accession number Y09749) and S2 – S6 (597 bp) were identified following subcloning into pBluescriptII KS+ (Stratagene, La Jolla, CA, USA), by sequencing and alignment with known plant K^+ channels. A *Vicia faba* cDNA library (ZAP

Express; Stratagene, kindly provided by H. Bäumlein, IPK Gatersleben, Germany) specific for stage V to VI cotyledons (Borisjuk *et al.*, 1995) was screened (1x 10^6 phages) using the S2–S6fragment as a homologous, ^{32}P-labelled probe. Filters were hybridised overnight at 68°C in PI-buffer (250 mM Sodium phosphate pH 7.2, 1% BSA Fraction V, 1 mM EDTA, 7% SDS) and washed three times in PI buffer at 68°C. Plaque-purified phage clones were converted to pBK-CMV (Stratagene) derivatives following the manufacturer's instructions.

Northern blot analysis

Total RNA was isolated from different *Vicia faba* organs using the Plant RNeasy Extraction kit (Qiagen, Hilden, Germany). Poly(A)$^+$ RNA was purified from total RNA using Dynabeads (Dynal, Hamburg, Germany) and subjected to Northern Blot analysis as described (Sambrook *et al.*, 1989). For quantification of transcript abundance dotted poly(A)$^+$ RNA was hybridised at 68°C in PI buffer against a ^{32}P-radiolabelled, specific PCR-amplified 814 bp fragment corresponding to the 3′-coding-region of the *VFK1* cDNA. The following Primers were used: VFK1probe fwd position 1639 (5′-CAG CTT AAG GAT TTG AGT ATC-3′) and VFK1probe rev position 2452 (5′-TTT TGA GTT TTT CTA ATG AAT-3′). In parallel poly(A)$^+$ RNA dots were hybridised at 42°C against a γ– ^{32}P dATP endlabelled oligo(dT) probe, modified according to Hollander and Fornace (1990), which served as a standard. The relative mRNA content was calculated by normalising the signal density of the specific channel probe to that of the oligo(dT) probe (mean of 15, 10 and 5 ng of dotted mRNA), untreated control values were set to 100%.

For induction experiments, petioles were cut under a liquid film and fed via the transpiration stream with solutions containing 50 mM potassium phosphate (pH 5.5) and 100 mM of sugar. Controls were treated with 50 mM potassium phosphate (pH 5.5) and mannitol at the same osmolarity.

In situ *techniques*

In situ RT–PCR was performed as described earlier (Johansen, 1997) with the following modifications: Plant material was fixed in FAA for 20 h at 20°C, slides were incubated with pepsin for 30 min. RT–PCR was carried out in a single-step reaction by use of rTth DNA-polymerase (PE Applied Biosystems, Weiterstadt, Germany) and 5 mM Mn^{2+} and Mg^{2+}, respectively, following the manufacturer's instructions. A VFK1 cDNA-fragment of 246 bp was amplified by (30 cycles) 94°C, 60 sec; 55°C, 60 sec; 72°C, 60 sec. *In situ* hybridisation on 2–5 mm thick hand-cuts of *Vicia faba* petioles was performed as described earlier (Marten *et al.*, 1999). Detection was carried out using a silver enhanced anti-Digoxigenin-gold-conjugate (5 nm, British BioCell, Cardiff, UK), according to the manufacturers advice. Subsequently the material was embedded in GMA (Glycolmethacrylate, Plano, Wetzlar, Germany). 10 μm slices were cut and stained with toluidineblue.

Two-electrode voltage-clamp

For heterologous expression in *Xenopus laevis* oocytes the *VFK1* cDNA was subcloned as a SmaI/HindIII-fragment into the pGEMHE vector. *In vitro* transcription of cRNA, preparation, injection and coinjection of oocytes as well as the generation of the KAT1 mutant T256G were performed as described earlier (Becker *et al.*, 1996). The two-electrode voltage-clamp technique was applied to characterise the electrophysiological channel properties (Hedrich *et al.*, 1995). The external solutions were composed of 30 mM either KCl or RbCl, 1 mM $CaCl_2$, 2 mM $MgCl_2$. The pH was adjusted with 10 mM MES/Tris (pH 5.6) and 10 mM Tris/MES (pH 7.4). The osmolarity of the solutions was adjusted to 220 mosmol kg^{-1} using sorbitol.

Membrane potential measurements

The aphid technique was carried out as described elsewhere (Fromm and Eschrich, 1988; Wright and Fisher, 1981). In brief: Before the measurements started, the plants were placed in the Faraday cage for 1day and an aphid cage with 10–15 aphids was applied to a petiole. The aphids were allowed to settle overnight. On the following day an aphid, which produced honeydew, was severed from its stylet by using a laser beam generator (Beck, Neu-Isenburg, Germany) connected to a Zeiss microscope (Carl Zeiss, Jena, Germany). When the stylet stump exuded sieve tube sap, all other aphids were brushed away and the stem was kept at about 90% relative humidity. The cut petiole was immersed in a vial containing artificial pond water (APW: 200 mM sorbitol, 1 mM NaCl, 0.1 mM KCl, 0.1 mM $CaCl_2$, 1 mM MES/Tris, pH 6.0). Into this vial, a window was cut through which the reference electrode (Ag/AgCl) was inserted, and through which the electrolyte solution was replaced by other test solutions. Attaching the tip of a microelectrode to the exudate droplet of the stylet by using a Leitz micromanipulator closed the circuit. The glass microelectrode had a tip diameter of approximately 1 μm and was fabricated from micro-capillaries on a vertical electrode puller and back-filled with 100 mM KCl. The microelectrode was clamped in an Ag/AgCl pellet holder and connected to a microelectrode pre-amplifier (input impedance 10^{12} ohms) to which a WPI-amplifier (Model 750, WPI, Sarasota, FL, USA) was attached. The resistance for an electric current inside the stylet is relatively low (around 10^9 ohms according to Wright and Fisher, 1981) compared with the high input impedance of the electric equipment used.

Acknowledgements

We thank Dr Helmut Bäumlein for providing the *Vicia faba* cotyledon cDNA library. We are grateful to Rob Roelfsema, Natalya Ivashikina and Benoit Lacombe for critical reading of the manuscript. This work was supported by grants of the Deutsche Forschungsgemeinschaft to RH.

References

Ache, P., Becker, D., Ivashikina, N., Dietrich, P., Roelfsema, M.R.G. and Hedrich, R. (2000) GORK, a delayed outward rectifier expressed in guard cells of *Arabidopsis thaliana*, is a K$^+$-selective, K$^+$-sensing ion channel. *FEBS Lett.* **486**, 93–98.

Anderson, J.A., Huprikar, S.S., Kochian, L.V., Lucas, W.J. and Gaber, R.F. (1992) Functional expression of a probable *Arabidopsis thaliana* potassium channel in *Saccharomyces cerevisiae*. *Proc. Natl Acad. Sci. USA*, **89**, 3736–3740.

Baizabal-Aguirre, V.M., Clemens, S., Uozumi, N. and Schroeder, J.I. (1999) Suppression of inward-rectifying K$^+$ channels KAT1 and AKT2 by dominant negative point mutations in the KAT1 a-subunit. *J. Membr. Biol.* **167**, 119–125.

Bauer, C.S., Hoth, S., Haga, K., Philippar, K., Aoki, N. and Hedrich, R. (2000) Differential expression and regulation of K$^+$ channels

in the maize coleoptile: molecular and biophysical analysis of cells isolated from cortex and vasculature. *Plant J.* **24**, 139–145.

Becker, D., Dreyer, I., Hoth, S., Reid, J.D., Busch, H., Lehnen, M., Palme, K. and Hedrich, R. (1996) Changes in voltage activation, Cs^+ sensitivity, and ion permeability in H5 mutants of the plant K^+ channel KAT1. *Proc. Natl Acad. Sci. USA*, **93**, 8123–8128.

Borisjuk, L., Weber, H., Panitz, R., Manteuffel, R. and Wobus, U. (1995) Embryogenesis of *Vicia faba* L. Histodifferentiation in relation to starch and storage protein synthesis. *J. Plant Physiol.* **147**, 203–218.

Brüggemann, L., Dietrich, P., Becker, D., Dreyer, I., Palme, K. and Hedrich, R. (1999) Channel-mediated high-affinity K^+ uptake into guard cells from *Arabidopsis*. *Proc. Natl Acad. Sci. USA*, **96**, 3298–3302.

Dreyer, I., Antunes, S., Hoshi, T., Müller-Röber, B., Palme, K., Pongs, O., Reintanz, B. and Hedrich, R. (1997) Plant K^+ channel α-subunits assemble indiscriminately. *Biophys. J.* **72**, 2143–2150.

Eschrich, W. and Eschrich, B. (1987) Control of phloem unloading by source activities and light. *Plant Physiol. Biochem.* **25**, 625–634.

Eschrich, W., Fromm, J. and Evert, R.F. (1988) Transmission of electric signals in sieve tubes of zucchini plants. *Bot. Acta*, **101**, 327–331.

Fromm, J. and Eschrich, W. (1988) Transport processes in stimulated and non-stimulated leaves of *Mimosa pudica*. *Trees*, **2**, 18–24.

Gaymard, F., Cerutti, M., Horeau, C., Lemaillet, G., Urbach, S., Ravallec, M., Devauchelle, G., Sentenac, H. and Thibaud, J.B. (1996) The baculovirus/insect cell system as an alternative to *Xenopus* oocytes. First characterization of the AKT1 K^+ channel from *Arabidopsis thaliana*. *J. Biol. Chem.* **271**, 22863–22870.

Gaymard, F., Pilot, G., Lacombe, B., Bouchez, D., Bruneau, D., Boucherez, J., Michaux-Ferriere, N., Thibaud, J.-B. and Sentenac, H. (1998) Identification and disruption of a plant Shaker-like outward channel involved in K^+ release into the xylem sap. *Cell*, **94**, 647–655.

Hedrich, R. and Becker, D. (1994) Green circuits – the potential of plant specific ion channels. *Plant Mol. Biol.* **26**, 1637–1650.

Hedrich, R. and Dietrich, P. (1996) Plant K^+ channels: Similarity and diversity. *Bot. Acta*, **109**, 1–8.

Hedrich, R., Moran, O., Conti, F., Busch, H., Becker, D., Gambale, F., Dreyer, I., Küch, A., Neuwinger, K. and Palme, K. (1995) Inward rectifier potassium channels in plants differ from their animal counterparts in response to voltage and channel modulators. *Eur. Biophys. J.* **24**, 107–115.

Hedrich, R. and Roelfsema, M.R.G. (1999) Plant ion transport. *Encyclopaedia of Life Sciences. Macmillan Reference Ltd.* A1307.

Hirsch, R., Lewis, B.D., Spalding, E.P. and Sussmann, M.R. (1998) A role for the AKT1 potassium channel in plant nutrition. *Science*, **280**, 918–921.

Hollander, C. and Fornace, A.J. (1990) Estimation of relative mRNA content by filter hybridisation to a polythymidylate probe. *Biotechniques*, **9**, 174–179.

Hoth, S., Dietrich, P., Becker, D., Müller-Röber, B. and Hedrich, R. (1997) Molecular basis of plant-specific acid activation of K^+ uptake channels. *Proc. Natl Acad. Sci. USA*, **94**, 4806–4810.

Hoth, S., Geiger, D., Becker, D. and Hedrich, R. (2001) The pore of plant, K., + channels is involved in voltage-, pH. and -sensing: domain-swapping between different, K. + channel α-subunits. *Plant Cell*, **13**, 943–952.

Jeschke, W.D. and Pate, J.S. (1991) Cation and chloride partitioning through xylem and phloem within the whole plant of *Ricinus communis* L. under conditions of salt stress. *J. Exp. Bot.* **42**, 1105–1116.

Johansen, B. (1997) *In situ* PCR on plant material with sub-cellular resolution. *Annal. Of Bot.* **80**, 697–700.

Kempers, R., Ammerlaan, A. and van Bel, A.J.E. (1998) Symplastic constriction and ultrastructural features of the sieve element/companion cell complex in the transport phloem of apoplasmically and symplasmically phloem-loading species. *Plant Physiol.* **116**, 271–278.

Knoblauch, M. and van Bel, A.J.E. (1998) Sieve tubes in action. *Plant Cell*, **10**, 35–50.

Kühn, C., Franceschi, V.R., Schulz, A., Lemoine, R. and Frommer, W.B. (1997) Macromolecular trafficking indicated by localization of sucrose transporters in enucleate sieve elements. *Science*, **275**, 1298–1300.

Lacombe, B., Pilot, G., Michard, E., Gaymard, F., Sentenac, H. and Thibaud, J.B. (2000) A shaker-like K^+ channel with weak rectification is expressed in both source and sink phloem tissues of *Arabidopsis*. *Plant Cell*, **12**, 837–851.

Lucas, W.J. (1993). Plant signals in interactions with other organisms. In: *Current Topics in Plant Physiology Series* (Schultz, J.C. and Raskin, I. eds). 11, 79–92.

Marschner, H., Kirkby, E.A. and Cakmak, I. (1996) Effect of mineral nutritional status on shoot-root partitioning of photoassimilates and cycling of mineral nutrients. *J. Exp. Bot.* **47**, 1255–1263.

Marschner, H., Kirkby, E.A. and Engels, C. (1997) Importance of cycling and recycling of mineral nutrients within plants for growth and development. *Bot. Acta*, **110**, 265–273.

Marten, I., Hoth, S., Deeken, R., Ache, P., Ketchum, K.A., Hoshi, T. and Hedrich, R. (1999) AKT3, a phloem-localized K^+ channel, is blocked by protons. *Proc. Natl Acad. Sci. USA*, **96**, 7581–7586.

Mühling, K.H. and Sattelmacher, B. (1997) Determination of apoplastic K^+ in intact leaves by ratio imaging of PBFI fluorescence. *J. Exp. Bot.* **48**, 1609–1614.

Philippar, K., Fuchs, I., Lüthen, H., Hoth, S., Bauer, C.S., Haga, K., Thiel, G., Ljung, K., Sandberg, G., Böttger, M., Becker, D. and Hedrich, R. (1999) Auxin-induced K^+ channel expression represents an essential step in coleoptile growth and gravitropism. *Proc. Natl Acad. Sci. USA*, **96**, 12186–12191.

Pilot, G., Lacombe, B., Gaymard, F., Cherel, I., Boucherez, J., Thibaud, J.B. and Sentenac, H. (2001) Guard cell inward K^+ channel activity in *Arabidopsis* involves expression of the twin channel subunits, KAT1 and KAT2. *J. Biol. Chem.* **79**, 631–641. (1989)

Sambrook, J., Fritsch, E.F. and Maniatis, T. *Molecular Cloning, a Laboratory Manual*. 2nd edn. Cold Spring Harbor, NY: Cold Spring Harbor Laboratory Press.

Schroeder, J.I., Ward, J.M. and Gassmann, W. (1994) Perspectives on the physiology and structure of inward-rectifying K^+ channels in higher plants. *Annu. Rev. Biophys. Biomol. Struct.* **23**, 441–471.

Sentenac, H., Bonneaud, N., Minet, M., Lacroute, F., Salmon, J.-M., Gaymard, F. and Grignon, C. (1992) Cloning and expression in yeast of a plant potassium ion transport system. *Science*, **256**, 663–665.

Sibaoka, T. (1982) Excitable cells in *Mimosa*. *Science*, **137**, 226.

Stadler, R., Brandner, J., Schulz, A., Gahrtz, M. and Sauer, N. (1995) Phloem loading by the PmSUC2 sucrose carrier from *Plantago major* occurs into companion cells. *Plant Cell*, **5**, 1545–1554.

Szyroki, A., Ivashikina, N., Dietrich, P., Roelfsema, M.R.G., Ache, P., Reintanz, B., Deeken, R., Godde, M., Felle, H., Steinmeyer,

R., Palme, K. and Hedrich, R. (2001) KAT1 is not essential for stomatal opening. *Proc. Nat. Acad. Sci. USA* (in press)

Uozumi, N., Gassmann, W., Cao, Y. and Schroeder, J.I. (1995) Identification of strong modifications in cation selectivity in an *Arabidopsis* inward rectifying potassium channel by mutant selection in yeast. *J. Biol. Chem.* **270**, 24276–24281.

van Bel, A.J.E. (1993) II. The transport phloem. Specifics of its functioning. *Prog. Bot.* **54**, 134–150.

van Bel, A.J.E. and van Rijen, H.V.M. (1994) Microelectrode-recorded development of the symplastic autonomy of the sieve element/companion cell complex in the stem phloem of *Lupinus luteus* L. *Planta*, **192**, 165–175.

van Bel, A.J.E. (1996) Interaction between sieve element and companion cell and the consequences for photoassimilate distribution. Two structural hardware frames with associated physiological software packages in dicotyledons?. *J. Exp. Bot.* **47**, 1129–1140.

Vreugdenhil, D. (1985) Source-to-sink gradient of potassium in the phloem. *Planta*, **163**, 238–240.

Walker, N.A., Zhang, W.-H., Harrington, G., Holdaway, N. and Patrik, J.W. (2000) Effluxes of solutes from developing seed coats of *Phaseolus vulgaris* L. & *Vicia faba* L. locating the effect of turgor in a coupled chemiosmotic system. *J. Exp. Bot.* **48**, 1047–1055.

Weber, H., Borisjuk, L., Heim, U., Sauer, N. and Wobus, U. (1997) A role for sugar transporters during seed development: Molecular characterization of a hexose and a sucrose carrier in fava bean seeds. *Plant Cell*, **9**, 895–908.

Wright, J.P. and Fisher, D.B. (1981) Measurement of sieve tube membrane potential. *Plant Physiol.* **67**, 845–848.

⇒ zurück zur Übersicht

1999

Brüggemann, Dietrich, Becker, **Dreyer**, Palme, Hedrich

Channel-mediated high-affinity K^+ uptake into guard cells from *Arabidopsis*.

Proc. Natl. Acad. Sci. USA **96**:3298-3302.

Proc. Natl. Acad. Sci. USA
Vol. 96, pp. 3298–3302, March 1999
Plant Biology

Channel-mediated high-affinity K^+ uptake into guard cells from *Arabidopsis*

LIOUBOV BRÜGGEMANN*, PETRA DIETRICH*, DIRK BECKER*, INGO DREYER*, KLAUS PALME†, AND RAINER HEDRICH*‡

*Julius-von-Sachs-Insititut für Biowissenschaften, Lehrstuhl für Molekulare Pflanzenphysiologie und Biophysik, Universität Würzburg, Julius-von-Sachs-Platz 2, 97082 Würzburg, Germany; and †Max-Delbrück-Laboratorium in der Max-Planck Gesellschaft, Carl-von-Linné Weg 10, 50829 Cologne, Germany

Communicated by Jozef S. Schell, Max Planck Institute for Breeding Research, Cologne, Germany, December 24, 1998 (received for review November 30, 1998)

ABSTRACT **Potassium uptake by higher plants is the result of high- or low-affinity transport accomplished by different sets of transporters. Although K^+ channels were thought to mediate low-affinity uptake only, the molecular mechanism of the high-affinity, proton-dependent K^+ uptake system is still scant. Taking advantage of the high-current resolution of the patch-clamp technique when applied to the small *Arabidopsis thaliana* guard cells densely packed with voltage-dependent K^+ channels, we could directly record channels working in the concentration range of high-affinity K^+ uptake systems. Here we show that the K^+ channel KAT1 expressed in *Arabidopsis* guard cells and yeast is capable of mediating potassium uptake from media containing as little as 10 μM of external K^+. Upon reduction of the external K^+ content to the micromolar level the voltage dependence of the channel remained unaffected, indicating that this channel type represents a voltage sensor rather than a K^+-sensing valve. This behavior results in K^+ release through K^+ uptake channels whenever the Nernst potential is negative to the activation threshold of the channel. In contrast to the H^+-coupled K^+ symport shown to account for high-affinity K^+ uptake in roots, pH-dependent K^+ uptake into guard cells is a result of a shift in the voltage dependence of the K^+ channel. We conclude that plant K^+ channels activated by acid pH may play an essential role in K^+ uptake even from dilute solutions.**

Since the initial observation of Epstein that K^+ uptake into plant cells can be decomposed into the activity of high- and low-affinity transport systems (1), the molecular structure of three different K^+ transporters, K^+ channels, and two distinct carrier types, has been identified. In 1992, AKT1 and KAT1 (2, 3) were shown to represent the first members of a large family of inward-rectifying K^+ channels (4), channel subtypes that had been recognized from patch-clamp studies in almost all plant cell types studied so far (5). In the presence of millimolar K^+ concentrations and upon hyperpolarization of the plasma membrane, these inward rectifiers mediate K^+ uptake. Based on studies in the whole-cell configuration of the patch-clamp technique applied to *Vicia faba* guard cell protoplasts, Schroeder and Fang (6) calculated an affinity constant of 3.5 mM for these guard cell K^+ channels. Analysis of the current–voltage relation obtained from guard cells and root cells exposed to varying external K^+ concentrations revealed that the activation potential of the inward currents shifted to 20- to 30-mV more negative values with decreasing K^+ concentrations (6–8), a behavior from which it was concluded that K^+ channels can sense the external potassium. Thus, channel opening was supposed to occur only when the K^+ gradient is inward, restricting these transporters to function as K^+-sensing K^+ uptake valves (9). Supporting this hypothesis, these channels were reported to not open in the absence of extracellular K^+ (9). Because of this effect, K^+ uptake channels were not supposed to form shunt pathways through which K^+, accumulated by high-affinity carriers, can leak out of the cells.

To date, two high-affinity plant K^+ carriers have been identified. In 1994, Schachtman and Schroeder reported on the discovery of HKT1, a proton-driven K^+ symporter from *Hordeum vulgare* (10). Later, however, detailed studies revealed that HKT1 mediates Na^+-driven rather than H^+-driven K^+ uptake (11). In search for the molecular entity generating the H^+/K^+ phenomenon, *Escherichia coli*-like K^+ transporters recently were identified in barley (12) and *Arabidopsis* (13). Later studies showed that members of this family mediate both high- and low-affinity K^+ transport (14, 15). It is, however, still unclear which members of the channel or carrier families account for acid-induced K^+ uptake observed *in vivo* (16).

Here we report that hyperpolarization-activated K^+ channels in guard cells are capable of mediating high-affinity K^+ uptake, the activity of which strongly depends on the external proton concentration. Supporting this finding we show that K^+ uptake-deficient yeast, when complemented with this guard cell K^+ channel, regained the ability to grow in micromolar K^+ media. Therefore, acid-activated K^+ uptake channels might represent a molecular equivalent contributing to the H^+/K^+ phenomenon.

MATERIALS AND METHODS

Yeast Genetics. Potassium-dependent growth assays were performed by using the *Saccharomyces cerevisiae* strain JR Y339 (17). KAT1 was subcloned into the yeast expression vector pGK (18) and transformed into JR Y339 using the lithium acetate method (19). Growth assays were performed on SDAP medium (20) containing 2% purified Agar (Sigma A7921) supplemented with potassium at concentrations indicated in the figure legends.

Patch-Clamp Experiments. *Arabidopsis thaliana* seedlings (L. cv. C24; Arabidopsis Stock Center, Columbus, Ohio) were grown in a growth chamber, and guard cell protoplasts were isolated as described before (21). Current measurements were performed by using an EPC-9 patch-clamp amplifier (HEKA Electronics, Lambrecht, Germany) and low-pass-filtered with an eight-pole Bessel filter. Whole-cell data were low-pass-filtered with a cut-off frequency of 2 kHz. Data were sampled at 2.5 times the filter frequency (for single-channel recording this factor was 5), digitized (ITC-16; Instrutech, Mineola, NY), stored on hard disk, and analyzed with the software PULSE and PULSEFIT from Instrutech on a Gravis TT200. Patch pipettes were prepared from Kimax-51 glass (Kimble Glass, Vineland, NJ) and coated with silicone (Sylgard 184 silicone elastomer kit; Dow-Corning). To determine membrane potentials, the

The publication costs of this article were defrayed in part by page charge payment. This article must therefore be hereby marked "*advertisement*" in accordance with 18 U.S.C. §1734 solely to indicate this fact.

PNAS is available online at www.pnas.org.

‡To whom reprint requests should be addressed.

command voltages were corrected off-line for series resistances and liquid junction potentials according to Neher (22). The standard pipette solution (cytoplasm) contained 300 mM potassium gluconate/2 mM $MgCl_2$/3 mM $CaCl_2$/5 mM EGTA/2 mM MgATP/10 mM Hepes-Tris, pH 7.5. The bathing medium contained 10 mM citrate-Tris, pH 4.5 or 6.0 or 10 mM Mes-Tris, pH 6.0, in addition to 0.26 mM $MgCl_2$ or 2.6 mM $MgCl_2$, respectively (0.1 mM free Mg^{2+}). Potassium was adjusted by using potassium gluconate as indicated in the figure legends. The K^+ content of all solutions was verified by atomic-absorption spectroscopy. Single-channel recordings were performed in 150 mM symmetrical potassium gluconate using standard pipette solution and a bathing medium containing 1 mM $CaCl_2$/10 mM citrate-Tris, pH 5.0. All solutions were adjusted to 540 mosmol/kg by using D-sorbitol. Chemicals were obtained from Sigma.

Biophysical Analysis. Relative open probabilities were deduced from a double voltage-step protocol. Time- and voltage-dependent K^+ currents were elicited in response to hyperpolarization. During the second voltage step, K^+ currents relaxed in a time-dependent manner. The instantaneous current–voltage relationship, obtained from extrapolating the relaxation time course of the second pulse to $t = 0$ with an exponential function, is proportional to the relative open probability, $p_O(V)$, at the end of the activation pulse. Relative open probabilities were fitted with a Boltzmann function:

$$P_O = \frac{1}{1 + \left(\frac{V - V_{1/2}}{V_S}\right)}.$$

Here, $V_{1/2}$ denotes the voltage at which 50% of the channels are active, and V_S is the slope factor that is correlated to the charge of the voltage sensor.

RESULTS AND DISCUSSION

When we complemented the yeast mutant lacking the K^+ transporters Δtrk1 and Δtrk2 with KAT1, a K^+ channel expressed in *A. thaliana* guard cells (23), growth was rescued in low-K^+ medium (Fig. 1), a behavior that has been used previously for cloning the first plant K^+ uptake channels, KAT1 and AKT1 (2, 3). Although the mutant containing the vector alone did not grow at K^+ concentrations below 10 mM, KAT1 supported yeast growth in as low as 10 μM K^+ in the culture medium, indicating that K^+ channels are able to catalyze high-affinity K^+ uptake.

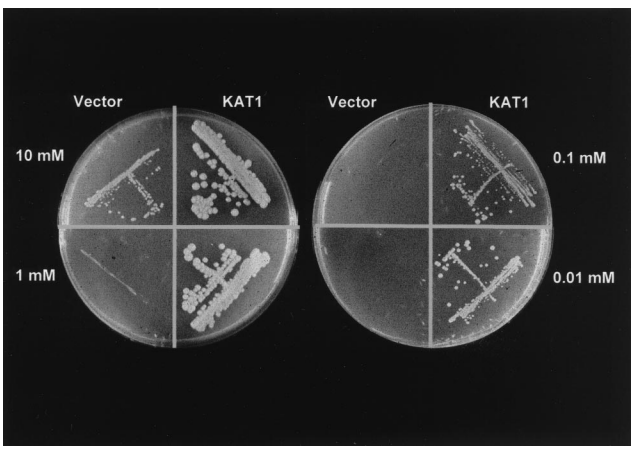

FIG. 1. Potassium concentration-dependent growth of the K^+ uptake-deficient yeast mutant JR Y339 complemented with the *A. thaliana* guard cell K^+ channel KAT1 or the empty vector.

In the presence of 150 mM K^+, inward-rectifying K^+ channels in guard cells as well as the gene products of KAT1 and KST1 [guard cell K channel of *Solanum tuberosum* (24)] expressed in *Xenopus* oocytes are characterized by a unitary conductance in the order of 5–8 pS (Fig. 2*A*; ref. 21). This conductance is the result of, e.g., 1.1-pA current driven by a voltage drop across the membrane of about –180 mV (Fig. 2*A*, Nernst potential for K^+, $E_K = 0$). According to the substrate dependency of K^+ currents (see Fig. 3*A*), in 100 μM K^+ or even less, the same potential difference ($E_K - E_M$) would elicit single-channel K^+ currents in the order of only a few femtoampere. This is far below the resolution limit of the patch-clamp technique [100 fA (25)]. To perform high-resolution current recordings at K^+ concentrations representing the high-affinity K^+ uptake range, we used *A. thaliana* guard cell protoplasts characterized by a "membrane patch-like" whole-cell surface area (capacitance = 1.4 ± 0.7 pF, $n = 253$) but high channel density [≈5–8 channels·μm^{-2} corresponding to around 500–1,000 channels per cell (21)].

In the presence of basically 300 mM K^+ in the pipette and 1.14 mM K^+ in the bath, inward currents were elicited upon hyperpolarization of the plasma membrane negative to around –130 mV (Fig. 2 *B* and *C*). At potentials more positive than, e.g., –60 mV, outward-rectifying K^+ channels were gated open (not shown here). Because this channel type is not involved in K^+ uptake but, rather, K^+ release, it will not be taken into account in this study. When we reduced the external K^+ concentration to, e.g., 60 μM (Fig. 2*B Right*), a concentration within the working range of high-affinity K^+ transporters (1), inward currents required membrane potentials negative of –200 mV because of the change in the driving force. At voltages positive to the Nernst potential for K^+, channel activity resulted in outward currents, which decreased with further depolarization. Detailed analysis of the current–voltage curves revealed that channel activation is K^+-independent from 30 mM down to the micromolar range (Fig. 2*D*; see also ref. 26). An identical behavior was seen with oocytes expressing KAT1 (down to 500 μM K^+, not shown), proving high-affinity uptake to represent an intrinsic property of the K^+ channel. Thus, in contrast to the current literature (see ref. 9 for review), this channel type conducts outward K^+ currents positive from E_K, whereas negative to the equilibrium potential it mediates K^+ uptake. Additional evidence for this hyperpolarization-activated K^+ channel to function as voltage sensor rather than K^+ sensor was obtained from the analysis of the open probability in the presence of 20, 60, 130, 330, and 1140 μM K^+ in the bath. As shown in Fig. 2*D*, the activation curves as well as half-activation potentials ($V_{1/2}$) superimposed for K^+ levels representing the high- and low-affinity range. Therefore, the voltage range at which K^+ efflux occurs is a function of the difference between the voltage threshold for K^+ channel activation and the Nernst potential for potassium. The whole-cell conductance of the inward current through the K^+ channel plotted as a function of the K^+ concentration displayed a Michaelis–Menten type of behavior characterized by an affinity constant of about 2 mM (Fig. 3*A*), a K_M similar to that of potassium channels in *V. faba* guard cells (6). This channel, therefore, represents a low-affinity transport system that, because of its K^+-independent gating, also operates in the high-affinity range.

Because this channel type is capable of conducting K^+ currents of the same order of magnitude as described for pH-dependent K^+ uptake in plants (9), we also explored the pH sensitivity of the high-affinity K^+ uptake component of the K^+ channel. After activating inward K^+ currents through membrane hyperpolarization to −220 mV in the presence of 60 μM K^+ and pH 6.0, we applied pulses of higher proton concentration to the guard cell protoplasts (Fig. 3*B*, pH 4.5). Upon this acidification the current amplitude increased dramatically (Fig. 3*B*), a feature reminiscent of H^+/K^+ symport-

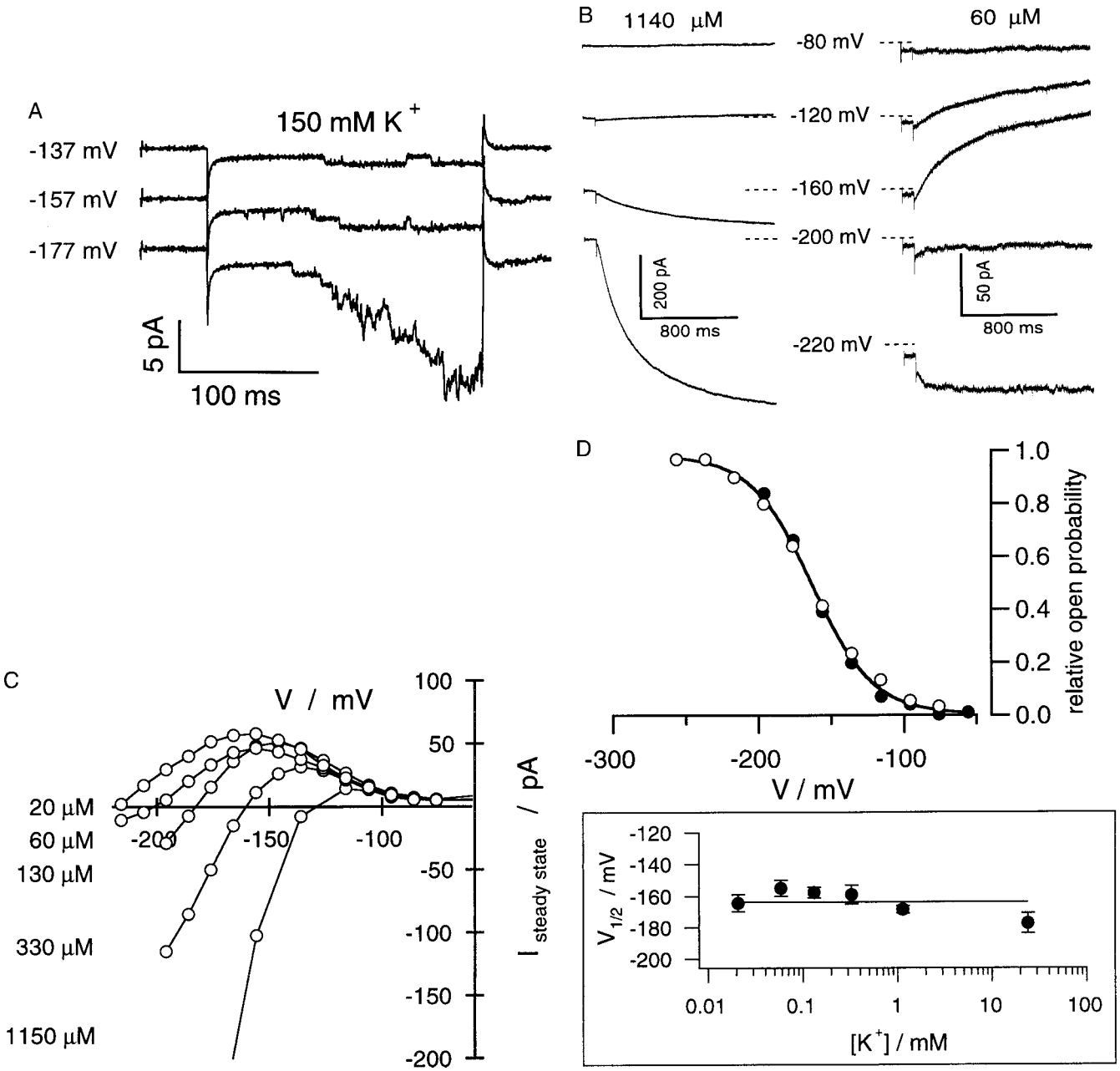

FIG. 2. Voltage-, time-, and K^+-dependent properties of the K^+ uptake channel in *A. thaliana* guard cells. (*A*) Activation of single K^+ uptake channels in an outside-out patch in response to hyperpolarizing voltage pulses to values indicated starting from a holding potential of –67 mV. For better resolution of current amplitudes, the K^+ concentration was 150 mM K^+ on both sides. The current–voltage relation of single channels from four to six individual measurements as a function of the membrane voltage corresponded to a slope conductance of 8.6 ± 0.3 pS (not shown). (*B*) Macroscopic outward and inward K^+ currents (whole-cell configuration) through the inward rectifier elicited by 1.5-s, too pulses to voltages indicated in the presence of 1140 μM K^+ (*Left*) and 60 μM K^+ (*Right*). Because of the experimental conditions K^+_{out} channels present in the plasma membrane, too, are not active in the voltage range shown. (*C*) Current–voltage curves of steady-state K^+ currents in the presence of different external K^+ concentrations. Pulse protocols are as in *B*. The data shown in *B* and *C* are representative of three to six independent experiments. (*D*) Voltage-dependent open probabilities (*Upper*) and half-activation potentials ($V_{1/2}$, *Lower*) as a function of the K^+ concentration. Open probabilities were recorded in the presence of 30 mM (*Upper*, ○) and 20 μM K^+ (*Upper*, ●) and 20, 60, 130, 330, and 1,140 μM K^+ (*Lower*, n = 3–9).

ers. When comparing the current–activation curves under both conditions, we could relate this increase in K^+ current to an acid-induced shift in the voltage dependence by 65 mV to less-negative membrane potentials (Fig. 3*C*). This facilitation of K^+ channel activation by protons thus is qualitatively similar to that recognized for guard cell channels from other plants as well as KAT1 and KST1 expressed in *Xenopus* oocytes in the presence of millimolar K^+ concentrations (21, 24, 27–30). Plotting the reversal potentials of the macroscopic currents against the external K^+ concentration showed that they perfectly followed the Nernst equation (Fig. 3*D*, 58.9 mV/decade). This indicates that acid activation of the channel is not superimposed by H^+/K^+ symporter activity, and, consequently, proton gradients do not energize K^+ channel-dependent K^+ uptake into guard cells.

From the experimental evidence presented here we conclude further that (*i*) K^+ uptake channels are capable of mediating high-affinity K^+ transport that is stimulated upon acidification, (*ii*) K^+ uptake channels are equipped with a channel-intrinsic voltage sensor rather than a K^+ sensor, (*iii*)

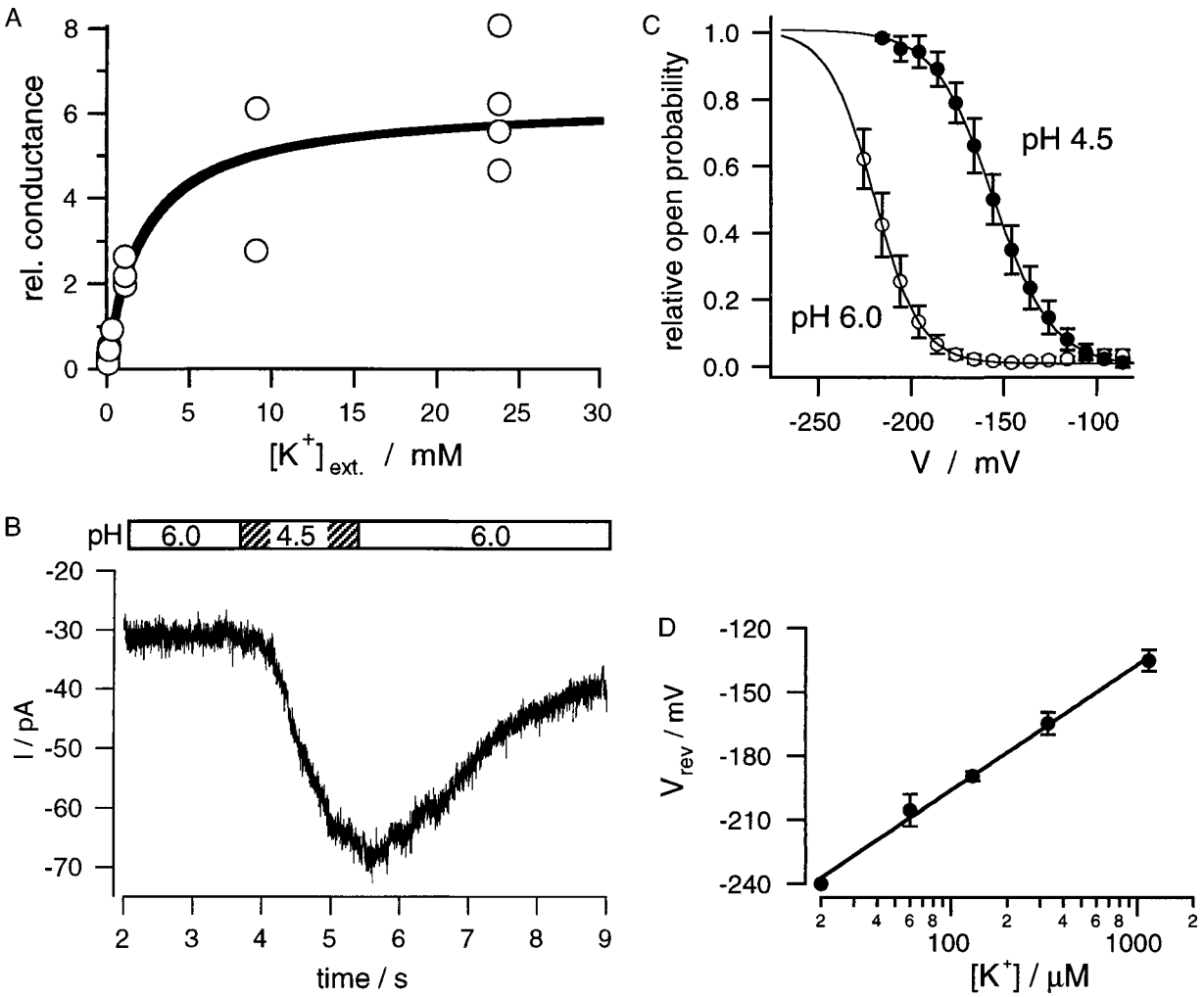

FIG. 3. High-affinity inward currents through guard cell plasma membrane K^+ channels is not driven by the proton gradient. (*A*) Potassium-dependent saturation of the K^+ channel conductance recorded in bath medium of pH 4.5 and K^+ concentrations ranging from 20 μM to 30 mM. Relative conductance was determined according to ref. 6 (n = 2–6). (*B*) Proton-dependent stimulation of inward K^+ currents during a solute pulse of pH 4.5 within 60 μM K^+ and pH 6.0. The membrane potential was clamped to −220 mV. The bar illustrates the duration of the acid pulse generated by a fast perfusion system. (*C*) Shift in voltage-dependent open probabilities of the K^+ channels in response to a pH change from 6.0 to 4.5. Relative open probabilities were normalized with respect to the maximum at pH 4.5. Lines represent Boltzmann fits to the voltage-dependent open probabilities at the two pH values. The data represent mean ± SD of seven measurements. (*D*) Ideal Nernstian behavior of the K^+ current reversal potentials. Reversal potentials (V_{rev}) were deduced from steady-state current–voltage relations as shown in Fig. 2*C* in the presence of 20–1,140 μM external K^+ at pH 4.5. The line represents a fit according to the Nernst equation, revealing a shift in V_{rev} of 58.9 mV per 10-fold change in the K^+ concentration.

the channel-intrinsic pH sensor (29, 31) is active under high- and low-affinity transport conditions, and (*iv*) K^+ uptake channels, upon potassium starvation, could represent a K^+-efflux pathway. In line with our high-resolution K^+ current measurements on *A. thaliana* guard cells, the K^+ uptake-deficient yeast mutant Δtrk1/2, when complemented with KAT1, took advantage of the voltage-dependent properties of this ion channel. Activated by hyperpolarization and acidic pH, KAT1 does not inactivate, allowing long-term K^+ accumulation, which is required for yeast growth (Fig. 1).

To drive channel-mediated K^+ influx with 10 μM K^+ in the culture medium, yeast cells containing, e.g., 100 mM cytoplasmic K^+ have to pump their membrane potential negative to −232 mV. Resting potentials even more negative have been recorded in guard cells as well as in root apex cells (32, 33). Our results also have shown that at micromolar extracellular potassium concentrations, K^+ uptake channels could represent a significant K^+ shunt if the membrane potential is positive to E_K. K^+ symporters that are driven by gradients other than or in addition to the electrical potential are able to operate in the voltage window between E_K and −100 mV or even more positive (10–13, 15, 34). In *A. thaliana* root protoplasts, net K^+ uptake currents carried by these symporters could at least balance channel-mediated K^+ efflux (35). Furthermore, conditions such as "K^+ depletion" or "K^+ starvation" seem to induce the expression of K^+ symporters probably to limit channel-mediated K^+ loss (12, 15). In this context, up-regulation of nonchannel K^+ transporters may explain why, in 10 μM K^+, plants lacking AKT1 still reach 50% of the fresh weight compared with the wild type (32).

In summary, we conclude that acid-activated, high-affinity K^+ uptake displays an intrinsic biophysical property of plant K^+ uptake channels extending the dynamic range of K^+ channel action. Because K^+ channels operate on the basis of a K^+ concentration-independent voltage sensor, K^+ uptake at potentials positive to E_K might represent the working range of nonchannel K^+ transporters.

We are grateful to J. Vanderleyden (Leuven, Belgium) and his group for stimulating discussion as well as to D. Sanders for comments on the manuscript. For atomic absorption measurements of K^+ concentrations, we thank W. Kaiser (Würzburg, Germany). We also thank J. D.

Reid for providing us with the yeast mutant $\Delta trk_{1/2}$. This work was funded by Deutsche Forschungsgemeinschaft grants to R.H.

1. Epstein, E. (1976) in *Encyclopedia of Plant Physiology*, eds. Lüttge, U. & Pitman, N. G. (Springer, Berlin), Vol. 2, pp. 70–94.
2. Anderson, J. A., Huprikar, S. S., Kochian, L. V., Lucas, W. J. & Gaber, R. F. (1992) *Proc. Natl. Acad. Sci. USA* **89,** 3736–3740.
3. Sentenac, H., Bonneaud, N., Minet, M., Lacroute, F., Salmon, J. M., Gaymard, F. & Grignon, C. (1992) *Science* **256,** 663–665.
4. Hedrich, R., Hoth, S., Becker, D., Dreyer, I. & Dietrich, P. (1998) in *Cellular Integration of Signalling Pathways in Plant Development*, NATO ASI Series, eds. LoSchiavo, R., Last, R. L., Morelli, G. & Raiknel, N. V. (Springer, Berlin), Vol. H104, pp. 35–45.
5. Hedrich, R. & Dietrich, P. (1996) *Bot. Acta* **109,** 94–101.
6. Schroeder, J. I. & Fang, H. H. (1991) *Proc. Natl. Acad. Sci. USA* **88,** 11583–11587.
7. Maathuis, F. J. & Sanders, D. (1995) *Planta* **197,** 456–464.
8. Schroeder, J. I., Ward, J. M. & Gassman, W. (1994) *Annu. Rev. Biophys. Biomol. Struct.* **23,** 411–471.
9. Maathuis, J. M., Ichida, A. M., Sanders, D. & Schroeder, J. I. (1997) *Plant Physiol.* **114,** 1141–1149.
10. Schachtman, D. P. & Schroeder, J. I. (1994) *Nature (London)* **370,** 655–658.
11. Rubio, F., Gassmann, W. & Schroeder, J. I. (1995) *Science* **270,** 1660–1663.
12. Santa-Maria, G. E., Rubio, F., Dubcovsky, J. & Rodriguez-Navarro, A. (1997) *Plant Cell* **9,** 2281–2289.
13. Quintero, F. J. & Blatt, M. R. (1997) *FEBS Lett.* **415,** 206–211.
14. Fu, H. H. & Luan, S. (1998) *Plant Cell* **10,** 63–73.
15. Kim, E. J., Kwak, J. M., Uozumi, N. & Schroeder, J. I. (1998) *Plant Cell* **10,** 51–62.
16. Walker, N. A., Sanders, D. & Maathuis, F. J. (1996) *Science* **273,** 977–979.
17. Becker, D., Dreyer, I., Hoth, S., Reid, J. D., Busch, H., Lehnen, M., Palme, K. & Hedrich, R. (1996) *Proc. Natl. Acad. Sci. USA* **93,** 8123–8128.
18. Kang, Y. S., Kane, J., Kurjan, J., Stadel, J. M. & Tipper, D. J. (1990) *Mol. Cell. Biol.* **10,** 2582–2590.
19. Gietz, R. D. & Schiestl, R. H. (1991) *Yeast* **7,** 253–263.
20. Rodriguez-Navarro, A. & Ramos, J. (1984) *J. Bacteriol.* **159,** 940–945.
21. Brüggemann, L., Dietrich, P., Dreyer, I. & Hedrich, R. (1999) *Planta* **207,** 370–376.
22. Neher, E. (1992) *Methods Enzymol.* **207,** 123–131.
23. Nakamura, R. L., McKendree, W. L. J., Hirsch, R. E., Sedbrook, J. C., Gaber, R. F. & Sussman, M. R. (1995) *Plant Physiol.* **109,** 371–374.
24. Mueller-Roeber, B., Ellenberg, J., Provart, N., Willmitzer, L., Busch, H., Becker, D., Dietrich, P., Hoth, S. & Hedrich, R. (1995) *EMBO J.* **14,** 2409–2416.
25. Sakmann, B. & Neher, E. (1995) *Single Channel Recording* (Plenum, New York).
26. Blatt, M. R. (1991) *J. Membr. Biol.* **124,** 95–112.
27. Blatt, M. R. (1992) *J Gen. Physiol.* **99,** 615–644.
28. Dietrich, P., Dreyer, I., Wiesner, P. & Hedrich, R. (1998) *Planta* **205,** 287.
29. Hoth, S., Dreyer, I., Dietrich, P., Becker, D., Mueller-Roeber, B. & Hedrich, R. (1997) *Proc. Natl. Acad. Sci. USA* **94,** 4806–4810.
30. Ilan, N., Schwartz, A. & Moran, N. (1996) *J. Membr. Biol.* **154,** 169–181.
31. Hedrich, R., Moran, O., Conti, F., Busch, H., Becker, D., Gambale, F., Dreyer, I., Kuech, A., Neuwinger, K. & Palme, K. (1995) *Eur. Biophys. J.* **24,** 107–115.
32. Hirsch, R. E., Lewis, B. D., Spalding, E. P. & Sussman, M. R. (1998) *Science* **280,** 918–921.
33. Lohse, G. & Hedrich, R. (1992) *Planta* **188,** 206–214.
34. Maathuis, F. J. & Sanders, D. (1994) *Proc. Natl. Acad. Sci. USA* **91,** 9272–9276.
35. Maathuis, F. J., Sanders, D. & Gradmann, D. (1997) *Planta* **203,** 229–236.

⇒ zurück zur Übersicht

1999

Brüggemann, Dietrich, **Dreyer**, Hedrich

Pronounced differences between the native K^+ channels and KAT1 and KST1 α-subunit homomers of guard cells.

Planta. **207**:370-376.

Planta (1999) 207: 370–376

Planta

Pronounced differences between the native K^+ channels and KAT1 and KST1 α-subunit homomers of guard cells

Lioubov Brüggemann, Petra Dietrich, Ingo Dreyer, Rainer Hedrich

Lehrstuhl für Molekulare Pflanzenphysiologie und Biophysik, Julius-von-Sachs-Institut, Universität Würzburg, Julius-von-Sachs-Platz 2, D-97082 Würzburg, Germany

Received: 6 March 1998 / Accepted: 9 July 1998

Abstract. Stomatal opening is the result of K^+-salt accumulation in guard cells. Potassium uptake in these motor cells is mediated by voltage-dependent, K^+-selective ion channels. Here we compare the in-vitro properties of two guard-cell K^+-channel α-subunits from *Arabidopsis thaliana* (L.) Heynh. (KAT1) and *Solanum tuberosum* L. (KST1) after heterologous expression with the respective K^+-transport characteristics in their mother cell. The KAT1 and KST1 subunits when expressed in *Xenopus* oocytes shared the basic features of the K^+-uptake channels in the corresponding guard cells, including voltage dependence and single-channel conductance. Besides these similarities, the electrophysiological comparison of K^+ channels in the homologous and the heterologous expression systems revealed pronounced differences with respect to modulation and block by extracellular cations. In the presence of 1 mM Cs^+, 50% of the guard-cell K^+-uptake channels ($GCKC1_{in}$) in *A. thaliana* and *S. tuberosum*, were inhibited upon hyperpolarization to −90 mV. For a similar effect on KAT1 and KST1 in oocytes, voltages as negative as −155 mV were required. In contrast, compared to the K^+ channels in vivo the functional α-subunit homomers almost lacked a voltage-dependent block by extracellular Ca^{2+}. Similar to the block by Cs^+ and Ca^{2+}, the acid activation of the α-homomers was less pronounced in oocytes. Upon acidification the voltage-dependence shifted by 82 and 90 mV for $GCKCL_{in}$ in *A. thaliana* and *S. tuberosum*, respectively, but only by 25 mV for KAT1 and KST1. From the differences in K^+-channel modulation in vivo and after heterologous expression we conclude that the properties of functional guard-cell K^+-uptake channels result either from the heterometric assembly of different α-subunits or evolve from cell-type-specific posttranslational modification.

Correspondence to: R. Hedrich;
E-mail: hedrich@botanik.uni-wuerzburg.de;
Fax: 49 (931) 8886157; Tel.: 49 (931) 8886101

Key words: *Arabidopsis* – Guard cell – Heterologous expression (K^+-channel subunits) – K^+channel – (KAT1, KST1 subunits) – *Solanum*

Introduction

Stomata in the outer epidermis of the leaf enable land plants to optimize the uptake of CO_2 and the loss of water vapor. Depending on the environmental conditions and individual habitats, species differ in their ability to regulate the stomatal aperture (Atkinson et al. 1989; MacRobbie 1989; Atkinson 1991; Allan et al. 1994). Differences were found in the kinetics of opening and closing movement, response to light, CO_2, and the phytohormones abscisic acid (ABA) and indole acetic acid (IAA), as well as external proton and calcium concentrations (Raschke 1979). Recent comparative patch-clamp studies on guard-cell protoplasts from *Solanum tuberosum*, *Nicotiana tabacum*, and *Vicia faba* have shown that the K^+-uptake channels of these major crop plants share the same voltage dependence, selectively and block by external Cs^+ (Dietrich et al. 1998). In contrast, they exhibited pronounced differences with respect to their activation upon external acidification and susceptibility to block by apoplastic Ca^{2+}. The cloning of KAT1 and KST1, K^+-channel α-subunits expressed in guard cells from *Arabidopsis thaliana* and *Solanum tuberosum* (Anderson et al. 1992; Müller-Röber et al. 1995; Nakamura et al. 1995) and their analysis after heterologous expression in *Xenopus* oocytes, Sf9 cells and yeast allowed the elucidation of channel protein-intrinsic properties (Bertl et al. 1995; Hedrich et al. 1995b; Hoshi 1995; Müller-Röber et al. 1995; Véry et al. 1995; Becker et al. 1996; Marten et al. 1996; Hoth et al. 1997).

Since guard-cell K^+ channels in vivo differ in their regulation by cations (Hedrich and Dietrich 1996; Dietrich et al. 1998), it is tempting to speculate that these variabilities are based on the structural diversity of

K^+-channel α-subunits (Hedrich and Dietrich 1996). The answer to this question requires a quantitative analysis of K^+-channel properties in vivo and their corresponding α-subunits in vitro. We therefore compared the biophysical features of *Arabidopsis thaliana* guard-cell K^+-uptake channels and those of *Solanum tuberosum* with those of the gene products of *kat1* and *kst1* following their heterologous expression in *Xenopus* oocytes.

Materials and methods

Plant material. Arabidopsis thaliana L. C24 cv. Columbia (*Arabidopsis* Stock Center, Columbus, Ohio, USA) and *Solanum tuberosum* L. cv. Desireé (Fritz Lange Saatzucht, Bad Schwartau, Germany) were grown in a growth chamber. The photoperiod was 8 h and the photon flux density 300 μmol m^{-2} s^{-1} (HQ1-TS 250 W/D; Osram, München, Germany). The temperature was 23 °C in the light and 16 °C in the dark. The humidity ranged between 50 and 60%.

Protoplast isolation and patch-clamp recordings. Guard-cell protoplast were enzymatically isolated from 5- to 7-week-old leaves of *A. thaliana* or *S. tuberosum* according to the method developed for *V. faba* (Hedrich et al. 1990). Ion fluxes were studied either in the whole-cell or outside-out configuration of the patch-clamp technique (Hamill et al. 1981). Current measurements were performed using an EPC-9 patch-clamp amplifier (HEKA, Lambrecht, Germany). Data were low-pass-filtered with an eight-pole Bessel filter, sampled at 200 μs corresponding to 2.5-fold the filter frequency (for single-channel recording this factor was 5), digitized (ITC-16; Instrutech Corp., Elmont, N.Y., USA), stored on hard disk, and analysed with software (Instrutech Corp.) on a Gravis TT200 (Gravis, Berlin, Germany). The Ca^{2+} and Cs^+ block were fitted using the non-linear Marquardt-Levenberg algorithm (Marquardt 1963). Patch pipettes were prepared from Kimax-51 glass (Kimble products, Vineland, N.Y., USA) and coated with silicone (Sylgard 184 silicone elastomer kit; Dow Corning, USA). In order to determine membrane potentials the command voltages were corrected off-line for series resistances and liquid-junction potentials (Neher 1992).

Heterologous expression in Xenopus oocytes. Experiments were performed on RNA-injected, voltage-clamped *Xenopus* oocytes using a two-electrode voltage-clamp approach as previously described by Hedrich et al. (1995b). Because some properties of K^+-uptake channels differ with the expression level (Véry et al. 1994; Cao et al. 1995), oocytes with similar K^+-current amplitudes were selected for analysis, only.

Solutions. In patch-clamp recordings the pipette solution (cytoplasm) contained either 150 mM K-gluconate, 2 mM $MgCl_2$, 3 mM $CaCl_2$, 5 mM EGTA, 2 mM MgATP, 10 mM Hepes-Tris (pH 7.5) or 2 mM $MgCl_2$, 10 mM EGTA, 2 mM MgATP, 10 mM Hepes-Tris (pH 7.4). The standard bathing medium contained 30 mM K-gluconate, 1 mM $CaCl_2$. The pH value was adjusted using 10 mM Mes-Tris (pH 5.5–6.5, pH 4.5 for control), Tris-Mes (pH 7.0–8.5) or citrate-Tris (pH 4.0–6.0). For experiments in the presence of citrate, $CaCl_2$ was added to give the desired free Ca^{2+} concentration (calculations were done using the program WINMAXC; Chris Patton, Stanford University, Calif., USA). Solutions for measurements on *A. thaliana* were adjusted to 540 mosmol kg^{-1} and for *S. tuberosum* to 400 mosmol kg^{-1} using D-sorbitol. Modifications in solute compositions are included in the figure legends. Chemicals were obtained from Sigma.

In double-electrode voltage-clamp recordings the external standard solution was composed of 30 mM KCl, 2 mM $MgCl_2$, 1 mM $CaCl_2$, and 10 mM Mes-Tris (pH 5.6), with modifications indicated in the figure legends. All solutions were adjusted to 200 mosmol kg^{-1} with D-sorbitol.

Biophysical analysis

Voltage-dependence. The voltage-dependence of a potassium channel was described by its relative open probability (p_o). In a double-voltage step protocol, time- and voltage-dependent inward currents (I) were induced during a first activation pulse to hyperpolarizing voltages (V). During the second pulse to a fixed voltage, inward currents relaxed. The $I_0 - V$ relationship obtained from extrapolating the relaxation time course of the second pulse to $t = 0$ ms with an exponential function is proportional to the relative open probability of the channel at the end of the activation pulse ($I_0 = N \cdot i \cdot p_o$), where N denotes the number of channels, I_0 the instantaneous tail current, and i the single-channel current at the fixed voltage of the second pulse. The values for $p_o(V)$ were fitted with a Boltzmann-function:

$$p_o = \frac{1}{1 + e^{\left(\frac{V - V_{1/2}}{V_S}\right)}} \quad . \qquad \text{(Eq. 1)}$$

Here V_S denotes the slope factor, which correlates to the apparent gating charge, and $V_{1/2}$ the half-activation voltage.

Channel block. To obtain the instantaneous current-voltage characteristic of the open channel [$I_T(V)$], after an activating pre-pulse (V_{pp}) the membrane voltage was stepped subsequently to various test potentials. The $I_T(V)$ relationships were deduced from extrapolating the channel deactivation ($V > V_{pp}$) or activation ($V \leq V_{pp}$) to $t = 0$ using a single exponential function.

Current-voltage relationships of tail and steady-state currents in the presence of external cations were fitted according to the Woodhull model for cationic block of ion channels (Woodhull 1973):

$$I(V) = I^o(V) \frac{1}{1 + e^{-\left(\frac{zF}{RT}\delta(V - V_{B1/2})\right)}} \qquad \text{(Eq. 2)}$$

where F, R, and T have their usual meaning, $I^0(V)$ denotes the current in the absence of the blocking ion, z its valence and δ the fraction of the transmembrane voltage sensed by the ion. The value for $V_{B1/2}$ denotes the voltage at which 50% of the channels are blocked and is a measure of the affinity of the channel for the blocking ions. A less negative value of $V_{B1/2}$ correlates to smaller currents thereby indicating a higher sensitivity of the channel to blocking ions.

pH-dependence. Measured open probabilities at different pH values were fitted with Eq. 1 whereby the half-activation voltage $V_{1/2}$ was determined for each pH value independently, whereas the slope factor V_S was adjusted for each cell (Hoth et al. 1997; Dietrich et al. 1998). Although the single-channel conductance is pH independent (Ilan et al. 1996; Dietrich et al. 1998) we cannot exclude additional effects on the maximum conductance due to the lack of saturating maximum conductances, especially at alkaline pH values. In order to assure reversibility of the pH-effect, control measurements were performed before and after changing the extracellular pH. The pH-dependence of the half-activation potential $V_{1/2}$ was fitted according to the Henderson-Hasselbalch equation

$$V_{1/2} = V_{1/2\,\min} + \Delta V_{1/2\,\max} \frac{1}{1 + 10^{pH - pK}} \qquad \text{(Eq. 3)}$$

with the maximum sensitivity of the channel at the apparent pK value. The term $V_{1/2\,\min}$ denotes the half-maximum activation-voltage of the fully deprotonized channel and $\Delta V_{1/2\,\max}$ the maximum pH-induced shift in the voltage-dependence.

Results

Voltage-dependence and conductance

When in the whole-cell configuration of the patch-clamp technique the guard-cell plasma membrane of *A. thaliana* or *S. tuberosum* was clamped at −67 mV with essentially 150 mM K^+ in the pipette and 30 mM K^+ in the bath, depolarization to >0 mV activated K^+-release channels (Fig. 1A; c.f. Roelfsema and Prins 1997). Hyperpolarizing pulses negative to around −100 mV induced inward currents which reversed direction at the Nernst potential for K^+ (Figs. 2, 3). Guard cell K^+-uptake channels ($GCKC1_{in}$) in *A. thaliana*, however, displayed a faster activation kinetics than those in *S. tuberosum* (around 5-fold faster at −217 mV). A similar difference was observed between the cloned guard-cell K^+-uptake channels KAT1 from *A. thaliana* (Nakamura et al. 1995) and KST1 from *S. tuberosum* (Müller-Röber et al. 1995) expressed in *Xenopus* oocytes (Fig. 1A).

The voltage- and time-dependence of the macroscopic currents could be related to the activation of single K^+-selective channels (Fig. 1B). In symmetrical 150 mM K^+ a single-channel conductance of 8.6 ± 0.3 pS ($n = 6$) was derived for $GCKCl_{in}$ in *A. thaliana*, a value comparable to the 5–8 pS determined for $GCKC1_{in}$ in *S. tuberosum* as well as KAT1- and KST1-expressing *Xenopus* oocytes (Hedrich et al. 1995b; Hoshi 1995; Müller-Röber et al. 1995; Dietrich et al. 1998). Similar to $GCKC1_{in}$ in *S. tuberosum* and its corresponding α-subunit KST1, the basic properties including voltage-dependence, kinetics and single-channel conductance of the K^+-uptake channel from *Arabidopsis* resembled those of KAT1 after heterologous expression in *Xenopus* ooctyes. From the steady-state K^+-current amplitudes as shown in Fig. 1A we determined channel numbers of around 2400 per *S. tuberosum* (Dietrich et al. 1998), 500 per *A. thaliana* guard cell, and 10^6 for a KST1- or KAT1-expressing oocytes. Given the difference in cell size these numbers translate into ca. 5–8 channels per μm^2 for *Arabidopsis* and *Solanum* guard cells and ca. 2 per μm^2 in oocytes.

Response to extracellular cations

Cesium. The susceptibility towards voltage-dependent block by Cs^+ represents a general feature of all plant K^+-uptake channels investigated so far (Draber and Hansen 1994; Hedrich et al. 1995a,b; Müller-Röber et al. 1995; Becker et al. 1996; Ichida and Schroeder 1996; Dreyer et al. 1997; Dietrich et al. 1998). We therefore used 1 mM of the blocker in the presence of 30 mM K^+ in the bath to compare the Cs^+-sensitivity of K^+ channels in vivo and after heterologous expression in oocytes. Having activated the channels during a prepulse to −197 mV, in the subsequent depolarizing pulse to −117 mV or −177 mV the current amplitude initially increased due to the release of Cs^+ from the blocked channel (Fig. 2A). Hyperpolarizing voltage steps, e.g. to

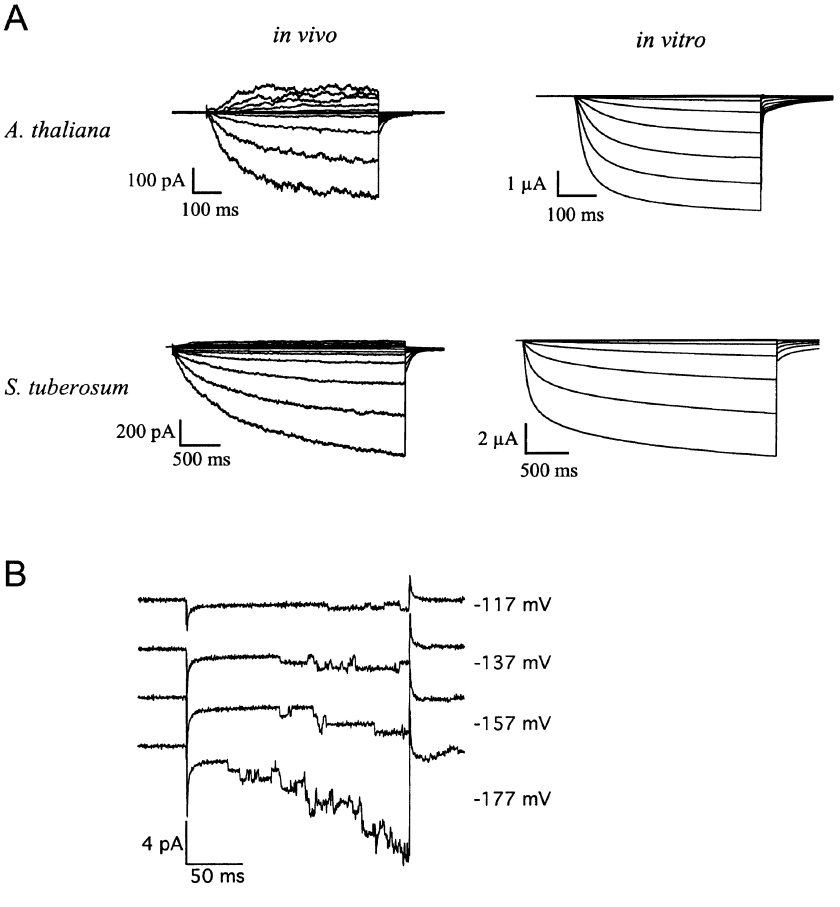

Fig. 1A,B. Voltage- and time-dependent properties of guard-cell K^+ channels in *Arabidopsis thaliana*. **A** Activation of K^+-uptake and K^+-release channels. Starting from a holding potential of −67 mV, in guard-cell protoplasts from *A. thaliana* (*top left*) and *S. tuberosum* (*bottom left*), pulses to voltages between +43 mV and −217 mV in 20-mV intervals elicited K^+ currents. Outward whole-cell currents activated positive to 0 mV while inward K^+ currents appeared negative of around −100 mV. In KAT1- (*top right*) and KST1-expressing oocytes (*bottom right*), the membrane potential was stepped from +20 mV to −180 mV in 20-mV decrements starting from a holding potential of −20 mV. Currents were recorded in the presence of 30 mM K^+ at pH 5.6 in the bath (pH 5.5 for *A. thaliana*). **B** Time-and voltage-dependent opening of single K^+-uptake channels in *Arabidopsis* guard-cell protoplasts during 200-ms pulses to the voltages indicated. Consecutive voltage pulses were applied from a holding potential of −67 mV. For better resolution of the single-channel amplitudes, the extracellular K^+ concentration was raised to 150 mM, a treatment not affecting the voltage-dependence of the channel

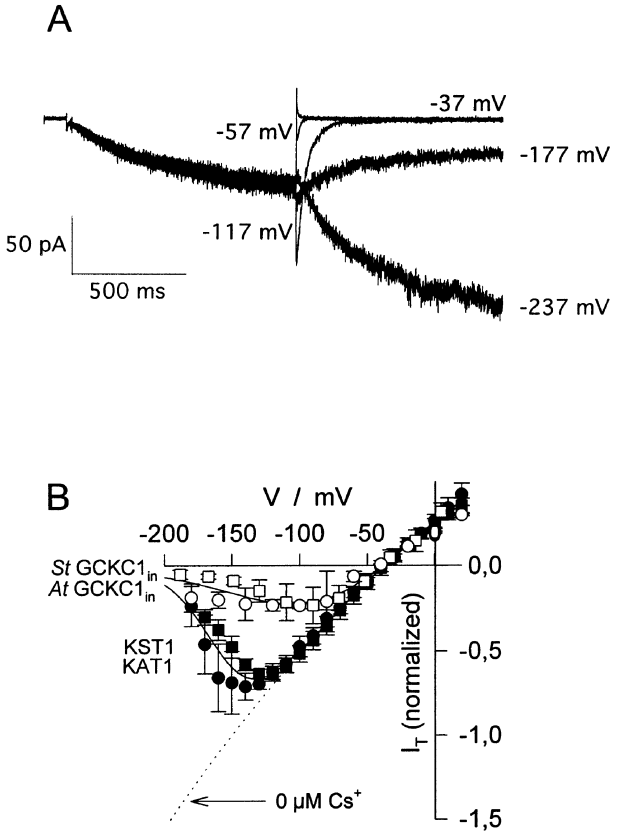

Fig. 2A,B. Voltage-dependent block of K^+-uptake channels by extracelluar Cs^+. **A** In the presence of 1 mM Cs^+, small steady-state inward K^+ currents could be recorded in *A. thaliana* at the end of the pre-pulse to −197 mV. Subsequent depolarization induced a fast unblock of K^+ channels superimposed by the deactivation kinetics. Due to the dramatic increase in the fraction of unblocked channels, open for the permeation of K^+, the instantaneous current amplitude at −117 exceeded that of the pre-pulse. At −237 mV, the fast voltage-dependent Cs^+-block induced an initial current decrease. **B** Instantaneous current-voltage characteristics of KAT1 (*closed circles*), KST1 (*closed squares*), $GCKC1_{in}$ in *A. thaliana* (*open circles*), and *S. tuberosum* (*open squares*) recorded in the presence of 1 mM Cs^+. The *dashed line* indicates the current voltage characteristics in the absence of Cs^+. *Solid lines* represent fits according to Eq. 2. Currents were normalized to I_T (−150 mV, 0 µM Cs^+) = −1. Each datum point reflects the mean ± SD of three to eight independent measurements

−237 mV, favoured channel block and decreased the instantaneous tail-current amplitude. The derived current-voltage relation of the extrapolated tail currents $[I_T(V)]$ in the presence of 1 mM Cs^+ could be fitted according to the Woodhull model for channel block (Fig. 2B; Eq. 2, Woodhull 1973). A half-maximal block of the channel ($V_{B1/2}$) was obtained at −86 mV and −95 mV for $GCKC1_{in}$ in *A. thaliana* and *S. tuberosum* and −162 mV and −150 mV for KAT1 and KST1, respectively. Thus, the Cs^+-sensitivity of the K^+ channels is more pronounced in guard cells.

Calcium. Potassium-uptake channels are blocked by extracellular Ca^{2+}, the degree of which depends on the concentration of both K^+ and Ca^{2+} (Dietrich et al. 1998). In the presence of 30 mM K^+ and 19 mM Mg^{2+}, 1 mM Ca^{2+} did not appreciably block the guard-cell K^+ channel in *A. thaliana* (Fig. 3A). Upon replacement of Mg^{2+} by Ca^{2+} the current amplitude decreased in a voltage-dependent manner (Fig. 3B). From the current-voltage curve of the extrapolated relaxation current $[I_T(V)]$ a half-maximal block was found at $V_{B1/2} = -165$ mV for *A. thaliana* and $V_{B1/2} = -204$ mV in *S. tuberosum* (Fig. 3C). To our surprise, the KAT1 and KST1 homomers almost lacked a Ca^{2+}-sensitivity under similar conditions (30 mM Ca^{2+}/30 mM K^+).

Protons. Due to the activity of the plasma-membrane proton ATPase, both membrane hyperpolarization and acidification of the extracellular medium accompany stomatal movement (Shimazaki et al. 1986; Edwards et al. 1988; Muehling et al. 1995). Since guard-cell K^+-uptake channels have been shown to activate at high extracellular proton concentration, their activity is strongly coupled to that of the proton ATPase (Blatt 1992; Ilan et al. 1994, 1996; Dietrich et al. 1998). In *S. tuberosum*, K^+ inward currents increased 3-fold when the apoplastic medium was acidified from pH 7.4 to pH 5.6 with the highest sensitivity to pH changes around pH 6.2 (Dietrich et al. 1998). In related measurements on *Arabidopsis* guard-cell protoplasts, the steady-state current amplitude increased only 1.6-fold when the pH was changed from either pH 7.5 to pH 6.0 or from pH 6.0 to pH 5.5 (Fig. 4A). Upon a pH-drop from pH 5.5 to pH 4.5, however, K^+ channel currents increased 3-fold. Boltzmann fits to the individual open probabilities revealed a proton-induced shift of the voltage-dependence to more-positive potentials (Eq. 1, Fig. 4B). Compared to an apparent pK of 6.2 in *S. tuberosum*, a pK of 4.8 for $GCKC1_{in}$ in *A. thaliana* indicates that these channels operate in the more acidic region of the pH-spectrum (for a similar acid activation in *V. faba*, see Ilan et al. 1996). In $GCKC1_{in}$ in *A. thaliana* and *S. tuberosum*, protonation-deprotonation reactions shifted $V_{1/2}$ by maximally 82 and 90 mV, respectively (Fig. 4C). By contrast, in KAT1 and KST1, pH changes induced a maximal shift in $V_{1/2}$ of 23 mV and 27 mV, only (Hoth et al. 1997). Together with an apparent pK of around 6.5 these data indicate that acid activation of KAT1 is comparable to KST1 rather than to its putative homologue in *Arabidopsis* guard cells. This provides further evidence that KAT1 and KST1 do not reflect all the properties of the K^+-uptake channels in their native environment of the guard cell.

Discussion

In this study, we compared the biophysical properties of K^+ channels in guard cells from *A. thaliana* and *S. tuberosum* with KAT1 and KST1 after heterologous expression in oocytes. Similar biophysical features, including kinectics and single-channel conductance, point to the structural relationship between the guard-cell channels in vivo and their proposed gene products in oocytes. However, a more detailed comparision

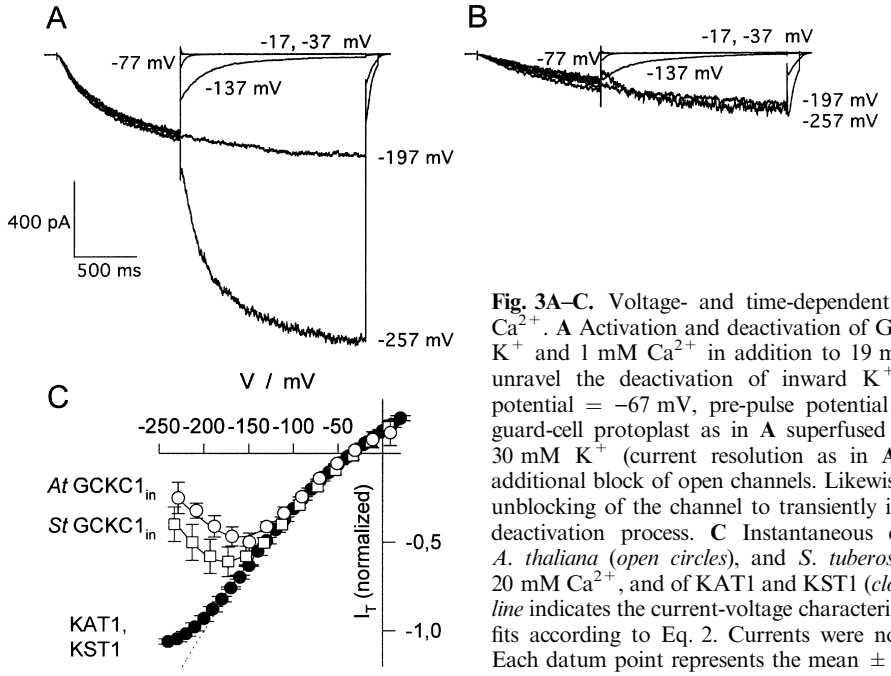

Fig. 3A–C. Voltage- and time-dependent block of K^+-uptake channels by extracellular Ca^{2+}. **A** Activation and deactivation of $GCKC1_{in}$ in *A. thaliana* in the presence of 30 mM K^+ and 1 mM Ca^{2+} in addition to 19 mM Mg^{2+}. Double-pulse protocols were used to unravel the deactivation of inward K^+ channels at depolarizing potentials (holding potential = −67 mV, pre-pulse potential = −197 mV). **B** Inward currents of the same guard-cell protoplast as in **A** superfused with extracellular 20 mM Ca^{2+} in addition to 30 mM K^+ (current resolution as in **A**). Hyperpolarization to −257 mV induced an additional block of open channels. Likewise, depolarization to e.g. −137 mV resulted in the unblocking of the channel to transiently increase the current before it decayed due to the deactivation process. **C** Instantaneous current-voltage characteristics of $GCKC1_{in}$ in *A. thaliana* (*open circles*), and *S. tuberosum* (*open squares*) recorded in the presence of 20 mM Ca^{2+}, and of KAT1 and KST1 (*closed circles*) recorded in 30 mM Ca^{2+}. The *dashed line* indicates the current-voltage characteristics in the absence of Ca^{2+} ions. *Solid lines* show fits according to Eq. 2. Currents were normalized to I_T (−200 mV, 0 mM Ca^{2+}) = −1. Each datum point represents the mean ± SD of three to seven independent measurements

elucidated dramatic differences between K^+ channels in the homologous and heterologous expression systems. Compared to the guard-cell channels in vivo, KAT1 and KST1 in the in-vitro system were characterized by their reduced sensitivity to the cationic blockers Cs^+ and Ca^{2+} as well as a less pronounced activation by extracellular protons. These differences may arise from variabilities in:

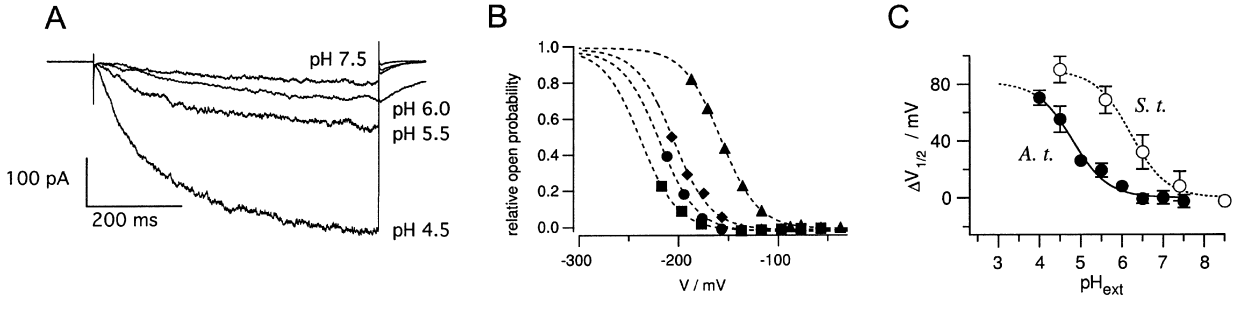

Fig. 4A–C. Acid activation of guard-cell K^+ channels. **A** Inward K^+ currents through *A. thaliana* $GCKC1_{in}$ upon voltage steps from −67 mV to −197 mV at the pH values indicated. **B** Relative open probabilities of $GCKC1_{in}$ *A. thaliana* as a function of voltage and extracellular pH. Open probabilities were normalized with respect to the maximum conductance (*triangles*, pH 4.5; *diamonds*, pH 5.5; *circles*, pH 6.0; *squares*, pH 7.5). *Dotted lines* represent Boltzmann fits to the voltage-dependent open probabilities at the individual pH. **C** pH-induced shift of the half-activation potential ($V_{1/2}$) calculated from the open-probability curves as shown in **B**. Values for $V_{1/2}$ at different pH values from three to nine independent experiments (*filled circles*, ±SD) were plotted relative to the minimum at alkaline pH ($V_{1/2min}$). The *solid line* represents a fit according to Eq. 3 with an apparent pK of 4.8 and a maximum pH-induced shift of 82 mV in $V_{1/2}$. The corresponding values obtained for $GCKCl_{in}$ in *S. tuberosum* have been added as *open circles* (c.f. Dietrich et al. 1998). The fit of the data from *S. tuberosum* (*dotted line*) revealed an apparent pK of 6.2 but a similar steepness of the pH-dependence

(i) techniques used

One could speculate that the differences in currents may arise from the two techniques used, especially since in the whole-cell configuration of the patch-clamp technique regulatory factors could have been lost from the cytosol. However, the effects of Cs^+, Ca^{2+}, protons and voltage could be observed right after whole-cell access, where cytosolic factors have not yet been lost (Pusch and Neher 1988). Ten to fifteen minutes later the responses were identical to those observed right after the breakthrough.

A comparison of measurements on K^+-uptake channels of *Vicia faba* guard cells performed with the patch-clamp technique as well as with impalement electrodes showed that this K^+-uptake channel – independent of the technique used – exhibits the same voltage-dependence, selectivity and sensitivity to, for example, ABA and Ca^{2+} (Schroeder 1988; Blatt 1992; Lemtiri-Clieh and MacRobbie 1994; Armstrong et al. 1995; Dietrich et al. 1998). Furthermore, the impalement studies on *A. thaliana* guard cells by Roelfsema and Prins (1997) obtained very similar voltage-dependent properties of this K^+ channel. The two techniques performed on the same cell type therefore exclude the possibility that the choice of the technique is responsible for the differences

observed between *A. thaliana* $GCKCl_{in}$ and KAT1, and *S. tuberosum* $GCKC1_{in}$ and KST1.

(ii) expression-levels

Véry et al. (1994) have shown that the Cs^+ sensitivity of KAT1 expressed in *Xenopus* oocytes strongly depends on the K^+-channel density. A decrease in the expression level of KAT1 was accompanied by an increase in its Cs^+ susceptibility and vice versa. From the low sensitivity of KAT1 and KST1 to Cs^+ and Ca^{2+} one would therefore assume these channels to be more abundant in the in vitro system than in the guard-cell membrane. Since we measured higher channel densities in guard cells and assuming equally distributed channels in both membrane types, expression-level-dependent variables do not account for the loss of cation sensitivity in oocytes.

(iii) post-translational modifications

Expression studies on *Xenopus* oocytes, yeast or Sf9 cells revealed that KAT1 displayed expression system-dependent variabilities with respect to voltage dependence and ammonium permeability (Schachtman et al. 1992; Bertl et al. 1995; Marten et al. 1996). Channel modifications such as glycosylation and phosphorylation have recently been shown to shift the voltage dependence of various animal K^+ channels without affecting their selectivity (Moran et al. 1991; Santacruz-Toloza et al. 1994; Schwalbe et al. 1995, 1996; Thornhill et al. 1996). While minor differences in the voltage-dependence of guard cell K^+ channels between different expression systems may be explained on the basis of individual glycosylation or phosphorylation patterns, alterations of Ca^{2+}- and Cs^+-sensitivities would require severe changes within the permeation pathway (Doyle et al. 1998). This region, however, which is conserved among all K^+ channels including KAT1 and KST1, lacks putative glycosylation and phosphorylation sites (Anderson et al. 1992; Müller-Röber et al. 1995). In this context ABA- and Ca^{2+}-dependent kinases were identified in guard cells (Armstrong et al. 1995; Li et al. 1998). These elements are likely to be involved in the down-regulation of K^+-uptake channels in response to elevated cytosolic Ca^{2+}/pH during stomatal closure. So far, however, this kind of regulation has not been shown to alter the sensitivity of K^+ channels to extracellular cations. In line with this conclusion, a 10-min treatment with the protein kinase inhibitor staurosporine or the phosphatase inhibitor okadaic acid did not alter the response of KAT1 to Cs^+ and Ca^{2+} (data not shown).

(iv) subunit composition: Is one α-subunit enough?

From the diversity of plant K^+-channel structures (Hedrich and Dietrich 1996) it may be assumed that different α-subunits co-localize in one cell type. Since a tetramerization domain in the C-terminus seems to be required for the assembly of functional channels (Daram et al. 1997) the cell-type-specific expression pattern of different K^+-channel genes may therefore determine the properties of the functional K^+-channel complex. In line with this hypothesis, Dreyer et al. (1997) could demonstrate that co-expression of KAT1 with SKT1 or AKT1 resulted in functional heteromers with Cs^+-phenotypes similar to those of K^+ channels in guard cells. The AKT-related α-subunits are thus assumed to express a high sensitivity to cationic blockers. Confirming this hypothesis, Bertl and Slayman (1996) could demonstrate that AKT1, when expressed in yeast, exhibits a more pronounced sensitivity to extracelluar Cs^+ compared to KAT1 or KST1 in oocytes. Whether AKT-related α-subunits are equipped with an increased proton sensitivity, too, remains to be elucidated. We conclude that a heteromeric assembly of α-subunits is likely to contribute to unique guard-cell K^+-current phenotypes in different species.

This work was supported by grants from the Deutsche Forschungsgemeinschaft.

References

Allan AC, Fricker MD, Ward JL, Beale MH, Trewavas AJ (1994) Two transduction pathways mediate rapid effects of abscisic acid in *Commelina* guard cells. Plant Cell 6: 1319–1328

Anderson JA, Huprikar SS, Kochian LV, Lucas WJ, Gaber RF (1992) Functional expression of a probable *Arabidopsis thaliana* potassium channel in *Saccharomyces cerevisiae*. Proc Natl Acad Sci USA 89: 3736–3740

Armstrong F, Leung J, Grabov A, Brearley J, Giraudat J, Blatt MR (1995) Sensitivity to abscisic acid of guard-cell K^+ channels is suppressed by *abil-1*, a mutant *Arabidopsis* gene encoding a putative protein phosphatase. Proc Natl Acad Sci. USA 92: 9520–9524

Atkinson CJ (1991) The influence of increasing rhizospheric calcium on the ability of *Lupinus luteus* L. to control water use efficiency. New Phytol 119: 207–216

Atkinson CJ, Mansfield TA, Kean AM, Davies WJ (1989) Control of stomatal aperture by calcium in isolated epidermal tissue and whole leaves of *Commelina communis* L. New Phytol 111: 9–18

Becker D, Dreyer I, Hoth S, Reid JD, Busch H, Lehnen M, Palme K, Hedrich R (1996) Changes in voltage activation, Cs^+ sensitivity, and ion permeability in H5 mutants of the plant K^+ channel KAT1. Proc Natl Acad Sci USA 93: 8123–8128

Bertl A, Slayman CL (1996) Comparative physiology of plant ion channels expressed in yeast. Annual Meeting of the Society for Experimental Biology: Plant Biology Abstracts, Lancaster, UK, March 24–29, 1996: 69–70

Bertl A, Anderson JA, Slayman CL, Gaber RF (1995) Use of *Saccharomyces cerevisiae* for patch-clamp analysis of heterologous membrane proteins: characterization of Kat1, an inward- rectifying K^+ channel from *Arabidopsis thaliana*, and comparison with endogenous yeast channels and carriers. Proc Natl Acad Sci USA 92: 2701–2705

Blatt MR (1992) K^+ channels of stomatal guard cells. Characteristics of the inward rectifier and its control by pH. J Gen Physiol 99: 615–644

Cao Y, Ward JM, Kelly WB, Ichida AM, Gaber RF, Anderson JA, Uozumi N, Schroeder JI, Crawford NM (1995) Multiple genes, tissue specificity, and expression-dependent modulation contribute to the functional diversity of potassium channels in *Arabidopsis thaliana*. Plant Physiol 109: 1093–1106

Daram P, Urbach S, Gaymard F, Sentenac H, Cherel I (1997) Tetramerization of the AKT1 plant potassium channel involves its C-terminal cytoplasmic domain. EMBO J 16: 3455–3463

Dietrich P, Dreyer I, Wiesner P, Hedrich R (1998) Cation sensitivity and kinetis of guard-cell potassium channels differ among species. Planta 205: 277–287

Doyle DA, Cabral JM, Pfuetzner RA, Kuo A, Gulbis JM, Cohen SL, Chait BT, MacKinnon R (1998) The structure of the potassium channel: molecular basis of K^+ conduction and selectivity. Science 280: 69–77

Draber S, Hansen UP (1994) Fast single-channel measurements resolve the blocking effect of Cs^+ on the K^+ channel. Biophys J 67: 120–129

Dreyer I, Antunes S, Hoshi T, Muller-Rober B, Palme K, Pongs O, Reintanz B, Hedrich R (1997) Plant K^+ channel alpha-subunits assemble indiscriminately. Biophys J 72: 2143–2150

Edwards MC, Smith GN, Bowling D-JF (1988) Guard cells extrude protons prior to stomatal opening – A study using fluorescence microscopy and pH micro-electrodes. J Exp Bot 39: 1541–1548

Hamill OP, Marty A, Neher E, Sakmann B, Sigworth FJ (1981) Improved patch-clamp techniques for high-resolution current recording from cells and cell-free membrane patches. Pflügers Arch 391: 85–100

Hedrich R, Dietrich P (1996) Plant K^+ channels: similarity and diversity. Bot Acta 109: 94–101

Hedrich R, Busch H, Raschke K (1990) Ca^{2+} and nucleotide dependent regulation of voltage dependent anion channels in the plasma membrane of guard cells. EMBO J 9: 3889–3892

Hedrich R, Bregante M, Dreyer I, Gambale F (1995a) The voltage-dependent potassium-uptake channel of corn coleoptiles has permeation properties different from other K^+ channels. Planta 197: 193–199

Hedrich R, Moran O, Conti F, Busch H, Becker D, Gambale F, Dreyer I, Küch A, Neuwinger K, Palme K (1995b) Inward rectifier potassium channels in plants differ from their animal counterparts in response to voltage and channel modulators. Eur Biophys J 24: 107–115

Hoshi T (1995) Regulation of voltage dependence of the KAT1 channel by intracellular factors. J Gen Physiol 105: 309–328

Hoth S, Dreyer I, Dietrich P, Becker D, Müller-Röber B, Hedrich R (1997) Molecular basis of plant-specific acid activation of K^+ uptake channels. Proc Natl Acad Sci USA 94: 4806–4810

Ichida AM, Schroeder JI (1996) Increased resistance to extracelluar cation block by mutation of the pore domain of the *Arabidopsis* inward-rectifying K^+ channel KAT1. J Membr Biol 151: 53–62

Ilan N, Schwartz A, Moran N (1994) External pH effects on the depolarization-activated K^+ channels in guard cells protoplast of *Vicia faba*. J Gen Physiol 103: 807–831

Ilan N, Schwartz A, Moran N (1996) External protons enhance the activity of the hyperpolarization-activated K^+ channels in guard cell protoplasts of *Vicia faba*. J Membr Biol 154: 169–181

Lemtiri-Clieh F, MacRobbie E (1994) Role of calcium in the modulation of *Vicia* guard cell potassium channels by abscisic acid, a patch-clamp study. J Membr Biol 137: 99–107

Li J, Lee YR, Assmann SM (1998) Guard cells possess a calcium-dependent protein kinase that phosphorylates the KAT1 potassium channel. Plant Physiol 116: 785–795

MacRobbie EAC (1989) Calcium influx at the plasmalemma of isolated guard cells of *Commelina communis*: effects of abscisic acid. Planta 178: 231–241

Marquardt D (1963) An algorithm for least-squares estimation of non-linear parameters. J Soc Ind App Math 11: 431–441

Marten I, Gaymard F, Lemaillet G, Thibaud JB, Sentenac H, Hedrich R (1996) Functional expression of the plant K^+ channel KAT1 in insect cells. FEBS Lett 380: 229–232

Moran O, Dascal N, Lotan I (1991) Modulation of a *Shaker* potassium A-channel by protein kinase C activation. FEBS Lett 279: 256–260

Muehling KH, Plieth C, Hansen UP, Sattelmacher B (1995) Apoplastic pH of intact leaves of *Vicia faba* as influenced by light. J Exp Bot 46: 377–382

Müller-Röber B, Ellenberg J, Provart N, Willmitzer L, Busch H, Becker D, Dietrich P, Hoth S, Hedrich R (1995) Cloning and electrophysiological analysis of KST1, an inward rectifying K^+ channel expressed in potato guard cells. EMBO J 14: 2409–2416

Nakamura RL, McKendree WLJ, Hirsch RE, Sedbrook JC, Gaber RF, Sussman MR (1995) Expression of an *Arabidopsis* potassium channel gene in guard cells. Plant Physiol 109: 371–374

Neher E (1992) Correction for liquid junction potentials in patch clamp experiments. Methods Enzymol 207: 123–131

Pusch M, Neher E (1988) Rates of diffusional exchange between small cells and a measuring patch pipette. Pflügers Arch 411: 204–211

Raschke K (1979) Movements of stomata. In: Haupt W, Feinleib M (eds) Enzyclopedia of plant physiology. Springer, Heidelberg, pp 383–441

Roelfsema MR, Prins HB (1997) Ion channels in guard cells of *Arabidopsis thaliana* (L.) Heynh. Planta 202: 18–27

Santacruz-Toloza L, Huang Y, John SA, Papazian DM (1994) Glycosylation of *shaker* potassium channel protein in insect cell culture and in *Xenopus* oocytes. Biochemistry 33: 5607–5613

Schachtman DP, Schroeder JI, Lucas WJ, Anderson JA, Gaber RF (1992) Expression of an inward-rectifying potassium channel by the *Arabidopsis* KAT1 cDNA. Science 258: 1654–1658

Schroeder JI (1988) K^+ transport properties of K^+ channels in the plasma membrane of *Vicia faba* guard cells. J Gen Physiol 92: 667–683

Schwalbe RA, Wang Z, Wible BA, Brown AM (1995) Potassium channel structure and function as reported by a single glycosylation sequon. J Biol Chem 270: 15336–15340

Schwalbe RA, Wang Z, Bianchi L, Brown AM (1996) Novel sites of N-glycosylation in ROMK1 reveal the putative pore-forming segment H5 as extracellular. J Biol Chem 271: 24201–24206

Shimazaki K, Iino M, Zeiger E (1986) Blue light-dependent proton extrusion by guard-cell protoplasts of *Vicia faba*. Nature 319: 324–326

Thornhill WB, Wu MB, Jiang X, Wu X, Morgan PT, Margiotta JF (1996) Expression of Kv1.1 delayed rectifier potassium channels in *Lec* mutant Chinese hamster ovary cell lines reveals a role for sialidation in channel function. J Biol Chem 271:19093–19098

Véry AA, Bosseux C, Gaymard F, Sentenac H, Thibaud JB (1994) Level of expression in *Xenopus* oocytes affects some characteristics of a plant inward-rectifying voltage-gated K^+ channel. Pflügers Arch 428: 422–424

Véry AA, Gaymard F, Bosseux C, Sentenac H, Thibaud JB (1995) Expression of a cloned plant K^+ channel in *Xenopus* oocytes: analysis of macroscopic currents. Plant J 7: 321–332

Woodhull AM (1973) Ionic blockage of sodium channels in nerve. J Gen Physiol 61: 687–708

⇒ zurück zur Übersicht

1998

Dreyer, Becker, Bregante, Gambale, Lehnen, Palme, Hedrich

Single mutations strongly alter the K^+-selective pore of the K_{in} channel KAT1.

FEBS Lett. **430**:370-376.

FEBS Letters 430 (1998) 370–376 FEBS 20458

Single mutations strongly alter the K^+-selective pore of the K_{in} channel KAT1

Ingo Dreyer[a], Dirk Becker[a], Monica Bregante[b], Franco Gambale[b], Michaela Lehnen[c], Klaus Palme[c], Rainer Hedrich[a,*]

[a] *Julius-von-Sachs-Institut für Biowissenschaften, Lehrstuhl Botanik I-Molekulare Pflanzenphysiologie und Biophysik, Julius-von-Sachs-Platz 2, D-97082 Würzburg, Germany*
[b] *Istituto di Cibernetica e Biofisica, CNR, Via de Marini 6, I-16149 Genoa, Italy*
[c] *Max-Delbrück-Laboratorium in der Max-Planck-Gesellschaft, Carl-von-Linne-Weg 10, D-50829 Cologne, Germany*

Received 6 April 1998; revised version received 28 May 1998

Abstract Voltage-dependent potassium uptake channels represent the major pathway for K^+ accumulation underlying guard cell swelling and stomatal opening. The core structure of these *Shaker*-like channels is represented by six transmembrane domains and an amphiphilic pore-forming region between the fifth and sixth domain. To explore the effect of point mutations within the stretch of amino acids lining the K^+ conducting pore of KAT1, an *Arabidopsis thaliana* guard cell K_{in} channel, we selected residues deep inside and in the periphery of the pore. The mutations on positions 256 and 267 strongly altered the interaction of the permeation pathway with external Ca^{2+} ions. Point mutations on position 256 in KAT1 affected the affinity towards Ca^{2+}, the voltage dependence as well as kinetics of the Ca^{2+} blocking reaction. Among these T256S showed a Ca^{2+} phenotype reminiscent of an inactivation-like process, a phenomenon unknown for K_{in} channels so far. Mutating histidine 267 to alanine, a substitution strongly affecting C-type inactivation in *Shaker*, this apparent inactivation could be linked to a very slow calcium block. The mutation H267A did not affect gating but hastened the Ca^{2+} block/unblock kinetics and increased the Ca^{2+} affinity of KAT1. From the analysis of the presented data we conclude that even moderate point mutations in the pore of KAT1 seem to affect the pore geometry rather than channel gating.

Key words: Gating; Inactivation; Pore structure; Site-directed mutagenesis; Voltage-dependent block

1. Introduction

Voltage-gated inwardly rectifying K^+ channels (K_{in} channels) play a fundamental role in plant physiology. These transporters allow plant cells to take up large quantities of potassium essential for cell growth and differentiation. The molecular cloning of plant K_{in} channels and the functional expression in heterologous expression systems provided the basis to relate structural motifs within the channel protein to distinct functions [1–15]. From the gating characteristics, kinetics, pharmacology, and the primary structure, K_{in} channels were grouped within a separate family of voltage-dependent potassium channels [2]. Based on the putative secondary structure with six transmembrane-spanning domains (S1–S6) and a pore region (P) between S5 and S6 (cf. [16] and references therein), plant K_{in} channels resemble voltage-gated outwardly rectifying animal K^+ channels of the *Shaker* type (K_V channels, for review see [17]). In contrast K_{in} channels do not activate at positive but at negative potentials and thus in vivo and in vitro predominantly mediate inward currents. These inward currents do not inactive even during sustained hyperpolarization (see [18] and references therein).

Like K_V channels K_{in} channels represent multisubunit proteins. When expressed in *Xenopus* oocytes plant K_{in} channel α-subunits assemble non-selectively among channel subtypes originating from different tissues, plant species and even different families [19]. An assembly region in the cytoplasmic C-terminal part of the protein has been identified as an essential element for subunit aggregation. This region is highly conserved among different subfamilies of plant K_{in} channels [20]. Similar findings were recently reported for the rat ether-à-go-go potassium channel, an animal K^+ channel with a high degree of homology to K_{in} channels [21].

Due to the structural similarity to K_V channels, differences in assembly and opposite gating, K_{in} channels represent a unique target for studies on the difference between structure and function within *Shaker*-related K^+ channel families. The two K_{in} channels, KST1 from *Solanum tuberosum* [10] and KAT1 from *Arabidopsis thaliana* [1], advanced to a model system for these studies. For both proteins it has recently been shown that the positively charged S4 segment together with the N- and C-termini contribute to the gating of K_{in} channels [19,22,23]. However, the pore region seems to play an extraordinary role, because this domain, besides its function as the permeation pathway [24–27], very likely interacts with the gating machinery as well [22,24,28].

In this study we investigated the influence of point mutations in the pore region of KAT1 on the pore geometry and related it to the crystal structure of the K^+ channel from *Streptomyces lividans* KcsA [29]. Probing the interaction between pore mutants and Ca^{2+} ions we were able to distinguish the effects of the divalent cation on permeation and gating.

2. Materials and methods

2.1. Electrophysiology

Experiments were performed on RNA-injected, voltage-clamped *Xenopus* oocytes using a two-electrode voltage clamp approach as previously described by Hedrich et al. [8]. Because some channel properties of K_{in} channels differ with the expression level [5,7], oocytes with similar K^+ current amplitudes were selected for analysis only.

2.1.1. Solutions. Experiments were performed either in 30 mM or in 10 mM KCl, 10 mM MES/Tris, pH 5.6. Various molar fractions of 30 mM between $CaCl_2$ and $MgCl_2$ were used to maintain the ionic strength. All solutions were adjusted to 220 mosmol/kg with sorbitol.

*Corresponding author.
E-mail: hedrich@botanik.uni-wuerzburg.de

PII: S0014-5793(98)00694-2

2.2. Biophysical analysis

2.2.1. Ion blockTo obtain the instantaneous current-voltage characteristic of the open channel ($I_T(V)$) the membrane voltage after approaching steady-state activation at $V=-150$ mV was stepped to various values. $I_T(V)$ relationships were deduced from extrapolating the tail current onset to $t=0$.

Current-voltage relationships of tail and steady-state currents in the presence of an antagonist were fitted according to the Woodhull model [30]:

$$I(V) = I^0(V)\frac{1}{1+\frac{[Ca^{2+}]^n}{\kappa}e^{-\left(\frac{zF}{RT}\delta V\right)}}$$

$$= I^0(V)\frac{1}{1+e^{-\left(\frac{zF}{RT}\delta(V-V_{Block1/2})\right)}} \quad (1)$$

where F, R, and T have their usual meanings. $I^0(V)$ denotes the current in the absence of the blocking ion, z its valence, δ the fraction of the transmembrane voltage sensed by the ion, $[Ca^{2+}]$ the blocker concentration, n the stoichiometry coefficient of the blocking reaction, and κ the K_i at 0 mV. κ is correlated with the energy which characterizes the affinity of the Ca^{2+} binding site (ΔG_B; Fig. 6C) Comparing two mutants characterized by κ_1 or ΔG_{B1} and κ_2 or ΔG_{B2} the difference

$$\ln\kappa_1-\ln\kappa_2 = \frac{1}{kT}(\Delta G_{B2}-\Delta G_{B1}) = \frac{1}{kT}\cdot\Delta G_{aff} \quad (2)$$

is a measure for the altered affinity to the blocking ion ΔG_{aff}.

Given a $[Ca^{2+}]$ value, the half-blocking voltage $V_{Block1/2}$ could be obtained from $I(V_{Block1/2}) = 1/2\ I^0(V_{Block1/2})$. From Eq. 1 it can be deduced:

$$\ln[Ca^{2+}] = \frac{zF}{RT}\frac{\delta}{n}V_{Block1/2} + \frac{1}{n}\ln\kappa \quad (3)$$

i.e. in a $\ln[Ca^{2+}]$-$V_{Block1/2}$ plot the slope is a measure for the voltage dependence of the block, and

$$\ln\frac{I^0-I}{I} = n\ln[Ca^{2+}]-\ln\kappa-\frac{zF}{RT}\delta V \quad (4)$$

i.e. in a $\ln[(I^0\text{-}I)/I]$-$\ln[Ca^{2+}]$ plot the slope is a measure for the concentration dependence of the block (stoichiometry coefficient n).

Combining Eqs. 2 and 3 the difference in the affinity energy can be calculated by

$$\Delta G_{aff} = kT\cdot\left(\frac{zF}{RT}\cdot(\delta_2 V^2_{Block1/2}-\delta_1 V^1_{Block1/2}) + (n_1-n_2)\cdot\ln[Ca^{2+}]\right) \quad (5)$$

2.3. Molecular biology

KAT1 single mutants were generated as previously described [24]. To construct the double mutants T256E/H267A and T256S/H267A the single mutants KAT1-T256E, KAT1-T256S, and KAT1-H267A in pGEMHE [31] were incubated with the restriction enzymes *Dsa*I and *Sal*I which resulted in the release of two fragments, one 800 bp fragment covering position 256 and a 4600 bp fragment representing the expression vector as well as the other parts of the KAT1 sequence including position 267. The 800 bp fragments containing the T256E and T256S mutations were isolated and ligated into the 4600 bp backbone of the KAT1-H267A restriction digest. The double mutants were verified by sequencing.

3. Results

3.1. Low-affinity Ca^{2+} block in KAT1 wild-type

In previous experiments performed in 30 mM K^+ in the bath, Ca^{2+} concentrations up to 30 mM, and voltages in the range of -170 mV to +20 mV no Ca^{2+} sensitivity of the KAT1 wild-type could be detected [24]. A recent study, however, showed that in guard cell protoplasts the degree of the voltage-dependent Ca^{2+} block of plasma membrane K^+_{in} channels increased when lowering the external K^+ concentration. In *Vicia faba* for example the Ca^{2+} block in media containing 20 mM Ca^{2+} in addition to 30 mM K^+ was comparable to the block in solutions based on 10 mM K^+ and 1 mM Ca^{2+} [32]. We therefore tested the Ca^{2+} sensitivity of KAT1 expressed in *Xenopus* oocytes in the presence of 10 mM K^+ only. Using Ca^{2+} concentrations up to 30 mM a divalent block was resolved at voltages negative of -200 mV (Fig. 1A). With more hyperpolarizing voltages the strength of the block increased. In this voltage range a weak Ca^{2+} block could be observed in media containing 30 mM K^+ and 30 mM Ca^{2+} as well (Fig. 1B). Thus the KAT1 wild-type channel when expressed in *Xenopus* oocytes exhibits a very low Ca^{2+} susceptibility, only.

3.2. Mutations at position T256 modify the Ca^{2+} sensitivity of KAT1

In the following we tested whether and in which way single site mutations within the pore of KAT1 modify the interaction with the divalent blocker. Since in a previous study [24] we observed that a pore mutant on position 256, T256E, is more sensitive to extracellular Ca^{2+} than the KAT1 wild-type

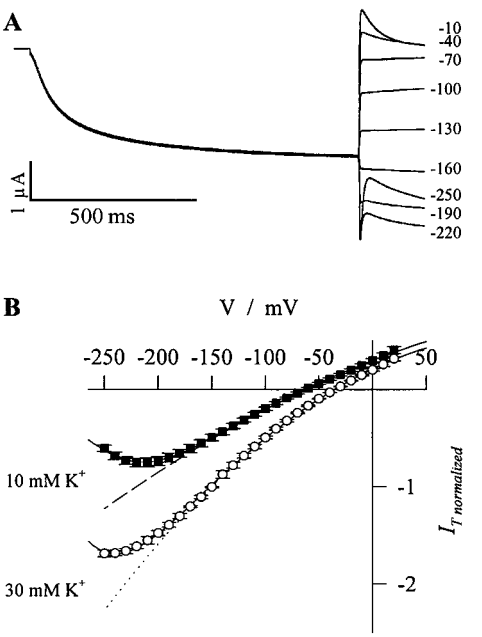

Fig. 1. Low affinity Ca^{2+} block in the K_{in} channel KAT1 expressed in *Xenopus* oocytes. Low affinity Ca^{2+} block was uncovered using a two step pulse protocol. The first pulse to -150 mV activated KAT1 channels but not oocyte-intrinsic channels. At the beginning of the second 300-ms pulse the driving force for the ions was altered while the open probability of KAT1, and oocyte-intrinsic channels remained unaffected. A: Representative current families from KAT1-expressing oocytes measured in 10 mM K^+/30 mM Ca^{2+}. Voltages of the second pulse are indicated in mV. B: Instantaneous current-voltage characteristics of the KAT1 wild-type measured in 10 mm K^+/1 mM Ca^{2+} (dashed line), 10 mM K^+/30 mM Ca^{2+} (closed squares), 30 mM K^+/1 mM Ca^{2+} (dotted line), and 30 mM K^+/30 mM Ca^{2+} (open circles). Solid lines represent best fits according to Eq. 1. This yielded $\delta = 0.43\pm0.03$, $V_{Block1/2}{}^{10mMK} = -250.1\pm1.8$ mV, and $V_{Block1/2}{}^{30mMK} = -280.2\pm1.8$ mV. Currents in B were normalized to $I(-150$ mV, 30 mM K^+/1 mM $Ca^{2+}) = -1$. Each data point represents the mean of three or four measurements. Error bars indicate the standard deviation.

we focused on this residue and further created the mutants T256D, T256H, T256K, T256Q, T256M, T256I, and T256S.

The substitution T256E increased the Ca^{2+} affinity of KAT1 by at least $\Delta G_{aff} \geq 6\ kT$ (Fig. 2A, left; Fig. 3; Table 1; Eq. 5). To prove whether this gain in sensitivity results from the negative charge introduced, we altered the charge density at that position by the mutations T→D, T→H, T→K, and T→Q. In line with previous observations the mutant T256D exhibited a pronounced Rb^+ permeability when compared to wild-type KAT1 [25]. However, in 30 mM K^+ and even in 100 mM K^+ the current amplitudes were too small to allow reliable Ca^{2+} interaction studies. From similar experiments we deduced that residues with large and positively charged side chains like histidine or lysine at position 256, T256H and T256K, seemed to hinder K^+ fluxes through the channel.

In contrast to T256E the mutant channel T256Q did not show an increase in Ca^{2+} sensitivity (not shown). This finding seemed to indicate that the negative charge in T256E is responsible for the pronounced Ca^{2+} block. The exchange of the hydrophilic polar threonine by amino acids with hydrophobic non-polar side chains (isoleucine and methionine), however, increased the Ca^{2+} sensitive of the channels as well. Similar to T256E, the mutant T256M was blocked by extracellular calcium in a voltage-dependent manner (Fig. 3A). The interaction of the open pore of both mutant channels, T256M and T256E, with the Ca^{2+} ion could be described with the Woodhull model [30]. δ values of 0.32 for T256E and 0.55 for T256M indicate that the blocking ion might move 32% and 55%, respectively, along the voltage drop across the selectivity filter. The block in the mutant T256M was, however, weaker than in T256E. This distinction could be expressed by the difference in the affinity energy, $\Delta G_{aff} \approx 4.6\ kT$ (Table 1, Eq. 5), on one hand, and by the inhibitory constant K_i (−150 mV), on the other. In the presence of 30 mM K^+ in the bath, 14.5 mM Ca^{2+} was sufficient to inhibit the K^+

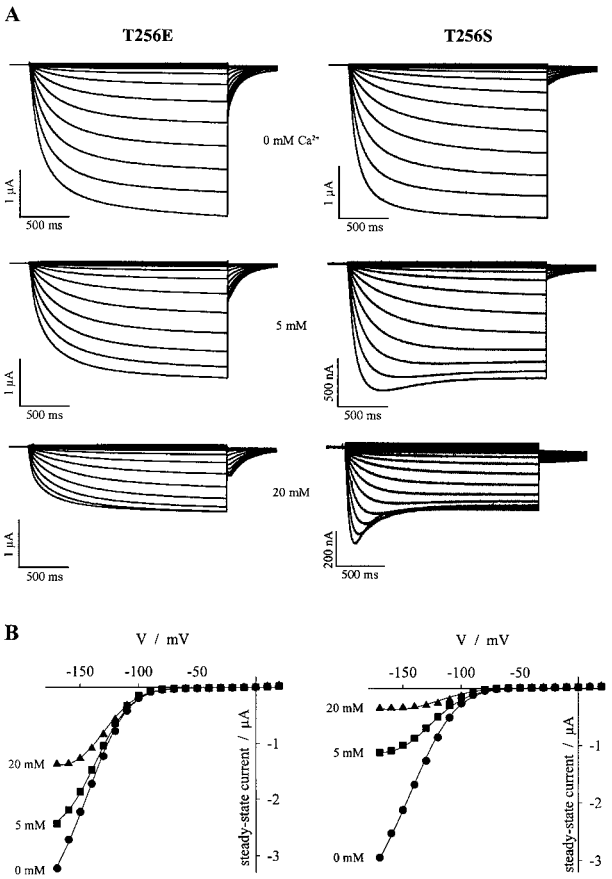

Fig. 2. Ca^{2+} modulation of inward potassium currents in the KAT1 mutants T256E (left) and T256S (right). A: Representative current families from oocytes measured in 30 mM K^+ and 0 mM (top), 5 mM (middle), and 20 mM Ca^{2+} (bottom) respectively. From a holding potential of −20 mV currents were elicited by 1-s voltage steps from −20 mV to −170 mV (10 mV steps) followed by a voltage step to −70 mV. B: Steady-state current-voltage characteristics for the oocytes shown in A. The symbols correspond to Ca^{2+} concentrations of 0 mM (circles), 5 mM (squares), and 20 mM (triangles) in bath. Solid lines represent best fits according to Eq. 1 ($\delta_{T256E} = 0.32 \pm 0.02$, $V_{Block1/2,\ T256E}{}^{5Ca} = -214.3 \pm 2.9$ mV, $V_{Block1/2,\ T256E}{}^{20Ca} = -160.1 \pm 0.8$ mV, $\delta_{T256S} = 0.24 \pm 0.01$, $V_{Block1/2,\ T256S}{}^{5Ca} = -144.4 \pm 1.2$ mV, and $V_{Block1/2,\ T256S}{}^{20Ca} = -68.0 \pm 5.3$ mV).

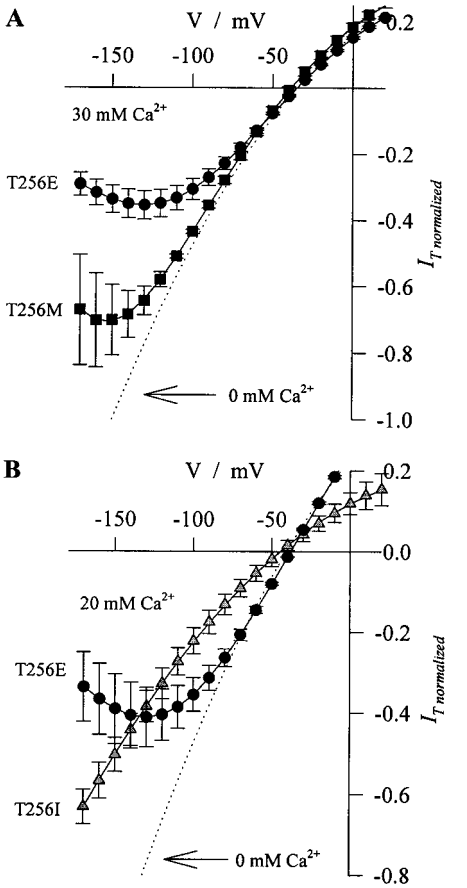

Fig. 3. Voltage-dependent and voltage-independent Ca^{2+}-block of KAT1-T256 mutants in 30 mM K^+. A: Instantaneous current-voltage characteristics of the mutants T256E (closed circles) and T256M (closed squares) measured in 30 mM Ca^{2+}. B: Instantaneous current-voltage characteristics of the mutants T256E (closed circles) and T256I (gray triangles) measured in 20 mM Ca^{2+}. The dotted lines indicate the current-voltage characteristics in the absence of Ca^{2+}. Solid lines represent best fits according to Eq. 1. This yielded in A $\delta_{T256E} = 0.32 \pm 0.03$, $V_{Block1/2}{}^{T256E} = -124.6 \pm 12.4$ mV, $\delta_{T256M} = 0.47 \pm 0.14$, $V_{Block1/2}{}^{T256M} = -174.7 \pm 6.0$ mV, and in B $\delta_{T256E} = 0.32 \pm 0.06$, $V_{Block1/2}{}^{T256E} = -133.5 \pm 19.6$ mV. The data for T256I were fitted according to the equation $I(V) = a \cdot I^0(V)$, $a = 0.51 \pm 0.01$. Currents were normalized to $I(-150$ mV, 0 mM $Ca^{2+}) = -1$. Each data point represents the mean of three or four measurements. Error bars indicate the standard deviation.

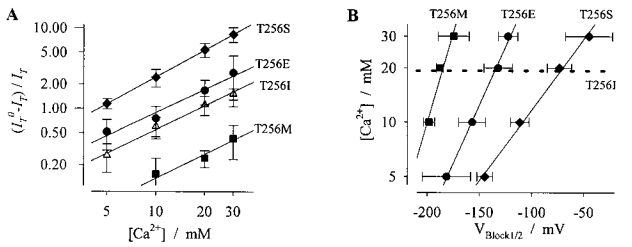

Fig. 4. Ca^{2+} inhibition of the K^+ currents in the KAT1 mutants T256E (circles), T256I (gray triangles), T256M (squares), and T256S (rhombi). Each data point represents the mean of three to ten measurements. Error bars indicate the standard deviation. A: Concentration dependence of the Ca^{2+} block displayed in a $\ln[I^0-I]$-$\ln[Ca^{2+}]$ plot. Data were generated at −150 mV. Solid lines represent best fits according to Eq. 4 ($n_{T256E} = 1.0 \pm 0.3$, $n_{T256M} = 1.0 \pm 0.1$, $n_{T256M} = 1.0 \pm 0.3$, and $n_{T256S} = 1.1 \pm 0.1$. B: Voltage dependence of the Ca^{2+} block displayed in a $\ln[Ca^{2+}]$-$V_{Block1/2}$ plot. Solid lines represent best fits according to Eq. 3. The dashed line indicates the voltage-independent Ca^{2+} block in the mutant T256I.

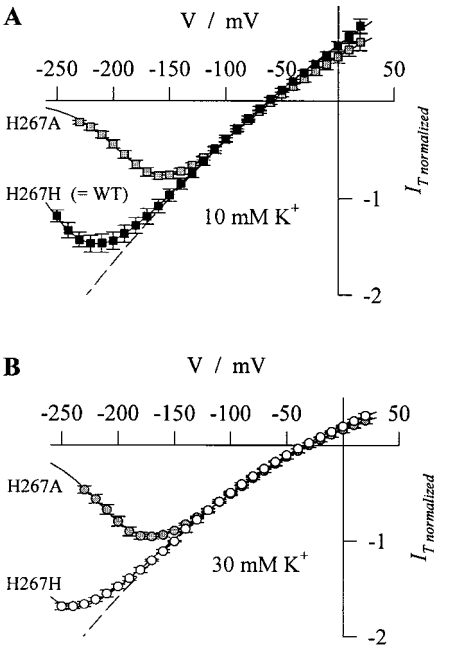

Fig. 5. The mutation of the highly conserved histidine in the GYGDxx**H** motif to alanine alters the affinity of KAT1 to Ca^{2+}. A: Instantaneous current-voltage characteristics of the KAT1 wild-type (closed squares) and the mutant KAT1-H267A (gray squares) measured in 10 mM K^+/30 mM Ca^{2+}. B: Instantaneous current-voltage characteristics of the KAT1 wild-type (open circles) and the mutant KAT1-H267A (gray circles) measured in 30 mM K^+/30 mM Ca^{2+}. The dashes lines indicate the current-voltage characteristics in 1 mM Ca^{2+}. Solid lines represent best fits according to Eq. 1. The data for the wild-type are presented in Fig. 1. The fits for H267A yielded $\delta_{10K} = 0.55 \pm 0.02$, $V_{Block1/2}{}^{10K} = -178.1 \pm 2.2$ mV, $\delta_{30K} = 0.52 \pm 0.02$, and $V_{Block1/2}{}^{30K} = -200.1 \pm 1.5$ mV. Currents were normalized to $I(-150$ mV, 1 mM $Ca^{2+}) = -1$. Each data point represents the mean of three or four measurements. Error bars indicate the standard deviation.

current through the mutant channel T256E by ∼50% while in T256M even in 30 mM Ca^{2+} a related blocking efficiency could not be achieved (Fig. 3A, Table 1). Like the K^+ channel mutants T256E and T256M, K^+ currents through KAT1-T256I were inhibited by Ca^{2+} as well. The Ca^{2+} block of the latter, however, characterized by a K_i of ∼19 mM (Table 1), was voltage-*in*dependent (Fig. 3B). Despite these large differences in sensitivity and voltage dependence of the Ca^{2+} block the mutants T256E, T256I, and T256M, a stoichiometry coefficient of $n \approx 1$ suggests that in all three mutants one Ca^{2+} ion occludes one channel (Fig. 4A, Table 1). Thus the Ca^{2+} block in T256E, T256I, and T256M is based on similar molecular mechanisms.

3.3. Does the mutant T256S inactivate?

In plant K_{in} channels in vivo and after heterologous expression of wild type and mutant channels inactivation has not been observed so far. The mutant T256S, however, which differs from the wild-type in a single methyl group, exhibited an inactivation-like behavior (Fig. 2A, right, lower traces). During a 2-s hyperpolarizing voltage pulse the current amplitude initially increased, before it slowly decreased. This apparent 'inactivation' was reminiscent of C-type inactivation in the *Shaker* channel [33,34] or P-type inactivation in Kv2.1 [35], processes caused by conformational changes of the outer pore. The rate of inactivation was dependent on the extracellular cation concentrations. When we increased the amount of Ca^{2+} the inactivation process speeded up. During voltage pulses to −150 mV the time course of the current decay followed a single exponential with a time constant $\tau = 946 \pm 203$ ms in 5 mM, $\tau = 555 \pm 184$ ms in 10 mM, $\tau = 248 \pm 40$ ms in 20 mM, and $\tau = 181 \pm 34$ ms in 30 mM Ca^{2+} ($n = 3$–5). With

Table 1
Characteristics of the Ca^{2+} phenotype of KAT1 mutants

		δ	K_i at −150 mV (mM)	$V_{Block1/2}$ 30 mM Ca^{2+} (mV)	Stoichiometry coefficient	Block kinetics
KAT1 WT 10 mM K^+		0.45 ± 0.08	> 30	< −250	n.d.	fast
T256E		0.32 ± 0.03	14.5 ± 6.3	−123 ± 9	1.0	fast
T256I		0	19.3 ± 6.9	–	1.0	–
T256M		0.55 ± 0.03	> 30	−175 ± 15	1.0	fast
T256S		0.27 ± 0.03	4.8 ± 0.8	−45 ± 23	1.1	slow
H267A	10 mM K^+	0.55 ± 0.01	> 30	−176 ± 3	n.d.	very fast
	30 mM K^+	0.52 ± 0.02	> 30	−201 ± 3	n.d.	very fast
T256E/H267A		n.d.	n.d.	n.d.	n.d.	very fast
T256S/H267A		0.23 ± 0.03	4.3 ± 0.7	−38 ± 28	1.1	medium

Susceptibility to block by Ca^{2+} ions in 30 mM KCl is given by the inhibition constant K_i at −150 mV. The electrical distance, δ, and half-blocking voltage, $V_{Block1/2}$, were determined according to Eq. 1 for each cell and the stoichiometry coefficient from the linear regression of the $\ln[(I^0-I)/I]$-$\ln[Ca^{2+}]$ plot (Fig. 4A, Eq. 3) for all data. K_i values were determined from interpolating the fits in $\ln[Ca^{2+}]$-$V_{Block1/2}$ plots (cf. Fig. 4B, Eq. 3) to $V_{Block1/2} = -150$ mV.
Data represent the mean of 3–5 measurements ± S.D.

increasing hyperpolarization τ decreased by a factor of 1.5 for a 10-mV change. A similar effect was obtained by lowering the extracellular K^+ concentration to 10 mM. This reduction in the monovalent cation concentration accelerated the apparent inactivation two-fold ($\tau_{10mMK} = 416 \pm 85$ ms, $n = 4$, instead of $\tau_{30mMK} = 946 \pm 203$ ms). Likewise the time course of the C-type inactivation in the *Shaker* channel was slowed when the external K^+ concentration was increased. Alterations in the Ca^{2+} concentration, however, did not affect inactivation kinetics of this channel [34]. Additionally, the inactivation process in *Shaker* was voltage-independent [33,36], while the current decay for the mutant KAT1-T256S shown here was strongly dependent on voltage. At −110 mV, for instance, no inactivation was seen whereas the K^+ current decayed with increasing hyperpolarization. When analyzing the steady-state current-voltage characteristics of the mutant T256S (Fig. 2B) with Eq. 1, the strong Ca^{2+} interaction could be described by the block parameters $\delta \approx 0.27$ and $n \approx 1$ (Fig. 4). The apparent inactivation in the mutant T256S might therefore result from a very slow Ca^{2+} block rather than C-type inactivation.

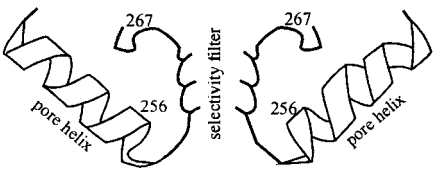

Fig. 7. Model of the inner pore region of the plant K_{in} channel KAT1. The model is based on the crystal structure obtained from the *Streptomyces lividans* channel KcsA [29] and a model designed for the *Shaker* channel [16]. From the four subunits building a functional channel [20], subunits one and three are displayed only. The numbers indicate the positions of the related residues.

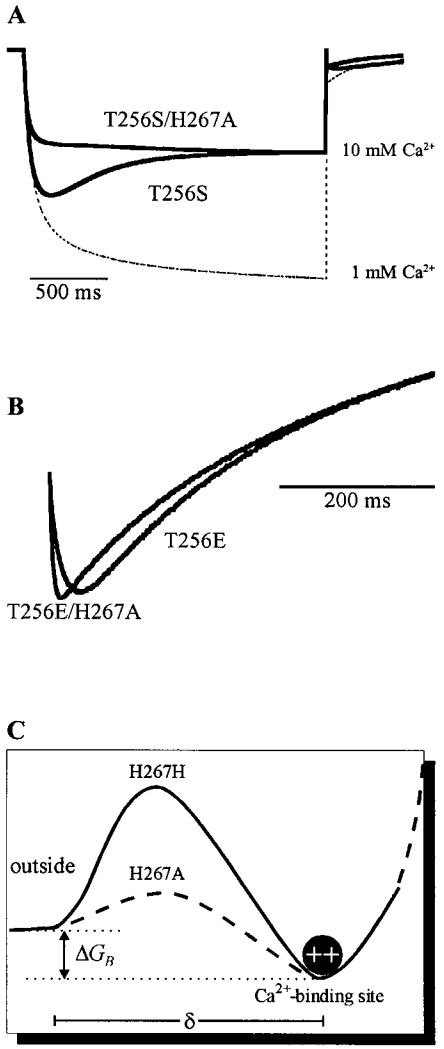

Fig. 6. Effect of H267 on the Ca^{2+} sensitivity of T256E and T256S. A: Elimination of the apparent inactivation due to the mutation H267A. Comparison of potassium currents mediated by T256S and T256S/H267A. Currents were elicited by 2-s activation pulses to −150 mV, measured in 30 mM K^+, 10 mM Ca^{2+}, pH 5.6, and normalized to the steady-state current. To visualize the inhibitory effect of Ca^{2+} the related current trace measured in 1 mM Ca^{2+} in T256S was superimposed. B: Acceleration of the Ca^{2+} unblock in T256E/H267A compared to T256E. Unblocking kinetics were resolved at a potential of −110 mV following an activation pulse to −150 mV (cf. [24]). Currents were measured in 30 mM Ca^{2+} and normalized to peak and steady-state values. C: Cartoon of the energetic profile sensed by the blocking Ca^{2+} ion in H267H (KAT1 wild-type) and H267A. The model is based on Eyring rate theory [37]. δ indicates the depth of the binding site in the transmembrane electrical field.

3.4. Does H267 represent the initial Ca^{2+} barrier?

In order to unequivocally distinguish between Ca^{2+} block and C-type inactivation we replaced the histidine 267 by alanine. The position KAT1-H267 is equivalent to *Shaker*-T449. Changes of this residue strongly affect C-type inactivation in the *Shaker* channel. The substitution T449H slows C-type inactivation while T449A accelerates this process [34]. KAT1-H267A, however, showed neither any kind of inactivation nor any other significant change in the gating behavior, but altered pharmacological properties. The mutation H267A increased the Ca^{2+} sensitivity of KAT1 by at least $\Delta G_{aff} \geq 1.3$ *kT* (Fig. 5A,B, Table 1, Eq. 5), while the voltage dependence of the block showed no significant difference. Similar to wild-type KAT1 the obstructing cation might move 52% along the voltage drop across the selectivity filter.

In order to test the effect of the mutation H267A on the apparent inactivation in the channel KAT1-T256S we created the double mutant T256S/H267A and tested its interaction with calcium ions. Although this channel was still Ca^{2+}-sensitive, in contrast to T256S, no inactivation-like behavior was detectable (Fig. 6A). Instead, the Ca^{2+} sensitivity of T256S/H267A showed all characteristics of a voltage-dependent block with parameters similar to those obtained for the single mutant T256S, $\delta \approx 0.23$ and $n \approx 1$. The apparent inactivation in the mutant T256S thus very likely results from a very slow Ca^{2+} block. Since in this channel the block was *slower* than channel activation an inactivation phenotype was mimicked. The substitution H→A on position 267 seemed to accelerate the interaction of the Ca^{2+} ion with the pore. In the double mutant T256S/H267A the blocking reaction was *faster* than channel activation so that the blocking process could be resolved during deactivation only (cf. [24]). In line with this hypothesis the voltage-dependent Ca^{2+} unblock in the double mutant T256E/H267A was five times as fast as in T256E (Fig. 6A; in 30 mM K^+/30 mM Ca^{2+} at −110 mV: $\tau_{T256E/H267A} = 4.6 \pm 0.8$ ms vs. $\tau_{T256E} = 23.7 \pm 2.2$ ms, $n = 3$). Thus in KAT1 channels carrying the mutation H267A the entry of the blocking Ca^{2+} ions into the pore was facilitated.

4. Discussion

In this study we examined structural motifs affecting the Ca^{2+} sensitivity of the K_{in} channel KAT1. Based on previous observations that mutations of the pore residues L251, T259, and T260 do not markedly alter the affinity of KAT1 to Ca^{2+} [24], we focused on positions T256 and H267. The related channel mutants exhibited a broad variety of Ca^{2+} phenotypes. Point mutations on position 256 affected the affinity for Ca^{2+}, the voltage dependence as well as kinetics of the blocking reaction. Whereas a non-conserved substitution, T256Q, did not influence these parameters, the conserved exchange T256S created a phenotype reminiscent of an inactivation-like behavior. Detailed experiments on the mutants T256S and T256S/H267A, however, indicate that this apparent inactivation originates from a very slow Ca^{2+} block. Moreover, the replacement of histidine by alanine right next to the selectivity filter (GYGDxx**H** motif) neither created inactivation nor fundamentally influenced the gating behavior of the channel.

From the presented data we conclude that the pore histidine which is highly conserved among K_{in} channels [28] serves as a first barrier for Ca^{2+} ions in entering the pore. This conclusion could be explained by a simple model based on the Eyring rate theory (Fig. 6C, [37]). To enter the binding site the Ca^{2+} ion has to cross an energy barrier. The rate of this reaction is inversely correlated with the height of the barrier, i.e. a high barrier implies low rate constants. Supposing that the histidine represents a high barrier and the alanine a low barrier, the model would account for faster blocking and unblocking reactions in the double mutants T256E/H267A and T256S/H267A due to the facilitated entry of Ca^{2+} ions. The height of the barrier in KAT1-H267H (wild-type) compared to the mutant KAT1-H267A, however, cannot explain the difference in Ca^{2+} sensitivity between the mutants T256Q, T256E, T256M, T256S, and T256I. In the mutant channel T256M the obstructing Ca^{2+} ion senses $\sim$55% of the voltage drop indicating a Ca^{2+} binding site deep in the pore. In T256E and T256S this interaction site locates less deep in the pore and in T256I it is even in the periphery. We therefore propose several Ca^{2+} interaction sites within the pore. Consequently the side chain at residue 256 might not represent the interaction site itself but affect the pore geometry. From the lack of correlation between the pattern of the Ca^{2+} sensitivity and the chemical properties as well as size of the side chain one would not expect this residue to line the pore.

In order to further explain our results on the molecular level we adapted the KAT1 sequence to the crystal structure of the pore of the potassium channel KcsA from *Streptomyces lividans* [29]. As shown in Fig. 7 the residue on position 256 appeared to be a component of the pore helix. In KcsA this tilted pore helix provides a rigid backbone which holds the selectivity filter. According to this model alterations of the side chain at position 256 could change the electrostatic and van der Waals interactions of the amino acids in the narrow pore. This in turn would alter the electrical field within the permeation pathway.

Acknowledgements: Current work was founded by grants of the Deutsche Forschungsgemeinschaft to R.H. (1640/1-3) and R.H. and K.P. (1640/9-10) as well as by a fellowship to I.D. We thank Kerstin Neuwinger (Würzburg) for expert technical assistance, and Irene Marten (Hannover), Benoît Lacombe, Hervé Sentenac, Jean-Baptiste Thibaud (Montpellier) as well as Gerald Schönknecht (Würzburg) for helpful discussions and comments on the manuscript.

References

[1] Anderson, J.A., Huprikar, S.S., Kochian, L.V., Lucas, W.J. and Gaber, R.F. (1992) Proc. Natl. Acad. Sci. USA 89, 3736–3740.
[2] Schachtman, D.P., Schroeder, J.I., Lucas, W.J., Anderson, J.A. and Gaber, R.F. (1992) Science 258, 1645–1658.
[3] Sentenac, H., Bonneaud, N., Minet, M., Lacroute, F., Salmon, J.M., Gaymard, F. and Grignon, C. (1992) Science 256, 663–665.
[4] Bertl, A., Anderson, J.A., Slayman, C.L., Sentenac, H. and Gaber, R.F. (1994) Folia Microbiol. (Prague) 39, 507–509.
[5] Véry, A.A., Bosseux, C., Gaymard, F., Sentenac, H. and Thibaud, J.B. (1994) Pflügers Arch. 428, 422–424.
[6] Bertl, A., Anderson, J.A., Salyman, C.L. and Gaber, R.F. (1995) Proc. Natl. Acad. Sci. USA 92, 2701–2705.
[7] Cao, Y., Ward, J.M., Kelly, W.B., Ichida, A.M., Gaber, R.F., Anderson, J.A., Uozumi, N., Schroeder, J.I. and Crawford, N. (1995) Plant Physiol. 109, 1093–1106.
[8] Hedrich, R., Moran, O., Conti, F., Busch, H., Becker, D., Gambale, F., Dreyer, I., Küch, A., Neuwinger, K. and Palme, K. (1995) Eur. Biophys. J. 24, 107–115.
[9] Hoshi, T. (1995) J. Gen. Physiol. 105, 309–328.
[10] Müller-Röber, B., Ellenberg, J., Provart, N., Willmitzer, L., Busch, H., Becker, D., Dietrich, P., Hoth, S. and Hedrich, R. (1995) EMBO J. 14, 2409–2416.
[11] Véry, A.A., Gaymard, F., Bosseux, C., Sentenac, H. and Thibaud, J.B. (1995) Plant J. 7, 321–332.
[12] Gaymard, F., Cerutti, M., Horeau, C., Lemaillet, G., Urbach, S., Ravallec, M., Devauchelle, G., Sentenac, H. and Thibaud, J.B. (1996) J. Biol. Chem. 271, 22863–22870.
[13] Ketchum, K.A. and Slayman, C.W. (1996) FEBS Lett. 378, 19–26.
[14] Marten, I., Gaymard, F., Lemaillet, G., Thibaud, J.B., Sentenac, H. and Hedrich, R. (1996) FEBS Lett. 380, 229–232.
[15] Zimmermann, S., Talke, I., Ehrhardt, T., Nast, G. and Müller-Röber, B. (1998) Plant Physiol. 116, 879–890.
[16] Durell, S.R. and Guy, H.R. (1996) Neuropharmacology 35, 761–773.
[17] Chandy, K.G. and Gutman, G.A. (1994) in: Handbook of Receptors and Channels (North, R.A., Ed.), pp. 1–71, CRC Press, Boca Raton, FL.
[18] Hedrich, R. and Dietrich, P. (1996) Bot. Acta 109, 94–101.
[19] Dreyer, I., Antunes, S., Hoshi, T., Müller-Röber, B., Palme, K., Pongs, O., Reintanz, B. and Hedrich, R. (1997) Biophys. J. 72, 2143–2150.
[20] Daram, P., Urbach, S., Gaymard, F., Sentenac, H. and Chérel, I. (1997) EMBO J. 16, 3455–3463.
[21] Ludwig, J., Owen, D. and Pongs, O. (1997) EMBO J. 16, 6337–6345.
[22] Hoth, S., Dreyer, I. and Hedrich, R. (1997) J. Exp. Bot. 48, 415–420.
[23] Marten, I. and Hoshi, T. (1997) Proc. Natl. Acad. Sci. USA 94, 3448–3453.
[24] Becker, D., Dreyer, I., Hoth, S., Reid, J.D., Busch, H., Lehnen, M., Palme, K. and Hedrich, R. (1996) Proc. Natl. Acad. Sci. USA 93, 8123–8128.
[25] Uozumi, N., Gassmann, W., Cao, Y. and Schroeder, J.I. (1995) J. Biol. Chem. 270, 24276–24281.
[26] Ichida, A.M. and Schroeder, J.I. (1996) J. Membrane Biol. 151, 53–62.
[27] Nakamura, R.I., Anderson, J.A. and Gaber, R.F. (1997) J. Biol. Chem. 272, 1011–1018.
[28] Hoth, S., Dreyer, I., Dietrich, P., Becker, D., Müller-Röber, B. and Hedrich, R. (1997) Proc. Natl. Acad. Sci. USA 94, 4806–4810.
[29] Doyle, D.A., Cabral, J.M., Pfuetzner, R.A., Kuo, A., Gulbis, J.M., Cohen, S.L., Chait, B.T. and MacKinnon, R. (1998) Science 280, 69–77.
[30] Woodhull, A.M. (1973) J. Gen. Physiol. 61, 687–708.
[31] Liman, E.R., Tytgat, J. and Hess, P. (1992) Neuron 9, 861–871.
[32] Dietrich, P., Dreyer, I., Wiesner, P. and Hedrich, R. (1998) Planta 205, 277–287.

[33] Hoshi, T., Zagotta, W.N. and Aldrich, R.W. (1991) Neuron 7, 547–556.
[34] López-Barneo, J., Hoshi, T., Heinemann, S.H. and Aldrich, R.W. (1993) Receptors Channels 1, 61–71.
[35] De Biasi, M., Hartmann, H.A., Drewe, J.A., Taglialatela, M., Brown, A.M. and Kirsch, G.E. (1993) Pflugers Arch. 422, 354–363.
[36] Choi, K.L., Aldrich, R.W. and Yellen, G. (1991) Proc. Natl. Acad. Sci. USA 88, 5092–5095.
[37] Glasstone, S., Laidler, K.J. and Eyring, H. (1941) The Theory of Rate Processes, McGraw-Hill, New York.

⇒ zurück zur Übersicht

1998

Dietrich, **Dreyer**, Wiesner, Hedrich

Cation-sensitivity and kinetics of guard cell potassium channels differ among species.

Planta. **205**:277-287.

Planta (1998) 205: 277–287

Planta

Cation sensitivity and kinetics of guard-cell potassium channels differ among species

Petra Dietrich, Ingo Dreyer, Peter Wiesner, Rainer Hedrich

Julius-von-Sachs-Institut für Biowissenschaften, Mittlerer Dallenbergweg 64, D-97082 Würzburg, Germany

Received: 19 July 1997 / Accepted: 2 October 1997

Abstract. In patch-clamp studies we compared the electrical properties of an inward rectifying guard cell K^+ channel, $GCKC1_{in}$, from three major crop plants *Solanum tuberosum* L., *Nicotiana tabacum* L., and *Vicia faba* L. Selecting guard cells for our analyses we aimed to test whether K^+ channels of the same cell type differ among species. The channels shared basic features including voltage-dependence, selectivity and single-channel conductance. They activated at hyperpolarization ($V_{1/2} \approx -164$ mV) with single channels of 7 pS underlying the whole-cell current. The channel density in *S. tuberosum* was higher than in *V. faba* and *N. tabacum* while the activation and deactivation kinetics were faster in the latter two species. Among different monovalent cations the K^+ channels discriminated strongly against Na^+, Li^+, and Cs^+. The sensitivity to Cs^+ was similar for the three species. Extracellular Ca^{2+} blocked the *V. faba* K^+ channel at concentrations ≥1 mM but only affected its functional homologs in *S. tuberosum* and *N. tabacum* at higher concentrations and more-negative membrane potentials. Like the differences in Ca^{2+}-sensitivity, protoplasts from the three species differed remarkably in their response towards extracellular pH changes. Whereas protons neither altered the open probability nor the kinetic parameters of the *V. faba* $GCKC1_{in}$, in *S. tuberosum* and *N. tabacum* this cation affected the voltage-dependent properties strongly. An increase in proton concentration from pH 8.5 to 4.5 shifted the potential of half-maximal open probability to less-negative values with a maximum effect around pH 6.2. The pH modulation of the K^+ channels could be described assuming a two-state model where the open and closed channel can be protonated. The observed differences in cation-sensitivity and voltage-dependent kinetics between K^+ channels reflect the diversification of guard-cell channels that may contribute to species-specific variations in the control of stomatal aperture.

Key words: Cation sensitivity – Guard cell – K^+ channel – *Nicotiana* – *Solanum* – *Vicia*

Introduction

In guard cells, K^+ channels represent the dominant transport mechanism for potassium uptake and release. The reversible accumulation of salts, and thus volume increase, drives the stomatal motor and regulates the gas exchange of the plant. Various voltage-dependent plant K^+ channels have been studied within their natural environment (for recent reviews, see Hedrich and Becker 1994; Schroeder et al. 1994; Hedrich and Dietrich 1996). Among them, the inward rectifying channels were classified according to their hyperpolarization-induced activation (e.g. Schroeder et al. 1987; Moran et al. 1988; Schroeder and Hagiwara 1989; Roberts and Tester 1995). Cloning the first plant K^+ channels (Anderson et al. 1992; Sentenac et al. 1992), inward and outward rectifiers were then separated on the molecular level. Some plant K^+-inward-rectifier genes have been analysed with respect to their expression pattern in planta and after heterologous expression (Kochian et al. 1993; Bertl et al. 1995; Cao et al. 1995; Hoshi 1995; Müller-Röber et al. 1995; Nakamura et al. 1995; Véry et al. 1995; Gaymard et al. 1996; Lagarde et al. 1996; Marten et al. 1996). Different expression systems such as *Xenopus* oocytes, Sf9-cells or yeast have been used for the structure-function analysis of these plant K^+ channels. Besides the channel-specific diversification, this approach revealed the biophysical properties of the channel gene product expressed by voltage-dependence, susceptibility to cations as well as kinetic parameters as expression-system-dependent variables. This variability may arise from differences in the expression level, post-translational modifications, membrane properties, and

Abbreviations: GCKC1 = guard-cell K^+ channel 1; KST1 = K^+ channel *Solanum tuberosum* 1

Correspondence to: R. Hedrich;
E-mail: hedrich@botanik.uni-wuerzburg.de; Fax: 49 (931) 8886158

cell-type-specific regulation (Véry et al. 1994; Bertl et al. 1995; Marten et al. 1996). Since the class of plant inward rectifiers seems to be highly diverse (Anderson et al. 1992; Sentenac et al. 1992; Müller-Röber et al. 1995; Hedrich and Dietrich 1996) and one cell type may express more than one channel α-subunit which have been shown to assemble to functional homo- as well as hetero-multimers (Daram et al. 1997; Dreyer et al. 1997; Ehrhardt et al. 1997) a detailed study of K^+ channels in vivo should help to correlate the increasing knowledge on structure-function relation to their contribution to physiological responses in vivo. With respect to K^+ uptake and release, as well as anion channels and the H^+-ATPase, *Vicia faba* guard cells represent the most intensively studied model system. In this species, plant hormones such as *cis*-abscisic acid (ABA) and auxin interact with ion channels of guard cells either directly (Marten et al. 1991; Lohse and Hedrich 1995) or via changes in the cytoplasmic calcium and proton concentrations (Schwartz et al. 1988; Schroeder and Hagiwara 1989; Irving et al. 1992; McAinsh et al. 1992; Gilroy and Trewavas 1994; Lemtiri-Chlieh and MacRobbie 1994; McAinsh et al. 1995). Elevation of the apoplastic Ca^{2+} concentration can act as a stimulus for stomatal closure (Schwartz 1985; Inoué and Katoh 1986; Schwartz et al. 1988; Mansfield et al. 1990; MacRobbie 1992; McAinsh et al. 1995). In contrast to a rise in the external calcium level, which seems to stimulate ion efflux, the increase in proton concentration on both membrane sides has been found to favour K^+ uptake and stomatal opening in *Vicia faba* (Blatt 1992; Blatt and Armstrong 1993; Lemtiri-Chlieh and MacRobbie 1994).

In order to understand how similar guard cells are, we compared the voltage-dependent K^+-uptake channels in the plasma membrane from the three different C3-crops *Vicia faba*, *Solanum tuberosum* and *Nicotiana tabacum* under similar experimental conditions, together with their susceptibility towards the block by extracellular Cs^+ and modulation by calcium ions and protons.

Materials and methods

Plant material. Broad bean (*Vicia faba* L. cv. Grünkernige Hangdown and Osnabrücker Markt, Gebag, Hannover, Germany), tobacco (*Nicotiana tabacum* L. cv. Samsun NN25, gift from Dr. U. Conrad, IPK Gatersleben, Germany) and potato plants (*Solanum tuberosum* L. cv. Desirée; Fritz Lange Saatzucht, Bad Schwartau, Germany) were grown in a growth chamber. The photoperiod was 14 h and the photon flux density 300 $\mu mol \cdot m^{-2} \cdot s^{-1}$ (HQI-TS 250 W/D; Osram, München, Germany). The temperature was 20 °C in the light and 14 °C in the dark. The humidity ranged between 60 and 70%.

Protoplast isolation and patch-clamp recordings. Guard cell protoplast were enzymatically isolated from two- to three-week-old leaves of *V. faba* and six-week-old leaves of *S. tuberosum* and *N. tabacum* according to the method developed for *V. faba* (Hedrich et al. 1990). Ion fluxes were studied either in the whole-cell or outside-out configuration of the patch-clamp technique (Hamill et al. 1981). Current measurements were performed using either an EPC-7 or EPC-9 patch-clamp amplifier (HEKA, Lambrecht, Germany) and low-pass-filtered with an eight-pole Bessel filter. Whole-cell data were low-pass-filtered with a cut-off frequency of 2 kHz or for 3-s activation pulses of 0.5 kHz. Data were sampled at 2.5-fold the filter frequency (for single-channel recording this factor was 5), digitized (ITC-16; Instrutech Corp., Elmont, N.Y., USA), stored on hard disk and analysed with software of Instrutech Corp. on a MacIntosh Quadra 650. The Ca^{2+} and Cs^+ block was fitted using the non-linear Marquardt-Levenberg algorithm (Marquardt 1963). Patch pipettes were prepared from Kimax-51 glass (Kimble products, Vineland, N.Y., USA) and coated with silicone (Sylgard 184 silicone elastomer kit; Dow Corning, Midland, Mich., USA). In order to determine membrane potentials the command voltages were corrected off-line for series resistances and liquid junction potentials according to Neher (1992).

Patch-clamp solutions. The pipette solution (cytoplasm) contained 150 mM K-gluconate, 2 mM $MgCl_2$, 2 mM MgATP, 10 mM EGTA, and 10 mM Hepes-Tris pH 7.2 (*V. faba*) or 7.4 (*S. tuberosum* and *N. tabacum*). The standard bathing medium contained 30 mM K-gluconate, 1 mM $MgCl_2$, and 1 mM $CaCl_2$. The pH value was adjusted using 10 mM Mes-Tris (pH 5.6–6.5), Hepes-Tris (pH 7.4–8.5) or citrate-Tris (pH 4.5). Modifications in solute compositions are included in the figure legends. Chemicals were obtained from Sigma (Deisenhofen, Germany).

Description of channel block. Assuming a single blocking site, the probability of a channel staying in the conductive state p_O* could be expressed by the product of the open probability obtained in the absence of blocking ions (p_O) and the probability of the channel not being blocked ($B(V)$), given by:

$$B(V) = \frac{1}{1 + \frac{[C]_{ext}}{K_i(V)}} = \frac{1}{1 + \frac{[C]_{ext}}{\kappa} \cdot e^{-\left(\frac{ze_0}{kT}\delta_B V\right)}} \quad \text{(Eq. 1)}$$

where $K_i(V) = \kappa \cdot \exp\{ze_0/(kT) \cdot \delta_B \cdot V\}$ indicates the voltage-dependent inhibition-constant and δ_B the electrical distance the blocking ion (C) moves into the pore. The function $B(V)$ is independent of the gating mechanism of the channel. The tail currents in the presence of the blocker (I_C) could then be described by

$$I_C = B(V) \cdot I_{0C} \quad \text{(Eq. 2)}$$

where I_{0C} denotes the K^+ current in the absence of the blocker and $B(V)$ the concentration- and voltage-dependent probability of the channel not being blocked. According to the Woodhull-model (Woodhull 1973) the potential causing half-maximal inhibition $V_{B^{1/2}}[B(V_{B^{1/2}}) = 1/2;$ cf. Eq. 1] depends on the logarithm of the blocker concentration

$$V_{B^{1/2}} = \frac{kT}{z\delta_B e_0} \cdot \ln \frac{[C]_{ext}}{\kappa}. \quad \text{(Eq. 3)}$$

Results

In patch-clamp studies on guard-cell protoplasts from *Vicia faba*, *Solanum tuberosum* and *Nicotiana tabacum*, K^+ currents were analysed using the whole-cell and excised-patch configuration in basically 150 mM K^+ in the pipette ('cytoplasm') and 30 mM K^+ in the bath solution. Double-voltage pulses activated inward K^+ currents upon voltage steps to −193 mV which deactivated during subsequent depolarization (Fig. 1A for *S. tuberosum*; for *V. faba*, see Schroeder et al. 1987). In addition to the inward K^+ channels, slowly activating outward K^+ currents could be detected at positive voltages (Fig. 1A, current traces at −3 and +47 mV). When compared to the whole-cell studies the activation

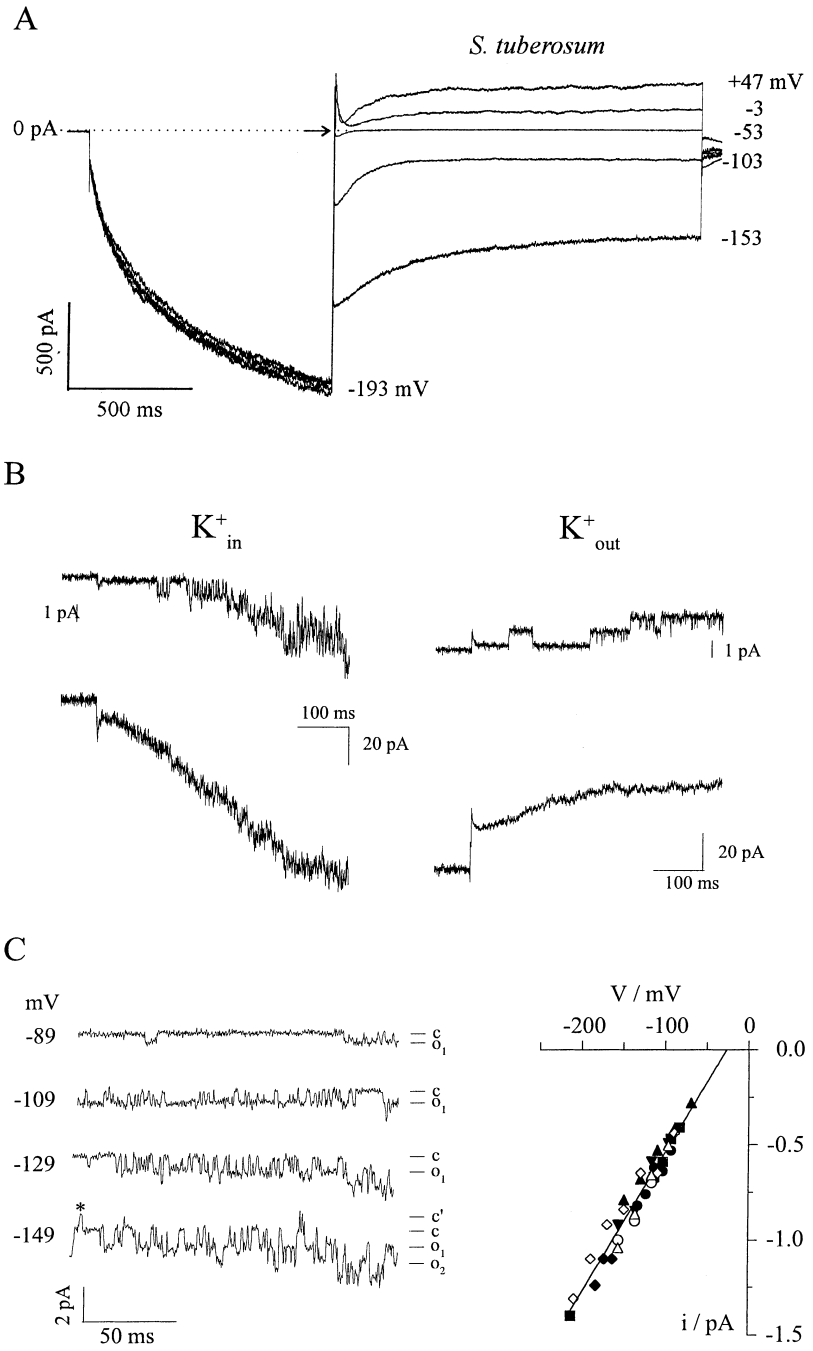

Fig. 1A–C. Activation and deactivation of $GCKC1_{in}$ in *Solanum tuberosum*. **A** Activation of whole-cell K^+ currents in response to repetitive 1-s prepulse steps to −193 mV followed by deactivation during depolarizing 1.5-s voltage pulses to −153, −103, −53, −3, and +47 mV (*arrow* indicates the reversion in the current direction). The double-voltage pulse series was applied from a holding potential of −63 mV. Note, that at −3 and +47 mV the deactivation of the inward current is superimposed by the slow activation of K^+-release channels. **B** Time-dependent activation of single inward (−129 mV, *left-hand traces*) and outward rectifying K^+ channels (+31 mV, *right-hand traces*) in a cell-free outside-out membrane patch. The external K^+ concentration was 100 mM to better resolve the single-channel fluctuations. Hyperpolarizing and depolarizing voltages were applied from a holding potential of −29 mV. Note, that the kinetics of the sum of currents from 27 individual sweeps resemble those of the macroscopic current in **A** and Fig. 2A, B. **C** *Left panel*, open-closed transitions of single inward K^+ channels in a cell-free outside-out membrane at voltages indicated. The holding potential was −29 mV (data not shown). Single-channel activities increase with hyperpolarizing membrane potentials. Frequently, open-channel amplitudes with long open times were observed (marked by an *asterisk*). *c′*, channels closed; *c*, fast channels closed and channel with longer open times open; o_1, one (fast) channel open; o_2, two (fast) channels open. *Right panel*, Current-voltage relation of single-channel amplitudes as shown in the left panel. The slope conductance was 7.4 ± 0.8 pS ($n = 8$) for the inward K^+ channel at an extracellular pH of 5.6 (*closed symbols*) or 7.4 (*open symbols*). The pipette solution contained either 10 mM EGTA (*circles*, *triangles*), 2 mM EGTA plus 3 mM $CaCl_2$ (*squares*) or 1 mM Ca^{2+} (*diamonds*) in addition to 150 mM K-gluconate, 2 mM $MgCl_2$, 2 mM MgATP, and 10 mM Hepes-Tris (pH 7.4). Note, that the single-channel conductance of $GCKC1_{in}$ in *S. tuberosum* is independent of the cytosolic Ca^{2+} concentration as was found in *Vicia faba* (Schroeder and Hagiwara 1989)

of the two different channel types[1] in excised outside-out patches resembled the time- and voltage-dependent behaviour of the macroscopic currents (Fig. 1B; cf. Figs. 1A and 2A).

Kinetics. The activation process of the *S. tuberosum* and *N. tabacum* inward rectifying guard cell K^+ channel ($GCKC1_{in}$) was slow compared to *V. faba*. The current of $GCKC1_{in}$ in *S. tuberosum* did not even saturate within a 3-s voltage pulse to −193 mV (Fig. 2A). The time-course of activation during 30-s pulses could be fitted by the sum of two exponentials with the slow time constant >1 s (data not shown). The fast time constant τ_1 of 171 ± 37.6 ms ($n = 11$) was obtained from 3-s pulses to −193 mV. In contrast, the activation of the $GCKC1_{in}$ in *V. faba* followed a single exponential with an activation time-constant τ of 100 ± 30 ms ($n = 10$). Like the activation process, the deactivation kinetics in response to depolarizing voltage pulses were faster for *V. faba* than for *S. tuberosum* (Fig. 2B). Deactivating pulses of 300 and 1500 ms were sufficient to obtain steady-state currents in *V. faba* and *S. tuberosum* protoplasts, respectively. In *S. tuberosum* and *N. tabacum* the description of the deactivation behaviour

[1]For the molecular identification of voltage-dependent K^+ channels in *S. tuberosum*, see Müller-Röber et al. (1995).

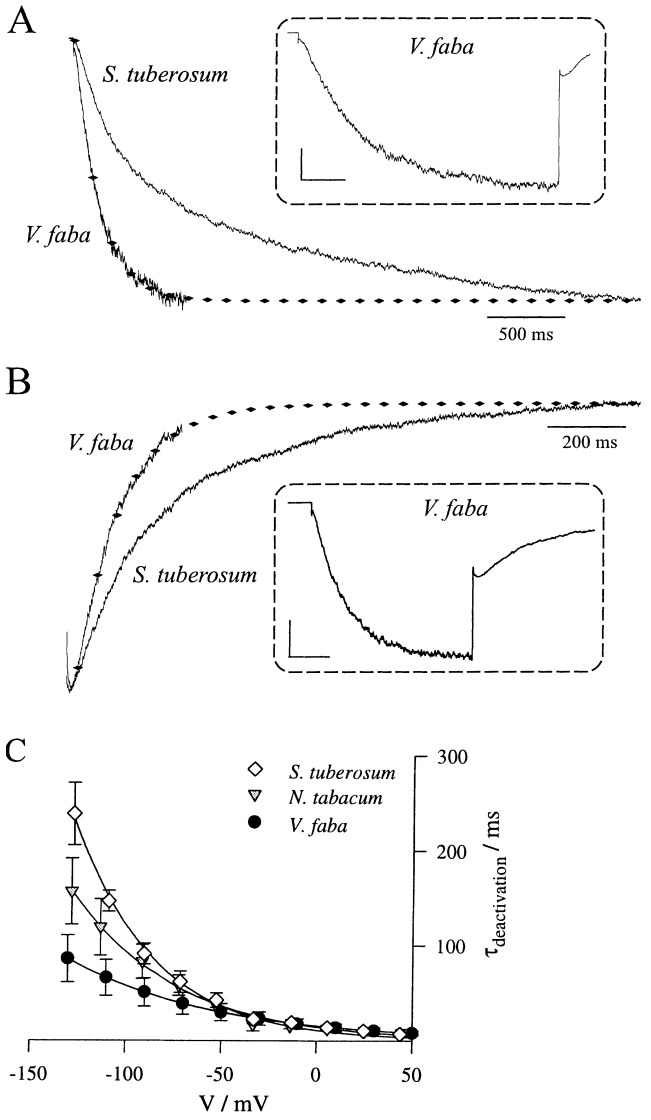

Fig. 2A–C. Pronounced differences in the activation and deactivation kinetics of inward K^+ channels in guard cells. **A** Clamped at a holding potential of −63 mV, $GCKC1_{in}$ in *Vicia faba* and *Solanum tuberosum* activates during a step to hyperpolarizing voltages. K^+ currents increase in response to a 600-ms (*V. faba*) and 3000-ms (*S. tuberosum*) voltage pulse to −193 mV. Currents were scaled with respect to their extrapolated steady-state value. **B** Decay of inward K^+ currents during a 300-ms (*V. faba*) and 1500-ms (*S. tuberosum*) depolarizing voltage pulse to −133 mV following the activation phase as shown in **A**. *Insets*, Time course of activation and deactivation for the *V. faba* channel at higher resolution. Bars denote 100 pA and 100 ms. **C** Voltage-dependence of the deactivation time constants of $GCKC1_{in}$ in *V. faba* ($n = 18$), *N. tabacum* ($n = 10$) and *S. tuberosum* ($n = 11$) determined from single exponential fits to current relaxations as shown in **B**

required one to two exponential functions whereas in *V. faba* a single exponential was sufficient to describe this process. Therefore, in Fig. 2C the kinetic properties of the three K^+ channels were compared on the basis of the fast deactivation time-constants of current relaxations. At −135 mV the deactivation of the *V. faba* K^+ uptake channel was almost three times as fast as that of *S. tuberosum*. The current relaxation of $GCKC1_{in}$ in *N. tabacum* was intermediate with respect to the other two species (Fig. 2C).

Channel density and unitary conductance. Since low-affinity K^+ uptake is assumed to be essential for volume increase in guard cells and finally stomatal opening (Schroeder and Fang 1991), in the following we focused on the K^+-transport capacities of the guard-cell membranes. When current-voltage curves were related to the membrane surface area (whole-cell capacitance) we recorded just one-third the current density for the inward K^+ channels of *V. faba* and *N. tabacum* than for *S. tuberosum* (Fig. 3A). The voltage-dependent open probability p_O, however, was very similar (Fig. 3B) and could be described by a single Boltzmann equation

$$p_O = \frac{1}{1 + e^{\left(\frac{V - V_{1/2}}{V_S}\right)}}. \qquad \text{(Eq. 4)}$$

A half-maximal activation potential of $V_{1/2} = -164$ mV and a voltage sensitivity (V_S) of 16 mV were calculated for the three species, corresponding to an effective gating charge z_g of 1.4. In order to determine whether the difference in potassium transport-capacity between *V. faba* and *S. tuberosum* results from either a higher unitary conductance or an increased channel density, single-channel conductances were compared. Under the same experimental conditions the slope conductance of 7.4 ± 0.8 pS ($n = 8$) of the *S. tuberosum* $GCKC1_{in}$ (Fig. 1C, right panel) and the inward rectifying $\underline{K}^+$ channel cloned from a guard cell library of *S. tuberosum* (KST1; Müller-Röber et al. 1995) were identical and were comparable to the *V. faba* channel (4–8 pS in internal 104 mM and external 13 mM K^+; Schroeder and Hagiwara 1989). As expected from a hyperpolarization-activated channel, single K^+-channel fluctuations in excised outside-out membrane patches from potato guard-cell protoplasts increased with negative-going voltages (Fig. 1B,C). From the open probability (p_O) – a parameter not depending on the driving-force for K^+ uptake (cf. Blatt 1992; Hedrich et al. 1995a) – and the single-channel conductance (σ) – which seems to be similar between external 13 and 100 mM K^+ (Schroeder and Hagiwara 1989 and this study, respectively) – the number of K^+ channels (N) was calculated according to:

$$I_{SS} = N \cdot p_O \cdot \sigma \cdot (V_m - V_{rev}) \qquad \text{(Eq. 5)}$$

where I_{SS} denotes the steady-state current. A number of 2400 ± 600 ($n = 9$) K^+ channels per guard cell for *S. tuberosum*, 1037 ± 518 ($n = 14$) for *N. tabacum* and 900 ± 600 ($n = 11$) calculated for *V. faba* corresponds to a channel density of 8, 2.5 and 1.2 channels per μm^2, respectively. The significance of the differences in channel densities was proven in a student *t*-test (probability of the data not differing < 0.13). Thus, the difference in channel density should fully account for the lower K^+-transport capacity of *V. faba* and *N. tabacum* guard cells compared to that of *S. tuberosum*. The low scattering in K^+-current densities compared to that of the anion channel *V. faba* GCAC1 (Schulz-Lessdorf et al. 1996) might furthermore indicate that under the

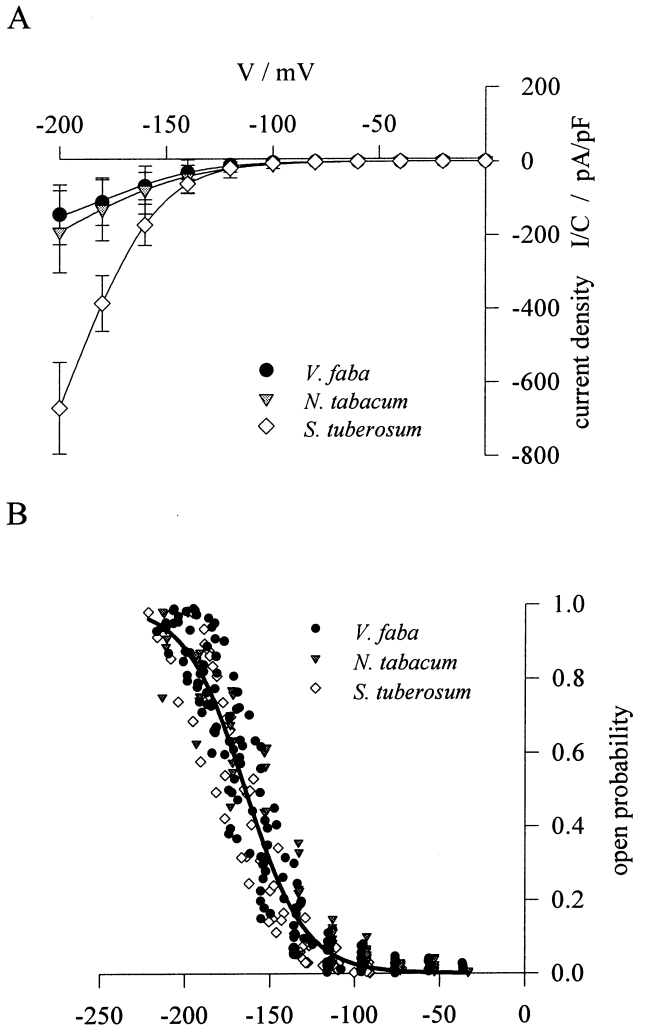

Fig. 3A,B. Current densities and open probabilities of $GCKC1_{in}$ in *Vicia faba*, *Nicotiana tabacum* and *Solanum tuberosum*. **A** Current-voltage relation of species-dependent steady-state inward current densities. Current densities were expressed by the ratio between the individual whole-cell current I and the related membrane capacitance C ($I/C = I/A \cdot C_m$; A, cell surface, C_m, 1 μF/cm^2, assumed specific membrane capacity). Current densities from 9 *S. tuberosum*, 12 *N. tabacum* and 11 *V. faba* guard cells were fitted taking the open probability and conductance of single K^+ channels into account. Channel densities of 8 ± 2.3, 2.5 ± 1.5 and 1.2 ± 0.7 per μm^2 membrane area were determined, respectively. **B** Open probabilities were obtained from either the instantaneous currents in response to a pulse to −93 mV following the steady-state activation in the range between −213 and −33 mV, or double-pulse experiments. In the latter pulse sequence the open probability was deduced from the ratio between the steady-state currents at the end of the deactivating test pulse (600 ms for *V. faba*, 1000 ms for *N. tabacum* and 1500 ms for *S. tuberosum*) and the tail-current amplitudes extrapolated to the pulse onset. Data points were fitted by a single Boltzmann distribution scaled to the maximum (*solid line*). Parameters were $V_{1/2} = -164$ mV and $V_S = 16$ mV corresponding to an effective gating charge z_g of 1.4 (*V. faba*: $V_{1/2} = -163$ mV, $z_g = 1.5$, $n = 15$; *N. tabacum*: $V_{1/2} = -159$ mV, $z_g = 1.2$, $n = 8$; *S. tuberosum*: $V_{1/2} = -167$ mV, $z_g = 1.6$, $n = 6$)

growth conditions and media used (see Materials and methods) the K^+-channel density and activity remained rather stable.

Cationic effectors. In addition to the close similarities in voltage-dependence and conductance, the ion selectivity for the *V. faba* (Schroeder 1988; Blatt 1992) and *S. tuberosum* (this study) channels was comparable, too. From the reversal potential under biionic conditions a selectivity sequence of $K^+ > Rb^+ > NH_4^+ > Na^+$, Li^+ was calculated (Table 1). In order to identify further differences or similarities between the properties of the three channel types we studied their susceptibility towards blocking ions as well as potential cationic modulators.

Cesium. Extracellular cesium ions have been previously described as voltage-dependent blockers of K^+ inward channels from higher plants and algae (Tester 1988; Klieber and Gradmann 1993; Draber and Hansen 1994; Hedrich et al. 1995a, b; Véry et al. 1995). The application of Cs^+ to the bath solution blocked the K^+-uptake channels in a concentration-dependent manner (Fig. 4A). The Cs^+-induced decrease in steady-state inward currents at −213 mV revealed an apparent dissociation constant K_i of 64, 48 and 40 μM for the $GCKC1_{in}$ of *S. tuberosum*, *N. tabacum* and *V. faba*, respectively (Fig. 4B). The voltage-dependence of the block was revealed in double-pulse experiments and could be described by the Woodhull-model assuming an electrical distance for the Cs^+-block of $\delta_B = 0.85 \pm 0.27$ ($n = 3$–5) in *S. tuberosum* (data not shown; Woodhull 1973, cf. chapter on Ca^{2+}-block).

Calcium. Between species the degree of stomatal closure in the presence of millimolar extracellular Ca^{2+} concentrations has been found to vary largely (Willmer and Mansfield 1969; Schwartz 1985). A voltage-dependent Ca^{2+} block of K^+-uptake channels similar to the Cs^+-block described above has already been described for guard cells of *Vicia faba* and *Zea mays* (Busch et al. 1990; Fairley-Grenot and Assmann 1992). We therefore compared the Ca^{2+}-sensitivity of K^+ channels in *S. tuberosum*, *V. faba* and *N. tabacum*. In the presence of high (20 mM) Ca^{2+} concentrations in addition to 30 mM K^+ in the bath, the deactivation currents of $GCKC1_{in}$ in *V. faba* were superimposed by an additional kinetic component (Fig. 5A right traces, and 5B upper trace) which results from the slow kinetics of the voltage-dependent unblocking of the channel at depolarizing potentials which thereby increases the K^+-current amplitude. The unblocking kinetics were eliminated when a 2-ms pulse to + 24 mV preceded the deactivation pulse (Fig. 5B, middle trace). Due to the channel unblocking at positive membrane potentials, the pre-depolarizing pulse removed the occluding calcium ion from the pore ('kick-out') and separated the deactivation from the unblocking reaction (Fig. 5B, lower trace). The unblocking reaction in the presence of Ca^{2+} could easily be resolved since it was slow compared to that in Cs^+-containing media (for kinetics of Cs^+-block see Becker et al. 1996). In contrast to GCKC1 in *V. faba* the K^+ channel *in S. tuberosum* was affected at more-negative potentials, only (Fig. 5A, left traces). Therefore, the blocking process of the *S. tuberosum* channel appeared

Table 1. Relative ion permeabilities of guard-cell K^+ channels from two different species. *n.d.*, not determined

	K^+	$> Rb^+$	$> NH_4^+$	$> Na^+$	$> Li^+$
S. tuberosum[a]	1	0.24 ± 0.039	0.04 ± 0.009	< 0.01	< 0.002
V. faba[b]	1	0.21 ± 0.03	n.d.	< 0.001	n.d.
V. faba[c]	1	0.2	n.d.	0.06	0.03

[a]This study
[b]Blatt 1992
[c]Schroeder 1988
From the shift in the reversal potential upon the exchange of extracellular K^+ against other monovalent cations, a sequence of relative permeabilities (P_{X^+}/P_{K^+}, n = 3–5) was deduced for the *S. tuberosum* $GCKC1_{in}$, according to the Nernst equation:

$$\frac{P_{X^+}}{P_{K^+}} = e^{\frac{F}{RT}\Delta V_{rev}} \quad \text{(Eq. 6)}$$

F, R and T have their usual meanings and ΔV_{rev} is expressed as $V_{rev}^X - V_{rev}^K$

upon hyperpolarization onset, only (Fig. 5A, inset). The difference in the voltage-dependence of the channel block between the three species could be quantified using the Woodhull model (Woodhull 1973, see Materials and methods, Eqs. 1–3). Whereas an electrical distance δ_B of 0.85 was found for the three species, they differed in the potential of half-maximal inhibition $V_{B^{1/2}}$ with respect to this cation (Eq. 3). The latter parameter represents a measure of the affinity of the blocking site for extracellular Ca^{2+}. In the presence of 20 mM Ca^{2+} in addition to 30 mM K^+, a half-maximal blocking voltage $V_{B^{1/2}}$ of −163 mV, −194 mV and −208 mV for the $GCKC1_{in}$ of *V. faba*, *N. tabacum* and *S. tuberosum* was determined (Fig. 6A). Although 20 mM Ca^{2+} induced a strong reduction of the K^+ current, 1 mM Ca^{2+} in addition to 30 mM K^+ proved rather uneffective in blocking the channel in the given voltage range. Following the reduction of the K^+ concentration to 10 mM the steady-state current amplitudes of $GCKC1_{in}$ in *V. faba* in the presence of 1 mM Ca^{2+} decreased by the same degree as in $30K^+/20Ca^{2+}$ with $V_{B^{1/2}} = -158$ mV (Fig. 6B). Compared to the effect of 1 mM Ca^{2+} in addition to 30 or 10 mM K^+ the block was even more pronounced in the presence of only 3 mM K^+ ($V_{B^{1/2}} = -126$ mV).

Protons. The opening and closing of stomata is accompanied by changes in the apoplastic pH (Raschke and Humble 1973; Shimazaki et al. 1986). During the opening phase the plasma-membrane H^+-ATPase is supposed to acidify the extracellular space to pH values around 5 (Edwards et al. 1988; Mühling et al. 1995). Potassium uptake and proton extrusion appear to be coupled to the energy status of the cell (Müller-Röber et al. 1995; Wu and Assmann 1995) and may respond directly to changes in the extracellular pH, too (Blatt 1992; Hedrich et al. 1995b; Müller-Röber et al. 1995; Ilan et al. 1996). In order to test whether guard-cell K^+-uptake channels differ in their response to extracellular pH changes we compared the pH-sensitivity of the K^+ channels of the three species (Fig. 7). With the cytoplasm buffered to pH 7.4 the steady-state potassium currents in *S. tuberosum* (Fig. 7A, left-hand traces) and *N. tabacum* (data not shown) were altered in a pH-dependent manner. When, at pH 5.6, the *S. tuberosum* $GCKC1_{in}$ was activated by a hyperpolarizing voltage pulse to −173 mV, K^+ currents saturated within the 30-s voltage step (Fig. 7A, left-hand traces). A change from pH 5.6 to 7.4 in the external medium during the following two voltage pulses, however, reduced the steady-state current by about 70%. Even though the protoplasts were isolated under identical experimental conditions, even together in the same enzyme solution, the *V. faba* channel remained unaffected upon pH changes between pH 5.6 and pH 7.4, a result different from that reported previously (Fig. 7A, right-hand

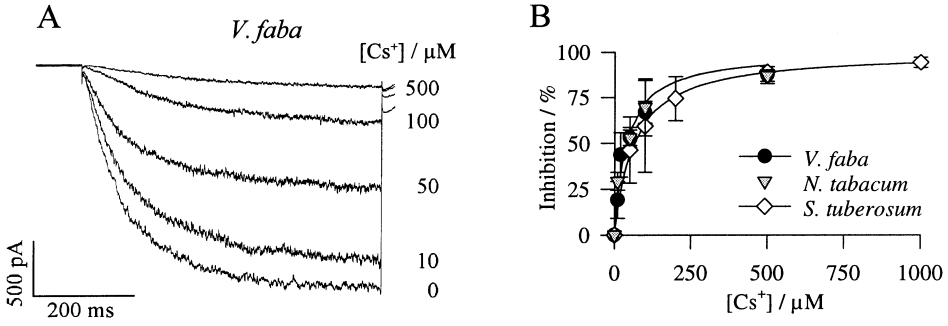

Fig. 4A,B. Cesium ions block inward K^+ channels of guard cells in a concentration-dependent manner. **A** Reduction of whole-cell inward K^+ currents in *Vicia faba* with increasing extracellular cesium concentrations at −213 mV. **B** The concentration-dependence of the steady-state Cs^+-block at −213 mV for three species (±SD; n = 3–5). The dose response was fitted by the Michaelis-Menten relation (*solid lines*) characterized by an inhibitor constant K_i of 40 (*V. faba*), 48 (*Nicotiana tabacum*) and 64 µM (*Solanum tuberosum*)

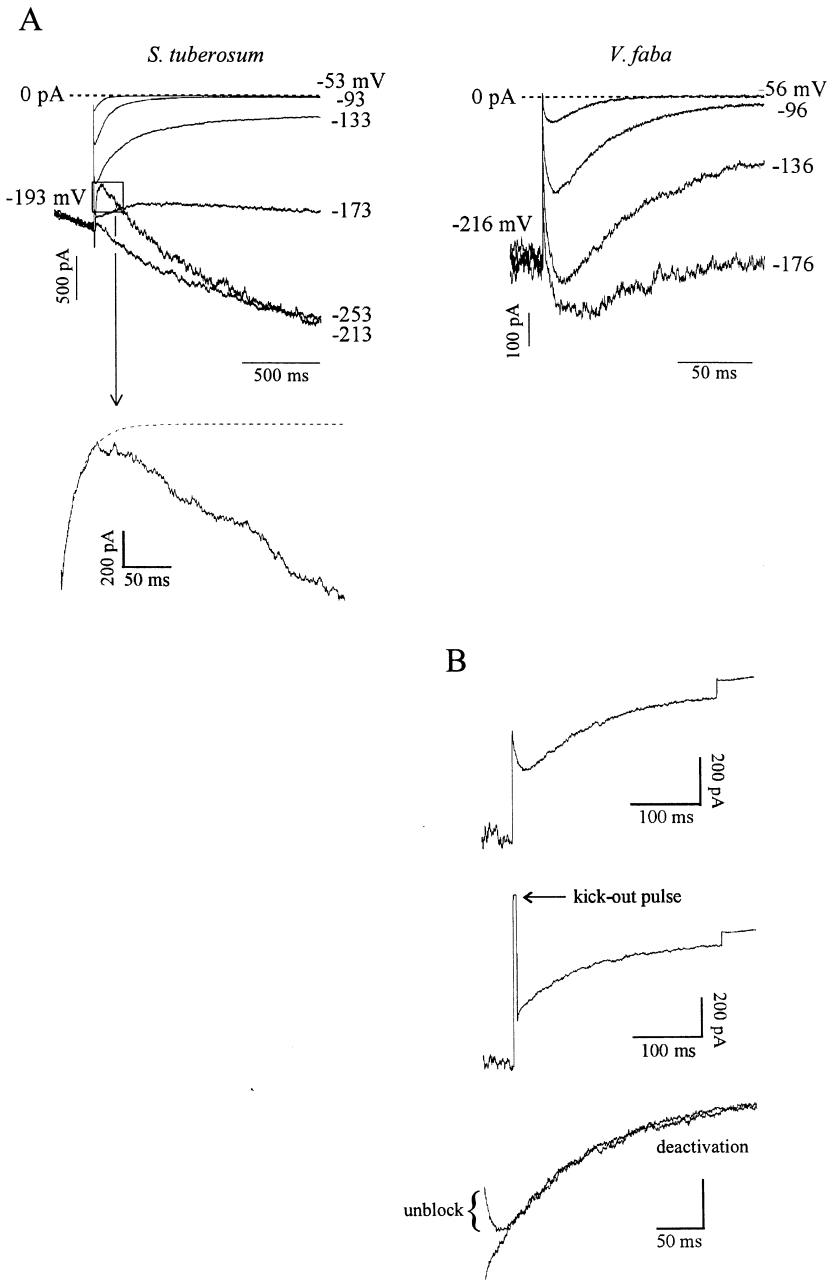

Fig. 5A,B. Kinetics of the Ca^{2+}-block of $GCKC1_{in}$ in *Solanum tuberosum* and *Vicia faba*. **A** Tail currents in the presence of 20 mM extracellular Ca^{2+} in response to depolarizing (*V. faba*) and hyperpolarizing voltage steps following a pre-pulse to −216 mV (*V. faba*) or −193 mV (*S. tuberosum*). *Inset*, tail current at −253 mV at higher resolution. Note, that as a result of the slow blocking reaction, the 'onblock' ($\tau \approx 17$ ms, *dotted line*) can be separated from the activation kinetics. **B** Time-dependent Ca^{2+} release from the channel K^+ pore of *V. faba*. *Upper trace*, after an activating pulse to −216 mV in the subsequent tail pulse to $V = -136$ mV, unblocking and deactivation kinetics superimpose. *Middle trace*, the unblocking kinetics are completely abolished after a pre-depolarizing step (2 ms) to +24 mV which kicks the blocking ion(s) out of the pore. *Lower trace*, superposition of tail currents obtained from pulse sequences with and without kickout pulse. Since during this 2-ms pre-pulse a fraction of the channel population deactivated ($I(t) = I_0 \cdot e^{-t/\tau}$ with $\tau \approx 10$ ms, Fig. 2C), the current declined by a factor of 0.8 ($= e^{-2ms/10ms}$, vertical bar = 100 and 120 pA). Currents were recorded in the presence of 5 mM Ca^{2+}

traces; cf. Blatt 1992) but well in agreement with recent findings (Ilan et al. 1996).

Current-voltage curves in the presence of different proton concentrations allowed the pH effect in *S. tuberosum* and *N. tabacum* to be related to a shift in the half-activation potential (Fig. 7B–D). Solid lines in Fig. 7B represent fits assuming a constant maximum whole-cell conductance as well as gating charge z_g. Reduced proton concentrations shifted the half-activation potential to more-negative potentials and thus did not reach maximal activation in the voltage range tolerated by the protoplasts (≈−200 mV). We therefore can not exclude pH effects on the maximal whole-cell conductance in addition to the change in voltage dependence.

From the analysis of the pH effect on the open probability of $GCKC1_{in}$ the dependence of the half-activation potential $V_{1/2}$ on the extracellular pH could be well fitted assuming that both states, open and closed, of a two-state model can be protonated (solid line for *S. tuberosum* in Fig. 7C):

$$V_{1/2} = V_{1/2}^{\infty} - V_S \cdot \ln \frac{10^{pH} + K_{closed}}{10^{pH} + K_{open}} \qquad \text{(Eq. 8)}$$

where $V_{1/2}$ denotes the pH-dependent half-activation potential, $V_{1/2}^{\infty}$ the half-activation potential of the completely deprotonated channel and V_S the voltage sensitivity which is related to the gating charge (Eq. 4). The parameters K_{closed} and K_{open} correspond to the reaction constants of the protonation reaction of the closed and open channel, respectively.

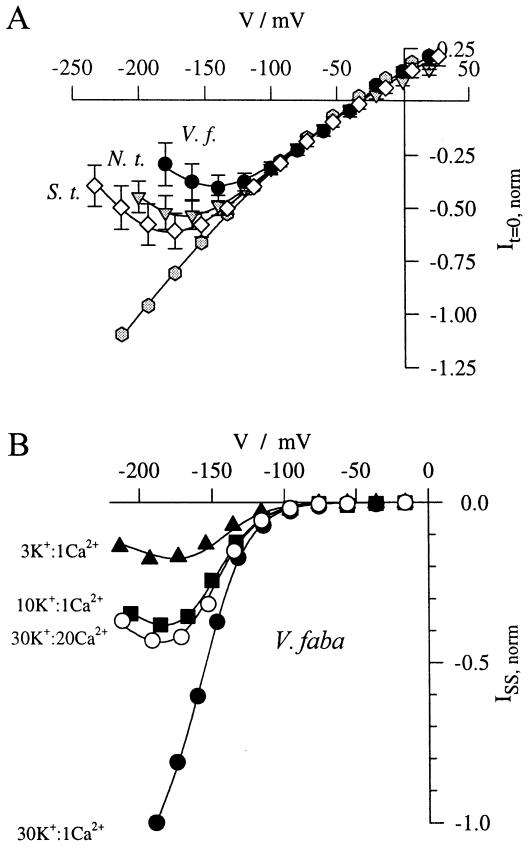

Fig. 6A,B. Inward K^+ currents through the plasma membrane of guard cells as a function of the potassium to calcium ratio. **A** Whole-cell tail current-voltage curves of the $GCKC1_{in}$ from *Vicia faba* ($n = 6$), *Nicotiana tabacum* ($n = 12$) and *Solanum tuberosum* ($n = 6$) in the presence of 1 (*hexagons*) and 20 mM (*circles*, *triangles*, *diamonds*) Ca^{2+} in addition to 30 mM K^+. Currents were scaled with respect to the slope of the tail in 1 mM Ca^{2+}. Data were fitted according to Eq. 2. **B** Whole-cell current-voltage relation of $GCKC1_{in}$ of a representative *V. faba* guard-cell protoplast at different K^+/Ca^{2+} ratios. Steady-state inward currents in different K^+ concentrations were related to a constant driving force (V), according to

$$I_{SS,norm} = \frac{V}{V - V_{rev}} \cdot I_{SS} \qquad \text{(Eq. 7)}$$

and normalized to $I_{ss}(30K^+: 1Ca^{2+})$ at −200 mV = −1

A similar acid activation was found for the K^+ channel in tobacco (Fig. 7C). In line with the hypothesis of protons interacting with the voltage sensor of the channel, the conductance of single inward K^+ channels proved to be pH-insensitive (Figs. 7D and 1C).

Discussion

In the work presented here we have compared the characteristics of the inward rectifying K^+ channels $GCKC1_{in}$ from *Vicia faba*, *Solanum tuberosum* and *Nicotiana tabacum*. Whereas the voltage dependence, conductance, selectivity as well as high-affinity block by extracellular Cs^+ were similar between species, pronounced differences in the kinetics, channel densities and susceptibility towards block by calcium and activation by protons have been discovered. Although the channel kinetics in *S. tuberosum* are slow compared to those in *V. faba* (Fig. 2) their physiological relevance remains unclear. Since in *S. tuberosum* the guard-cell K^+ inward current density is almost three times that in *V. faba* (Fig. 3A), in the short term this high channel abundance may be balanced in *S. tuberosum* by the slow activation kinetics.

Ion permeation and cation sensitivity. Inward rectifying K^+ channels in *V. faba*, *N. tabacum* and *S. tuberosum* were blocked by extracellular Ca^{2+} in a concentration- and voltage-dependent manner (Figs. 5, 6). Since Ca^{2+} and K^+ interact within the channel pore (Fig. 6B), an inhibitory effect of extracellular Ca^{2+} at concentrations of about 1 mM is likely to contribute to the reduction of stomatal aperture in vivo where K^+ concentrations around open stomata vary in the low-millimolar range (Bowling 1987). The voltage inducing a half-maximal block and thus the binding affinity of the blocker was far more negative for *S. tuberosum* than for *V. faba* (−208 versus −163 mV, Fig. 6). The target site for extracellular Ca^{2+} was, however, located at the same electrical distance ($\delta = 0.85$) within the membrane. Together with the similarities in the sensitivity to extracellular Cs^+ the permeation pathway near the narrow pore might be identical.

Besides species-dependent differences in the Ca^{2+}-sensitivity between K^+ uptake channels in vivo the susceptibility to extracellular cations is reduced in KST1, a guard-cell K^+ channel from *S. tuberosum* after heterologous expression in *Xenopus laevis* oocytes (Müller-Röber et al. 1995) when compared to $GCKC1_{in}$ in the corresponding guard-cell protoplast. When in KAT1, another guard-cell K^+-uptake channel cloned from *Arabidopsis thaliana* (Anderson et al. 1992; Nakamura et al. 1995), the threonine at position 256 was replaced by glutamate (T256E), this initially Ca^{2+}-insensitive channel developed a voltage-dependent susceptibility towards extracellular Ca^{2+} (Becker et al. 1996). Along with the Ca^{2+}-sensitivity this mutation increased the Cs^+-sensitivity as well. Variations in this region could therefore contribute to the species-dependent differences in Ca^{2+}-modulated stomatal movement.

The K^+ channel and H^+-ATPase interact via the apoplastic pH. Acid activation of the inward rectifying K^+ channel from *S. tuberosum* and *N. tabacum* is mediated through a shift towards less-hyperpolarized potentials (Fig. 7) which is maintained in *kst1* after heterologous expression (Hoth et al. 1997). In the derived amino acid sequence the histidine at the rim of the channel pore (H271) as well as within the extracellular loop linking the transmembrane helices S3 and S4 (H160) has been shown to relate to the pH-sensor at least in KST1. Thus, pH-sensitive and ATP-dependent K^+ channels (Hoshi 1995; Müller-Röber et al. 1995; Wu and Assmann 1995; Ilan et al. 1996) together with ATP- and pH-dependent anion channels in this motor cell (Hedrich et al. 1990; Schulz-Lessdorf et al. 1996) could link the membrane potential to the energy status and acid metabolism of the guard cell.

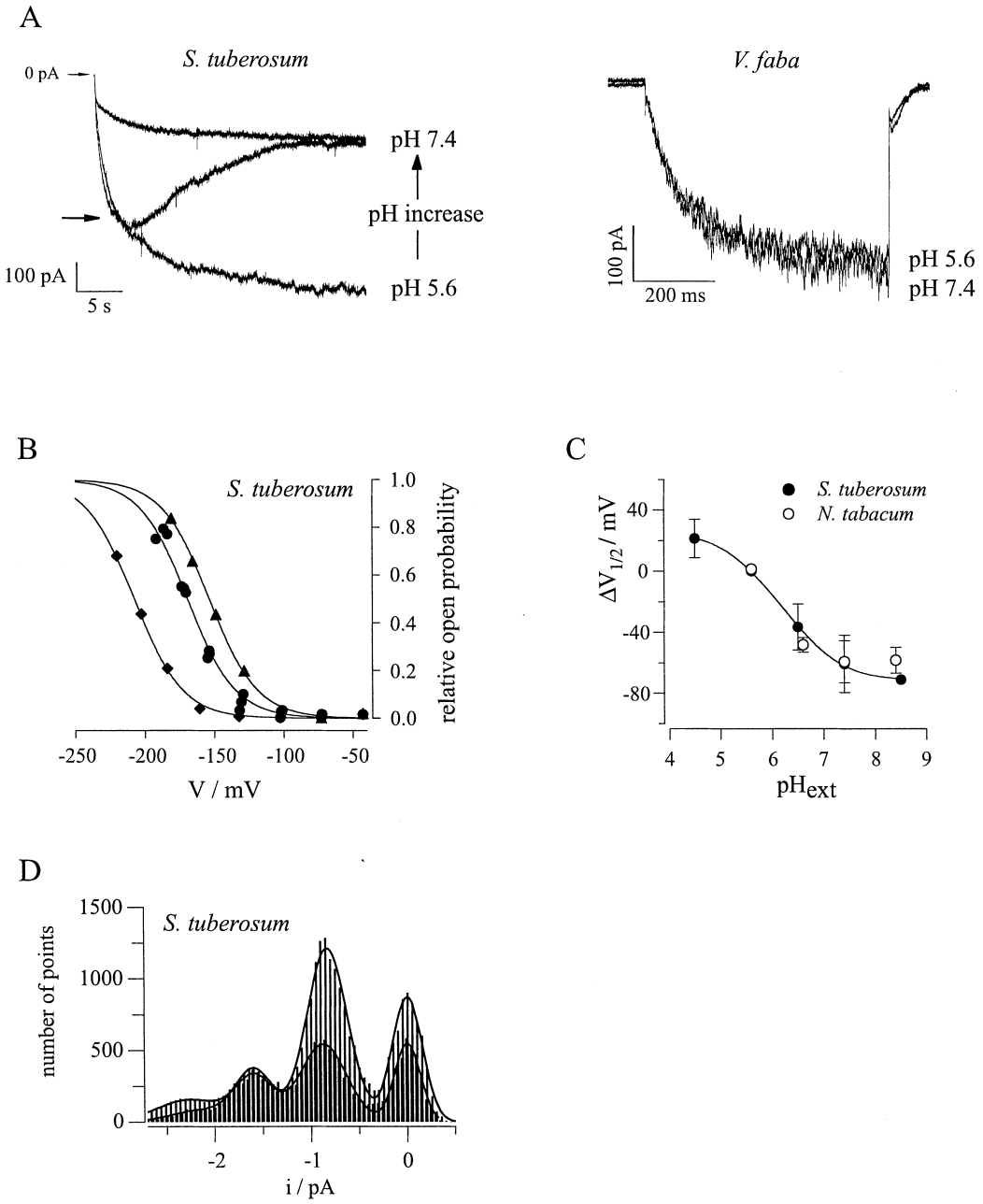

Fig. 7A–D. Difference in pH-dependent activity of $GCKC1_{in}$ from *Vicia faba* and *Solanum tuberosum*. **A** *Left-hand traces*, time-course of the K^+-current response before, during, and after a pH change from 5.6 to 7.4 in *S. tuberosum* guard cells. From a holding potential of −63 mV (100 ms) three subsequent 30-s voltage pulses to −173 mV were applied. During the second voltage step the bath solution was changed from pH 5.6 to pH 7.4 (flux rate 4.1 ml · min^{-1}, *arrow* indicates the onset of solution exchange). *Right-hand traces*, time-dependent activation of the *V. faba* channel in response to 600-ms pulses to −193 mV. Current traces recorded in pH 5.6 and pH 7.4 superimposed. **B** pH- and voltage-dependent open probabilities of $GCKC1_{in}$ from *S. tuberosum*. Open probabilities of $GCKC1_{in}$ from a representative measurement were fitted on the basis of a constant gating charge as well as constant maximum whole-cell conductance. pH values were 4.5 (*triangles*), 5.6 (*circles*) and 6.5 (*diamonds*). Control currents at pH 5.6 (*circles*) were recorded before and after the application of solutions of pH values indicated. **C** Shift of the half-activation potential $V_{1/2}$ as a function of the external pH. Open-probabilities for *S. tuberosum* (*filled circles*, ±SD, $n \geq 3$, for pH 8.5 $n = 2$) and *Nicotiana tabacum* (*open circles*, $n = 3$) were determined from instantaneous currents at −93 mV after a pre-pulse to the test voltages (see figure legend 3B). Data points were fitted by single Boltzmann equations (Eq. 4) assuming a constant maximum conductance and gating charge. The pH dependence of the half-activation potentials of $GCKC1_{in}$ in *S. tuberosum* were then fitted according to Eq. 8 (*solid line*). Note that the pH dependence is similar for $GCKC1_{in}$ in *N. tabacum*. **D** Superposition of amplitude histograms of two different patches from *S. tuberosum* protoplasts derived from consecutive 27–30 current traces at −129 mV in pH 5.6 or 7.4 (dark). Data points were fitted using four gaussian distributions to describe one closed (0 pA) and three open levels with an open-channel amplitude of 0.80 pA (pH 5.6) and 0.78 pA (pH 7.4, cf. Fig. 1C)

Diversification of inward rectifying guard cell K^+ channels. In contrast to *S. tuberosum* and *N. tabacum* the K^+-uptake channel from *V. faba* is insensitive in the pH range between 7.4 and 5.6 (Fig. 7A). Stimulation of potassium uptake in the latter channel type seems to require more acidic pH values (Ilan et al. 1996). In addition, the mechanism of acid activation in *Vicia* is not based on changes of the voltage dependence but involves activation of formerly silent K^+ channels (Ilan et al. 1996). Before finishing the cloning of $GCKC1_{in}$ from *V. faba* and comparing its structure to KST1 we can only speculate about the target amino acid(s) in the broad-bean channel.

The strong pH dependence of the heterologously expressed potato channel (KST1) compared to its homolog (KAT1) cloned from *Arabidopsis thaliana* (Hedrich et al. 1995b) could be related to the KST1-specific histidine (H160) not present in the guard-cell channel from *A. thaliana* (Hoth et al. 1997). Since plant K^+ channels cloned so far are conserved with respect to the pore-histidine (H271 in *kst1*; Hoth et al. 1997) the differences in pH-sensitivity of K^+ channels in vivo may be based on variabilities in the region around H160. It is, however, unclear whether the observed species-dependent differences in Ca^{2+}- and H^+-sensitivity of inward rectifying K^+ channels in vivo and after heterologous expression in vitro result from structural implications due to variabilities within the corresponding channel genes, only (Becker et al. 1996; Hoth et al. 1997) or also point to a heteromultimeric structure of the functional K^+ channel in vivo (Dreyer et al. 1997). Detailed future analysis of the expression patterns of different α-subunits will therefore help to better relate the results from molecular cloning and structure-function analysis to the physiology of an individual species or cell type.

This work was funded by Deutsche Forschungsgemeinschaft grants to R.H.

References

Anderson JA, Huprikar SS, Kochian LV, Lucas WJ, Gaber RF (1992) Functional expression of a probable *Arabidopsis thaliana* potassium channel in *Saccharomyces cerevisiae*. Proc Natl Acad Sci USA 89: 3736–3740

Becker D, Dreyer I, Hoth S, Busch H, Küch A, Palme K, Hedrich R (1996) Pronounced changes in Cs^+ sensitivity and ion permeability in H5 mutants of a plant K^+ channel. Proc Natl Acad Sci USA 93: 8123–8128

Bertl A, Anderson JA, Slayman CL, Gaber RF (1995) Use of *Saccharomyces cerevisiae* for patch-clamp analysis of heterologous membrane proteins: Characterization of Kat1, an inward-rectifying K^+ channel from *Arabidopsis thaliana*, and comparison with endogeneous yeast channels and carriers. Proc Natl Acad Sci USA 92: 2701–2705

Blatt MR (1992) K^+ channels of stomatal guard cells – characteristics of the inward rectifier and its control by pH. J Gen Physiol 99: 615–644

Blatt MR, Armstrong F (1993) K^+ channels of stomatal guard cells, abscisic-acid-evoked control of the outward rectifier mediated by cytoplasmic pH. Planta 191: 330–341

Bowling DJF (1987) Measurement of the apoplastic activity of K^+ and Cl^- in the leaf epidermis of *Commelina communis* in relation to stomatal activity. J Exp Bot 38: 1351–1355

Busch H, Hedrich R, Raschke K (1990) External calcium blocks inward rectifier potassium channels in guard cell protoplasts in a voltage and concentration dependent manner. (Abstr) Plant Physiol 93: 14

Cao Y, Ward JM, Kelly WB, Ichida AM, Gaber RF, Anderson JA, Uozumi N, Schroeder JI, Crawford NM (1995) Multiple genes, tissue specificity, and expression-dependent modulation contribute to the functional diversity of potassium channels in *Arabidopsis thaliana*. Plant Physiol 109: 1093–1106

Daram P, Urbach S, Gaymard F, Sentenac H, Charel I (1997) Tetramerization of the AKT1 plant potassium channel involves its C-terminal cytoplasmic domain. EMBO J 16: 3455–3463

Draber S, Hansen U-P (1994) Fast single-channel measurements resolve the blocking effect of Cs^+ on the K^+ channel. Biophys J 67: 120–129

Dreyer I, Antunes S, Hoshi T, Müller-Röber B, Palme K, Pongs O, Reintanz B, Hedrich R (1997) Plant K^+ channel α-subunits assemble indiscriminately. Biophys J 72: 2143–2150

Edwards MC, Smith GN, Bowling DJF (1988) Guard cells extrude protons prior to stomatal opening – a study using fluorescence microscopy and pH micro-electrodes. J Exp Bot 39: 1541–1547

Ehrhardt T, Zimmermann S, Müller-Röber B (1997) Association of plant K^+_{in} channels is mediated by conserved C-termini and does not affect subunit assembly. FEBS Lett 409: 166–170

Fairley-Grenot KA, Assmann SM (1992) Whole-cell K^+ current across the plasma membrane of guard cells from a grass: *Zea mays*. Planta 186: 282–293

Gaymard F, Cerutti M, Horeau C, Lemaillet G, Urbach S, Ravallec M, Devauchelle G, Sentenac H, Thibaud J-B (1996) The baculovirus/insect cell system as an alternative to *Xenopus* oocytes. Am Soc Biochem Mol Biol 271: 22863–22870

Gilroy S, Trewavas T (1994) A decade of plant signals. BioEssays 16: 677–682

Hamill OP, Marty A, Neher E, Sakmann B, Sigworth FJ (1981) Improved patch-clamp technique for high resolution current recording from cells and cell-free membrane patches. Pflügers Arch 391: 85–100

Hedrich R, Becker D (1994) Green circuits – the potential of plant specific ion channels. Plant Mol Biol 26: 1637–1650

Hedrich R, Dietrich P (1996) Plant K^+ channels: similarity and diversity. Bot Acta 109: 81–176

Hedrich R, Busch H, Raschke K (1990) Ca^{2+} and nucleotide dependent regulation of voltage dependent anion channels in the plasma membrane of guard cells. EMBO J 9: 3889–3892

Hedrich R, Bregante M, Dreyer I, Gambale F (1995a) The voltage-dependent potassium uptake channel of corn coleoptiles has permeation properties different from other K^+ channels. Planta 197: 193–199

Hedrich R, Moran O, Conti F, Busch H, Becker D, Gambale F, Dreyer I, Küch A, Neuwinger K, Palme K (1995b) Inward rectifier potassium channels in plants differ from their animal counterparts in response to voltage and channel modulators. Eur Biophys J 24: 107–115

Hoshi T (1995) Regulation of voltage dependence of the KAT1 channel by intracellular factors. J Gen Physiol 105: 309–328

Hoth S, Dreyer I, Dietrich P, Becker D, Müller-Röber B, Hedrich R (1997) Molecular basis of plant-specific acid activation of K^+ uptake channels. Proc Natl Acad Sci USA: 4806–4810

Ilan N, Schwartz A, Moran N (1996) External protons enhance the activity of the hyperpolarization-activated K channels in guard cell protoplasts of *Vicia faba*. J Membr Biol 154: 169–181

Inoué H, Katoh Y (1986) Calcium inhibits ion-stimulated stomatal opening in epidermal strips of *Commelina communis* L. J Exp Bot 38: 142–149

Irving HR, Gehring CA, Parish RW (1992) Changes in cytosolic pH and calcium of guard cells precede stomatal movements. Proc Natl Acad Sci USA 89: 1790–1794

Klieber HG, Gradmann D (1993) Enzyme kinetics of the prime K^+ channel in the tonoplast of *Chara*, selectivity and inhibition. J Membr Biol 132: 253–265

Kochian LV, Garvin DF, Shaff JE, Chilcott TC, Lucas WJ (1993) Towards an understanding of the molecular basis of plants K^+ transport: characterization of cloned K^+ transport cDNA's. Plant Soil 155/156: 115–118

Lagarde D, Basset M, Lepetit M, Conejero G, Gaymard F, Astruc S, Grignon C (1996) Tissue-specific expression of *Arabidopsis* AKT1 gene is consistent with a role in K^+ nutrition. Plant J 9: 195–203

Lemtiri-Chlieh F, MacRobbie EAC (1994) Role of calcium in the modulation of *Vicia* guard cell potassium channels by abscisic acid, a patch-clamp study. J Membr Biol 137: 99–107

Lohse G, Hedrich R (1995) Anions modify the response of guard-cell anion channels to auxin. Planta 197: 546–552

MacRobbie EAC (1992) Calcium and ABA-induced stomatal closure. Phil Trans R Soc Lond B 338: 5–18

Mansfield TA, Hetherington AM, Atkinson CJ (1990) Some current aspects of stomatal physiology. Annu Rev Plant Physiol Plant Mol Biol 41: 55–75

Marquardt DW (1963) An algorithm for least-squares estimation of non-linear parameters. J Soc Ind App Math 11: 431–441

Marten I, Lohse G, Hedrich R (1991) Plant growth hormones control voltage-dependent activity of anion channels in the plasma membrane of guard cells. Nature 353: 1–4

Marten I, Gaymard F, Lemaillet G, Thibaud J-B, Sentenac H, Hedrich R (1996) Cytoplasmic Ca^{2+} and nucleotides do not affect the voltage-dependent activity of KAT1. FEBS Lett 380: 229–232

McAinsh MR, Brownlee C, Hetherington AM (1992) Visualizing changes in cytosolic free Ca^{2+} during the response of stomatal guard cells to abscisic acid. Plant Cell 4: 1113–1122

McAinsh MR, Webb AAR, Taylor JE, Hetherington AM (1995) Stimulus-induced oscillations in guard cell cytosolic free calcium. Plant Cell 7: 1207–1219

Moran N, Ehrenstein G, Iwasa K, Mischke C, Bare C, Satter RL (1988) Potassium channels in motor cells of *Samanea saman*: a patch-clamp study. Plant Physiol 88: 643–648

Mühling K-H, Plieth C, Hansen U-P, Sattelmacher B (1995) Apoplastic pH of intact leaves of *Vicia faba* as influenced by light. J Exp Bot 46: 377–382

Müller-Röber B, Ellenberg J, Provart N, Willmitzer L, Busch H, Becker D, Dietrich P, Hoth S, Hedrich R (1995) Cloning and electrophysiological analysis of KST1, an inward-rectifying K^+ channel expressed in potato guard cells. EMBO J 14: 2409–2416

Nakamura RL, McKendree WL Jr, Hirsch RE, Sedbrook JC, Gaber RF, Sussman MR (1995) Expression of an *Arabidopsis* potassium channel gene in guard cells. Plant Physiol 109: 371–374

Neher E (1992) Corrections for liquid junction potentials in patch clamp experiments. Methods Enzymol 207: 123–131

Raschke K, Humble GD (1973) No uptake of anions required by opening stomata of *Vicia faba*, guard cells release hydrogen ions. Planta 115: 47–57

Roberts SK, Tester M (1995) Inward and outward K^+-selective currents in the plasma membrane of protoplasts from maize root cortex and stele. Plant J 8: 811–825

Schroeder JI (1988) K^+ transport properties of K^+ channels in the plasma membrane of *Vicia faba* guard cells. J Gen Physiol 92: 667–683

Schroeder JI, Fang HH (1991) Inward-rectifying K^+ channels in guard cells provide a mechanism for low-affinity K^+ uptake. Proc Natl Acad Sci USA 88: 11583–11587

Schroeder JI, Hagiwara S (1989) Cytosolic calcium regulates ion channels in the plasma membrane of *Vicia faba* guard cells. Nature 338: 427–430

Schroeder JI, Raschke K, Neher E (1987) Voltage dependence of K^+ channels in guard-cell protoplasts. Proc Natl Acad Sci USA 84: 4108–4112

Schroeder JI, Ward JM, Gassmann W (1994) Perspectives on the physiology and structure of inward-rectifying K^+ channels in higher plants: Biophysical implications for K^+ uptake. Annu Rev Biophys Biomol Struct 23: 441–471

Schulz-Lessdorf B, Lohse G, Hedrich R (1996) GCAC1 recognizes the pH-gradient across the plasma membrane – a pH-sensitive and ATP-dependent anion channel links guard cell membrane potential to acid- and energy-metabolism. Plant J 10: 993–1004

Schwartz A (1985) Role of Ca^{2+} and EGTA on stomatal movements in *Commelina communis* L. Plant Physiol 79: 1003–1005

Schwartz A, Ilan N, Gantz DA (1988) Calcium effects on stomatal movement in *Commelina communis* L. Plant Physiol 87: 583–587

Sentenac H, Bonneaud N, Minet M, Lacroute F, Salmon J-M, Gaymard F, Grignon C (1992) Cloning and expression in yeast of a plant potassium ion transport system. Science 256: 663–665

Shimazaki K, Iino M, Zeiger E (1986) Blue light-dependent proton extrusion by guard-cell protoplasts of *Vicia faba*. Nature 319: 324–326

Tester M (1988) Pharmacology of K^+ channels in the plasmalemma of the green alga *Chara corallina*. J Membr Biol 103: 159–169

Véry A-A, Bosseux C, Gaymard F, Sentenac H, Thibaud J-B (1994) Level of expression in *Xenopus* oocytes affects some characteristics of a plant inward-rectifying voltage-gated K^+ channel. Pflügers Arch 428: 422–424

Véry A-A, Gaymard F, Bosseux C, Sentenac H, Thibaud J-B (1995) Expression of a cloned plant K^+ channel in *Xenopus* oocytes, analysis of macroscopic currents. Plant J 7: 321–332

Willmer CM, Mansfield TA (1969) A critical examination of the use of detached epidermis in studies of stomatal physiology. New Phytol 68: 363–375

Woodhull AM (1973) Ionic blockage of sodium channels in nerves. J Gen Physiol 61: 687–708

Wu W-H, Assmann SM (1995) Is ATP required for K^+ channel activation in *Vicia* guard cells? Plant Physiol 107: 101–109

⇒ zurück zur Übersicht

1997

Hoth, **Dreyer**, Dietrich, Becker, Mueller-Roeber, Hedrich

Molecular basis of plant-specific acid activation of K^+ uptake channels.

Proc. Natl. Acad. Sci. USA **94**:4806-4810.

Proc. Natl. Acad. Sci. USA
Vol. 94, pp. 4806–4810, April 1997
Plant Biology

Molecular basis of plant-specific acid activation of K^+ uptake channels

STEFAN HOTH*, INGO DREYER*, PETRA DIETRICH*, DIRK BECKER*, BERND MÜLLER-RÖBER†, AND RAINER HEDRICH*‡

*Institut für Biophysik, Universität Hannover, Herrenhäuser Strasse 2, 30419 Hannover, Germany; and †Max-Planck-Institut für Molekulare Pflanzenphysiologie, Karl-Liebknecht Strasse 25, Haus 20, 14476 Golm, Germany

Communicated by Erwin Neher, Max Planck Institute for Biophysical Chemistry, Goettingen, Germany, February 11, 1997 (received for review December 10, 1996)

ABSTRACT **During stomatal opening potassium uptake into guard cells and K^+ channel activation is tightly coupled to proton extrusion. The pH sensor of the K^+ uptake channel in these motor cells has, however, not yet been identified. Electrophysiological investigations on the voltage-gated, inward rectifying K^+ channel in guard cell protoplasts from *Solanum tuberosum* (KST1), and the *kst1* gene product expressed in *Xenopus* oocytes revealed that pH dependence is an intrinsic property of the channel protein. Whereas extracellular acidification resulted in a shift of the voltage-dependence toward less negative voltages, the single-channel conductance was pH-insensitive. Mutational analysis allowed us to relate this acid activation to both extracellular histidines in KST1. One histidine is located within the linker between the transmembrane helices S3 and S4 (H160), and the other within the putative pore-forming region P between S5 and S6 (H271). When both histidines were substituted by alanines the double mutant completely lost its pH sensitivity. Among the single mutants, replacement of the pore histidine, which is highly conserved in plant K^+ channels, increased or even inverted the pH sensitivity of KST1. From our molecular and biophysical analyses we conclude that both extracellular sites are part of the pH sensor in plant K^+ uptake channels.**

Plant growth, differentiation, cell and tissue polarity, as well as movements strongly depend on the formation of pH gradients across individual cell types (1–3). Stomata that are formed by two guard cells represent a unique model for plant movement. Regulation of stomatal movement in higher plants is essential for efficient uptake of CO_2 at minimal water loss. Stomatal opening requires accumulation of potassium ions into guard cells. K^+ uptake is mediated by K^+ uptake channels, a process accompanied by the acidification of the apoplast (4–7). Due to differential pumping activity of the plasma membrane H^+-pump the apoplastic pH around closed and open stomata varies between 7 and 5 (8, 9). Within this range changes in the extracellular proton concentration affect the activity of guard cell inward rectifying K^+ channels (10–13). In contrast to their functional and structural animal counterparts, which are either not activated or even inhibited by protons (14, 15), the guard cell K^+ channel is activated upon extracellular acidification (10–13).

The molecular cloning of plant K^+ inward rectifiers revealed a structural homology to animal outward rectifying K^+ channels of the *Shaker* gene family (12, 16, 17). Hydrophobicity analyses of their primary structure predicted six transmembrane domains (S1–S6) (12, 16, 17). Whereas S4 is likely to represent the voltage sensor of these voltage-dependent channels, the amphiphilic linker between S5 and S6 (P) forms the conductive pore (18). Based on the current molecular model of the *Shaker* channel we were able to relate structural elements of guard cell K^+ inward rectifiers to stomatal physiology. In this context we have previously shown that a putative ATP-binding site in the amino acid sequence together with the requirement of KST1 for cytoplasmic ATP pointed to a tight coupling between channel activity and guard cell energy metabolism (12).

Here, we demonstrate that protonation and deprotonation in response to the H^+ pumping activity and acid metabolism modulates the K^+ uptake channel. Proton-induced increase in whole cell currents of KST1 is due to a shift in the half-maximum activation voltage rather than an increase in the single-channel conductance. To understand this mechanism of acid activation we studied the role of external histidine residues in the pH sensing of KST1.

MATERIALS AND METHODS

Generation of *kst1* Mutants. For mutants H160D, H160R, and H160A, the *Pfl*MI/*Bse*RI segment of the *kst1*-coding region in pGEMHE (12) was replaced by PCR-generated fragments obtained with forward primer P1 (5′-CTGTGTGGACGAGTTCCAAATGG-3′) and reverse primers P2XXX (5′-AGCAATCTGAATCCAACTCCTCCGCTTTCTTTXXXACCCGTGAAG-3′, with XXX = GTC for aspartate, TCG for arginine, and GGC for alanine). To produce H271 and N274 mutants, a silent mutation creating a novel *Bgl*II site was first introduced into the *kst1* coding region upstream of the H271 codon. This modification was achieved by exchanging the *Sph*I fragment of the *kst1* cDNA in the plasmid pKST1#8–1 (12) by a corresponding PCR fragment amplified with primers P3 (5′-CCATTCCAATCATTGATCCTCG-3′) and P4 (5′-CTCAGCATGCAGATCTCCATAACCG-3′). To obtain H271 mutants, the *Bgl*II/*Sty*I fragment of the modified *kst1* sequence was replaced by fragments generated via PCR using reverse primer P5 (5′-TTGCTTCGGAGGGAAGTATTCAGCTTC-3′) and forward primers P6XXX (5′-CGGTTATGGAGATCTGXXXGCTGAGAACTC-3′, with XXX = GAC for aspartate, CGA for arginine, and GCA for alanine). For N274 mutants forward primers P7XXX (5′-ATGGAGATCTGCATGCTGAGXXXTCTAGAGAGATGC-3′, with XXX = GAC for aspartate and GCA for alanine) and reverse primer P5 were employed. Mutated *kst1* cDNAs were cloned as *Asp*718/*Bam*HI fragments (blunt-ended; sense orientation) into the *Sma*I site of vector pGEMHE (19). All modifications were verified by DNA sequence analysis using the T7 Sequencing Kit from Pharmacia. Double mutants were derived from the corresponding single mutants by exchange of DNA fragments.

The publication costs of this article were defrayed in part by page charge payment. This article must therefore be hereby marked "*advertisement*" in accordance with 18 U.S.C. §1734 solely to indicate this fact.

0027-8424/97/944806-5$2.00/0
PNAS is available online at **http://www.pnas.org**.

Data deposition: The sequences reported in this paper have been deposited in the GenBank database (accession nos. Y07632, Y09748, Y09749, Y09750, Y09751, Y09752, Y09753, Y09747, and X86021).
‡To whom reprint requests should be sent at the present address: Julius-von-Sachs-Institut für Biowissenschaften, Lehrstuhl Botanik I, Mittlerer Dallenbergweg 64, 97082 Würzburg, Germany.

Patch-Clamp Recordings on Potato Guard Cell Protoplasts (*in Vivo*). Patch-clamp studies on potato guard cell protoplasts were performed as described (12). The bath medium was adjusted to pH 8.5 and to pH 7.4 with 10 mM Hepes-Tris, to pH 6.5 and to pH 5.6 with 10 mM Mes-Tris, and to pH 4.5 with 10 mM citrate-Tris. Single-channel events recorded from excised outside–out patches with 100 mM K^+ in the bath and 150 mM K^+ in the pipette were filtered at 1 kHz.

Expression of *kst1* and Mutants in *Xenopus* Oocytes and Voltage-Clamp Recordings (*in Vitro*). *Xenopus* frogs were purchased from Nasco (Fort Atkinson, WI). Oocytes were isolated as described elsewhere (20) and injected with 1–10 ng of cRNA per oocyte using a General Valve (Fairfield, NJ) Picospritzer II microinjector. Forty-eight hours after injection whole-cell K^+ currents were measured with a two-microelectrode voltage-clamp amplifier (Turbotec-01C; NPI Instruments, Tamm, Germany) using 0.5–2 MΩ pipettes filled with 3 M KCl (12). Solutions were composed of 30 mM KCl, 2 mM $MgCl_2$, and 1 mM $CaCl_2$. pH values were buffered with 10 mM Mes-Tris (pH 5.2–6.5) and 10 mM Tris-Mes (pH 7.0–9.2), respectively. All solutions were adjusted to 220 mOsm with D-sorbitol.

Biophysical Analyses. Open probabilities (p_o) were deduced from a double-voltage step protocol. In two-electrode voltage-clamp measurements time- and voltage-dependent K^+ currents were induced during the first 5 s activation pulse to hyperpolarizing voltages (V) between −50 mV and −170 mV in −10 mV increments.§ During the second pulse to a fixed voltage (V_F = −70 mV) inward currents relaxed. The I_0–V relationship, obtained from extrapolating the relaxation time course of the second pulse to t = 0 ms with an exponential function, is proportional to the open probability of the channel at the end of the activation pulse:

$$I_0(V) = N \cdot i(V_F) \cdot p_o(V) = const. \cdot p_o(V),$$

where N denotes the number of KST1 channels within the membrane, I_0 the instantaneous tail current, V_F the voltage of the following-pulse, and $i(V_F)$ the single channel current at V_F ($N \cdot i(V_F) = const.$). Patch-clamp data analyses were performed based on the same equations and similar voltage protocols.

To obtain biophysical parameters that allow a comparative analysis of acid activation, we described the channel by a two state model (closed and open). Independent of its state the channel can be protonated or deprotonated. According to the law of mass action the distribution between protonated and deprotonated states can be described by

$$K_{closed} = \frac{p_{cp}}{p_{cd} \cdot [H^+]} \quad \text{and} \quad K_{open} = \frac{p_{op}}{p_{od} \cdot [H^+]},$$

where p_{cp}, p_{cd}, p_{op}, and p_{od} denote the probabilities to find the channel in one of the different states (c = closed, o = open, p = protonated, and d = deprotonated), $[H^+]$ the proton concentration, and K_{closed} and K_{open} the reaction constants of the protonation reaction.

Using Boltzmann statistics as well as the equation $p_{cp} + p_{cd} + p_{op} + p_{od} = 1$ the measurable open probability $p_{open} = p_{op} + p_{od}$ derives to

$$p_{open} = \frac{1}{1 + e^{\left(\frac{V - V_{1/2}}{V_s}\right)}}. \qquad [1]$$

Here V_s denotes the slope factor, which is correlated to the gating charge, and $V_{1/2}$ the pH-dependent half-activation voltage

$$V_{1/2} = V_{1/2}^{\infty} - V_s \cdot \ln \frac{10^{pH} + K_{closed}}{10^{pH} + K_{open}}, \qquad [2]$$

where $V_{1/2}^{\infty}$ corresponds to the half-activation voltage of the completely deprotonated channel.

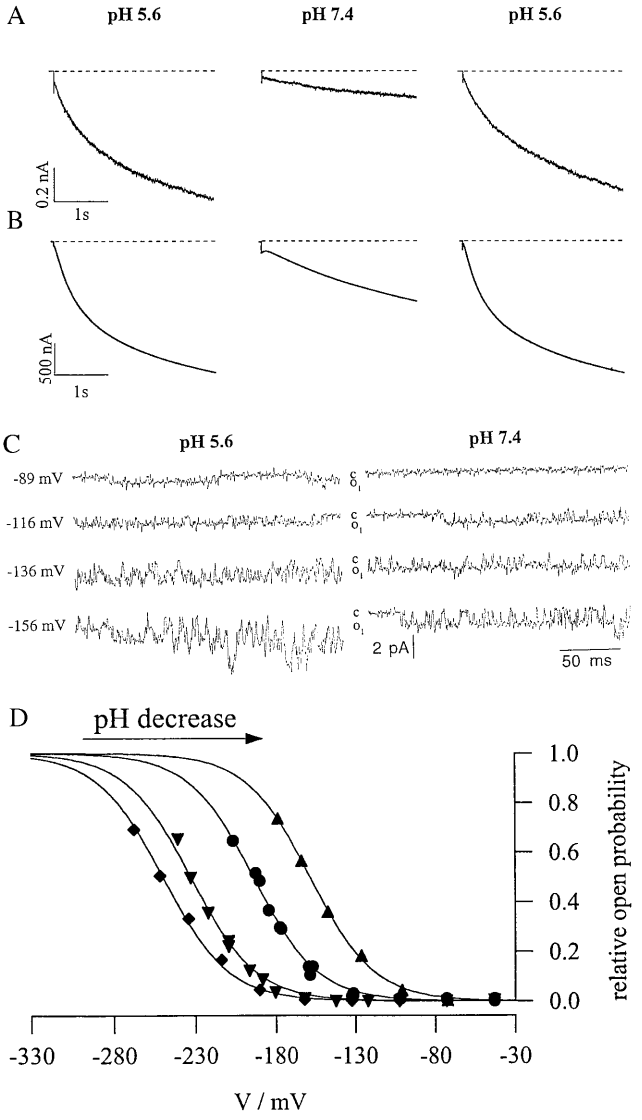

FIG. 1. Acid activation of a guard cell inward rectifying K^+ channel *in vivo* and *in vitro*. (*A*) In the whole-cell configuration guard cell protoplasts from *Solanum tuberosum* were clamped at −63 mV to elicit inward K^+ currents during subsequent 3-s pulses to −180 mV. (*B*) Two-electrode voltage-clamp recordings of inward K^+ currents through *kst1* expressed in *Xenopus* oocytes. With the oocyte clamped at −20 mV KST1-specific inward K^+ currents were induced by membrane hyperpolarization to −170 mV. In contrast to KAT1 an artificial acidification of the cytoplasm of oocytes using acetate did not affect the gating behavior of KST1 (data not shown). In both systems channel activity of the inward rectifier increased with the extracellular proton concentration (pH 7.4–5.6). (*C*) Open–closed transitions of single inward K^+ channels in cell-free outside–out membrane patches from isolated protoplasts exposed to pH 5.6 and 7.4. Single channels were recorded between t = 100 and 300 ms during steps to voltages indicated from a holding potential of −46 mV. Note that open-channel amplitudes (o_1) were identical for both proton concentrations. (*D*) pH- and voltage-dependent open probability of the K^+ uptake channel from one representative guard cell protoplast. Data points were fitted by Boltzmann functions ($po = N \cdot \{1 + \exp[(V - V_{1/2})/V_s]\}^{-1}$) and scaled to the value N obtained in pH 4.5. The activation threshold shifts to less negative potentials with a decrease in pH (◆, pH 7.4; ▼, pH 6.5; ●, pH 5.6; ▲, pH 4.5).

§Due to the slow activation kinetics of KST1 steady state was not reached within 3-s, 5-s, or even 20-s pulses. However, we have previously shown that results obtained with 3-s or 5-s pulses are qualitatively similar to those obtained with 20-s pulses (11, 12).

Measured open probabilities were fitted with Eq. **1** whereby the half-activation voltage $V_{1/2}$ was determined for each pH value independently, whereas the slope factor V_s was adjusted for each cell.

Cloning of K^+ Channel Sequences. Additional K^+ channel sequences were identified by reverse transcriptase–PCR experiments. For this purpose poly(A)$^+$ RNA was isolated from different plant species and tissues using the RNeasy extraction kit (Qiagen, Chatsworth, CA) in conjunction with paramagnetic beads (Dynal, Oslo). Obtained mRNA was reverse transcribed using Superscript RT (GIBCO/BRL) and an oligo(dT) 16-mer primer according to the manufacturers instructions. The resulting 1st strand cDNA was used in PCR experiments as template for the amplification of K^+ channel fragments. The primers used were designed on the basis of the plant K^+ channel consensus sequences FFAIDI (forward primers) and MLFNLG (reverse primers). Whenever possible codon usage-based primers were designed. In other cases inositoles substituted for variable bases within certain codons. Due to the choice of primers a 600-bp PCR fragment could be expected which was extracted from the agarose gel (Jet-Pure; Genomed, Bad Oeynhausen) and cloned into the *Eco*RV site of the pZERO plasmid (Invitrogen). Cloned K^+ channel fragments were verified by sequencing and sequences were deposited in GenBank database.

RESULTS

Protons Modulate the Voltage Dependence. To elucidate the molecular mechanism of pH sensing, K^+ uptake was studied after heterologous expression of *kst1* in *Xenopus* oocytes (*in vitro*) and in in its natural environment in isolated guard cell protoplasts from *Solanum tuberosum* (*in vivo*). Using the whole-cell configuration of the patch-clamp technique (21), we recorded inward K^+ currents in protoplasts in response to plasma membrane hyperpolarization. When changing the pH of the extracellular solution from 5.6 to 7.4, the currents of the inward rectifying K^+ channel decreased in a reversible manner (Fig. 1*A*). These two pH values reflect apoplastic conditions around closed (pH 7) and open stomata (pH 5) (8, 9). To test whether protons directly act on the channel protein we heterologously expressed *kst1* in *Xenopus* oocytes. Because the capability to activate upon acidification has been maintained in KST1 (Fig. 1*B*), the interaction with protons, like voltage and ATP activation (11, 12, 22), seems to reflect an intrinsic property of the K^+ channel protein. While the single-channel conductance of the guard cell channel (7.4 ± 0.8 pS, $n = 8$) (P.D. and R.H., unpublished data) was pH-insensitive (Fig. 1*C*) like the parameter $N{\cdot}i(V_F)$ obtained from experiments in oocytes (see *Materials and Methods*), the voltage-dependent activation of the K^+ uptake channel in isolated protoplasts changed as a function of the extracellular pH (Fig. 1*D*). With decreasing pH the half-maximum-activation potential $V_{1/2}$ shifted to less negative potentials.

The Role of Histidines in pH Sensing. Histidines, cysteines, and glutamates are proposed to mediate the proton block of animal inward-rectifying K^+ and cyclic nucleotide-gated channels (15, 23). Most strikingly KST1 contains no external cysteine, but two external histidines. One histidine is located within the linker between S3 and S4 (H160) and another in the outer pore (P) of the potato guard cell K^+ channel (H271) (Fig. 2*A*). To determine whether these histidines represent key amino acids of the pH sensor we generated histidine mutants of KST1. When both extracellular histidines were replaced by alanines, the double mutant KST1–H160A/H271A completely lost its pH dependence (Fig. 2 *B* and *C*). To distinguish between the relative contribution of these two sites we initially focused on the role of the pore histidine 271. Single mutations at this position affected the pH dependence drastically. Substitution by aspartate (KST1–H271D) further increased the pH sensitivity, whereas replacement of histidine by arginine (KST1-H271R) even inverted the pH dependence (Fig. 3 *A* and *B*). Following the removal of the charge at position 271 (KST1–H271A), KST1 still exhibits a significant but less pronounced pH sensitivity (Fig. 3*B*). In the next step we

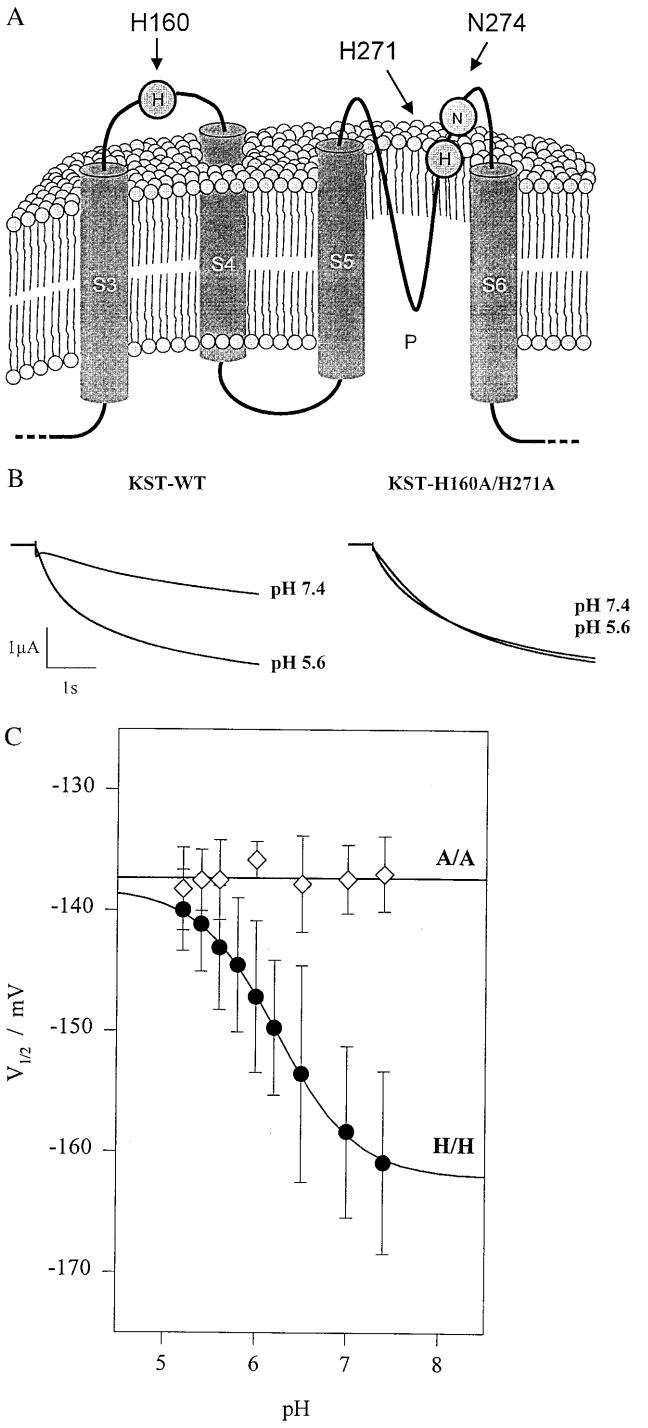

FIG. 2. pH-dependence of wild-type KST1 and the histidine double mutant. (*A*) Cartoon of the predicted topology of segments S3 to S6, including the pore region P and the extracellular linker between S3 and S4 [in relation to the *Shaker* K^+ channel structure (18)]. (*B*) Compared with wild-type (left traces) inward currents of the double mutant KST1-H160A/H271A were not affected by changes in the extracellular proton concentration (right traces). (*C*) In contrast to the wild-type (H/H) substitution of both histidines by alanine (A/A) resulted in a loss of pH-sensitivity of the half-maximum activation potential. Data points represent the mean ± SE of three to six measurements, and solid lines represents best fits according to Eq. **2**.

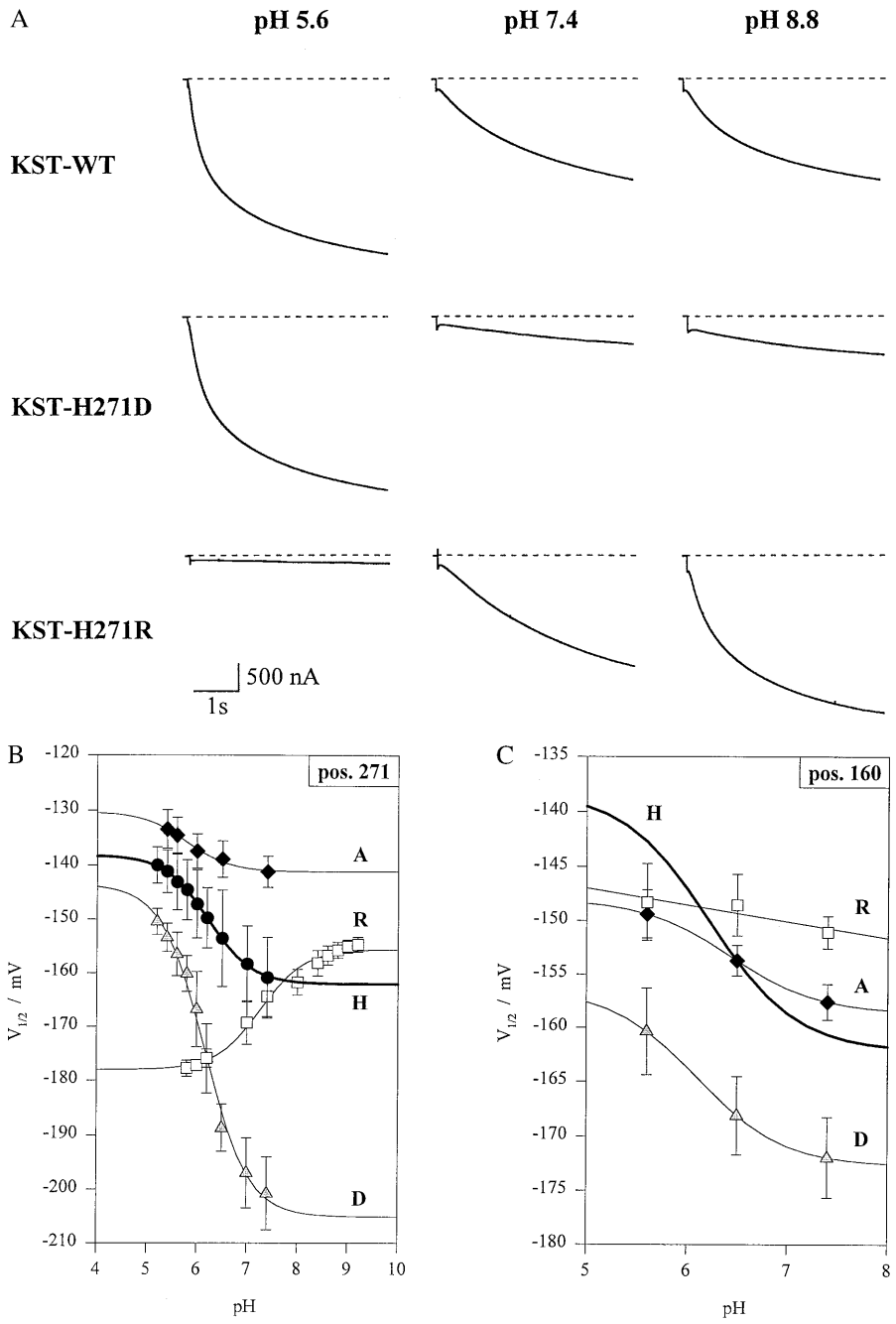

FIG. 3. pH-sensitivity of wild-type KST1 and single mutants. (*A Top*) Wild-type inward currents in response to pH 5.6, 7.4, and 8.8 in the bath medium. (*Middle*) Pronounced reduction of K^+ current in mutant KST1–H271D in response to an increase in extracellular pH from 5.6 to 7.4 and 8.8 with respect to wild-type KST1 and KST1–H271R. (*Bottom*) The mutant KST1–H271R converts the acid activation into an alkaline activation. Note the absence of inward K^+ current at pH 5.6 compared with wild-type KST1 and KST1–H271D. (*B*) pH-sensitivity of the half-activation potential ($V_{1/2}$) in wild-type KST1 (H) and the mutants KST1–H271R (R), –H271D (D), and –H271A (A) (n = 3–6). (*C*) Reduction in pH dependence of the mutants KST1–H160R (R), –H160A (A), and –H160D (D) compared with the wild-type channel (H) (n = 3–6). Solid lines represent best fits according to Eq. **2**.

analyzed H271-related mutations at position 160 (KST1–H160A, –H160D, –H160R). All these mutants independent of the charge at this site were less pH-sensitive, when compared with the wild type (Fig. 3*C*). Identical mutations in the pore asparagine 274 (Fig. 2*A*), however, did not alter the pH dependence (not shown). We therefore propose that both histidines in KST1 are required for the pH sensing mechanism.

The Pore Histidine Together with Asparagine Represent Plant-Specific Residues. To decide whether pH sensing based on histidines may represent a guard cell-specific feature, we identified further K^+ channel sequences from various plant species and cell types (Fig. 4). These new sequences (marked by an asterisk in Fig. 4) were aligned to known sequences of plants, yeast, bacteria, and animals. This comparison revealed that the histidine at position 271 together with asparagine N274 is highly conserved among plants, but is not restricted to the guard cell channels KST1 and KAT1. Kv1.3, a mammalian lymphocyte K^+ channel, contains the pore histidine, too (ref. 24 and Fig. 4). However, the pH sensitivity of Kv1.3 does not depend on this histidine (25).

DISCUSSION

In this study we demonstrated that acid activation of the potato guard cell K^+ uptake channel KST1 is due to a shift in the

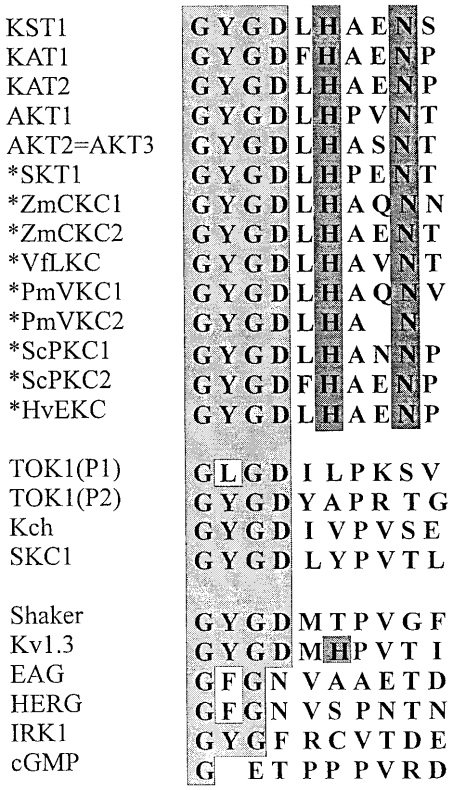

FIG. 4. Alignment of amino acids of the outer pore region C terminal to the GXG sequence from K^+ channels of plants, yeast, bacteria, and animals. We cloned *KAT*- and *AKT*-related K^+ channels (16, 17) (marked by an asterisk) from *Solanum tuberosum* epidermal fragments (SKT1), *Zea mays* coleoptiles (ZmCKC1 and -2), *Vicia faba* developing leafs (VfLKC), veins of *Plantago major* (PmVKC1 and -2), pollen of *Secale cereale* (ScPKC1 and -2), and *Hordium vulgare* epidermis (HvEKC). Note the conservation of a histidine (H271) close to an asparagine (N274) in plant K^+ channels only. The GenBank accession numbers of the aligned channel sequences are as follows: KST1 (X79779), KAT1 (M86990), KAT2 (U25694), AKT1 (X62907), AKT2 and AKT3 appear to be identical (U40154 and U44745), SKT1 (X86021), ZmCKC2 (Y07632), VfLKC1 (Y09749), ZmCKC1 (Y09747), PmVKC1 (Y09750), PmVKC2 (Y09751), ScPKC1 (Y09752), ScPKC2 (Y09753), HvEKC1 (Y09748), TOK1 (U28005), Kch (L12044), SKC1 (Z37969), Shaker (M17211), Kv1.3 (M30312), EAG (M61157), HERG (U04270), IRK1 (X73052), cGMP (X51604).

voltage dependence rather than an increase in the single-channel conductance (Fig. 1). This mechanism fundamentally differs from that found for cyclic nucleotide-gated and inward-rectifying K^+ channels in animals. In the latter protons block the open channel and thereby reduce the single-channel conductance (15, 23). Consequently, we would expect a different molecular basis for pH dependence in plant K^+ channels. In line with this hypothesis we identified a plant-specific histidine in the outer pore of K^+ uptake channels in all plant species and tissues investigated (Fig. 4). Because mutations of this residue in KST1 drastically affected the pH sensitivity we conclude that H271 plays a central role in the pH sensing mechanism. The conservation of the pore histidine may implicate that acid activation represents a common regulation mechanism of plant K^+ uptake channels. The histidine (H160) of the potato K^+ channel which seems to be related to the pH dependence of KST1 too, was not found in other plant K^+ uptake channels cloned so far. Variations at this position may therefore result in a species- and cell type-specific fine-tuning of the pH effect.

Because the pH-dependent shift of the half-activation voltage implicates interaction between pH sensing and gating, future detailed analyses will address the question about the molecular link between the pH and the voltage sensor.

We thank A. Basner and K. Zander as well as K. Neuwinger for technical assistance as well as Katrin Philippar and Peter Ache for supporting us with new K^+ channel sequences. We gratefully acknowledge E. Liman for providing us with the pGEMHE vector, and O. Pongs (Hamburg) for helpful comments on the manuscript. B.M.-R. is a Junior Scientist of the Max-Planck Society. These investigations were funded by Deutsche Forschungsgemeinschaft grants to R.H.

1. Weisenseel, M. H. & Jaffe, L. F. (1976) *Planta* **133,** 1–7.
2. Satter, R. L., Morse, M. J., Lee, Y., Crain, R. C., Coté, G. G. & Moran, N. (1988) *Bot. Acta* **101,** 205–213.
3. Cosgrove, J. (1993) *Plant Physiol.* **102,** 1–6.
4. Raschke, K. (1979) in *Encyclopedia of Plant Physiology: Physiology of Movements*, eds. Haupt, W. & Feinleib, M. E. (Springer, Berlin), pp. 383–441.
5. Shimazaki, K., Iino, M. & Zeiger, E. (1986) *Nature (London)* **319,** 324–326.
6. Behl, R. & Raschke, K. (1987) *Planta* **172,** 531–538.
7. Kochian, L. V. & Lucas, W. J. (1988) *Adv. Bot. Res.* **15,** 93–174.
8. Edwards, M. C., Smith, J. N. & Bowling, D. J. F. (1988) *J. Exp. Bot.* **39,** 1541–1547.
9. Mühling, K. H., Plieth, C., Hansen, U.-P. & Sattelmacher, B. (1995) *J. Exp. Bot.* **46,** 377–382.
10. Blatt, M. R. (1992) *J. Gen. Physiol.* **99,** 615–644.
11. Hedrich, R., Moran, O., Conti, F., Busch, H., Becker, D., Gambale, F., Dreyer, I., Küch, A., Neuwinger, K. & Palme, K. (1995) *Eur. Biophys. J.* **24,** 107–115.
12. Müller-Röber, B., Ellenberg, J., Provart, N., Willmitzer, L., Busch, H., Becker, D., Dietrich, P., Hoth, S. & Hedrich, R. (1995) *EMBO J.* **14,** 2409–2416.
13. Ilan, N., Schwartz, A. & Moran. N. (1996) *J. Membr. Biol.* **154,** 169–181.
14. Suzuki, M., Takahashi, K., Ikeda, M., Hayakawa, H., Ogawa, A., Kawaguchi, Y. & Sakai, O. (1994) *Nature (London)* **367,** 642–645.
15. Coulter, K. L., Périer, F., Radeke, C. M. & Vandenberg, C. A. (1995) *Neuron* **15,** 1157–1168.
16. Anderson, J. A., Huprikar, S. S., Kochian, L. V., Lucas, W. J. & Gaber, R. F. (1992) *Proc. Natl. Acad. Sci. USA* **89**, 3736–3740.
17. Sentenac, H., Bonneaud, N., Minet, M., Lacroute, F., Salmon, J.-M., Gaymard, F. & Grignon, C. (1992) *Science* **256,** 663–665.
18. Durell, S. R. & Guy, H. R. (1992) *Biophys. J.* **62,** 238–250.
19. Liman, E. R., Tytgat, J. & Hess, P. (1992) *Neuron* **9**, 861–871.
20. Stühmer, W. & Parekh, A. B. (1995) in *Single Channel Recording*, eds. Sakmann, B. & Neher, E. (Plenum, New York), pp. 341–355.
21. Hamill, O. P., Marty, A., Neher, E., Sakmann, B. & Sigworth, F. J. (1981) *Pflügers Arch.* **391,** 85–100.
22. Hoshi, T. (1995) *J. Gen. Physiol.* **105,** 309–328.
23. Root, M. J. & MacKinnon (1994) *Science* **265,** 1852–1856.
24. North, R. A. (1995) *Handbook of Receptors and Channels: Ligand- and Voltage-Gated Ion Channels* (CRC, Boca Raton, FL).
25. Kavanaugh, M. P., Varnum, M. D., Osborne, P. B., Christie, M. J., Busch, A. E., Adelman, J. P. & North, R. A. (1991) *J. Biol. Chem.* **266,** 7583–7587.

⇒ zurück zur Übersicht

1997

Dreyer, Antunes, Hoshi, Moeller-Roeber, Palme, Pongs, Reintanz, Hedrich

Plant K^+ channel α-subunits assemble indiscriminately.

Biophys. J. **72**:2143-2150.

Biophysical Journal Volume 72 May 1997 2143–2150

Plant K^+ Channel α-Subunits Assemble Indiscriminately

Ingo Dreyer,* Sónia Antunes,* Toshinori Hoshi,# Bernd Müller-Röber,§ Klaus Palme,¶ Olaf Pongs,‖ Birgit Reintanz,¶ and Rainer Hedrich*

*Institut für Biophysik, Universität Hannover, D-30419 Hannover, Germany, #Department of Physiology and Biophysics, The University of Iowa, College of Medicine, Iowa City, Iowa 52242 USA, §Max-Planck-Institut für Molekulare Pflanzenphysiologie, D-14476 Golm, Germany, ¶Max-Delbrück-Laboratorium in der Max-Planck-Gesellschaft, D-50829 Köln, Germany, and ‖Zentrum für Molekulare Neurobiologie, Institut für Neuronale Signalverarbeitung, D-20246 Hamburg, Germany

ABSTRACT In plants a large diversity of inwardly rectifying K^+ channels (K_{in} channels) has been observed between tissues and species. However, only three different types of voltage-dependent plant K^+ uptake channel subfamilies have been cloned so far; they relate either to KAT1, AKT1, or AtKC1. To explore the mechanisms underlying the channel diversity, we investigated the assembly of plant inwardly rectifying α-subunits. cRNA encoding five different K^+ channel α-subunits of the three subfamilies (KAT1, KST1, AKT1, SKT1, and AtKC1) which were isolated from different tissues, species, and plant families (*Arabidopsis thaliana* and *Solanum tuberosum*) was reciprocally co-injected into *Xenopus* oocytes. We identified plant K^+ channels as multimers. Moreover, using K^+ channel mutants expressing different sensitivities to voltage, Cs^+, Ca^{2+}, and H^+, we could prove heteromers on the basis of their altered voltage and modulator susceptibility. We discovered that, in contrast to animal K^+ channel α-subunits, functional aggregates of plant K_{in} channel α-subunits assembled indiscriminately. Interestingly, AKT-type channels from *A. thaliana* and *S. tuberosum*, which as homomers were electrically silent in oocytes after co-expression, mediated K^+ currents. Our findings suggest that K^+ channel diversity in plants results from nonselective heteromerization of different α-subunits, and thus depends on the spatial segregation of individual α-subunit pools and the degree of temporal overlap and kinetics of expression.

INTRODUCTION

Inwardly rectifying K^+ channels (K_{in} channels) have been found in all plant cells studied so far. Whereas their voltage-dependent properties were similar, their kinetics, selectivity, and susceptibility toward cationic blockers varied among cells, tissues, and plant species (see Hedrich and Dietrich, 1996, for review). Besides this large variety found in vivo, up to now on the molecular level only three different subfamilies of voltage-dependent inward K_{in} channels have been identified: they relate either to *Arabidopsis* KAT1 (Anderson et al., 1992), AKT1 (Sentenac et al., 1992) or AtKC1 (Reintanz et al., in preparation, GenBank accession no. U73325). Although these subtypes contain six transmembrane domains (S1–S6) and a pore region (P), they differ strongly in the putative extramembrane regions and in their expression pattern. The two KAT-type channels cloned as full-length clones so far, KAT1 from *Arabidopsis thaliana* and KST1 from *Solanum tuberosum*, are expressed in guard cells (Müller-Röber et al., 1995; Nakamura et al., 1995). They share an overall identity of 61%. Members of the AKT subfamily harbor, in contrast to KAT1 and KST1, a conserved ankyrin-binding domain within their C-termini. The two AKT-type channels used in this study, AKT1 from *A. thaliana*, which is predominantly expressed in roots (Basset et al., 1995; Lagarde et al., 1996), and SKT1 from *S. tuberosum* cloned from a leaf library (Müller-Röber et al., GenBank accession no. X86021) share an identity of 70%. A comparison of the AKT-type and KAT-type channels, however, revealed reciprocal identities of only ~45%. Recently, AtKC1 from *A. thaliana*, a member of a new subfamily, has been cloned (Reintanz et al., unpublished data). This channel shares identities of ~42% with KAT-type channels and of ~37% with AKT-type channels.

Functionally, plant K_{in} channels of the different types behave similarly. When expressed in yeast and animal cells like *Xenopus* oocytes or Sf9 insect cells, the gene products mediate hyperpolarization-activated, noninactivating, K^+-selective currents (Schachtman et al., 1992; Bertl et al., 1994; Bertl et al., 1995; Hedrich et al., 1995; Hoshi, 1995; Müller-Röber et al., 1995; Véry et al., 1995; Gaymard et al., 1996; Ketchum and Slayman, 1996; Marten et al., 1996). An in vivo–in vitro comparison between a cloned channel and the K^+ channel in its natural environment has only been performed for KST1 so far. When expressed in *Xenopus* oocytes this channel seems to possess all of the basic properties, such as voltage-dependence, kinetics, and selectivity, of the inward rectifier in *S. tuberosum* guard cells (Müller-Röber et al., 1995). Its pH-sensitivity and susceptibility toward Cs^+ ions, however, were less pronounced (Dietrich et al., unpublished data). This difference might indicate that KST1 is posttranslationally modified in the guard cell, or alternatively interacts with other cellular components, such as other α-subunits, β-subunits, or metabolites.

Plant voltage-dependent K_{in} channels represent members of the large gene family of potassium channels (Jan and Jan,

Received for publication 7 October 1996 and in final form 18 February 1997.

Address reprint requests to R. Hedrich, Julius-von-Sachs-Institut für Biowissenschaften, Lehrstuhl Botanik I, Mittlerer Dallenbergweg 64, 97082 Würzburg, Germany. Fax: 49-931-888-6157; E-mail: hedrich@botanik.uni-wuerzburg.de.

0006-3495/97/05/2143/08 $2.00

1994). On the level of the amino acid sequence they are structurally related to animal voltage-dependent outward rectifiers (K_v; Chandy and Gutman, 1994) or *eag* channels (Warmke et al., 1991) containing the *Shaker*-channel-like motives S1–S6 and P. Functionally, however, they are different. Like animal inward rectifiers (K_{ir}, Doupnik et al., 1995), upon hyperpolarization K_{in} channels catalyze K^+ uptake into the cytoplasm. In the related animal field the large functional diversity of K^+ channels at least partially seems to result from heterooligomerization of α-subunits (Christie et al., 1990; Isacoff et al., 1990; Ruppersberg et al., 1990; Covarrubias et al., 1991). Voltage-dependent outwardly rectifying channels as well as inwardly rectifying channels segregate structurally and functionally into diverse subfamilies (e.g., *Shaker*, *Shal*, *Shab*, and *Shaw*, Salkoff et al., 1992; Doupnik et al., 1995). With a few recently reported notable exceptions (Glowatzki et al., 1995; Shahidullah et al., 1995; Chen et al., 1996; Hugnot et al., 1996; Pessia et al., 1996), heteromultimers are assumed not to be formed among different subclasses, but between subunits from the same subfamily only. The assembly within subfamilies seems to require highly conserved N-terminal tetramerization domains (Li et al., 1992; Shen et al., 1993).

The structural similarity of cloned plant K^+ channels to the K_v channel family and the fact that KST1 after heterologous expression differ from its in vivo counterpart suggests that also in plants K^+ channel diversity is caused by heteromultimerization.

MATERIALS AND METHODS

Electrophysiology

Experiments were performed on RNA-injected, voltage-clamped *Xenopus* oocytes using a two-electrode voltage clamp approach as previously described by Hedrich et al. (1995). RNA concentrations were quantified spectroscopically (Spectrometer DU-64, Beckmann, Germany). Because some channel properties of plant K^+-channels differ with the expression level (Véry et al., 1994, Cao et al., 1995), oocytes with similar K^+ current amplitudes were selected for analysis only.

Solutions

External standard solution was composed of 30 mM KCl, 2 mM $MgCl_2$, 1 mM $CaCl_2$, and 10 mM MES/Tris, pH 5.6. Solutions for Cs^+ experiments contained additionally 200 μM–2 mM CsCl. Experiments with regard to the Ca^{2+} sensitivity were performed in 30 mM KCl, and 10 mM MES/Tris, pH 5.6. Various mol fractions of 30 mM between $CaCl_2$ and $MgCl_2$ were used to maintain the ionic strength. All solutions were adjusted to 220 mosmol/kg with sorbitol.

Biophysical analysis

Relative open probability

Relative open probabilities were deduced from a double voltage-step protocol. Time- and voltage-dependent K^+ currents were elicited in response to activation pulses (1 s) to voltages between +100 mV and −170 mV in −10-mV increments. During the second voltage step (1 s) to V_F = −70 mV K^+ currents relaxed in a time-dependent manner. The instantaneous current voltage relationship [$I_0(V)$], obtained from extrapolating the relaxation time course of the second pulse to $t = 0$ with an exponential function, is proportional to the relative open probability [$p_O(V)$] at the end of the activation pulse: $I_0(V) = N \cdot i(V_F)p_O(V) = const.\ p_O(V)$, where N denotes the number of potassium channels within the membrane and $i(V_F)$ the single channel current at −70 mV [$N \cdot i(V_F) = const.$]. To make sure not to measure a leak, in the mutant KAT1-S168R, which is not entirely closed in the voltage range tolerated by the oocyte (≈−180 mV–+100 mV), 10 mM Cs^+ were used to completely block the channels at negative potentials (cf. Becker et al., 1996). Theoretical predictions for relative open probabilities in Fig. 1 *B* were calculated according to the equation

$$p_O(V) = \frac{c_{KAT1} p_O^{KAT1}(V) + c_{KAT1\text{-}S168R} p_O^{KAT1\text{-}S168R}(V)}{c_{KAT1} + c_{KAT1\text{-}S168R}},$$

where c_{KAT1} and $c_{KAT1\text{-}S168R}$ denotes the relative amount of injected KAT1- and KAT1-S168R-RNA, respectively. The relative open probabilities $p_O^{KAT1}(V)$ and $p_O^{KAT1\text{-}S168R}(V)$ were determined experimentally (cf. Fig. 1 *A*).

Ion block

To obtain the instantaneous current-voltage characteristic of the open channel [$I_T(V)$] the membrane voltage after approaching steady-state acti-

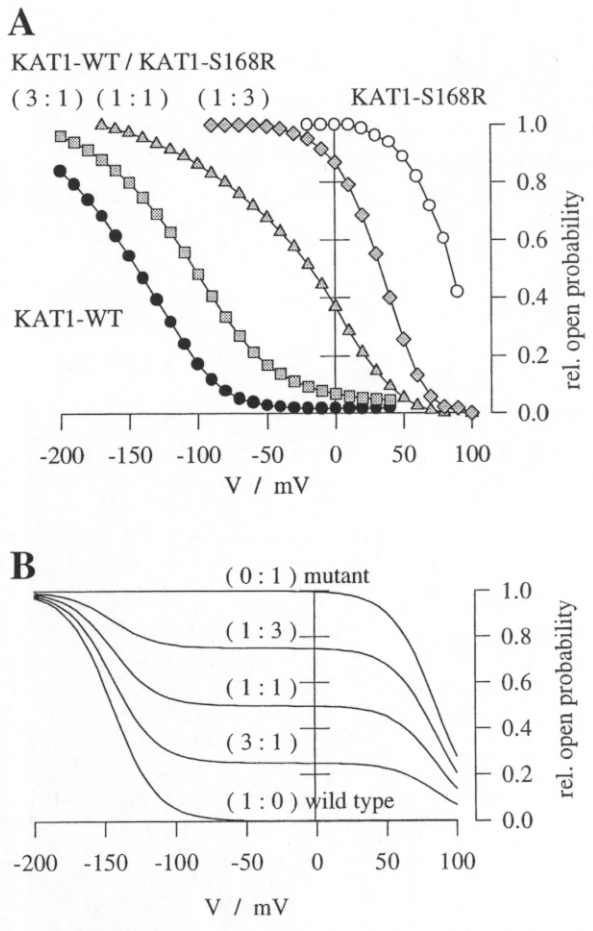

FIGURE 1 Co-expression of wild-type KAT1 and mutant KAT1-S168R in *Xenopus* oocytes. (*A*) Voltage-dependent relative open-probabilities of the K^+ channel homomers and heteromers recorded in representative oocytes injected with different fractions of KAT1-WT/KAT1-S168R cRNA: wild type (*closed circles*), KAT1-S168R (*open circles*), and 3:1 (*squares*), 1:1 (*triangles*), and 1:3 (*rhombi*) mixtures. (*B*) Theoretical predictions for relative open-probabilities for the experiment shown in (*A*) under the assumption that plant K_{in} channels are monomers.

vation at $V = -150$ mV was stepped subsequently to various values between +20 mV and −180 mV. $I_T(V)$ relationships were deduced from extrapolating the tail current onset to $t = 0$. Current-voltage relationships of tail-currents in the presence of an antagonist were fitted according to the Woodhull model (Woodhull, 1973):

$$I_T(V) = I_T^0(V)\frac{1}{1 + e^{-((zF/RT)\delta(V - V_{Block1/2}))}}$$

where $I_T^0(V)$ denotes the current in the absence of the blocking ion, z its valence and δ the fraction of the transmembrane voltage sensed by the ion. F, R, and T have their usual meaning. The half-blocking voltage $V_{Block1/2}$ could be obtained from $I_T(V_{Block1/2}) = \frac{1}{2}I_T^0(V_{Block1/2})$.

Molecular biology

The mutant KAT1-T256E was generated according to Becker et al. (1996). KAT1S168R*pYES2–2 is based on the wild-type KAT1*pYES2–2 received from Rick Gaber. The mutation was introduced by using standard polymerase chain reaction-mediated cassette mutagenesis. The segment between *Eco*R1 and *Xcm*1 of the coding sequence area was amplified using two oligonucleotides, with one of them containing the S168R mutation. The amplified segment was digested with *Eco*R1 and *Xcm*1 and ligated into KAT1*pYES2–2 digested with *Eco*R1 and partially with *Xcm*1. The PCR-amplified segment was sequenced by the University of Iowa DNA core (ABI sequencer). Finally, the reconstituted mutant cDNA was cloned into the pGEMHE expression cassette (Liman et al., 1992). To produce the mutant KST1-H271R, a silent mutation creating a novel *Bgl*II site was first introduced into the KST1 coding region upstream of the H271 codon. This modification was achieved by exchanging the *Sph*I fragment of the *KST1* cDNA in the plasmid pKST1#8–1 (Müller-Röber et al., 1995) with a corresponding PCR fragment amplified with primers P1 (5′-CCATTC-CAATCATTGATCCTCG-3′) and P2 (5′-CTCAGCATGCAGATCTC-CATAACCG-3′). In the following step, the *Bgl*II/*Sty*I fragment of the modified *KST1*-sequence was replaced by a fragment generated via PCR using reverse primer P3 (5′-TTGCTTCGGAGGGAAGTATTCAGCTTC-3′) and forward primer P4 (5′-CGGTTATGGAGATCTGCGAGCT-GAGAACTC-3′).

Vectors used for the production of cRNA were based on plasmid pGEMHE (Liman et al., 1992). Construction of the *KST1* plasmid was described in Müller-Röber et al. (1995) and of the *KAT1* plasmid in Hedrich et al. (1995). For SKT1 the complete *SKT1* cDNA (GenBank accession no. X86021) was cloned as an *Asp*718/*Eco*R1 fragment into the *Sma*I site of pGEMHE. The *AKT1* cDNA was kindly provided by Dr. H. Sentenac. The AKT1 coding region was excised, subcloned, and inserted into the pGEMHE expression cassette. The AtKC1 coding region was excised from the *AtKC1* cDNA (GenBank accession no. U73325) and inserted into the pGEMHE expression cassette. cRNA was produced as described by Hedrich et al. (1995).

RESULTS

Plant K^+ channel α-subunits form multimers

The outward-rectifying *Shaker*-related K^+ (K_v channels), (MacKinnon, 1991; Liman et al., 1992) and the inward-rectifying IRK-related potassium channels (K_{ir} channels), (Glowatzki et al., 1995; Yang et al., 1995) show a tetrameric structure. To demonstrate whether or not the plant K_{ir} channels also form multimers, wild-type KAT1 and KAT1-S168R were co-expressed in *Xenopus* oocytes. The latter, modified in the putative voltage sensor S4, half-activates ($V_{1/2}$) at ~+85 mV compared to −140 mV for KAT1 (Fig. 1 *A*). When co-injected into oocytes, K^+ channels with intermediate gating behavior were created. With an increasing relative amount of mutant cRNA the voltage-dependent relative open probability shifted toward $V_{1/2}$ of KAT1-S168R (Fig. 1 *A*). This behavior could not be described by the sum of the relative open probabilities of the α-subunit homomers (see Materials and methods), indicating the formation of heteromeric channels rather than assembly within independent homomeric pools (Fig. 1 *B*). In contrast, co-expression of a mutant of the plant inward rectifier KAT1, KAT1-T256E, which differs from wild-type KAT1 in its susceptibility to blocking ions (Becker et al., 1996), and the structurally related outward rectifier *reag* cloned from rat brain (Ludwig et al., 1994) elicited inward and outward K^+ currents (Fig. 2 *A*). For this combination steady-state current-voltage characteristics as well as voltage-dependent relative open probabilities could be resolved and demonstrated as arising from two homomeric entities (Fig. 2, *B* and *C*), indicating differential assembly of KAT1 and *reag*. In line with the hypothesis that not even the animal K^+

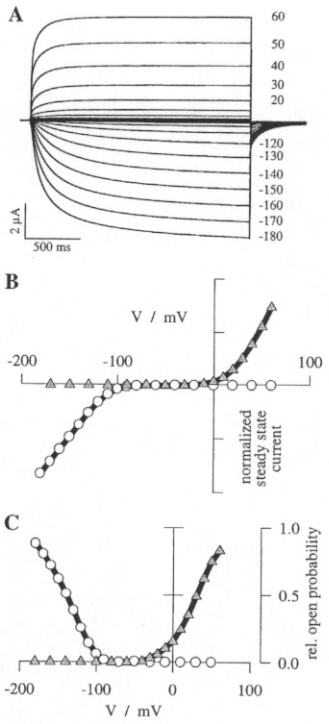

FIGURE 2 Co-expression of plant KAT1-T256E and *reag* (5:1 mixture) in *Xenopus* oocytes. The fraction of 5:1 was used to obtain inward and outward currents of similar amplitudes. Different fractions did not change the result qualitatively. (*A*) Representative inward and outward K^+ currents. From a holding potential of −30 mV currents were evoked by activating voltage-pulses to voltages indicated in millivolts. (*B*) Steady-state current-voltage characteristic (*solid lines*) and (*C*) voltage-dependent relative open probability (*solid lines*) for the oocyte shown in (*A*) superimposed with the respective relationships of homomeric KAT1-T256E (*open circles*) and *reag* (*gray triangles*). Relative open probabilities and steady-state current-voltage relationships of the homomers were determined in oocytes into which similar amounts of either KAT1-T256E- or *reag*-RNA, respectively, were injected. Steady-state current voltage characteristics of the single transporters were normalized to maximum currents measured in the mixture.

channels with the highest degree of homology to the plant inward rectifiers assemble with the "green" channels, permeation properties of K^+ inward currents were not altered (cf. next paragraphs). Inward currents could, e.g., be entirely suppressed by 1 mM Cs^+ (data not shown) as has been shown for KAT1-T256E homomers [Becker et al., 1996; cf. Fig. 2, *B* and *C* (*gray triangles*)].

Strategy to investigate assembly of plant K^+ channels

To test whether α-subunits from different plant species and tissues form heteromers we used the following strategy (Fig. 3): α-subunits "A" and "B" were co-expressed in *Xenopus* oocytes. Whereas "A" exhibited a pronounced phenotype, homomeric "B" did not carry K^+ currents. A change in the phenotype "A" thus provides evidence for the heteromerization of the two different α-subunits.

K^+ channel α-subunits from guard cells of different species co-aggregate

Initially we probed for the assembly of the guard cell K^+ channels KAT1 from *A. thaliana* (Anderson et al., 1992; Nakamura et al., 1995) and KST1 from *S. tuberosum* (Müller-Röber et al., 1995). Because both channels differ in their kinetics but are similar in their selectivity and in their sensitivity to blocking ions, to discriminate between selective and nonselective assembly more easily we used mutants with distinct properties: besides the increased Cs^+ sensitivity, KAT1-T256E, in contrast to the wild-type KAT1, is characterized by a voltage-dependent Ca^{2+} block (Becker et al., 1996), whereas KST1-H271R is altered in its pH-dependence. At pH 5.6 the latter activates more negative than −180 mV. At higher pH values the activation threshold shifts more positive (Hoth et al., 1997). Therefore, under our experimental conditions (an external pH of 5.6 and voltages between −170 mV and +20 mV) the homomeric KST1-H271R channel was electrically silent. In contrast to the Ca^{2+}-sensitive KAT1 mutant KAT1-T256E, KST1-H271R like the KST1 wild type was insensitive to extracellular Ca^{2+} (data not shown). When co-injected at a ratio of 1:3, kinetics of K^+ currents mediated by the hybrid channels were slowed more than threefold compared to KAT1-T256E (Fig. 4 *A*). Moreover, K^+ currents exhibited an intermediate susceptibility toward Ca^{2+} ions. Whereas

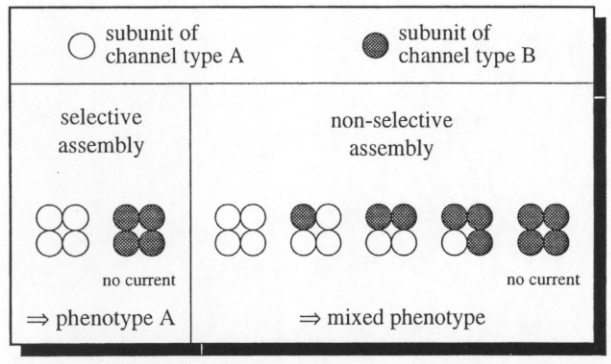

FIGURE 3 Cartoon of K^+ channel phenotypes following selective and nonselective assembly from a current-mediating ("A") and an electrically silent ("B") subunit. Because plant K^+ channels might be formed by four subunits, like the *Shaker* and IRK K^+ channels (MacKinnon, 1991; Liman et al., 1992; Glowatzki et al., 1995; Yang et al., 1995), in the presence of subunits from two different channel types, subunits could either assemble indiscriminately or form homomultimers.

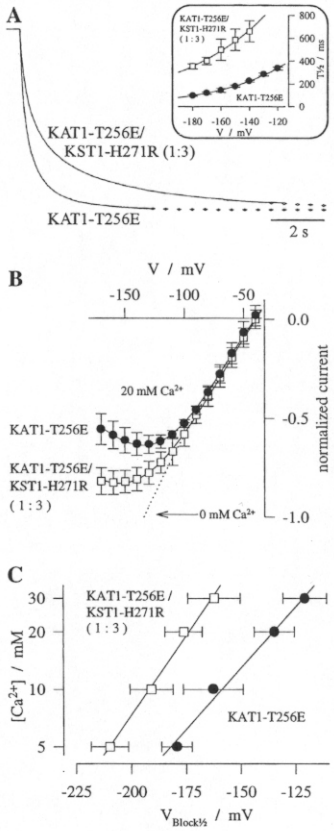

FIGURE 4 Co-expression of the Ca^{2+}-sensitive KAT1 mutant KAT1-T256E and the Ca^{2+}-insensitive KST1 mutant KST1-H271R. At pH 5.6 KST1-H271R activates more negatively than −180 mV (Hoth et al., 1997). Each data point represents the mean of five measurements ± standard error of the mean. (*A*) Co-expression slows activation kinetics of KAT1-T256E. Representative K^+ currents mediated by KAT1-T256E and KAT1-T256E/KST1-H271R mixtures (1:3). Currents were evoked by activation pulses to −150 mV starting from a holding potential of −30 mV. Current amplitudes were normalized to the steady-state value of −2.2 μA for KAT1-T256E and −2.4 μA for the KAT1-T256E/KST1-H271R mixture (1:3). *Inset*: Comparison of the voltage-dependence of the half-activation time ($T_{1/2}$). Solid lines represent best fits with an exponential function. (*B*) Co-expression reduces the Ca^{2+} sensitivity of KAT1-T256E. Tail currents recorded in 20 mM Ca^{2+} for KAT1-T256E (*closed circles*) and KAT1-T256E/KST1-H271R (1:3, *open squares*) after an activating pre-pulse to −150 mV are superimposed. The dotted line represents tail currents through KAT1-T256E and KAT1-T256E/KST1-H271R in the absence of Ca^{2+} ions, and solid lines represent best fits according to the Woodhull model (Woodhull, 1973). (*C*) Concentration- and voltage-dependence of the Ca^{2+} block. Half-blocking voltages ($V_{Block1/2}$) were determined in different Ca^{2+} concentrations (5, 10, 20, and 30 mM). Note the logarithmic scale of the concentration axis.

for KAT1-T256E 7 mM Ca^{2+} were sufficient to inhibit the K^+ current at −170 mV by ~50%, a related block of the hybrid channels required more than three times the Ca^{2+} concentration (Fig. 4, *B* and *C*).

Guard cell and root K^+ channels from different species form heteromers

Because the two guard cell channels from *A. thaliana* and *S. tuberosum*, KAT1 and KST1, belong to the same K^+ channel subfamily, we could not exclude the possibility that the assembly was tissue- or subtype-dependent. Therefore, we co-injected the guard cell KAT1-related mutants with AKT1 (Sentenac et al., 1992) and SKT1 (GenBank accession no. X86021), members of the AKT subtype, as well as with AtKC1 (Reintanz et al., GenBank accession no. U73325), a member of a new subfamily. AKT1 and AtKC1 from *A. thaliana* are predominantly expressed in roots (Basset et al., 1995, Lagarde et al., 1996; Reintanz et al., unpublished data) whereas SKT1 was cloned from a leaf library of *S. tuberosum* but also showed expression in roots (Müller-Röber et al., unpublished data). When injected alone into *Xenopus* oocytes these channels were electrically silent. After co-injection of SKT1 with the KAT1 mutant T256E, however, K^+ currents were present that were less Ca^{2+} sensitive (Fig. 5 *A*) and had slower kinetics than KAT1-T256E homomers (data not shown, cf. Fig. 4 *A*). Co-expression of SKT1 and KST1 wild type, both cloned from an epidermal fragment library, resulted in channels with increased Cs^+ sensitivity (Fig. 5 *B*). When co-injecting the two silent subunits, KST1-H271R and SKT1, together they created K^+ currents of intermediate pH dependence compared to the mutant and KST1 wild type (data not shown). This might indicate that the presence of SKT1 α-subunits rescues KST1-H271R from the inability to activate at moderate voltages under acidic conditions. Similar results were obtained by co-expressing AKT1 with KAT1-T256E and KST1, respectively. K^+ currents resulting from hybrid AKT1/KAT1-T256E channels were less susceptible to Ca^{2+} (Fig. 5 *C*). At −170 mV the K_i was 25 mM compared to 7 mM for homomeric KAT1-T256E multimers. K^+ currents obtained from AKT1/KST1 mixtures had an increased Cs^+-sensitivity (Fig. 5 *D*). The K_i at −150 mV was 40 μM compared to 500 μM for the KST1 wild type.

The heterooligomerization between AtKC1 and KST1 on one side, and AtKC1 and KAT1-S168R on the other, has already been apparent during steady-state activation of the multimers. These subunit mixtures shifted the voltage dependence ($V_{1/2}$) to more negative potentials than KAT1-S168R and KST1, respectively (Fig. 5, *E* and *F*). An unusual S4 segment of AtKC1 may bring about a $V_{1/2}$ more negative than −200 mV, which is not tolerated by *Xenopus* oocytes. When heterooligomerized with other channel subunits, however, its activation threshold is shifted positive into the voltage range tolerated by *Xenopus* oocytes. Like SKT1 and AKT1, the presence of AtKC1 significantly

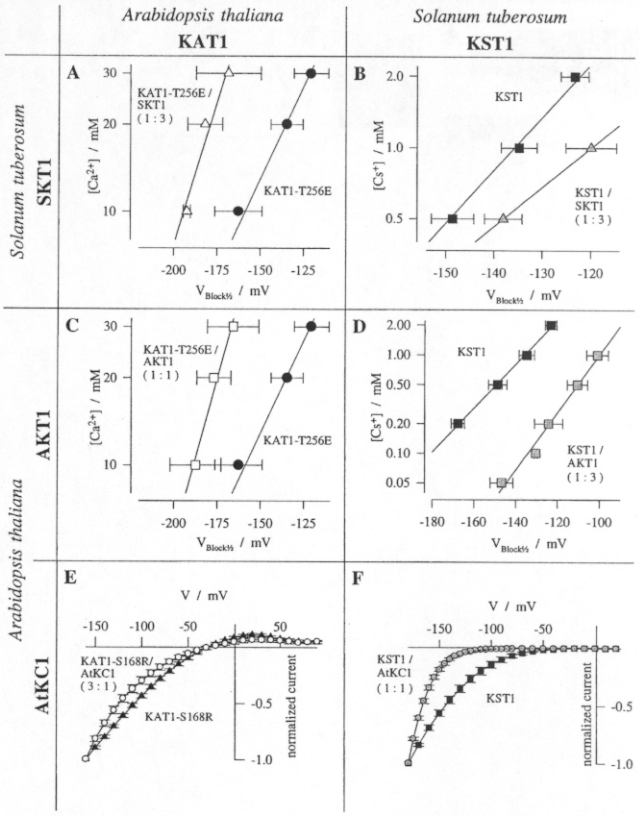

FIGURE 5 Co-expression of K^+ channel α-subunits from different cells/tissues and plant species. KAT-homologs (KAT1, KST1) and AKT-homologs (AKT1, SKT1) were from *Arabidopsis thaliana* and *Solanum tuberosum* and AtKC1 from *A. thaliana*. AKT1 and AtKC1, as well as SKT1 homomultimers, were electrically silent when expressed alone in oocytes. Each data point represents the mean of 3 to 10 measurements ± standard error of the mean. (*A* and *C*) Concentration- and voltage-dependence of the Ca^{2+} block in KAT1-T256E (*closed circles*), and in the subunit mixtures KAT1-T256E/SKT1 (1:3, *A*, *open triangles*), and KAT1-T256E/AKT1 (1:1, *C*, *open squares*). (*B* and *D*) Cs^+-sensitivity of KST1 wild type (*closed squares*), and the mixtures KST1/SKT1 (1:3, *B*, *gray triangles*), and KST1/AKT1 (1:3, *D*, *gray squares*). (*E* and *F*) Steady-state current-voltage relationships of KAT1-S168R (*E*, *closed triangles*), KAT1-S168R/AtKC1 (3:1, *F*, *open circles*), KST1 wild type (*F*, *closed squares*), and KST1/AtKC1 (1:1, *F*, *gray circles*). Here a normalized current of −1.0 corresponds to a whole-cell current of ~−1.1 μA in KAT1-S168R/AtKC1-, −1.8 μA in KAT1-S168R-, −4.5 μA in KST1-, and −1 μA in KST1/AtKC1-oocytes. Note the logarithmic scale of the concentration axes in (*A*—*D*).

increased the Cs^+-sensitivity of the K^+ currents compared to wild-type KST1 and KAT1-S168R (data not shown).

Since neither AtKC1 alone nor in combination with the electrically silent subunits SKT1 and AKT1 did carry measurable K^+ currents, a proof for or against assembly between these α-subunits could not be furnished. To our surprise, however, co-expression of the two silent channels SKT1 and AKT1 produced K^+ currents in *Xenopus* oocytes (Fig. 6). These currents show the highest Cs^+ sensitivity observed so far. The Cs^+ block was already visible at a concentration of 2 μM. At −150 mV the half-blocking concentration was 15 μM, a K_i ~70-fold lower than for

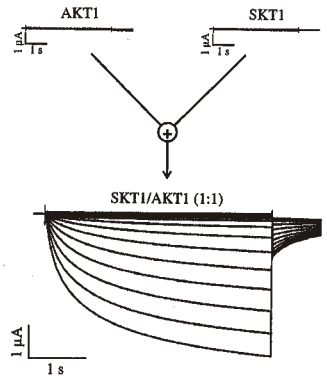

FIGURE 6 The two silent subunits, AKT1 and SKT1, form active channels upon co-expression. Representative current families from oocytes expressing AKT1, SKT1, and AKT1/SKT1 (1:1 mixture), respectively. Currents were elicited by 4-s voltage steps from +10 mV to −150 mV (10-mV steps) followed by a voltage step to −70 mV from a holding potential of −30 mV.

KAT1 and KST1 when studied at comparable current amplitudes. Thus the Cs^+ sensitivity of AKT1 and SKT1 might account for the increased Cs^+ sensitivity in KST1/SKT1 and KST1/AKT1 heteromers as well (cf. Fig. 5, *B* and *D*).

DISCUSSION

By taking advantage of K^+ channel mutants affected in sensitivity toward changes in voltage, pH, Cs^+, and Ca^{2+}, we could demonstrate, from the change of two independent biophysical parameters (gating and permeation), heteromeric assembly of plant K_{in} channel α-subunits. Although heteromerization within a K^+ channel subfamily (KAT1 with KST1) was not a surprising result, assembly of plant K^+ channel subunits was different from processes known for the animal K_v and K_{ir} channel families (Covarrubias et al., 1991; Salkoff et al., 1992; Pessia et al., 1996). Whereas in animals a molecular barrier to heteropolymerization seems to exist, for plants we could show the nonselective assembly among channel subtypes originating from different tissues and even different plant families.

The most striking result was the oligomerization of KAT1 with SKT1 α-subunits and of KST1 with AKT1 or AtKC1 α-subunits. This indiscriminate assembly would be comparable to a heteromultimerization of, e.g., *Shaker*-type subunits from rat brain and *Shal*-type subunits from human heart.

Physiologically significant, however, was the heterooligomerization of α-subunits of different channel subfamilies within one and the same species (KST1 with SKT1, and KAT1 with AKT1 or AtKC1). This interesting finding might explain the above-mentioned (see Introduction) difference between the heterologously expressed channel KST1 and the channel in its natural environment. For example, the Cs^+ sensitivity of the inwardly rectifying potassium channel in *S. tuberosum* guard cells is ~10-fold more pronounced than in KST1 expressed in oocytes. Heteromerization of KST1 α-subunits with subunits of the AKT-type (not necessarily SKT1) in guard cells could be responsible for this contrariety.

Less striking but more spectacular was the result of co-injecting *SKT1*- and *AKT1*-RNA. In contrast to the SKT1 and AKT1 homomers that were inactive in *Xenopus* oocytes, their heteromers formed active K^+ channels of the highest Cs^+ sensitivity observed so far. This result becomes even more strange when taking into account that AKT1 and SKT1 homomers were functionally expressed in Sf9 insect cells and yeast (Sentenac et al., 1992; Bertl et al., 1994; Gaymard et al., 1996; Müller-Röber et al., unpublished data). Although the genuine reason for this discrepancy is still unknown, some recent experimental findings indicate modifications of heterologously expressed channels by the expression system. First evidence for expression system-dependent functional differences have been observed with KAT1. Like all investigated plant inward rectifiers in vivo (Hedrich and Dietrich, 1996), when expressed in oocytes KAT1 is characterized by a significant NH_4^+ permeability (Schachtman et al., 1992). Expressed in Sf9 cells and yeast, however, KAT1 lost its NH_4^+ permeability (Bertl et al., 1995; Marten et al., 1996). This change in the permeation properties might result either from differences in protein glycosylation and phosphorylation, or that native peptides assemble with K^+ channel α-subunits. In a similar way cytoplasmic factors or even β-subunits present in individual expression systems may enable functional expression of channels. Recently, putative plant β-subunits (Tang et al., 1995) with a high degree of homology with the animal K^+ channel β-subunits (Heinemann et al., 1994; Pongs, 1995) have been discovered. Inasmuch as the latter contain amino acid stretches similar to regions in the N-terminus of the *Shaker* channels, they might be able to interact with the α-subunit.

Even if plant K^+ channel α-subunits seem to heterooligomerize without preference, to date we cannot exclude defined stoichiometries within the aggregates. Nevertheless, the physiological aspects of the following questions can be discussed: why is the assembly within the plant K_{in} family different from that in the animal K_v or K_{ir} families? Why is the molecular barrier to heteropolymerization—if it actually exists in the K_{in} family—so weak? What could be the advantage for the plant?

In contrast to animal potassium channels, plant K_{in} channels are not involved in fast signal transduction but are predominantly required for long-term potassium uptake. The centralized processing of signals in animals demands a maximum amount of synchronization of the transducing cells. To reduce their sensitivity to disturbances, blending of multiple K^+ channel types might be the best way for each cell to fine-tune its electrical properties. Inevitably the cells accept the disadvantage to have to drive a high expenditure in protein expression. The local decentralized perception and response to environmental signals, on the other hand, makes plants less sensitive to disturbances in signal transduction. Not facing this handicap, nonselective assembly of

K^+ channel α-subunits could be advantageous for the plant to be able to adapt more easily to its environment. By temporal overlap and kinetics of α-subunit expression, plants might obtain a maximum of flexibility to alter the whole-cell K^+ current features during cell growth, development, and reproduction with a minimum of expenditure.

We thank Michaela Lehnen (MDL, Köln), Gabriele Nast (Institut für Genbiologische Forschung Berlin GmbH), and Kerstin Neuwinger (Hannover) for expert technical assistance. Furthermore, we are grateful to Chris Readhead (Köln), and Stefan Hoth and Dirk Becker (Hannover) for helpful comments on the manuscript.

This work was supported by Deutsche Forschungsgemeinschaft Grants 1640/1-3 (to R.H.) and 1640/9-10 (to R.H. and K.P.). Partial support was provided by National Institutes of Health Grant GM51474 (to T.H.).

REFERENCES

Anderson, J. A., S. S. Huprikar, L. V. Kochian, W. J. Lucas, and R. F. Gaber. 1992. Functional expression of a probable *Arabidopsis thaliana* potassium channel in *Saccharomyces cerevisiae*. *Proc. Natl. Acad. Sci. U.S.A.* 89:3736–3740.

Basset, M., G. Conejero, M. Lepetit, D. Fourcroy, and H. Sentenac. 1995. Organization and expression of the gene coding for the potassium channel transport system AKT1 of *Arabidopsis thaliana*. *Plant Mol. Biol.* 29:947–958.

Becker, D., I. Dreyer, S. Hoth, J. D. Reid, H. Busch, M. Lehnen, K. Palme, and R. Hedrich. 1996. Changes in voltage activation, Cs^+ sensitivity, and ion permeability in H5 mutants of the plant K^+ channel KAT1. *Proc. Natl. Acad. Sci. U.S.A.* 93:8123–8128.

Bertl A., J. A. Anderson, C. L. Slayman, H. Sentenac, and R. F. Gaber. 1994. Inward and outward rectifying potassium currents in *Saccharomyces cerevisiae* mediated by endogenous and heterologously expressed ion channels. *Folia Microbiol. (Praha).* 39:507–509.

Bertl, A., J. A. Anderson, C. L. Slayman, and R. S. Gaber. 1995. Use of *Saccharomyces cerevisiae* for patch-clamp analysis of heterologous membrane proteins: characterization of KAT1, an inward-rectifying K^+ channel from *Arabidopsis thaliana*, and comparison with endogenous yeast channels and carriers. *Proc. Natl. Acad. Sci. U.S.A.* 92:2701–2705.

Cao, Y., J. M. Ward, W. B. Kelly, A. M. Ichida, R. F. Gaber, J. A. Anderson, N. Uozumi, J. I. Schroeder, and N. Crawford. 1995. Multiple genes, tissue specificity, and expression-dependent modulation contribute to the functional diversity of potassium channels in *Arabidopsis thaliana*. *Plant Physiol.* 109:1093–1106.

Chandy, K. G., and G. A. Gutman. 1994. Voltage-gated potassium channel genes. *In* Handbook of Receptors and Channels. R. A. North, editor. CRC Press, Inc., Boca Raton, FL. 1–71.

Chen, M. L., T. Hoshi, and C. F. Wu. 1996. Heteromultimeric interactions among K^+ channel subunits from *Shaker* and *eag* families in *Xenopus* oocytes. *Neuron.* 17:535–542.

Christie, M. J., R. A. North, P. B. Osborne, J. Douglass, and J. P. Adelman. 1990. Heteropolymeric potassium channels expressed in *Xenopus* oocytes from cloned subunits. *Neuron.* 4:405–411.

Covarrubias, M., A. Wei, and L. Salkoff. 1991. *Shaker*, *Shal*, *Shab*, and *Shaw* express independent K^+ current systems. *Neuron.* 7:763–773.

Doupnik, C. A., N. Davidson, and H. A. Lester. 1995. The inward rectifier potassium channel family. *Curr. Opin. Neurobiol.* 5:268–277.

Gaymard, F., M. Cerutti, C. Horeau, G. Lemaillet, S. Urbach, M. Ravallec, G. Devauchelle, H. Sentenac, and J. B. Thibaud. 1996. The baculovirus/insect cell system as an alternative to *Xenopus* oocytes. First characterization of the AKT1 K^+ channel from *Arabidopsis thaliana*. *J. Biol. Chem.* 271:22863–22870.

Glowatzki, E., G. Fakler, U. Brändle, U. Rexhausen, H. P. Zenner, J. P. Ruppersberg, and B. Fakler. 1995. Subunit-dependent assembly of inward-rectifier K^+ channels. *Proc. R. Soc. Lond. B Biol. Sci.* 261: 251–261.

Hedrich, R., and P. Dietrich. 1996. Plant K^+ channels: similarity and diversity. *Bot. Acta.* 109:94–101.

Hedrich, R., O. Moran, F. Conti, H. Busch, D. Becker, F. Gambale, I. Dreyer, A. Küch, K. Neuwinger, and K. Palme. 1995. Inward rectifier potassium channels in plants differ from their animal counterparts in response to voltage and channel modulators. *Eur. Biophys. J.* 24: 107–115.

Heinemann, S., J. Rettig, V. E. S. Scott, D. N. Parcej, C. Lorra, J. Dolly, and O. Pongs. 1994. The inactivation behaviour of voltage-gated K-channels may be determined by association of α- and β-subunits. *J. Physiol. (Paris)* 88:173–180.

Hoshi, T. 1995. Regulation of voltage dependence of the KAT1 channel by intracellular factors. *J. Gen. Physiol.* 105:309–328.

Hoth, S., I. Dreyer, P. Dietrich, D. Becker, B. Müller-Röber, and R. Hedrich. 1997. Molecular basis of plant-specific acid activation of K^+ uptake channels. *Proc. Natl. Acad. Sci. USA.* in press.

Hugnot, J. P., M. Salinas, F. Lesage, E. Guillemare, J. de Weille, C. Heurteaux, M. G. Matéi, and M. Lazdunski. 1996. Kv8.1, a new neuronal potassium channel subunit with specific inhibitory properties toward *Shab* and *Shaw* channels. *EMBO J.* 15:3322–3331.

Isacoff, E. Y., Y. N. Jan, and L. Y. Jan. 1990. Evidence for the formation of heteromultimeric potassium channels in *Xenopus* oocytes. *Nature.* 345:530–534.

Jan, L. Y., and Y. N. Jan. 1994. Potassium channels and their evolving gates. *Nature.* 371:119–122.

Ketchum, K. A., and C. W. Slayman. 1996. Isolation of an ion channel gene from *Arabidopsis thaliana* using the H5 signature sequence from voltage-dependent K^+ channels. *FEBS Lett.* 378:19–26.

Lagarde, D., M. Basset, M. Lepetit, G. Conejero, F. Gaymard, S. Astruc, and C. Grignon. 1996. Tissue-specific expression of *Arabidopsis AKT1* gene is consistent with a role in K^+ nutrition. *Plant J.* 9:195–203.

Li, M., Y. N. Jan, and L. Y. Jan. 1992. Specification of subunit assembly by the hydrophilic amino-terminal domain of the *Shaker* potassium channel. *Science.* 257:1225–1230.

Liman, E. R., J. Tytgat, and P. Hess. 1992. Subunit stoichiometry of a mammalian K^+ channel determined by construction of multimeric cDNAs. *Neuron.* 9:861–871.

Ludwig, J., H. Terlau, F. Wunder, A. Brüggemann, L. A. Pardo, A. Marquardt, W. Stühmer, and O. Pongs. 1994. Functional expression of a rat homologue of the voltage gated ether a go-go potassium channel reveals differences in selectivity and activation kinetics between the *Drosophila* channel and its mammalian counterpart. *EMBO J.* 13: 4451–4458.

MacKinnon, R. 1991. Determination of the subunit stoichiometry of a voltage-activated potassium channel. *Nature.* 350:232–235.

Marten, I., F. Gaymard, G. Lemaillet, J. B. Thibaud, H. Sentenac, and R. Hedrich. 1996. Functional expression of the plant K^+ channel KAT1 in insect cells. *FEBS Lett.* 380:229–232.

Müller-Röber, B., J. Ellenberg, N. Provart, L. Willmitzer, H. Busch, D. Becker, P. Dietrich, S. Hoth, and R. Hedrich. 1995. Cloning and electrophysiological analysis of KST1, an inward rectifying K^+ channel expressed in potato guard cells. *EMBO J.* 14:2409–2416.

Nakamura, R. L., W. L. McKendree, Jr., R. E. Hirsch, J. C. Sedbrook, R. F. Gaber, and M. R. Sussman. 1995. Expression of an *Arabidopsis* potassium channel gene in guard cells. *Plant Physiol.* 109:371–374.

Pessia, M., S. J. Tucker, K. Lee, C. T. Bond, and J. P. Adelman. 1996. Subunit positional effects revealed by novel heteromeric inwardly rectifying K^+ channels. *EMBO J.* 15:2980–2987.

Pongs, O. 1995. Regulation of the activity of voltage-gated potassium channels by β-subunits. *Sem. Neurosci.* 7:137–146.

Ruppersberg, J. P., K. H. Schröter, B. Sakmann, M. Stocker, S. Sewing, and O. Pongs. 1990. Heteromultimeric channels formed by rat brain potassium channel proteins. *Nature.* 352:711–714.

Salkoff, L., K. Baker, A. Butler, M. Covarrubias, M. D. Pak, and A. Wei. 1992. An essential "set" of K^+ channels conserved in flies, mice and humans. *Trends Neurosci.* 15:161–166.

Schachtman, D. P., J. I. Schroeder, W. J. Lucas, J. A. Anderson, and R. F. Gaber. 1992. Expression of an inward-rectifying potassium channel by the *Arabidopsis* KAT1 cDNA. *Science.* 258:1645–1658.

Sentenac, H., N. Bonneaud, M. Minet, F. Lacroute, J. M. Salmon, F. Gaymard, and C. Grignon. 1992. Cloning and expression in yeast of a plant potassium ion transport system. *Science.* 256:663–665.

Shahidullah, M., N. Hoshi, S. Yokohama, and H. Higashida. 1995. Micro-heterogeneity in heteromultimeric assemblies formed by *Shaker* (Kv1) and *Shaw* (Kv3) subfamilies of voltage-gated K^+ channels. *Proc. R. Soc. Lond. B Biol. Sci.* 261:309–317.

Shen, N. V., X. Chen, M. M. Boyer, and P. J. Pfaffinger. 1993. Deletion analysis of K^+ channel assembly. *Neuron.* 11:67–76.

Tang, H., A. C. Vasconcelos, and G. A. Berkowitz. 1995. Evidence that plant K^+ channel proteins have two different types of subunits. *Plant Physiol.* 109:327–330.

Véry, A. A., C. Bosseux, F. Gaymard, H. Sentenac, and J. B. Thibaud. 1994. Level of expression in *Xenopus* oocytes affects some characteristics of a plant inward-rectifying K^+ channel. *Pflügers Arch.* 428: 422–424.

Véry, A. A., F. Gaymard, C. Bosseux, H. Sentenac, and J. B. Thibaud. 1995. Expression of a cloned plant K^+ channel in *Xenopus* oocytes: analysis of macroscopic currents. *Plant J.* 7:321–332.

Warmke, J., R. Drysdale, and B. Ganetzky. 1991. A distinct potassium channel polypeptide encoded by the *Drosophila eag* locus. *Science.* 252:1560–1562.

Woodhull, A. M. 1973. Ionic blockage of sodium channels in nerves. *J. Gen. Physiol.* 61:687–708.

Yang, J., Y. N. Jan, and L. Y. Jan. 1995. Determination of the subunit stoichiometry of an inwardly rectifying potassium channel. *Neuron.* 15:1441–1447.

⇒ zurück zur Übersicht

1996

Becker, **Dreyer**, Hoth, Reid, Busch, Lehnen, Palme, Hedrich

Changes in voltage activation, Cs^+ sensitivity, and ion permeability in H5 mutants of the plant K^+ channel KAT1.

Proc. Natl. Acad. Sci. USA **93**:8123-8128.

Proc. Natl. Acad. Sci. USA
Vol. 93, pp. 8123–8128, July 1996
Plant Biology

Changes in voltage activation, Cs^+ sensitivity, and ion permeability in H5 mutants of the plant K^+ channel KAT1

DIRK BECKER*, INGO DREYER*, STEFAN HOTH*, JOHN D. REID†, HEINER BUSCH*, MICHAELA LEHNEN‡, KLAUS PALME‡, AND RAINER HEDRICH*§

*Institut für Biophysik, Universität Hannover, Herrenhäuserstraβe 2, 30419 Hannover, Germany; †Department of Molecular Biology, Glaxo Institute for Molecular Biology, Chemin des Aulx 14, 1228 Geneva, Switzerland; and ‡Max-Delbrück-Laboratorium in der Max-Planck-Gesellschaft, Carl von Linne Weg 10, 50829 Köln, Germany

Communicated by Winslow R. Briggs, Carnegie Institution of Washington, Stanford, CA, December 26, 1995

ABSTRACT **KAT1 is a voltage-dependent inward rectifying K^+ channel cloned from the higher plant *Arabidopsis thaliana* [Anderson, J. A., Huprikar, S. S., Kochian, L. V., Lucas, W. J. & Gaber, R. F. (1992) *Proc. Natl. Acad. Sci. USA* 89, 3736–3740]. It is related to the Shaker superfamily of K^+ channels characterized by six transmembrane spanning domains (S1–S6) and a putative pore-forming region between S5 and S6 (H5). The H5 region between Pro-247 and Pro-271 in KAT1 contains 14 additional amino acids when compared with Shaker [Aldrich, R. W. (1993) *Nature (London)* 362, 107–108]. We studied various point mutations introduced into H5 to determine whether voltage-dependent plant and animal K^+ channels share similar pore structures. Through heterologous expression in *Xenopus* oocytes and voltage-clamp analysis combined with phenotypic analysis involving a potassium transport-defective *Saccharomyces cerevisiae* strain, we investigated the selectivity filter of the mutants and their susceptibility toward inhibition by cesium and calcium ions. With respect to electrophysiological properties, KAT1 mutants segregated into three groups: (*i*) wild-type-like channels, (*ii*) channels modified in selectivity and Cs^+ or Ca^{2+} sensitivity, and (*iii*) a group that was additionally affected in its voltage dependence. Despite the additional 14 amino acids in H5, this motif in KAT1 is also involved in the formation of the ion-conducting pore because amino acid substitutions at Leu-251, Thr-256, Thr-259, and Thr-260 resulted in functional channels with modified ionic selectivity and inhibition. Creation of Ca^{2+} sensitivity and an increased susceptibility to Cs^+ block through mutations within the narrow pore might indicate that both blockers move deeply into the channel. Furthermore, mutations close to the rim of the pore affecting the half-activation potential ($U_{1/2}$) indicate that amino acids within the pore either interact with the voltage sensor or ion permeation feeds back on gating.**

KAT1 was cloned from an *Arabidopsis thaliana* cDNA library by functional complementation of a yeast mutant deficient in K^+ uptake (1, 2). Using the oocyte-expression system, Schachtman *et al.* (3) were the first who demonstrated that KAT1 carries a voltage-dependent inward-rectifying K^+ current. Further studies have shown that KAT1, the "green" inward rectifier, gains its voltage dependence through an intrinsic voltage sensor (4) rather than a block through cytoplasmic Mg^{2+} as shown for its animal counterpart (5). With respect to the gating mechanism, KAT1 is therefore more closely related to the outward-rectifying Shaker-type channels. In common with Shaker, KAT1, a member of the plant inward rectifiers, shares an overall molecular structure of six hydrophobic domains (S1–S6), one of which is positively charged (S4), and an amphiphilic stretch of amino acids (H5) between S5 and S6 (Fig. 1*A*) (7). The latter two motifs are very likely to be part of the voltage sensor (S4) and part of the ion permeation pathway (H5) (8, ¶, ‖). So far, however, chimera between KAT1 and Shaker on one side (9) and eag on the other**, including S4, did not affect inward rectification. Therefore, other membrane domains as well as intra- or extracellular sites may contribute to the voltage-sensing mechanism.†† ‡‡

Whereas different laboratories found an increase in macroscopic current through the green K^+ channel at hyperpolarized membrane potentials (3, 4, 10–12), conflicting single channel conductances have been reported. Hedrich *et al.* (4) and Hoshi (12) could show that a single 5-pS rather than a 34 pS (3, 13, 14) channel generated the inward currents following the expression of KAT1 in *Xenopus* oocytes.

A KAT1-related K^+ channel, KST1, cloned from an epidermal fragment library of potato (*Solanum tuberosum*), is expressed in guard cells and flowers (15). KST1 is characterized by a voltage- and ATP-dependent 7-pS K^+ channel when functionally expressed in oocytes. An apparently plant-specific feature of KAT1 and KST1 is their activation by acidic pH (refs. 4, 10, 12, and 15; cf. ref. 16). pH activation is achieved by a shift in the half-activation potential ($U_{1/2}$) toward less negative or even positive potentials (refs. 4 and 12; for lack of modulation of the voltage sensor, see ref. 10). In addition to the Shaker-related features of KAT1, a putative ATP- and cyclic nucleotide-binding domain was deduced from the primary structure of this plant K^+ channel (17). In line with the postulated role of these structural motifs, activation of KAT1 and KST1 by ATP and cGMP has been demonstrated (12, 15).

Herein we show that mutations in H5 alter the Rb^+ permeability, the susceptability to block by Cs^+ and Ca^{2+}, as well as voltage sensitivity of the green Shaker channel.

MATERIALS AND METHODS

Generation of KAT1 Mutants. KAT1 mutants were generated by polymerase chain reaction (PCR) as described by H.A. Erlich (18). The mutations were introduced into the 3′ oligonucleotide used for PCR amplification. The PCR was performed using AmpliTaq polymerase (Perkin–Elmer/Cetus) on an Applied Biosystems PCR machine. The amplified PCR

The publication costs of this article were defrayed in part by page charge payment. This article must therefore be hereby marked "*advertisement*" in accordance with 18 U.S.C. §1734 solely to indicate this fact.

Abbreviation: TEA, tetraethylammonium.

§To whom reprint requests should be addressed.

¶Becker, D., Dreyer, I., Palme, K. & Hedrich, R. (1995) 10th International Workshop on Plant Membrane Biology, Regensburg, abstr. C51.

‖Chilcott, T. C., Frost-Schartzer, S., Iverson, M. W., Garvin, D., Kochian, L. V. & Lucas, W. J. (1995) 10th International Workshop on Plant Membrane Biology, Regensburg, abstr. C54.

**Hoshi, T., Marten, I. & Henneger, D. J. (1995) 10th International Workshop on Plant Membrane Biology, Regensburg, abstr. L15.

††Bosseux, C., Daram, P., Lemaillet, G., Sentenac, H. & Thibaud, J. B. (1995) 10th International Workshop on Plant Membrane Biology, Regensburg, abstr. C53.

‡‡Lemaillet, G., Ros, R. & Sentenac, H. (1995) 10th International Workshop on Plant Membrane Biology, Regensburg, abstr. C61.

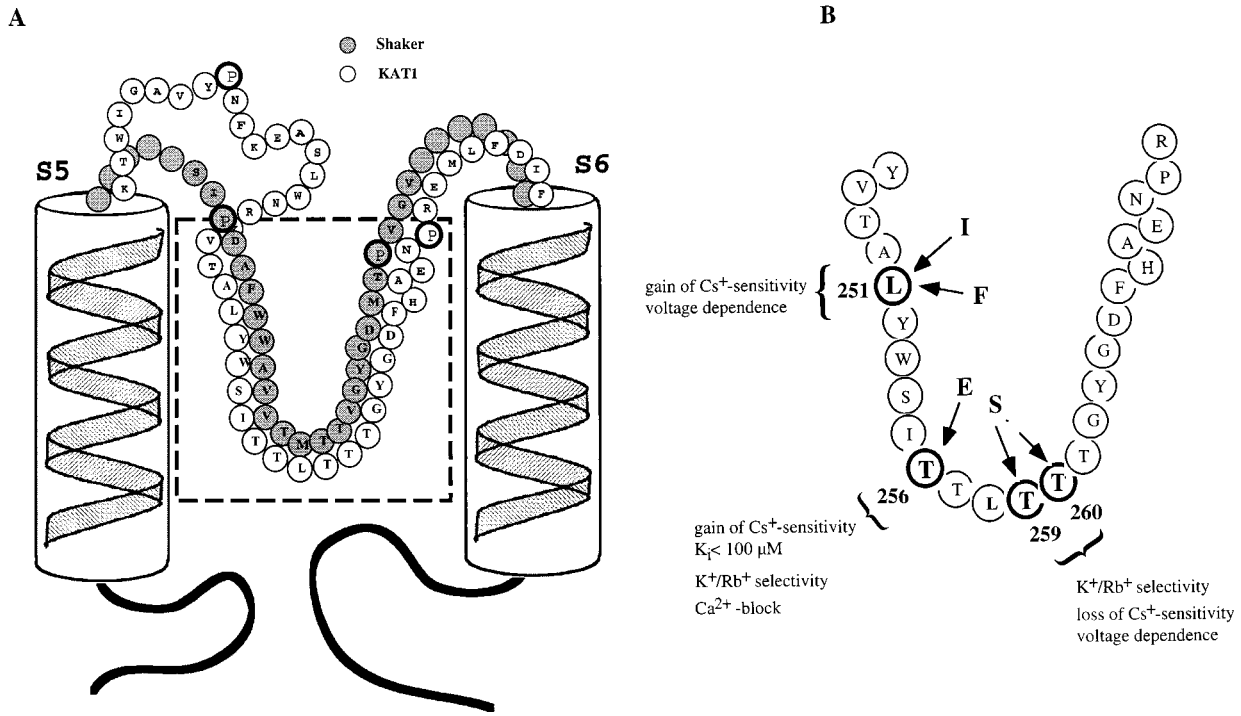

FIG. 1. Diagram of the putative pore of KAT1 and Shaker. (*A*) Residues forming the loop between predicted transmembrane segments 5 and 6. The stretch of amino acids between the marked Pro residues have been shown to line the narrow pore in Shaker (6). In KAT1, 14 additional amino acids were found between Pro-247 and Pro-271, the supposed bounds for the entry and exit of the plant pore region. (*B*) Leu-251, Thr-256, Thr-259, and Thr-260, the four residues that were mutated within this study, are indicated by arrows.

fragments were subcloned into pUC19 and sequenced. The mutated fragments were inserted into the KAT1 cDNA as a *Bsp*HI fragment and the reconstituted mutant cDNA was cloned into the pGEMHE expression cassette (19).

Yeast Genetics. The construction of the *Saccharomyces cerevisiae* strain used in this study: JRY339, *MAT***a** *trk1*::*ura3*Δ*456*, *trk2*Δ*1*::*hisG*, *ura3*Δ, is described in Lichtenberg-Frate *et al.* (20). Yeast strains were maintained on SDAP medium (21) containing 2% purified agar (Sigma A-7921) supplemented with KCl. KAT1 and mutants were subcloned in the expression vector pPGK (22) containing the 3-phosphoglycerate kinase promoter and terminator. Yeast transformations were performed using the lithium acetate method (23).

Injection of cRNA in *Xenopus* Oocytes. *Xenopus* frogs were purchased from Nasco (Fort Atkinson, WI). Oocytes were isolated as described by Stühmer *et al.* (24) and injected with cRNA (100 ng/μl) using a General Valve Picospritzer II microinjector [40 psi (1 psi = 6.89 kPa) for 5–10 ms].

Voltage-Clamp Recordings. Whole-cell K^+ currents were measured with a two-microelectrode voltage-clamp (Turbotec 01C, NPI Germany), by using 0.5- to 2-MΩ pipettes filled with 3 M KCl as described (15). Since Véry *et al.* (10) described that some channel properties of KAT1 differ with the expression rate, we selected for further analysis oocytes with similar KAT1 expression.

Single-Channel Recordings (Patch-Clamp). Data acquisition and single-channel experiments were performed as described (4, 15). The bath solution contained 100 mM potassium gluconate, 2 mM $MgCl_2$, 2 mM EGTA, 10 mM Tris/Mes (pH 7.4), and 1 mM MgATP. Patch pipettes were loaded with 100 mM potassium gluconate/2 mM $MgCl_2$/1 mM $CaCl_2$/10 mM Mes/Tris (pH 5.6). The osmolality in both media was balanced with D-sorbitol to 220 milliosmoles.

Solutions. Solutions for selectivity experiments contained 2 mM $MgCl_2$, 1 mM $CaCl_2$, 10 mM Mes/Tris (pH 5.6), 100 mM KCl, 100 mM RbCl, 100 mM NH_4Cl, 100 mM LiCl, and 100 mM NaCl, respectively. Solutions for Cs^+ experiments contained 30 mM KCl, 2 mM $MgCl_2$, 1 mM $CaCl_2$, 10 mM Mes/Tris (pH 5.6), and 10 μM to 10 mM CsCl. Solutions for Ca^{2+} experiments on the mutant T256E contained 30 mM KCl, 2 mM $MgCl_2$, 10 mM Mes/Tris (pH 5.6), and various mole fractions at 30 mM of $CaCl_2$ and $MgCl_2$ used to maintain the ionic strength. All solutions were adjusted to 220 milliosmolal with sorbitol.

Data Analyses. *Selectivity.* Relative permeability for Rb^+ and NH_4^+ was calculated according to

$$\frac{P_X}{P_K} = \frac{[K^+]}{[X^+]} \exp\left[\left(\frac{F}{RT}\right)\cdot\Delta U_{rev}\right]$$

from the shift in reversal potential ($\Delta U_{rev.}$) after replacement of 100 mM KCl with RbCl or NH_4Cl in the bath.

Cs^+ sensitivity. Current–voltage relationships of tail currents were fitted according to Woodhull model (25):

$$I(U) = I_0(U)\left\{\frac{1}{1 + \exp\left[-(zF/RT)\delta(U - U_{Block1/2})\right]}\right\},$$

where $I_0(U)$ denotes the current in the absence of Cs^+. The half-blocking voltage $U_{Block1/2}$ could be obtained from $I(U_{Block1/2}) = \frac{1}{2} \times I_0(U_{Block1/2})$.

Table 1. Characteristics of pore mutants of KAT1

	Relative permeability			$K_i(Cs^+)$,		Shift in
	K^+	Rb^+	NH_4^+	μM	$\delta_{Cs+block}$	$U_{1/2}$
KAT1 WT	100	34 ± 2	5 ± 1	335 ± 93	1.6 ± 0.3	−
T199S	100	29 ± 3	5 ± 1	312 ± 120	1.5 ± 0.1	−
L251I	100	34 ± 5	6 ± 2	112 ± 43	1.4 ± 0.3	+
L251F	100	41 ± 5	5 ± 1	212 ± 43	1.3 ± 0.1	−
T256E	100	64 ± 9	9 ± 1	20 ± 2	—	−
T259S	100	48 ± 5	6 ± 1	1110 ± 238	1.7 ± 0.2	−
T260S	100	80 ± 18	7 ± 1	1703 ± 302	0.8 ± 0.2	+
T259/260S	100	49 ± 4	6 ± 1	622 ± 129	1.3 ± 0.2	+

Susceptability toward block by Cs^+ ions in 30 mM KCl is given by the inhibition constant K_i at −180 mV. The electrical distance $\delta_{Cs+Block}$ in 30 mM KCl was determined according to Woodhull (25). Data represent the mean ± SD of three to nine measurements.

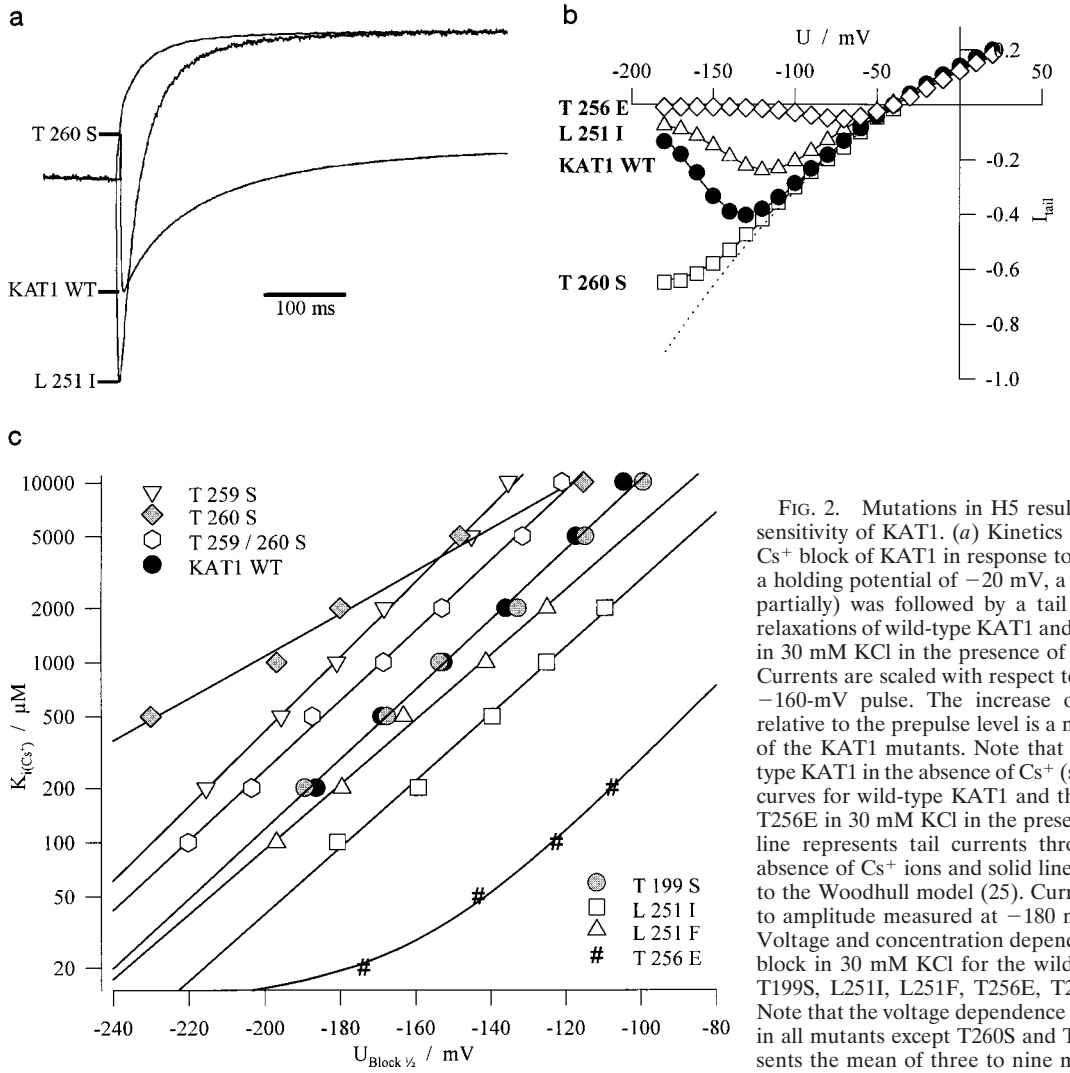

FIG. 2. Mutations in H5 result in the alteration of the Cs^+ sensitivity of KAT1. (*a*) Kinetics of deactivation and release of Cs^+ block of KAT1 in response to a double-voltage pulse. From a holding potential of −20 mV, a 1-s pulse to −160 mV (shown partially) was followed by a tail pulse to −120 mV. Current relaxations of wild-type KAT1 and the mutants T260S and L251I in 30 mM KCl in the presence of 1 mM Cs^+ are superimposed. Currents are scaled with respect to the current at the end of the −160-mV pulse. The increase of the tail current (unblock) relative to the prepulse level is a measure for the Cs^+ sensitivity of the KAT1 mutants. Note that T260S is comparable to wild-type KAT1 in the absence of Cs^+ (see *b*). (*b*) Tail current–voltage curves for wild-type KAT1 and the mutants T260S, L251I, and T256E in 30 mM KCl in the presence of 1 mM Cs^+. The dotted line represents tail currents through wild-type KAT1 in the absence of Cs^+ ions and solid lines represent best fits according to the Woodhull model (25). Currents were normalized relative to amplitude measured at −180 mV in the absence of Cs^+. (*c*) Voltage and concentration dependence ($U_{Block1/2}$, K_i) of the Cs^+ block in 30 mM KCl for the wild-type KAT1 and the mutants T199S, L251I, L251F, T256E, T259S, T260S, and T259/260S. Note that the voltage dependence of the Cs^+ block is maintained in all mutants except T260S and T256E. Each data point represents the mean of three to nine measurements.

RESULTS AND DISCUSSION

Selectivity. Most inward rectifiers in plant cells studied so far, including the gene products of *Kat1* and *Kst1*, are permeable to K^+ and Rb^+ but often impermeable to Na^+ and Li^+ (13). A corn coleoptile K^+ channel, however, is an exception in that its Rb^+ permeability is strongly reduced (26). In addition, both the plant inward rectifiers, which have been

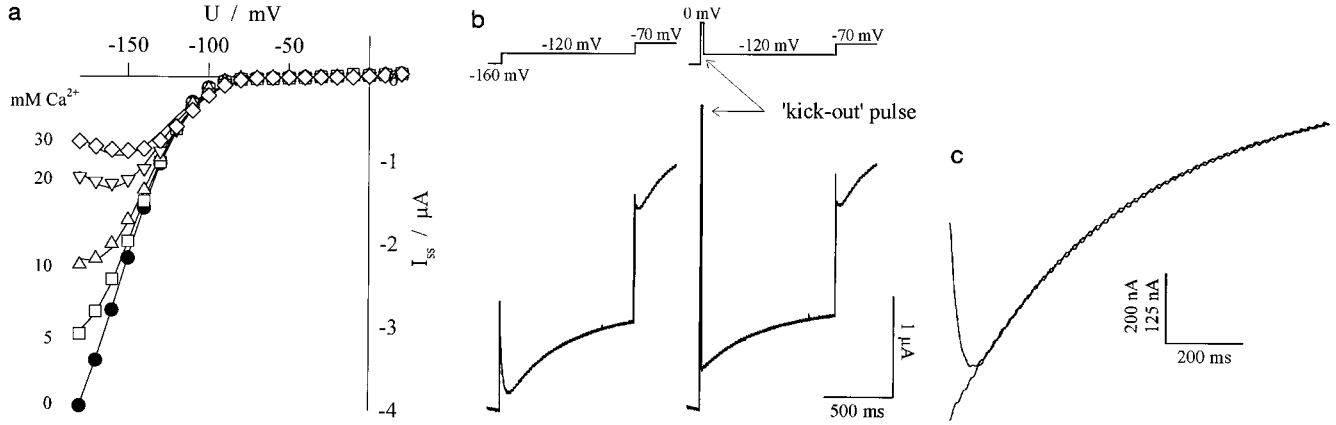

FIG. 3. Calcium ions block inward K^+ currents of the KAT1 mutant T256E. (*a*) Steady-state current–voltage relationship in the presence of Ca^{2+} in the external solution. Since Mg^{2+} did not block the inward currents, the ionic strength was balanced with $MgCl_2$. Solid lines represent best fits according to the Woodhull model (25). (*b*) The Ca^{2+} unblock kinetics of T256E resolved by tail experiments. After an activating prepulse to $U = -160$ mV for $t = 1$ s (shown partially) in the following tail pulse to $U = -120$ mV unblock and deactivation kinetics superimpose (left trace). The unblock kinetics is completely eliminated by an initial short depolarizing step (10 ms) to 0 mV (kick-out pulse). The deactivation process procedes as in the absence of Ca^{2+} (right trace). (*c*) During the intermediate depolarizing pulse, not only were the blocking ions removed from the pore but also some channels were deactivated according to $I(t) = I_0 \times \exp(-t/\tau)$, with $\tau \approx 20$ ms (12). Since the amplitude of the current was thus smaller by a factor of $\exp(-10 \text{ ms}/20 \text{ ms}) \approx 0.6$ than without the deactivating prepulse, the superposition shows the normal and the scaled tail after a kick-out pulse.

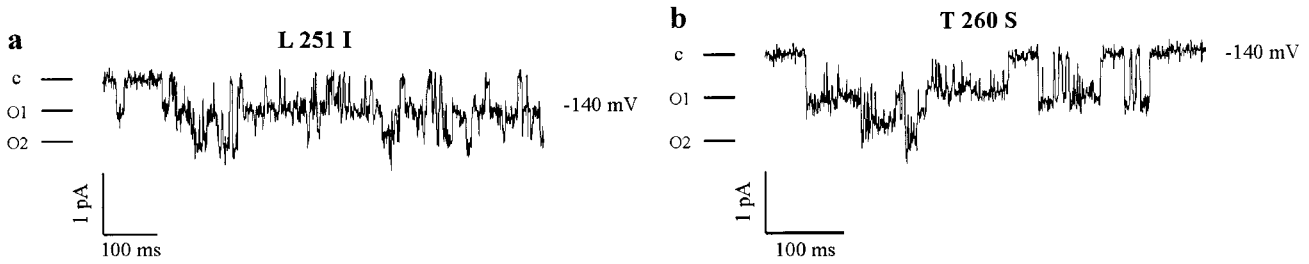

FIG. 4. The most diverse Cs^+-sensitive mutants L251I and T260S are not affected in their single-channel conductance when compared with wild-type KAT1. Inside-out patches were excised from *Xenopus* oocytes expressing the H5 mutants T260S and L251I of KAT1. o, Open channel; c, closed channel.

studied in their natural environment, as well as the gene products of *Kat1* and *Kst1* analyzed in *Xenopus* oocytes, are characterized by a high NH_4^+ conductance (3, 4, 15, 26). We therefore generated channel mutants in H5 and analyzed them with respect to their permeability for Rb^+ and NH_4^+.

Inward K^+ current through these mutated channels showed the slow activation kinetics charactistic of the wild-type channel (3, 4), when elicited by hyperpolarizing voltage pulses. None of the introduced replacements significantly affected the relative NH_4^+ permeability $P_{NH4}+/P_K+$. Although a ratio of 0.06 ± 0.01 in wild type and mutants (Table 1) indicated that the selectivity filter favors K^+ transport, the half-saturation constants for both ions, $K_m(K^+) = 39$ mM (in line with previous findings, ref. 27) and $K_m(NH_4^+) = 47$ mM, however, were rather similar.

Since Thr-441 in Shaker is part of the selectivity filter (28), we mutated the corresponding amino acid Thr-259 in KAT1 to Ser (Fig. 1). The T259S mutation as well as the mutation of Thr-260 to Ser (T260S) altered the relative Rb^+ permeability ($P_{Rb}+/P_K+$) from 0.34 in the wild-type channel to 0.48 and 0.80 in the mutants. The simultaneous mutation of both Thr-259 and Thr-260 to Ser resulted in a relative permeability ratio for $P_{Rb}+/P_K+$ of 0.49, indicating that in the double mutant T259S is dominant (for inverse behavior with respect to shifts in the activation curve, see Fig. 5 and corresponding text below).

Susceptability to Blocking Cations. In contrast to their animal counterparts, which subdivide into two classes according to their tetraethylammonium (TEA^+) sensitivity (<1 mM and >20 mM; refs. 29 and 30), all plant K^+ channels studied have exhibited a low affinity for external TEA^+ ($K_i \approx 10$–30 mM), the cationic K^+ channel blocker. This behavior is possibly due to the lack of corresponding high-affinity amino acids in H5 (31, 32) including Thr-449 and Asp-431 in Shaker or Tyr-380 in Kv2.1 (6) compared with Thr-249 and His-267 in KAT1 (Fig. 1). Plant growth and K^+ channel activity, however, are extremely sensitive to Cs^+ (4, 10, 15, 26, 33), which in contrast to TEA^+ causes voltage-dependent blockade (4, 10). To elucidate whether the change in Cs^+ sensitivity correlates with the location of the mutated amino acid relative to the transmembrane electrical field, we measured the relative voltage drop sensed by the Cs^+ according to the Woodhull model (25). The block of KAT1 by Cs^+ is strongly voltage-dependent, increasing its strength with increasing negative voltages (Fig. 2*b*). An electrical distance δ of >1 was calculated (Table 1). Therefore, for KAT1, like the inward rectifier in the starfish egg (34, 35), a multi-ion single-file pore has to be assumed to describe permeation through the K^+ channel and the observed features of the interaction with Cs^+ (36). A supposed competition of both ions for at least two common binding sites was additionally supported by the finding that δ changed with the external K^+ concentration (data not shown).

The various point mutations in H5 could be distinguished by their differences in Cs^+ sensitivity up to a hundredfold (Table 1). When we replaced Thr-259 or Thr-260 with Ser (T259S or T260S), the K_i for Cs^+ at -180 mV increased by a factor of 3 or 5, respectively, compared with wild type. Interestingly, the double mutant T259/260S is more sensitive to Cs^+ than any of the two single mutants. (Fig. 2 *a* and *b* and Table 1). In addition to residues Thr-259 and Thr-260, which were presumed to contribute to the selectivity filter, we mutated Leu-251 in KAT1, because at this position there is an Ile in a corn coleoptile and broad bean leaf channel, and a Phe in Shaker (unpublished results). In contrast to the conserved exchanges at positions 259 and 260, mutations L251I and L251F resulted in an increase in Cs^+ sensitivity (Table 1). In Fig. 2*a*, the response of wild-type KAT1, L251I, and T260S to a double voltage pulse is superimposed. In the presence of 1 mM Cs^+, K currents through these channels slowly activate during a 1-s prepulse to -160 mV. Upon the subsequent step to -120 mV, the tail current decreased toward a new steady state in T260S (zero current level in the case of T260S and L251I, but not wild type, see Fig. 5). In contrast, KAT1 wild-type and L251I tails initially increased (Fig. 2*a*). This increase in current has previously been demonstrated to result from unblock of Cs^+ from the open channel (4, 15, 26). Thus, T260S in the presence of 1 mM Cs^+ responded almost like the wild-type KAT1 in the absence of the inhibitor (data not shown). In contrast to the reduced Cs^+ sensitivity and voltage dependence of the Cs^+ block in the mutant T260S channel, other exchanges altered the Cs^+ sensitivity while leaving the voltage dependence unaffected (Fig. 2 *b* and *c*). As a control for nonspecific effects of mutagenesis in this experiment, a change of Thr-199 to Ser, outside the

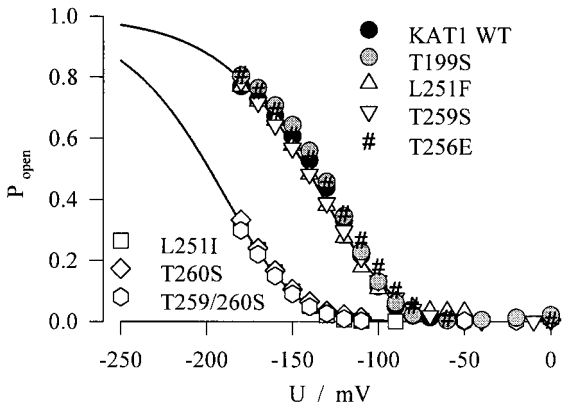

FIG. 5. Mutations within H5 shift the voltage-dependent open probability of KAT1. The mutants L251I and T260S and the double mutant T259/260S but not T199S, L251F, T256E, and T259S are characterized by an half-activtion potential ($U_{1/2}$) shifted by about 60 mV more negative than wild-type KAT1. The determination of the half-activation potentials was based on activation-curve analyses as described (4). When plotting the ratio between the steady-state currents and the corresponding tails as a function of voltage, a measure for the voltage-dependent open probability, P_{open}, of single KAT1 channels, best fits for wild-type and mutant channels were obtained when a cooperativity of four identical channel subunits (S4 segments) was assumed, an approach described for potassium channels (12). The solid lines represent the best fits according to $P_0 = \{1/[1 + \exp(ZF/RT)(U - U_{1/2})]\}^n$, with $z = 1.3$ and $n = 4$.

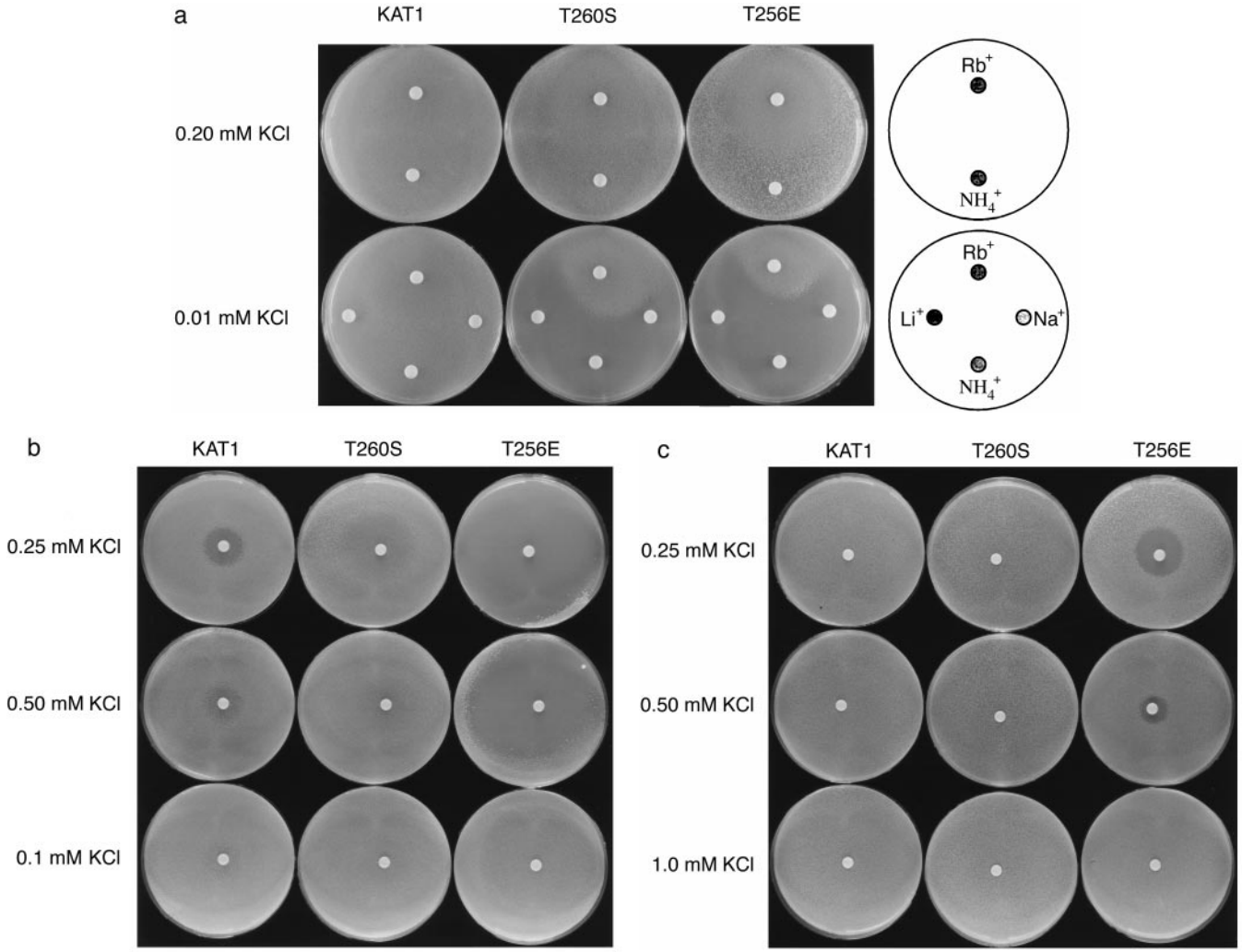

FIG. 6. Selectivity and blockade of wild-type KAT1, T260S, and T256E mutant channels *in vivo*. The effect of monovalent and divalent cations on growth was detected by the halo assay. A lawn of 10^5 cells of JRY339 expressing KAT1, T260S, or T256E was plated in 1% agar on SDAP plates supplemented with the indicated concentration of KCl. A paper disk containing 10 μl of the test cation solution was placed on the agar surface and the plates were incubated at 30°C for 36 h. In the growth zone around the disk, inhibition creates a dark halo whereas stimulation creates a reverse halo. Concentration and position of each test solution: (*a*) RbCl (1 M), upper disk; NH_4Cl (1 M), lower disk; LiCl (10 M), left disk, lower row; NaCl (5 M), right disk, bottom row. (*b*) CsCl (1 M). (*c*) $CaCl_2$ (1 M).

putative pore region, exhibited properties indistinguishable from wild-type KAT1 (Fig. 2*c* and Table 1; see Fig. 5).

In contrast to the guard-cell K^+ uptake channels from *Vicia faba*, *Zea mays* (37, 38), *Solanum tuberosum*, and *Nicotina tabaccum* (unpublished results), KAT1 is not blocked by external Ca^{2+} up to 30 mM. We therefore introduced a charged amino acid at position 256, corresponding to Val-438 in Shaker, which is supposed to interact with the GYG and thus to line the narrow pore. Replacing Thr with Glu, T256E, drastically altered the permeation properties of the channel. Whereas the selectivity sequence was within the range described for the other mutants (Table 1), the sensitivity toward Cs^+ increased by a factor of 15 compared with the wild type and up to 100 compared with T260S. Even more interesting, this mutant developed a Ca^{2+} sensitivity similar in voltage and concentration dependence to that described for the inward rectifying K^+ channel in guard cells of *Vicia faba* (Fig. 3) (37, 38). In Fig. 3, the blocking Ca^{2+} is released by a depolarizing voltage pulse to -120 mV. In contrast to the Cs^+ block, the voltage-dependent interaction of the calcium with the open pore could be described with a δ of 0.5, indicating that a single Ca^{2+} might move 50% of the voltage drop (25). The unblock could be described by a single exponential. The deactivation in the absence of Ca^{2+} and after unblock was identical (Fig. 3*c*).

Single-Channel Conductance and Voltage Dependence. Patch-clamp studies revealed that the single-channel conductances of the most diverse and conservative amino acid exchanges containing Cs^+-sensitive mutants L251I and T260S of 5 ± 1 pS ($n = 3$) and 7 ± 2 pS ($n = 2$) were comparable with 5–6 pS for wild-type KAT1 and 7 pS for KST1 (Fig. 4) (4, 12, 15). When we compared the voltage dependence of the H5 mutants, however, two groups could be identified: L251F and T259S had half-activation potentials ($U_{1/2}$) comparable to wild type, whereas L251I, T260S, and T259/260S exhibited activation curves shifted by about 60 mV toward more negative voltages (Fig. 5). An apparent gating charge of $z = 1.3$ indicated that the voltage sensitivity of the KAT1 mutants remained unaffected. It should be noted that the double mutant T259S/T260S shifted the activation curve in the same way as T260S (Table 1 and Fig. 5). Hence, in the double mutant the T259S exchange was dominant with respect to ion permeation (see above) while the T260S exchange was dominant with respect to activation-threshold shifts. An analogous mutation to KAT1 T260S in Shaker (T442S) caused a similar shift in the activation threshold (28). Since this effect was not analyzed further, we cannot distinguish between the possibilities that in KAT1, where the shift was even more pronounced, amino acids within the pore either interact with the voltage sensor or the

permeating ion affects its own gating. The complex interaction between the pore-forming domain and the voltage sensor was illustrated by the fact that a conservative exchange at position 251 from Leu to Ile strongly influenced the voltage dependence of activation, whereas the more drastic exchange from Leu to Phe did not affect this parameter. Likewise, the introduction of a negative charge into the narrow pore left the voltage dependence unaffected.

Functional Expression in Yeast. *S. cerevisiae* strain JRY339, in which the *TRK1* and *TRK2* genes (2) have been deleted, does not grow on growth medium containing less than 1 mM KCl; growth can be rescued by expression of KAT1 (1). We tested whether KAT1 with either of two mutations in the H5 region would allow growth in low K^+ medium. The T256E and T260S mutant channels restored the growth of strain JRY339 on medium containing 0.2 mM KCl but unlike KAT1 they did not grow with only 0.01 mM KCl. The effect of other ions on growth was tested by placing an impregnated paper disk on a nascent lawn of yeast cells suspended in growth agar. After incubation for 36 h, growth inhibition was reflected by a clear halo around the disk and growth stimulation by an increased density (reverse halo). RbCl strongly stimulated growth of T256E and T260S, but slightly inhibited growth of the KAT1 strain (Fig. 6*a*). $NHCl_4$ and $MgCl_2$ had no effect. In contrast to KAT1, cells expressing T256E were supersensitive to inhibition by CsCl (Fig. 6*b*) and $CaCl_2$ (Fig. 6*c*). The T260S mutant cells were unaffected by $CaCl_2$ and less sensitive to CsCl than either T256E or KAT1 (Fig. 6*b*); however, when measured at 24 h, there was clear inhibition by CsCl. NaCl and LiCl were strongly inhibitory to T260S cells, but only weakly inhibitory to T256E and KAT1. Whenever growth inhibition was observed (for KAT1 and both mutants), the diameter of the halo was larger at lower potassium concentrations.

These results demonstrate that both KAT1T256E and KAT1T260S express functional K^+ uptake channels in yeast. Growth on low K^+ was strongly affected by certain cations and was different for each mutant. Despite the qualitative nature of the growth assay, the diameter of the reverse halos produced by Rb^+ stimulation was in line with the PK/PRb permeability ratios of the mutant channels (Table 1), and the degree of inhibition by Cs^+ or Ca^{2+} correlated with data obtained from voltage-clamp recordings of whole cell K^+ currents (Figs. 2 and 3). Therefore, the phenotype conferred by each mutation most likely resulted from the direct action of specific cations on ion-uptake through the mutant channels. Thus, the removal of a methyl group from the sidechain of a conserved Thr in the signature sequence allowed Rb^+ to permeate the T260S channel and thereby activate intracellular processes that are required for growth. The substitution of an acidic Glu residue at T256 resulted in increased permeation by Rb^+ and a dramatic increase in inhibition by Cs^+ and Ca^{2+}. The finding that the degree of inhibition by Cs^+ and Ca^{2+} changed with the external KCl concentration, suggests a competition between K^+ ions and blocking cations for residues in the P region that are exposed to the aqueous lumen of the pore.

We are grateful to Chris Readhead (Köln) for helpful comments on the manuscript. Furthermore, we thank Alan North (Geneva), Mohamed El Alama, and Kerstin Neuwinger for expert technical assistance and Angelika Küch and Birgit Reintanz for support in the generation of H5 mutants. This work was funded by Deutsche Forschungsgemeinschaft grants to R.H. (1640/1–3) and R.H. and K.P. (1640/9–10).

1. Anderson, J. A., Huprikar, S. S., Kochian, L. V., Lucas, W. J. & Gaber, R. F. (1992) *Proc. Natl. Acad. Sci. USA* **89,** 3736–3740.
2. Ko, C. H. & Gaber, R. F. (1991) *Mol. Cell. Biol.* **11,** 4266–4273.
3. Schachtman, D. P., Schroeder, J. I., Lucas, W. J., Anderson, J. A. & Gaber, R. F. (1992) *Science* **258,** 1654–1658.
4. Hedrich, R., Moran, O., Conti, F., Busch, H., Becker, D., Gambale, F., Dreyer, I., Küch, A., Neuwinger, K. & Palme, K. (1995) *Eur. Biophys. J.* **24,** 107–115.
5. Kubo, Y., Baldwin, T. J., Jan, Y. N. & Jan, L. Y. (1993) *Nature (London)* **362,** 127–132.
6. Brown, A. M. (1993) *Annu. Rev. Biophys. Biomol. Struct.* **22,** 173–198.
7. Aldrich, R. W. (1993) *Nature (London)* **362,** 107–108.
8. Uozumi, N., Gassmann, W., Cao, Y. & Schroeder, J. I. (1995) *J. Biol. Chem.* **270,** 24276–24281.
9. Cao, Y., Crawford, N. M. & Schroeder, J. I. (1995) *J. Biol. Chem.* **270,** 17697–17701.
10. Véry, A. A., Gaymard, F., Bosseux, C., Sentenac, H. & Thibaud, J. B. (1995) *Plant J.* **7,** 321–332.
11. Bertl, A., Anderson, J. A., Slayman, C. L., Sentenac, H. & Gaber, R. F. (1995) *Proc. Natl. Acad. Sci. USA* **92,** 2701–2705.
12. Hoshi, T. (1995) *J. Gen. Physiol.* **105,** 309–328.
13. Hedrich, R. & Becker, D. (1994) *Plant Mol. Biol.* **26**, 1637–1649.
14. Methfessel, C., Witzemann, V., Takahashi, T., Mishima, M., Numa, S. & Sakmann, B. (1986) *Pflügers Arch.* **407,** 577–588.
15. Müller-Röber, B., Ellenberg, J., Provart, N., Willmitzer, L., Busch, H., Becker, D., Dietrich, P., Hoth, S. & Hedrich, R. (1995) *EMBO J.* **14,** 2409–2416.
16. Blatt, M. R. (1992) *J. Gen. Physiol.* **99,** 615–644.
17. Schroeder, J. I., Ward, J. M. & Gassmann, W. (1994) *Annu. Rev. Biophys. Biomol. Struct.* **23,** 441–471.
18. Erlich, H. A. (1989) *PCR Technology: Principles and Applications for DNA Amplification* (Stockton, New York).
19. Liman, E. R., Tytgat, J. & Hess. P. (1992) *Neuron* **9,** 861–871.
20. Lichtenberg-Frate, H., Reid, J. D., Heyer, M. & Höfer, M. (1996) *J. Membr. Biol.*, in press.
21. Rodriguez-Navarro, A. & Ramos, J. (1984) *J. Bacteriol.* **159,** 940–945.
22. Kang, Y., Kane, J., Kurjan, J., Stadel, J. M. & Tipper, D. J. (1990) *Mol. Cell. Biol.* **10,** 2582–2590.
23. Geitz, R. D. & Schiestl, R. H. (1991) *Yeast* **7,** 253–263.
24. Stühmer, W., Methfessel, C., Sakmann, B., Noda, M. & Numa, S. (1987) *Eur. Biophys.* **14,** 131–138.
25. Woodhull, A. (1973) *J. Gen. Physiol.* **61,** 687–708.
26. Hedrich, R., Bregante, M., Dreyer, I. & Gambale, F. (1995) *Planta* **197,** 193–199.
27. Kochian, L. V., Garvin, D. F., Shaff, J. E., Chilcott, T. C. & Lucas, W. J. (1993) *Plant and Soil* **155/156,** 115–118.
28. Yool, J. A. & Schwarz, T. L. (1991) *Nature (London)* **349,** 700–704.
29. Hille, B. (1967) *J. Gen. Physiol.* **50,** 1287–1302.
30. Heginbotham, L. & MacKinnon, R. (1992) *Neuron* **8,** 483–491.
31. Kavanaugh, M. P., Varnum, M. D., Osborne, P. B., Christie, M. J., Busch, A. E., Adelman, J. P. & North, R. H. (1991) *J. Biol. Chem.* **266,** 7583–7587.
32. Hidalgo, P. & MacKinnon, R. (1995) *Science* **268,** 307–310.
33. Sheahan, J. J., Ribeiro-Neto, L. & Sussman, M. R. (1993) *Plant J.* **3,** 647–656.
34. Hagiwara, S. S., Miyazaki, S. & Rosenthal, N. P. (1976) *J. Gen. Physiol.* **67,** 621–638.
35. Hagiwara, S. S., Miyazaki, S., Krasne, S. & Ciani, S. (1977) *J. Gen. Physiol.* **70,** 269–281.
36. Hille, B. & Schwarz, W. (1978) *J. Gen. Physiol.* **72,** 409–442.
37. Busch, H., Hedrich, R. & Raschke, K. (1990) *Plant Physiol.* **93,** 96A.
38. Fairley-Grenot, K. A. & Assmann, S. M. (1992) *J. Membr. Biol.* **128,** 103–113.
39. Lü, Q. & Miller, C. (1995) *Science* **268,** 304–307.

⇒ zurück zur Übersicht

1995

Hedrich, Bregante, **Dreyer**, Gambale

The voltage-dependent potassium-uptake channel of corn coleoptiles has permeation properties different from other K^+ channels.

Planta. **197**:193-199.

Planta (1995) 197:193–199

Planta

The voltage-dependent potassium-uptake channel of corn coleoptiles has permeation properties different from other K^+ channels

Rainer Hedrich[1], Monica Bregante[2], Ingo Dreyer[1], Franco Gambale[2]

[1] Institut für Biophysik, Universität Hannover, Herrenhäuser Strasse 2, D-30419 Hannover, Germany
[2] Istituto di Cibernetica e Biofisica, CNR, Via de Marini 6, I-16149 Genova, Italy

Received: 2 January 1995 / Accepted: 11 May 1995

Abstract. The initial response of coleoptile cells to growth hormones and light is a rapid change in plasma-membrane polarization. We have isolated protoplasts from the cortex of maize (*Zea mays* L.) coleoptiles to study the electrical properties of their plasma membrane by the patch-clamp technique. Using the whole-cell configuration and cell-free membrane patches we could identify an H^+-ATPase, hyperpolarizing the membrane potential often more negative than –150 mV, and a voltage-dependent, inward-rectifying K^+ channel (unit conductance ≈5–7 pS) as the major membrane conductances. Potassium currents through this channel named $CKC1_{in}$ (for *C*oleoptile *K*$^+$ *C*hannel *in*ward rectifier) were elicited upon voltage steps negative to –80 mV, characterized by a half-activation potential of –112 mV. The kinetics of activation, well described by a double-exponential process, were strongly dependent on the degree of hyperpolarization and the cytoplasmic Ca^{2+} level. Whereas at nanomolar Ca^{2+} concentrations K^+ currents increased with a $t_{1/2}$=16 ms (at –180 mV), higher calcium levels slowed the activation process about four- to fivefold. Upon changes in the extracellular K^+ concentration the reversal potential of the K^+ channel followed the Nernst potential for potassium with a 56-mV shift for a tenfold increase. The absence of a measurable conductance for Na^+, Rb^+, Cs^+ and a permeability ratio $P_{NH_4^+}/P_{K^+}$ around 0.25 underlines the high selectivity of $CKC1_{in}$ for K^+. In contrast to Cs^+, which at submillimolar concentration blocks the channel in a voltage-dependent manner, Rb^+, often used as a tracer for K^+, does not permeate this type of K^+ channel. The lack of Rb^+ permeability is unique with respect to other K^+ transporters. Therefore, future molecular analysis of $CKC1_{in}$, considered as a unique variation of plant inward rectifiers, might help to understand the permeation properties of K^+ channels in general.

Key words: Coleoptile (K^+ uptake) – K^+ channel selectivity, voltage-dependence – *Zea*

Introduction

The coleoptile is an organ specific to members of the Poaceae. This tissue was the object of the pioneering work on growth hormone action as well as perception and transduction of stimulation by gravity and the red and blue range of the electromagnetic spectrum (Hager et al. 1971, and references therein). The tip region of this organ is the site of auxin synthesis. It delivers this growth factor longitudinally to the homogeneous cell layer(s) of the epidermis and cortex covering the primary leaf. Both tissues have been shown to respond to auxin by a change in the electrical properties of the plasma membrane and cell expansion (Peters and Felle 1990). On the level of the plasma membrane of coleoptile cells, auxin action is initiated by a rapid depolarization (Bates and Goldsmith 1983). The mechanism underlying the auxin stimulation has been studied by patch-clamp analysis in guard cells of *Vicia faba*. Following the application of auxin, GCAC1, the *G*uard *C*ell *A*nion *C*hannel (for review, see Hedrich 1994), is activated through a shift in its activation threshold towards the resting potential of the cell (Marten et al. 1991). While the immediate activation of an anion conductance may account for the initial depolarization, the delayed but sustained increase in H^+ extrusion through the P-type ATPase may underly the hyperpolarization phase (Lohse and Hedrich 1992; Rück et al. 1993).

In both experimental systems, coleoptiles and guard cells, the auxin response in the long term is accompanied by an increase in the K^+-salt concentration, volume and turgor. In guard cells, however, this process is reversible. Thus, K^+-uptake channels have recently been postulated to present targets for this growth factor, too (Blatt and Thiel 1994). Whereas there is no evidence for a direct auxin (ligand) interaction as shown for GCAC1 (Marten

Abbreviations: $CKC1_{in}$=Coleoptile *K*$^+$ *C*hannel *in*ward rectifier; U= membrane voltage; I_{ss}=steady-state currents; I_{tail}=tail currents

Correspondence to: R. Hedrich; FAX: 49 (511) 7622606

et al. 1991; Lohse and Hedrich 1992), the hormone, as well as antibodies against the maize auxin-binding protein and specific peptides thereof, have been shown to affect the K^+ channel through changes in the cytosolic pH (Thiel et al. 1994, and references therein).

In this report we have elucidated whether the plasma membranes of the two highly specialized, auxin-sensitive cell types are equipped with similar sets of ionic pathways or whether cell-specific subtypes are expressed.

Materials and methods

Protoplast isolation. Seeds of *Zea mays* L. (Dekalb, strain "Serse") were germinated on wet filter paper in the dark at room temperature. On days 3–5 coleoptiles of about 1–2 cm length were harvested. A small cut at the base of this organ enabled its removal while leaving the primary leaf on the seedling. After excision of the very tip, coleoptile segments were incubated with 0.8% (w/v) Onozuka RS cellulase (Yakult, Tokyo, Japan), 0.08% (w/v) pectolyase (Sigma, Deisenhofen, Germany), 0.5% bovine serum albumin (Sigma), 0.5% polyvinilpyrrolidone (Sigma), 500 mM sorbitol, 1 mM $CaCl_2$ and 5 mM Mes-KOH (pH 5.5) for 1 h at 30°C. Since the coleoptile segments were not abraded, only cortical cell protoplasts were released, as indicated by microscopic observations (not shown). Cortical protoplasts were filtered through nylon nets with mesh diameters of 100 and 50 µm, centrifuged for 5 min at 80·*g*. Protoplasts of 20–40 µm diameter and 20–50 pF capacitance, containing several amyloplasts, were selected for patch-clamp measurements.

Patch-clamping coleoptile protoplasts. Patch pipettes were sealed against the plasma membrane to study ion fluxes in the whole-cell configuration and in cell-free, outside-out membrane patches (Hedrich and Schroeder 1989). Currents were measured with an Axon 200A patch-clamp amplifier (Axon Instruments, Inc., Foster City, Calif., USA) and low-pass-filtered with the four-pole Bessel filter of the amplifier. Data were digitized with a minimum sampling rate of 0.4 ms (ITC 16; Instrutech Corp., Elmont, N.Y., USA) and stored on hard disk. Activation and deactivation kinetics were analyzed on a MacIntosh Quadra 950 personal computer, using Pulsefit software from HEKA (Lambrecht, Germany). Tail currents were determined by fitting an exponential function to data points (for details, see Hedrich et al. 1995). Data are representative of three to four independent experiments.

Solutions. Pipette: 100 mM KCl, 2 mM $MgCl_2$, 5 mM MgATP, 1 mM EGTA, 5 mM Hepes-Tris (pH 7.2). Bath: 30 mM KCl (RbCl, NaCl, LiCl or NH_4Cl), 0–1 mM $CaCl_2$, 2 mM $MgCl_2$, 10 mM Mes-Tris (pH 5.6). All solutions were adjusted with sorbitol to 600–700 mOsmol. External monovalent and divalent cations and auxin were applied by bath perfusion at a rate of 1 ml·min^{-1} (Gambale et al. 1994). For details with respect to variations in solute composition, see figure legends.

Results

Proton-ATPase. With solutions containing 100 mM KCl plus 5 mM MgATP buffered to pH 7.2 in the pipette and 30 mM KCl at pH 5.6 in the bath, 2- to 4-MΩ patch pipettes were sealed onto coleoptile cortical cell protoplasts. After breaking the membrane patch underlying the pipette tip by a short suction pulse we measured the free-running membrane potential in the current-clamp mode (cf. Lohse and Hedrich 1992). In the absence of MgATP in the pipette, membrane potentials between –150 and –200 mV were recorded until the pipette solution equilibrated with the cytosol and depleted the cell of ATP (usually 5–10 min in 20- to 40-pF cells; for diffusion in guard-cell protoplasts, see Marten et al. 1992). These values are far more negative than the Nernst potentials for K^+ (E_{K^+}=–20 mV), Cl^- (E_{Cl^-}=+20 mV), Mg^{2+} ($E_{Mg^{2+}}$=0 mV) and Ca^{2+} ($E_{Ca^{2+}}$>+200 mV). In the presence of MgATP, however, hyperpolarized potentials could be maintained for prolonged times, indicating that MgATP suffices to maintain the residual H^+-ATPase activity. Since the voltage profile of the electrogenic pump of coleoptile protoplasts and its sensitivity to auxins (Felle et al. 1986; Palme et al. 1991) were similar to those of the guard-cell enzyme (Lohse and Hedrich 1992; Rück et al. 1993), in the following we will focus on the peculiar properties of the other major conductance of the coleoptile protoplast, the K^+-uptake channel. This channel will be denoted as $CKC1_{in}$ for *C*oleoptile *K*$^+$ *C*hannel *in*ward rectifier throughout the text.

Potassium-uptake channels. When in the presence of 100 mM KCl in the pipette and 30 mM KCl in the bath the membrane potential was clamped around the diffusion potential for K^+ (E_{K^+}=–20 mV but 0 to –40 mV under conditions used in Fig. 2), 0.3–1.2-s voltage steps between +70 and –80 mV neither elicited K^+-release currents nor anion currents of either direction (Fig. 1c). Upon hyperpolarization negative to –80 mV, inward currents activated in a voltage- and time-dependent manner (Fig. 1a, c). Activation-curve analyses showed a half-activation potential $U_{1/2}$ of –112 mV (Fig. 1d), at this voltage 50% of the K^+ channels were open. In order to determine the charge carrier of this current we performed tail-current analyses (for details, see Hedrich et al. 1986). During the pre-pulse to –200 mV the majority of the voltage-dependent conductances were induced [I_{ss}=N·i(U)·P_o(U), where I_{ss} is the steady-state current, i is the single-channel current, U is the membrane voltage, P_o is the open probability of a single channel, and N is the number of channels) to deactivate during a subsequent series of depolarizing voltage steps (Fig. 1b). The tail current at t= 0 of the second pulse represents the ion flux through the open channel at a given voltage (tail current: I_{tail}=N·i(U), N= constant). Based on the Goldman-equation, the potential at which the current reverses direction, the zero-current potential ($U_{reversal}$, i($U_{reversal}$)= 0), is a measure of the nature of charge carrier(s) (Hedrich et al. 1986).

Potassium sensitivity. During the replacement of 30 mM KCl by 3, 10, and 100 mM KCl the reversal of the tail currents followed the Nernst potential for K^+ with a 56-mV shift per tenfold change in the K^+ activity (Figs. 1b, 2a). As a result of an increase in the external K^+ activity, steady-state K^+ currents saturated in a Michaelis-Menten type manner (Fig. 2b, c), indicating that K^+ uptake is limited by the transport capacity of the K^+ channel. The K_m of about 6 mM is in the same order of magnitude as described for the guard-cell homologue (Schroeder and Fang 1991). Alterations in the extracellular K^+ level did not significantly affect the threshold potential of activa-

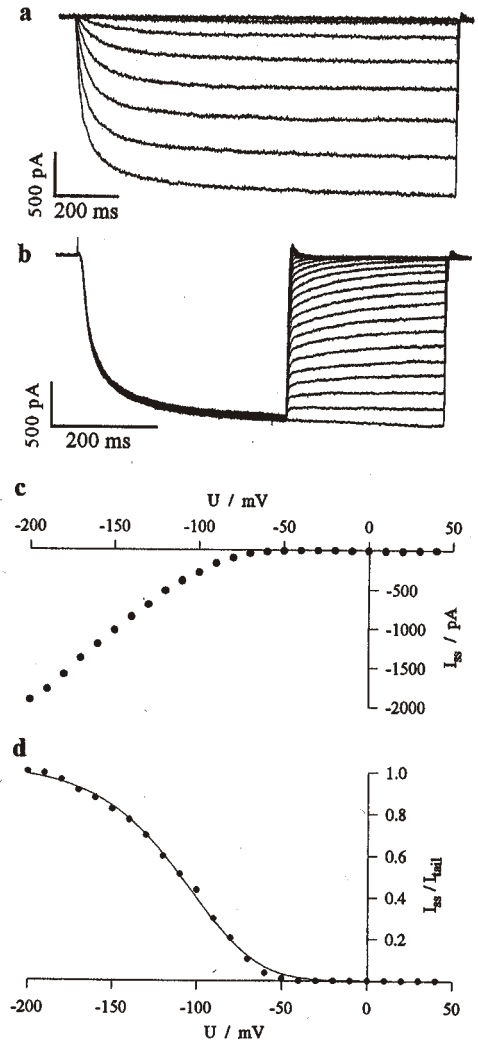

Fig. 1a–d. Inward-rectifying whole-cell currents in maize coleoptile protoplasts mediated by $CKC1_{in}$. **a** Time- and voltage-dependent inward currents elicited by voltage steps (of 1.2 s duration) to hyperpolarized potentials from a holding potential of 0 mV. Current traces during consecutive voltage steps from –200 mV to 0 mV in 20-mV increments are superimposed. Note that the activation threshold was around –80 mV. The P/4 procedure was used to correct for capacitive and leakage currents. **b** Voltage-dependent relaxations of inward currents in response to a double-voltage-step protocol. Within the first pulse to –200 mV, K^+ currents were induced to deactivate during the second pulse to depolarizing voltages (from –200 mV to +40 mV in 10-mV increments) in a voltage-dependent manner. Note that the current reverts direction at the Nernst potential for potassium (cf. Fig. 2a). **c** Current-voltage relation of inward-rectifying K^+ currents. Data points were obtained from a voltage protocol described in **a** but with a pulse interval of 10 mV. **d** Activation-curve analysis of $CKC1_{in}$. Activation curves are based on the current ratio I_{ss}/I_{tail} (extrapolated to t=0, see *Materials and methods*), normalized to the value obtained at –200 mV (see **a** and **b**) and thus represent a measure of the open probability of the K^+ channel. Assuming that four identical subunits form the active channel, data points were fitted well with the modified Boltzmann equation, $N/(1+\exp(\alpha U+\beta))^4$; half-activation voltage $U_{½}$=–112 mV (=–(1.67+β)/α) and a slope factor 1/α=31 mV were obtained. N is a scaling factor

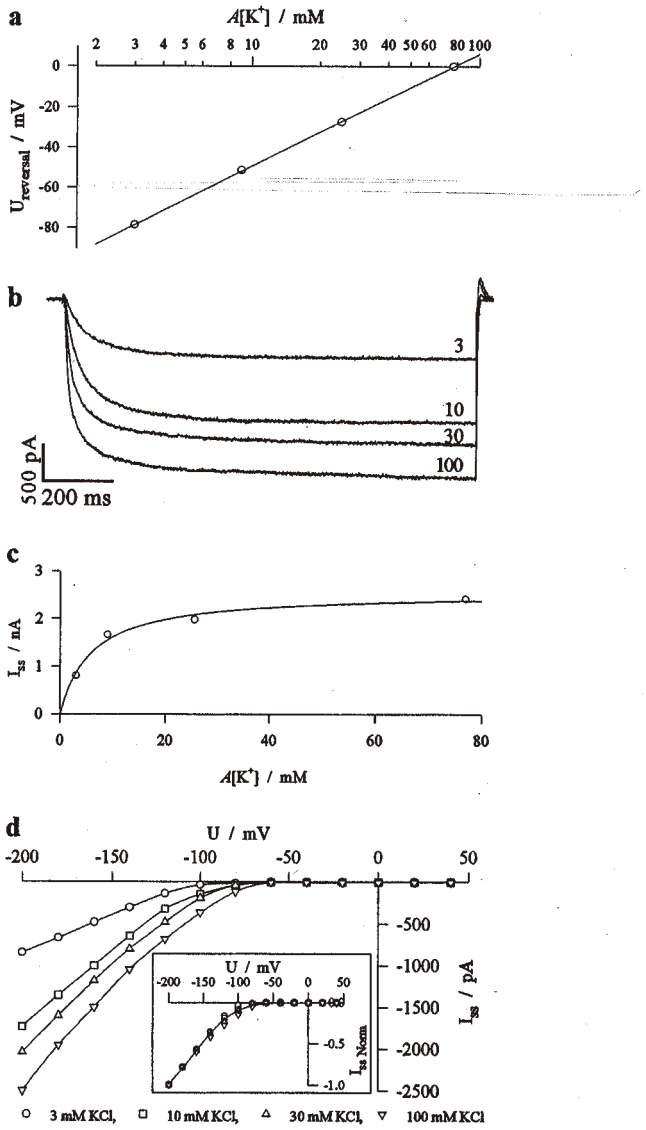

Fig. 2. a Reversal potential of K^+ currents through $CKC1_{in}$ as a function of external K^+ activity. With 100 mM potassium inside the maize coleoptile protoplast, changes in the extracellular K^+ level from 100 to 30, 10, and 3 mM caused the reversal potential of the tail currents to shift with the Nernst potential for K^+. Note that data are presented as a semilogarithmic plot and fitted with a linear regression function with a slope of 56 mV for a tenfold change in K^+ activity. **b** Steady-state whole-cell currents, in response to 1.2-s voltage pulses to –200 mV, in the presence of 3, 10, 30 and 100 mM K^+ in the bath solution. **c** Steady-state inward currents at –200 mV as a function of the external K^+ activity. Data points were well fitted by a Michaelis-Menten function characterized by a K_m value of 6 mM. **d** Current-voltage relation of $CKC1_{in}$ in the presence of extracellular 3, 10, 30 and 100 mM K^+. Note that the activation threshold is not affected by the K^+ gradient (*insert*)

tion (Fig. 2d), in line with impalement-electrode studies on guard cells (Blatt 1992) but in contrast to patch-clamp studies on guard-cell protoplasts (Schroeder and Fang 1991).

Selectivity and block. Upon substitution of K^+ by other monovalent inorganic cations, inward currents were completely abolished (Fig. 3b, c). Only NH_4^+, another

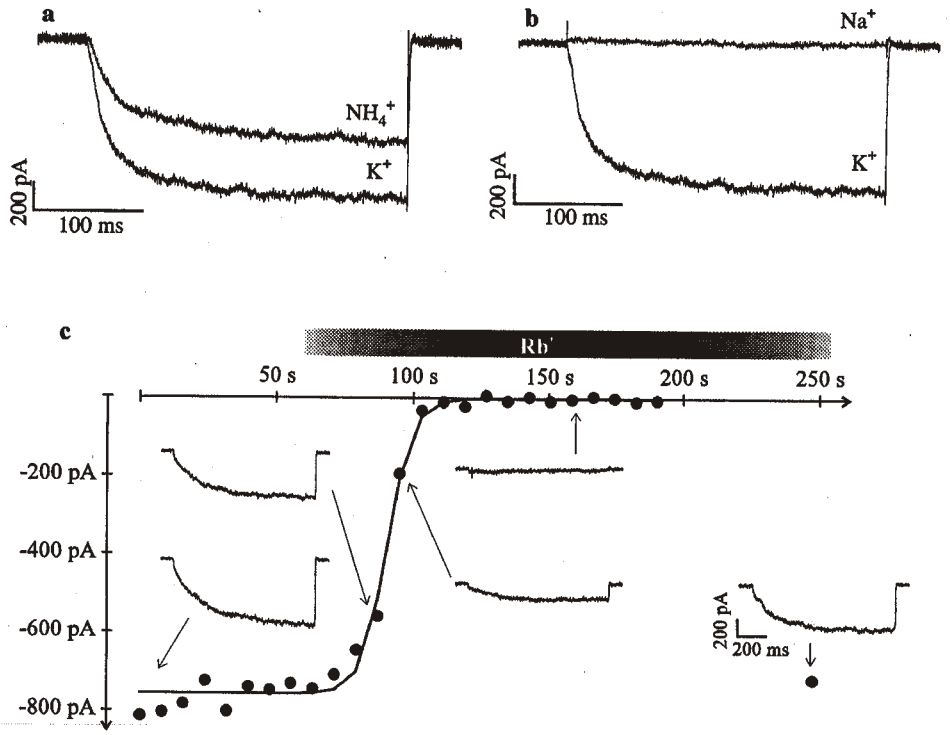

Fig. 3a–c. Selectivity of $CKC1_{in}$ with respect to monovalent cations. **a** After replacement of 30 mM K^+ by NH_4^+, steady-state currents in response to voltage steps to –200 mV (Fig. 1a), were reduced by 30–40%, indicating that the K^+ channel is less permeable to NH_4^+ than to K^+. **b** Replacement of potassium by sodium. In sodium solution, inward currents were largely suppressed, $P_{Na^+}/P_{K^+}<0.03$. This value results from tail-current analysis before complete exchange of K^+ by Na^+ via the bath perfusion system. **c** Steady-state currents in response to hyperpolarizing voltage pulses (as in **a**) during the exchange of K^+ by Rb^+. Data points reflect K^+ currents at times after onset of K^+-Rb^+ exchange and *vice versa*. The relative time is proportional to the mole fraction of Rb^+/K^+. *Insets*: Current traces illustrate the magnitude and kinetics of $CKC1_{in}$ during Rb^+ treatment. Note the recovery around t = 250 s in Rb^+-free solution

important nutrient besides K^+, significantly permeated through the channel. The relative permeability $P_{NH_4^+}/P_{K^+}$, evaluated from tail-current experiments, was around 0.25 and the ratio $I_{NH_4^+}/I_{K^+}$ of the steady-state current in the range of 60–70% (Fig. 3a).

Unlike the guard-cell channel or other K^+ channels (Hille 1992), even Rb^+, often used as a tracer for potassium, was unable to pass the inward rectifier (Fig. 3c). This observation is in line with the findings of Behl and Jeschke (1982, and references therein), which showed that Rb^+ is not a suitable tracer for K^+-flux measurements with barley roots and possibly with other grasses as well. The lack of Rb^+ permeability, however, has no consequence for the life of a maize plant, but it does for the data obtained from flux analysis where $^{86}Rb^+$ was used as a tracer for K^+.

In contrast to 1 mM Rb^+, which did not affect $CKC1_{in}$ when applied against a background of 30 mM K^+, the same concentration of Cs^+ almost completely blocked the inward rectifier (Fig. 4). The block imposed by Cs^+, a well-known K^+-channel blocker, was strongly voltage- and concentration-dependent (Fig. 4c). When drawn into the extracellular mouth of the channel by hyperpolarized voltages (e.g. at –200 mV in the tail experiment shown in Fig. 4a, b), subsequent depolarizing voltage pulses unblocked the channel. Whereas the block was faster than the time-resolution of the whole-cell clamp, the unblocking kinetics, and thus the amplitude of the "Cs^+-free" tail (at t=0), could be separated from the on-going deactivation process (Fig. 4a, b). In order to prove whether cesium ions, which sense the electrical field across the channel pore, interfere with the gating process, we superimposed the deactivation kinetics of the K^+ current in the presence and absence of 200 μM Cs^+ (Fig. 4b). While deviating at potentials negative to –80 mV (data not shown), the kinetics at more-depolarized values were indistinguishable from each other (Fig. 4b, black and grey traces at –80, –50, and –20 mV). This behaviour indicates that positive to –80 mV (i) K^+ channels were completely unblocked and that (ii) Cs^+ does not affect the voltage-dependent gating. Additional evidence for the latter was provided by the fact that the activation curves (I_{ss}/I_{tail} as a function of voltage) for the two experimental conditions were similar (data not shown).

Modulation by calcium. In guard cells of broad bean and maize, both external Cs^+ and Ca^{2+} block the inward rectifier in a voltage-dependent manner (Rudy 1988; Fairley-Grenot and Assmann 1992a; own data, not shown). When the Ca^{2+} concentration on the external face of the K^+-uptake channel $CKC1_{in}$ was raised from nominally 0 to 1 mM the coleoptile channel remained unaffected. On the cytosolic side, however, a rise in Ca^{2+} concentration from the nanomolar range (no Ca^{2+}, 1 mM EGTA) to levels above 1 μM (1 mM Ca^{2+}, no EGTA) increased the kinetics of activation about four to fivefold (Fig. 5a); likewise the deactivation kinetics were slowed by an increase in this divalent ion (Fig. 5b). Since these measurements were performed in the presence of at least 2 mM internal Mg^{2+} an effect of Ca^{2+} on the surface charge density could be excluded (Hille 1992).

Compared with guard cells, elevated internal Ca^{2+} levels neither blocked nor shifted the activation threshold of $CKC1_{in}$ towards more-negative potentials (Schroeder and Hagiwara 1989; Fairley-Grenot and Assmann 1992b). Thus K^+-uptake channels from coleoptiles and guard cells, even within the same plant (*Zea mays*),

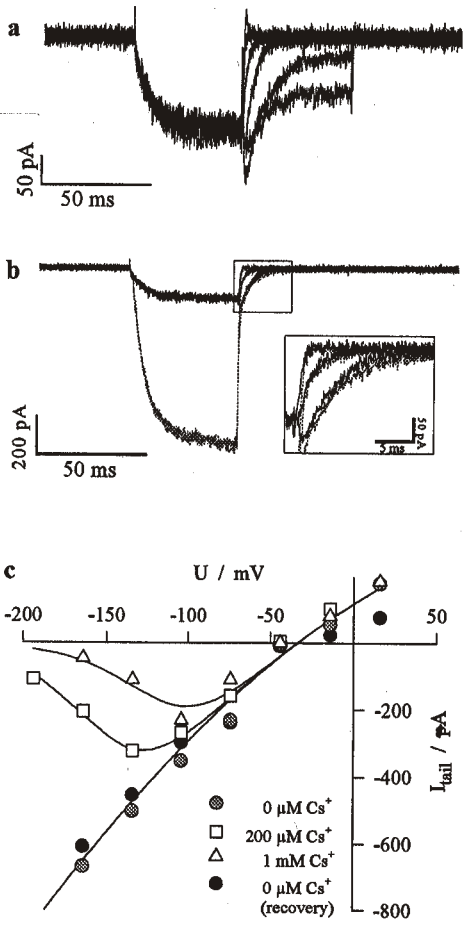

Fig. 4a–c. The channel $CKC1_{in}$ is blocked by Cs^+ in a voltage-dependent manner. **a** Activation and deactivation of $CKC1_{in}$ in the presence of Cs^+ and in response to voltage protocols similar to that in Fig. 1b. Note that, in the presence of 200 µM Cs^+ in the bath solution, tail currents at –140, –110, and –80 mV even exceed the current amplitude at the end of the prepulse to –200 mV. **b** Superimposition of inward currents during tail pulses to –80, –40, –20 mV in the presence (*black*) and absence (*grey line*) of 200 µM Cs^+. **c** Current-voltage relation of tail currents (at t=0) in the presence of 200 µM and 1 mM Cs^+, as well as before and after (*controls*) challenge with the inhibitor. Note that the peak potential varies with cesium concentration

strongly differ in their sensitivity toward external and internal changes of this second messenger.

Single-channel equivalent of $CKC1_{in}$. When cell-free outside-out membrane patches were excised from whole cells, characterized by a pronounced $CKC1_{in}$ activity, 5-7-pS channel openings appeared at potentials more negative than –100 mV (data not shown).

Discussion

The electrical properties of the plasma membrane of cortical cells of maize coleoptiles were dominated by two major conductances, the H^+-ATPase and the voltage-dependent K^+-uptake channel $CKC1_{in}$. Under our experimental conditions, which in other cell types were used to study, for example K^+ release and Cl^- channels (Bush et al. 1988; Keller et al. 1989), no additional conductances were observed in the voltage-range between –200 and +70 mV. The absence or low activity of K^+-release channels is in agreement with measurements on barley aleurone and oat mesophyll cells but in contrast to barley mesophyll cells (Bush et al. 1988; Hedrich et al. 1990; Kourie and Goldsmith 1992). Although coleoptile cells are programmed for rapid salt uptake, volume increase, turgor formation and finally cell expansion, we cannot exclude the possibility that channels for K^+ and anion release are expressed or activated under certain conditions.

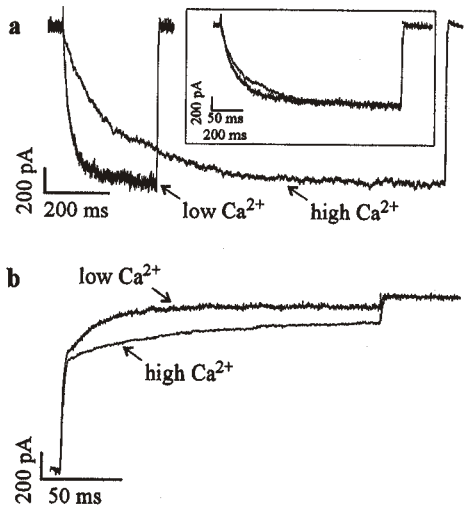

Fig. 5a, b. Changes in cytosolic calcium levels affect the voltage-dependent kinetics of $CKC1_{in}$. **a** Activation kinetics during hyperpolarizing voltage pulses of 300 ms duration in nanomolar Ca^{2+} concentrations are plotted together with those obtained for a 1.2-s pulse at 1 mM Ca^{2+}. *Inset*: Superimposition of activation kinetics scaled to the length of the saturating voltage pulse. **b** Deactivation kinetics at –110 mV under the same conditions as in **a**

It is known from the early experiments on auxin action that the ability to respond to the growth hormone requires the presence of extracellular Ca^{2+} (cf. Hager et al. 1971). Recent studies have indicated that in coleoptile cells the cytosolic Ca^{2+} level rises during auxin treatment (Gehring et al. 1990). Under physiological external Ca^{2+} concentrations (1–5 mM), however, we have found neither voltage-dependent nor ATP-dependent Ca^{2+} conductances (Lohse and Hedrich 1992; Thuleau et al. 1994) positive to the threshold potential of the inward rectifier nor a Ca^{2+} permeability of the K^+ channel itself[1]. We cannot, however, exclude the possibility that mechano-sensitive Ca^{2+}-permeable channels (Cosgrove and Hedrich 1991) activate in response to an auxin-induced turgor increase.

Our initial experiments showed that the voltage-dependent properties of the K^+ uptake channel in growth-hormone-sensitive cells were not affected by micromolar

[1] Recently Gassmann and Schroeder (1994) were able to demonstrate that the putative Ca^{2+} permeability of the Ca^{2+}-sensitive K^+-uptake channel of guard cells only appeared when the shift in liquid-junction potential was not compensated (Fairley-Grenot and Assmann 1992a). For discussion of another discrepancy, putative Ca^{2+} permeability but lack of cytosolic Ca^{2+}-sensitivity, see Schulz-Lessdorf et al. 1994

amounts of the auxin 2,4D in the bath (cf. Marten et al. 1991) or the presence of MgATP in the pipette (cf. Spalding and Goldsmith 1993; Müller-Röber et al. 1995).

Do Ca^{2+} sensitivity and the selectivity profiles of $CKC1_{in}$ represent cell-type-specific features or properties of channel subtypes associated with the Gramineae? The properties of $CKC1_{in}$ with respect to changes in Ca^{2+} concentration are in line with the extra- and intracellular levels of Ca^{2+} observed during auxin action (Gehring et al. 1990). In contrast to the guard-cell channel, the transport capacity of $CKC1_{in}$ is not affected by elevated levels of calcium on both sides. Whereas a rise in the cytosolic Ca^{2+} only slowed the activation and deactivation kinetics (Fig. 5) of the coleoptile channel, the guard-cell channel is characterized by (i) a voltage-dependent block through millimolar concentrations of extracellular Ca^{2+} as well as (ii) modification of gating by micromolar cytosolic concentrations of this divalent cation (Schroeder and Hagiwara 1989; Fairley-Grenot and Assmann 1992a). Consequently both channels might differ in their pore structure and presence of a regulatory Ca^{2+}-site. Additional evidence for a unique selectivity filter within the coleoptile channel, compared with other K^+-channel types, is provided by the lack of Rb^+ permeability (Fig. 3c). The lack of detailed selectivity studies on *Zea mays* L. guard cells, however, prevents further comparison[2]. In guard cells of broad bean the permeability of Rb^+ relative to K^+, $P_{Rb}+/P_K+$, is about 0.3, in agreement with the ratio found for the K^+-uptake channel cloned from potato guard cells (Müller-Röber et al. 1995).

To date, plasma-membrane K^+ channels in the Gramineae have been studied in corn cell-suspension cultures (Ketchum et al. 1989), wheat roots (Gassmann and Schroeder 1994), root hairs (Schachtman et al. 1991) and cortex (Findlay et al. 1994), barley xylem parenchyma and aleurone, as well as barley and oat mesophyll cells (Bush et al. 1988; Hedrich et al. 1990; Kourie and Goldsmith 1992; Wegner and Raschke 1994). Potassium-uptake channels of barley xylem parenchyma and wheat root hair protoplasts were readily permeable to Rb^+. In parenchyma cells even Cs^+, a blocker of the K^+ channel in coleoptiles, root hairs and mesophyll cells, could penetrate the inward rectifier. These cells, concerned with the loading the xylem with macro- and micronutrients (among them K^+ and Ca^{2+}), are equipped with K^+-uptake channels sensitive to external Ca^{2+} but insensitive to elevated cytoplasmic levels of this divalent cation (Wegner et al. 1994).

[2] By comparing the voltage-dependent activation kinetics of the broad-bean and *Zea mays* guard-cell K^+-uptake channels it has been emphasized that differences of milliseconds in the activation half-times account for variations in stomatal opening in both plants (Fairley-Grenot and Assmann 1993). Even faster kinetics have been measured for barley aleurone (Bush et al. 1988) and maize coleoptile K^+ channels, cells which are not poised for reversible change in the K^+-salt concentration within tens of minutes; thus the difference between stomata of dicotyledons and monocotyledonous grasses might relate to the hydrodynamics of the two stoma types rather than their K^+-channel kinetics

Conclusion. Apart from pronounced differences in activation kinetics, the voltage-dependent properties of the coleoptile channel are similar to inward-rectifying K^+ channels in vivo and to cloned K^+ channels from *Arabidopsis thaliana* (cellular location still unknown) and *Solanum tuberosum* guard cells functionally expressed in frog oocytes (Hedrich et al. 1995; Müller-Röber et al. 1995; for review, see Hedrich and Becker 1994). With respect to the exclusion of Rb^+ the selectivity filter of the coleoptile channel is exceptional. Therefore we are currently investigating (i) whether this is a property of coleoptile cells in particular or C_4 grasses in general and (ii), by molecular analysis, whether the pore region of this channel is structurally related to *Shaker* and KAT1 mutants; and (iii) the involvement of this channel in auxin-induced signal transduction as well as co-expression of its gene along with that of the H^+-ATPase and the *aux* genes (genes coding for auxin-binding-proteins, e.g. Palme et al. 1992).

Experiments were conducted in the laboratory of F. G. during the stay of R. H. as a guest professor sponsored by Special Project RAISA, subproject N. 2.1, paper N. 2155.

References

Bates GW, Goldsmith MHM (1983) Rapid response of the plasma-membrane potential in oat coleoptiles to auxin and other weak acids. Planta 159:231–237

Behl R, Jeschke WD (1982) Potassium fluxes in excised barley roots. J Exp Bot 33:584–600

Blatt MR (1992) K^+ channels of stomatal guard cells: characteristics of the inward rectifier and its control by pH. J Gen Physiol 99:615–644

Blatt MR, Thiel G (1994) K^+ channels of stomatal guard cells: Bimodal control of the K+ inward-rectifier evoked by auxin. Plant J 5:55–68

Bush DS, Hedrich R, Schroeder JI, Jones RL (1988) Channel-mediated K^+ flux in barley aleurone protoplasts. Planta 176: 368–377

Cosgrove DJ, Hedrich R (1991) Stretch-activated chloride, potassium, and calcium channels coexisting in plasma membranes of guard cells of *Vicia faba* L. Planta 186:143–153

Fairley-Grenot KA, Assmann SM (1992a) Permeation of Ca^{2+} through K^+ channels in the plasma membrane of *Vicia faba* guard cells. J Membr Biol 128:103–113

Fairley-Grenot KA, Assmann SM (1992b) Whole-cell K^+ current across the plasma membrane of guard cells from a grass: *Zea mays*. Planta 186:282–293

Fairley-Grenot KA, Assmann SM (1993) Comparison of K^+-channel activation and deactivation in guard cells from a dicotyledon (*Vicia faba* L.) and a graminaceous monocotyledon (*Zea mays*). Planta 189:410–419

Felle H, Brummer B, Bertl A, Parish RW (1986) Indole-3-acetic acid and fusicoccin cause cytosolic acidification of corn coleoptile cells. Proc Natl Acad Sci USA 83:8992–8995

Findlay GP, Tyerman SD, Skerrett AG (1994) Pump and K^+ inward rectifiers in the plasmalemma of wheat root protoplasts. J Membr Biol 139:103–116

Gambale F, Kolb HA, Cantù AM, Hedrich R (1994) The voltage-dependent H^+-ATPase of the sugar beet vacuole is reversible. Eur Biophys J 22:399–403

Gassmann W, Schroeder JL (1994) Inward-rectifying K^+ channels in root hairs of wheat. Plant Physiol 105:1399–1408

Gehring CA, Irving HR, Parish RW (1990) Effect of auxin and abscisic acid on cytosolic calcium and pH in plant cells. Proc Natl Acad Sci USA 87:9645–9649

Hager A, Menzel H, Krauss A (1971) Versuche und Hypothese zur Primärwirkung des Auxins beim Streckungswachstum. Planta 100:1–15

Hedrich R (1994) Voltage-dependent chloride channels in plant cells: Identification, characterization, and regulation of a guard cell anion channel. Curr Top Membr 42:1–33

Hedrich R, Becker D (1994) Green circuits – The potential of plant specific ion channels. Plant Mol. Biol 26, 1637–1650

Hedrich R, Flügge UI, Fernandez JM (1986) Patch-clamp studies of ion transport in isolated plant vacuoles. FEBS Lett 204:228–232

Hedrich R, Busch H, Raschke K (1990) Ca^{2+} and nucleotide dependent regulation of voltage dependent anion channels in the plasma membrane of guard cells. EMBO J 9:3889–3892

Hedrich R, Schroeder JI (1989) The physiology of ion channels and electrogenic pumps in higher plants. Annu Rev Plant Physiol 40:539–569

Hedrich R, Moran O, Conti F, Busch H, Becker D, Gambale F, Dreyer I, Küch A, Neuwinger K, Palme K (1995) Inward rectifier potassium channels in plants differ from their animal counterparts in response to voltage and channel modulators. Eur Biophys J 23: in press

Hille B (1992) Ionic channels of excitable membranes. Sinauer Associates, Sunderland, Massachusetts

Keller B, Hedrich R, Raschke K (1989) Voltage-dependent anion channels in the plasma membrane of guard cells. Nature 341: 450–453

Ketchum KA, Shrier A, Poole RJ (1989) Characterization of potassium-dependent currents in protoplasts of corn suspension cells. Plant Physiol 89:1184–1192

Kourie J, Goldsmith MHM (1992) K^+ channels are responsible for an inwardly rectifying current in the plasma membrane of mesophyll protoplasts of *Avena sativa*. Plant Physiol 98:1087–1097

Lohse G, Hedrich R (1992) Characterization of the plasma-membrane H^+-ATPase from *Vicia faba* guard cells. Planta 188: 206–214

Marten I, Lohse G, Hedrich R (1991) Plant growth hormones control voltage-dependent activity of anion channels in the plasma membrane of guard cells. Nature 353:1–4

Marten I, Zeilinger C, Redhead C, Landry DW, Al-Awqati Q, Hedrich R (1992) Identification and modulation of a voltage dependent anion channel in the plasma membrane of guard cells by high-affinity ligands. EMBO J 11:3569–3575

Müller-Röber B, Ellenberg J, Provart N, Willmitzer L, Busch H, Becker D, Dietrich P, Hoth S, Hedrich R (1995) Cloning and electrophysiological analysis of KST1, an inwardly rectifying K^+ channel expressed in potato guard cells. EMBO J 14:2409–2416

Palme K, Hesse T, Moore I, Campos N, Feldwisch J, Garbers C, Hesse F, Schell J (1991) Hormonal modulation of plant growth: the role of auxin perception. Mech Devel 33:97–106

Palme K, Hesse T, Campos N, Garbers C, Yanofsky MF, Schell J (1992) Molecular analysis of an auxin binding protein gene located on chromosome 4 of *Arabidopsis*. Plant Cell 4:193–201

Peters WS, Felle H (1990) Control of apoplast pH in corn coleoptile segments. I: The endogenous regulation of cell wall pH. J Plant Physiol 137:1–8

Rudy B (1988) Diversity and ubiquity of K channels. Neuroscience 25:729–749

Rück A, Palme K, Venis MA, Napier RM, Felle HH (1993) Patch-clamp analysis establishes a role for an auxin binding protein in the auxin stimulation of plasma membrane current in *Zea mays* protoplasts. Plant J 4:41–46

Schachtman DP, Tyerman SD, Terry BR (1991) The K^+/Na^+ selectivity of a cation channel in the plasma membrane of root cells does not differ in salt-tolerant and salt-sensitive wheat species. Plant Physiol 97:598–605

Schroeder JI, Fang HH (1991) Inward-rectifying K^+ channels in guard cells provide a mechanism for low-affinity K^+ uptake. Plant Biol 88:11583–11587

Schroeder JI, Hagiwara S (1989) Cytosolic calcium regulates ion channels in the plasma membrane of *Vicia faba* guard cells. Nature 338:427–430

Schulz-Lessdorf B, Dietrich P, Marten I, Lohse G, Busch H, Hedrich R (1994) Coordination of plasma membrane and vacuolar membrane ion channels during stomatal movement. In: Leigh RA (eds) The SEB Symposium 48, Membrane transport in plants and fungi. SEB, Cambridge 1994, pp 99–112

Spalding EP, Goldsmith MHM (1993) Activation of K^+ channels in the plasma membrane of *Arabidopsis* by ATP produced photosynthetically. Plant Cell 5:477–484

Thiel G, Blatt MR, Fricker MD, White IR, Millner P (1994) Modulation of K^+ channels in *Vicia* stomatal guard cells by peptide homologs to the auxin-binding protein C terminus. Proc Natl Acad Sci USA 90:11493–11497

Thuleau P, Ward JM, Ranjeva R, Schroeder JI (1994) Voltage-dependent calcium-permeable channels in the plasma membrane of a higher plant cell. EMBO J 13/13:2970–2975

Wegner LH, Raschke K (1994) Ion channels in the xylem parenchyma of barley roots. Plant Physiol 105:799–813

Wegner LH, De Boer AH, Raschke K (1994) Properties of the K^+ inward rectifier in the plasma membrane of xylem parenchyma cells from barley roots: Effects of TEA^+, Ca^{2+}, Ba^{2+} and La^{3+}. J Membr Biol 142:363–379

Note added in proof

We have just succeeded in the isolation of two corn coleoptile cDNA clones with structural homology to members of plant K^+ channel families.

⇒ zurück zur Übersicht

1995

Hedrich, Moran, Conti, Busch, Becker, Gambale, **Dreyer**, Küch, Neuwinger, Palme

Inward rectifier potassium channels in plants differ from their animal counterparts in response to voltage and channel modulators.

Eur. Biophys. J. **24**:107-115.

Eur Biophys J (1995) 24: 107–115

European Biophysics Journal

Inward rectifier Potassium channels in plants differ from their animal counterparts in response to voltage and channel modulators

R. Hedrich[1], O. Moran[2], F. Conti[2], H. Busch[1], D. Becker[1], F. Gambale[2], I. Dreyer[1], A. Küch[3], K. Neuwinger[1], K. Palme[3]

[1] Institut für Biophysik, Universität Hannover, Herrenhäuserstrasse 2, D-30419 Hannover, Germany
[2] Istituto di Cibernetica e Biofisica, C.N.R., Via DeMarini 6, I-16149 Genova, Italy
[3] Max-Planck-Institut für Züchtungsforschung, Carl-von-Linne-Weg 10, D-50829 Köln, Germany

Received: 9 September 1994 / Accepted in revised form: 2 February 1995

Abstract. We have investigated the electrophysiological basis of potassium inward rectification of the *KAT1* gene product from *Arabidopsis thaliana* expressed in *Xenopus* oocytes and of functionally related K^+ channels in the plasma membrane of guard and root cells from *Vicia faba* and *Zea mays*. The whole-cell currents passed by these channels activate, following steps to membrane potentials more negative than –100 mV, with half activation times of tens of milliseconds. This voltage dependence was unaffected by the removal of cytoplasmic magnesium. Consequently, unlike inward rectifier channels of animals, inward rectification of plant potassium channels is an intrinsic property of the channel protein itself. We also found that the activation kinetics of *KAT1* were modulated by external pH. Decreasing the pH in the range 8.5 to 4.5 hastened activation and shifted the steady state activation curve by 19 mV per pH unit. This indicates that the activity of these K^+ channels and the activity of the plasma membrane H^+-ATPase may not only be coordinated by membrane potential but also by pH. The instantaneous current-voltage relationship, on the other hand, did not depend on pH, indicating that H^+ do not block the channel. In addition to sensitivity towards protons, the channels showed a high affinity voltage dependent block in the presence of cesium, but were less sensitive to barium. Recordings from membrane patches of *KAT1* injected oocytes in symmetric, Mg^{2+}-free, 100 mM-K^+, solutions allowed measurements of the current-voltage relation of single open *KAT1* channels with a unitary conductance of 5 pS. We conclude that the inward rectification of the currents mediated by the *KAT1* gene product, or the related endogenous channels of plant cells, results from voltage-modulated structural changes within the channel proteins. The voltage-sensing or the gating-structures appear to interact with a titratable acidic residue exposed to the extracellular medium.

Correspondence to: R. Hedrich

Key words: Potassium channel – *KAT1* – Voltage dependence – Cesium block – pH dependence – Kinetics

Introduction

Since the application of the patch-clamp technique to higher pants, K^+-selective channels have been identified in various species and cell types such as guard cells, mesophyll cells, aleuron cells, and root cells (Schroeder et al. 1984, 1987; Moran et al. 1988; Bush et al. 1988; Spalding et al. 1993; Colombo and Cerana 1991; Schachtmann et al. 1991; for review see Hedrich and Schroeder 1989). In the different cell types two major classes of voltage-dependent K^+ channels have been distinguished: inward rectifiers, that pass inward K^+ fluxes at negative membrane potentials, and outward rectifiers, activated by depolarisation. Both classes are characterised by their long activation and deactivation times (tens of ms), lack of inactivation, and pronounced selectivity for K^+ over the monovalent cations, with a permeability sequence $K^+ > Rb^+ > Na^+ >> Cs^+$ (Schroeder et al. 1987).

Two cDNAs encoding plant K^+ channels (*KAT1* and *AKT1*) have been isolated from *Arabidopsis thaliana* by complementation of K^+ transport deficient yeast mutants (Sentenac et al. 1992; Anderson et al. 1992). Following heterologous expression of *KAT1* in *Xenopus* oocytes and of *AKT1* in *Sf9* cells, it was demonstrated that both gene products mediate inward rectifying K^+ currents, as expected from the cloning strategy (Schachtmann et al. 1992). The predicted structure of the gene products comprise a membrane domain containing a putative pore forming region, which is highly homologous to the transmembrane segments S1–S6 and to the H5 segment common to all members of the voltage-gated K^+ channels of the *Shaker* gene family from animal cells (Pongs 1992), indicating a common ancestor (Jan and Jan 1992). Only very recently two members of a new family of inward rectifying K^+ channels from animal cells (*IRK1* and *ROMK1*) have been identified. Compared to the *Shaker*-type K^+ channels they

contain a much smaller membrane domain, which lacks the first four transmembrane segments, including the putative voltage sensor S4 (Kubo et al. 1993; Ho et al. 1993). Thus, plant K^+ channels present an apparent paradox of structure-function relation, having more functional similarities with the new K^+ channel family to which they are structurally more distantly related. A tentative explanation is that the membrane domain S1–S4, which seems to be a determinant of the activation of *Shaker* channels at more positive voltages, is simply not functional in *KAT1*. Consequently *KAT1* might share with *IRK1* and *ROMK1* the block by intracellular Mg^{2+}, a mechanism of voltage-dependence that obviates intrinsic voltage sensors (Matsuda et al. 1987; Vandenberg 1987; Matsuda 1988). Contrary to this hypothesis, it has already been shown that, unlike *IRK1* and *ROMK1*, the voltage range of activation of plant inward rectifiers is only weakly dependent on the extracellular K^+ concentration (Schroeder and Fang 1991; Schachtmann et al. 1992; Blatt 1992). The experiments reported here aim at further characterising the functional properties of these channels. We concentrated on the effects of potential channel-blockers: cytoplasmic Mg^{2+}, extracellular Cs^+ and Ba^{2+}, as well as extracellular protons.

Our results indicate that plant inward rectifier K^+ channels have voltage-sensing mechanisms profoundly distinct from those adopted by their functional relatives in the animal kingdom. This encourages speculation that apart from the voltage-dependence of voltage-gated channels, their property to either pass inward or outward K^+-flux, may be founded independently in the channel structure.

Material and methods

Molecular biology

KAT1 was recloned from an *Arabidopsis thaliana* cDNA library (Elledge et al. 1991) by PCR as described by Nitschke et al. (1992). The sequences of the oligonucleotides used were: 5 prime end: 5′TTC CTC GAG CTC CGT CAG GGA AAA GAT ATC GAT CTC TTG G 3′. 3 prime end: 5′TTC CTC GAG CTA CGT CAG GGG ATA ATC TAG ACT TTT C 3′. The resulting PCR product was subcloned in pBluescript. The DNA sequence analysis was performed using an automated DNA sequence analyzer (A.L.F., Pharmacia). The open reading frame was identical to the one reported by Anderson et al. (1992). However, it contained a mutation in the 3′ non-translated region. The PCR product was subcloned as an Xba I/BamH I fragment into the pGEMHE vector (Liman et al. 1992) (kind gift of E. Liman). Plasmid DNA was prepared using standard recombinant DNA techniques with minor variations according to Sambrook et al. (1989). In vitro transcription was performed using the T7 MegaScript Kit (Ambion).

Injection of cRNA in Xenopus oocytes

Experiments were performed in Hannover and Genova. *Xenopus* frogs (Hannover) were purchased from Nasco (Wisconsin). Genova frogs were orginally purchased from Korlh (Hamburg) in 1991 and cultured in a small pond in the garden of Dr. R. Fioravanti in Camogli. Oocytes were isolated as described by Stühmer et al. (1987) and injected with *KAT1* cRNA (100 ng/µl) using a General Valve Picospritzer II microinjector (40 psi for 5–10 ms; Hannover) or Drumond "Nanoject" (46 nl, Genova). In order to compare *KAT1* expression in oocytes originating from the two different sources, preinjected oocytes and *KAT1* cRNA (Hannover) were transferred and analyzed in Genova.

Voltage-Clamp recordings

Whole cell K^+ currents were measured with a two microelectrode voltage-clamp (GeneClamp 500, Axon Instruments USA and Turbotec 01C, NPI Germany), using 0.2–0.4 MΩ (Genova) or 0.5–2 MΩ pipettes (Hannover) filled with 3 M KCl. Oocyte high potassium solution, KD98, contained (in mM): 98 KCl, 1 $CaCl_2$, 2 $MgCl_2$, 10 TRIS-HCl, pH 7.4. The low potassium solution, KD10, was essentially the same as KD98, but contained only 10 mM KCl. All solutios were adjusted to 270 mOsm with sorbitol. Currents were filtered with a cut-off frequency of 3 kHz before acquisition.

Single channel recordings

Patch pipettes were made from aluminium silicate glass capillaries, silicone rubber coated, and fire polished to a final resistance of 0.6–1.2 MΩ. Pipettes were filled with 120 mM KCl, 20 mM TRIS-HCl pH 7.4, 5 mM EDTA and oocytes were bathed in the same solution. The membrane of the oocyte was partially broken to equilibrate the intracellular space with the bathing solution. Single channel properties of *KAT1* expressed in oocytes were studied in cell attached patches formed on the intact membrane. Currents were recorded with a standard patch-clamp amplifier (EPC-7, List, Germany), filtered with a low-pass four-pole Bessel filter at a cut-off frequency of 1–5 kHz. Single channel events were sampled at 5–20 kHz. Linear capacities and leak currents were digitally subtracted using appropriate scaled current traces without channel openings. Measurements were performed at 21.5 ± 1.5 °C.

Single channel events were analysed from >4 patches excised from different oocytes. Currents were studied during test pulses ranging from –60 to –200 mV from a holding potential of –40 mV. Average currents from single and multichannel patches to reconstruct macroscopic currents were performed on the basis of at least 30 consecutive voltage pulses.

Patch-clamp studies on guard cell and root protoplasts

Guard cell protoplasts were enzymatically isolated from 2–3 week old leaves of the broad bean, *Vicia faba* (Hedrich et al. 1990). Root protoplasts were enzymatically isolated from 3 day old *Zea mays* seedlings as described by Schachtmann et al. (1991). Ionic currents were studied

in the whole-cell configuration of the patch clamp technique (Hedrich and Schroeder 1989). Currents were elicited by voltage-steps from –80 to –200 mV and 300–600 ms duration, from a holding potential of –40 mV, and measured with either EPC-7, EPC-9 (HEKA, Germany) or Axoclamp 200A (Axon Instruments, USA) patch clamp amplifiers, and low-pass filtered with an eight-pole Bessel filter.

Guard cells were bathed in a solution containing (in mM): 30 Kgluconate, 0.1–1 $CaCl_2$, 2 $MgCl_2$, 10 MES/TRIS pH 5.6. The pipette (intracellular) solution contained (in mM): 146 Kgluconate, 4 KCl, 10 HEPES/TRIS pH 7.2 and 2 Na_2ATP, 0.1 EGTA. Root cell extracellular solution contained (in mM): 10 KCl, 88 Kgluconate, 1 $MgCl_2$, 10 MES/TRIS pH 5.6 in the bath and 10 KCl, 88 Kgluconate, 10 HEPES/TRIS pH 7.4 in the intracellular solution. The final osmolarity of the solutions of 450 mOsm was adjusted with sorbitol.

Results

General features of KAT1 currents

Members of the family of the plant inward rectifying K^+ channels were studied in vitro and in vivo. In vitro we analyzed the *KAT1* gene product following cRNA injection in *Xenopus* oocytes; in vivo we studied inward rectifying K^+ currents in the plasma membranes of *Vicia faba* guard and *Zea mays* root cells.

In voltage-clamped oocytes, inward currents resulting from *KAT1* expression were elicited by membrane potentials, V, more negative than –80 mV (Fig. 1 a). Stepping the membrane potential from a holding potential of –40 mV to various values between –80 and –200 mV activated voltage-dependent, slowly rising, K^+ currents, that did not reach a steady plateau even after 300 ms. Following long stimulation pulses of 3 s duration, the fraction of the steady-state current reached after 300 ms increased with more hyperpolarized potentials from 70% at –120 mV to 95% at –200 mV. The time course of the activation process at pH 7.4 was initially sigmoidal, but neither was of the Hodgkin-Huxley type (Hille 1992) nor could it be fitted by the sum of ≤2 exponentials (Fairley-Grenot and Assmann 1993). During a 300 ms step to –180 mV the current reached 50% of the plateau level after 37 ms, but at the end of the pulse still comprised only 92% of the steady state current reached after 3 s of activation. Since prolonged voltage stimulation tends to be deleterious to the cells, 300 ms pulses were routinely used in most of our experiments. Therefore, we characterised the voltage dependence of activation and kinetics by measurements of the late current, I_l, in response to 300 ms voltage pulses and the time, t_a, required to reach 50% of I_l. Both t_a and I_l are underestimates of the values that would characterise long stimulations, but their systematic use in comparative situations allowed us to extrapolate qualitatively our findings with respect to steady state conditions. Figure 1 c shows that t_a and the true half-activation time differed by up to 50%; however, they exhibited very similar voltage dependencies. The plot of I_l versus V in Fig. 1 b shows that activation became significant for $V \leq -100$ mV, but does not seem to saturate even for $V = -200$ mV, beyond which measurements were impaired by electrical breakdown phenomena. A better description of the voltage dependence of activation is obtained by converting the data of Fig. 1 b into estimates of activation probabilities, P(V), as shown in Fig. 1 d. This was per-

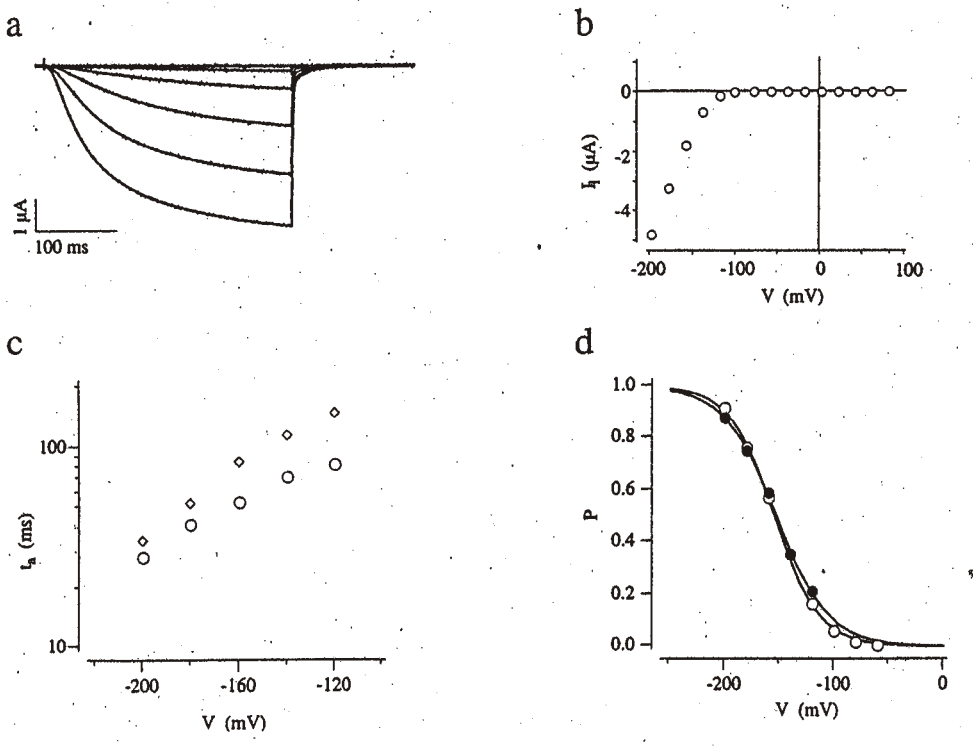

Fig. 1 a–d. Voltage-dependent properties of *KAT1* following expression in *Xenopus* oocytes. **a** Inward currents were elicited in response to voltage pulses from –80 to –200 mV of 300 ms duration, from a holding potential of –40 mV. **b** Late currents, measured at the end of the 300 ms voltage pulse, I_l, are plotted against the pulse potential, V. **c** The activation kinetics were evaluated as the time to reach the half of the amplitude at 300 ms (*circles*) and at 3 s (*diamonds*). **d** Activation curves corresponding to the current at the end of 300 ms voltage pulses (*open circles*) and at the end of 3 s pulses (*filled circles*). Data were fitted by a Boltzmann function (Eq. (1)), and normalized to the maximum value, yielding $V_o = -154$ mV and $V_a = 20.7$ mV for 300 ms pulses, and $V_o = -153$ mV and $V_a = 24.1$ mV for 3 s pulses

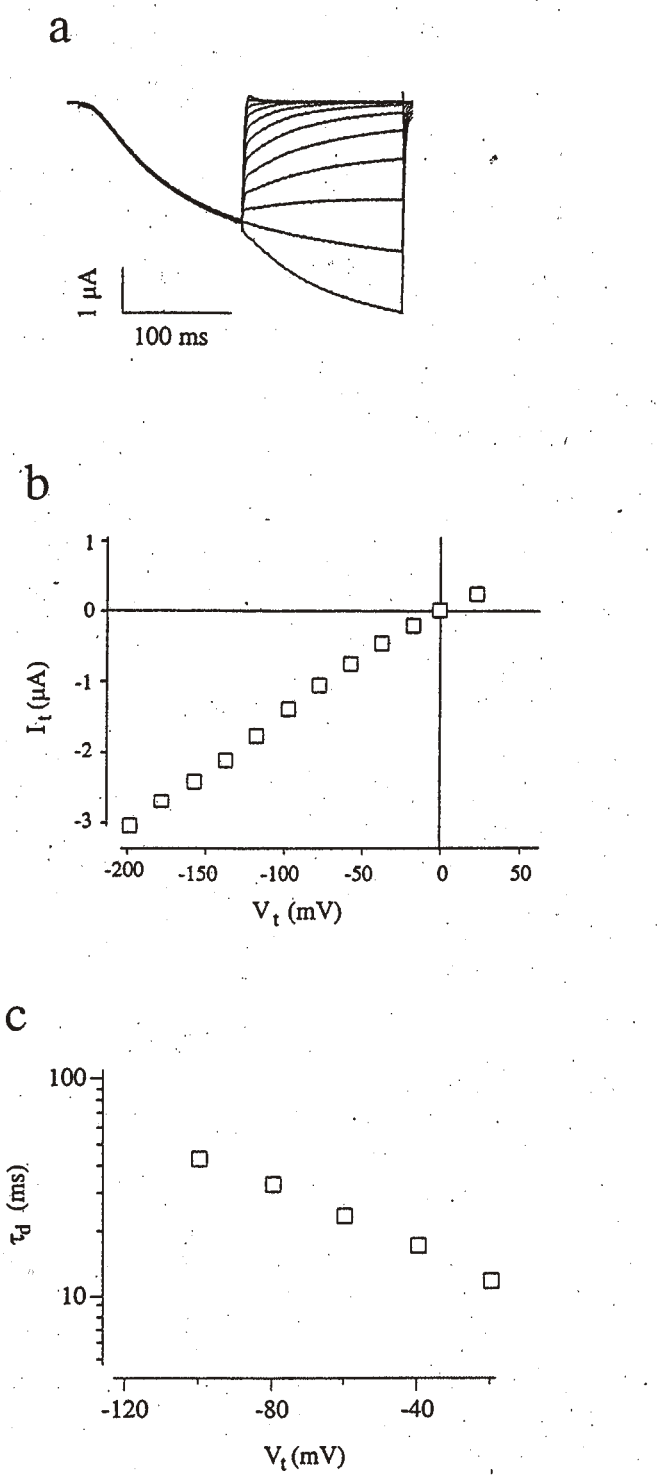

Fig. 2. **a** *KAT1* Currents elicited in oocytes by a tail pulse V_t from −200 to +20 mV (20 mV increments) following a conditioning prepulse to −180 mV for 150 ms, from a holding potential of −40 mV. Note further activation at tail potentials −180 and −200 mV indicating that activation was not yet completed during the prepuls. **b** Instantaneous current I_t is plotted against V_t. Notice the almost ohmic behaviour of the tails, which reverse direction at 2.5 mV in KD 98. **c** Voltage dependence of deactivation time constants τ_d, obtained by fitting the tail currents by a single exponential

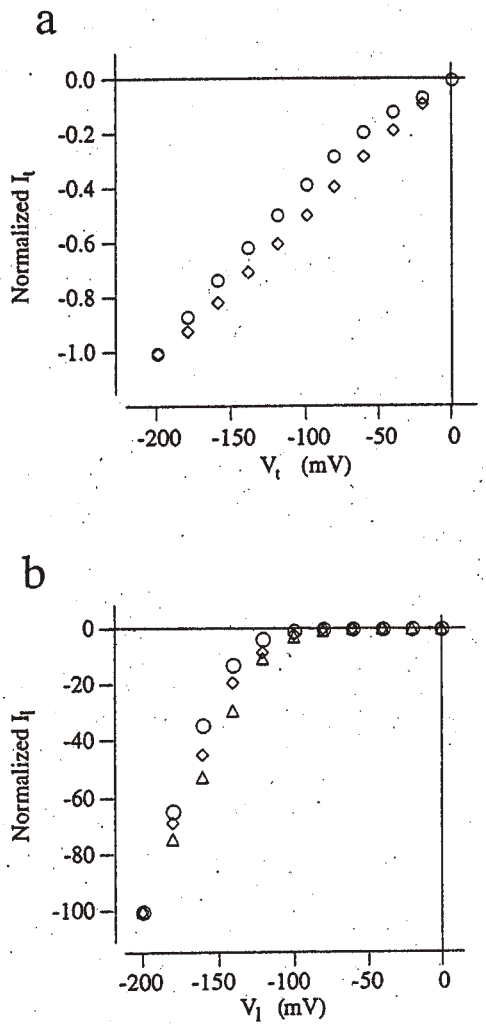

Fig. 3 a, b. Effect of intracellular Mg^{2+} on plant K^+ channels. **a** Instantaneous current-voltage relationships evaluated from a control *KAT1* injected oocytes (*circles*) and from an oocyte with zero intracellular Mg^{2+}, obtained by injecting EDTA, to an intracellular concentration of ~10 mM (diamonds). Values of I_t were normalized to the instantaneous current obtained at −200 mV. Note that the slight rectification in the control experiment almost diappeared after injection with EDTA. **b** Voltage-dependent inward K^+ currents in the plasma membrane of *KAT1* injected oocytes (*circles*), guard cell (diamonds), and root cell protoplasts (*triangles*) in the absence of cytoplasmic Mg^{2+}. I_l were normalized to the I_l obtained at −200 mV

formed by dividing $I_1(V)$ by the instantaneous tail current, $I_t(V)$, measured as described below, and normalizing the results to the asymptotic value (A) at infinite negative voltage, estimated from a Boltzmann fit of the data:

$$\frac{I_l}{I_t} = A \cdot P(V) = \frac{A}{1 + e^{\frac{(V - V_0)}{V_a}}}. \quad (1)$$

For the experiment illustrated in Fig. 1 the latter fit yields an half-activation voltage, $V_o = -154$ mV, and a voltage sensitivity, $V_a = 21$ mV. In Fig. 1 d we also plotted the P(V) estimates that would have been obtained from true steady-state currents measured for 3 s stimuli. A fit of the latter with Eq. (1) yields estimates of V_o and V_a, of −153 mV

and 24 mV, respectively, justifying the use of I_i for our routine analyses.

Instantaneous current-voltage relationships and the effect of intracellular Mg^{2+}

The kinetics of the deactivation following the return from an hyperpolarizing prepulse to less negative voltages, were studied by tail current analysis (Fig. 2 a). Following an activating prepulse of 150 ms at V = −180 mV, steps to tail potentials, V_t, between −160 and +20 mV, elicited tail currents, I_t, that decayed exponentially with time constants decreasing with V_t from 50 ms to 10 ms (Fig. 2 c). The tail current-voltage relationship, between the early I_t and V_t, showed some non-linearity upon approaching the zero-current potential, near the estimated Nernst potential for K^+ (−3 ± 5 mV in KD98, Fig. 2 b; −60 mV in KD10). However, this rectification is insignificant in comparison with that of the late currents, shown in Fig. 1 b. Protoplasts from *Vicia faba* guard cells and *Zea mays* root cells as well exhibited slowly activating and voltage dependent inward rectifier K+ channels (data not shown), indicating the existence of *KAT1* related currents in these two preparations.

In order to determine whether the strong inward rectification of the late currents results from a voltage-dependent block by cytoplasmic Mg^{2+} ions, as suggested for animal inward rectifiers (Matsuda et al. 1987; Vandenberg 1987; Matsuda 1988), we performed experiments at low intracellular Mg^{2+} concentrations. Injection of oocytes with 40 nl of 200 mM EDTA solution was expected to result in ~10 mM final concentration of EDTA inside the cell, buffering intracellular Mg^{2+} to below 100 nM. Voltage-clamp measurements on EDTA treated oocytes were performed 5 min to 2 h after EDTA injection. In all 10 oocytes tested, K^+ currents with the same properties as described before were observed (Fig. 3 a, circles). Likewise, in the two plant cell types in the absence of Mg^{2+} and addition of 2 mM cytoplasmic EDTA in whole-cell recordings, we found the voltage-dependence of the K^+ currents not to depend on the presence of intracellular Mg^{2+} (Fig. 3 b). The only difference found in Mg^{2+}-free conditions was the absence of significant non-linearities in the instantaneous I_t–V_t relation (Fig. 3 a). This indicates that cytoplasmic Mg^{2+} may act as a fast voltage-dependent blocker of inward currents, as in most other cation selective channels (Matsuda 1988; Johnson and Ascher 1990; Horie et al. 1987; Lin et al. 1991; Pusch 1990), but does not play an important role in the voltage dependence of the slow activation of plant inward rectifier K^+ channels.

5 pS channels underlie KAT1 currents

Single-channel properties were analysed from patch-clamp recordings of *KAT1*-cRNA injected oocytes. Using 0.8–1 MΩ pipettes filled with KD98 solution, attached-patch seal resistances larger than 10 GΩ were obtained. This allowed the analysis of single channel events, with recording from 5–40 channels. In patches, lacking stretch activated channels, we never detected any channel activity at a steady holding potential of −40 mV, whereas 300 ms pulses from −120 to −200 mV caused channel openings, whose frequency increases with pulse duration and the amplitude of the voltage step (Fig. 4 a). This activity was clearly attributable to *KAT1* channels because the average of many (25–40) responses to the same voltage step reproduced the behaviour of the macroscopic current recorded in whole oocytes in response to the same type of stimulation (Fig. 4 b). Owing to the low steady state probability of opening for V = −120 or −140 mV, a large number of distinct single-channel events could be resolved at these potentials, even in patches showing up to 40 active channels at −200 mV (see upper trace of Fig. 4 a, c). Unitary events were occasionally observed also at the beginning of pulses to V = −160 mV, when the open channel probability was still small. However, the presence of multiple channel openings did not allow a reliable statistical analysis of single-channel kinetics.

Single-channel currents were estimated from raw data amplitude histograms, as shown in Fig. 4 d for measurements at V = −160 mV. Several peaks were observed, corresponding to current amplitudes fairly equally spaced at an interval of 0.8 pA, the unitary current flowing through a single *KAT1* channel at that potential. Similar data could also be obtained for membrane potentials positive to −100 mV by analysis of the tail currents at various voltages following hyperpolarizing prepulses. The single-channel current-voltage relation shown in Fig. 4 e was obtained from 5 different membrane patches (4 oocytes). In agreement with the measurements of macroscopic currents described above, this current-voltage relation is linear in the range of −200 mV to +60 mV and intersects the voltage axis near the origin, as expected for Mg^{2+}-free symmetric K^+ conditions. Under these conditions a voltage independent conductance, γ, of *KAT1* channels of the order of 5 pS was calculated from the single channel current-voltage relation in Fig. 4 e. Occasionally, we saw discrete current events corresponding to much higher γ values (34 pS, Fig. 4 f), close to those reported by Schachtmann et al. (1992). However, the correlation of these events with *KAT1* channels is very doubtful, because in these membrane patches the average of many records failed to reproduce the time course and the voltage dependence of macroscopic *KAT1* currents.

High-affinity Cs^+ block

A characteristic feature of K^+ inward rectifiers is their sensitivity to blockage by extracellular Cs^+ and Ba^{2+} (Hagiwara et al. 1976; Standen and Stanfield 1978; Kubo et al. 1993; for review see Hille 1992). We also expected *KAT1* channels to be blocked by Cs^+ because this cation was recently found to suppress K^+ uptake and growth in *Arabidopsis* at concentrations between 50 μM and 2 mM (Sheahan et al. 1993). Indeed, when Cs^+ was applied to the bath solution in this concentration range, *KAT1* currents were strongly affected: the current amplitude was reduced and the activation kinetics were slowed. In KD98 the current at the end of a 300 ms voltage pulse to −160 mV was halved in the presence of 1 mM Cs^+, and the reduction was larger at more negative voltages and at higher Cs^+ concentrations

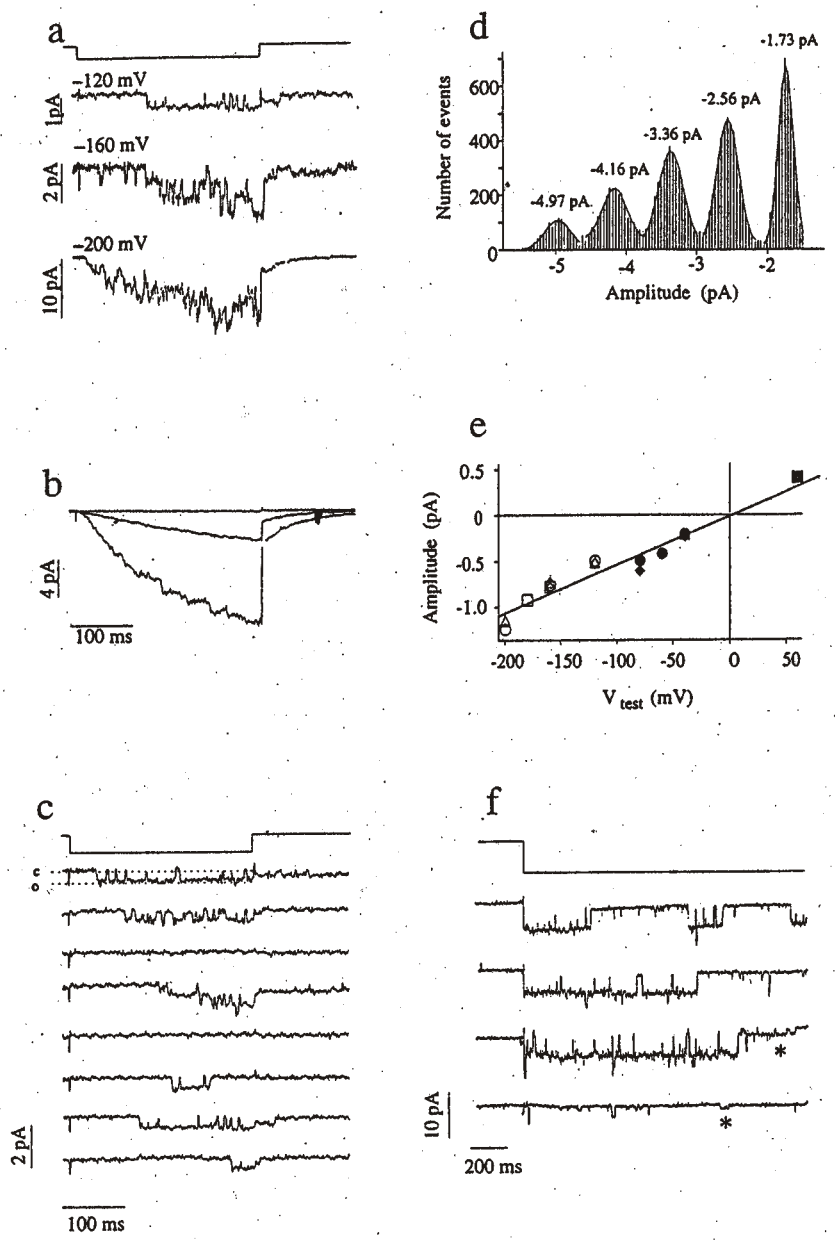

Fig. 4 a–f. Unitary events of *KAT1* channels expressed in oocytes measured from attached membrane patches. **a** Currents elicited by voltage pulses to −120, −160 and −200 mV, from a holding potential of −40 mV. The linear capacity and leakage was digitally subtracted by appropriate scaled responses to positive potentials. The patch contained at least 32 active channels. **b** Averages of 25–40 current traces as those shown in **a** reconstruct the macroscopic inward currents (compare with Fig. 1 a, time scale as in Fig. 1 a). **c** Single channel events in a membrane patch with few channels (5), stimulated by voltage pulses to −120 mV. Closed (c) and open (o) states are indicated. **d** Raw data histogram of single *KAT1* channels in a patch was constructed from 40 consecutive pulses to V = −160 mV. Each peak was well fitted by a Gaussian distribution. The first peak at −1.73 pA corresponds to the closed state. **e** Current-voltage relation of single *KAT1* channels obtained from four different experiments (different symbols). Channel amplitudes marked with filled symbols were measured during channel closure (tails) following a double-voltage pulse experiment (in analogy to Fig. 2 a). **f** In some patches we observed 34 pS channels (c.f. Schachtman et al. 1992) superimposed to 5 pS *KAT1* channels (*asterisks*)

(Fig. 5 a). A tenfold reduction of the K^+ concentration in the control solution (KD10) increased the Cs^+ sensitivity, e.g. the blocking effect of 2 mM Cs^+ in KD98 was comparable to that of 200 μM Cs^+ in KD10 (not shown). This suggests a competition between K^+ and Cs^+ for the same site.

The voltage-dependence of the Cs^+ block is more clearly seen in the instantaneous tail currents following an activating prepulse to −180 mV (Fig. 5 b). In 2 mM Cs^+, for $V_t = -200$ mV the early tail current is smaller, and for V_t between −160 and −60 mV larger than the current at the end of the prepulse. This indicates a further block at −200 mV and a partial unblock of the channels between −160 and −60 mV that was faster than our time resolution. Thus, the instantaneous current-voltage relation exhibits a region of negative resistance. The absolute value of the current reaches a maximum at a voltage that is about −120 mV in 1 mM Cs^+ and increases with increasing Cs^+ concentration (Fig. 5 c).

In contrast to Cs^+, extracellular Ba^{2+} did not affect the *KAT1* currents at concentrations up to 5 mM (c.f. 30 μM in *IRK1*, Kubo et al. 1993).

pH-dependence

We studied the effect of extracellular pH on the properties of *KAT1* channels because K^+ uptake in plants and fungi is often accompanied by changes in the extracellular proton concentrations. We explored whether titratable amino acids in the *KAT1* polypeptide are susceptible to extracellular pH changes. In particular, low pHs might modify Asp and His residues located at or close to the putative pore region H5. Furthermore, protons are known blockers of some

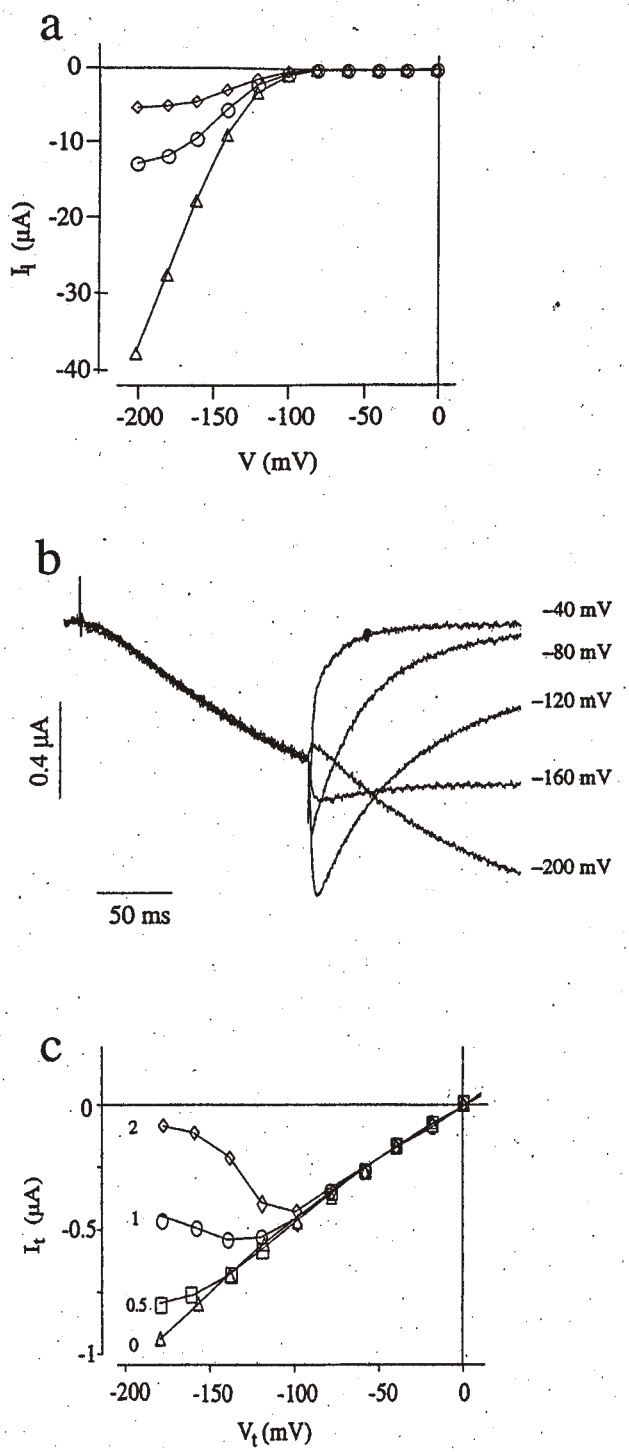

Fig. 5 a–c. Block of *KAT1* currents in oocytes by Cs^+. **a** I_1-V relation measured in control conditions and in the presence of 1 mM (*circles*) and 2 mM extracellular Cs^+ (diamonds). **b** Tail currents measured in the presence of 2 mM extracellular Cs^+. Currents were elicited by a prepulse to –180 mV for 150 ms, followed by a tail pulse to –200 mV to –40 mV. The value of V_t is indicated near to each trace. **c** Instantaneous currents determined by extrapolation of single exponential fits (t=0) at different extracellular Cs^+ concentrations were plotted against V_t. The Cs^+ concentration (mM) is given next to each curve

cation-selective channels, notably the voltage-gated Na^+ and K^+ channels (Hille 1992), as well as the SV-type channel in plant vacuoles (Schulz-Lessdorf and Hedrich unpublished).

By raising the H^+ concentration from pH 7.4 to 6.5, 5.6 as well as pH 4.5, which is closer to the physiological pH range in the extracellular space of plant cells, the currents at the end of 300 ms pulses were increased, but the effect became progressively smaller at more negative voltages (Fig. 6 a). This observation might be explained by a pH-induced positive shift of the activation curve rather than modification of the open-channel conductance. This interpretation was further supported by measurements of instantaneous current-voltage characteristics, which were independent of pH, apart from a scaling factor related to the differences in the extent of activation at the end of the prepulse (data not shown). Figure 6 b shows activation curves at pH 7.4 and pH 4.5 on the same oocyte (obtained as described for Fig. 1 d). These data demonstrate that the increase in pH by one unit produces a positive shift of approximately 19 mV in the voltage-dependence of activation of *KAT1* channels (Fig. 6 b inset). Consistent with this observation we found a pronounced pH-dependence of the gating kinetics of *KAT1* channels. As shown in Fig. 6 c, d the activation times decreased and the deactivation times increased upon the decrease in extracellular pH.

Discussion

Cloned members of plant homologues of the *Shaker* potassium channel family showed striking structural similarities, but significant differences in their physiological function from their animal counterparts (shown here and in Anderson et al. 1992; Sentenac et al. 1992; Schachtmann et al. 1992). Unlike animal *Shaker*-related channels these plant K^+ channels are inwardly rectifying. The inwardly rectifying K^+ channels from animals do belong to a different, distantly related family (Aldrich 1993) and rectification rather than being an intrinsic property appears to be dependent on the presence of intracellular magnesium (Ho et al. 1993; Kubo et al. 1993; Matsuda 1988). The results reported here now show that inward rectification of *KAT1* and functionally-related channels in guard and root cells does not require the presence of cytoplasmic Mg^{2+}. In retrospect, this result is not surprising, since the overall structures of the animal inward rectifiers cloned so far, *IRK1*, *ROMK1* and *RACTK1* (Suzuki et al. 1994), are not related to *KAT1*. Thus, like their outwardly rectifying relatives in animals, the voltage dependence of *KAT1* is genuine and may be attributed to an intrinsic voltage sensor.

Voltage sensitivity of the animal *Shaker* channels appears to lie in the S4 transmembrane domain. This region contains repeating basic amino acids at every third or fourth residue, whose presence appears to be important for the sensitivity of the channel to voltage (Papazian et al. 1991). Such repeating basic residues are also evident in the S4 region of *KAT1*. However, what is lacking in *KAT1* are leucine heptat repeats, another structural motif found in the S4 and S5 region of *Shaker* related channels. These

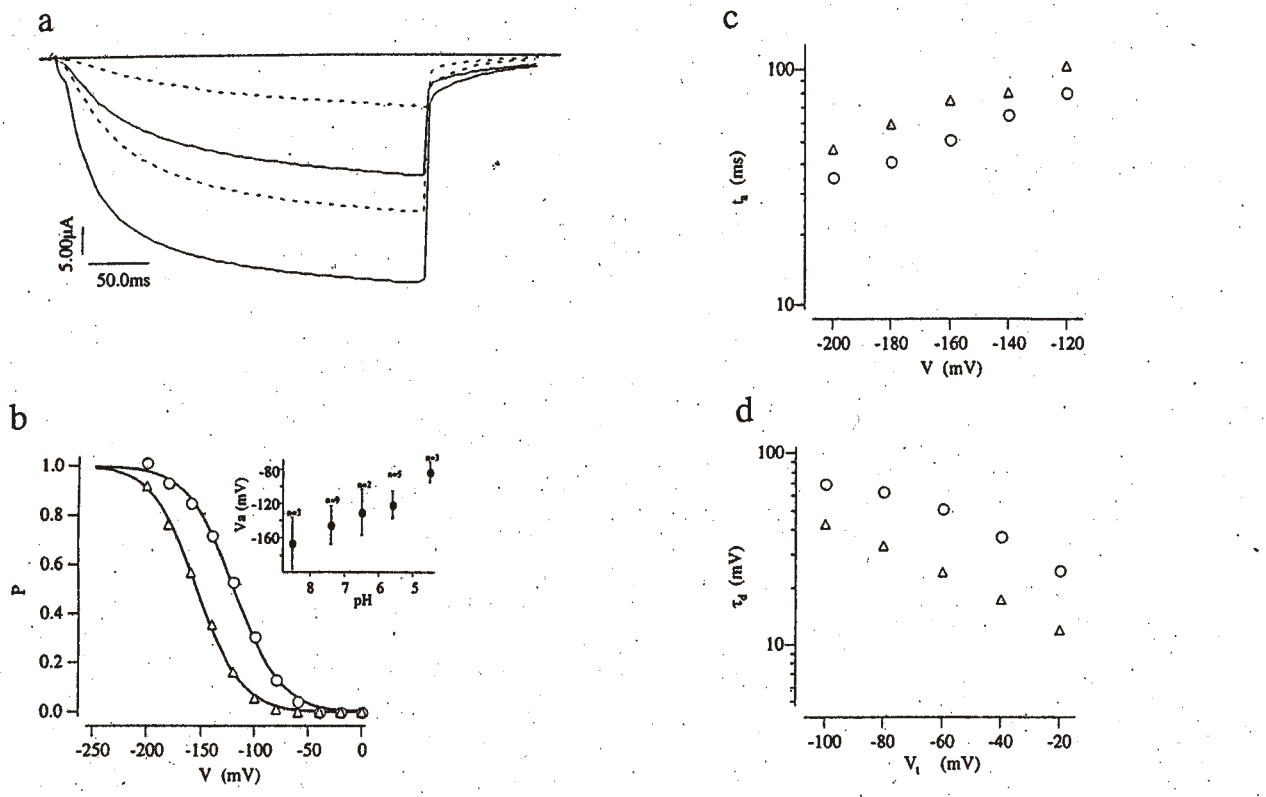

Fig. 6a–d. Effect of protons on *KAT1* currents in oocytes. **a** Currents elicited by a voltage pulse to –140 and –160 mV, with an extracellular proton concentration of pH=7.4 (*broken lines*) and pH=4.5 (*continuous lines*), from a holding potential of –40 mV. Inset: pH-dependent shift in the half-activation voltage, V_a **b**. The corresponding activation curves reveal a shift of the half activation potential, from V_o=–154 mV at pH=7.4 (*triangles*) to V_o=–119 mV at pH=4.5 (*circles*), without a significant change on V_a=20 mV. Voltage dependence of the activation time t_a **a** and deactivation time constants τ_d **d**, evaluated at pH=7.4 (*triangles*) and pH=4.5 (*circles*)

heptad repeats are also supposed to be involved in voltage sensing possibly through interactions with other helices (McCormack et al. 1991). Consequently, the absence of these heptads in the *KAT1* sequence may suggest that the interaction of the S4 helices with other parts of the channel molecule may be altered, leading to opposed rectification.

The only highly conserved motif in *Shaker*, *IRK1*, *ROMK1*, and *KAT1* is the pore region, including the selectivity filter. In order to prove whether the plant and animal inward rectifiers share other properties related to the pore, besides K^+ selectivity, we compared their susceptibility to inhibition by Cs^+ and Ba^{2+}. A high-affinity voltage-dependent block by Cs^+ is a characteristic feature of most K^+ selective channels that is also apparent in *KAT1*. However, we found that Ba^{2+}, the other common blocker of animal voltage-dependent K^+ channels, had no effect on *KAT1*, even at millimolar concentrations. An observation in contrast to Schachtmann et al. (1992).

What is possibly even more significant is the sensitivity of these plant channels to pH. For most potassium and sodium channels protons act as a blocker (Hille 1992; Suzuki et al. 1994). In contrast, *KAT1* has an increased probability of opening in response to decreasing pH, showing an increased current amplitude resulting from a shift in the voltage-threshold for activation. This sensitivity to pH is particularly interesting given the role of the H^+-ATPase in generating the membrane potential negative to –100 mV. Thus H^+ pumping and potassium channel activity may be coordinated in a voltage and pH dependent manner as has been discussed for the inwardly rectifying potassium channel in guard cells (Blatt 1992). Compared to their animal counterparts, acid-activation, a consequence of H^+ extrusion (Shimazaki and Zeiger 1986), as shown for *KAT1* constitutes a plant K^+ channel specific property.

In conclusion, we think that the present work has provided evidence that *KAT1* differs from animal counterparts in response to voltage and channel modulators. With respect to the susceptibility of *KAT1* towards inhibition by low Cs^+ concentrations, our studies together with those on the cesium toxicity (Sheahan et al. 1993) may underline the vital function of K^+ channels for plant growth and development.

Acknowledgements. We gratefully acknowledge E. Liman for providing us with pGEMHE vector. We thank C. Redhead for helpful comments on the manuscript. This work was funded by DFG grants to RH, CNR target project Genetic Engeneering to FC, special project RAISA, subproject N.2.1 paper 1142 to FG and RH and HSFPO to KP.

References

Anderson JA, Huprikar SS, Kochian LV, Lucas WJ, Gaber RF (1992) Functional expression of a probable *Arabidopsis thaliana* potassium channel in *Saccharomyces cerevisiae*. Proc Natl Acad Sci 89:3736–3740

Aldrich R (1993) Advent of a new family. Nature 362:107–108

Blatt MR (1992) K^+ channels of stomatal guard cells – Characteristics of the inward rectifier and its control by pH. J Gen Physiol 99:615–644

Bush DS, Hedrich R, Schroeder JI, Jones RL (1988) Channel-mediated K^+ flux in barley aleurone protoplasts. Planta 176:368–377

Colombo R, Cerana R (1991) Inward rectifying K^+ channels in the plasma membrane of *Arabidopsis thaliana*. Plant Physiol 9:1130–1135

Elledge SE, Mulligan JT, Ramer SW, Spottswood M, Davis (1991) λYES: A multifunctional cDNA expression vector for the isolation of genes by complementation of yeast and *Escherichia coli* mutations. Proc Natl Acad Sci, USA 88:1731–1735

Fairley-Grenot KA, Assmann SM (1993) Comparison of K^+-channel activation and deactivation in guard cells from a dicotyledon (*Vicia faba*) and an graminaceous monocotyledon (*Zea mays*). Planta 189:410–419

Hagiwara S, Miyazaki S, Rothenthal NP (1976) Potassium current and the effect of cesium on this current during anomalous rectification of the egg cell membrane of a starfish. J Gen Physiol 67:621–638

Hedrich R, Schroeder JI (1989) The physiology of ion channels and electrogenic pumps in higher plants. Ann Rev Plant Physiol 40:539–569

Hedrich R, Busch H, Raschke K (1990) Ca^{2+} and nucleotide dependent regulation of voltage dependent anion channels in the plasma membrane of guard cells. EMBO J 9:3889–3892

Hille B (1992) Ionic Channels of Excitable Membranes. Sinauer, Sunderland, MA, USA

Ho K, Nichols CG, Lederer WJ, Lytton J, Vassilev PM, Kanazirska MV, Herbert SC (1993) Cloning and expression of an inwardly rectifying ATP-regulated potassium channel. Nature 362:31–38

Horie M, Irisawa H, Noma A (1987) Voltage-dependent magnesium block of adenosine-triphosphate-sensitive potassium channel in guinea-pig ventricular cells. J Physiol (London) 387:251–271

Jan LY, Jan YN (1992) Tracing the roots of ion channels. Cell 69:715–718

Johnson JW, Ascher P (1990) Voltage-dependent block by intracellular Mg^{2+} of *N*-methyl-D-aspartate-activated channels. Biophys J 57:1085–1090

Kubo Y, Baldwin TJ, Jan YN, Jan LY (1993) Primary structure and functional expression of a mouse inward rectifier potassium channel. Nature 362:127–133

Liman ER, Tytgat J, Hess P (1992) Subunit stoichiometry of a mammalian K^+ channel determined by construction of multimeric cDNAs. Neuron 9:861–871

Lin F, Conti F, Moran O (1991) Competitive blockage of the sodium channel by intracellular magnesium ions in central mammalian neurones. Eur Biophys J 19:109–118

Matsuda H (1988) Open-state substructure of inwardly rectifying potassium channels revealed by magnesium block in guinea-pig heart cells. J Physiol (London) 397:237–258

Matsuda H, Saigusa A, Irisawa H (1987) Ohmic conductance through the inwardly rectifying K channel and blocking by internal magnesium. Nature 325:156–159

McCormack K, Tanouye MA, Iverson LE, Lin J-W, Ramaswami M, McCormack T, Capanelli JT, Mathew MK, Rudy B (1991) A role for hydrophobic residues in the voltage-dependent gating of shaker K^+ channels. Proc Natl Acad Sci USA 88:2931–2935

Moran N, Ehrenstein G, Iwasa K, Mischke C, Bare C, Sutter RI (1988) Potassium channels in motor cells of *Samanea saman* – A patch-clamp study. Plant Physiol 88:643–648

Nitschke K, Fleig U, Schell J, Palme K (1992) Complementation of the cs *dis2* – 11 cell cycle mutant of *Schizosaccharomyces pombe* by a protein phosphatase from *Arabidopsis thaliana*. EMBO J 11:1327–1333

Papazian DMT, Timpe LC, Jan YN, Jan LY (1991) Alteration of voltage-dependence of *Shaker* potassium channels by mutations in the S4 sequence. Nature 349:305–310

Pongs O (1992) Voltage-gated K^+ channels. In: Molecular aspects of transport proteins. Amsterdam, Elsevier

Pusch M (1990) Open-channel block of Na^+ channels by intracellular Mg^{2+}. Eur Biophys J 18:317–326

Sambrook J, Fritsch EF, Maniatis T (1989) Molecular Cloning: A Laboratory Manual 2nd. Cold Spring Habour Laboratory Press, Cold Spring Habour N.Y.

Schachtmann DP, Tyerman SD, Terry BR (1991) The K^+/Na^+ selectivity of a cation channel in the plasma membrane of root cells does not differ in salt-tolerant and salt-sensitive wheat species. Plant Physiol 97:598–605

Schachtmann DP, Schroeder JI, Lucas WJ, Anderson JA, Gaber RF (1992) Expression of an inward-rectifying potassium channel by the *Arabidopsis KAT1* cDNA. Science 258:1654–1658

Schroeder JI, Fang MM (1991) Inward-rectifying K^+ channels in guard cells provide a mechanism for low affinity K^+ uptake. Proc Natl Acad Sci 88:11583–11587

Schroeder JI, Hedrich R, Fernandez JM (1984) Potassium-selective single channels in guard cell protoplasts of *Vicia faba*. Nature 312:361–362

Schroeder JI, Raschke K, Neher E (1987) Voltage dependence of K^+ channels in guard-cell protoplasts. Proc Natl Acad Sci 84:4108–4112

Sentenac H, Bonneaud N, Minet M, Lacroute F, Salmon J-M, Gaymard F, Grignon C (1992) Cloning and expression in Yeast of a plant potassium ion transport system. Science 256:663–665

Sheahan JJ, Ribeiro-Neto L, Sussman MR (1993) Cesium insensitive mutants of *Arabidopsis thaliana*. Plant J 3:647–656

Shimazaki K, Iino N, Zeiger E (1986) Blue-light-dependent proton extrusion by guard cell protoplasts. Nature 319:324–326

Spalding EP, Goldsmith MH (1993) Activation of K^+ channels in the plasma membrane of *Arabidopsis* by ATP produced photosynthetically. Plant Cell 5:477–484

Standen NB, Stanfield PR (1978) A potential- and time-dependent blockade of inward rectification in frog skeletal muscle fibres. J Physiol 280:169–191

Stühmer W, Methfessel C, Sakmann B, Noda M, Numa S (1987) Patch clamp characterization of sodium channels expressed from rat brain cDNA. Eur Biophys J 14:131–138

Suzuki M, Takahashi K, Ikeba M, Hayakawa H, Ogawa A, Kawaguchi Y, Sakai O (1994) Cloning of a pH-sensitive K^+ channel possessing two transmembrane segments. Nature 367:642–645

Vandenberg CA (1987) Inward rectification of a potassium channel in cardiac ventricular cells depends on internal magnesium ions. Proc Natl Acad Sci 84:2560–2564

⇒ zurück zur Übersicht

1997

Hoth, **Dreyer**, Hedrich

Mutational analysis of functional domains within plant K^+ uptake channels.

J. Exp. Bot. **48**:415-420.

Journal of Experimental Botany, Vol. 48, Special Issue, pp. 415–420, March 1997

Journal of Experimental Botany

Mutational analysis of functional domains within plant K^+ uptake channels

Stefan Hoth, Ingo Dreyer and Rainer Hedrich[1]

Institut für Biophysik, Universität Hannover, Herrenhäuser Str. 2, D-30419 Hannover, Germany

Received 27 August 1996; Accepted 6 November 1996

Abstract

Site-directed mutations have been generated in the pore and voltage sensor regions of the inwardly rectifying potassium channels KAT1 and KST1. The properties of mutant channels have been analysed in *Xenopus* oocytes, and give insights into the structure-function relations of these channels.

Key words: Functional domains, potassium channels, site-directed mutagenesis.

Introduction

In plant cells, electrophysiological studies have identified both depolarization- and hyperpolarization-activated K^+ channels. Their biophysical and physiological properties *in vivo* have been characterized using the patch clamp technique (for a review see Hedrich and Becker, 1994). Since 1992, the cloning of several plant K^+ channels enabled the relation of various channel functions to structural elements. Mutational analyses, heterologous expression, and transgenic plants in combination with electrophysiological investigations now represent suitable tools to unravel the molecular mechanisms underlying channel action.

Plant channel cDNAs cloned from *Arabidopsis thaliana* and *Solanum tuberosum* so far encode inwardly rectifying K^+ channels only. Whereas K^+ currents through the gene products of *kat1*, *akt1*, *akt3*, *kst1*, and *skt1* have been shown already, the channel function of *kat2* (GenBank accession number U25694) and *akt2* was deduced from sequence homology only (Anderson *et al.*, 1992; Sentenac *et al.*, 1992; Cao *et al.*, 1995*a*; Müller-Röber *et al.*, 1995; Ehrhardt *et al.*, 1996; Ketchum and Slayman, 1996).

Besides the striking homology between amino acid sequences of all cloned plant K^+ channels, they are related to animal outward rectifying K^+ channels of the *Shaker* gene family, too. Like *Shaker*-type channels, six transmembrane segments (S1 through S6) and an amphiphilic pore-forming loop P between the transmembrane helices S5 and S6 were predicted from hydrophobicity analyses (Anderson *et al.*, 1992; Sentenac *et al.*, 1992; Cao *et al.*, 1995*a*; Müller-Röber *et al.*, 1995; Ehrhardt *et al.*, 1996, Ketchum and Slayman, 1996). Although the plant inward-rectifiers in contrast to the outward rectifying *Shaker*-related K^+ channels are activated by hyperpolarization, both channel types harbour a positively charged S4 segment, which may take part in voltage sensing.

In order to prove the proposed K^+ channel structure (Fig. 1) (for *Shaker* see Durell and Guy, 1992) mutant channels have been generated, and their functional properties compared to those of the wild-type channel (Pongs, 1992; Perozo *et al.*, 1994; Uozumi *et al.*, 1995; Becker *et al.*, 1996). A prerequisite for related studies on plant K^+ channels was their successful expression in heterologous systems such as *Xenopus* oocytes, insect cells (Sf9), and K^+ transport-deficient yeast strains (Anderson *et al.*, 1992; Bertl *et al.*, 1995; Marten *et al.*, 1996; Uozumi *et al.*, 1995; Becker *et al.*, 1996; for a review see Hedrich, 1995). In the following paper the channel structure will be related to the biophysical properties and regulation of the guard cell K^+ uptake channels KAT1 and KST1.

The selectivity filter

K^+ channels conduct K^+, while they discriminate against other mono- and divalent cations. Mutant channels with selectivities different from wild-type K^+ channels may help to pinpoint the location of the selectivity filter and

[1] To whom correspondence should be addressed at: Julius-von-Sachs Institut für Biowissenschaften, Lehrstuhl Botanik 1, Mittlerer Dallenbergweg 64, D-97082 Wurzburg, Germany. Fax: +49 931 888 6157.

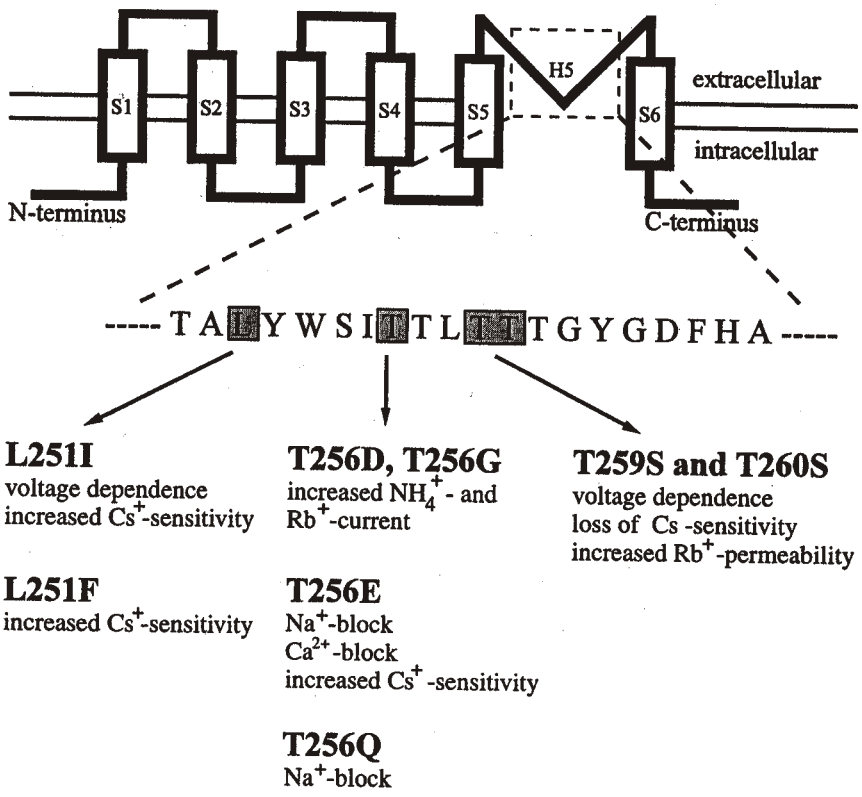

Fig. 1. Phenotype of KAT1 pore mutants. Site-directed mutagenesis of amino acid residues in the inner pore region of the plant inward rectifier KAT1 generated mutant channels with altered properties. These mutations in the channel protein affected the permeability, voltage dependence, and the susceptibility to blocking cations (Uozumi *et al.*, 1995; Becker *et al.*, 1996).

the underlying mechanism involved in selection by size, charge density or binding affinity.

When expressed in *Xenopus* oocytes KAT1, an *Arabidopsis thaliana* guard cell channel, is characterized by a conductance ratio sequence of $K^+ > Rb^+ \cong NH_4^+ > Cs^+ \cong Na^+ \cong Li^+$ (Schachtman *et al.*, 1992; Nakamura *et al.*, 1995), very similar to relative permeabilities found for the potato guard cell K^+ channel equivalent KST1 (Müller-Röber *et al.*, 1995). The significant conductance for both Rb^+ and NH_4^+ was used to screen for selectivity mutants in *Kat1* (Uozumi *et al.*, 1995). Complementation of K^+ uptake-deficient yeast strains with *Kat1* in combination with random site-directed mutagenesis selected for mutants with pronounced increase in the NH_4^+ and Rb^+ uptake. Besides positions 259 and 260 (Becker *et al.*, 1996), the ion permeation seems to be extremely sensitive towards amino acid substitutions at position 256 (Uozumi *et al.*, 1995). Since T256 seems to interact with amino acids of the consensus sequence TXTTXGYG, these sites may constitute the selectivity filter in both animal and plant K^+ channels (Yool and Schwarz, 1991; Kirsch *et al.*, 1992; Heginbotham *et al.*, 1994). When in KAT1 threonine residues T259 and T260 of the putative pore region were mutated to serine, the relative Rb^+ permeability (P_{Rb}/P_K) of both mutants T259S and T260S increased (Becker *et al.*, 1996), while the NH_4^+ permeability remained unaffected. These observations indicate that the selectivity filter is constituted by a stretch of amino acids in the pore-forming region (T256, T259, T260). Among them, the hydroxyl-groups of the threonines, on the one hand, could play a crucial role in the interaction of the pore with the permeating ion. On the other hand, threonine and serine differ in the position of their hydroxyl-group, which could alter the capability to form hydrogen bonds and finally the overall pore structure.

Cation block

A characteristic feature of K^+ channels is their susceptibility towards block by extracellular cations (Hille, 1992). Whereas both KAT1 and KST1 were blocked by Cs^+, TEA^+ (*t*etra*e*thyl*a*mmonium), and Ba^{2+} (Hedrich *et al.*, 1995; Véry *et al.*, 1995; Müller-Röber *et al.*, 1995; Anderson *et al.*, 1992), KST1 is blocked by extracellular Zn^{2+} as well (Fig. 2). Binding motifs for Zn^{2+} have been described to contain cysteine and histidine residues (Berg and Shi, 1996). Since KST1 does not possess any extracellular cysteine, the two external histidines might be responsible for the Zn^{2+} sensitivity of this plant K^+ channel.

Up to now, in KAT1 several mutants in the channel

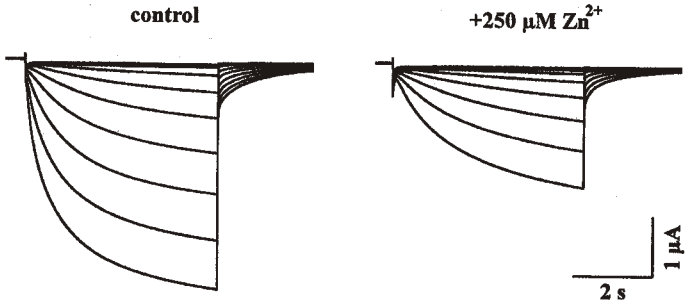

Fig. 2. Zn^{2+} sensitivity of the potato guard cell K^+ uptake channel KST1. The *kst1* gene product was heterologously expressed in *Xenopus* oocytes and K^+ currents were analysed as described previously (Müller-Röber *et al.*, 1995). From a holding potential of −20 mV hyperpolarization of the membrane to −160 mV in steps of 10 mV elicited large inward currents. Note the decrease in the current amplitude upon addition of 250 μM Zn^{2+}. Solutions were composed of 30 mM KCl, 2 mM $MgCl_2$, 1 mM $CaCl_2$ and buffered with 10 mM TRIS/MES to pH 7.4.

pore affected the block by Cs^+, Ca^{2+}, and Na^+ (Uozumi *et al.*, 1995; Becker *et al.*, 1996). Among them, the mutants L251I and T256E are more sensitive to Cs^+ than the wild-type channel, whereas T259S and T260S lost their Cs^+ susceptibility. The competition between K^+ and Cs^+ for at least two binding sites (Becker *et al.*, 1996) may, however, ask for a more complex binding motif.

In contrast to the guard-cell K^+ uptake channel in *Vicia faba* (Busch *et al.*, 1990; Fairley-Grenot and Assmann, 1992), KAT1 is not blocked by external Ca^{2+} up to 30 mM concentrations. Upon substitution of threonine 256 by the negatively charged amino acid glutamate KAT1, however, gains a Ca^{2+} susceptibility similar to that of the *Vicia faba* channel *in vivo* (Becker *et al.*, 1996). The complementation of a K^+ transport-deficient yeast with the KAT1 mutant T256E created a Ca^{2+}-sensitive phenotype (Becker *et al.*, 1996), while T256E and T256Q introduced a Na^+ sensitivity (Uozumi *et al.*, 1995).

The gate

Although the amino acid sequences of the S4 segment are highly homologous, the depolarization-activated animal K^+ release channels and the hyperpolarization-activated plant K^+ uptake channels exhibit inverse voltage gating. Very recently, the simultaneous mutation of three amino acids (R365, L366, R371) in the putative voltage sensor S4 inverted the outward-rectifiying *Shaker* ShB channel successfully into an inward-rectifier (Miller and Aldrich, 1996). This S4 segment, which is proposed to move during activation of the channel (Yang *et al.*, 1996), thus seems to play a crucial role in the gating of the animal K^+ channel. Although the inward-rectification of this *Shaker* triple mutant appears to be KAT1-like, it still does not consequently explain inward rectification of the plant K^+ channel. Since chimera between *kat1* (N-terminus including S4 and the S4-S5 linker) and animal outward rectifiers (C-terminus including S5 and P) did not affect inward rectification (Cao *et al.*, 1995*b*), the N-terminal part of Kat1 containing the S4 segment might be sufficient for plant-specific gating. Furthermore, single mutations in S4 (S168, S180, S176) shifted the activation threshold of Kat1 without changing the steepness of the G(V) curve (Hoshi, personal communication). The KST1 channel mutant R181Q shifted in its activation about 90 mV more positive than the wild type and reduced the apparent gating charge equivalent from 2 to 0.8 (Fig. 3). Therefore, single mutants in S4 may suffice to alter the voltage dependence of activation, but not to invert the rectification of the channel protein.

Animal inward-rectifying K^+ channels with only two membrane-spanning segments and a putative pore-forming loop gain their gating from soluble particles such as cytosolic Mg^{2+} and polyamines (Lopatin *et al.*, 1994; Taglialatela *et al.*, 1994). The gating of plant inward rectifiers, however, does not depend on the presence of intracellular Mg^{2+} or Ca^{2+} (Hedrich *et al.*, 1995; Hoshi, 1995). It was noticed with surprise that single mutations in the pore of KAT1 (L251I and T260S) introduced a shift in the activation curve similar to some S4 mutants (Becker *et al.*, 1996). In contrast to mutations in S4, however, the activation threshold in L251I and T260S shifted to more negative voltages, leaving the apparent gating charge and the single channel conductance unaffected. Therefore, an interaction of the pore or the permeating ion with the voltage sensor cannot be excluded.

Kinetics

Since the kinetics of channel proteins expressed in *Xenopus* oocytes strongly depends on the expression level (Véry *et al.*, 1994), oocytes were selected for comparable K^+ channel amplitudes.

Whereas the rates of activation of the pore mutant channels L251I, T260S, and T259S/T260S were identical to those of the wild-type channel KAT1 (unpublished data), the single mutants L251I (Fig. 4) and L251F (not

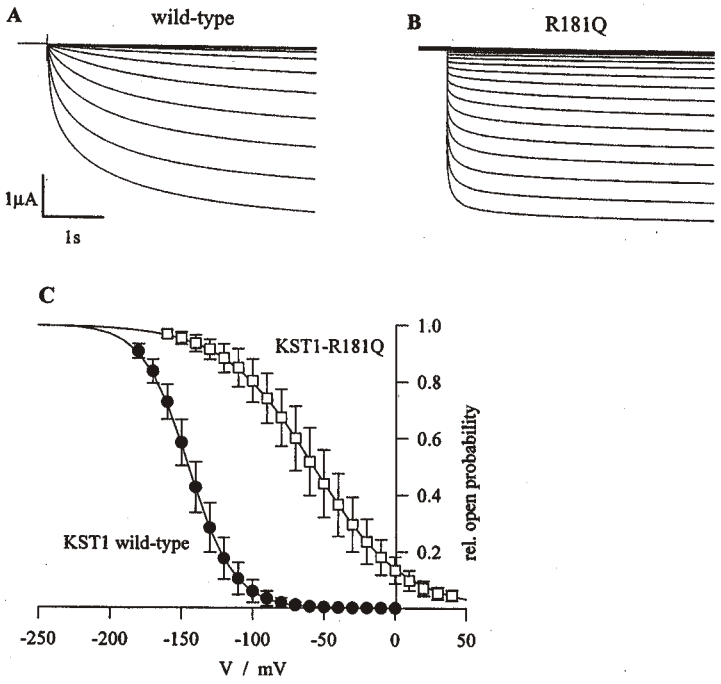

Fig. 3. Replacement of the charged arginine residue in the putative voltage sensor S4 of KST1 altered the voltage dependence. From the resting potential of −20 mV the membrane potential was changed to more negative voltages. Beside a much faster activation kinetics (A, B), the activation threshold of the mutant channel R181Q was shifted to more positive voltages (C). Solid lines represent best fits according to the Boltzmann equation: *relative open probability* $= 1/(1+e^{zF/RT(U-U1/2)})$ where F, R, and T have their usual meanings. $U_{1/2}$ denotes the half-activation voltage and z the apparent gating charge. Compared to the wild-type in the mutant R181Q the gating charge z was reduced from 2 to 0.8. The external solution was composed of 30 mM KCl, 2 mM $MgCl_2$, 1 mM $CaCl_2$ and buffered to pH 5.6 with 10 mM MES/TRIS.

shown) showed a significantly faster deactivation kinetics. The resulting time constants of deactivation for the mutant channel L251I (and L251F) were smaller compared to the wild type (Fig. 4c), equivalent to a higher energy requirement for mutant channel activation (see above).

Regulation through pH

Since inward-rectifying guard cell K^+ channels KST1 and KAT1 seem to play a crucial role in stomatal opening, their activation should be linked to the starch-malate interconversion and thus energy and acid metabolism.

Plant K^+ uptake channels have been reported to activate upon extracellular acidification (Blatt, 1992; Hedrich *et al.*, 1995; Müller-Röber *et al.;* 1995, Véry *et al.*, 1995). The apoplastic acidification and, in turn, activation of K^+ influx, is a consequence of H^+ extrusion through the plasma membrane H^+ ATPase (Shimazaki *et al.*, 1986). Both the membrane hyperpolarization and the apoplastic acidification activate voltage-dependent and pH-sensitive K^+ uptake channels and thereby tightly couple the state of activity of the two membrane proteins.

Since the pH sensitivity of K^+ influx is a property of the K^+ channel protein rather than the cellular background (Müller-Röber *et al.*, 1995; Hedrich *et al.*, 1995; Véry *et al.*, 1995), through mutational analysis of extracellular pH-sensitive residues the molecular mechanism of proton-channel interaction was recently elucidated (Hoth *et al.*, 1997).

Compared to KST1 the pH dependence in KAT1, upon changes in the external pH, was less pronounced. The voltage dependence of the *Arabidopsis thaliana* K^+ channel, however, was altered by intracellular pH, too. An increase in the cytosolic proton concentration shifted the activation threshold to more positive voltages (Hoshi and Marten, 1996).

Nucleotide dependence

The coupling between the membrane potential and the energy metabolism might be reflected by the nucleotide dependence of the guard cell K^+ channel (Hoshi, 1995; Müller-Röber *et al.*, 1995). In line with the activation of the inward rectifier by MgATP, the KST1 amino acid sequence contains a putative ATP-binding motif (Müller-Röber *et al.*, 1995). Future site-directed mutagenesis may locate the amino acids interacting with the nucleotide and identify nucleotide selectivity and sensitivity.

In conclusion, the mutational analysis on plant K^+ uptake channels is a very suitable tool to characterize the channel protein biophysically. This approach allows the identification of the position of amino acids within structural elements harboring general and plant-specific

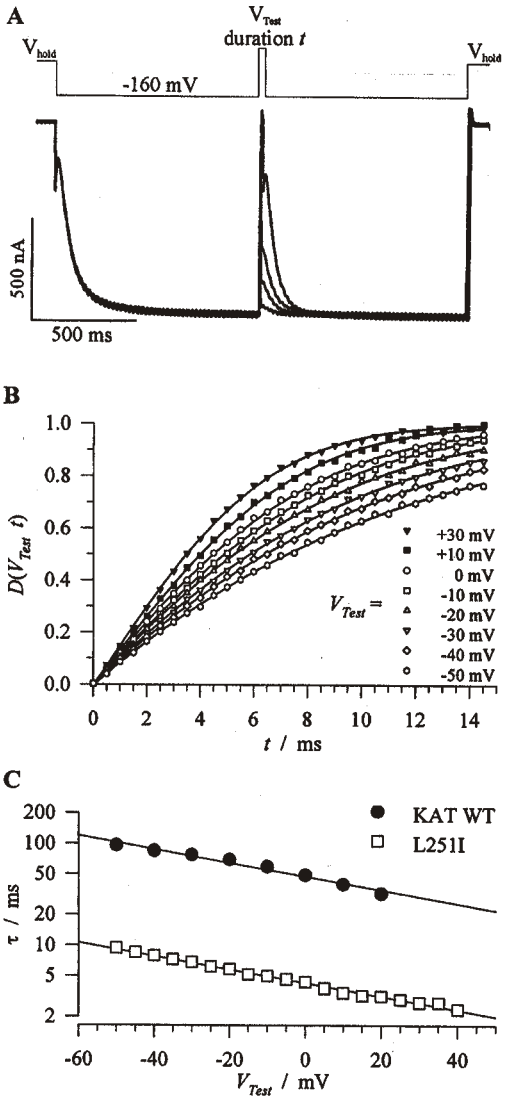

Fig. 4. Rapid deactivation in the Katl mutant channel L251I in 30 mM KCl. Since deactivation time-constants were too small to be resolved from tail-pulses, they were determined during recovery. (A) From a holding potential of $V_{hold} = -20$ mV the membrane potential was stepped to $V = -160$ mV. An intermediate voltage step to the test voltage V_{Test} with duration t deactivated the channels. For the different test voltages the duration was changed subsequently. The current families in (A) show a superposition of four pulses at constant $V_{test} =$ 0 mV ($t = 0.5$, 2, 4, and 14.5 ms). (B) To obtain a deactivation time-course, at constant V_{Test} the degree of deactivation, $D(V_{Test}, t)$, was calculated according to: $D(V_{Test},t) = I_{SS} - I_R(V_{Test},t)/I_{SS} - I_O$ where I_{SS} denotes the steady-state current at the end of the activating pulse, I_O the extrapolated current amplitude at the beginning of the activation pulse, and $I_R(V_{Test},t)$ the current amplitude extrapolated to the onset of the recovery pulse. These time-courses were fitted with a sum of two exponential functions: $D(V_{Test},t) = 1 - A_1 e^{-1/t} + A_2 e^{-1/\tau capacity}$. For each V_{Test} the deactivation time-constant τ and the amplitude A_1 ($A_2 = A_1 - 1$), were adjusted separately, whereas the capacity time-constant was fitted simultaneously for all measured V_{Test}. In line with a capacity time-constant for an oocyte, $\tau_{capacity}$ was in the range of 2 ms. In (B) the deactivation time-courses as well as the fits for V_{Test} of +30 to −50 mV are shown. (C) The voltage-dependence of the deactivation time constant τ for this representative cell is displayed in a semi-logarithmic plot. Experiments on several oocytes ($n = 5$) showed identical results. The corresponding data for wild-type Katl ($n = 6$) were obtained on one hand as described in (A) and (B), on the other hand by fitting the deactivation time-course of tail-pulse experiments with an exponential function. Both fits produced identical results.

channel properties. The exploration of the physiological consequence of channel mutants with changed or novel properties will be performed in the *in vivo* system. Plants, which are transgenic with respect to the mutated channel, will allow the identification of the role of structural domains for stomatal action and K^+ channel function in the plasma membrane of higher plants.

Acknowledgement

We gratefully acknowledge E Liman for providing us with the pGEMHE vector. We thank B Müller-Röber for helpful comments on the manusscript. These investigations were funded by DFG grants to RH (1640/1–3).

References

Anderson JA, Huprikar SS, Kochian LV, Lucas WJ, Gaber RF. 1992. Functional expression of a probable *Arabidopsis thaliana* potassium channel in *Saccharomyces cerevisiae*. *Proceedings of the National Academy of Sciences, USA* **89,** 3736–40.

Becker D, Dreyer I, Hoth S, Reid JD, Busch H, Lehnen M, Palme K, Hedrich R. 1996. Changes in voltage activation, Cs^+ sensitivity, and ion permeability in H5 mutants of the plant K^+ channel KAT1. *Proceedings of the National Academy of Sciences, USA* **93,** 8123–8.

Berg JM, Shi Y. 1996. The galvanization of biology: a growing appreciation for the roles of zinc. *Science* **271,** 1081–5.

Bertl A, Anderson JA, Slayman CL, Gaber RF. 1995. Use of *Saccharomyces cerevisiae* for patch-clamp analysis of heterologous membrane proteins: characterization of Katl, an inward-rectifying K^+ channel from *Arabidopsis thaliana*, and comparison with endogenous yeast channels and carriers. *Proceedings of the National Academy of Science, USA* **92,** 2701–5.

Blatt MR. 1992. Characteristics of the inward rectifier and its control by pH. *Journal of General Physiology* **99,** 615–44.

Busch H, Hedrich R, Raschke K. 1990. External calcium blocks inward rectifier potassium channels in guard cell protoplasts in a voltage and concentration dependent manner. *Plant Physiology* **93,** 14 (Abstract).

Cao Y, Ward JM, Kelly WB, Ichida AM, Gaber, RF, Anderson JA, Uozumi N, Schroeder JI, Crawford NM. 1995*a*. Multiple genes, tissue specificity, and expression-dependent modulation contribute to the functional diversity of potassium channels in *Arabidopsis thaliana*. *Plant Physiology* **109,** 1093–1106.

Cao Y, Crawford NM, Schroeder JI. 1995*b*. Amino terminus and the first four membrane-spanning segments of the *Arabidopsis* K^+ channel KAT1 confer inward-rectification property of plant-animal chimeric channels. *The Journal of Biological Chemistry* **270,** 17697–701.

Durell SR, Guy HR. 1992. Atomic scale structure and functional models of voltage-gated potassium channels. *Biophysical Journal* **62,** 238–50.

Ehrhardt T, Zimmermann S, Müller-Röber B. 1996. Molecular studies towards understanding guard-cell K^+ channel KST1. *Journal of Experimental Botany* **47,** Supplement, 67.

Fairley-Grenot KA, Assmann SM. 1992. Permeation of Ca^{2+} through K^+ channels in the plasma membrane of *Vicia faba* guard cells. *Journal of Membrane Biology* **128,** 103–13.

Hedrich R. 1995. Technical approaches to studying specific

properties of ion channels in plants. In: Sakmann and Neher, eds. *Single-channel recording*, 2nd edn. Plenum Press.

Hedrich R, Moran O, Conti F, Busch H, Becker D, Gambale F, Dreyer I, Küch A, Neuwinger K, Palme K. 1995. Inward rectifier potassium channels in plants differ from their animal counterparts in response to voltage and channel modulators. *European Biophysical Journal* **24,** 107–15.

Hedrich R, Becker D. 1994. Green circuits—the potential of plant specific ion channels. *Plant Molecular Biology* **26,** 1637–50.

Heginbotham L, Lu Z, Abramson T, MacKinnon R. 1994. Mutations in K^+ channel signature sequence. *Biophysical Journal* **66,** 1061–7.

Hoshi T. 1995. Regulation of voltage dependence of the KAT1 channel by intracellular factors. *Journal of General Physiology* **105,** 309–28.

Hoshi T, Marten I. 1996. Effect of cytoplasmic pH on the gating behaviour of the K^+ channel KAT1. *Biophysical Journal* **A123,** (Abstract).

Hoth S, Dreyer I, Dietrich P, Becker D, Müller-Röber B, Hedrich R. 1997. Molecular basis of plant-specific acid activation of K^+ uptake channels. *Proceedings of the National Academy of Sciences, USA* (in press).

Hille B. 1992. *Ionic channels of excitable membranes.* Sunderland, MA: Sinauer Associates Inc.

Ketchum KA, Slayman CW. 1996. Isolation of an ion channel gene from *Arabidopsis thaliana* using the H5 signature sequence from voltage-dependent K^+ channels. *FEBS Letters* **378,** 19–26.

Kirsch GE, Drewe JA, Taglialatela M, Joho RH, DeBiasi, M, Hartmann HA, Brown AM. 1992. A single nonpolar residue in the deep pore of related K^+ channels acts as a K^+:Rb^+ conductance switch. *Biophysical Journal* **62,** 136–44.

Lopatin AN, Makhina EN, Nichols CG. 1994. Potassium channel block by cytoplasmic polyamines as the mechanism of intrinsic rectification. *Nature* **372,** 366–9.

Marten I, Gaymard F, Lemaillet G, Thibaud J-B, Sentenac H, Hedrich R. 1996. Functional expression of the plant K^+ channel KAT1 in insect cells. *FEBS Letters* **380,** 229–32.

Miller AG, Aldrich RW. 1996. Conversion of a delayed rectifier K^+ channel to a voltage-gated inward rectifier K^+ channel by three amino acid substitutions. *Neuron* **16,** 853–8.

Müller-Röber B, Ellenberg J, Provart N, Willmitzer L, Busch H, Becker D, Dietrich P, Hoth S, Hedrich R. 1995. Cloning and electrophysiological analysis of KST1, an inward rectifying K^+ channel expressed in potato guard cells. *The EMBO Journal* **14,** 2409–16.

Nakamura RL, McKendree Jr WL, Hirsch RE, Sedbrook JC, Gaber RF, Sussman MR. 1995. Expression of an *Arabidopsis* potassium channel gene in guard cells. *Plant Physiology* **109,** 371–4.

Perozo E, Santacruz-Toloza L, Stefani E, Bezanilla F, Papazian DM. 1994. S4 mutations alter gating currents of shaker K channels. *Biophysical Journal* **66,** 345–54.

Pongs O. 1992. Voltage-gated K^+ channels. In: De Pont, ed. *Molecular aspects of transport proteins.* Elsevier Science Publishers bv.

Schachtman DP, Schroeder JI, Lucas WJ, Anderson JA, Gaber RF. 1992. Expression of an inward-rectifying potassium channel by the *Arabidopsis* KAT1 cDNA. *Science* **258,** 1654–8.

Sentenac H, Bonneaud N, Minet M, Lacroute F, Salmo J-M, Gaymard F, Grignon C. 1992. Cloning and expression in Yeast of a plant potassium ion transport system. *Science* **256,** 663–5.

Shimazaki K, Iino M, Zeiger E. 1986. Blue light-dependent proton extrusion by guard-cell protoplasts of *Vicia faba. Nature* **319,** 324–6.

Taglialatela M, Wible BA, Caporaso R, Brown A. 1994. Specification of pore properties by the carboxyl terminus of inwardly rectifying K^+ channels. *Science* **264,** 844–7.

Uozumi N, Gassmann W, Cao Y, Schroeder JI. 1995. Identification of strong modifications in cation selectivity in an *Arabidopsis* inward rectifying potassium channel by mutant selection in yeast. *The Journal of Biological Chemistry* **270,** 24276–81.

Véry A-A, Bosseux C, Gaymard F, Sentenac H, Thibaud J-B. 1994. Level of expression in *Xenopus* oocytes affects some characteristics of a plant inward-rectifying voltage-gated K^+ channel. *Pflügers Archiv* **428,** 422–4.

Véry A-A, Gaymard F, Bosseux C, Sentenac H Thibaud J-B. 1995. Expression of a cloned plant K^+ channel in *Xenopus* oocytes: analysis of macroscopic currents. *The Plant Journal* **7,** 321–32.

Yang N, George Jr AL, Horn R. 1996. Molecular basis of charge movement in voltage-gated sodium channels. *Neuron* **16,** 113–22.

Yool JA, Schwarz TL. 1991. Alteration of ionic selectivity of a K^+ channel by mutation of the H5 region. *Nature* **349,** 700–4.

⇒ zurück zur Übersicht

1998

Hedrich, Hoth, Becker, **Dreyer**, Dietrich

On the structure and function of plant K^+ channels.

In: *Cellular integration of signalling pathways in plant developement.*
F. Lo Schiavo, R.L. Last, G. Morelli, and N.V. Raikhel (eds.) NATO ASI Series. H **104**:35-45.

On the Structure and Function of Plant K^+ Channels

Rainer Hedrich, Stefan Hoth, Dirk Becker, Ingo Dreyer and Petra Dietrich

Institut für Molekulare Pflanzenphysiologie und Biophysik, Mittlerer Dallenbegweg 64, 97082 Würzburg, Germany

Abstract. K^+ uptake is essential throughout the plant life cycle. Transport and accumulation of this macronutrient in large quantities have been recognized e.g. during germination, cell division and growth, differentiation, movement and reproduction. Since K^+ transport is electrogenic - accompanied by the movement of charges - electrophysiological techniques have been used to unravel the molecular mechanisms of K^+ transporters and ion channels, pumps and carriers in general (Hedrich, 1995). This review will concentrate on the biophysical and molecular biological approaches the results of which have shaped our current picture of the structure and function of plant ion channels. For related studies on carriers and pumps see (Hedrich and Schroeder, 1989; Lohse and Hedrich, 1992; Walker et al., 1996; for review see Chasan and Schroeder, 1992; Maathuis and Sanders, 1992).

Patch clamp studies have identified K^+ uptake and K^+ release channels, two major channel types which are inversely activated by the membrane voltage (Blatt, 1988, 1992; Schroeder, 1988, 1989; for review see Schroeder et al., 1994; Hedrich and Dietrich, 1996). Besides, voltage-independent cation channels with often very broad selectivity were described as well (Hedrich and Neher, 1987; Enz et al., 1993; Schulz-Lessdorf and Hedrich, 1995; Allen and Sanders, 1996). Since for K^+ uptake and K^+ release channels extensive *in vivo*-studies, molecular cloning and functional expression analyses are available this review will focus on these channel types, only

Keywords: K^+ channel, plant physiology, heterologous expression, cation sensitivity

Plant K^+ Channels Group into Families

K^+ channels have been found to be present in archaebacteria such as *Methanococcus* (Bult et al., 1996), eubacteria like *Streptomyces* (Schrempf et al., 1995), yeasts (Ketchum et al., 1995; Zhou et al., 1995; Lesage et al., 1996a; Reid et al., 1996), plants (Anderson et al., 1992; Sentenac et al., 1992; Müller-Röber et al., 1995; Ketchum and Slayman, 1996; Czempinski et al., 1997) and animals (for review see Warmke and Ganetzky, 1994; Jan and Jan, 1997). Genome sequencing projects have revealed evidence for the existence of novel K^+ channel genes thereby discovering eight K^+ channel families in the nematode *Caenorhabditis elegans* (Wei et al., 1996). From the existence of four different K^+ channel structural classes characterized by either 2, 4, 6 or 8 putative transmembrane domains in ancient bacteria to man one might conclude that survival of

NATO ASI Series, Vol. H 104
Cellular Integration of Signalling Pathways in Plant Development
Edited by F. Lo Schiavo, R. L. Last, G. Morelli, and N. V. Raikhel

organisms required the control of K^+ fluxes and membrane potential (Fig. 1). From the basic structural elements of 2,4 and 6 putative transmembrane domains in yeast and human and possibly in plants too, 8 transmembrane segments seem to evolve from assembly of a K^+ channel with 6 transmembrane domains and one with just two (Fig. 1, see Lesage et al., 1996a; Zhou et al., 1995).

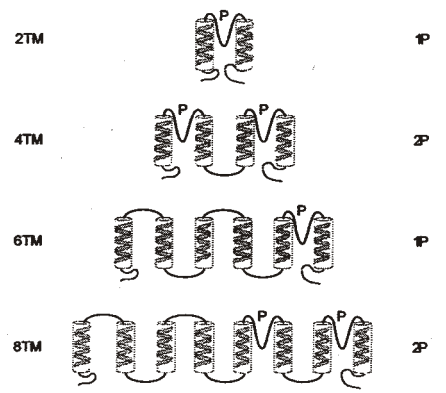

Fig. 1 K^+ channel structures. K^+ channel classes with 2, 4, and 8 transmembrane domains (TM) have been identified. They are characterized by either one or two pore domains (P).

So far the *2-transmembrane-channels* seem to represent voltage-independent K^+ uptake channels known as the 'classical' inward rectifiers (for review see Hille, 1992). Inward rectification - asymmetrical K^+ current in response to hyperpolarization - in these channels is a function of cytoplasmic gating particles such as divalent cations or polyamines (Ficker et al., 1994; Lu and MacKinnon, 1994; for review see Jan and Jan, 1997).The *4-transmembrane-channels* structurally look like two 2-transmembrane channels in tandem. In contrast to the latter the *4-transmembrane channels* are either K^+ release or uptake channels (Lesage et al., 1996b; Fink et al., 1996; Czempinski et al., 1997). ORK1 which is expressed in *Drosophila* neuromuscular tissue, however, appears to be ungated (Goldstein et al., 1996). The *6-transmembrane-channels* found in excitable animal cells comprise the 'classical' outward rectifiers (Hodgkin and Huxley, 1952) first identified in the *Shaker* mutant of *Drosophila melanogaster* (e.g. Papazian et al., 1987; Tempel et al., 1987). Upon depolarization these channels release K^+ and thus repolarize the membrane potential following an action potential. In plants, however, channels with related structure seem to mediate K^+ uptake upon hyperpolarization, only (for review see Hedrich and Becker, 1994; Hedrich and Dietrich, 1996).

From current sequences available the plant K^+ channels group into the two families of inward (K^+_{in}) and outward (K^+_{out}) rectifyiers (Fig. 2). While only recently the first member of the K^+_{out} rectifiers has been cloned (Czempinski et al., 1997) the identification and sequence analyses of several K^+ uptake channel genes groups this family into at least four subfamilies (Fig. 2).

After initial patch-clamp studies on guard cells in 1984 (Schroeder et al., 1984) the K^+ uptake channel in these plant motor cells has been cloned from potato in 1995 (KST1 for K^+ channel *Solanum tuberosum* 1, Müller-Röber et al., 1995). The molecular identification of kst1 in a guard cell library was based on a homology screen taking advantage of *Shaker*-like sequences found in *Arabidopsis thaliana* (kat1: Anderson et al., 1992; akt1: Sentenac et al., 1992). With these members of two different K^+ channel families (Fig. 2) the door to structure-function, antisense and knock out analyses was thrown open.

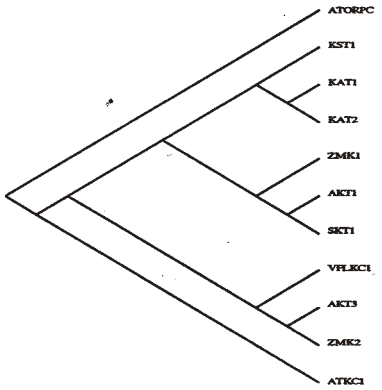

Fig. 2 Evolutionary tree of K^+ channels. The alignment of plant potassium channel sequences was performed using ClustalW (Thompson et al., 1994) and the tree was drawn with the program TreeView (R.D.M. Page, division of environmental and evolutionary biology, University of Glasgow).

K^+ Channel Properties *in vivo* and *in vitro*

Cloning of K^+ channel genes from cell types of specialized physiology such as guard cells (movement), coleoptile cells (growth), phloem cells (sugar loading and unloading) or pollen (polarity and tip growth- fertilization) allowed to relate the K^+ channel properties identified in patch-clamp studies on the 'mother' cells *in vivo* to those of the gene product after heterologous expression *in vitro* (Müller-Röber et al., 1995; Hoth et al., 1997a). This comparison further enabled to distinguish between channel-intrinsic properties and those resulting from plant- or cell-specific regulators present in the 'mother' cells, only.

K^+ uptake channels (Fig. 2) functionally express either in *Xenopus* oocytes (Schachtman et al., 1992; Véry et al., 1994, 1995; Hedrich et al., 1995; Müller-Röber et al., 1995), insect (Sf9, Sf21, Gaymard et al., 1996; Marten et al., 1996; Ehrhardt et al., 1997) or mammalian cell lines (CHO, own unpublished results) or yeast (Bertl et al., 1995). Selecting the expression system depends on three basic requirements:

1. Functional expression of plant channels in general: AKT1 and SKT1 α-subunit homomers so far do not form active channels in *Xenopus* oocytes (for functional coexpression of AKT1 and SKT1, see Dreyer et al., 1997).

2. Low background of endogenous channels (for oocyte-intrinsic channels see Yang and Sachs, 1989; Krause et al., 1996).

3. Sufficient membrane stability to withstand the voltage protocols required to analyse the voltage-dependence of the plant channels properly.

While activation by protons and block by calcium ions already difers between guard

cell K^+ channels from different species *in vivo* (Dietrich et al., 1997), comparative studies to the *in vitro* properties revealed that the selectivity and voltage-dependence is conserved between K^+ channels in different cell types, species and expression systems (Hedrich et al., 1995; Müller-Röber et al., 1995; Véry et al., 1995; Becker et al., 1996; Dietrich et al., 1997). The lack of NH_4^+ permeability found with Sf9 cells and yeast (Marten et al., 1996; Bertl et al., 1995) compared to K^+ channels *in vivo* or after heterologous expression in oocytes (Müller-Röber et al., 1995; Becker et al., 1996; Dietrich et al., 1997) might result from posttranslational modifications such as phosphorylation and glycosylation.

Functional Domains

Since the voltage sensor of the K^+ channel which responds to membrane hyperpolarization in K^+ uptake channels should locate within a transmembrane domain the primary sequence was screened for regions with charged residues within the hydrophobic core. In analogy to the *Shaker* channels (Papazian et al., 1991; Perozo et al., 1994; Yusa et al., 1996) mutations in the fourth putative transmembrane segment (S4, Fig. 3) of KST1 and KAT1 strongly affected the voltage-dependence of the corresponding channel (Dreyer et al., 1997; Hoth et al., 1997b). This result is in line with S4 as a dipole moved by the electrical field which thereby changes the size of the permeation pore (Durell and Guy 1992, 1996; Mannuzzu et al., 1996). Although having S4-segments in common it is however still unclear why the 'red' *Shaker* activates upon depolarization and the 'green' *Shaker* (KAT1, KST1) upon hyperpolarization. It is therefore tempting to speculate that besides S4, C- and N-terminal regions make the difference (Marten and Hoshi, 1997).

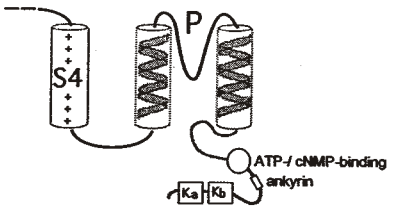

Fig. 3 Functional domains of plant *6-transmembrane K^+ channels*. The transmem-brane domains S4, S5 and S6 are shown with the charged (+) voltage sensor in S4 and the pore region (P). ATP-/cNMP-binding: putative (cyclic) nucleotide-binding domain; ankyrin: ankyrin-binding domain; Kb: basic consensus sequence; Ka: acid consensus sequence.

The selectivity filter is the site of interaction between the potassium ion and blockers with residues lining the permeation pathway the pore (P). In order to allow the movement of the hydrophilic potassium ions through an hydrophobic membrane protein the pore should be formed by amphiphilic residues. Based on the stuctural model for the *Shaker* channel exhibiting one pore domain (P) between S5 and S6 (Durell and Guy 1992, 1996) point mutations in the amphiphilic linker between S5 and S6 in KAT1 identified this domain as a major part of the plant K^+ channel pore as well (Fig. 3 and Becker et al., 1996; Uozumi et al., 1995; Nakamura et al., 1997). Mutations in the inner and outer mouth of the pore resulted in a change in selectivity as well as an alteration of the susceptibility towards the ion channel blockers Cs^+ and Ca^{2+} (Fig. 4). When expressed in yeast they showed a strong phenotype with respect to Cs^+- and Ca^{2+}-dependent growth. The K^+ channel mutant carrying a negatively charged residue in the inner pore developed a Ca^{2+} block absent in the KAT1 wild type. In all cases tested the yeast phenotype could be predicted from the electrophysiology and *vice versa* (Becker et al., 1996; Uozumi et al., 1995).

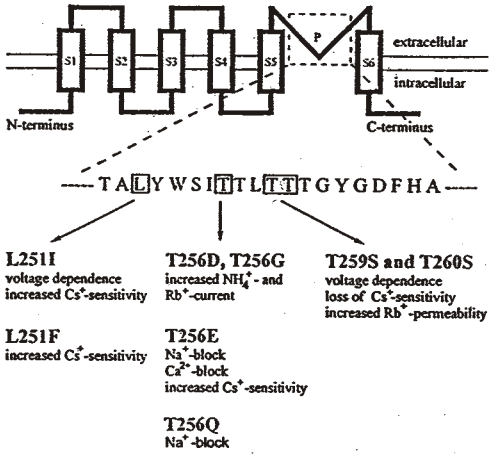

Fig. 4 Structure-function analysis of KAT1 residues. Point mutations in the pore alter cation selectivity and suceptibility to ionic blockers (Hoth et al., 1997b).

pH-sensor: During stomatal movement, coleoptile and pollen growth as well as phloem loading K^+ uptake is always accompanied by changes in external pH in a manner that K^+ uptake is dependent or at least strongly stimulated upon acidification (Weisenseel and Jaffe, 1976; Satter et al., 1988; Cosgrove, 1993). Since in KST1 the pH-sensitivity was most pronounced at pH-changes around 6.2 extracellular histidines were examined in detail (Hoth et al., 1997a; Dietrich et al., 1997). In all plant K^+ uptake channels but not K^+ release channels the motif HXXN was apparent (Fig. 5) pointing to a possible signature sequence for pH-dependent K^+ uptake. Indeed, when this histidine in the outer pore (H271 in KST1, Fig. 5) in addition to the only other histidine in the linker between S2-S3 (H160) was replaced by alanines (A) the activity of this *S. t.* guard cell K^+ channel mutant KST1-H160A/ H271A was pH-insensitive. This fact together with an inversion of the pH-dependence when the histidine was replaced by an aginine (alcaline- instead of acid-activation) provided good evidence for a major role of this residue in the pH-sensing.

Nucleotide-sensor: In the C-terminus of the KAT- and AKT-related channel sequences sites for interaction with ATP or cyclic nucleotides were found (Fig. 3). On the other hand KAT1- and KST1-activity strongly depend on cytoplasmic ATP (Hoshi, 1995; Müller-Röber et al., 1995). The role of this ATP-binding site in KST1 as well as a cNMP-binding domain in AKT-related channels for nucleotide activation now awaits detailed mutational analysis.

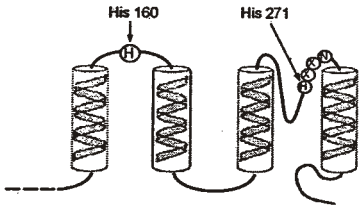

Fig. 5 Putative pH-sensing domains in KST1. The transmembrane segments S3 to S6 and the apparent consensus sequence HXXN are shown.

Heterologous Assembly - a Basis for Functional Diversity

From the biophysical analyses and in analogy to the *Shaker* channels one could propose that the plant K^+ uptake channels functionally assemble as tetramers (Dreyer et al., 1997). Recently, Daram et al. (1997) applying the two-hybrid system to AKT1 found that the cytoplasmic C-terminus alone formed tetrameric structures when expressed in Sf9 cells. For this interaction within AKT1 α-subunits two sides were required, the cNMP-binding domain specific to the AKT-related families (see Fig. 2) and an acidic and basic domain common to all plant K^+ uptake channels (Fig. 4; Daram et al., 1997; Ehrhardt et al., 1997). Furthermore, Dreyer et al. (1997) were able to demonstrate that plant K^+ channel α-subunits from different subfamilies assemble indiscriminately when coinjected into *Xenopus* oocytes. Using α-subunits with different strong phenotypes or creating them by site-directed mutagenesis they could show that in contrast to animal K^+ channels plant α-subunits formed functional heteromers even when originated from different species (Fig. 6 and Dreyer et al., 1997).

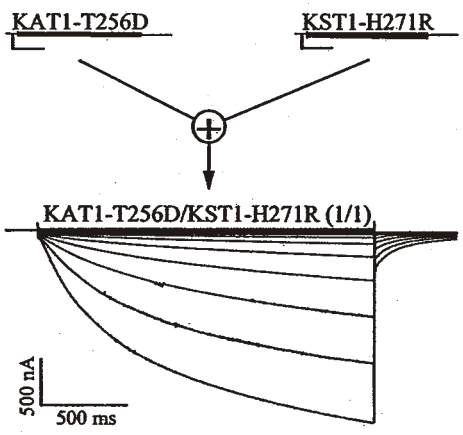

Fig.6 Rescue of the K^+ channel phenotype by coexpression of two silent subunits. The KAT1 mutant KAT1-T256D does not mediate potassium currents (Uozumi et al., 1995) whereas the mutant KST1-H271R is unable to activate at moderate voltages under acidic conditions (Hoth et al., 1997a). Representative current families from oocytes expressing KAT1-T256D, KST1-H271R, and KAT1-T256D/KST1-H271R (1:1 mixture), respectively. Currents were elicited by 2-s voltage steps from +20 mV to -170 mV (10-mV steps) followed by a voltage step to -70 mV from a holding potential of -20 mV.Experiments were performed in 30 mM KCl, pH 5.6.

Outlook

Besides studies on the stucture-function analysis of sites common to K^+ channels and those specific for the 'green' ones cellular expression patterns of plant K^+ channels and their relation to developmental processes are under current investigation. Knowing the cellular localization and developmental pattern the relation between channel distribituion and cell polarity will come to a central question. In epithelia for example cell polarity is directly linked to membrane protein distribution between apical and basolateral sites as a result of immobilization by the cytoskeleton. Within the family of AKT-related channels the ankyrin binding domain might point to a potential site for interaction with the cytoskeleton (see Fig. 3). Despite the absence of the ankyrin binding motif in KAT1, inhibitiors of cytoskeleton dynamics affect K^+ channel activity (Marten and Hoshi, 1997). The molecular mechanism of this interaction has to await further characterization using methods suited to resolve protein-protein interactions like the yeast two-hybrid system or phage display.

Many examples have shown that the electrical properties of a cell membrane depend on the existence of a single predominant channel type or just a few channel types. Thus, ongoing studies aimed on the identification of channel 'knock-out' mutants in transgenic plants very likely will enable to relate phenotypes in for example K^+ uptake efficiency, growth rate, or even plant architecture to the presence or absence of an ion channel.

References

Allen G.J. & Sanders D. 1996. Control of ionic currents in guard cell vacuoles by cytosolic and luminal calcium. *Plant J.* 10, 1055-1069.

Anderson, J. A., Huprikar, S. S., Kochian, L. V., Lucas, W. J. & Gaber, R. F. 1992. Functional expression of a probable *Arabidopsis thaliana* potassium channel in *Saccharomyces cerevisiae*. *Proc. Natl. Acad. Sci. USA* 89, 3736-3740.

Becker, D., Dreyer, I., Hoth, S., Reid, J.D., Busch, H., Lehnen, M., Palme, K. & Hedrich, R. 1996. Changes in voltage-activation, Cs^+ sensitivity, and ion permeability in H5 mutants of a plant K^+ channel, KAT1. *Proc. Natl. Acad. Sci. USA*, 93, 8123-8128.

Bertl, A., Anderson, J. A., Slayman, C. L. & Gaber, R. F. 1995. Use of *Saccharomyces cerevisiae* for patch-clamp analysis of heterologous membrane proteins: Characterization of Kat1, an inward-rectifying K^+ channel from *Arabidopsis thaliana*, and comparison with endogeneous yeast channels and carriers. *Proc. Natl. Acad. Sci. USA* 92, 2701-2705.

Blatt, M. R. 1988. Potassium-dependent, bipolar gating of K^+ channels in guard cells. *J. Membr. Biol.* 102, 235-246.

Blatt, M. R. 1992. K^+ channels of stomatal guard cells / Characteristics of the inward rectifier and its control by pH. *J. Gen. Physiol.* 99, 615-644.

Bult C.J., White O, Olsen G.J., Zhou L., Fleischmann R.D., Sutton G.G., Blake J.A., FitzGerald L.M., Clayton R.A., Gocayne J.D., KerlavageA.R., Dougherty B.A., Tomb J.F., Adams M.D., Reich C.I., Overbeek R., Kirkness E.F, Weinstock K.G., Merrick J.M., Glodek A., Scott J.L., Geoghagen N.S.M., Weidman J.F., Fuhrmann J.L., Venter J.C., et al. 1996. Complete genome sequence of the methanogenic archaeon, *Methanococcus jannaschii. Science* 273, 1058-1073.

Chasan, R. and Schroeder, J.I. 1992. Excitation in plant membrane biology. *The Plant Cell*, 1180-1188.

Cosgrove, J. 1993. How do plant cell walls extend? *Plant Physiol.* 102, 1-6.

Czempinski, K., Zimmermann, S., Ehrhardt, T. & Müller-Röber, B. 1997. New structure and function in plant K^+ channels: KCO1, an outward rectifier with a steep Ca^{2+} dependency. *EMBO J.* 16, 2565-2575.

Daram, P., Urbach, S., Gaymard, F., Sentenac, H. & Charel, I. 1997. Tetramerization of the AKT1 plant potassium channel involves its C-terminal cytoplasmic domain. *EMBO J.* 16, 3455-3463.

Dietrich, P., Dreyer, I., & Hedrich. 1997. Cation-sensitivity and kinetics of guard cell potassium channels differ among species-dependent. *Plant J.*, submitted.

Dreyer, I., Antunes, S., Hoshi, T., Müller-Röber, B., Palme, K., Pongs, O., Reintanz, B. & Hedrich, R. 1997. Plant K^+ channel α-subunits assemble indiscriminately. *Biophysical Journal* 72, 2143-2150.

Durell, S. R. & Guy, H. R. 1992. Atomic scale structure and functional models of voltage-gated potassium channels. *Biophys. J.* 62, 238-250.

Durell, S. R. & Guy, H. R. 1996. Structural model of the outer vestibule and selectivity filter of the *Shaker* voltage-gated K^+ channel. *Neuropharmacology* 35, 761-773.

Ehrhardt, T., Zimmermann, S. & Müller-Röber, B. 1997. Association of plant K^+ channels is mediated by conserved C-termini and does not affect subunit assembly. *FEBS Lett.* 409, 166-170.

Enz, C., Steinkamp, T. & Wagner, R. 1993. Ion channels in the thylakoid membrane. *Biochim. Biophys. Acta* 1143, 67-76.

Ficker, E., Taglialatela, M., Wible, B.A., Henley, C.M. & Brown, A.M. 1994. Spermine and spermidine as gating molecules for inward rectifier K^+ channels. *Science* 266, 1068-1072.

Fink, M., Duprat, F., Lesage, F., Reyes, R., Romey, G., Heurteaux, C. & Lazdunski, M. 1996. Cloning, functional expression and brain localization of a novel unconventional outward rectifier K^+ channel. *EMBO J.* 15, 6854-6862.

Gaymard, F., Cerutti, N., Horeau, C., Lemaillet, G., Urbach, S., Ravallec, M., Devauchelle, G., Sentenac, H. & Thibaud, J.B. 1996. The baculovirus/insect cell system is an alternative to *Xenopus* oocytes. First characterization of the AKT1 K^+ channel from *Arabidopsis thaliana*. *J. Biol. Chem.* 271, 22863-22870.

Goldstein, S.A., Price, L.A., Rosenthal, D.N. & Pausch, M.H. 1996. ORK1, a potassium-selective leak channel with two pore domains cloned from *Drosophila melanogaster* by expression in *Saccharomyces cerevisiae*. *Proc. Natl. Acad. Sci. USA* 93, 13256-13261.

Hedrich, R. 1995. Technical approaches to studying specific properties of ion channels in plants. In: *Single Channel Recording*, 2nd edition, Sakmann, B. & Neher, E., eds., Ch. 12, 277-305.

Hedrich, R. & Becker, D. 1994. Green circuits - The potential of plant specific ion channels. In: *Plant Molecular Biology*, 26. Ausg. Palme, K. Hrsg., Kluwer Academic Publishers, Dordrecht, Belgium, 1637-1650.

Hedrich, R. & Dietrich, P. 1996. Plant K^+ channels: Similarity and diversity. *Bot. Acta* 109, 94-101.

Hedrich, R. & Neher, E. 1987. Cytoplasmic calcium regulates voltage-dependent ion channels in plant vacuoles. *Nature* 329, 833-836.

Hedrich, R. & Schroeder, J. I. 1989. The physiology of ion channels and electrogenic pumps in higher plants. *Ann. Rev. Plant Physiol.* 40, 539-569.

Hedrich, R., Moran, O., Conti, F., Busch, H., Becker, D., Gambale, F., Dreyer, I., Küch, A., Neuwinger, K. & Palme, K. 1995. Inward rectifier potassium channels in plants differ from their animal counterparts in response to voltage and channel modulators. *Eur. Biophys. J.* 24, 107-115.

Hille, B. 1992. *Ionic channels of excitable membranes*, Sinauer Associates Inc., Sunderland, Massachusetts.

Hodgkin, A. L. & Huxley, A. F. 1952. A quantitative description of membrane current and its application to conduction and excitation in nerve. *J. Physiol.* 117, 500-544.

Hoshi, T. 1995. Regulation of voltage dependence of the KAT1 channel by intracellular factors. *J. Gen. Physiol.* 105, 309-328.

Hoth, S., Dreyer, I., Dietrich, P., Becker, D., Müller-Röber, B. & Hedrich, R. 1997a. Molecular basis of plant-specific acid activation of K^+ uptake channels. *Proc. Natl. Acad. Sci. USA* 94, 4806-4810.

Hoth, S., Dreyer, I. & Hedrich, R. 1997b. Mutational analysis of functional domains within plant K^+ uptake channels. *J. Exp. Bot.* 48 Special Issue, 415-420.

Jan, L.Y. & Jan, Y.N. 1997. Cloned potassium channels from eukaryotes and prokaryotes. *Annu. Rev. Neurosci.* 20, 91-123.

Ketchum, K. A. & Slayman, C. W. 1996. Isolation of an ion channel gene from *Arabidopsis thaliana* using the H5 signature sequence from voltage-dependent K^+ channels. *FEBS Lett.* 378, 19-26.

Ketchum, K. A., Joiner, W. J., Sellers, A. J. Kaczmarek, L. K. & Goldstein, S.A. 1995. A new family of outwardly rectifying potassium channel proteins with two pore domains in tandem. *Nature* 376, 690-695.

Krause, J.D., Foster, C.D. & Reinhart, P. H. 1996. *Xenopus laevis* oocytes contain endogenous large conductance Ca^{2+}-activated K^+ channels. *Neuropharmacology*. 35, 1017-1022.

Lesage, F., Guillemare, E., Fink, M., Duprat, F., Lazdunski, M. Romey, G. & Barhanin, J. 1996a. A pH-sensitive yeast outward rectifier K^+ channel with two pore domains and novel gating properties. *J. Biol. Chem.* 271, 4183-4187.

Lesage, F., Guillemare, E., Fink, M., Duprat, F., Lazdunski, M., Romey, G. & Barhanin, J. 1996b. TWIK-1, a ubiquitous human weakly inward rectifying K^+ channel with a novel structure. *EMBO J.* 15, 1004-10011.

Lohse, G. & Hedrich, R. 1992. Characterization of the plasmamembrane HATPase from *Vicia faba* guard cells. *Planta* 188, 206-214.

Lu, Z. & MacKinnon, R. 1994. Electrostatic tuning of Mg^{2+} affinity in an inward-rectifier K^+ channel. *Nature* 371, 243-246.

Maathuis, F.J.M. & Sanders, D. 1992. Plant membrane transport. *Current Opinion in Cell Biology* 4, 661-669.

Mannuzzu, L. M., Moronne M. M., & Isacoff E. Y, 1996. Direct physical measure of conformational rearrangement underlying potassium channel gating. *Science* 271, 213-216.

Marten, I. & Hoshi, T. 1997. Voltage-dependent gating characteristics of the K^+ channel KAT1 depend on the N and C termini. *Proc. Natl. Acad. Sci.* USA 94, 3448-3453.

Marten, I., Gaymard, F., Lemaillet, G., Thibaud, J.-B., Sentenac, H., & Hedrich, R. 1996. Cytoplasmic Ca^{2+} and nucleotides do not affect the voltage-dependent activity of KAT1, *FEBS Lett.* 380, 229-232.

Müller-Röber, B., Ellenberg, J., Provart, N., Willmitzer, L., Busch, H., Becker, D., Dietrich, P., Hoth, S. & Hedrich, R. 1995. Cloning and electrophysiological analysis of KST1, an inward-rectifying K^+ channel expressed in potato guard cells. *EMBO J.* 14, 2409-2416.

Nakamura, R.L., Anderson, J.A. & Gaber R.F 1997. Determination of key structural requirements of a K^+ channel pore. *J. Biol. Chem.* 272, 1011-1018.

Papazian, D. M., Schwarz, T. L., Tempel, B. L., Jan, Y. N. & Jan, L. Y. 1987. Cloning of genomic and complementary DNA from *Shaker*, a putative potassium channel gene from *Drosophila*. *Science* 237, 749-753.

Papazian, D. M., Timpe, L. C., Jan, Y. N. & Jan, L. Y. 1991. Alteration of voltage-dependence of *Shaker* potassium channel by mutations in the S4 sequence. *Nature* 349, 305-310.

Perozo, E., Santacruz-Toloza, L., Stafani, E., Bezanilla, F & Papazian, D. M. 1994. S4 mutations alter gating currents of *Shaker* K^+ channels. *Biophys. J.* 66, 345-354.

Reid, J. D., Lukas, W., Shafaatian, R., Bertl, A., Scheurmann-Kettner, C., Guy, H. R. & North, R. A. 1996. The *S. cerevisiae* outwardly-rectifying potassium channel (DUK1) identifies a new family of channels with duplicated pore domains. *Recept. Channels* 4, 51-62.

Satter, R.L., Morse, M.J., Lee, Y., Crain, R.C. Coté, G.G. & Moran, N. 1988. Light- and clock-controlled leaflet movements in *Samanea saman*: A physiological, biophysical and biochemical analysis. *Bot. Acta* 101, 205-213.

Schachtman, D.P., Schroeder, J.I., Lucas, W.J., Anderson, J.A. & Gaber R.F. 1992. Expression of an inward-rectifying potassium channel by the *Arabidopsis* KAT1 cDNA. *Science* 258, 1645-1658.

Schrempf, H., Schmidt, O., Kümmerlen, R., Hinnah, S., Müller, D., Betzler, M., Steinkamp, T. & Wagner, R. 1995. A procaryotic potassium ion channel with two predicted transmembrane segments from *Streptomyces lividans*. *EMBO J.* 14, 5170-5178.

Schroeder, J. I. 1988. K^+ transport properties of K^+ channels in the plasma membrane of *Vicia faba* guard cells. *J. Gen. Physiol.* 92, 667-683.

Schroeder, J. I. 1989. Qantitative analysis of outward rectifying K^+ channel currents in guard cell protoplasts from *Vicia faba*. *J. Membr. Biol.* 107, 229-235.

Schroeder, J.I., Hedrich, R. & Fernandez, J.M. 1984. Potassium-selective single channels in guard cell protoplasts of *Vicia faba*. *Nature* 312, 361-362.

Schroeder, J. I., Ward, J. M. & Gassmann, W. 1994. Perspectives on the physiology and structure of inward-rectifying K^+ channels in higher plants: Biophysical implications for K^+ uptake. *Annu. Rev. Biophys. Biomol. Struct.* 23, 441-4471.

Schulz-Lessdorf, B. & Hedrich, R. 1995. Protons and calcium modulate SV-type channels in the vacuolar-lysosomal compartment - channel interaction with calmodulin inhibitors. *Planta* 197, 655-671.

Sentenac, H., Bonneaud, N., Minet, M., Lacroute, F., Salmon, J. -M., Gaymard, F. & Grignon, C. 1992. Cloning and expression in yeast of a plant potassium ion transport system. *Science* 256, 663-665.

Tempel, B., Papazian, D. M., Schwarz, T. L., Jan, Y. N. & Jan, L. Y. 1987. Sequence of a probable potassium channel component encoded at the *Shaker* locus of *Drosophila*. *Science* 237, 770-775.

Thompson, J.D., Higgins, D.G. & Gibson, T.J. 1994. CLUSTAL W: improving the sensitivity of progressive multiple sequence alignment through sequence weighting, position-specific gap penalties and weight matrix choice. *Nucleic Acids Res.* 22, 4673-4680.

Uozumi, N., Gassmann, W., Cao, Y.& Schroeder, J.I. Identification of strong modifications in cation selectivity in an Arabidopsis inward rectifying potassium channel by mutant selection in yeast. *Biol. Chem.* 270, 24276-24281.

Véry, A.-A., Bosseux, C., Gaymard, F., Sentenac, H. & Thibaud, J. -B. 1994. Level of expression in *Xenopus* oocytes affects some characteristics of a plant inward-rectifying voltage-gated K^+ channel. *Pflügers Arch.* 428, 422-424.

Véry, A.-A., Gaymard, F., Bosseux, C., Sentenac, H. & Thibaud, J. -B. 1995. Expression of a cloned plant K^+ channel in *Xenopus* oocytes: analysis of macroscopic currents. *Plant J.* 7, 321-332.

Walker N.A., Sanders D., & Maathuis FJ. 1996. High-affinity potassium uptake in plants. *Science* 273, 977-979.

Warmke, J. W. & Ganetzky, B. 1994. A family of potassium channel genes related to *eag* in *Drosophila* and mammals. *Proc. Natl. Acad. Sci. USA* 91, 3438-3442.

Wei, A., Jegla, T. & Salkoff, L. 1996. Eight potassium channel families revealed by the C. elegans genome project. *Neuropharmacology* 35, 805-829.

Weisenseel, M.H. & Jaffe, L.F. 1976. Natural H^+ currents traverse growing roots and root hairs of barley (*Hordeum vulgare* L.). *Planta* 133, 1-7.

Yang, X.-C. & Sachs, F. 1989. Block of stretch-activated ion channels in *Xenopus laevis* oocytes by gadolinium and calcium ions. *Science* 243, 1068-1071.

Yusa, S.P., Wray, D.& Sivaprasadarao, A. 1996. Measurement of the movement of the S4 segment during the activation of a voltage-gated potassium channel. *Pflügers Arch.* 433, 91-97.

Zhou, X. L., Vaillant, B., Loukin, S. H., Kung C. & Saimi Y. 1995. YKC1 encodes the depolarization-activated K^+ channel in the plasma membrane of yeast. *FEBS Lett.* 373, 170-176.

⇒ zurück zur Übersicht

1999

Dreyer, Horeau, Lemaillet, Zimmermann, Bush, Rodríguez-Navarro, Schachtman, Spalding, Sentenac, Gaber

Identification and characterization of plant transporters using heterologous expression systems.

J. Exp. Bot. **50** (Special Issue):1073-1087.

Journal of Experimental Botany, Vol. 50, Special Issue, pp. 1073–1087, June 1999

Journal of Experimental Botany

Identification and characterization of plant transporters using heterologous expression systems

Ingo Dreyer[1,8], Christèle Horeau[1], Guy Lemaillet[1], Sabine Zimmermann[2], Daniel R. Bush[3], Alonso Rodríguez-Navarro[4], Daniel P. Schachtman[5], Edgar P. Spalding[6], Hervé Sentenac[1,8] and Richard F. Gaber[7,8]

[1] *Biochimie et Physiologie Moléculaire des Plantes, UMII/Agro-M/INRA/CNRS URA 2133, Place Viala, F-34060 Montpellier cedex 1, France*

[2] *Max-Planck-Institut für Molekulare Pflanzenphysiologie, D-14476 Golm/Potsdam, Germany*

[3] *Department of Plant Biology and Photosynthesis Research Unit, US Department of Agriculture–Agricultural Research Service, University of Illinois at Urbana-Champain, Urbana, IL 61801, USA*

[4] *Departamento de Biotecnologia, Escuela Técnica Superior de Ingenieros Agrónomos, E-28040 Madrid, Spain*

[5] *Department of Botany, University of Adelaide, Adelaide, SA 5005, Australia*

[6] *Department of Botany and Program in Cellular and Molecular Biology, University of Wisconsin, Madison, WI 53706, USA*

[7] *Department of Biochemistry, Molecular Biology and Cell Biology, Northwestern University, Evanston, IL 60208, USA*

Received 28 November 1998; Accepted 8 December 1998

Abstract

In recent years major progress has been achieved in the understanding of transport processes in higher plants. The boom in the field of molecular plant physiology led to the identification and characterization of membrane transporters with transport activities for potassium, calcium, sugars, nitrate, ammonium, sulphate, phosphate, amino acids, peptides, and metal ions. Such progress was hardly feasible without heterologous expression of the isolated transport proteins. This review summarizes the different approaches in characterizing plant membrane transporters using heterologous expression systems. By presenting concrete examples, it outlines different cloning strategies, displays the methods used for (i) expression of transport proteins and detection of their function, (ii) biochemical analyses, (iii) explorations of the structure–function relationship through mutational analysis, and concludes with a discussion about the physiological relevance of the analyses in heterologous expression systems.

Key words: Membrane transporters, transport processes, heterologous expression systems, transport proteins, cloning strategies.

Introduction

Plants are fully autotrophic organisms, with aerial parts fixing CO_2 from the atmosphere and roots taking up mineral ions from the earth's crust. Obviously, together with the photosynthetic machinery, this autotrophic way of life requires controlled expression of a large set of membrane transport systems, responsible for mineral uptake from the soil and translocation towards the shoots, coupled to transport of photosynthetates in the opposite direction. These transporters are therefore integral systems underlying the autotrophic status of plants.

Particularly during the last decade new and detailed insights into the biology of plant transport have been obtained. As is true elsewhere, the field of plant science has been revolutionized by the development and use of molecular biology techniques. Molecular genetic approaches have, for the first time, afforded the opportunity to extract single transporters from the complicated

[8] To whom correspondence should be addressed. Gaber: Fax: +1 847 4671422. E-mail: r-gaber@nwu.edu; Sentenac: Fax: +33 4 67 52 57 37. E-mail: sentenac@ensam.inra.fr; Dreyer: Fax: +33 4 67 52 57 37. E-mail: dreyer@ensam.inra.fr

network of the plant and have allowed their detailed investigation in isolation. Now seen, with increasing frequency, is the molecular characterization of individual transport proteins that begins with the cloning of the gene or the gene transcript, determination of the nucleotide and amino acid sequences, expression of the gene product and detection of its function followed by biochemical analyses and further elaborated explorations of the structure–function relationship through mutational analysis (for recent reviews see Tanner and Caspari, 1996; Logan *et al.*, 1997; Maurel, 1997; Rentsch *et al.*, 1997; Eng *et al.*, 1998; Fox and Guerinot, 1998). These steps were hardly feasible without the utilization of heterologous expression systems. In this article, the different expression systems used for the characterization of plant transport proteins are described, both the advantages and the risks of heterologous systems are pointed out and the physiological significance of some of the results obtained is discussed. This analysis refers mainly to plasma membrane transporters, with rather special emphasis on K^+ carriers and channels.

Heterologous expression systems

Several heterologous expression systems have been used for the identification and characterization of plant membrane transporter proteins (Frommer and Ninnemann, 1995).

Escherichia coli

Although the prokaryote *Escherichia coli* serves as a well-established system for protein production, the heterologous expression of membrane proteins has been successful only in some exceptional cases (e.g. the light-harvesting chlorophyll *a/b* binding protein from pea, Kühlbrandt and Wang, 1991) and even then the protein is not always obtained in a functional form. Although the main problem might be the failure of the expressed protein to fold correctly, many membrane proteins seem to be toxic when expressed in bacteria. Probably because of these limitations, *E. coli* has not become an expression system of choice for plant membrane transporters. Nevertheless, *E. coli* is occasionally used to produce plant transporter proteins for reconstitution, and very recently for direct flux-measurements and complementation assays (Kim *et al.*, 1998; Uozumi *et al.*, 1998).

Yeast

Most of the basis of our current knowledge on plant membrane transporters has been obtained by skilful use of the yeasts *Saccharomyces cerevisiae* and *Schizosaccharomyces pombe*. These organisms have short generation times and can easily be handled. Moreover, the great progress in using yeasts as heterologous systems for the expression of plant transporters was facilitated by the engineering of yeast strains with deficiencies in specific transport pathways (Riesmeier *et al.*, 1992). By functional complementation, such strains were used for proving the functionality of cloned transporters and for screening cDNA libraries to identify new transporters. In addition, yeast is well suited for flux measurements allowing the determination of substrate specificity of particular transporters. The yeast system has also been used in biochemical approaches, for example, for analysing functional properties of H^+-ATPases (Palmgren and Christensen, 1994), and to a lesser extent for electrophysiological characterization of ion channels (Bertl *et al.*, 1995).

Xenopus *oocytes*

Oocytes of the South-African clawed toad *Xenopus laevis* have been used as a powerful tool to study heterologous gene expression for more than 25 years (Gurdon *et al.*, 1971). The popularity of this expression system is due to several factors. On the one hand, *Xenopus* oocytes are quite robust and easy to handle because of their large size ($\sim$1 mm in diameter), and on the other they can efficiently synthesize and assemble a variety of proteins after injection of DNA or RNA either isolated from various tissues or synthesized *in vitro* from cDNA clones. Size and ease of handling have made oocytes well-suited to the measurement of water and solute fluxes, enzymatic activity and, in particular, to electrophysiological and biophysical characterization of electrogenic membrane transporters (for the use of *Xenopus* oocytes as an expression system for plant proteins see Schroeder, 1994; Theodoulou and Miller, 1995).

Insect cells

An alternative to the expression systems outlined so far is the infection of insect cells by recombinant baculoviruses. The use of this system for producing recombinant proteins has become more widespread due to many factors including potentially high protein expression levels, ease and speed of genetic engineering, and ease of insect cell growth in suspension cultures. Furthermore the recombinant proteins are often biologically active and, for the most part, appear to undergo faithful post-translational processing to produce recombinant products that are very similar to those of the authentic proteins (for reviews see McCarroll and King, 1997; Possee, 1997). Baculovirus-infected cells of the moth *Spodoptera frugiperda* (*Sf*9 and *Sf*21 cell lines) have been used for biochemical and electrophysiological characterization of plant K^+ channels (Gaymard *et al.*, 1996).

Mammalian cell lines

Mammalian cell lines have seldom been used for the the study of plant transporters. The exceptions mentioned in

this study note the utilization of COS cells, an engineered line of African green monkey kidney cells which can easily be transfected (Gluzman, 1981). Transiently transfected COS cells express the protein at relatively high levels over a short period of time in a burst starting about 24 h post-transfection and lasting for up to 1 week. With regard to the characterization of plant membrane transporters, thus far COS cells have only been used for a few cloning strategies and structure–function relationship studies (Kammerloher *et al.*, 1994; Kristoffersen *et al.*, 1996; Chang and Bush, 1997).

Characterization of plant membrane transporters

Cloning

By the beginning of this decade various membrane transporters were characterized *in planta* (for a contemporary review see Hedrich and Schroeder, 1989) but only two were identified at the molecular level. The plasma membrane H^+-ATPase from *Arabidopsis thaliana* was cloned with the aid of microsequencing of the purified protein (Boutry *et al.*, 1989; Harper *et al.*, 1989; Pardo and Serrano, 1989) whereas the H^+-hexose co-transporter from *Chlorella kessleri*, HUP1, was identified by differential screening of a cDNA library taking advantage of the fact that the expression of this transporter in *Chlorella* is hexose-induced (Sauer and Tanner, 1989). The demonstration of HUP1 as a glucose transporter was subsequently confirmed by heterologous expression in yeast (Sauer *et al.*, 1990).

More recently, the identification of most plant transporters has been achieved through the use of heterologous expression systems. The first successes resulted in the cloning of K^+ channels from *Arabidopsis thaliana* (Anderson *et al.*, 1992; Sentenac *et al.*, 1992) by complementation of mutant yeast cells. Yeast mutants deleted for the K^+ transporter genes *TRK1* and *TRK2* (required for high affinity K^+ uptake) are unable to grow on low K^+ media. The single mutant *trk1* and the double mutant *trk1 trk2* require high concentrations of K^+ (*c.* 3 mM and 50 mM, respectively) in the medium to grow at rates achieved by wild-type cells on medium containing micromolar quantities of the ion (Ramos *et al.*, 1985; Ko and Gaber, 1991). The K^+ uptake-defective yeast mutants were transformed with cDNA libraries from *Arabidopsis thaliana* and screened on low K^+ media for rescue of the growth phenotype. A major surprise was that the two inward-rectifying K^+ channels cloned by this approach, KAT1 (Anderson *et al.*, 1992) and AKT1 (Sentenac *et al.*, 1992), are remarkably similar to the animal voltage-dependent outward rectifiers of the *Shaker* type. This underscores another advantage of functional cloning: the ability to identify transporter proteins without implementing a structurally-biased constraint on the search.

The ability to restore K^+ uptake in *S. cerevisiae* mutants has also led to the identification of other classes of plant transport proteins. For example, a K^+ and a cation carrier from wheat roots have been cloned by complementation of yeast *trk* mutants: HKT1, which comprises 10–12 membrane spanning domains (Schachtman and Schroeder, 1994), and LCT1, which contains 8 to 10 transmembrane segments (Schachtman *et al.*, 1997). Interestingly, HKT1 and LCT1 exhibit no significant sequence similarities with other transport proteins.

The strategy of cloning by functional complementation has not only proven successful for the isolation of K^+ transporters but also, using yeast strains with appropriate deficiencies in other transport activities, plant carriers have been cloned that have transport activities for sucrose (Riesmeier *et al.*, 1992), amino acids (Frommer *et al.*, 1993; Hsu *et al.*, 1993; Kwart *et al.*, 1993), peptides (Steiner *et al.*, 1994), ammonium (Ninnemann *et al.*, 1994), copper (Kampfenkel *et al.*, 1995), sulphate (Smith *et al.*, 1995), calcium (Hirschi *et al.*, 1996), iron (Eide *et al.*, 1996), and zinc (Grotz *et al.*, 1998).

In theory, functional cloning by expression in *Xenopus* oocytes should provide an alternative means of identifying plant transporters. In this approach, cRNA synthesized from a subdivided plant cDNA library is injected into *Xenopus* oocytes and followed by assessment of individual oocytes for the detection of transport activity and subdivision of the positive cDNA pools, ultimately to identify the transporter cDNA. This type of expression cloning has been shown to be very powerful for the isolation of animal membrane receptors and ion channels (Jentsch *et al.*, 1990). However, although initial reports were promising (Cao *et al.*, 1992) this procedure has yet to be used successfuly for the isolation of a plant membrane transporter.

A different and elegant method for identifying plant membrane proteins resulted in the cloning of plant plasma membrane water channels. COS cells were transfected with an *Arabidopsis thaliana* root cDNA library and screened with an antiserum raised against purified integral plasma membrane proteins from *A. thaliana* roots. The immunoselection led to the identification of five genes which could be shown to code for proteins with water transport-facilitating activities when expressed in *Xenopus* oocytes (Kammerloher *et al.*, 1994). Further improvements of this immunoscreening method have been developed using either *E. coli* or COS cells for the systematic rapid cloning of plant cDNAs encoding proteins with membrane spanning domains (Shi *et al.*, 1995; Kristoffersen *et al.*, 1996). The function of the newly detected proteins, however, remains to be identified.

Functional characterization

Despite noteworthy exceptions (Lesage *et al.*, 1994), cloning by functional complementation of a yeast mutant

defective for the transport of a specific solute simultaneously demonstrates that the cloned transporter is indeed endowed with transport activity for the corresponding solute. In other cloning strategies, the activity of the expressed protein must be assessed separately. To date, in all cases where the substrate specificity of a plant transporter has been unambiguously determined, the approaches have relied on the use of heterologous expression systems. While yeasts have proven to be the systems of choice for many studies (Sauer *et al.*, 1990; Hechenberger *et al.*, 1996; Muchhal *et al.*, 1996) other systems including *Xenopus* oocytes (Müller-Röber *et al.*, 1995; Ketchum and Slayman, 1996; Gaymard *et al.*, 1998), the insect cell system (Gaymard *et al.*, 1996; Czempinski *et al.*, 1997; Zimmermann *et al.*, 1998), and *E. coli* (Kim *et al.*, 1998; Uozumi *et al.*, 1998) are also being exploited. Indeed, the first example of such a strategy has been provided by the cloning and characterization of the HUP1 glucose carrier from *Chlorella* (Sauer and Tanner, 1989; Sauer *et al.*, 1990; see above). Recently, K^+ transporters identified among EST clones from the *Arabidopsis* genome sequencing project, or through a PCR strategy based on sequence alignments and identification of highly conserved regions, have been shown to be endowed with K^+ transport activity by complementing *S. cerevisiae trk* mutants (Quintero and Blatt, 1997; Santa-Maria *et al.*, 1997; Fu and Luan, 1998) or *E. coli* (Kim *et al.*, 1998). However, in this context it should be noted that there are still several putative plant transport systems (Köhler and Neuhaus, 1998; Schuurink *et al.*, 1998) and ionotropic receptors (Lam *et al.*, 1998) which have to be assigned a function.

Beyond providing a means for revealing the transport activity of a given system, the heterologous expression of cloned transporters can provide additional information about transport kinetics (K_m values for various substrates), transport mechanisms (energetic coupling to the transmembrane proton electrochemical gradient), and pharmacological properties (Riesmeier *et al.*, 1993, for sucrose carriers). It should be noted, however, that the transport properties and bioenergetics of the sucrose and amino acid symporters were initially defined using purified plasma membrane vesicles and imposed proton electrochemical differences (Bush, 1993*a*).

With regard to K^+ transport, flux studies in *S. cerevisiae* using K^+ and Rb^+ allowed the characterization of high-affinity K^+ uptake systems (Schachtman and Schroeder, 1994; Fu and Luan, 1998), and the identification of the transporter mediating the high-affinity K^+ uptake of barley roots (Santa-Maria *et al.*, 1997). Using $^{42}K^+$ and $^{22}Na^+$ the transport mechanism of the wheat K^+ carrier HKT1 was revealed to be a Na^+-coupled co-transport with a stoichiometry of $K^+ : Na^+ \approx 2$ (Rubio *et al.*, 1995). To elaborate the transport characteristics of the transporter LCT1, radiotracer measurements were combined with a negative yeast growth assay. Flux studies showed that LCT1 mediates $^{45}Ca^{2+}$ as well as $^{109}Cd^{2+}$ uptake. A prolonged exposure of LCT1-expressing cells to these cations led to toxic accumulations of Ca^{2+} or Cd^{2+}, which manifested itself in inhibited growth (Clemens *et al.*, 1998).

Flux measurements have also been performed with *Xenopus* oocytes. Swelling experiments to show the function of water channels is but one example (Maurel *et al.*, 1993). By far the greatest use of this expression system has been to analyse the electrical features of expressed transporters (Boorer *et al.*, 1992; Aoshima *et al.*, 1993; Tsay *et al.*, 1993; Schachtman and Schroeder, 1994). The combination of electrical and radiotracer flux measurements revealed the dependence of the transport activity on both extracellular pH and membrane voltage for several carriers (hexose, nitrate, amino acids, and sucrose). Based on such observations, the transport mechanism of these transporters has been deduced to be an electrogenic proton co-transport with stoichiometries of H^+:sucrose = 1, H^+:amino acid = 1, and $H^+ : NO_3^- > 1$ (Boorer *et al.*, 1992, 1996*a*, *b*; Tsay *et al.*, 1993; Boorer and Fischer, 1997). Furthermore, for the amino acid transporter, freeze–fracture electron microscopy allowed an estimate of the number of transporters expressed in the oocyte plasma membrane. With this information, the transport rate of a single carrier molecule could be calculated to be 350–800 transport cycles per second (Boorer *et al.*, 1996*a*). In this context it should be noted that, due to such relatively low transport rates, the electrophysiological analyses of carriers are difficult and could lead to distorted conclusions. Thus, since the membrane current is proportional to the cell surface × the transporter density × the turnover rate of the transporter (Tyerman and Schachtman, 1992), low rates of transport are more likely to be detected with large cells such as *Xenopus* oocytes.

Ion channels have transport rates (in the range of 10^7 ions per second or even higher) that are much higher than those of carriers (10–1000 transport events per second), and electrophysiological analysis of their transport activity is therefore easier. To date, several plant ion channels have been cloned (including chloride channels, Hechenberger *et al.*, 1996; Lurin *et al.*, 1996) but thus far, only plant potassium channels have been investigated in detail. All but one of the K^+ channels share a common structure of six transmembrane spanning helices. The exception, KCO1 from *Arabidopsis*, comprises only four transmembrane domains (Czempinski *et al.*, 1997). Using the oocyte expression system with the two-electrode voltage-clamp technique, the pharmacological and biophysical features of some of these channels were determined (Schachtman *et al.*, 1992; Kochian *et al.*, 1993; Véry *et al.*, 1994, 1995; Cao *et al.*, 1995*b*; Hedrich *et al.*, 1995; Hoshi, 1995; Müller-Röber *et al.*,

1995; Ketchum and Slayman, 1996; Gaymard *et al.*, 1998; Lacombe and Thibaud, 1998; Moroni *et al.*, 1998).

Several channels which were not functional in oocytes have been characterized in insect cells applying the patch-clamp technique (Gaymard *et al.*, 1996; Czempinski *et al.*, 1997; Zimmermann *et al.*, 1998). Additional information could be acquired from patch-clamped yeast cells expressing KAT1 or AKT1 (Bertl *et al.*, 1994, 1995, 1997). Besides the two-electrode voltage-clamp technique, the patch-clamp technique has been adapted to the oocyte system to explore the activity of a single transport molecule (Schachtman *et al.*, 1992; Cao *et al.*, 1995*b*; Hedrich *et al.*, 1995; Hoshi, 1995; Müller-Röber *et al.*, 1995; Zei and Aldrich, 1998). From these observations transport rates in the range of millions of ions per second could be estimated.

The data obtained so far indicate that plant K^+ channels are not only potassium-selective pores in the membrane, but can be directly regulated by the membrane voltage, intracellular and extracellular protons, and cytoplasmic nucleotides. Furthermore, based on the transport direction under physiological conditions, plant potassium channels have been segregated into two groups: inwardly rectifying channels (KAT1, AKT1, AKT2/3 from *Arabidopsis*; KST1, SKT1 from potato) and outwardly rectifying channels (KCO1, SKOR from *Arabidopsis*; for references see Table 1).

Biochemical characterization

In addition to the investigation of the function of plant transporters, other methods have been used to gain further information. Biochemical approaches have been developed for the characterization of phosphorylation and glycosylation status of the transporter proteins and also the assembly of the components of several transport systems. Such analyses require the isolation of large quantities of protein in a controlled environment. Since, as mentioned above, expression in *E. coli* does not seem to offer particular advantages, most success in this field has up to now relied on expression in yeast or in insect cells. However, even in these eukaryotic systems, problems regarding correct targeting of the heterologously expressed protein to the cell membrane can occur. Most, or even all, of the synthesized polypeptides may be trapped in internal membranes (Villalba *et al.*, 1992; Regenberg *et al.*, 1995; Gaymard *et al.*, 1996; Erhardt *et al.*, 1997). Yet problems in the targeting of heterologously expressed proteins do not exclude the development of biochemical approaches and the purification of the protein in a functional state. Absence of targeting to the cell membrane can facilitate purification protocols (Villalba *et al.*, 1992). By the same token, the use of yeast strains defective in the secretion pathway (sec mutants) has yielded insights in the phosphorylation processes occurring during the movement of newly synthesized ATPases from the ER to the cell surface (Chang and Slayman, 1991).

Illustrative approaches for the purification of plant membrane transport proteins have been developed for K^+ channels and plasma membrane H^+-ATPases. Direct purification of K^+ channels from plant tissue is highly challenging work (Zeilinger, 1994) due to the very low

Table 1. *Functionality of potassium transporters in different heterologous expression systems*

Transporter	Expression system				Reference
	Yeast	*Xenopus* oocytes	*Sf*9 cells	*E. coli*	
AKT1	+	−[a]	+		Sentenac *et al.*, 1992 Gaymard *et al.*, 1996
SKT1	−	−[a]	+		Zimmermann *et al.*, 1998
KAT1	+	+	+	+	Anderson *et al.*, 1992 Schachtman *et al.*, 1992 Gaymard *et al.*, 1996 Marten *et al.*, 1996 Uozumi *et al.*, 1998
KST1		+	+		Müller-Röber *et al.*, 1995 Zimmermann *et al.*, 1998
AKT2[b]	−	−	−	+	Cao *et al.*, 1995*b* Uozumi *et al.*, 1998
AKT3[b]		+			Ketchum and Slayman, 1996
KCO1		−[c]	+		Czempinski *et al.*, 1997
AtKUP1	+[d]/−[e]	−		+	Fu and Luan, 1998[d] Kim *et al.*, 1998[e]

[a] AKT1 and SKT1 build functional channels when co-expressed in *Xenopus* oocytes (Dreyer *et al.*, 1997). Meanwhile it could also be shown that SKT1 alone is functional in oocytes (S Zimmermann and B Müller-Röber, unpublished results).

[b] AKT2 and AKT3 are encoded by the same gene showing two start-codons in the same open reading frame. AKT2 is the protein synthesized if the first start codon is used, and AKT3 the protein if the second codon is used.

[c] Injection of KCO1-encoding cRNA into *Xenopus* oocytes seems to be poisonous for the cells (S Zimmermann and B Müller-Röber, unpublished results).

abundance of these proteins in the membrane. In contrast, the heterologous expression of K^+ channels in the baculovirus/insect cell system and their subsequent purification has proven to be much more effective. The *Arabidopsis* K^+ channel AKT1 has been obtained with high purity (a single band on a silver stained gel) in sufficiently large amounts (*c.* 1 mg protein from a 1.0 l cell culture) to allow the demonstration that, like its *Shaker* family counterparts in animal cells, AKT1 takes on a tetrameric structure (Daram *et al.*, 1997).

Although by comparison to K^+ channels, the plasma membrane H^+-ATPase is much more abundant, its functional characterization after purification from plant tissues remains problematic due to the presence and the similarity of multiple isoforms in many tissues. The first comparison of the functional properties of isoforms of the plant plasma membrane H^+-ATPase was obtained by expression in *S. cerevisiae* (Palmgren and Christensen, 1994). Using inducible promoters, which allowed independent control for the expression of the endogenous yeast H^+-ATPase and that of the heterologous pump, three isoforms of the *Arabidopsis* pump, AHA1, AHA2 and AHA3, were produced individually and their biochemical properties characterized. Each of the isoforms displayed qualitatively similar enzymatic properties, but quantitative differences were found in turnover rates for ATP hydrolysis, the apparent affinities for ATP or sensitivity to pH. This first demonstration of functional differences between members of the same gene family led to the suggestion that such diversity is central to solute transport integration at the whole plant level, allowing each tissue to express the set of transport systems suited to the role that this tissue plays in the plant (Sussman, 1994).

Analyses of structure–function relationships

Determination of the amino acid sequence of a transporter through the sequence of its cloned cDNA can provide an initial glimpse of its putative structure. Based on the inferred hydrophilic and lipophilic character of different parts of the protein, transmembrane domains and sometimes extramembraneous regions can be postulated. However, as such analyses can lead to strongly distorted models, the need for direct experimental approaches, such as the investigations aimed at elucidating the structure of the *Drosophila* Shaker K^+ channel (compare the initially proposed topology, Kamb *et al.*, 1987, with the latest model, Durell *et al.*, 1998) and the *Arabidopsis* NAT2/AAP1 amino acid carrier (Chang and Bush, 1997), is inescapable.

To elucidate the topology of NAT2, NAT2, c-myc epitopes that are readily detectable by immunolabelling were fused to the C-terminus and the N-terminus of the protein. Expression in yeast revealed that this engineering did not disrupt the function of the protein. After heterologous expression in COS cells, only the C-terminal epitope was detected on the cell surface indicating the C-terminus is oriented on the outside and the N-terminus on the inside. In addition, the epitope-tagged proteins were expressed in a cell free translation system, incorporated into microsome membranes, and digested with a protease. From the resultant proteolytic fragments it could be concluded that NAT2 contains 11 transmembrane domains, a cytosolic N-terminus and an extracellular C-terminus (Chang and Bush, 1997). In contrast, hydropathy analysis of the NAT2 sequence had suggested 12 membrane-spanning segments (Frommer *et al.*, 1993; Hsu *et al.*, 1993).

The topology of the *Arabidopsis* K^+ channel KAT1 has been investigated by a different technique. Varying lengths of the N-terminus of the protein were fused with alkaline phosphatase (PhoA), and the resulting chimaeric proteins were expressed in *E. coli*. The enzyme activity of the PhoA moiety indicated the localization of the phosphatase, since PhoA is active when it is exported into the periplasm, whereas it remains inactive in the cytoplasm (Manoil and Beckwith, 1986). Based on this screen, the postulated topology of the channel, with six transmembrane domains (Anderson *et al.*, 1992), was confirmed (Uozumi *et al.*, 1998).

Obviously, to gain an understanding of the molecular basis of the catalysis of transmembrane transport, detailed structural information beyond the elucidation of topology of the transporter proteins is required. With notable exceptions, including the recently solved structure of the *Streptomyces lividans* K^+ channel KcsA (Doyle *et al.*, 1998), there is a paucity of direct structural data on transport proteins. Most of our knowledge in this field originates from the manipulation of transport proteins using recombinant DNA techniques and subsequent assays in heterologous systems for effects on function. In accordance with this, three different approaches have been used: random mutagenesis, site-directed mutagenesis, and creation of chimaeric proteins.

In the case of random mutagenesis, a preparation of randomly mutated transporter cDNA is generated and screened upon expression in a heterologous host, such as *S. cerevisiae*. Clues regarding structure–function relationships are subsequently gleaned from the sequence and detailed characterization of the mutants exhibiting altered transport function. In many cases, this approach can be the most efficient way of investigating the structure of the protein. However, the usefulness of random mutagenesis can be limited unless the output of the system can be designed to distinguish between mutations, such nonsense or frameshift mutations (Ros *et al.*, 1999), that confer trivial loss-of-function phenotypes and those that alter sites specifically required for transporter function.

Site-directed mutagenesis presupposes a concrete

suspicion that a specific part(s) of the protein determines a distinct feature. This suspicion can arise from sequence comparison with homologous proteins, from random mutagenesis, or from the pharmacological attributes of the transporter. The chemical properties of inhibitors, as well as their molecular interactions with the transporter, often provide information about amino acid residues that are involved in substrate binding and translocation (Crestfield *et al.*, 1963; Westhead, 1965). Accordingly, single amino acids are selectively changed or parts of the protein are truncated and the functional features of the mutant system investigated. One limitation of this approach is the intrinsic bias in selecting specific regions for mutagenesis while another is the inefficiency of site-directed mutagenesis compared to random mutagenesis when the targeted region is large.

The third approach, creation and analysis of chimaeric proteins, is applicable to homologous proteins strongly differing in only a few functional characteristics. Creation of chimaeric proteins between both transporters can help to localize the sites in the proteins being responsible for the difference.

Structure–function studies have been performed for different plant transporters, among them several water channels, the Na^+-coupled K^+ carrier HKT1, the hexose-H^+ symporters HUP1 and HUP2, the sucrose-H^+ symporter AtSUC1, as well as the potassium channels KAT1 and KST1. Results of studies on these transporters are summarized below.

Plant water channels (aquaporins) belong to the major intrinsic proteins (MIP family) with six putative transmembrane segments (for a review, see Maurel, 1997). The water flux through many aquaporins can be blocked by extracellular mercury. Using site-directed mutagenesis, the mercury-sensitive site of γ-TIP and δ-TIP (aquaporins expressed on the tonoplast) was shown to be a cysteine residue in the third transmembrane domain (Daniels *et al.*, 1996). In contrast, the plasma membrane water channel RD28 is not sensitive to Hg^{2+}. Engineering of a cysteine residue in the fifth transmembrane helix created a mercury sensitivity (Daniels *et al.*, 1994) indicating that both the third and the fifth transmembrane segment are involved in the formation of the aqueous pore. In a further study, it was shown that the activity of α-TIP is regulated by phosphorylation (Maurel *et al.*, 1995). Mutating putative targets for a phosphorylation, three serines were identified which each can independently modulate water transport by the α-TIP protein (Maurel *et al.*, 1995). The control of permeability by channel phosphorylation has also been investigated for the plasma membrane channel PM28A. Mutational analysis revealed two serines which were phosphorylated when the protein was expressed in *Xenopus* oocytes. However, biochemical investigations led to the conclusion that only one of these two sites is used to modulate the channel activity *in planta* (Johansson *et al.*, 1998).

A model system for structure–function studies on plant transporters belonging to the major facilitator superfamily is the *Chlorella* glucose-H^+ symporter HUP1 (for review see Tanner and Caspari, 1996). Transporters in this family are believed to contain 12 transmembrane segments. To determine structural elements of HUP1 involved in sugar binding and transport, randomly produced mutants of the *HUP1* gene were screened in *Schizosaccharomyces pombe* for an altered affinity toward the toxic sugar analogue 2-deoxyglucose. Whereas yeast cells transformed with the wild-type HUP1 were highly sensitive to 2-deoxyglucose, mutations that altered the protein in either the 5th, 7th or 11th transmembrane domains conferred decreased sensitivity (Will *et al.*, 1994, 1998). In addition, site-directed mutagenesis revealed that a residue at the end of the first transmembrane domain (D44) is essential for the activity of the transporter (Caspari *et al.*, 1994). In subsequent studies this region of the protein was shown to be crucial for substrate specificity as well.

HUP2, another monosaccharide-H^+ symporter in *Chlorella*, shares 74% homology to HUP1, but differs significantly from HUP1 in the former's higher specificity for D-galactose. The expression of chimaeric proteins in yeast led to the conclusion that this difference involves the amino-terminal part of the first extracellular loop, and site-directed mutagenesis pinpointed the distinction to a single amino acid (N45; Will and Tanner, 1996; Will *et al.*, 1998). As a whole, the data support the proposal that the 1st, 5th, 7th, and 11th transmembrane segments line the sugar translocation path and determine its specificity. Additionally, the role of histidine residues in the transport of hexoses has been investigated. The substitution of all of the histidine residues in HUP1 to arginine has no effect on the transport activity in *S. pombe* indicating that the extracellular histidines are not required for substrate binding nor for coupling of transport of the solute with co-transported protons (Caspari *et al.*, 1994).

In comparison, a histidine highly conserved among plant sucrose-H^+ transporters has been identified to be part of the sucrose binding pocket of the sucrose carrier AtSUC1. Previous biochemical investigations showed that, when the classical histidine denaturating agent diethyl pyrocarbonate (DEPC) was applied from the outside face of the plasma membrane, the sucrose carrier was inhibited. Significantly, DEPC inhibition was blocked when sucrose was present in the reaction mixture, suggesting the DEPC-sensitive residue was at, or conformationally linked to, the sucrose binding site (Bush, 1993*b*). Site-directed mutagenesis subsequently inferred that the corresponding residue was located in the loop between the first and second transmembrane segment (Lu and Bush, 1998), supporting the hypothesis that this region of sugar transporters determines the substrate specificity.

In contrast to aquaporins or sugar carriers which both belong to large protein families sharing structural and functional similarities, nothing was known regarding the structure of the sodium-coupled potassium carrier HKT1. To identify regions of this protein involved in the binding and transport of Na^+ and K^+, two approaches involving both random and site-directed mutagenesis have been developed. Analysis of the mutant proteins expressed in *S. cerevisiae* indicate that HKT1 harbours distinct and separate binding sites for Na^+ and K^+. The loop between the putative 9th and 10th transmembrane segments appears to be part of the Na^+ binding site, whereas the 6th transmembrane segment is evidently involved in the binding of K^+ (Rubio *et al.*, 1995; Diatloff *et al.*, 1998).

At the present time, the most detailed information on structure–function relationships of a plant transporter family is available for plant K^+ channels. In this connection, KAT1 (*Arabidopsis thaliana*) and KST1 (*Solanum tuberosum*), which are both expressed in guard cells, have evolved into model systems for these studies. These plant potassium channels belong to the large family of voltage-gated potassium channels showing a topology of six transmembrane domains (see above) and a pore region with the typical signature sequence TxxTxGYGD (Heginbotham *et al.*, 1994) between the 5th and 6th segment. Extensive use of site-directed mutagenesis and the biophysical characterization of the resulting mutants expressed in oocytes identified this region as the permeation pathway for potassium ions. Accordingly, altered pharmacology and selectivity of the channel mutants could be correlated to an altered growth phenotype of complemented yeast cells (Anderson *et al.*, 1994; Uozumi *et al.*, 1995; Becker *et al.*, 1996; Ichida and Schroeder, 1996; Nakamura *et al.*, 1997; Dreyer *et al.*, 1998).

By exploiting both the microbial aspects and the genetic capabilities of the yeast system, elements of the GYG motif within the pore signature sequence of the K^+ channel KAT1 have been shown to play a key role in recognition of potassium and the ability of the channel to discriminate between ions (Nakamura *et al.*, 1997). It was possible to perform a combinatorial analysis in which all possible amino acid substitutions at the YG sites within this signature sequence were tested for function and for ion selectivity by expression of the mutant channels in yeast (and subsequently supported by independent analysis in *Xenopus* oocytes). The results of this study established specific roles for these sites and revealed structural constraints that could not have been discovered by other (non-combinatorial) strategies. For example, it was shown that only the wild-type YG and the conservative mutant FG channels are completely selective for K^+ over other ions. It was also learned that essentially any amino acid substitution at the site normally occupied by glycine abolishes channel function yet glycine substitution mutants can function if accompanied by compensatory mutations that decrease the size of the side chain at the adjacent site, normally occupied by tyrosine. Thus, the absolute requirement for glycine in an otherwise wild-type channel was concluded to arise from an intrinsic physical restraint on the channel pore. Evidently, the tyrosine side chain interferes with channel function if the amino acid beside it (normally G) contains a side chain of any size. Importantly, the basic structure–function features of the KAT1 pore gleaned from numerous studies involving heterologous expression in yeast (Anderson *et al.*, 1994; Uozumi *et al.*, 1995; Becker *et al.*, 1996; Nakamura *et al.*, 1997) are generally supported by the recently solved structure of the K^+ channel KcsA from *Streptomyces lividans* (Doyle *et al.*, 1998), underscoring the relevance, in this case, of data generated from a heterologous system.

Besides altering the ionic selectivity and pharmacological properties of the K^+ channel, mutations in the pore region can also affect the voltage-dependent activity (Becker *et al.*, 1996; G Lemaillet, unpublished data), indicating that this region is involved in the conformational changes during opening and closing. Plant K^+ uptake channels like KAT1 and KST1 open upon hyperpolarization, and close when the membrane is depolarized. This voltage-dependent activity (gating) is likely to be triggered by movement of the 4th transmembrane domain which displays a high density of positively charged amino acids (Cao *et al.*, 1995*a*; Dreyer *et al.*, 1997; Hoth *et al.*, 1997*a*; Marten and Hoshi, 1997, 1998; Zei and Aldrich, 1998). The gating machinery of plant K^+ channels is further modulated by both intracellular and extracellular protons (Hedrich *et al.*, 1995; Hoshi, 1995; Müller-Röber *et al.*, 1995). For the K^+ channel KST1, it has been shown that extracellular histidines are involved in a pH-sensing mechanism (Hoth *et al.*, 1997*b*). The deletion of all extracellular histidine residues removed the pH-effect on the steady-state activity of KST1. In contrast, a similar approach carried out on the closely related channel KAT1 did not influence its pH-sensitivity at all (Ichida and Schroeder, 1996), indicating that other amino acids besides histidine are involved in the pH-sensing mechanism.

Finally, further approaches, aimed at elucidating the structure–function relationships of plant K^+ channels, based on expression of green fluorescent protein (GFP)-tagged channels in the insect cell system and/or in the two-hybrid system, have revealed domains involved in channel clustering (Erhardt *et al.*, 1997) and/or channel tetramerization (Daram *et al.*, 1997). In the former approach, a yeast two-hybrid screen (Fields and Song, 1989; for a recent review see Niethammer and Sheng, 1998) using a C-terminal fragment of the potato guard cell K^+ channel KST1 as bait led to the identification of the two novel K^+ channel proteins SKT2 and SKT3. Interactions between the C-terminal fragment of KST1

and C-terminal fragments of SKT2 and SKT3 were independently confirmed by Western blot-related assays, utilizing K^+ channel C-termini fused to green fluorescent proteins. Analysis of fluorescence microscopy images of insect cells expressing GFP or a fusion of GFP to the complete KST1 polypeptide revealed formation of channel clusters within the cell membrane. In contrast, a fusion protein between GFP and KST1 deleted for the C-terminus region, the so-called K_{HA} domain (corresponding to about the last 80 amino acids) which is highly conserved among plant K^+ channels, clearly displayed an even, i.e. non-clustered, distribution of fluorescence along the plasma membrane. Additional electrophysiological studies showed that both fusion proteins displayed functional features similar to those of the wild-type channel. Taken as a whole, these data support the hypothesis that domain K_{HA} mediates channel protein interactions, leading to channel clustering, but is not essential to channel subunit tetramerization (see section on Biochemical characterization) and channel activity (Erhardt *et al.*, 1997). In the latter approach, the entire cytoplasmic C terminus (the 564 amino acids downstream of the 6th transmembrane segment) of *Arabidopsis* AKT1 channel was expressed in the baculovirus system and shown to form highly stable tetrameric structures, suggesting a role for this region in channel tetramerization (Chérel *et al.*, 1996; Daram *et al.*, 1997). Expressing various domains from this region as bait and prey in yeast two-hybrid tests revealed subsets of interactions, that could be involved in the tetramerization process as suggested by Daram *et al.* (1997) or in channel-protein interactions or clustering. It might be likely that interactions between C-termini of different channel subunits as revealed by Ehrhardt *et al.* (1997) between KST1 and SKT2 and SKT3 have a physiological significance. Co-expression of different wild type as well as mutant K^+ channel proteins has unveiled that plant potassium channels have the potential to form heteromultimeric structures composed of different of α-subunits (Dreyer *et al.*, 1997). Such phenomena, also reported for animal K^+ channels (for a review see Jan and Jan, 1997), could allow the cell to increase and control the functional diversity of the channels expressed on its membrane.

Problems with expression systems

The previous sections have demonstrated the powerful application of heterologous expression systems for the cloning and functional characterization of plant membrane transporters. Nevertheless, there are problems and risks involved in the utilization of the particular heterologous systems and these are now outlined. However, it is emphasized that the utility of an expression system should not be judged by the quantity of the statements below. It is obvious that the more a system is used and the more sophisticated the measurements are, the more is known about the limitations. *Xenopus* oocytes, for instance, represent the most documented system in this regard.

A simple example might point out one of the uncertainties in the use of the oocyte expression system. The determination of the single channel conductance of the plant K^+ channel KAT1 expressed in *Xenopus* oocytes led to partially inconsistent results (compare Schachtman *et al.*, 1992, with Cao *et al.*, 1995*b*; Hedrich *et al.*, 1995; Hoshi, 1995; Zei and Aldrich, 1998), raising the discussion as to whether the observed currents are caused by the heterologously expressed gene or originate from oocyte-intrinsic transporters (Methfessel *et al.*, 1986). Oocytes possess endogenous transport systems that influence their growth, maturation and fertilization. Thus it is important to be aware of endogenous currents that may already be present in the native oocyte, although the amplitude of most of the endogenous ionic conductances is highly variable among oocytes from different batches and frogs and it is not uncommon for several of the native currents to be absent altogether or to be present at only very low levels. A frequently used strategy to estimate the errors by intrinsic currents is to compare the electrical features of RNA-injected oocytes with those of oocytes from the same batch being untreated or injected with water or antisense RNA. However, this strategy does not provide absolute controls since it has been shown that expression of heterologous membrane proteins in *Xenopus* oocytes can induce endogenous currents (Tzounopoulos *et al.*, 1995). Thus it is possible that even non-functional transporters expressed in oocytes might induce significant currents which are not present in control cells. Therefore, not only the presence of a current but also, when possible, additional pharmacological characterizations may be required to prove unequivocally the functional expression of the heterologous protein.

The occurrence of intrinsic currents set another limit to the use of the oocyte system for the investigation of plant membrane transporters. On the one hand, the plant plasma membrane can be strongly polarized (< -200 mV) and its transporters can require strongly negative potentials for their activation or energetic coupling, while on the other hand, even in oocytes with low background currents, hyperpolarizing the membrane beyond -170 mV can result in activation of large endogenous negative currents possibly exceeding the magnitude of the current of the heterologously expressed transporter. Hence, the most trustworthy voltage range of an oocyte is limited from -170 mV to $+90$ mV. However, in special cases this limitation could partially be overcome by using appropriate voltage-pulses (Dreyer *et al.*, 1998). Finally, it must be noted that in several experiments aimed at characterizing new channels and carriers, functional expression was not observed. For example, the injection of certain channel cRNAs into

oocytes did not result in significant changes in the membrane conductance (Table 1; Cao *et al.*, 1995*b*, Gaymard *et al.*, 1996; Dreyer *et al.*, 1997; Kim *et al.*, 1998; Zimmermann *et al.*, 1998). The baculovirus–insect cell system has provided an alternative system for characterizing those plant K^+ channels, e.g. AKT1, whose expression in *Xenopus* oocytes fails to produce electrical signals (Gaymard *et al.*, 1996). The reasons why a channel or transporter is or is not expressed in a functional state according to the expression system used remain unknown.

Beyond providing an alternative for functional expression, the baculovirus insect cell system has another advantage compared to *Xenopus* oocytes. *Sf*9 or *Sf*21 cells are more directly amenable to patch-clamp studies, because they are not surrounded by a vitelline membrane that must be removed before electrodes can be attached. However, the insect cell system has its own inconveniences. The expression vectors, i.e. the recombinant baculovirus encoding for the gene of interest, are by comparison rather difficult to construct and to purify routinely. In addition, the usefulness of these expression vectors is essentially limited to *Sf*9 or *Sf*21 cells whereas vectors that function for heterologous expression in oocytes can also be used in cell types such as COS and Chinese hamster ovary cells (CHO cells) and thus offer complementary opportunities of investigation on the channel of interest. Furthermore, *Sf*9 cells die within only 1–3 d after infection, allowing fewer experimental possibilities compared to transfected oocytes, which can be used up to 1 week after injection of cRNA or DNA vectors. Besides these technical inconveniences the use of infected *Sf*9 or *Sf*21 cells for electrophysiological purposes is limited as well. Endogenous currents, which are less documented in the literature than those of oocytes but which occasionally resemble those of the transporters under investigation, can disturb the measurements (Cao *et al.* 1995*b*; Gaymard *et al.*, 1996; Marten *et al.*, 1996; Czempinski *et al.*, 1997; S Zimmermann, unpublished data). In addition, the cell membrane withstands poorly the large hyperpolarizations that may be required to study plant channels.

Problems regarding the use of mutant yeast strains for the identification and characterization of plant K^+ transporters have been stressed recently (Madrid *et al.*, 1998). The strains of *S. cerevisiae* used for these approaches contain null alleles of one or both of the high-affinity K^+ transporter genes, *TRK1* and *TRK2*. These mutations cause hyperpolarization of the membrane potential. In the case of the *trk1 trk2* double mutant, membrane hyperpolarization is extreme and can lead to artefacts in the estimation of the K_m values of K^+ carriers complementing the yeast mutant. Potentially more serious than this, *trk1 trk2* mutants show an ectopic low-affinity potassium uptake in which K^+ is accumulated through many proteins whose normal role is not that of K^+ transport. If the hyperpolarized membrane potential of these mutants can transform their own non-K^+ transporters into K^+ transporters, it is evident that the same may occur with some plant transporters. One example in this context might be the cloning of the low affinity cation transporter LCT1 (Schachtman *et al.*, 1997).

Physiological relevance of analyses in heterologous systems and perspectives

A reliable characterization of the functional and pharmacological features of a given transporter, leading to an unequivocal fingerprint, is a prerequisite towards the elucidation of its role *in planta*. Unfortunately, together with the problem mentioned regarding ectopic K^+ uptake in yeast *trk1 trk2* mutants, a wide set of observations advise that caution should be taken with the data obtained from heterologous systems. By way of illustration, several studies on potassium channels show that the results acquired from heterologous expression systems are ambiguous. Véry *et al.* (1994) and Cao *et al.* (1995*b*), for example, reported that changes in the expression level of the heterologous channel within the same expression system (*Xenopus* oocytes in these studies) can induce changes in both functional and pharmacological features of the channel. Moreover, comparisons of the features of the same K^+ channel expressed in various systems, yeast, insect cells or oocytes, unveiled further inconsistencies (Table 2). For instance, KAT1 showed a high permeability for NH_4^+ ions when expressed in oocytes, but was rather impermeant to this ion when expressed in yeast or insect cells (Schachtman *et al.*, 1992; Uozumi *et al.*, 1995; Bertl *et al.*, 1995; Marten *et al.*, 1996). By the same token, KST1 was 15-fold more sensitive to extracellular Cs^+ in insect cells than it was in oocytes (Zimmermann *et al.*, 1998).

Differences between features of transporters expressed in oocytes and those derived *in planta* for the native protein have also been reported. The two channels KAT1 and KST1 are believed to be the guard cell K^+ uptake channels of *Arabidopsis thaliana* and *Solanum tuberosum*, respectively (Müller-Röber *et al.*, 1995; Nakamura *et al.*, 1995). However, when expressed in *Xenopus* oocytes, these channels are less sensitive to Ca^{2+}, Cs^+, and H^+ than are the channels of the guard cells (Table 2; Brüggemann *et al.*, 1999). Similar findings were reported for the hexose carrier HUP1. The isolated protein in oocytes differs from the native transporters in *Chlorella* at least in its pH and voltage dependence (Tanner and Caspari, 1996). Such differences clearly indicate that (i) the functional features and the activity of a transporter not only depend on the right ligation of the amino acid chain but also on its correct folding and further transcriptional processes, and (ii) the expressed sequences do not form single proteins, isolated in a virtual membrane, but

Table 2. *Electrophysiological properties of the plant potassium channels KAT1 and KST1 in different expression systems*

Channel feature	Expression system			
	Xenopus oocytes	*Sf*9 cells	Yeast	*in situ* (guard cells)
Voltage-dependence, activation threshold	~ -80 mV	~ -60 mV	~ -120 mV	~ -100 mV
pH-dependence, maximum shift in $V_{\frac{1}{2}}$	$\sim$ 20 mV			$\sim$100 mV
Sensitivity to blocking ions				
TEA^+, Inhibition (10 mM)	$\sim$70%		$\sim$70%	
Cs^+, K_i at -130 mV	$\sim$1100 μM	$\sim$90 μM		
Cs^+, $V_{Block\frac{1}{2}}$ (1 mM Cs^+)	~ -155 mV			~ -90 mV
Ca^{2+}, $V_{Block\frac{1}{2}}$ (20 mM Ca^{2+})	< -250 mV			~ -190 mV
Permeability for NH_4^+	+	−	−	+

Data were obtained from KAT1, KST1, and potato and *Arabidopsis* guard cell K^+ uptake channels (Schachtman *et al.*, 1992; Bertl *et al.*, 1995; Müller-Röber *et al.*, 1995; Uozumi *et al.*, 1995; Véry *et al.*, 1995; Marten *et al.*, 1996; Dreyer *et al.*, 1997; Dietrich *et al.*, 1998; Zimmermann *et al.*, 1998; Brüggemann *et al.*, 1999).

rather pieces of a three-dimensional puzzle, interacting with other surrounding proteins present within the membrane, in the cytoskeleton or in the cytosol, in the heterologous host cell as well as in the original cell. One must be aware that such interactions within a heterologous host cell may result in distorted features. In addition, reconstitution in the heterologous host cell of the variety of interactions that normally occur in the original cell, by co-expression experiments, is probably beyond of our reach at the present time. Several reports regarding plant K^+ channels have highlighted the variety of interactions that could occur *in planta*, by providing evidence for the existence of mechanisms such as interactions between various α-subunits leading to heteromultimeric channels (Dreyer *et al.*, 1997), interactions with β-subunits (Tang *et al.*, 1996; Fang *et al.*, 1998), channel clustering (Ehrhardt *et al.*, 1997), and channel activity probably tuned by phosphorylation and dephosphorylation events (Li *et al.*, 1998). From what is known for animal K^+ channels, regulatory mechanisms involving, for example, interactions with intracellular compounds that reduce or oxidize cysteine and methionine residues (Ruppersberg *et al.*, 1991; Ciorba *et al.*, 1997), phospholipids (Honoré *et al.*, 1994; Baukrowitz *et al.*, 1998; Shyng and Nichols, 1998) or *N*-glycosylation events (Schwalbe *et al.*, 1995) are also likely.

To circumvent misunderstandings that might arise from the investigation of plant transporters only within a heterologous expression system, recent studies have allowed cloned transporters to journey back to their roots (and leaves). Homologous expression in guard cells, mesophyll cells, and suspension culture cells (Ichida *et al.*, 1997; Bei and Luan, 1998; Kim *et al.*, 1998) allowed electrophysiological analyses and radiotracer flux measurements in a cell environment closely related to that of the native cell of the cloned transporter. To elaborate aspects of the physiological roles of plant transporter molecules further, it is likely that the establishment of homologous expression systems, in combination with the development of reverse genetic approaches, allowing comparison of the transport features in the wild-type plant and in a knock out mutant (Gaymard *et al.*, 1998; Hirsch *et al.*, 1998), is now inescapable.

Acknowledgement

We are grateful to Rick Aldrich, Stanford, for providing us with a manuscript before publication.

References

Anderson JA, Huprikar SS, Kochian LV, Lucas WJ, Gaber RF. 1992. Functional expression of a probable *Arabidopsis thaliana* potassium channel in *Saccharomyces cerevisiae*. *Proceedings of the National Academy of Sciences, USA* **89,** 3736–3740.

Anderson JA, Nakamura RL, Gaber RF. 1994. Heterologous expression of K^+ channels in *Saccharomyces cerevisiae*: strategies for molecular analysis of structure and function. *Symposium of the Society for Experimental Biology* **48,** 85–97.

Aoshima H, Yamada M, Sauer N, Komor E, Schobert C. 1993. Heterologous expression of the H^+/hexose cotransporter from *Chlorella* in *Xenopus* oocytes and its characterization with respect to sugar specificity, pH and membrane potential. *Journal of Plant Physiology* **141,** 293–297.

Baukrowitz T, Schulte U, Oliver D, Herlitze S, Krauter T, Tucker SJ, Ruppersberg JP, Fakler B. 1998. PIP_2 and PIP as determinants for ATP inhibition of K_{ATP} channels. *Science* 282, 1141–1144.

Becker D, Dreyer I, Hoth S, Reid JD, Busch H, Lehnen M, Palme K, Hedrich R. 1996. Changes in voltage activation, Cs^+ sensitivity, and ion permeability in H5 mutants of the plant K^+ channel KAT1. *Proceedings of the National Academy of Sciences, USA* **93,** 8123–8128.

Bei Q, Luan S. 1998. Functional expression and characterization of a plant K^+ channel gene in a plant cell model. *The Plant Journal* **13,** 857–865.

Bertl A, Anderson JA, Slayman CL, Sentenac H, Gaber RF. 1994. Inward and outward rectifying potassium currents in *Saccharomyces cerevisiae* mediated by endogenous and heterologously expressed ion channels. *Folia Microbiologia (Praha)* **39,** 507–509.

Bertl A, Anderson JA, Slayman CL, Gaber RF. 1995. Use of

Saccharomyces cerevisiae for patch-clamp analysis of heterologous membrane proteins: characterization of Kat1, an inward-rectifying K^+ channel from *Arabidopsis thaliana*, and comparison with endogeneous yeast channels and carriers. *Proceedings of the National Academy of Sciences, USA* **92,** 2701–2705.

Bertl A, Reid JD, Sentenac H, Slayman CL. 1997. Functional expression of plant inward-rectifier channels expressed in yeast. *Journal of Experimental Botany* **48,** 405–413.

Boorer KJ, Forde BG, Leigh RA, Miller AJ. 1992. Functional expression of a plant plasma membrane transporter in *Xenopus* oocytes. *FEBS Letters* **302,** 166–168.

Boorer KJ, Frommer WB, Bush DR, Kreman M, Loo DD, Wright EM. 1996*a*. Kinetics and specificity of a H^+/amino acid transporter from *Arabidopsis thaliana*. *Journal of Biological Chemistry* **271,** 2213–2220.

Boorer KJ, Loo DDF, Frommer WB, Wright EM. 1996*b*. Transport mechanism of the cloned potato H^+/sucrose cotransporter StSUT1. *Journal of Biological Chemistry* **271,** 25139–25144.

Boorer KJ, Fischer WN. 1997. Specificity and stoichiometry of the *Arabidopsis* H^+/amino acid transporter AAP5. *Journal of Biological Chemistry* **272,** 13040–13046.

Boutry M, Baudouin M, Goffeau A. 1989. Molecular cloning of a family of plant genes encoding a protein homologous to plasma membrane H^+-translocating ATPases. *Biochemical and Biophysical Research Communications* **162,** 567–574.

Brüggemann L, Dietrich P, Dreyer I, Hedrich R. 1999. Pronounced differences between the native K^+ channels and KAT1 and KST1 alpha-subunit homomers of guard cells. *Planta* **207,** 370–376.

Bush DR. 1993*a*. Proton-coupled sugar and amino acid transporters in plants. *Annual Review of Plant Physiology and Plant Molecular Biology* **44,** 513–542.

Bush DR. 1993*b*. Inhibitors of the proton-sucrose symport. *Archives of Biochemistry and Biophysics* **307,** 355–360.

Cao Y, Anderova M, Crawford NM, Schroeder JI. 1992. Expression of an outward-rectifying potassium channel from maize mRNA and complementary RNA in *Xenopus* oocytes. *The Plant Cell* **4,** 961–969.

Cao Y, Crawford NM, Schroeder JI. 1995*a*. Amino terminus and the first four membrane-spanning segments of the *Arabidopsis* K^+ channel KAT1 confer inward-rectification property of plant-animal chimeric channels. *Journal of Biological Chemistry* **270,** 17697–17701.

Cao Y, Ward JM, Kelly WB, Ichida AM, Gaber RF, Anderson JA, Uozumi N, Schroeder JI, Crawford NM. 1995*b*. Multiple genes, tissue specificity, and expression-dependent modulation contribute to the functional diversity of potassium channels in *Arabidopsis thaliana*. *Plant Physiology* **109,** 1093–1106.

Caspari T, Stadler R, Sauer N, Tanner W. 1994. Structure/function relationship of the *Chlorella* glucose/H^+ symporter. *Journal of Biological Chemistry* **269,** 3498–3502.

Chang A, Slayman CW. 1991. Maturation of the yeast plasma membrane H^+-ATPase involves phosphorylation during intracellular transport. *Journal of Cell Biology* **115,** 289–295.

Chang HC, Bush DR. 1997. Topology of NAT2, a prototypical example of a new family of amino acid transporters. *Journal of Biological Chemistry* **272,** 30552–30557.

Chérel I, Daram P, Gaymard F, Horeau C, Thibaud JB, Sentenac H. 1996. Plant K^+ channels: structure, activity and function. *Biochemical Society Transactions* **24,** 964–971.

Ciorba MA, Heinemann SH, Weissbach H, Brot N, Hoshi T. 1997. Modulation of potassium channel function by methionine oxidation and reduction. *Proceedings of the National Academy of Sciences, USA* **94,** 9932–9937.

Clemens S, Antosiewicz DM, Ward JM, Schachtman DP, Schroeder JI. 1998. The plant cDNA LCT1 mediates the uptake of calcium and cadmium in yeast. *Proceedings of the National Academy of Sciences, USA* **95,** 12043–12048.

Crestfield AM, Stein WH, Moore S. 1963. Alkylation and identification of the histidine residues at the active site of ribonuclease. *Journal of Biological Chemistry* **238,** 2413–2419.

Czempinski K, Zimmermann S, Ehrhardt T, Müller-Röber B. 1997. New structure and function in plant K^+ channels: KCO1, an outward rectifier with a steep Ca^{2+} dependency. *EMBO Journal* **16,** 2565–2575.

Daniels MJ, Mirkov TE, Chrispeels MJ. 1994. The plasma membrane of *Arabidopsis thaliana* contains a mercury-insensitive aquaporin that is a homolog of the tonoplast water channel protein TIP. *Plant Physiology* **106,** 1325–1333.

Daniels MJ, Chaumont F, Mirkov TE, Chrispeels MJ. 1996. Characterization of a new vacuolar membrane aquaporin sensitive to mercury at a unique site. *The Plant Cell* **8,** 587–599.

Daram P, Urbach S, Gaymard F, Sentenac H, Cherel I. 1997. Tetramerization of the AKT1 plant potassium channel involves its C-terminal cytoplasmic domain. *EMBO Journal* **16,** 3455–3463.

Diatloff E, Kumar R, Schachtman DP. 1998. Site-directed mutagenesis reduces the Na^+ affinity of HKT1, an Na^+ energized high affinity K^+ transporter. *FEBS Letters* **432,** 31–36.

Dietrich P, Dreyer I, Wiesner P, Hedrich R. 1998. Cation sensitivity and kinetics of guard-cell potassium channels differ among species. *Planta* **205,** 277–287.

Doyle DA, Cabral JM, Pfuetzner RA, Kuo A, Gulbis JM, Cohen SL, Chait BT, MacKinnon R. 1998. The structure of the potassium channel: molecular basis of K^+ conduction and selectivity. *Science* **280,** 69–77.

Dreyer I, Antunes S, Hoshi T, Muller-Rober B, Palme K, Pongs O, Reintanz B, Hedrich R. 1997. Plant K^+ channel alpha-subunits assemble indiscriminately. *Biophysical Journal* **72,** 2143–2150.

Dreyer I, Becker D, Bregante M, Gambale F, Lehnen M, Palme K, Hedrich R. 1998. Single mutations strongly alter the K^+-selective pore of the K_{in} channel KAT1. *FEBS Letters* **430,** 370–376.

Durell SR, Hao Y, Guy HR. 1998. Structural models of the transmembrane region of voltage-gated and other K^+ channels in open, closed, and inactivated conformations. *Journal of Structural Biology* **121,** 263–284.

Eide D, Broderius M, Fett J, Guerinot ML. 1996. A novel iron-regulated metal transporter from plants identified by functional expression in yeast. *Proceedings of the National Academy of Sciences, USA* **93,** 5624–5628.

Ehrhardt T, Zimmermann S, Müller-Röber B. 1997. Association of plant K channels is mediated by conserved C-termini and does not affect subunit assembly. *FEBS Letters* **409,** 166–170.

Eng BH, Guerinot ML, Eide D, Saier Jr MH. 1998. Sequence analyses and phylogenetic characterization of the ZIP family of metal ion transport proteins. *Journal of Membrane Biology* **166,** 1–7.

Fang Z, Kamasani U, Berkowitz GA. 1998. Molecular cloning and expression characterization of a rice K^+ channel beta subunit. *Plant Molecular Biology* **37,** 597–606.

Fields S, Song O. 1989. A novel genetic system to detect protein-protein interactions. *Nature* **340,** 245–246.

Fox TC, Guerinot ML. 1998. Molecular biology of cation transport in plants. *Annual Reviews of Plant Physiology and Plant Molecular Biology* **49,** 669–696.

Frommer WB, Hummel S, Riesmeier JW. 1993. Expression

cloning in yeast of a cDNA encoding a broad specificity amino acid permease from *Arabidopsis thaliana*. *Proceedings of the National Academy of Sciences, USA* **90,** 5944–5948.

Frommer WB, Ninnemann O. 1995. Heterologous expression of genes in bacteria, fungal, animal, and plant cells. *Annual Review of Plant Physiology and Plant Molecular Biology* **46,** 419–444.

Fu HH, Luan S. 1998. AtKuP1: a dual-affinity K^+ transporter from *Arabidopsis*. *The Plant Cell* **10,** 63–73.

Gaymard F, Cerutti M, Horeau C, Lemaillet G, Urbach S, Ravallec M, Devauchelle G, Sentenac H, Thibaud JB. 1996. The baculovirus/insect cell system as an alternative to *Xenopus* oocytes. First characterization of the AKT1 K^+ channel from *Arabidopsis thaliana*. *Journal of Biological Chemistry* **271,** 22863–22870.

Gaymard F, Pilot G, Lacombe B, Bouchez D, Bruneau D, Boucherez J, Michaux-Ferriere N, Thibaud JB, Sentenac H. 1998. Identification and disruption of a plant *shaker*-like outward channel involved in K^+ release into the xylem sap. *Cell* **94,** 647–655.

Gluzman Y. 1981. SV40-transformed simian cells support the replication of early SV40 mutants. *Cell* **23,** 175–182.

Grotz N, Fox T, Connolly E, Park W, Guerinot ML, Eide D. 1998. Identification of a family of zinc transporter genes from *Arabidopsis* that respond to zinc deficiency. *Proceedings of the National Academy of Sciences, USA* **95,** 7220–7224.

Gurdon JB, Lane CD, Woodland HR, Marbaix G. 1971. Use of frog eggs and oocytes for the study of messenger RNA and its translation in living cells. *Nature* **233,** 177–182.

Harper JF, Surowy TK, Sussman MR. 1989. Molecular cloning and sequence of cDNA encoding the plasma membrane proton pump (H^+-ATPase) of *Arabidopsis thaliana*. *Proceedings of the National Academy of Sciences, USA* **86,** 1234–1238.

Hechenberger M, Schwappach B, Fischer WN, Frommer WB, Jentsch TJ, Steinmeyer K. 1996. A family of putative chloride channels from *Arabidopsis* and functional complementation of a yeast strain with a CLC gene disruption. *Journal of Biological Chemistry* **271,** 33632–33638.

Hedrich R, Schroeder JI. 1989. The physiology of ion channels and electrogenic pumps in higher plants. *Annual Review of Plant Physiology and Plant Molecular Biology* **40,** 539–569.

Hedrich R, Moran O, Conti F, Busch H, Becker D, Gambale F, Dreyer I, Kuch A, Neuwinger K, Palme K. 1995. Inward rectifier potassium channels in plants differ from their animal counterparts in response to voltage and channel modulators. *European Biophysics Journal* **24,** 107–115.

Heginbotham L, Lu Z, Abramson T, MacKinnon R. 1994. Mutations in the K^+ channel signature sequence. *Biophysical Journal* **66,** 1061–1067.

Hirsch RE, Lewis BD, Spalding EP, Sussmann MR. 1998. A role for the AKT1 potassium channel in plant nutrition. *Science* **280,** 918–921.

Hirschi KD, Zhen RG, Cunningham KW, Rea PA, Fink GR. 1996. CAX1, an H^+/Ca^{2+} antiporter from *Arabidopsis*. *Proceedings of the National Academy of Sciences, USA* **93,** 8782–8786.

Honoré E, Barhanin J, Attali B, Lesage F, Lazdunski M. 1994. External blockade of the major cardiac delayed-rectifier K^+ channel (Kv1.5) by polyunsaturated fatty acids. *Proceedings of the National Academy of Sciences, USA* **91,** 1937–1941.

Hoshi T. 1995. Regulation of voltage dependence of the KAT1 channel by intracellular factors. *Journal of General Physiology* **105,** 309–328.

Hoth S, Dreyer I, Dietrich P, Becker D, Muller-Rober B, Hedrich R. 1997*a*. Molecular basis of plant-specific acid activation of K^+ uptake channels. *Proceedings of the National Academy of Sciences, USA* **94,** 4806–4810.

Hoth S, Dreyer I, Hedrich R. 1997*b*. Mutational analysis of functional domains within plant K^+ uptake channels. *Journal of Experimental Botany* **48,** 415–420.

Hsu LC, Chiou TJ, Chen L, Bush DR. 1993. Cloning a plant amino acid transporter by functional complementation of a yeast amino acid transport mutant. *Proceedings of the National Academy of Sciences, USA* **90,** 7441–7445.

Ichida AM, Schroeder JI. 1996. Increased resistance to extracellular cation block by mutation of the pore domain of the *Arabidopsis* inward-rectifying K^+ channel KAT1. *Journal of Membrane Biology* **151,** 53–62.

Ichida AM, Pei ZM, Baizabal-Aguirre VM, Turner KJ, Schroeder JI. 1997. Expression of a Cs^+-resistant guard cell K^+ channel confers Cs^+-resistant, light-induced stomatal opening in transgenic *Arabidopsis*. *The Plant Cell* **9,** 1843–1857.

Jan LY, Jan YN. 1997. Cloned potassium channels from eukaryotes and prokaryotes. *Annual Review of Neuroscience* **20,** 91–123.

Jentsch TJ, Steinmeyer K, Schwarz G. 1990. Primary structure of *Torpedo marmorata* chloride channel isolated by expression cloning in *Xenopus* oocytes. *Nature* **348,** 510–514.

Johansson I, Karlsson M, Shukla VK, Chrispeels MJ, Larsson C, Kjellbom P. 1998. Water transport activity of the plasma membrane aquaporin PM28A is regulated by phosphorylation. *The Plant Cell* **10,** 451–459.

Kamb A, Iverson LE, Tanouye MA. 1987. Molecular characterization of *Shaker*, a *Drosophila* gene that encodes a potassium channel. *Cell* **50,** 405–413.

Kammerloher W, Fischer U, Piechottka GP, Schaffner AR. 1994. Water channels in the plant plasma membrane cloned by immunoselection from a mammalian expression system. *The Plant Journal* **6,** 187–199.

Kampfenkel K, Kushnir S, Babiychuk E, Inze D, Van Montagu M. 1995. Molecular characterization of a putative *Arabidopsis thaliana* copper transporter and its yeast homologue. *Journal of Biological Chemistry* **270,** 28479–28486.

Ketchum KA, Slayman CW. 1996. Isolation of an ion channel gene from *Arabidopsis thaliana* using the H5 signature sequence from voltage-dependent K^+ channels. *FEBS Letters* **378,** 19–26.

Kim EJ, Kwak JM, Uozumi N, Schroeder JI. 1998. *AtKUP1*: an *Arabidopsis* gene encoding high-affinity potassium transport activity. *The Plant Cell* **10,** 51–62.

Ko CH, Gaber RF. 1991. *TRK1* and *TRK2* encode structurally related K^+ transporters in *Saccharomyces cerevisiae*. *Molecular and Cellular Biology* **11,** 4266–4273.

Kochian LV, Garvin DF, Shaff JE, Chilcott TC, Lucas WJ. 1993. Towards an understanding of the molecular basis of plants K^+ transport: characterization of cloned K^+ transport cDNAs. *Plant and Soil* **155/156,** 115–118.

Köhler C, Neuhaus G. 1998. Cloning and partial characterization of two putative cyclic nucleotide-regulated ion channels from *Arabidopsis thaliana*, designated CNGC1 and CNGC2. *Plant Physiology* **116,** 1604.

Kristoffersen P, Teichmann T, Stracke R, Palme K. 1996. Signal sequence trap to clone cDNAs encoding secreted or membrane-associated plant proteins. *Analytical Biochemistry* **243,** 127–132.

Kühlbrandt W, Wang DN. 1991. Three-dimensional structure of plant light-harvesting complex determined by electron crystallography. *Nature* **350,** 130–134.

Kwart M, Hirner B, Hummel S, Frommer WB. 1993. Differential expression of two related amino acid transporters with

differing substrate specificity in *Arabidopsis thaliana*. *The Plant Journal* **4,** 993–1002.

Lacombe B, Thibaud JB. 1998. Evidence for a multi-ion pore behavior in the plant potassium channel KAT1. *Journal of Membrane Biology* **166,** 91–100.

Lam HM, Chiu J, Hsieh MH, Meisel L, Oliveira IC, Shin M, Coruzzi G. 1998. Glutamate-receptor genes in plants. *Nature* 396, 125–126.

Lesage F, Hugnot JP, Amri EZ, Grimaldi P, Barhanin J, Lazdunski M. 1994. Expression cloning in K^+ transport defective yeast and distribution of HBP1, a new putative HMG transcriptional regulator. *Nucleic Acids Research* **22,** 3685–3688.

Li J, Lee YR, Assmann SM. 1998. Guard cells possess a calcium-dependent protein kinase that phosphorylates the KAT1 potassium channel. *Plant Physiology* **116,** 785–795.

Logan H, Basset M, Véry AA, Sentenac H. 1997. Plasma membrane transport systems in higher plants: from black boxes to molecular physiology. *Physiologia Plantarum* **100,** 1–15.

Lu JM, Bush DR. 1998. His-65 in the proton-sucrose symporter is an essential amino acid whose modification with site-directed mutagenesis increases transport activity. *Proceedings of the National Academy of Sciences, USA* **95,** 9025–9030.

Lurin C, Geelen D, Barbier-Brygoo H, Guern J, Maurel C. 1996. Cloning and functional expression of a plant voltage-dependent chloride channel. *The Plant Cell* **8,** 701–711.

Madrid R, Gomez MJ, Ramos J, Rodriguez-Navarro A. 1998. Ectopic potassium uptake in *trk1 trk2* mutants of *Saccharomyces cerevisiae* correlates with a highly hyperpolarized membrane potential. *Journal of Biological Chemistry* **273,** 14838–14844.

Manoil C, Beckwith J. 1986. A genetic approach to analysing membrane protein topology. *Science* **233,** 1403–1408.

Marten I, Gaymard F, Lemaillet G, Thibaud JB, Sentenac H, Hedrich R. 1996. Functional expression of the plant K^+ channel KAT1 in insect cells. *FEBS Letters* **380,** 229–232.

Marten I, Hoshi T. 1997. Voltage-dependent gating characteristics of the K^+ channel KAT1 depend on the N and C termini. *Proceedings of the National Academy of Sciences, USA* **94,** 3448–3453.

Marten I, Hoshi T. 1998. The N-terminus of the K channel KAT1 controls its voltage-dependent gating by altering the membrane electric field. *Biophysical Journal* **74,** 2953–2962.

Maurel C, Reizer J, Schroeder JI, Chrispeels MJ. 1993. The vacuolar membrane protein gamma-TIP creates water specific channels in *Xenopus* oocytes. *EMBO Journal* **12,** 2241–2247.

Maurel C, Kado RT, Guern J, Chrispeels MJ. 1995. Phosphorylation regulates the water channel activity of the seed-specific aquaporin alpha-TIP. *EMBO Journal* **14,** 3028–3035.

Maurel C. 1997. Aquaporins and water permeability of plant membranes. *Annual Review of Plant Physiology and Plant Molecular Biology* **48,** 399–429.

McCarroll L, King LA. 1997. Stable insect cell cultures for recombinant protein production. *Current Opinion in Biotechnology* **8,** 590–594.

Methfessel C, Witzemann V, Takahashi T, Mishina M, Numa S, Sakmann B. 1986. Patch clamp measurements on *Xenopus laevis* oocytes: currents through endogenous channels and implanted acetylcholine receptor and sodium channels. *Pflugers Archiv European Journal of Physiology* **407,** 577–588.

Moroni A, Bardella L, Thiel G. 1998. The impermeant ion methylammonium blocks K^+ and NH_4^+ currents through KAT1 channel differently: evidence for ion interaction in channel permeation. *Journal of Membrane Biology* **163,** 25–35.

Muchhal US, Pardo JM, Raghothama KG. 1996. Phosphate transporters from the higher plant *Arabidopsis thaliana*. *Proceedings of the National Academy of Sciences, USA* **93,** 10519–10523.

Müller-Röber B, Ellenberg J, Provart N, Willmitzer L, Busch H, Becker D, Dietrich P, Hoth S, Hedrich R. 1995. Cloning and electrophysiological analysis of KST1, an inward rectifying K^+ channel expressed in potato guard cells. *EMBO Journal* **14,** 2409–2416.

Nakamura RL, McKendree Jr WL, Hirsch RE, Sedbrook JC, Gaber RF, Sussman MR. 1995. Expression of an *Arabidopsis* potassium channel gene in guard cells. *Plant Physiology* **109,** 371–374.

Nakamura RL, Anderson JA, Gaber RF. 1997. Determination of key structural requirements of a K^+ channel pore. *Journal of Biological Chemistry* **272,** 1011–1018.

Niethammer M, Sheng M. 1998. Identification of ion channel-associated proteins using yeast two-hybrid system. *Methods in Enzymology* **293,** 104–122.

Ninnemann O, Jauniaux JC, Frommer WB. 1994. Identification of a high affinity NH_4^+ transporter from plants. *EMBO Journal* **13,** 3464–3471.

Palmgren MG, Christensen G. 1994. Functional comparisons between plant plasma membrane H^+-ATPase isoforms expressed in yeast. *Journal of Biological Chemistry* **269,** 3027–3033.

Pardo JM, Serrano R. 1989. Structure of a plasma membrane H^+-ATPase from the plant *Arabidopsis thaliana*. *Journal of Biological Chemistry* **264,** 8557–8562.

Possee RD. 1997. Baculoviruses as expression vectors. *Current Opinion in Biotechnology* **8,** 569–572.

Quintero FJ, Blatt MR. 1997. A new family of K^+ transporters from *Arabidopsis* that are conserved across phyla. *FEBS Letters* **415,** 206–211.

Ramos J, Contreras P, Rodriguez-Navarro A. 1985. A potassium transport mutant of *Saccharomyces cerevisiae*. *Archives of Microbiology* **143,** 88–93.

Regenberg B, Villalba JM, Lanfermeijer FC, Palmgren MG. 1995. C-terminal deletion analysis of plant plasma membrane H^+-ATPase: yeast as a model system for solute transport across the plant plasma membrane. *The Plant Cell* **7,** 1655–1666.

Rentsch D, Boorer KJ, Frommer W. 1997. Structure and function of plasma membrane amino acid, oligopeptide and sucrose transporters from higher plants. *Journal of Membrane Biology* **162,** 177–190.

Riesmeier JW, Willmitzer L, Frommer WB. 1992. Isolation and characterization of a sucrose carrier cDNA from spinach by functional expression in yeast. *EMBO Journal* **11,** 4705–4713.

Riesmeier JW, Hirner B, Frommer WB. 1993. Potato sucrose transporter expression in minor veins indicates a role in phloem loading. *The Plant Cell* **5,** 1591–1598.

Ros R, Lemaillet G, Fonrouge AG, Daram P, Enjuto M, Salmon JM, Thibaud JB, Sentenac H. 1999. Molecular determinants of the *Arabidopsis* AKT1 K^+ channel ionic selectivity investigated by expression in yeast of randomly mutated channels. *Physiologia Plantarum* **105,** 459–468.

Rubio F, Gassmann W, Schroeder JI. 1995. Sodium-driven potassium uptake by the plant potassium transporter HKT1 and mutations conferring salt tolerance. *Science* **270,** 1660–1663.

Ruppersberg JP, Stocker M, Pongs O, Heinemann SH, Frank R, Koenen M. 1991. Regulation of fast inactivation of cloned mammalian IK(A) channels by cysteine oxidation. *Nature* **352,** 711–714.

Santa-Maria GE, Rubio F, Dubcovsky J, Rodriguez-Navarro A.

1997. The *HAK1* gene of barley is a member of a large gene family and encodes a high-affinity potassium transporter. *The Plant Cell* **9,** 2281–2289.

Sauer N, Tanner W. 1989. The hexose carrier from *Chlorella*. cDNA cloning of a eukaryotic H^+-cotransporter. *FEBS Letters* **259,** 43–46.

Sauer N, Caspari T, Klebl F, Tanner W. 1990. Functional expression of the *Chlorella* hexose transporter in *Schizosaccharomyces pombe*. *Proceedings of the National Academy of Sciences, USA* **87,** 7949–7952.

Schachtman DP, Schroeder JI, Lucas WJ, Anderson JA, Gaber RF. 1992. Expression of an inward-rectifying potassium channel by the *Arabidopsis* KAT1 cDNA. *Science* **258,** 1654–1658.

Schachtman DP, Schroeder JI. 1994. Structure and transport mechanism of a high-affinity potassium uptake transporter from higher plants. *Nature* **370,** 655–658.

Schachtman DP, Kumar R, Schroeder JI, Marsh EL. 1997. Molecular and functional characterization of a novel low-affinity cation transporter (LCT1) in higher plants. *Proceedings of the National Academy of Sciences, USA* **94,** 11079–11084.

Schroeder JI. 1994. Heterologous expression and functional analysis of higher plant transport proteins in *Xenopus* oocytes. *Methods* **6,** 70–81.

Schuurink RC, Shartzer SF, Fath A, Jones RL. 1998. Characterization of a calmodulin-binding transporter from the plasma membrane of barley aleurone. *Proceedings of the National Academy of Sciences, USA* **95,** 1944–1949.

Schwalbe RA, Wang Z, Wible BA, Brown AM. 1995. Potassium channel structure and function as reported by a single glycosylation sequon. *Journal of Biological Chemistry* **270,** 15336–15340.

Sentenac H, Bonneaud N, Minet M, Lacroute F, Salmon JM, Gaymard F, Grignon C. 1992. Cloning and expression in yeast of a plant potassium ion transport system. *Science* **256,** 663–665.

Shi J, Dixon RA, Gonzales RA, Kjellbom P, Bhattacharyya MK. 1995. Identification of cDNA clones encoding valosin-containing protein and other plant plasma membrane-associated proteins by a general immunoscreening strategy. *Proceedings of the National Academy of Sciences, USA* **92,** 4457–4461.

Shyng SL, Nichols CG. 1998. Membrane phospholipid control of nucleotide sensitivity of K_{ATP} channels. *Science* **282,** 1138–1141.

Smith FW, Ealing PM, Hawkesford MJ, Clarkson DT. 1995. Plant members of a family of sulphate transporters reveal functional subtypes. *Proceedings of the National Academy of Sciences, USA* **92,** 9373–9377.

Steiner HY, Song W, Zhang L, Naider F, Becker JM, Stacey G. 1994. An *Arabidopsis* peptide transporter is a member of a new class of membrane transport proteins. *The Plant Cell* **6,** 1289–1299.

Sussman MR. 1994. Molecular analysis of proteins in the plant plasma membrane. *Annual Review of Plant Physiology and Plant Molecular Biology* **45,** 211–234.

Tang H, Vasconcelos AC, Berkowitz GA. 1996. Physical association of KAB1 with plant K^+ channel alpha subunits. *The Plant Cell* **8,** 1545–1553.

Tanner W, Caspari T. 1996. Membrane transport carriers. *Annual Review of Plant Physiology and Plant Molecular Biology* **47,** 595–626.

Theodoulou FL, Miller AJ. 1995. *Xenopus* oocytes as a heterologous expression system for plant proteins. *Molecular Biotechnology* **3,** 101–115.

Tsay YF, Schroeder JI, Feldmann KA, Crawford NM. 1993. The herbicide sensitivity gene *CHL1* of *Arabidopsis* encodes a nitrate-inducible nitrate transporter. *Cell* **72,** 705–713.

Tyerman SD, Schachtman DP. 1992. The role of ion channels in plant nutrition and prospects for their genetic manipulation. *Plant and Soil* **146,** 137–144.

Tzounopoulos T, Maylie J, Adelman JP. 1995. Induction of endogenous channels by high levels of heterologous membrane proteins in *Xenopus* oocytes. *Biophysical Journal* **69,** 904–908.

Uozumi N, Gassmann W, Cao Y, Schroeder JI. 1995. Identification of strong modifications in cation selectivity in an *Arabidopsis* inward rectifying potassium channel by mutant selection in yeast. *Journal of Biological Chemistry* **270,** 24276–24281.

Uozumi N, Nakamura T, Schroeder JI, Muto S. 1998. Determination of transmembrane topology of an inward-rectifying potassium channel from *Arabidopsis thaliana* based on functional expression in *Escherichia coli*. *Proceedings of the National Academy of Sciences, USA* **95,** 9773–9778.

Véry AA, Bosseux C, Gaymard F, Sentenac H, Thibaud JB. 1994. Level of expression in *Xenopus* oocytes affects some characteristics of a plant inward-rectifying voltage-gated K^+ channel. *Pflügers Archive* **428,** 422–424.

Véry AA, Gaymard F, Bosseux C, Sentenac H, Thibaud JB. 1995. Expression of a cloned plant K^+ channel in *Xenopus* oocytes: analysis of macroscopic currents. *The Plant Journal* **7,** 321–332.

Villalba JM, Palmgren MG, Berberian GE, Ferguson C, Serrano R. 1992. Functional expression of plant plasma membrane H^+-ATPase in yeast endoplasmic reticulum. *Journal of Biological Chemistry* **267,** 12341–12349.

Westhead EW. 1965. Photooxidation with rose bengal of a critical histidine residue in yeast enolase. *Biochemistry* **4,** 2139–2144.

Will A, Caspari T, Tanner W. 1994. K_m mutants of the *Chlorella* monosaccharide/H^+ cotransporter randomly generated by PCR. *Proceedings of the National Academy of Sciences, USA* **91,** 10163–10167.

Will A, Tanner W. 1996. Importance of the first external loop for substrate recognition as revealed by chimeric *Chlorella* monosaccharide/H^+ symporters. *FEBS Letters* **381,** 127–130.

Will A, Grassl R, Erdmenger J, Caspari T, Tanner W. 1998. Alteration of substrate affinities and specificities of the *Chlorella* hexose/H^+ symporters by mutations and construction of chimeras. *Journal of Biological Chemistry* **273,** 11456–11462.

Zei PC, Aldrich RW. 1998. Voltage-dependent gating of single wild-type and S4 mutant KAT1 inward rectifier potassium channels. *Journal of General Physiology* **112,** 679–713.

Zeilinger C. 1994. Isolation of a potassium-selective ion channel from the plasma membrane of the broad bean *Vicia faba* L. *FEBS Letters* **348,** 278–282.

Zimmermann S, Talke I, Ehrhardt T, Nast G, Müller-Röber B. 1998. Characterization of SKT1, an inwardly rectifying potassium channel from potato, by heterologous expression in insect cells. *Plant Physiology* **116,** 879–890.

⇒ zurück zur Übersicht

2002

Dreyer, Mueller-Roeber, Köhler

New challenges in plant ion transport research: from molecules to phenomena.

In: *Recent Research Developments in Molecular & Cellular Biology.*
Research Signpost, Kerala, India. **3**:379-395.

Research Signpost
37/661 (2), Fort P.O., Trivandrum-695 023, Kerala, India

Recent Res. Devel. Mol. Cell. Biol., 3(2002): 379-395 ISBN: 81-7736-148-1

New challenges in plant ion transport research: From molecules to phenomena

Ingo Dreyer, Bernd Mueller-Roeber and Barbara Köhler
Universität Potsdam, Institut für Biologie und Biochemie, Abteilung Molekularbiologie, Karl-Liebknecht-Strasse 24-25, Haus 20, D-14476 Golm/Potsdam, Germany

Abstract

Ion transporters are membrane spanning proteins, which mediate transport of minerals through membranes. They are often selective for one compound and their activities are tightly regulated. Therefore, fluxes through membranes, which are virtually impermeable for most compounds, can be controlled. The selective movement and redistribution of ions is essential for plant growth and cellular homeostasis like turgor generation, nutrient acquisition, and signal transduction. A large number of different transporters have been identified both in vivo and at the molecular level. Arabidopsis thaliana is a model organism for plant research. Due to the efforts of the Arabidopsis Genome Initiative (AGI) the genomic sequences of all five chromosomes are publicly available since the end of year 2000. On the basis of these data, analysis of the expression and function of the ca. 25,000 genes can be performed in a previously not possible context. About one-fifth of the predicted protein sequences were identified as

Correspondence/Reprint request: Dr. Ingo Dreyer, Universität Potsdam, Institut für Biologie und Biochemie, Abteilung Molekularbiologie, Karl Liebknecht-Strasse 24-25, Haus 20, D-14476 Golm/Potsdam, Germany . E-mail: dreyer@rz.uni-potsdam.de

containing two or more membrane spanning domains. Based on sequence homologies to previously characterized plant or animal transporter proteins, the predicted genes putatively coding for similar proteins could be classified [1]. In this classification currently around 129 genes are assigned to code for ATP binding cassette (ABC)-transporters, about 120 genes for antiporters, ca. 86 genes for inorganic solute cotransporters, more than 350 genes for organic solute cotransporters, up to 60 genes for ATPases, around 35 for major intrinsic proteins (MIPs), and 63 for ion channels (Table I).

Table 1. Brief overview over selected ion transporter gene families identified in *Arabidopsis thaliana*. For further details see: Arabidopsis Membrane Protein Library: http://www.cbs.umn.edu/arabidopsis/, Arabidopsis Transporters: http://www.biology.ucsd.edu/~ipaulsen/transport/, PlantsT: http://plantst.sdsc.edu/, Milton Saier: http://www-biology.ucsd.edu/~msaier/transport/, and TAIR: http://www.arabidopsis.org/info/genefamily/genefamily.html

Family name	No. of genes in the *A. thaliana* genome	Transported ions	References
Trk/HKT Family	1	K^+	[2]
KUP/HAK/KT Family	13	K^+	[3-7]
AMT Family	5	NH_4^+	[8-10]
Natural Resistance-Associated Macrophage Proteins (NRAMP)	6	Fe^{2+}, Cd^{2+}, other heavy metal ions	[7,11,12]
Cation-H^+ Antiporter	56	Ca^{2+}, Cd^{2+}, Mn^{2+}, Mg^{2+}, Zn^{2+}, Na^+, K^+	[7,13-15]
Zinc Iron Permeases (ZIP, IRT)	15	Cd^{2+}, Fe^{2+}, Mn^{2+}, Zn^{2+}	[16]
Cation Diffusion Facilitator (CDF)	8	Zn^{2+}, Co^{2+}, Cd^{2+}	[17]
Sulphate Transporter (Sultr)	14	SO_4^{2-}	[18,19]
Phosphate:H^+ Symporter (PHS)	11	$H_2PO_4^-$	[20]
Inorganic Phosphate Transporter (PiT)	1	$H_2PO_4^-$	[21]
Magnesium Transport Proteins (AtMGT)	10	Mg^{2+}, Ni^{2+}, Co^{2+}, Fe^{2+}, Mn^{2+}, Cu^{2+}	[22]
High Affinity Nitrate Transporter (NRT2)	7	NO_3^-	[23]
Peptide/Nitrate Transporter (PTR) Family	51	NO_3^-, amino acids, peptides	[10,24]
ATP-Binding Cassette (ABC) Protein Superfamily	129	glutathione conjugates, chlorophyll catabolites, anthocyanins, phytoalexins	[25,26]

This article focuses on the role and characterization of plant ion channels with an emphasis on Arabidopsis thaliana. Ion transport through channels is a passive process with ion fluxes of 10^6 to 10^8 ions s^{-1}. In contrast turnover rates of carriers are appreciably lower, i.e. in the range of 10^3 molecules s^{-1}. After giving an overview about the diversity of ion channels characterized in planta we address the question how this variability can be achieved on the molecular level. Differences have been observed between electrophysiologically characterized ion channels in planta and cloned ion channels expressed in heterologous expression systems. Some results addressing these differences like channel subunit heteromerization and posttranslational modifications by kinases and phosphatases are presented exemplarily.

Role, characterization and molecular identification of ion channels in planta

It is generally assumed that the major physiological role of ion channels is to transport inorganic ions for processes such as salt absorption and secretion, cell volume regulation, signal transduction, and control of the membrane potential. One of the best characterized cellular system in this respect is the guard cell [27,28]. The change in turgor during opening and closing of stomata is mediated by ion fluxes through K^+ and anion channels. Furthermore guard cells are a valuable system to study the role of ion channels in signal transduction. Several stresses like drought and cold trigger stomatal closing. One of the first events is the activation of Ca^{2+} channels [29-31]. Ion channels play an important role in plant nutrition [32-34]. K^+ and anion channels have been characterized in xylem parenchyma cells from roots which contribute to xylem loading with salts [35-38]. Some anion channels in root apices are aluminium activated and mediate the efflux of organic acids, thus providing a mechanism for Al tolerance in plants [39-41].

Electrophysiological characterization revealed a diversity of ion channels. K^+, anion, Ca^{2+} and non-specific cation channels have been identified. Their classification was mainly based on selectivity and voltage dependence. In all cases channels which activate with more negative potentials (= hyperpolarization activated), and channels which activate with more positive potentials (= depolarization activated), have been reported (Fig. 1). Some channels like the non-selective cation channels are only weakly voltage dependent (Fig. 1C). That means that their open probability changes only slightly with a change in membrane potential. In addition to voltage, ligand binding is in some cases required for enhanced channel activity. Ligands may include inositol trisphosphate, cyclic ADP-ribose [42,43], Al^{3+} [40,41] or elicitors [44,45]. In addition, non-selective stretch-activated channels have been reported in plants [46,47]. To come back to the initial examples of stomatal movement and xylem loading, both - guard cells and xylem parenchyma cells - possess typical K^+ inward rectifying (hyperpolarization activated) and K^+ outward rectifying (depolarization activated) channels, which mediate K^+ influx and efflux, respectively (Fig. 1A; [35,48-51]. Both cell types possess depolarization activated anion channels through which Cl^- or NO_3^- efflux can occur (Fig. 1B; [52])[38,53,54]. They differ in their activation kinetics. QUAC, from guard cells, and X-QUAC, from xylem parenchyma, are rapidly activating (in the ms range), whereas SLAC and X-SLAC are slowly activating ion channels (in the s range). In xylem parenchyma cells a third type, an inward rectifying anion channel, named X-IRAC, exists (dotted line in Fig. 1B; [38]). The Al^{3+} activated anion current from root apices is another example for a hyperpolarization activated anion channel [39-41]. The hyperpolarization activated Ca^{2+} channel from the plasma membrane of guard cells can account for Ca^{2+} influx triggered by ABA (indicated as HACC in Fig. 1D; [29,30]). For a detailed summary with listings of the characteristics of the different channel types observed so far, see [55] for anion and cation channels, [56] for anion channels, and [57-60] for cation and calcium channels.

As mentioned above the sequencing of the *Arabidopsis* genome revealed the existence of about 98 channels, including 35 MIPs and 63 ion channels (Table II). Since membranes are water permeable the discovery of water channels was surprising [72]. Aquaporins represent some of the most abundant proteins in plant cell membranes. They are permeable for H_2O, glycerol, and urea. Their significance in the physiology of water transport in plants remains uncertain. Aquaporins may be needed to facilitate intense water flow across tissues. They also may be involved in solute distribution, gas transfer (CO_2, NH_3) and in micronutrient uptake (boric acid) [62,73,74].

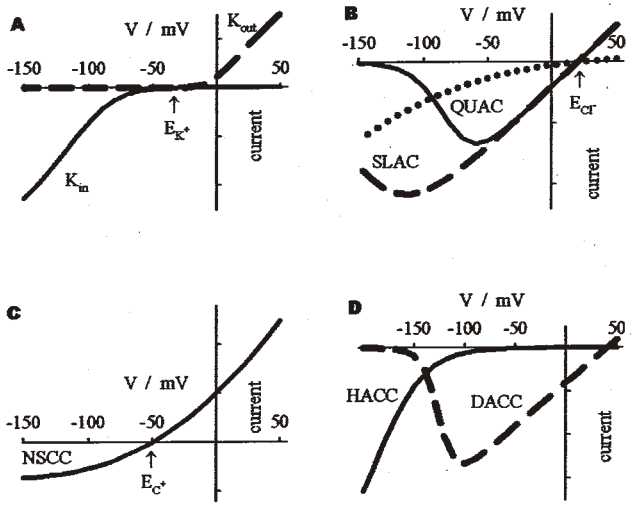

Figure 1. Plant ion channels *in vivo*.
In patch-clamp experiments several ion channels have been identified in plant cells. Among them are inward rectifying potassium channels (K_{in}, *A, solid line*), outward rectifying potassium channels (K_{out}, *A, dashed line*), rapidly activating chloride channels (QUAC, *B, solid line*), slowly activating chloride channels (SLAC, *B, dashed line*), inward rectifying chloride channels (B, *dotted line*), non-specific cation channels (NSCC, *C*), hyperpolarization activated calcium channels (HACC, *D, solid line*), and depolarization activated calcium channels (DACC, *D, dashed line*). Schematic current voltage curves are drawn. E indicats the reversal potential for K^+, Cl^- and cations, respectively. For details on the different channel types see the references given in the text.

K^+ channels

Most is known about K^+ channels. This group is well characterized both on the electrophysiological and on the molecular level. In contrast to non-specific cation channels, K^+ channels are highly selective for K^+. So far two families have been identified, the *Shaker*-like and the KCO family (Table II). Whereas inward and outward rectifying channels belong to the *Shaker*-like family, K^+ channels from the KCO family are presumably outward rectifying. In two different insect cell lines (*Sf*9

Table II. Brief overview over (ion) channel genes identified in *Arabidopsis thaliana*. For further details see web sites given in Tab. I.

Family name	No. of genes in the *A. thaliana* genome	Transported substrates	References
Major Intrinsic Protein (MIP) Family	35 genes, subdivided into PIPs (13 genes) and TIPs (10), NLM1 (12, 9 NIPs and 3 SIPs)	H_2O, urea, glycerol, Formamid, CO_2, NH_3	[61,62][3]
Shaker-like K^+ Channel Family	9 genes, subdivided into inward rectifying (6), outward rectifyimg (2) and weakly rectifying channels (1)	K^+, NH_4^+	[57,63]
KCO Family	6		[64]
Two Pore Putative Calcium Channels, candidate gene: AtTPC1	1	Ca^{2+}	[65]
Ionotropic Glutamate Receptor Channel (GLR) Family	20	Ca^{2+} (?), not shown yet	[66,67]
Cyclic Nucleotide-Gated Nonselective Cation Channel (CNGC) Family	20	K^+, Na^+, Ca^{2+}	[68-71]
Chloride Channel (CLC) Family	7	Cl^-	[56]

[3] http://www-biology.ucsd.edu/others/chrispeels/Research-Aquaporins.htm

and *Sf*21) infected with KCO1 K^+ outward currents activated positive of -30 mV [64]. Notice that in some later experiments similar currents were detected in *Sf*21 control cells which might have been caused by specific culture and/or stress conditions [75]. For further details on channel structure see the reviews [57,76]. Maathuis et al. [77] summarized the role of K^+ channels in membrane voltage control, in participation of osmotically driven movements, in cation nutrition, and in intracellular K^+ redristibution and cytosolic volume control. Genes encoding inward rectifying K^+ channel α-subunits were amongst the first membrane transport systems to be identified in plants at the molecular level. The first inward rectifying K^+ channels were cloned in 1992 [78,79]. Through mutational analysis on inward K^+ channels we have knowledge of the proteins and how individual amino acids determine functional characteristics such as ion conductivity, pH sensitivity, ion selectivity and voltage sensing [80-84]. Furthermore, the physiological functions of inward and outward rectifying K^+ channels in plants have been clarified. KAT1 and SKOR were identified as the K^+ inward channel from guard cells and the K^+ outward rectifier from xylem parenchyma cells, respectively [37,85-87]. Meanwhile biophysical properties and expression patterns of several other members of the *Shaker*-like family are known ([57] and

references therein). The *Shaker*-like family belongs to one of the best characterized ion transporter families in plants.

The functional role of the K^+ channels from the KCO family is not clear yet. It has been shown that KCO1 is localized in the tonoplast [88,89] and that it is activated by an increasing Ca^{2+} concentration [64]. K^+ accumulation in the vacuole is a major contributor to the intracellular osmotic pressure. Several types of potassium channels are present in the tonoplast and vacuolar K^+ release has been postulated to occur via these channels [90]. One ubiquitous type is the slowly activating vacuolar (SV) channel. Although the calcium dependence [64] and a reduction of currents through SV channels in vacuoles from *Arabidopsis KCO1* knockout plants [88] indicate that *KCO1* might encode or at least be involved in the formation of SV channels, this assumption awaits further elucidation.

Non-selective cation channels

Non-selective cation channels (NSCC) - in contrast to K^+ selective channels of the *Shaker*-like family - do not discriminate between monovalent, and only partly between divalent cations. Non-selective cation channels are permeable to NH_4^+, Rb^+, K^+, Cs^+, Na^+, Li^+, and Ca^{2+} [58]. In addition, a low selectivity for cations and anions has been described [91]. The channels have been named NSCC for non-selective cation channel, or VIC for voltage-independent channel. They have been investigated over the last decade [32,58,92] and may act as pathways for Na^+ entry into plants under salinity stress [32,92], as pathways for NH_4^+ in symbiosomes [93], and as general nutrient release mechanisms [50]. As pointed out in Fig. 1 non-selective cation channels are weakly voltage dependent. Other factors such as divalent cations [93] and cyclic nucleotides [94] can control their activity. So far the molecular identity of the NSCCs is not clear. Possible candidates are the cyclic nucleotide-activated channels (CNGC) and the ionotropic glutamate receptors (GLR) (Table II). These gene families have been identified by homology to animal counterparts and have been reviewed recently [57,58,71]. So far only AtCNGC2 from *Arabidopsis* could be successfully expressed in *Xenopus* oocytes and mammalian cells (HEK 293) although expression was difficult due to a toxic effect of the protein [70]. In this study AtCNGC2 was non-selective for several monovalent cations but excluded Na^+. The channel was permeable for Ca^{2+} as well. In contrast to the activation of AtCNGC2 by cyclic nucleotides, micromolar concentrations of cAMP or cGMP led to a decrease in channel activity in *Arabidopsis* roots [94]. A clear connection to the non-selective cation channels characterized *in planta* is still lacking. So far evidence for the existence of cyclic nucleotide-sensitive transport and glutamate receptor-mediated transport is indirect. Cyclic nucleotide-gated channels have been shown to play a role in Pb^{2+} transport [95], and glutamate receptors are likely to be involved in Ca^{2+} allocation and adaptation to ionic stresses [96].

Ca^{2+} channels

Likewise, the molecular identity of plant Ca^{2+} channels characterized *in vivo* is another open question. Ca^{2+} channels represent central signalling components which integrate several signal transduction pathways [28,97]. Ca^{2+} is an important second

messenger in signal transduction. A number of different stimuli evoke an increase of the cytosolic Ca^{2+} concentration by influx of Ca^{2+} from intracellular Ca^{2+} pools or from the extracellular space. Plasma membrane Ca^{2+} channels, for instance, can be activated by elicitors [44,45], ABA and reactive oxygen species [29,30], and vacuolar Ca^{2+} currents are activated by inositol trisphosphate and cyclic ADP-ribose [42,43]. A wide variety of Ca^{2+} channels have been identified at the plasma membrane, endoplasmatic reticulum, tonoplast, nuclear and plastidic membranes. Besides Ca^{2+} they are permeable for Ba^{2+} and Mg^{2+} [29,30,98]. For a review on electrical properties of Ca^{2+} channels see [59,60,99]. In a recent review [71], White et al. focus on the molecular identity of the Ca^{2+} channels. In *Arabidopsis* AtTPC1, a homologue of the two-pore channel (TPC1) from rat, was cloned [65]. Ca^{2+} transport was shown by yeast complementation. However, it was not possible to measure significant ionic currents in heterologous expression systems.

As pointed out in the previous paragraph, non-selective cation channels are permeable for Ca^{2+} as well and can be involved in Ca^{2+} signaling. Therefore, cyclic nucleotide-gated channels and ionotropic glutamate receptors are also candidate genes for Ca^{2+} selective channels [57,58,71]. Again, a clear correlation to the electrophysiological data could not be drawn yet.

Anion channels

For anion channels the situation is similar. A variety of different anion currents has been identified in various membranes and tissues using electrophysiological techniques [56,100]. Anion channels are permeable for various anions including NO_3^- and sulfate. They function in stomatal movement [56] and plant nutrition [32,33,40]. Now science focuses on the identification of the molecular structure of these channels. Based on homology to animal chloride channels the Chloride Channel (CLC) family from *Arabidopsis* was identified [101,102]. Localisation studies showed that they are located in internal membranes [101,102]. However, none of the electrophysiologically characterized anion channels has been identified at the molecular level so far.

One of the current challenges is the characterization of transporter gene products at the functional level. This has just started. There are still hundreds of predicted membrane proteins with unknown functions (see http://www.cbs.umn.edu/arabidopsis/). Regulation of ion transporters makes this task much more complicated. Even in a single cell type several types of channels occur, like it was mentioned for anion channels in guard cells and xylem parenchyma cells (Fig. 1B). Part of this channel diversity may be attributed to posttranslational regulation, even if these channels are encoded by a single gene. Notably, regulation can already occur by substrates themselves. The voltage dependence of K^+ and anion channels, for instance, is modified by K^+ and NO_3^-, respectively [50,103,104]. Other regulatory mechanisms expected to have a large impact on ion channel properties are subunit heteromerization and posttranslational modification of channel proteins (see below).

From molecules to phenomena

The identification of genes (putatively) coding for plant transporters opened the door to prove current pictures on ion transport in plants. On the one hand, the possibility to

functionally express cloned transporters in heterologous expression systems allowed to characterize them in -so far unknown- biophysical detail [105]. On the other hand, it was now possible to disturb systematically the function of individual transporter genes and analyze its consequences on the plant level. Over the recent years, *Agrobacterium tumefaciens* was used to introduce randomly a segment of transferred DNA (T-DNA) containing a selectable marker into the plant genome [106]. By this strategy ten-thousands of T-DNA insertion lines have been generated for the model plant *Arabidopsis thaliana* and made available to the research comunity[1]. Alternatively, transposable elements like *En-1* from *Zea mays* [107] were used to mutagenize populations of *A. thaliana*[2].

Among all these lines, a line containing a T-DNA or transposon insertion in the gene of interest can be identified by PCR-based techniques taking advantage of the known sequences of the gene and the inserted T-DNA/transposon [108]. In the ideal case, the selected line contains only a single DNA insertion. Generally, an insertion of the T-DNA into the coding region (or the promoter) leads to the expression of a truncated, non-functional gene product, or disrupts the expression of the gene. Thus, plants lacking a transporter gene can be obtained by generating homozygous plants from the selected (heterozygous) T-DNA insertion line. In addition to this reverse-genetics approach, T-DNA insertion lines are also used in forward genetic screens that allow the identification of phenotypic abnormalities. Subsequently, the disrupted genes containing the T-DNA insertion are identified by PCR-based techniques [109].

So far, "knock-out" plants have been identified and analysed for a variety of different transporter genes. Among them are the K^+ channels AKT1 [110], SKOR [37], AKT2 [111], KAT1 [112], AtKC1 [113], AtSPIK [114], AtKCO1 [88], the putative Cl^- channel AtCLC-a [115], the putative cyclic nucleotide-gated channel AtCNGC1 [95], the nitrate transporters AtNRT2.1 and AtNRT2.2 [116,117], the iron transporter IRT1 [118,119], the sulfate transporter Sultr1.2 [120], the plasma membrane H^+-ATPase AHA4 [121], the metal ion transporter AtNramp3 [12], the high affinity K^+ transporter AtHKT1 [122], and the ABC transporter AtMRP5 [123,124].

From the analyses of the insertion lines it became evident that the disruption of one gene in some cases has dramatic consequences for the plant. Very often, however, a gene knock-out does not cause an easily visible phenotypic difference between the wild-type and the mutant plant under normal growth conditions. For example, the knock-out lines for the K^+ channels KAT1, SKOR, and AKT1 betrayed their slight phenotypic abnormality only after detailed physiological analyses. An immediate working hypothesis to explain the weak (or nearly absent) phenotype in the knock-out lines may be illustrated linguistically: "rdndncy". Similarly, also the expression of plant K^+ channels may be redundant to a certain extend.

Heteromerization - A strategy to gain diversity?

Compared to the number of specialized cell types with different functions and geometries, the number of transporter genes in each family is rather small. To fine-tune

[1] http://tmri.org/pages/collaborations/garlic_files/GarlicDescription.html
http://signal.salk.edu/cgi-bin/tdnaexpress
http://flagdb-genoplante-info.infobiogen.fr/projects/fst/DocsIntro/introCollection.html
http://www.biotech.wisc.edu/arabidopsis/

[2] http://www.jic.bbsrc.ac.uk/Sainsbury-Lab/jonathan-jones/SINS-database/sins.htm

the transport characteristics of a certain cell type other control mechanisms beyond genetic diversity must have been developed during evolution. One of the possible mechanisms is protein-protein interaction between transporter proteins of the same but also of different types. In recent years, protein-protein interactions have been uncovered experimentally by using different experimental approaches (an overview about different techniques can be found in [125]). The "classical" molecular approach established to study protein-protein interactions is the yeast two-hybrid system. However, its application to probe for the interaction of membrane proteins is limited. Therefore also other techniques were used extensively. A modified yeast two-hybrid system has been applied to investigate protein-protein interactions between sugar transporters. With a split-ubiquitin approach [126], it was possible to demonstrate that heterologously expressed sucrose transporters physically interact in the plasma membrane [127]. The clustering of plant potassium channels was studied by fusing the green fluorescent protein (GFP) to the C-terminal end of a K^+ channel. The fluorescence of the marker protein showed an uneven distribution on the cell surface pointing to protein-protein interactions which result in the polarized agglomeration of transporter molecules [128]. The clustering of aquaporins was investigated after biochemical purification of the protein and reconstitution into lipid bilayers. Electron cryo-crystallography revealed that the aquaporin alpha-TIP aggregates as a tetramer [129]. The physiological significance of all these protein-protein interactions remains to be elucidated. It is possible that clustering of transporters plays an important role in polarized cell expansion. Additionally, clustered plant transporters may differ in their transport characteristics from single, isolated transporters. Findings on a human glucose transporter tend to this direction. Through cooperative conformational changes the activity status of a glucose transporter complex is affected by the status of an individual subunit [130].

For one class of plant transporters the physiological significance of protein-protein interactions has recently become obvious. Plant K^+ channels are functional as tetramers. Initially the oligomerization of plant K^+ channel subunits has been uncovered by two completely different approaches. Daram et al. [131] showed in a "classical" two-hybrid assay that the cytoplasmic C-terminus of the plant K^+ channel AKT1 physically self-interacts. Biochemical studies revealed further that this isolated part of the protein assembles into a tetrameric structure [131,132]. Independently, electrophysiological co-expression studies in *Xenopus oocytes*, using diverse mutants of plant K^+ channels, also indicated, that plant K^+ channels are functional as oligomeric aggregates [133]. Moreover, analysing the biophysical features of the expressed channels, it had to be concluded that plant K^+ channel α-subunits have the potential to form heteromeric potassium channels. Such heteromeric channels combine the features of the different underlying α-subunits. Thus, the phenotype of the mediated current differs from those of the homomeric channels composed of only one type of subunit. This finding could explain some of the biophysical differences observed for K^+ channels *in vivo* and their putative molecular counterparts after expression in heterologous expression systems [105,134]. Recent analyses of knock-out plants support this hypothesis [112,113].

Heterooligomerization of α-subunits allow plants to combine features of a few α-subunits to fine-tune their regulation of K^+ transport just by slight changes in the expression level. Fig. 2 illustrates the theoretical number of possible channels that can form, if one, two, three or four different α-subunits are expressed in the same cell at the

same time. This figure clarifies that heterooligomerization is indeed a possible strategy to gain diversity. The experimental findings on K^+ channels indicate that for this transporter type plants indeed take advantage from such a strategy. In guard cells, for example, it could be shown that more than one K^+ channel α-subunit is expressed [112]: In *Arabidopsis* the twin channel subunits KAT1 and KAT2, and in potato the channel subunits KST1 and SKT1 have the ability to form heteromeric channels [135,136]. Whether a similar situation exists also for other transporter types remains to be elucidated.

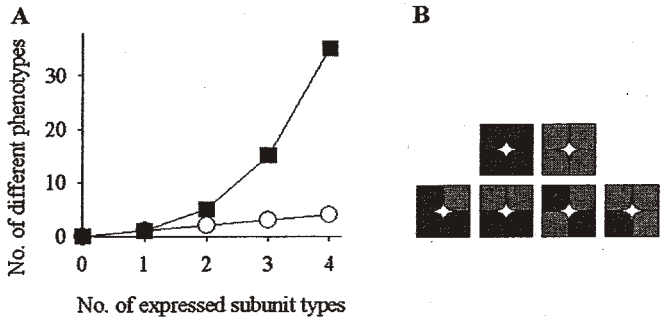

Figure 2. Heteromerization - the power of combinatorial assembly.
A potassium channel is built of 4 subunits. (*A*) If only subunits of the same type assemble into functional channels, a cell could generate only a small number of different channel phenotypes, respectively the number of expressed genes (*circles*). Assuming, in contrast, that all subunits can freely interact with each other, a small number of expressed subunit types would be sufficient to generate a large number of different channel phenotypes (*squares*). (*B*) Example for 2 expressed subunits types. In the case of selective assembly only two homomeric channel types are created (*upper row*). In the case of non-selective assembly up to 4 additional channel types are possible (*lower row*).

Regulation of transporter properties by post-translational modifications

The activity and functionality of plant transporters is regulated and modulated by a variety of signalling cascades most of which are only know in part. The final trigger in these cascades, however, is often a change in the cytosolic free Ca^{2+} concentration, the intracellular pH or the phosphorylation status of the target protein. The interaction of these second messenger molecules with the transporter changes the energy status of certain conformational states of the transporter protein, which in turn may have consequences for the transport rates of the transporter. Fig. 3 depicts these effects exemplarily on the guard cell K^+ uptake channel. This K^+ channel is activated by negative transmembrane voltages. At 0 mV the probability to find one channel open is almost zero. With more negative voltages this probability increases. These activities are affected by protons and Ca^{2+} ions. Whereas an acidification of the extracellular space as well as the cytoplasm shifts the activity curve towards positive voltages [137-140],

elevated cytoplasmic Ca^{2+} concentrations have the inverse effect [141]. Under some circumstances, this shift can be that large that the affected channel is not active anymore under physiological conditions. In these cases the modulation of the transporter may be considered as an on/off switch. The outlined regulations are not restricted to voltage-regulated transporters. A nearly perfect on/off switch for example has been reported for the aquaporin alpha-TIP. Although this water channel is not regulated by changes in the transmembrane voltage, its activity is determined by the phosphorylation status of three cytoplasmic serine residues [142].

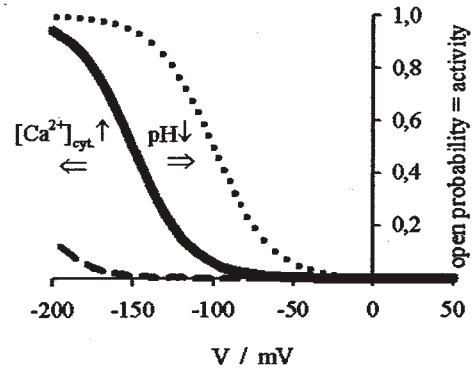

Figure 3. Modulation of K_{in} channel activity by second messengers.
Plant K_{in} channels are voltage-activated. With more negative voltages the probably to find a channel in the open conformation increases (*solid line*). Interaction of the channel protein with second messenger molecules can alter the energies of its conformational states. Interaction with protons favour the open configuration, i.e. the channel activates at more positive voltages (*dotted line*). Interaction with cytoplasmic Ca^{2+} ions increases the energy needed to activate the channel. The open probability curve is shifted to more negative voltages (*dashed line*).

In plants, the activities of K^+ and Cl^- channels are sensitive to protein (de)phosphorylation [143-145]. Phosphorylation of the hyperpolarization-activated Ca^{2+} channel from *Vicia faba* guard cells (or of closely associated proteins) facilitates channel opening [31]. Addition of phosphatase antagonists led to a profound shift in the voltage sensititvity for evoked $[Ca^{2+}]_{cyt}$ increases. In this case dephosphorylation was mediated by a serine/threonine, 1/2A-type protein phosphatase. In guard cells the abi1 and abi2 protein phosphatase 2C mutants are known to affect $[Ca^{2+}]_{cyt}$ increases in response to ABA [29]. Effects of both phosphatases, the 1/2A-type and 2C-type, must reflect distinct targets of the phosphatases and their functional proximity to them.

An interesting finding in this context has recently been made in the case of the *Arabidopsis* K^+ channel AKT2 [146,147]. In contrast to all other cloned *Arabidopsis* K^+ channels, which are either K^+ uptake or K^+ release channels, this phloem-expressed channel shows unique characteristics. It is able to mediate both, K^+ uptake as well as K^+ release [148,149]. The reason for this behaviour has been uncovered through biophysical analyses of the gating properties of the channel. When expressed in heterologous

expression systems, it became evident that the AKT2 channel population subdivides into two distinct fractions that have different gating modes (mode 1 and mode 2). Channels gating in mode 1 exhibit a voltage-dependent activation like typical K^+ uptake channels (e.g. KAT1), whereas channels which gate in mode 2 were not affected by the transmembrane voltage. Mode 2 channels remained open in the tested voltage interval from −180 mV to +50 mV (Fig. 4). Importantly, further studies suggested that a single AKT2 channel can switch between the two distinct gating modes by some reversible post-translational events [150]. Coincidentally, a candidate protein responsible for the reversible post-translational event has been discovered in molecular studies. Two groups identified independently an interaction between AKT2 and a protein phosphatase. By screening two-hybrid cDNA libraries with the C-terminal part of AKT2 as the bait, one group isolated a protein phosphatase 2C, called AtPP2CA, as an interacting protein [151]. Another group used this phosphatase as a bait and isolated AKT2 [152]. Thus, it is very likely that different phosphorylation statuses underlie the different gating modes in AKT2. However, whether (de)phosphorylation is the only mechanism to shift AKT2 between gating modes still remains to be investigated.

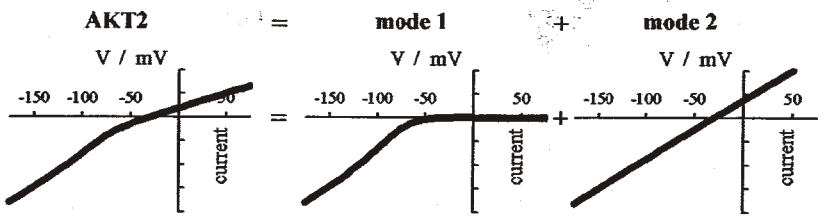

Figure 4. Separation of the currents mediated by AKT2 into two components.
Two types of AKT2 channels co-exist in the membrane of *Xenopus* oocytes after heterologous expression. The two fractions are characterized by different gating modes. One fraction shows the characteristics of K_{in} channels mediating inward K^+ currents (*mode 1*). The other fraction displays leak-like K^+ currents (*mode 2*). For details see [150].

Whether the *in vivo* targets of kinases and phosphatases are directly the ion channels or associated proteins has not been shown in most cases. KAT1 has been shown to be phosphorylated by a Ca^{2+}-dependent protein kinase and by an ABA induced protein kinase from *Vicia faba* guard cells [153,154]. Application of protein kinase A (PKA) and ATP restored KAT1 channel activity expressed in *Xenopus* oocytes, which otherwise decreases after patch excision. Opening transitions of KAT1 are enhanced not only by hyperpolarization but also by PKA-mediated phosphorylation [155]. Indirect evidence has been given, that also Cl^- channels are controlled by a ABA activated protein kinase [156]. Like heteromerization, phosphorylation and the formation of protein complexes, where i.g. channel proteins, phosphatases, kinases, and other regulatory subunits are associated, can potentially increase the observed diversity. The latter is of great interest because protein complexes of different composition would allow local specificity to be established which is thought to be important in decoding different Ca^{2+} signatures.

Conclusion – future challenges

The introduction of the molecular technology into the field of plant physiology dramatically changed membrane transport research in recent years. The increase in knowledge during the past few years is breath-taking. However, as outlined in this review, many questions still remain to be answered. Certainly, future challenges will differ from past ones. Whereas in the last ten years most effort was taken to identify and clone plant genes, the future will be dominated by assigning functions to still orphan genes. Once a function has been identified, its role in the cellular network has to be found. This network, from which we currently know only small pieces, is probably far more complex than we can imagine. Therefore, without any doubt computer models simulating individual cellular processes or even complete cells are needed [157]. A long way to go …

References

1. Ward, J.M. 2001, Bioinformatics., 17, 560.
2. Schachtman, D.P., and Schroeder, J.I. 1994, Nature, 370, 655.
3. Quintero, F.J., and Blatt, M.R. 1997, FEBS Lett., 415, 206.
4. Santa-Maria, G.E., Rubio, F., Dubcovsky, J., and Rodriguez-Navarro, A. 1997, Plant Cell, 9, 2281.
5. Kim, E.J., Kwak, J.M., Uozumi, N., and Schroeder, J.I. 1998, Plant Cell, 10, 51.
6. Fu, H.H., and Luan, S. 1998, Plant Cell, 10, 63.
7. Maser, P., Thomine, S., Schroeder, J.I., Ward, J.M., Hirschi, K., Sze, H., Talke, I.N., Amtmann, A., Maathuis, F.J., Sanders, D., Harper, J.F., Tchieu, J., Gribskov, M., Persans, M.W., Salt, D.E., Kim, S.A., and Guerinot, M.L. 2001, Plant Physiol, 126, 1646.
8. von Wiren, N., Gazzarrini, S., Gojon, A., and Frommer, W.B. 2000, Curr. Opin. Plant Biol., 3, 254.
9. Howitt, S.M., and Udvardi, M.K. 2000, Biochim. Biophys. Acta, 1465, 152.
10. Williams, L., and Miller, A. 2001, Annu. Rev. Plant Physiol Plant Mol. Biol., 52, 659.
11. Curie, C., Alonso, J.M., Le Jean, M., Ecker, J.R., and Briat, J.F. 2000, Biochem. J., 347, 749.
12. Thomine, S., Wang, R., Ward, J.M., Crawford, N.M., and Schroeder, J.I. 2000, Proc. Natl. Acad. Sci. U. S. A, 97, 4991.
13. Gaxiola, R.A., Rao, R., Sherman, A., Grisafi, P., Alper, S.L., and Fink, G.R. 1999, Proc. Natl. Acad. Sci. U. S. A, 96, 1480.
14. Hirschi, K. 2001, Trends Plant Sci., 6, 100.
15. Quintero, F.J., Blatt, M.R., and Pardo, J.M. 2000, FEBS Lett., 471, 224.
16. Guerinot, M.L. 2000, Biochim. Biophys. Acta, 1465, 190.
17. Van Der Zaal, B.J., Neuteboom, L.W., Pinas, J.E., Chardonnens, A.N., Schat, H., Verkleij, J.A., and Hooykaas, P.J. 1999, Plant Physiol, 119, 1047.
18. Takahashi, H., Yamazaki, M., Sasakura, N., Watanabe, A., Leustek, T., Engler, J.A., Engler, G., Van Montagu, M., and Saito, K. 1997, Proc. Natl. Acad. Sci. U. S. A, 94, 11102.
19. Grossman, A., and Takahashi, H. 2001, Annu. Rev. Plant Physiol Plant Mol. Biol., 52, 163.
20. Muchhal, U.S., Pardo, J.M., and Raghothama, K.G. 1996, Proc. Natl. Acad. Sci. U. S. A, 93, 10519.
21. Daram, P., Brunner, S., Rausch, C., Steiner, C., Amrhein, N., and Bucher, M. 1999, Plant Cell, 11, 2153.
22. Li, L., Tutone, A.F., Drummond, R.S., Gardner, R.C., and Luan, S. 2001, Plant Cell, 13, 2761.

23. Orsel, M., Filleur, S., Fraisier, V., and Daniel-Vedele, F. 2002, J. Exp. Bot., 53, 825.
24. Tsay, Y.F., Schroeder, J.I., Feldmann, K.A., and Crawford, N.M. 1993, Cell, 72, 705.
25. Sanchez-Fernandez, R., Davies, T.G., Coleman, J.O., and Rea, P.A. 2001, J. Biol. Chem., 276, 30231.
26. Martinoia, E., Klein, M., Geisler, M., Bovet, L., Forestier, C., Kolukisaoglu, U., Mueller-Roeber, B., and Schulz, B. 2002, Planta, 214, 345.
27. Schroeder, J.I., Allen, G.J., Hugouvieux, V., Kwak, J.M., and Waner, D. 2001, Annu. Rev. Plant Physiol Plant Mol. Biol., 52, 627.
28. Blatt, M.R. 2000, Annu. Rev. Cell Dev. Biol., 16, 221.
29. Pei, Z.M., Murata, Y., Benning, G., Thomine, S., Klusener, B., Allen, G.J., Grill, E., and Schroeder, J.I. 2000, Nature, 406, 731.
30. Hamilton, D.W., Hills, A., Kohler, B., and Blatt, M.R. 2000, Proc. Natl. Acad. Sci. U. S. A, 97, 4967.
31. Köhler, B., and Blatt, M.R. 2002, Plant J., in press,
32. Tyerman, S.D., and Skerrett, I.M. 1999, Sci. Hortic. -Amsterdam, 78, 175.
33. White, P.J., and Broadley, M.R. 2001, Annals of Botany, 88, 967.
34. Tester, M., and Leigh, R.A. 2001, J. Exp. Bot., 52, 445.
35. Wegner, L.H., and Raschke, K. 1994, Plant Physiol, 105, 799.
36. Roberts, S.K., and Tester, M. 1995, Plant J., 8, 811.
37. Gaymard, F., Pilot, G., Lacombe, B., Bouchez, D., Bruneau, D., Boucherez, J., Michaux-Ferriere, N., Thibaud, J.B., and Sentenac, H. 1998, Cell, 94, 647.
38. Köhler, B., and Raschke, K. 2000, Plant Physiol, 122, 243.
39. Ryan, P.R., Skerrett, M., Findlay, G.P., Delhaize, E., and Tyerman, S.D. 1997, Proc. Natl. Acad. Sci. U. S. A, 94, 6547.
40. Ryan, P.R., Delhaize, E., and Jones, D.L. 2001, Annu. Rev. Plant Physiol Plant Mol. Biol., 52, 527.
41. Pineros, M.A., Magalhaes, J.V., Carvalho, A., V, and Kochian, L.V. 2002, Plant Physiol, 129, 1194.
42. Leckie, C.P., McAinsh, M.R., Allen, G.J., Sanders, D., and Hetherington, A.M. 1998, Proc. Natl. Acad. Sci. U. S. A, 95, 15837.
43. Muir, S.R., Bewell, M.A., Sanders, D., and Allen, G.J. 1997, J. Exp. Bot., 48, 589.
44. Gelli, A., Higgins, V.J., and Blumwald, E. 1997, Plant Physiol, 113, 269.
45. Zimmermann, S., Nurnberger, T., Frachisse, J.M., Wirtz, W., Guern, J., Hedrich, R., and Scheel, D. 1997, Proc. Natl. Acad. Sci. U. S. A, 94, 2751.
46. Ding, J.P., and Pickard, B.G. 1993, Plant J., 3, 83.
47. Cosgrove, D.J., and Hedrich, R. 1991, Planta, 186, 143.
48. Schroeder, J.I., Raschke, K., and Neher, E. 1987, Proc. Natl. Acad. Sci. U. S. A, 84, 4108.
49. Fairley-Grenot, K.A., and Assmann, S.M. 1992, Planta, 186, 282.
50. Wegner, L.H., and de Boer, A.H. 1997, Plant Physiol, 115, 1707.
51. Dietrich, P., Dreyer, I., Wiesner, P., and Hedrich, R. 1998, Planta, 205, 277.
52. Keller, B.U., Hedrich, R., and Raschke, K. 1989, Nature, 341, 450.
53. Linder, B., and Raschke, K. 1992, FEBS Lett., 313, 27.
54. Schmidt, C., and Schroeder, J.I. 1994, Plant Physiol, 106, 383.
55. Krol, E., and Trebacz, K. 2000, Ann. Bot. (Lond), 86, 449.
56. Barbier-Brygoo, H., Vinauger, M., Colcombet, J., Ephritikhine, G., Frachisse, J., and Maurel, C. 2000, Biochim. Biophys. Acta, 1465, 199.
57. Very, A.A., and Sentenac, H. 2002, Trends Plant Sci., 7, 168.
58. Demidchik, V., Davenport, R.J., and Tester, M. 2002, Ann. Rev. Plant Biol., 53, 67.
59. White, P.J. 1998, Ann. Bot. (Lond), 81, 173.
60. White, P.J. 2000, Biochim. Biophys. Acta, 1465, 171.
61. Johanson, U., Karlsson, M., Johansson, I., Gustavsson, S., Sjovall, S., Fraysse, L., Weig, A.R., and Kjellbom, P. 2001, Plant Physiol, 126, 1358.

62. Quigley, F., Rosenberg, J.M., Shachar-Hill, Y., and Bohnert, H.J. 2002, Genome Biol., 3, research0001.1.
63. Schachtman, D.P. 2000, Biochim. Biophys. Acta, 1465, 127.
64. Czempinski, K., Zimmermann, S., Ehrhardt, T., and Mueller-Roeber, B. 1997, EMBO J., 16, 2565.
65. Furuichi, T., Cunningham, K.W., and Muto, S. 2001, Plant Cell Physiol, 42, 900.
66. Lam, H.M., Chiu, J., Hsieh, M.H., Meisel, L., Oliveira, I.C., Shin, M., and Coruzzi, G. 1998, Nature, 396, 125.
67. Lacombe, B., Becker, D., Hedrich, R., DeSalle, R., Hollmann, M., Kwak, J.M., Schroeder, J.I., Le Novere, N., Nam, H.G., Spalding, E.P., Tester, M., Turano, F.J., Chiu, J., and Coruzzi, G. 2001, Science, 292, 1486.
68. Kohler, C., Merkle, T., and Neuhaus, G. 1999, Plant J., 18, 97.
69. Leng, Q., Mercier, R.W., Yao, W., and Berkowitz, G.A. 1999, Plant Physiol, 121, 753.
70. Leng, Q., Mercier, R.W., Hua, B.G., Fromm, H., and Berkowitz, G.A. 2002, Plant Physiol, 128, 400.
71. White, P.J., Bowen, H., Demidchik, V., Nichols, C., and Davies, J. 2002, Biochim. Biophys. Acta, 1564, 299.
72. Maurel, C., Reizer, J., Schroeder, J.I., and Chrispeels, M.J. 1993, EMBO J., 12, 2241.
73. Maurel, C., Javot, H., Lauvergeat, V., Gerbeau, P., Tournaire, C., Santoni, V., and Heyes, J. 2002, Int. Rev. Cytol., 215, 105.
74. Tyerman, S.D., Niemietz, C.M., and Bramley, H. 2002, Plant Cell Environ., 25, 173.
75. Czempinski, K., Zimmermann, S., Ehrhardt, T., and Mueller-Roeber, B. 1997, EMBO J., 16, 6896.
76. Czempinski, K., Gaedeke, N., Zimmermann, S., and Mueller-Roeber, B. 1999, J. Exp. Bot., 50, 955.
77. Maathuis, F.J., Ichida, A.M., Sanders, D., and Schroeder, J.I. 1997, Plant Physiol, 114, 1141.
78. Anderson, J.A., Huprikar, S.S., Kochian, L.V., Lucas, W.J., and Gaber, R.F. 1992, Proc. Natl. Acad. Sci. U. S. A, 89, 3736.
79. Sentenac, H., Bonneaud, N., Minet, M., Lacroute, F., Salmon, J.M., Gaymard, F., and Grignon, C. 1992, Science, 256, 663.
80. Becker, D., Dreyer, I., Hoth, S., Reid, J.D., Busch, H., Lehnen, M., Palme, K., and Hedrich, R. 1996, Proc. Natl. Acad. Sci. U. S. A, 93, 8123.
81. Dreyer, I., Becker, D., Bregante, M., Gambale, F., Lehnen, M., Palme, K., and Hedrich, R. 1998, FEBS Lett., 430, 370.
82. Hoth, S., Dreyer, I., Dietrich, P., Becker, D., Mueller-Roeber, B., and Hedrich, R. 1997, Proc. Natl. Acad. Sci. U. S. A, 94, 4806.
83. Nakamura, R.L., Anderson, J.A., and Gaber, R.F. 1997, J. Biol. Chem., 272, 1011.
84. Uozumi, N., Gassmann, W., Cao, Y., and Schroeder, J.I. 1995, J. Biol. Chem., 270, 24276.
85. Schachtman, D.P., Schroeder, J.I., Lucas, W.J., Anderson, J.A., and Gaber, R.F. 1994, Science, 258, 1654.
86. Nakamura, R.L., McKendree, W.L., Hirsch, R.E., Sedbrook, J.C., Gaber, R.F., and Sussman, M.R. 1995, Plant Physiol, 109, 371.
87. Lacombe, B., Pilot, G., Gaymard, F., Sentenac, H., and Thibaud, J.B. 2000, FEBS Lett., 466, 351.
88. Schonknecht, G., Spoormaker, P., Steinmeyer, R., Bruggeman, L., Ache, P., Dutta, R., Reintanz, B., Godde, M., Hedrich, R., and Palme, K. 2002, FEBS Lett., 511, 28.
89. Czempinski, K., Frachisse, J.M., Maurel, C., Barbier-Brygoo, H., and Mueller-Roeber, B. 2002, Plant J., 29, 809.
90. Tikhonova, L.I. 1998, Membr. Cell Biol., 12, 301.
91. Zhang, W.H., Skerrett, M., Walker, N.A., Patrick, J.W., and Tyerman, S.D. 2002, Plant Physiol, 128, 388.

92. Amtmann, A., and Sanders, D. 1999, Adv. Bot. Res., 29, 75.
93. Roberts, D.M., and Tyerman, S.D. 2002, Plant Physiol, 128, 370.
94. Maathuis, F.J., and Sanders, D. 2001, Plant Physiol, 127, 1617.
95. Sunkar, R., Kaplan, B., Bouche, N., Arazi, T., Dolev, D., Talke, I.N., Maathuis, F.J., Sanders, D., Bouchez, D., and Fromm, H. 2000, Plant J., 24, 533.
96. Kim, S.A., Kwak, J.M., Jae, S.K., Wang, M.H., and Nam, H.G. 2001, Plant Cell Physiol, 42, 74.
97. Sanders, D., Pelloux, J., Brownlee, C., and Harper, J.F. 2002, Plant Cell, 14 Suppl, S401.
98. Very, A.A., and Davies, J.M. 2000, Proc. Natl. Acad. Sci. U. S. A, 97, 9801.
99. Thuleau, P., Ward, J.M., Ranjeva, R., and Schroeder, J.I. 1994, EMBO J., 13, 2970.
100. Tyerman, S.D. 1992, Annu. Rev. Plant Physiol Plant Mol. Biol., 43, 351.
101. Hechenberger, M., Schwappach, B., Fischer, W.N., Frommer, W.B., Jentsch, T.J., and Steinmeyer, K. 1996, J. Biol. Chem., 271, 33632.
102. Lurin, C., Guclu, J., Cheniclet, C., Carde, J.P., Barbier-Brygoo, H., and Maurel, C. 2000, Biochem. J., 348, 291.
103. Blatt, M.R., and Gradmann, D. 1997, J. Membr. Biol., 158, 241.
104. Köhler, B., Wegner, L.H., Osipov, V., and Raschke, K. 2002, Plant J., 30, 133.
105. Dreyer, I., Horeau, C., Lemaillet, G., Zimmermann, S., Bush, D.R., Rodriguez-Navarro, A., Schachtman, D.P., Spalding, E.P., Sentenac, H., and Gaber, R.F. 1999, J. Exp. Bot., 50, 1073.
106. Feldmann, K.A., Coury, D.A., and Christianson, M.L. 1997, Genetics, 147, 1411.
107. Wisman, E., Cardon, G.H., Fransz, P., and Saedler, H. 1998, Plant Mol. Biol., 37, 989.
108. Krysan, P.J., Young, J.C., Tax, F., and Sussman, M.R. 1996, Proc. Natl. Acad. Sci. U. S. A, 93, 8145.
109. Krysan, P.J., Young, J.C., Jester, P.J., Monson, S., Copenhaver, G., Preuss, D., and Sussman, M.R. 2002, OMICS., 6, 163.
110. Hirsch, R.E., Lewis, B.D., Spalding, E.P., and Sussman, M.R. 1998, Science, 280, 918.
111. Dennison, K.L., Robertson, W.R., Lewis, B.D., Hirsch, R.E., Sussman, M.R., and Spalding, E.P. 2001, Plant Physiol, 127, 1012.
112. Szyroki, A., Ivashikina, N., Dietrich, P., Roelfsema, M.R., Ache, P., Reintanz, B., Deeken, R., Godde, M., Felle, H., Steinmeyer, R., Palme, K., and Hedrich, R. 2001, Proc. Natl. Acad. Sci. U. S. A, 98, 2917.
113. Reintanz, B., Szyroki, A., Ivashikina, N., Ache, P., Godde, M., Becker, D., Palme, K., and Hedrich, R. 2002, Proc. Natl. Acad. Sci. U. S. A, 99, 4079.
114. Mouline, K., Very, A.A., Gaymard, F., Boucherez, J., Pilot, G., Devic, M., Bouchez, D., Thibaud, J.B., and Sentenac, H. 2002, Genes Dev., 16, 339.
115. Geelen, D., Lurin, C., Bouchez, D., Frachisse, J.M., Lelievre, F., Courtial, B., Barbier-Brygoo, H., and Maurel, C. 2000, Plant J., 21, 259.
116. Cerezo, M., Tillard, P., Filleur, S., Munos, S., Daniel-Vedele, F., and Gojon, A. 2001, Plant Physiol, 127, 262.
117. Filleur, S., Dorbe, M.F., Cerezo, M., Orsel, M., Granier, F., Gojon, A., and Daniel-Vedele, F. 2001, FEBS Lett., 489, 220.
118. Vert, G., Grotz, N., Dedaldechamp, F., Gaymard, F., Guerinot, M.L., Briat, J.F., and Curie, C. 2002, Plant Cell, 14, 1223.
119. Varotto, C., Maiwald, D., Pesaresi, P., Jahns, P., Salamini, F., and Leister, D. 2002, Plant J., 31, 589.
120. Shibagaki, N., Rose, A., McDermott, J.P., Fujiwara, T., Hayashi, H., Yoneyama, T., and Davies, J.P. 2002, Plant J., 29, 475.
121. Vitart, V., Baxter, I., Doerner, P., and Harper, J.F. 2001, Plant J., 27, 191.
122. Rus, A., Yokoi, S., Sharkhuu, A., Reddy, M., Lee, B.H., Matsumoto, T.K., Koiwa, H., Zhu, J.K., Bressan, R.A., and Hasegawa, P.M. 2001, Proc. Natl. Acad. Sci. U. S. A, 98, 14150.
123. Gaedeke, N., Klein, M., Kolukisaoglu, U., Forestier, C., Muller, A., Ansorge, M., Becker, D., Mamnun, Y., Kuchler, K., Schulz, B., Mueller-Roeber, B., and Martinoia, E. 2001, EMBO J., 20, 1875.

124. Klein, M., Perfus-Barbeoch, L., Frelet, A., Gaedeke, N., Reinhardt, D., Mueller-Roeber, B., Martinoia, E., and Forestier, C. 2002, Plant J., in press.
125. Veenhoff, L.M., Heuberger, E.H., and Poolman, B. 2002, Trends Biochem. Sci., 27, 242.
126. Stagljar, I., Korostensky, C., Johnsson, N., and te, H.S. 1998, Proc. Natl. Acad. Sci. U. S. A, 95, 5187.
127. Reinders, A., Schulze, W., Kuhn, C., Barker, L., Schulz, A., Ward, J.M., and Frommer, W.B. 2002, Plant Cell, 14, 1567.
128. Ehrhardt, T., Zimmermann, S., and Mueller-Roeber, B. 1997, FEBS Lett., 409, 166.
129. Daniels, M.J., Chrispeels, M.J., and Yeager, M. 1999, J. Mol. Biol., 294, 1337.
130. Hamill, S., Cloherty, E.K., and Carruthers, A. 1999, Biochemistry, 38, 16974.
131. Daram, P., Urbach, S., Gaymard, F., Sentenac, H., and Cherel, I. 1997, EMBO J., 16, 3455.
132. Urbach, S., Cherel, I., Sentenac, H., and Gaymard, F. 2000, Plant J., 23, 527.
133. Dreyer, I., Antunes, S., Hoshi, T., Mueller-Roeber, B., Palme, K., Pongs, O., Reintanz, B., and Hedrich, R. 1997, Biophys. J., 72, 2143.
134. Bruggemann, L., Dietrich, P., Dreyer, I., and Hedrich, R. 1999, Planta, 207, 370.
135. Zimmermann, S., Hartje, S., Ehrhardt, T., Plesch, G., and Mueller-Roeber, B. 2001, Plant J., 28, 517.
136. Pilot, G., Lacombe, B., Gaymard, F., Cherel, I., Boucherez, J., Thibaud, J.B., and Sentenac, H. 2001, J. Biol. Chem., 276, 3215.
137. Blatt, M.R. 1992, J. Gen. Physiol, 99, 615.
138. Hedrich, R., Moran, O., Conti, F., Busch, H., Becker, D., Gambale, F., Dreyer, I., Kuch, A., Neuwinger, K., and Palme, K. 1995, Eur. Biophys. J., 24, 107.
139. Mueller-Roeber, B., Ellenberg, J., Provart, N., Willmitzer, L., Busch, H., Becker, D., Dietrich, P., Hoth, S., and Hedrich, R. 1995, EMBO J., 14, 2409.
140. Ilan, N., Schwartz, A., and Moran, N. 1996, J. Membr. Biol., 154, 169.
141. Schroeder, J.I., and Hagiwara, S. 1989, Nature, 338, 427.
142. Maurel, C., Kado, R.T., Guern, J., and Chrispeels, M.J. 1995, EMBO J., 14, 3028.
143. Thiel, G., and Blatt, M.R. 1994, Plant J., 5, 727.
144. Luan, S., Li, W.W., Rusnak, F., Assmann, S.M., and Schreiber, S.L. 1993, Proc. Natl. Acad. Sci. U. S. A, 90, 2202.
145. Schmidt, C., Schelle, I., Liao, Y.J., and Schroeder, J.I. 1995, Proc. Natl. Acad. Sci. U. S. A, 92, 9535.
146. Cao, Y., Ward, J.M., Kelly, W.B., Ichida, A.M., Gaber, R.F., Anderson, J.A., Uozumi, N., Schroeder, J.I., and Crawford, N.M. 1995, Plant Physiol, 109, 1093.
147. Ketchum, K.A., and Slayman, C.W. 1996, FEBS Lett., 378, 19.
148. Lacombe, B., Pilot, G., Michard, E., Gaymard, F., Sentenac, H., and Thibaud, J.B. 2000, Plant Cell, 12, 837.
149. Marten, I., Hoth, S., Deeken, R., Ache, P., Ketchum, K.A., Hoshi, T., and Hedrich, R. 1999, Proc. Natl. Acad. Sci. U. S. A, 96, 7581.
150. Dreyer, I., Michard, E., Lacombe, B., and Thibaud, J.B. 2001, FEBS Lett., 505, 233.
151. Cherel, I., Michard, E., Platet, N., Mouline, K., Alcon, C., Sentenac, H., and Thibaud, J.B. 2002, Plant Cell, 14, 1133.
152. Vranova, E., Tahtiharju, S., Sriprang, R., Willekens, H., Heino, P., Palva, E.T., Inze, D., and Van Camp, W. 2001, J. Exp. Bot., 52, 181.
153. Li, J.X., Lee, Y.R.J., and Assmann, S.M. 1998, Plant Physiol, 116, 785.
154. Mori, I.C., Uozumi, N., and Muto, S. 2000, Plant Cell Physiol, 41, 850.
155. Tang, X.D., and Hoshi, T. 1999, Biophys. J., 76, 3089.
156. Li, J., Wang, X.Q., Watson, M.B., and Assmann, S.M. 2000, Science, 287, 300.
157. Tomita, M. 2001, Trends Biotechnol., 19, 205.

⇒ zurück zur Übersicht

2004

Dreyer, Mueller-Roeber, Koehler

Voltage-gated ion channels.

In: *Membrane Transport in Plants.*
Blatt M.R. (ed). pp 150-192. Oxford, Blackwell.

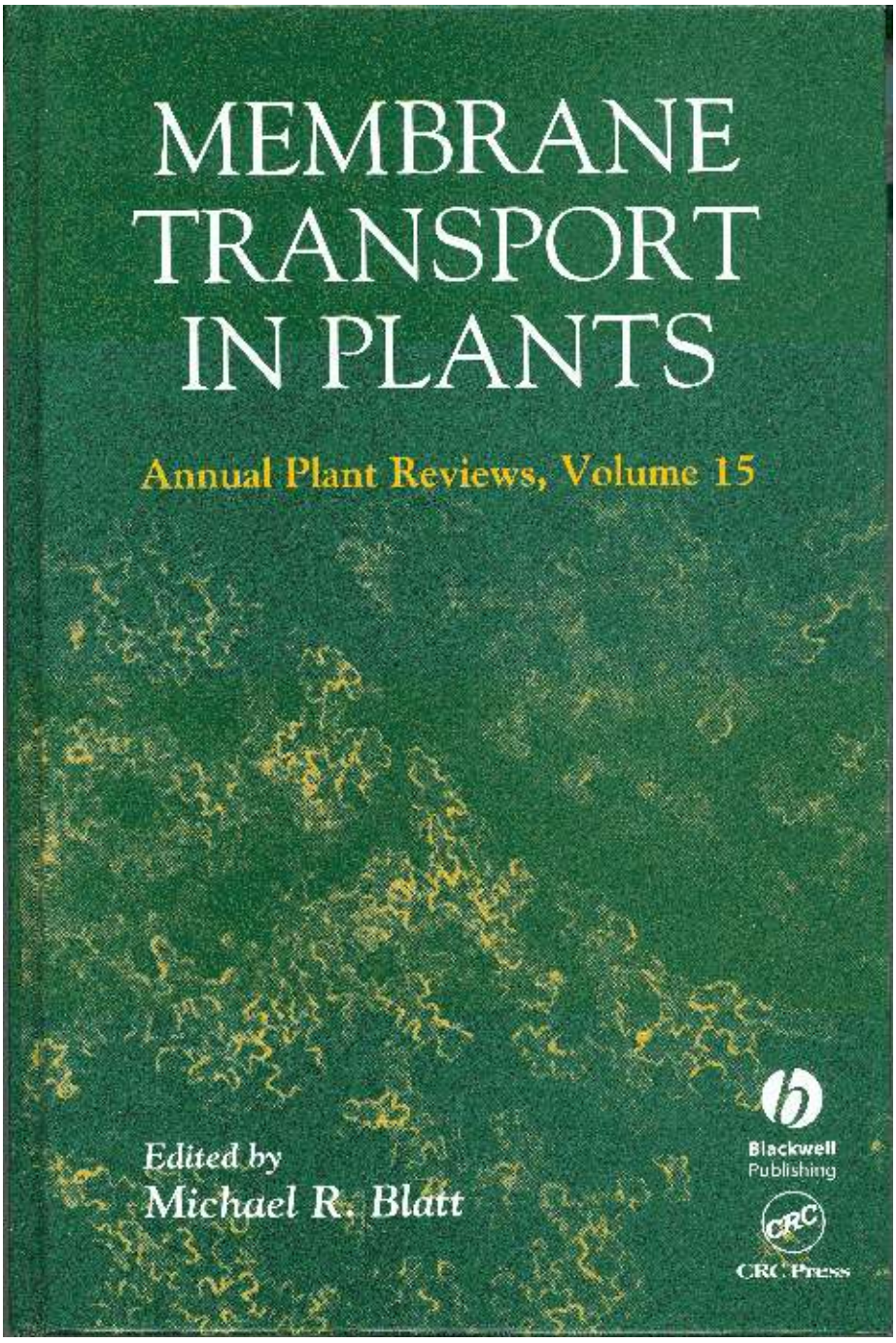

Chapter 6. Voltage-gated ion channels

Ingo Dreyer, Bernd Müller-Röber and Barbara Köhler

Universität Potsdam, Institut für Biochemie und Biologie, Golm, Germany

6 Voltage-gated ion channels

Ingo Dreyer, Bernd Mueller-Roeber and Barbara Köhler

6.1 Introduction

Voltage-regulated ion channels represent one (of several) type(s) of plant transport proteins. The similarity of voltage-gated ion channels found in prokaryotes and eukaryotes suggests that the basic structures responsible for voltage-regulated transmembrane ion transport have evolved more than 2 billion years ago. These similarities facilitated the investigation of plant ion channels. Indeed, in several cases, the knowledge obtained for channels from the different kingdoms served as a good basis for the understanding of the biological role of a plant ion channel. For example, plant potassium channels show the same selectivity filter, i.e. the structural entity that determines the selectivity, as animal K^+ channels (see below), and also in their overall topology they are similar. Considered in more detail, however, a number of plant-specific features show divergent patterns in structure and function. Before this chapter portrays voltage-gated ion channels identified in plants (see section 6.3), some basic structural and mechanistic aspects of voltage-gated ion channels are presented.

A voltage-gated ion channel can be defined as a membrane-spanning protein (i) that facilitates the passive passage of a certain species of ions, and (ii) the activity of which is controlled by the transmembrane voltage. In the following, aspects of this definition will be illustrated exemplarily on the basis of potassium channels since for this channel type most knowledge is available. Fig. 6.1 shows schematically the topology of a plant K^+ channel of the Shaker-type (Uozumi *et al.*, 1998). This channel is a tetramer composed of four subunits. Each subunit consists of six transmembrane-spanning domains (S1–S6) and a loop between the fifth and sixth domain (Fig. 6.1A). The loops of the four subunits together form a central rigid pore (P), which allows the passage of K^+ ions across the membrane (Fig. 6.1B). Usually the pore shows a high selectivity supporting the permeation of a single-ion species (here K^+ ions) along its electrochemical gradient while excluding others from transmembrane passage even when they are chemically related (e.g. Na^+ ions). The selectivity of the channel is determined by the structure of the pore and the chemical properties of the amino acid side chains facing it (Fig. 6.1C; Doyle *et al.*, 1998). Changes in the P-loop of the plant K^+ channel KAT1 by site-directed mutagenesis, for example, caused strong alterations of the selectivity of this channel (Uozumi *et al.*, 1995; Becker *et al.*, 1996; Nakamura *et al.*, 1997; Dreyer *et al.*, 1998).

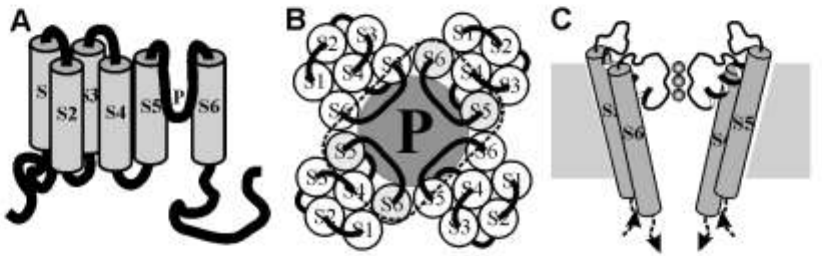

Fig. 6.1 Structure of a voltage-gated potassium channel. Potassium channels are multimeric proteins comprising four α-subunits. (A) Each subunit is built of six transmembrane domains (S1–S6) and an amphiphilic linker (P) between S5 and S6. (B) The four subunits assemble in a way that the P domains create a pore in the membrane. Here displayed in a top view. (C) Parts of the four P domains line the ion permeation pathway and determine the selectivity of the channel. Here only the S5–P–S6 segments of two subunits are displayed.

Thus, in a first simple sketch, an ion channel can be considered as a selective hole in a membrane. This hole *per se* would not be of essential benefit for a cell since it only facilitates the passage of a specific ion species along its electrochemical gradient but does not restrain this flow. To control the flux through an ion channel, mechanisms evolved that regulate the activity of the channel, i.e., those that close and open it. In most of these cases, energy from mechanical tension, the binding of a ligand, or the transmembrane voltage is used to cause conformational changes of the channel protein, which in turn result in blocking or opening of the selective permeation pathway.

6.2 Voltage gating from a mechanistic point of view

Concepts describing voltage-gated membrane conductivity were already developed before the existence of ion channels had been proven. The first model, describing selective voltage-dependent changes of the membrane permeability for different ion species, postulated the regulation of ion flux by so-called gating particles (Hodgkin & Huxley, 1952; honoured with the Nobel Prize in 1963). During the last half century, the original gating concept has been modified and refined. In particular, the cloning of channel genes in the course of the molecular revolution, e.g., the first cloning of a gene coding for a voltage-dependent ion channel (Noda *et al.*, 1984), gave an identity to structural elements of channel proteins involved in the gating process. The huge efforts in this field and the increasing knowledge were crowned recently by the publication of the first X-ray structure of a voltage-dependent K^+ channel (Jiang *et al.*, 2003). R. MacKinnon and P. Agre were honoured with the Nobel Prize in 2003 for their new molecular insights into channel structures enabled by employing crystallographic techniques.

The activity of ion channels can be modulated by the membrane voltage in two ways: indirectly/passively or directly/actively. In the first case, particles (e.g. charged molecules like Mg^{2+}) enter the pathway and obstruct the pore. This is identical to a voltage-dependent block of the permeation pathway. In the second case (voltage gating), the channel protein itself senses the transmembrane electrical gradient and undergoes conformational changes. In the case of voltage-dependent K^+ channels, for example, one part of the channel (the S4 segment containing a high density of charged amino acid residues) is affected by the transmembrane voltage and is displaced some distance across the electrical gradient. This movement of the voltage sensor in turn provokes structural rearrangements of the entire protein, resulting in channel opening or closing of the permeation pathway (Fig. 6.2).

The consequences of the conformational changes of an ion channel protein for its permeation properties were monitored in detail for the first time with the patch-clamp technique (Neher & Sakmann, 1976; honoured with the Nobel Price in 1991). As illustrated in Fig. 6.3A, an ion channel opens (O) and closes (C) in a stochastic manner. The process of opening and closing proceeds on a timescale that is beyond the experimental resolution of the patch-clamp technique. If we consider a single type of ion channel, each opening of the ion channel results in a current flux of the same amplitude. Under constant environmental conditions, the current flowing through the open channel is constant. The size of the single-channel current amplitude depends on the channel type and on two parameters: the electrical gradient, which influences the movement of the charged ions, and the composition of the extracellular and intracellular solutions, reflecting mainly the chemical gradient of the permeating ion. The voltage dependence of the single-channel amplitude is more or less linear when physiological voltages are applied. Its slope defines the single-channel conductance, which depends strongly on the structure of the permeation pathway, and which is therefore an intrinsic property of the ion channel type.

A living cell does not express a single-ion channel of one type, but instead, an ensemble of channels. In guard cells, for example, 600–2500 potassium uptake

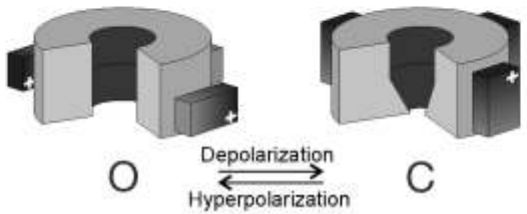

Fig. 6.2 A principle mechanism of voltage gating. Special parts of the channel protein that are characterised by a high density of charged amino acids (indicated as '+') are able to sense the transmembrane voltage. Upon changes in the electrical gradient, these parts move a bit and force the ion channel to undergo conformational changes, which in turn open or close the ion permeation pathway. Here the gating of inward-rectifying plant potassium channels is represented, postulated on the basis of the X-ray structure of a bacterial voltage-gated potassium channel (Jiang *et al.*, 2003).

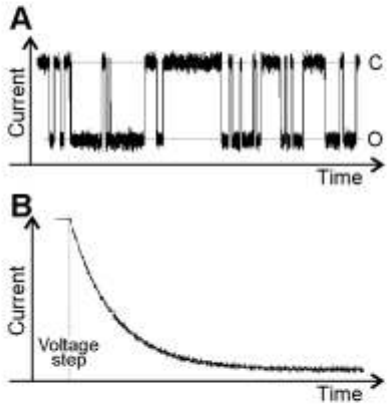

Fig. 6.3 Stochastic opening of single channels and kinetics of a channel ensemble. (A) A single channel opens (current level O) and closes (current level C) in a stochastic manner. The current amplitude is a constant that depends on the channel type, the ionic composition at both sides of the membrane and the membrane voltage. (B) An ensemble of several channels activate with a characteristic kinetics upon changes of the membrane voltage.

channels were detected (Dietrich *et al.*, 1998). The coordinated action of such a channel ensemble differs strongly from the behaviour of a single channel (Fig. 6.3B). Kinetic components are easily visible upon changes of the membrane voltage.

To comprehend the biological function of ion channels, it is useful to illustrate their behaviour with the help of biophysical/mathematical models. At a membrane voltage E and at time point t, the current flowing through an ensemble of channels, $I(E, t)$, can be described mathematically by the equation

$$I(E, t) = N\, i(E) p_O(E, t) \tag{6.1}$$

where $i(E)$ is the current flowing through a single channel and $p_O(E, t)$ the time- and voltage-dependent open probability, which is defined by the quotient N_O/N, i.e., the number of open channels (N_O) divided by the total number of channels (N). Equation 6.1 is fundamental to describe the dynamic behaviour of ion channels and to analyse their elementary properties. In the following we will provide some more mathematical background in order to fill this equation with life. To reduce the degree of complexity, a simplified channel will be considered that exists in only two conformations (Fig. 6.4), with the pore either open (O) or closed (C). Like an enzyme, the channel in the two configurations can be represented by two distinct levels of free energy: G_O and G_C. For a conformational change (O → C, or C → O), the channel has to overcome an energy peak, represented by the energy level G_P. Thus, the activation of the channel (C → O) is impeded by the energy barrier $\Delta G_{PC} = G_P - G_C$, and the deactivation (O → C) by the barrier $\Delta G_{PO} = G_P - G_O$.

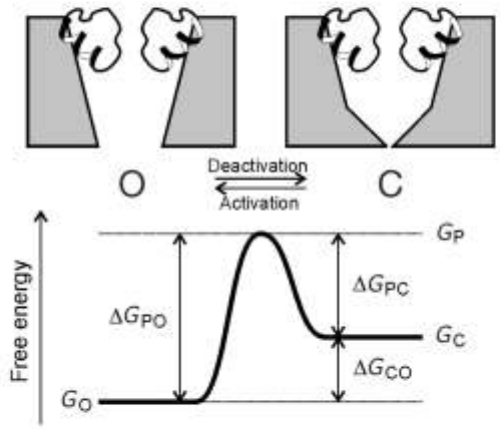

Fig. 6.4 An idealistic two-state model to illustrate ion channel gating. A simplified ion channel can exist in two states: open and closed. The two states correspond to two distinct conformations that differ in their free intrinsic energy (G_O and G_C). For a conformational change (activation or deactivation) the energy barrier (G_P) has to be overcome.

6.2.1 *Static – steady-state equilibrium*

The energy levels G_O, G_C and G_P depend on the surrounding conditions, e.g., the transmembrane voltage in the case of voltage-gated ion channels. Therefore, a frequently used experimental approach is to keep as many parameters as possible constant (e.g., clamp the voltage to a constant level) and allow the channels to relax into a steady-state equilibrium. Under this condition the probability of finding the channel in the open ($p_{O\infty}$) or in the closed ($p_{C\infty}$) configuration follows the Boltzmann statistics: $p_{C\infty}/p_{O\infty} = \exp(-(G_C - G_O)/(kT))$. Here, k denotes the Boltzmann constant and T the absolute temperature. Taking into account that $p_{O\infty} + p_{C\infty} = 1$, i.e., the probability to find the channel either in the open or in the closed state is 1, the open probability can be directly correlated with the energy difference between the open and the closed state ($\Delta G_{CO} = G_C - G_O$):

$$p_{O\infty} = \frac{1}{1 + e^{-\Delta G_{CO}/kT}} \tag{6.2}$$

As indicated above, in voltage-gated ion channels the free energy of the different configurations depends on the transmembrane voltage E. Detailed studies on the animal Shaker channel have shown that in the physiological voltage range this dependency can be expressed by a linear function (Perozo *et al.*, 1993): $G(E) = G(0) + E \cdot q$. (Mathematically, this is the first-order Taylor approximation of the function $G(E)$ (Stevens, 1978): $G(E) = G(0) + E\ \mathrm{d/d}E[G(E)]|_{E=0} + 0(E^2)$. Higher order terms do not significantly contribute to the free energy.) This implies

a voltage dependence of the open probability of the channel:

$$p_{O\infty}(E) = \frac{1}{1 + e^{-(QE + \Delta G_{CO}(0))/(kT)}} = \frac{1}{1 + e^{-Q(E - E_{1/2})/(kT)}} \tag{6.3}$$

with $\Delta G_{CO}(0) = G_C(0) - G_O(0)$ and $E_{1/2} = -\Delta G_{CO}(0)/Q$, the half-maximal activation voltage ($p_{O\infty}(E_{1/2}) = 0.5$). The parameter Q ($= q_C - q_O$) is often called the (apparent) gating charge and is correlated to the (fractional) charge movement of the channel voltage sensor. The so-called Boltzmann equation (Equation 6.3) describes (in the steady state) the mean behaviour of a single channel observed over a long period of time, or the mean behaviour of a channel ensemble in equilibrium at one time point. As shown in Fig. 6.5, the Boltzmann equation describes hyperpolarisation-activated channels when $Q < 0$ and depolarisation-activated channels when $Q > 0$. The parameter $\Delta G_{CO}(0)$ (ΔG_a, ΔG_b, ΔG_c and ΔG_d in Fig. 6.5) is a measure for the activity range of the ion channel. Several physiologically relevant channel-modulatory mechanisms influence this parameter and therefore change the activity range of the channel. We may exemplarily consider the binding of a signalling molecule (ligand) to the ion channel. The ligand binding alters the stability of the different channel conformations. Thus the parameters $G_C(0)$, $G_O(0)$ and hence $\Delta G_{CO}(0)$ change. This value can become larger (Fig. 6.5, $\Delta G_b \rightarrow \Delta G_a$), which results in channel stimulation, or it can become smaller (even negative), which causes an inhibition (Fig. 6.5, $\Delta G_b \rightarrow \Delta G_c$). Therefore, analyses using the Boltzmann equation allow a first biophysical categorisation of the observed channel and its modulation, which often is a prerequisite for assigning a biological function to this protein.

6.2.2 *Kinetic – relaxation into an equilibrium*

In the previous paragraph the idealised channel was considered in thermal equilibrium. Additional characteristic information on the channel can be obtained by

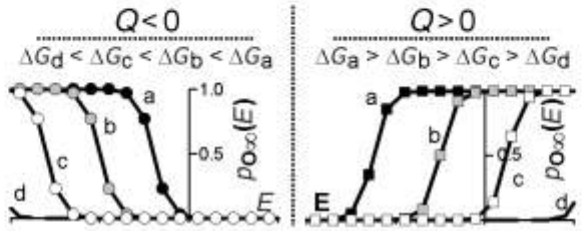

Fig. 6.5 Illustration of the Boltzmann equation. The Boltzmann equation describes the voltage dependence of the open probability of an ion channel in thermal equilibrium [$p_{O\infty}(E)$]. The graphical representation of the Boltzmann equation varies depending on the parameters Q (gating charge) and ΔG (difference in the free energy between open and closed state). Eight different $p_{O\infty}(E)$ curves ($Q > 0$, a–d; $Q < 0$, a–d) for eight Q-ΔG parameter sets are displayed.

analysing *transitions* between different equilibriums. Just by changing the environmental circumstances, e.g., in voltage-step protocols, the equilibrium conditions of the channels can be altered almost instantaneously. Upon such a change of the experimental condition, the channels relax more or less slowly into the new equilibrium. Experimentally, this relaxation kinetics is difficult to analyse on a single, isolated channel. Instead, in most cases the mean behaviour of an ensemble of many channels is studied. The experimentally observed relaxation kinetics can be described by an (or a sum of) exponential function(s). The reason why this is the general case will be illustrated again on the basis of the idealised two-state model (Fig. 6.4). A transition of a channel from the closed to the open state (activation) depends on the energy barrier ΔG_{PC} ($= G_P - G_C$), and a transition from the open to the closed state (deactivation) on the barrier ΔG_{PO} ($= G_P - G_O$). The corresponding transition rates, k_a and k_d, can be expressed according to the Eyring rate theory (Glasstone *et al.*, 1941), which is based on quantum mechanics, as:

$$k_a = kT/h e^{-\Delta G_{PC}/(kT)} \tag{6.4}$$

$$k_d = kT/h e^{-\Delta G_{PO}/(kT)} \tag{6.5}$$

With these transition rates, the changes of the open (dp_O) and closed probability (dp_C) of the channel in the small time interval dt are calculated as

$$\left.\begin{aligned} dp_O &= (-k_d p_O + k_a p_C)\, dt \\ dp_C &= (k_d p_O - k_a p_C)\, dt \end{aligned}\right\} \tag{6.6}$$

This system of differential equations determines the dynamic behaviour of the channel. Under certain conditions, e.g., when the voltage-dependent parameters k_a and k_d are kept constant, an analytic solution for the time course of the relaxation of the channel ensemble into a new equilibrium can be deduced:

$$p_O(t) = p_{O\infty} + (p_O(0) - p_{O\infty})\, e^{-\lambda t} \tag{6.7}$$

Here $p_{O\infty} = 1/(1 + k_d/k_a) = 1/(1 + \exp(-(G_C - G_O)/(kT)))$ is the open probability in thermal equilibrium (compare Equation 6.2), $\lambda = k_a + k_d$ the characteristic (voltage-dependent) time constant of the channel, and $p_O(0)$ the open probability at $t = 0$ (e.g., at the time of the voltage step). Since the measured current mediated by the channel ensemble is proportional to the open probability, the current amplitude is expected to relax in an exponential manner. From the analysis of the decay constant λ, further insights into the energetic properties of the ion channel protein can be obtained. Fig. 6.6 illustrates the consequences of a change in the free energy of the peak, G_P. While the steady-state characteristics remain unaffected, the higher the peak energy is, the smaller is the rate of channel activation and deactivation. Such a

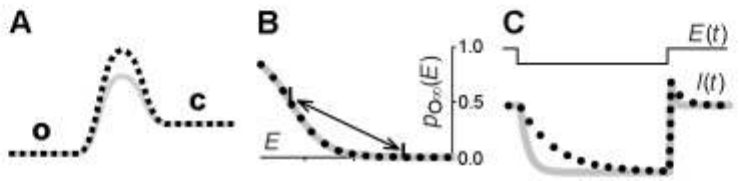

Fig. 6.6 Changes in the peak energy (A) do not affect open probability (B) but alter channel kinetics (C). For the simplified two-state model, the predictions for a higher free peak energy G_P (*dotted lines*) were compared with those for a lower free peak energy (*grey lines*).

difference in the peak energy can explain the variation observed in the kinetics between the two guard-cell-expressed K^+ channels KAT1 and KST1 (Mueller-Roeber *et al.*, 1995; Dietrich *et al.*, 1998). In comparison to KAT1, KST1 relaxes more slowly into equilibrium. Both channels exhibit, however, similar steady-state open probabilities. At this point an important aspect should be emphasised: slower relaxation kinetics does not mean that a single channel opens or closes more slowly. A single channel is still gating rapidly in a stochastic manner (Fig. 6.3A). Instead, slower relaxation kinetics means that the ensemble of channels relaxes more slowly into the new equilibrium because the number of transitions (O → C, or C → O) is smaller.

6.2.3 *Comparison of the model with the* in vivo *situation*

In vivo, an ion channel can exist in more than two configurations, adding to the complexity of the mathematics presented above (see Colquhoun & Hawkes, 1995). However, even if an ion channel can exist in more than two stable conformations, in general only one open state is observed and multiple closed states are manifested indirectly through kinetic relaxations with several time constants λ_i. In this case the open probability at equilibrium is described by

$$p_{O\infty} = \frac{1}{1 + \sum_i e^{-\Delta G_{iO}/(kT)}} \tag{6.8}$$

where ΔG_{iO} is the difference in the free energy between the ith closed state and the open state.

In most cases, however, it is sufficient to describe an ion channel by a two-state model to explain qualitatively the observed effects and to get a good idea about their biological relevance. This is the reason why in a large number of publications the Boltzmann function is used instead of a more precise, but also more complex function as exemplified by Equation 6.8. An interesting comparison between several alternative models for a plant channel *in vivo* is discussed in Blatt and Gradmann (1997).

6.3 Voltage-gated ion channels uncovered in plants and their involvements in physiological processes

In 1976, the patch-clamp technique allowed for the first time to monitor the action of a single transporter molecule in denervated frog muscle fibres (Neher & Sakmann, 1976). Two years later, a similar technique was employed to document single voltage-gated ion channels in the plasma membrane of the alga *Nitellopsis obtusa* (Krawczyk, 1978), and in 1984 the first single-channel recordings from angiosperms were reported (Moran *et al.*, 1984; Schroeder *et al.*, 1984). Combined use of diverse electrophysiological techniques (see Chapter 1) has since increased tremendously our knowledge of plant transport systems and especially of plant ion channels. The following presentation categorises the different types of channels in a more general way in terms of subcellular localisation, selectivity and voltage-regulation. In most of the cases, this classification already allows to illustrate the physiological function of a channel, independent of its exact spatial expression pattern at the tissue level. In this review we will refer to the membrane voltage according to the convention $E = \varphi_{\text{cytosol}} - \varphi_{\text{lumen}}$ (Bertl *et al.*, 1992). Here, φ_{cytosol} and φ_{lumen} denote the electrical potentials in the cytosol and the lumen (e.g., vacuole or extracellular space), respectively. This convention unifies currents and flux directions with respect to the cytosol. For example, a negative current of cations denotes an influx of these ions into the cytosol, independent of whether the ions come from the extracellular space (across the plasma membrane) or from endocellular compartments.

6.3.1 *Plasma membrane potassium channels*

Potassium is the most abundant cation in plants and is involved in many physiological processes. Therefore, it is not unexpected that the first single-ion channels recorded from a land plant were voltage-gated potassium channels (Schroeder *et al.*, 1984). Potassium channels have been identified in every living tissue and cell type investigated, including mesophyll cells, root cells, xylem parenchyma cells, pollen, coleoptiles, and, notably, guard cells. Voltage-gated potassium channels are involved in membrane voltage control, in osmotically driven movements, in cytosolic volume control, in cation nutrition and in K^+ redistribution at the intracellular-, tissue- and the whole plant-level (see Maathuis *et al.*, 1997, and Chapter 11). The categorisation as 'potassium channels' is based on the strong selectivity of these channels for K^+ against, e.g., Na^+. In the plasma membrane of plant cells, three distinct types of voltage-gated potassium channels were identified, which are active in different voltage ranges: hyperpolarisation-activated, depolarisation-activated, and weakly rectifying K^+ channels (see Very & Sentenac, 2002, 2003, for recent reviews).

6.3.1.1 *Hyperpolarisation-activated K^+ channels – K_{in} channels*

Hyperpolarisation-activated K^+ channels (K_{in} channels) open at membrane voltages more negative (cytosol) than around –100 mV, whereas at more positive voltages they are closed (Fig. 6.7A; Schroeder *et al.*, 1987; Blatt, 1992). In terms of the Boltzmann

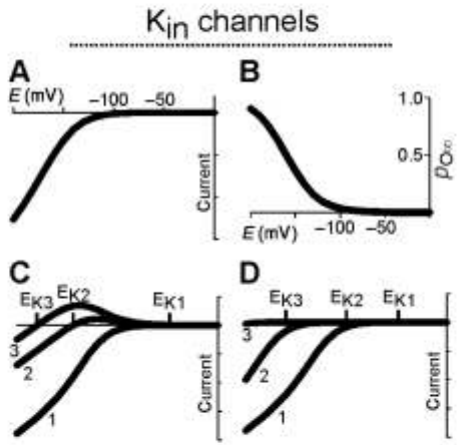

Fig. 6.7 Characteristics of K_{in} channels. (A) Current–voltage characteristics in the steady state. (B) The corresponding open probability in thermal equilibrium. (C and D) Two types of K_{in} channels have been reported: (C) One type does not sense the K^+ concentration, activates also positive of E_K , and thus mediates at certain voltages potassium efflux as well (Bruggemann *et al.* , 1999). (D) The other type senses the extracellular potassium concentration and activates only negative of E_K , the equilibrium potential for potassium (Maathuis & Sanders, 1995). Curves representing three different extracellular potassium concentrations (1–3) are displayed.

equation (Equation 6.3), this is equivalent to $Q < 0$ (Fig. 6.7B). Because of this activity range, K_{in} channels serve as potassium-uptake channels. They equip plant cells with the ability to accumulate high amounts of potassium in a reasonably short time. The driving force for potassium uptake is provided by the negative membrane voltage established by the activity of the H^+-ATPase that pumps H^+ ions out of the cell. Well-known examples for hyperpolarisation-activated potassium channels are guard-cell potassium-uptake channels playing a role in stomatal movement (Dietrich *et al.*, 1998), or root K_{in} channels playing a role in potassium uptake from the soil (Maathuis & Sanders, 1995). In general, hyperpolarisation-activated potassium channels show slow activation kinetics upon voltage steps (Equation 6.7; $1/\lambda$ is in the range of hundreds of milliseconds to seconds), and do not inactivate even under sustained hyperpolarisation (Schroeder, 1988). A characteristic fingerprint for this channel type is the activation upon extracellular acidification and the block by extracellular Cs^+, Ba^{2+}, and tetraethylammonium (TEA^+).

The first K^+ channel genes from plants were cloned in 1992 by two groups independently. cDNA libraries from *Arabidopsis thaliana* were expressed in mutant strains of the yeast *Saccharomyces cerevisiae*, lacking the endogenous potassium-uptake transport systems and, hence, unable to grow on media containing less than 1 mM K^+. Screening on low-K^+ media identified two cDNA clones that complemented this deficiency. These clones encoded the two K_{in} channels AKT1 and KAT1, which both belong to the Shaker family of K^+ channels (Anderson *et al.*,

1992; Sentenac *et al.*, 1992). We know now that the genome of *Arabidopsis thaliana* contains at least four genes (*KAT1*, *AKT1*, *KAT2*, *SPIK*) coding for potassium-uptake channels (Very & Sentenac, 2002). *KAT1* and *KAT2* are mainly expressed in guard cells (Nakamura *et al.*, 1995; Pilot *et al.*, 2001; Szyroki *et al.*, 2001), *SPIK* in pollen grains (Mouline *et al.*, 2002) and *AKT1* in roots (Lagarde *et al.*, 1996). The function of a fifth putative K_{in} channel encoded by the gene *AKT6* is still to be proven. Additionally, a sixth K_{in}-related gene has been identified (*AtKC1*), which shows an expression pattern similar to that of AKT1 (Reintanz *et al.*, 2002). *AtKC1* appears not to be functional alone, but rather to modulate the current carried by other K^+ channels (Dreyer *et al.*, 1997; Reintanz *et al.*, 2002).

Experiments employing heterologous expression systems and biochemical studies revealed that K_{in} channels are multimeric proteins consisting of four α-subunits (Daram *et al.*, 1997; Dreyer *et al.*, 1997). This result and fundamental pharmacological differences, observed e.g., between guard-cell potassium-uptake channels *in vivo* and their putative molecular counterparts, led to the model that *in planta* hyperpolarisation-activated potassium channels are (at least in part) heteromultimeric proteins (Dreyer *et al.*, 1997; Bruggemann *et al.*, 1999b; Pilot *et al.*, 2001).

6.3.1.2 *Depolarisation-activated K^+ channels – K_{out} channels*

Depolarisation-activated K^+ channels (K_{out} channels) open at membrane voltages more positive than the equilibrium potential for potassium, E_K. At more negative voltages they are closed (Fig. 6.8A). In terms of the Boltzmann equation (Equation 6.3), this is equivalent to $Q > 0$ (Fig. 6.8B; Blatt, 1988; Hosoi *et al.*, 1988; Schroeder, 1988). To guarantee that the channel is closed at voltages negative of E_K, its activation threshold varies with the extracellular potassium concentration (Fig. 6.8; see Section 6.4.5 for details). Because of their activity range, K_{out} channels serve as potassium release channels. In general, depolarisation-activated potassium channels exhibit slow delayed activation kinetics upon voltage-steps (Equation 6.7; $1/\lambda$ is in the range of hundreds of milliseconds to seconds), and do not inactivate even under sustained depolarisation (Schroeder, 1988). A characteristic fingerprint

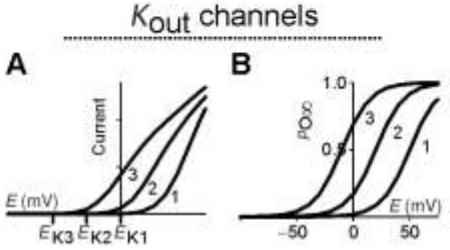

Fig. 6.8 Characteristics of K_{out} channels. (A) Current–voltage characteristics in the steady state. (B) The corresponding open probability in thermal equilibrium. K_{out} channels sense the extracellular potassium concentration. Curves representing three different extracellular potassium concentrations (1–3) are displayed.

for this channel type is the activation upon extracellular alkalinisation and the block by extracellular Ba^{2+} (Schroeder *et al.*, 1987).

The first gene coding for a plant K_{out} channel was cloned on the basis of sequence homologies to K_{in} channel genes. A DNA-based strategy, employed to identify further proteins belonging to the Shaker K^+ channel family, resulted in the identification of SKOR, which turned out to be a potassium release channel (Gaymard *et al.*, 1998). In total, the genome of *Arabidopsis thaliana* contains two genes coding for potassium release channels of the Shaker type: SKOR and GORK (Gaymard *et al.*, 1998; Ache *et al.*, 2000). For these two genes the expression patterns have been determined, and null-allele mutants of *Arabidopsis* have been investigated. SKOR has been proposed to play a major role in K^+ release from the stelar parenchyma into the xylem and therefore in the transport of potassium from roots towards shoots (Gaymard *et al.*, 1998). GORK is the potassium release channel of guard cells and plays an important role in stomatal closure (Hosy *et al.*, 2003).

6.3.1.3 *Weakly rectifying K^+ channels – K_{weak} channels*

K_{weak} channels belong to the Shaker K^+ channel family. These channels appear to be active in the entire physiological voltage range and thus mediate both, potassium inward and potassium outward fluxes. A characteristic fingerprint of weakly rectifying K^+ channels is the block by extracellular protons and Ca^{2+}. *In vivo*, this channel type has been unambiguously uncovered in protoplasts derived from vascular tissues of maize seedlings (Bauer *et al.*, 2000) and possibly in protoplasts from *Arabidopsis* mesophyll cells (Spalding *et al.*, 1992). Most knowledge, however, was obtained by investigating the cloned molecular counterparts (AKT2, ZmKT2) after expression in heterologous expression systems (Marten *et al.*, 1999; Philippar *et al.*, 1999; Lacombe *et al.*, 2000). As is the case for AKT2 from *Arabidopsis*, K_{weak} channels can act in two different gating modes: while in mode 1, AKT2 activates like a hyperpolarisation-activated K^+ channel, in mode 2 it is open in the entire physiological voltage range (Dreyer *et al.*, 2001; Fig. 6.9). It was proposed, that the setting of the gating mode is determined by the phosphorylation status of the protein. Thus, AKT2 can be switched from an inward-rectifying channel to a leak-like K^+ channel by phosphorylation events (Dreyer *et al.*, 2001; Cherel *et al.*, 2002). At the

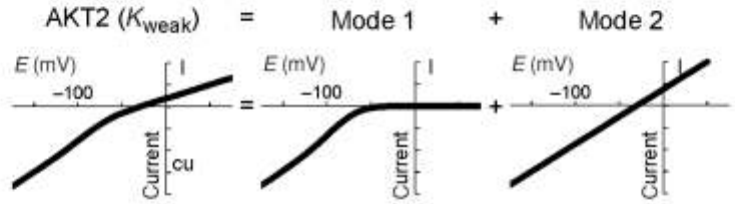

Fig. 6.9 Currents mediated by K_{weak} channels are composed of two components. The K_{weak} channel AKT2 can exist in two gating modes. In mode 1, AKT2 is comparable to K_{in} channels mediating potassium inward currents. In mode 2, AKT2 mediates leak-like potassium currents.

present time, K_{weak} channels are supposed to provide a background conductance that stabilises the membrane voltage, e.g., in phloem loading processes (Ache *et al.*, 2001; Deeken *et al.*, 2002).

6.3.2 *Vacuolar potassium channels*

Vacuoles are storage organelles that typically comprise 90–95% of the cell volume. They play important roles in the osmotic adjustment of plant cells. For example, during unidirectional and reversible turgor-driven processes, like cell elongation or motor cell and guard cell movements, vacuoles accumulate (and release during stomatal closure) the additional osmotically active molecules (e.g. ions). The cytoplasm is mainly only a thoroughfare in these processes. Additionally, vacuoles seem to serve as a buffer for cytosolic potassium. It has been observed that, under conditions of severe K^+ deficiency, the cytosolic potassium level in a variety of plant cells is kept constant at the expense of the vacuolar K^+ pool (Leigh & Wyn Jones, 1984; Walker *et al.*, 1996). In most plant cells, ATP- and PP_i-dependent H^+-pumps generate a small cytosol-negative electrical voltage across the vacuolar membrane (Rea & Sanders, 1987). Therefore, under most conditions vacuolar cation uptake requires active transport (for recent reviews on vacuolar transporters see, e.g., Luttge *et al.*, 2000; Martinoia *et al.*, 2000; Maeshima, 2001; Gaxiola *et al.*, 2002), whereas cation release is proposed to occur via ion channels.

6.3.2.1 *Slow-activating vacuolar channel*

The slow-activating vacuolar (SV) channel was the first tonoplast channel that was characterised (Hedrich & Neher, 1987). The SV channel is ubiquitous in all higher plants tested, and in view of the multitude of factors that regulate this channel, it is likely an essential element in most cells. The SV channel is non-selective for monovalent cations (Kolb *et al.*, 1987; Colombo *et al.*, 1988), and shows significant permeabilities for the divalent cations Ca^{2+}, Ba^{2+} and Mg^{2+} (Pantoja *et al.*, 1992b; Ward & Schroeder, 1994; Allen & Sanders, 1995; Gambale *et al.*, 1996). A replacement of cytosolic Cl^- by gluconate led to an increase of the permeability ratio of Ca^{2+} over Na^+ (Miedema & Pantoja, 2001). The SV channel is blocked by TEA^+, Ba^{2+} and Zn^{2+} (Hedrich & Kurkdjian, 1988). It activates slowly after the application of (cytosol) positive voltages (Fig. 6.5, $Q > 0$) and does not inactivate. However, SV channel activity is strongly modulated. The channels are blocked by luminal Ca^{2+} and cytosolic protons, and are activated by cytosolic Ca^{2+}, calmodulin, cytosolic Mg^{2+} and reducing agents, and are bimodally regulated by phosphorylation (Miedema & Pantoja, 2001; and references therein; for details, see Section 6.4). A putative candidate for the SV channel is the two-pore K^+ channel KCO1, which has been shown to be targeted to the vacuolar membrane (Czempinski *et al.*, 2002). In a *kco1* knockout line of *Arabidopsis*, the current density of SV currents, measured on vacuoles from mesophyll cells, was reduced by a factor of 3 (Schonknecht *et al.*, 2002).

Despite extensive research over the past years, the physiological function of the SV channels is not clear yet. SV channels are usually closed at resting (low) cytosolic Ca^{2+} levels and physiological tonoplast membrane voltages. Because of the activation of SV channels by increasing cytosolic Ca^{2+}, this channel has been proposed to play a role in Ca^{2+}-induced vacuolar Ca^{2+}-release (Ward & Schroeder, 1994) although this concept has been questioned (Pottosin *et al.*, 1997). Recent investigations on SV channels with gating-modulatory effectors, like Mg^{2+} and reducing agents (Carpaneto *et al.*, 1999, 2001; Pei *et al.*, 1999), however, have renewed the discussion of such a role (Bewell *et al.*, 1999).

6.3.2.2 *Fast-activating vacuolar channel*

Fast-activating vacuolar (FV) channels were observed as a second type of vacuolar cation channels (Hedrich & Neher, 1987) that activated without delay by extreme negative or positive voltages. At around (cytosolic) −40 mV, they mainly reside in the closed state (Allen & Sanders, 1996; Tikhonova *et al.*, 1997). In contrast to SV channels, FV channels are active at cytosolic Ca^{2+} levels <100 nM. Therefore, FV channels are proposed to represent the principle passive pathway for cation uptake and release across the vacuolar membrane under resting cytosolic Ca^{2+} conditions. In the sugar beet tonoplast, several fast-activating channels have been characterised with slightly different single-channel amplitudes (Gambale *et al.*, 1996). Thus, it is tempting to speculate that 'the FV channel' in fact comprises a class of several similar but still distinct channels. FV channels poorly select between monovalent cations (Bruggemann *et al.*, 1999c). They are blocked by cytosolic polyamines (Bruggemann *et al.*, 1998), by cytosolic and luminal Mg^{2+} and by luminal Ca^{2+} (Tikhonova *et al.*, 1997; Pei *et al.*, 1999).

6.3.2.3 *Vacuolar K^+ channels*

Vacuolar K^+ (VK) channels have been observed in vacuoles from *Vicia faba* guard cells and *Beta vulgaris* taproots (Ward & Schroeder, 1994; Allen & Sanders, 1996; Pottosin *et al.*, 2003). They are K^+-selective, voltage-independent, and active at cytosolic Ca^{2+} levels greater than 100 nM. The conductance of VK channels is pH-dependent, with an optimum at around pH 6.5.

6.3.3 *Plasma membrane calcium channels*

The importance of Ca^{2+} as a second messenger in response to a number of stimuli and in regulating the growth of 'tip-growing' systems like pollen tubes and root hairs is beyond dispute (Sanders *et al.*, 1999). Activation of plasma membrane calcium channels and resulting Ca^{2+} influx contributes to the observed increase in cytosolic Ca^{2+} concentration. Direct evidence for calcium channels was provided in the mid 1990s (Thuleau *et al.*, 1994b; Gelli & Blumwald, 1997). To date, hyperpolarisation- and depolarisation-activated calcium channels from a number of cell types have been characterised electrophysiologically (see below). Since the cytosolic Ca^{2+} concentration is buffered in the nanomolar range, the equilibrium potential of Ca^{2+}

is positive of zero, so that both types serve as Ca^{2+} influx channels. If charges are not compensated, activation of calcium channels leads to membrane depolarisation.

Calcium channels conduct several divalent ions including Mg^{2+} and Ba^{2+} and are selective for divalent over monovalent ions. This clearly distinguishes them from non-selective ion channels (see Chapter 7), which can also serve as Ca^{2+} entry pathways. Ba^{2+} often permeates even better than Ca^{2+} and is therefore used in experiments. In contrast, non-selective ion channels are inhibited by Ba^{2+}. Another difference is the inhibition of calcium channels by TEA^+ (Gelli & Blumwald, 1997; Pineros & Tester, 1997; Hamilton *et al.*, 2000, 2001; Kiegle *et al.*, 2000; Pei *et al.*, 2000; Very & Davies, 2000; White, 2000). The mechanism of permeation for Ca^{2+} channels is thought to be different from K^+ channels. Selectivity of animal calcium channels is explained by the existence of two specific binding sites for Ca^{2+} in the pore so that Na^+ entry is excluded. Ion permeation occurs by electrostatic repulsion between two Ca^{2+} ions. If there is no Ca^{2+} in the pore, the channel becomes much more permeable to Na^+ (Sather & McCleskey, 2003). Indeed, depolarisation-activated Ca^{2+} channels from plants conduct monovalent ions in the absence of Ca^{2+} (Pineros & Tester, 1997; White, 1998, 2000).

The molecular structure of plant voltage-gated Ca^{2+} channels is still unknown. In *Arabidopsis thaliana*, a homologue to the two-pore channel (TPC1) from rat has been cloned, and indirect evidence has been given that this channel is voltage-dependent and opens with depolarisation (Furuichi *et al.*, 2001). However, a clear correlation between the molecular structure and calcium currents through depolarisation- and hyperpolarisation-activated Ca^{2+} channels is lacking. For an overview about calcium channels and candidate genes, the reader is referred to White (2000) and White *et al.* (2002).

6.3.3.1 *Hyperpolarisation-activated Ca^{2+} channels*

Hyperpolarisation-activated Ca^{2+} channels (HACCs) open at membrane voltages more negative than −100 mV (Fig. 6.10A, HACC; Fig. 6.5, $Q < 0$, ΔG_c). The

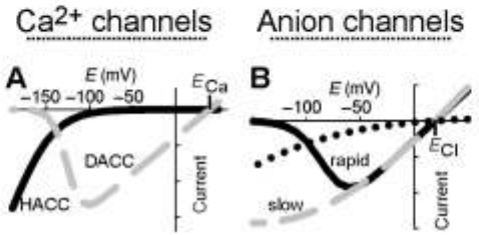

Fig. 6.10 Current–voltage characteristics of plant ion channels in the steady state. (A) Hyperpolarisation-activated (HACC; *solid line*) and depolarisation-activated Ca^{2+} channels (DACC; *grey dashed line*). (B) Rapid-activating anion channels (QUAC, R-type, GCAC1; *rapid*; *solid line*), slow-activating anion channels (SLAC, S-type; *slow*; *grey dashed line*) and inward-rectifying anion channels (*dotted line*).

first HACC was described in tomato (Gelli & Blumwald, 1997). Reports from hyperpolarisation-activated calcium channels in roots, guard cells and mesophyll cells followed (Hamilton *et al.*, 2000, 2001; Kiegle *et al.*, 2000; Pei *et al.*, 2000; Very & Davies, 2000; Stoelzle *et al.*, 2003). The hyperpolarisation-activated Ca^{2+} channels characterised so far are similar with respect to activation threshold, kinetics, selectivity and pharmacology. It is striking that although at negative voltages the open probability is largest, the absolute values remain low. This suggests a strong regulation preventing huge Ca^{2+} influx. Indeed, open probability is suppressed by elevated Ca^{2+} inside (Hamilton *et al.*, 2000, 2001) and is increased dramatically by various stimuli like ABA (abscisic acid), H_2O_2, elicitors and blue light (Gelli *et al.*, 1997; Hamilton *et al.*, 2000; Pei *et al.*, 2000; Klusener *et al.*, 2002; Stoelzle *et al.*, 2003). Activation comes along with a shift in the activation threshold towards more positive potentials (see Section 6.4). HACC activation and deactivation kinetics are fast. Mean open times are in the range of milliseconds (Hamilton *et al.*, 2001).

HACCs are involved in Ca^{2+} signalling. The observation in fluorescence-based imaging experiments under voltage control, that a hyperpolarisation-activated Ca^{2+} influx (not a depolarisation-activated one) was important in ABA signalling (Grabov & Blatt, 1998b) and the later identification of such a channel which is activated by ABA (Hamilton *et al.*, 2000; see Section 6.4.7), highlights its role in ABA-mediated cytosolic Ca^{2+} increase. HACC from guard cells is a target for several stimuli like phytohormones and elicitors (Hamilton *et al.*, 2000; Pei *et al.*, 2000; Klusener *et al.*, 2002) and might serve as a focal point, integrating signal transduction pathways and, thus, linking them to membrane voltage (Blatt, 2000b). HACCs also are well suited for nutritive Ca^{2+} uptake. They could maintain a sustained Ca^{2+}, Mg^{2+} and Mn^{2+} influx, provided the charge is compensated for. The voltage sensitivity of HACCs and the H^+-pump can ensure an effective 'clamp' at hyperpolarisation, preventing a depolarisation of the membrane potential, which in turn would lead to deactivation of HACCs (Miedema *et al.*, 2001). This mechanism is likely in root hairs, where tip growth is associated with an apex-high cytosolic-free calcium gradient generated by a local Ca^{2+} influx (Very & Davies, 2000).

6.3.3.2 *Depolarisation-activated Ca^{2+} channels*

Depolarisation-activated calcium channels (DACCs) have been characterised from suspension cells, mesophyll cells and root cells (Thuleau *et al.*, 1994a,b; Pineros & Tester, 1997; White, 1998, 2000). All of them activate at voltages above −140 mV (Fig. 6.10A, DACC; Fig. 6.5, $Q > 0$, ΔG_b) but differ in kinetics with open times ranging from tens and hundreds of milliseconds up to several seconds. Because of their voltage dependence, DACCs are assumed to function in Ca^{2+} uptake during Ca^{2+} signalling, mediating Ca^{2+} spikes and transient depolarisation. The fact that channel activity was detected in few cells only and that measurements were not stable owing to loss of cytosolic factors indicate tight control of DACCs (Thuleau *et al.*, 1994a,b).

6.3.4 *Vacuolar calcium release channels*

In addition to the Ca^{2+}-permeable SV channel, several types of Ca^{2+} release channels have been characterised in vacuolar membranes that open over the physiological range of cytosol negative voltages (Fig. 6.5, $Q < 0$; Alexandre *et al.*, 1990; Johannes *et al.*, 1992; Gelli & Blumwald, 1993; Allen & Sanders, 1994). They are permeable for divalent cations (Ba^{2+}, Sr^{2+}, Ca^{2+}, Mg^{2+}), and selective for divalents over K^+. Physiologically, the gating characteristics and the permeation properties suggest a role of these channels in vacuolar Ca^{2+} release.

6.3.5 *Calcium channels in the endoplasmatic reticulum*

The endoplasmatic reticulum (ER) serves as an intracellular Ca^{2+} pool. Voltage-dependent Ca^{2+} channels, which allow the passage of Ca^{2+} from the lumen of the ER into the cytosol, have been identified by functional reconstitution in planar lipid bilayers from touch-sensitive tendrils (BCC1, Klusener *et al.*, 1995) and from root tips (LCC1, Klusener & Weiler, 1999). Ca^{2+} channels from the ER may play an important role in regulation of the cytosolic-free Ca^{2+} concentration. Their role in Ca^{2+} signalling is supported by the fact that Gd^{3+} inhibits both calcium channel activity and the response of tendrils to touch (Klusener *et al.*, 1995). Furthermore, channel activity is modulated by cytosolic H_2O_2 and pH (Klusener *et al.*, 1997).

6.3.6 *Plasma membrane anion channels*

One of the first anion channels identified in higher plants was the quickly activating anion channel from guard cells (Keller *et al.*, 1989). After the establishment of the role of potassium channels for K^+ uptake and K^+ loss in the opening and closing of stomata, the presence of anion channels had already been postulated, because in processes in which massive salt flux is involved, electroneutrality has to be maintained by an equivalent flow of cations and anions. To date, anion channels are known from various tissues and cell types like guard cells, roots (cortex and stele), hypocotyls and suspension cells (for compilations, see Barbier-Brygoo *et al.*, 2000; Krol & Trebacz, 2000; White & Broadley, 2001). Anion channels can be classified into depolarisation-activated and inward-rectifying anion channels (Fig. 6.10B). Except for the anion channel in wheat roots, which only mediate anion influx (Skerrett & Tyerman, 1994), they serve as anion efflux pathways. Anion channels are highly selective for anions over cations. A larger permeability for NO_3^- than for Cl^- is a common feature of plant anion channels. Some are permeable for malate, citrate and sulphate. Anion channels play a role in volume regulation (as an example stomatal movement was already mentioned), in plant nutrition and in membrane potential control.

Animal voltage-dependent chloride channels (CLCs) show amazing differences to voltage-gated cation channels. CLCs are thought to be homodimers, with each subunit forming a pore, and gating exhibits tight coupling to Cl^- permeation (for a review see, e.g., Pusch, 2004). Plant homologues of CLCs exist, but the ones investigated so far are located in endomembranes (Hechenberger *et al.*, 1996; Barbier-Brygoo *et al.*, 2000). Furthermore, it has been suggested that the slow anion channel from guard cells is an ATP-binding cassette transporter (Leonhardt *et al.*, 1999). However, aside from the existence of some candidate genes, the molecular identity of plant anion channels remains a matter of speculation.

6.3.6.1 *Depolarisation-activated anion channels*

Depolarisation-activated anion channels belong to the best-investigated plant anion channels. Interestingly, the presence of two types of depolarisation-activated anion channels in one cell type is common. The quickly activating anion channel (QUAC; R-type, GCAC1) and the slowly activating anion channel (SLAC; S-type) have been identified in guard cells, xylem parenchyma cells and epidermal cells (Keller *et al.*, 1989; Linder & Raschke, 1992; Schroeder & Keller, 1992; Thomine *et al.*, 1995; Frachisse *et al.*, 2000; Köhler & Raschke, 2000). QUAC (Fig. 6.10B, *rapid*; Fig. 6.5, $Q > 0$, ΔG_b) is characterised by steep voltage dependence. Activation occurs positive of -100 mV and is completed within milliseconds. During sustained depolarisation, QUAC inactivates. A new activation is possible only after QUAC deactivates at negative membrane voltages. In contrast, SLAC (Fig. 6.10B, *slow*) displays weak voltage dependence. Complete activation and deactivation need seconds. Although there is no proof, it has been proposed that SLAC and QUAC from guard cells represent two switching modes of the same anion channel (Dietrich & Hedrich, 1994; Raschke, 2003; Raschke *et al.*, 2003). SLAC and QUAC are probably dedicated to specific functions: the first channel is able to mediate sustained anion efflux, while the second channel is a good candidate to be involved in fast electrical signalling. Oscillations in the free-running membrane voltage in guard cells were correlated with periodic activations and inactivations of QUAC (Dreyer & Hedrich, 1996; Raschke, 2003; see also Section 6.5).

A dominant theme among depolarisation-activated anion channels is the activation by a rise in cytosolic calcium and the need of nucleotides (Hedrich *et al.*, 1990; Skerrett & Tyerman, 1994; Thomine *et al.*, 1995, 1997; Schulz-Lessdorf *et al.*, 1996; Frachisse *et al.*, 2000). An exception is QUAC from xylem parenchyma cells, which is preferably active at low cytosolic Ca^{2+} concentrations matching its role in xylem loading (Köhler & Raschke, 2000). Raising the cytosolic ATP concentration shifts the activation curve towards less negative potentials (Fig. 6.5, $Q > 0$, $\Delta G_a \rightarrow \Delta G_b$; Colcombet *et al.*, 2001). Other major regulatory mechanisms involve protein phosphorylation and shift of the voltage dependence by auxin and anions (Marten *et al.*, 1991; Hedrich & Marten, 1993; Skerrett & Tyerman, 1994; Zimmermann *et al.*, 1994; Schmidt *et al.*, 1995; Grabov *et al.*, 1997; Dietrich & Hedrich, 1998; Frachisse *et al.*, 2000; Köhler *et al.*, 2002; see also Sections 6.4.6 and 6.4.7).

6.3.6.2 *Inward-rectifying anion channels*

Inward-rectifying anion channels have been described in mesophyll cells, suspension cells and xylem parenchyma cells (Schauf & Wilson, 1987; Terry *et al.*, 1991; Barbara *et al.*, 1994; Elzenga & Van Volkenburgh, 1997; Köhler & Raschke, 2000). This type of channel activates with hyperpolarisation (Fig. 6.10B, *dotted line*). Voltage dependence can be weak. Activators are high cytosolic Ca^{2+} concentration and light, in which the effect of light could be indirect (Cho & Spalding, 1996; Elzenga & Van Volkenburgh, 1997; Köhler & Raschke, 2000). Inward-rectifying anion channels are considered to provide a path for counter ions, e.g., for H^+ during the activity of the H^+-ATPase, and to participate in membrane voltage control.

Recently, much attention was paid to a new class of inward-rectifying anion channels in root cells, which are activated by extracellular Al^{3+} possibly indirectly via signalling cascades involving Ca^{2+} or inositol 1,4,5-trisphosphate (Ryan *et al.*, 1997; Kollmeier *et al.*, 2001; Pineros *et al.*, 2002; Zhang *et al.*, 2002). Al^{3+}-activated anion channels were proposed to be important in aluminium tolerance, since they mediate Al^{3+}-induced release of Al^{3+}-chelating ligands (primarily malate and citrate) into the rhizosphere from the root apex.

6.3.7 *Vacuolar anion channels*

In contrast to cation uptake into the vacuole (see introduction to Section 6.3.2), ion channels are well suited to facilitate anion uptake. Chloride and malate are the major charge-balancing anions present in the vacuole.

In the vacuolar membrane of both C3 and CAM (crassulacean acid metabolism) plants, malate-selective channels (VMAL) have been identified (Iwasaki *et al.*, 1992; Pantoja *et al.*, 1992a; Cerana *et al.*, 1995). These channels activate with an instantaneous and a slow, time-dependent component upon (cytosol) negative voltages (Fig. 6.5, $Q < 0$, ΔG_a). VMAL channels are mainly permeable for fumarate^{2-} and malate^{2-}, and to a smaller extent for Cl^-. VMAL channels are insensitive to changes in cytosolic Ca^{2+} and in the vacuolar proton concentration. However, decreasing cytosolic pH results in strong current reduction very likely caused by a block mechanism (Pantoja & Smith, 2002; Hafke *et al.*, 2003). The distinctive properties of VMAL suggest that this channel is likely to present the principal route for malate^{2-} uptake into the vacuole. Especially in plants performing CAM, the vacuole acts as a temporary repository for large amounts of malic acid synthesised as a result of nocturnal CO_2 fixation. In the vacuole, malate^{2-} is chelated or protonated, ensuring that the malate^{2-} gradient across the vacuolar membrane remains directed into the vacuole, which is required for passive transport.

Another Cl^- and malate^{2-} permeable channel (VCL) activated upon (cytosol) negative potentials (Fig. 6.5, $Q < 0$, ΔG_a). Activation was dependent on the phosphorylation status of the channel and was mediated specifically by CDPK, a Ca^{2+}-dependent protein kinase (Pei *et al.*, 1996). VCL channels were proposed to provide a pathway for kinase-dependent anion uptake into the vacuole.

6.4 Gating modifiers

Research during the past decade revealed that ion channels are part of diverse signalling cascades and/or serve as their final targets (MacRobbie, 1998; Blatt, 2000b; Schroeder *et al.*, 2001). Since most of these signals are transmitted chemically (by direct interaction with other molecules) rather than electrically (by the membrane voltage), the activity of voltage-gated ion channels is, in most cases, additionally modulated by chemical stimuli. The following sections present specific stimuli, and illustrate their modulatory influence on the biophysical gating properties of the target ion channel. In order to focus on the principles of the direct interaction of voltage-gated ion channels with signalling molecules, all possible further upstream signalling steps are mostly left aside. The interested reader is referred to MacRobbie (1998), Blatt (2000b), Schroeder *et al.* (2001), and Assmann (2002) (see also Chapter 8).

6.4.1 *Phosphorylation*

Phosphorylation (adding of PO_4^{2-} to OH groups of, e.g., serines) and dephosphorylation events are all-purpose tools enabling to switch a channel on or off. Mechanistically, this is a rather simple process. Attaching (detaching) of phosphate groups to (from) the channel protein by kinases (phosphatases) changes the stability of the different channel conformations. For phospho-activation in terms of the idealised two-state model, the removal of phosphate groups reduces strongly $\Delta G_{CO}(0)$, in some cases even to negative values (Fig. 6.5, $\Delta G_b \rightarrow \Delta G_d$). Thus, the open configuration is energetically disfavoured. The activity range of the channel is shifted to far more negative ($Q < 0$), or far more positive ($Q > 0$), voltages. The shift may have an extent that, theoretically, very high membrane voltages would be needed to open the channel (Fig. 6.5, ΔG_d). In practice, the channel is closed (switched off) at all times.

Channel control by phosphorylation is a widely observed phenomenon. Several voltage-gated ion channels undergo a rundown upon ATP depletion at the cytosolic face (see, e.g., Schmidt *et al.*, 1995; Moran, 1996; Kohler & Blatt, 2002). Since ATP is the substrate of kinases, ATP depletion disturbs the equilibrium of kinase/phosphatase reactions and results in dephosphorylated channel proteins.

The control of ion channel activity by phosphorylation exposes these transporter proteins as downstream targets in several diverging and converging signalling cascades. However, despite the simple mechanism, the tight control of channel activity by (de)phosphorylation is far more complicated and the understanding of these processes is just in the initial stage. An example is the complex phosphoregulation of guard cell K_{in} channels. On the one hand side, they are inhibited by the Ca^{2+}-stimulated phosphatase 2B (calcineurin; Luan *et al.*, 1993). On the other hand, the application of okadaic acid and calyculin, inhibitors of protein phosphatases 1 and 2A, strongly reduced K_{in}-mediated currents, indicating a negative regulation of K_{in} channels also by phosphorylation events (Li *et al.*, 1994; Thiel & Blatt, 1994).

A similar complexity to (de)phosphorylation control also applies to the SV channel (Allen & Sanders, 1995; Bethke & Jones, 1997).

Phosphorylation is not only used to switch a channel on or off. The different gating modes of weakly rectifying potassium channels, K_{weak}, are hypothesised to be determined by the phosphorylation status of the channel protein (Fig. 6.9; Dreyer *et al.*, 2001; Cherel *et al.*, 2002). Additionally, it is discussed that the slow and the rapid guard cell anion channels represent two modes of the same channel, which are distinguished by their phosphorylation status (Dietrich & Hedrich, 1994).

Despite the strong evidence for channel regulation by phosphorylation, the knowledge on enzymes involved in these processes is still poor. To date, a direct interaction with voltage-gated channels was proven for the kinase AAPK and a CDPK (Li & Assmann, 1996; Pei *et al.*, 1996; Li *et al.*, 1998, 2000) and the phosphatase AtPP2CA (Cherel *et al.*, 2002).

6.4.2 *Nitrosylation and other redox reactions*

Analogous to phosphorylation, it has been proposed that channel activity can be controlled via S-nitrosylation of cysteine residues by nitric oxide (NO) or via other redox reactions mediated by, e.g., glutathione or H_2O_2. In the case of animal channels, it has been demonstrated that redox compounds regulate important ion channel properties such as channel gating, inactivation and permeation (see references in Carpaneto *et al.*, 1999, and Garcia-Mata *et al.*, 2003). Redox agents are known to affect the ER Ca^{2+} channel BCC1 (Klusener *et al.*, 1997), the SV channel (Carpaneto *et al.*, 1999) and the plasma membrane K_{in} and K_{out} channels in guard cells (Kohler *et al.*, 2003). All are inactivated by oxidising agents. The physiological role of redox regulation is still speculative, but it may have fundamental physiological implications that wait to be uncovered.

Most effects of reactive oxygen species (ROS) on plant ion channels are indirect. In guard cells, for example, it was observed that NO increases the cytosolic Ca^{2+} level via a set of signalling cascades, which in turn has a direct regulatory effect on potassium and chloride channels (Garcia-Mata *et al.*, 2003; for the effect of Ca^{2+}, see Section 6.4.3). Additionally, recent reports identified a hyperpolarisation-activated plasma membrane Ca^{2+} channel, which is activated by the oxidising agent H_2O_2 indirectly via a phosphatase 2C (Pei *et al.*, 2000; Murata *et al.*, 2001; Kohler *et al.*, 2003).

6.4.3 *Calcium ions*

Calcium is a multifunctional signal transducer in plant cells. Usually, plant cells, like many other cells, maintain their cytosolic-free Ca^{2+} concentration between 10^{-7} and 10^{-8} M by actively extruding Ca^{2+} from the cytosol towards the vacuole or out of the cell and sequestering it within the ER and mitochondria. Diverse external stimuli (e.g., application of abscisic acid) mobilise Ca^{2+} from different subcellular pools and induce an array of responses including dark-induced inhibition of sucrose

synthesis, bending responses to gravity and blue light, turgor regulation and stomatal closure (for review see, e.g., Trewavas & Malho, 1998; Sanders *et al.*, 1999; Blatt, 2000a; Sanders *et al.*, 2002). Some of the responses are mediated by ion channels. In guard cells, for example, increased cytosolic Ca^{2+} levels regulate voltage-gated ion channels in different ways, which results in a depolarisation of the plasma membrane. Transporters that serve for ion accumulation close and those being responsible for ion release open. These are prerequisites for stomatal closure.

K_{in} channels are downregulated upon a rise in cytosolic-free Ca^{2+} (Fig. 6.5, $Q < 0$, $\Delta G_b \rightarrow \Delta G_c \rightarrow \Delta G_d$; Schroeder & Hagiwara, 1989; Grabov & Blatt, 1999). Whether this is a direct effect of Ca^{2+}-binding to the channel protein, whether downregulation is mediated via Ca^{2+}-dependent kinases/phosphatases, or whether other modulatory effectors sensitise K_{in} channels to cytosolic calcium remains to be investigated with cloned K_{in} channels after heterologous expression. It should be emphasised that under certain conditions, K_{in} channels appear to be insensitive to elevated cytosolic Ca^{2+} concentrations (Luan *et al.*, 1993; Armstrong *et al.*, 1995; Wang *et al.*, 1998). K_{out} channels in mesophyll cells also appear to be downregulated by increasing cytosolic Ca^{2+} concentrations (Li & Assmann, 1993). However, in general, guard cell K_{out} channels are known to be Ca^{2+}-insensitive (Hosoi *et al.*, 1988; Schroeder & Hagiwara, 1989; Blatt *et al.*, 1990; Blatt & Armstrong, 1993; Lemtiri-Chlieh & MacRobbie, 1994; Grabov & Blatt 1999). By contrast, increased cytosolic Ca^{2+} levels activate both slowly and rapidly activating guard cell anion currents (SLAC, S-type, Schroeder & Hagiwara, 1989; GACA1, QUAC, R-type, Hedrich *et al.*, 1990), apparently by increasing the number of actively gated channels, N (see Equation 6.1).

Control of hyperpolarisation-activated Ca^{2+} channels by cytosolic Ca^{2+} apparently is connected to their physiological function. While the open probability of the HACC from guard cells is suppressed by micromolar cytosolic Ca^{2+}, the HACC from root hairs is stimulated. Stimulation results from a shift of the activation threshold towards more positive membrane potentials ($Q < 0$, $\Delta G_c \rightarrow \Delta G_b$; Hamilton *et al.*, 2000; Very & Davies, 2000). Thus, *in vivo*, elevated cytosolic Ca^{2+} may form a negative feedback on Ca^{2+} influx in guard cells in accordance with its role in signalling and a positive feedback in root hairs for continued apical Ca^{2+} influx during tip growth. Interestingly, extracellular divalent cations activate the HACC from guard cells by shifting the voltage dependence towards more positive voltages (Hamilton *et al.*, 2000, 2001).

Cytosolic Ca^{2+} also influences voltage-gated ion channels in endomembranes. The SV channel is activated by cytosolic Ca^{2+}. Increasing cytosolic Ca^{2+} from 0.1 to 10 μM shifts the activation threshold of the channel to less positive voltages (Hedrich & Neher, 1987; Fig. 6.5, $Q > 0$, $\Delta G_d \rightarrow \Delta G_c$). Thus, SV channels mostly appear to be closed at physiological tonoplast voltages. Recent studies, however, have indicated that cytosolic Mg^{2+} and reducing agents also serve as gating-modulatory effectors, and thus may sensitise the SV channel to physiological cytosolic Ca^{2+} concentrations Cytosolic Mg^{2+} stimulates SV channels (Fig. 6.5, $Q > 0$, $\Delta G_d \rightarrow \Delta G_c$; Pei *et al.*, 1999; Carpaneto *et al.*, 2001).

Voltage-gated vacuolar calcium release channels separate into two classes with respect to their susceptibility towards cytosolic calcium. While one class is activated by increasing vacuolar Ca^{2+} (Fig. 6.5, $Q < 0$, $\Delta G_d \rightarrow \Delta G_c \rightarrow \Delta G_b \rightarrow \Delta G_a$; Johannes & Sanders, 1995), however insensitive towards cytosolic Ca^{2+} (Johannes *et al.*, 1992; Allen & Sanders, 1994), the other inactivates when Ca^{2+} reaches 1 μM (Gelli & Blumwald, 1993). Also the ER Ca^{2+} channel BCC1 is modulated by Ca^{2+} ions. The channel's open probability is governed largely by the chemical gradient of Ca^{2+}. Applying a 100-fold Ca^{2+} gradient, which reflects more the physiological situation, shifted the activation potential towards more negative membrane potentials (Fig. 6.5, $Q > 0$, $\Delta G_c \rightarrow \Delta G_b$; Klusener *et al.*, 1995). The different regulations of endomembrane Ca^{2+} channels may point to a convergence of diverse signalling cascades and a fine-tuning at the level of channel-mediated Ca^{2+}-release from subcellular pools.

6.4.4 *Protons*

A physiologically important regulatory trigger for ion channel activity is the proton concentration on one or both sides of the respective membrane. Ion channels can be very sensitive towards changes in the pH. The protonation of a channel protein at susceptible amino acid residues (e.g. histidines) alters its surface charge, which in turn may affect the permeation properties or the stability of certain channel conformations thereby affecting gating.

6.4.4.1 *Cytosolic pH changes*

The cytosolic pH in plant cells is strongly buffered at values around pH 7.0. Guard cells, for example, have a buffer capacity that corresponds to an apparent buffer concentration of 275 mM with $pK_a = 6.9$ (Grabov & Blatt 1997, 1998a). Nevertheless, external stimuli, e.g., application of hormones like ABA or auxins, are capable of provoking changes in the cytosolic pH in the range of 0.2–0.4 pH units. These apparently moderate changes have dramatic regulatory effects on diverse voltage-gated ion channels. An increase in cytosolic pH activates K_{out} channels and inactivates K_{in} channels (Blatt, 1992; Blatt & Armstrong, 1993; Miedema & Assmann, 1996). Similarly, a decrease in cytosolic pH activates K_{in} channels (Fig. 6.5, $Q < 0$, $\Delta G_c \rightarrow \Delta G_b$; Blatt, 1992; Blatt & Armstrong, 1993; Hoshi, 1995) and inactivates K_{out} channels, SV channels (Fig. 6.5, $Q > 0$, $\Delta G_c \rightarrow \Delta G_d$; Schulz-Lessdorf & Hedrich, 1995) as well as vacuolar voltage-gated calcium release channels (Fig. 6.5, $Q < 0$, $\Delta G_b \rightarrow \Delta G_c \rightarrow \Delta G_d$; Allen & Sanders, 1994). Changes in cytosolic pH appeared not to affect voltage gating of K_{out} channels, but rather the number N (Equation 6.1) of actively gated channels. Whether this effect is the result of a 'switch on/off' shift (Fig. 6.5, $Q > 0$, $\Delta G_d \rightarrow \Delta G_c$; cf. Section 6.4.1) remains to be investigated. Physiologically, the different responses to cytosolic pH adjust the guard cell cation channels for cation uptake when the pH drops and for cation release when the pH increases.

The guard cell anion channel GCAC1 is also regulated by cytosolic pH, namely it is upregulated by a more acidic cytoplasmic pH. More importantly, extracellular acidification slows down the inactivation process of GCAC1 and this modulation depends on the transmembrane pH gradient (Schulz-Lessdorf *et al.*, 1996). Thus, in the presence of a small transmembrane gradient (e.g. in closed stomata when H^+-ATPase activity is low), the inactivation process of GCAC1 would be accelerated compared to the presence of a pronounced pH gradient observed in open stomata.

6.4.4.2 *Extracellular/luminal pH changes*

In contrast to the moderate changes in cytosolic pH, the apoplastic pH can vary from pH 7.2 to pH 5.1 (Edwards *et al.*, 1988). The inactivation of guard cell K_{out} channels by lowering pH arises in part from a shift of the activation threshold (Fig. 6.5, $Q > 0$, $\Delta G_b \rightarrow \Delta G_c$; Ilan *et al.*, 1994), but mainly from a decrease in N, the number of actively gated channels (Blatt, 1992). Conversely, guard cell K_{in} channels are activated on lowering extracellular pH over this same range and the effect results in a shift of the activation threshold of these channels towards more positive voltages (Fig. 6.5, $Q < 0$, $\Delta G_b \rightarrow \Delta G_a$; Blatt, 1992; Ilan *et al.*, 1994; Hedrich *et al.*, 1995; Mueller-Roeber *et al.*, 1995). In biophysical terms this means that a protonation of specific amino acid residues of the outer part of the channel protein changes the stability of the different channel conformations to favour the open channel, i.e., $\Delta G_{CO}(0)$ increases. In the guard cell potassium channel KST1 from potato, two histidine residues were identified to be involved in the pH modulation (Hoth *et al.*, 1997). Physiologically, the acid activation of K_{in} channels guarantees a less negative membrane potential during long-term proton pump-driven potassium accumulation (Blatt, 1992), and therefore a more efficient use of ATP-hydrolysis energy.

For channels in the vacuolar membrane, the equivalent process to an apoplastic acidification is the decrease of the pH in the vacuolar lumen (physiological range: $3.8 \leq$ vacuolar pH ≤ 6; Felle, 1988). The activity of the SV channel was reduced at low vacuolar pH values (Fig. 6.5, $Q > 0$, $\Delta G_c \rightarrow \Delta G_d$; Schulz-Lessdorf & Hedrich, 1995). The importance of this regulation can be understood when considering the physiology of vacuolar solute uptake. Solute transport into the vacuole is an active process. Several vacuolar solute transporters are antiporters and use the tonoplastic proton gradient as energy source (Martinoia *et al.*, 2000; Maeshima, 2001). An open cation release channel (SV) would serve as a counteractive shunt pathway in vacuolar solute accumulation.

6.4.5 *Potassium ions*

So far potassium has been presented as a transported substrate. However, in certain cases this permeating ion modulates the activity of its transporting channel by itself. The effect is illustrated here exemplarily on depolarisation-activated K^+ channels. The activation threshold of these channels varies with the extracellular potassium concentration (Fig. 6.8B). Thus, depolarisation-activated K^+ channels are closed at voltages negative of E_K (Fig. 6.8A), at which the driving force for potassium is directed inwardly (Blatt, 1988, 1991; Schroeder, 1988). Biophysically, this means that potassium ions interact with the channel protein and favour energetically a closed conformation (Blatt & Gradmann, 1997).

Physiologically, the dependency of the activation threshold on the extracellular potassium concentration guarantees that depolarisation-activated K^+ channels are active over a wide range of physiological K^+ concentrations without providing a pathway for potassium leakage into the cell. Similarly, the K^+-dependency of an unusual hyperpolarisation-activated K^+ channel of *Arabidopsis* protects root cells from potassium leakage out of the cell when the extracellular K^+ concentration is very low (Fig. 6.7D; Maathuis & Sanders, 1995). Usually, hyperpolarisation-activated K^+ channels also mediate potassium efflux under unfavourable conditions (Fig. 6.7C; Bruggemann *et al.*, 1999a). Besides the modulation of the gating, another effect is observed when reducing the potassium concentration to extremely low levels (e.g., to nominal zero): some plant K^+ channels do not mediate currents in the absence of extracellular potassium. Even though the electrochemical gradient for potassium would favour strong outward currents, no or only tiny K^+ efflux is registered. This observation has fuelled the hypothesis that K_{in} channels also can sense the K^+ concentration (Maathuis *et al.*, 1997). However, this type of sensing differs from the sensing mechanism described above for K_{out} channels, in which the gating has been modified. In this case the gating appears to be unaffected. It is rather the pore that adopts a different conformation or even collapses, when the extracellular potassium concentration is lowered (Zhou *et al.*, 2001). At which K^+ concentration this collapse occurs apparently differs among the different channels.

Vacuolar potassium modulates the activity of FV channels. Lowering luminal potassium reduces the channel activity at (cytosol) negative voltages (Fig. 6.5, $Q < 0$; $\Delta G_a \rightarrow \Delta G_b \rightarrow \Delta G_c$), whereas the other branch of the bimodal gating ($Q > 0$) remains unaffected. Physiologically, this feedback mechanism likely guarantees that at low vacuolar K^+ concentrations no potassium leaks from the cytosol into the K^+-starved vacuole (Pottosin & Martinez-Estevez, 2003). This process may contribute to stabilise the cytosolic potassium concentration.

6.4.6 *Anions*

Anions like malate, chloride, nitrate and sulphate modulate the activity of plasma membrane anion channels. Slight increases in the extracellular $malate^{2-}$ concentration in the physiological concentration range shift the activation threshold of the guard cell anion channel GCAC1 towards hyperpolarised potentials (Fig. 6.5, $Q > 0$, $\Delta G_b \rightarrow \Delta G_a$; Hedrich & Marten, 1993; Raschke, 2003). Since cytosolic $malate^{2-}$ proved ineffective, the binding site for shifting the gate must be located on the extracellular face of the channel. Therefore, $malate^{2-}$ activates GCAC1 to feed forward anion release and promote stomatal closure. Since alterations in the ambient CO_2 level can modify the extracellular $malate^{2-}$ level, it has been suggested that this mechanism serves as a sensor of the apoplastic CO_2 concentration and thus of the metabolic status of the photosynthetic tissue to adjust stomatal aperture in relation to the photosynthetic capacity (Hedrich *et al.*, 1994). Interestingly, extracellular $malate^{2-}$ caused a conversion of the slowly activating anion channel from guard cells to the quickly activating anion channel GCAC1 and initiated a depolarisation

of the membrane voltage (Raschke, 2003). Similar to the malate effect, an increase in extracellular Cl^- also shifted the voltage dependence of GCAC1 towards negative potentials (Fig. 6.5, $Q > 0$, $\Delta G_b \rightarrow \Delta G_a$) supporting anion efflux (Dietrich & Hedrich, 1998). Chloride reduces the gate-shifting effect of extracellular malate and therefore seems to compete for the same binding site (Hedrich *et al.*, 1994; Dietrich & Hedrich, 1998).

The quickly activating anion conductance (X-QUAC) from root xylem parenchyma cells is a potential control point for NO_3^- release into the xylem (Köhler & Raschke, 2000; Köhler *et al.*, 2002). In contrast to GCAC1, X-QUAC appeared to be insensitive to $malate^{2-}$. However, extracellular NO_3^- strongly affected its voltage dependence. Extracellular, but not cytosolic, NO_3^- caused a shift of the activation threshold towards more negative voltages (Fig. 6.5, $Q > 0$, $\Delta G_b \rightarrow \Delta G_a$), increasing the transport capacity of the membrane for NO_3^- and all other permeating ions. X-QUAC may possess a binding site for NO_3^- that is exposed to the apoplast.

Another example for anion regulation of an ion channel is the anion channel from hypocotyl cells. Sulphate is not only a substrate of this channel but has a strong regulatory effect on its activity (Frachisse *et al.*, 1999). It prevented channel rundown and shifted the activation potential towards negative potentials (Fig. 6.5, $Q > 0$, $\Delta G_b \rightarrow \Delta G_a$). Remarkably, sulphate acts from the cytosolic site. Channel activation by sulphate is speculated to be part of a mechanism of cellular ion homeostasis, namely to avoid the cytosolic accumulation of SO_4^{2-} when it cannot be extensively metabolised.

Additional to these examples for plasma membrane anion channels, a modification of the gating by Cl^- is also known from the anion channel of vacuoles (Plant *et al.*, 1994). Rising vacuolar chloride concentrations increased the open probability of the channel and induced increases in the levels of nitrate and phosphate inward currents. Remarkably, malate currents are reduced. Vacuolar chloride concentrations regulate the influx of anions into the vacuole, favouring the uptake of nutrients for storage, but reducing vacuolar malate uptake, leaving it for use in mitochondrial oxidation and cytosolic pH control (Plant *et al.*, 1994).

6.4.7 *Phytohormones*

Plant hormones, like auxins, giberillic acids, cytokinines, abscisic acid, brassinosteroids and ethylene,serve an extremely broad spectrum of plant development and abiotic stress responses. Phytohormones are transported throughout the plant body, or from cell to cell, and reactions are evoked in the perceiving cell(s) through an intracellular signal transduction cascade. The specific 'make-up' of the cell's interior that is required to pass on the hormone signal towards a cellular response is highly diverse, allowing cell- and hormone-specific reactions to occur. The action of hormones may involve protein kinases and phosphatases that alter the phosphorylation status, and hence the activity, of target proteins (see Section 6.4.1). Also phospholipases can be involved (see Section 6.4.8). Cellular reactions may involve transient or sustained, and often rhythmic, increases in the cytosolic Ca^{2+}

concentration, which is, for example, a frequent response in ABA-mediated signal transduction.

6.4.7.1 *Auxins*

Hormones of the auxin class influence root initiation, cell expansion and division, apical dominance and responses to light and gravity (for reviews see, e.g., Kaldewey, 1976; Leyser, 2002). Closely connected to auxin-mediated stimuli are changes of the electrical properties of the plasma membrane (Barbier-Brygoo *et al.*, 1991). The effect of auxins on channel activity, however, is mostly indirect, e.g., via auxin-induced transients in the cytosolic pH (Blatt & Thiel, 1993, 1994; Thiel *et al.*, 1993) but also by changing the expression level of channel genes (Philippar *et al.*, 1999). In exceptional contrast, plasma membrane chloride channels of the rapid type (GCAC1) appear to be directly modulated by auxins (Fig. 6.5, $Q > 0$, $\Delta G_b \rightarrow \Delta G_a$) when applied from the extracellular side (Marten *et al.*, 1991).

6.4.7.2 *Abscisic acid*

The hormone (*RS*)-2-*cis*,4-*trans*-abscisic acid (ABA) is generally recognised to signal conditions of water stress. It is synthesised during periods of drought and accumulates in the leaf tissues, causing alterations in gene expression and evoking the closure of stomata, thereby reducing transpirational water loss. Directly applied to stomatal guard cells, ABA causes increases in the cytosolic Ca^{2+} concentration and pH via a cascade of signalling events (Gehring *et al.*, 1990; McAinsh *et al.*, 1990; Schroeder & Hagiwara, 1990; Irving *et al.*, 1992; Blatt & Armstrong, 1993). Thus, ABA mainly modulates membrane conductance and therefore channel activity indirectly. The rise in cytosolic-free Ca^{2+} inactivates K_{in} channels and activates anion channels, and the parallel rise in cytosolic pH activates outward-rectifying potassium channels, biasing in combination the plasma membrane for solute efflux and stomatal closure (see MacRobbie, 1998; Blatt, 2000b; Schroeder *et al.*, 2001; and references therein). An initial trigger being responsible for a part of the ABA-induced rise in cytosolic Ca^{2+} might be a hyperpolarisation-activated Ca^{2+} channel in the plasma membrane. This channel activated upon direct application of ABA (Fig. 6.5, $Q < 0$, $\Delta G_d \rightarrow \Delta G_b$; Hamilton *et al.*, 2000). The activation process might occur either by direct binding of ABA to the channel or via modulation by an ABA-sensitive protein that is closely attached to the Ca^{2+} channel. The action of protein phosphatase 1 and 2A antagonists and ABA is remarkably similar, including the displacement of the voltage sensitivity. This indicates that phosphorylation of sites on or close to the Ca^{2+} channel facilitate channel opening (Kohler & Blatt, 2002).

6.4.8 *Lipids and their hydrolysis products*

Lipid signalling is widespread in plants (for reviews see, e.g., Mueller-Roeber & Pical, 2002; Weber, 2002; Bogre *et al.*, 2003). Phospholipases produce phosphatidic acid and choline (in the case of phospholipase D), inositol 1,4,5-trisphophate and diacylglycerol (in the case of phospholipase C) or arachidonate and lysophosphatidylcholine (in the case of phospholipase A_2), which then have structural and regulatory functions including ion channel control.

The fatty acids linolenic acid (LN) and arachidonic acid (AA) activate guard cell K_{in} channels and inactivate K_{out} channels. Likewise, LN and AA induces stomatal opening and inhibits stomatal closure (Lee *et al.*, 1994). Other fatty acids, like linoleic acid (LA), have failed to induce a similar response. Whether LN and AA directly act on K_{in} and K_{out} channels or via signalling pathways remains to be investigated.

A voltage-dependent Ca^{2+}-release channel in the tonoplast was specifically activated by inositol 1,4,5-trisphosphate ($Ins(1,4,5)P_3$; Fig. 6.5, $Q < 0$, $\Delta G_d \rightarrow \Delta G_c \rightarrow \Delta G_b \rightarrow \Delta G_a$; Alexandre *et al.*, 1990), the product of phospholipase C activity. The channel was insensitive to other polyphosphoinositides including $Ins(1,4)P_2$, $Ins(1,3,4)P_3$, $Ins(2,4,5)P_3$ and $Ins(1,3,4,5)P_4$. This high selectivity towards the agonist may reflect a role of the Ca^{2+}-release channel in specific signalling processes while not being involved in others. This $Ins(1,4,5)P_3$-induced Ca^{2+} release into the cytoplasm in turn provokes secondary effects on other voltage-gated channels as, e.g., the inactivation of K_{in} channels (Section 6.4.3; Blatt *et al.*, 1990), and therefore initiates stomatal closure (Gilroy *et al.*, 1990). A similar Ca^{2+}-mediated effect on hyperpolarisation-activated guard cell potassium channels was evoked by inositol hexakisphosphate ($InsP_6$). Actually, $InsP_6$ was around 100-fold more potent than $Ins(1,4,5)P_3$ in (Ca^{2+}-mediated) modulating K_{in} channel activity (Lemtiri-Chlieh *et al.*, 2000, 2003). Since $InsP_6$ levels were increased upon guard cell stimulation with ABA, these results indicate a role of phosphoinositides in the ABA-induced signalling cascades preceding stomatal closure.

An exciting new finding is that sphingolipids, which play important signalling functions in animals and yeast, also regulate important processes in plants (Worrall *et al.*, 2003). More specifically, it has been discovered that the sphingosine metabolite sphingosine-1-phosphate (S1P) is involved in ABA regulation of the guard cell turgor (Ng *et al.*, 2001). Recently, S1P was shown to inhibit K_{in} channels in *Arabidopsis thaliana* guard cell protoplasts. This inhibition was dependent on the presence of the G-protein α-subunit gene *gpa1* (Coursol *et al.*, 2003). S1P was also able to stimulate slow anion currents in wild-type guard cells, but not in the *gpa1* null mutant (Coursol *et al.*, 2003).

6.4.9 *Proteins and peptides*

In addition to kinases and phosphatases, other proteins and peptides have been identified to modulate the gating behaviour of voltage-gated ion channels. Among them are G-proteins, 14-3-3 proteins and calmodulin.

6.4.9.1 *G-proteins*

Heterotrimeric G-proteins are guanine nucleotide-binding proteins composed of three subunits (α, β, γ). They are generally associated with plasma membrane receptors. Receptor activation stimulates the exchange of GTP for GDP and induces the dissociation into the $G\alpha$ and $G\beta\gamma$ components. These activated components

serve as second messengers, which then in turn activate messengers of higher order (Assmann, 2002). Several reports indicate that G-protein-mediated signalling modulates voltage-gated potassium channels indirectly via cytosolic factors (e.g., changes in free Ca^{2+} concentrations; Fairley-Grenot & Assmann, 1991; Li & Assmann, 1993; Kelly *et al.*, 1995). Anion channels are affected by G-proteins as well, probably in an indirect way. Guard cells defective in the sole prototypical heterotrimeric G-protein α-subunit gene lack pH-independent ABA activation of anion channels (Wang *et al.*, 2001).

There is evidence for a more direct (cytosol-independent) modulation. Single-channel experiments indicate a membrane-delimited stimulation of ion channels by G-proteins. The activation of G-proteins by the non-hydrolysable GTP analogue guanosine 5′-*O*-(3-thiotriphosphate) (GTP-γ-S), or by the mastoparan analogue mas7, inhibited guard cell K_{in} channels, favouring stomatal closure (Wu & Assmann, 1994; Fig. 6.5, $Q < 0$, $\Delta G_b \rightarrow \Delta G_c$; Armstrong & Blatt, 1995; Kelly *et al.*, 1995). In contrast, certain types of K_{in} channels in xylem parenchyma cells are activated by non-hydrolysable derivatives of GTP, enabling K^+ uptake (Wegner & de Boer, 1997). Also hyperpolarisation-activated Ca^{2+} channels were activated by GTP-γ-S and by a recombinant G-protein α-subunit. In fact, GTP-γ-S produced a similar response like a fungal elicitor. Since channel activation by the elicitor was abolished by locking G-proteins in their inactivated state, a role of heterotrimeric G-proteins in response to pathogens has been proposed (Gelli *et al.*, 1997; Aharon *et al.*, 1998).

6.4.9.2 14-3-3

14-3-3 proteins are phosphoserine-binding proteins that regulate the activities of a variety of targets via direct protein–protein interactions. Recent reports indicate that 14-3-3 proteins also interact with plant voltage-gated ion channels (for reviews see, e.g., Bunney *et al.*, 2002; Roberts, 2003). Overexpression of plant 14-3-3 proteins in tobacco doubled the number of active plant K_{out} channels in mesophyll cells (Saalbach *et al.*, 1997). Likewise, the application of recombinant 14-3-3 via the patch-pipette increased the measured potassium efflux currents in tomato cell protoplast (Booij *et al.*, 1999). In contrast, the application of recombinant barley 14-3-3B to mesophyll vacuoles resulted in a reduction of SV-channel-mediated currents. The effects on K_{out} and SV channels could not be explained by a regulation of the gating, but rather by an increase/reduction of the number of functional channels. It is concluded that 14-3-3 either interacted directly with K_{out} and SV channels or indirectly via an intermediate protein (van den Wijngaard *et al.*, 2001). The physiological implication of this interaction is yet unknown.

6.4.9.3 Calmodulin

In plants many Ca^{2+}-induced processes are amplified by Ca^{2+}-binding proteins like cytosolic or membrane-associated calmodulins (CaMs; for a recent review see, e.g., Luan *et al.*, 2002). CaM acts in concert with cytoplamic Ca^{2+} and intriguing evidence suggests that CaM is part of the transduction chain for environmental signals.

The application of calmodulin at high concentrations of about 3.5 μM sensitised the SV channel to lower cytosolic Ca^{2+} concentrations (Bethke & Jones, 1994).

Note that lower calmodulin concentrations ranging from 100 nM to 1 μM were without effect (Allen & Sanders, 1995; Schulz-Lessdorf & Hedrich, 1995). Likewise, calmodulin antagonists applied from the cytosolic side inactivated SV channels via a modulation of the gating (e.g., Fig. 6.5, $Q > 0$, $\Delta G_c \rightarrow \Delta G_d$; Weiser *et al.*, 1991; Bethke & Jones, 1994; Schulz-Lessdorf & Hedrich, 1995). It is still unclear whether CaM antagonists interacted directly with the SV channel or via channel-associated CaMs.

6.5 Outlook – voltage-gated ion channels in 'Systems Biology'

The past years were dominated by the separate consideration of isolated voltage-gated ion channels. This approach provided valuable detailed information on the different transporters, facilitating in turn to assign certain physiological roles to them. In some cases the concerted action of different voltage-gated ion channels have provided intuitive models for more complex physiological processes, for example, aspects of long-term ion fluxes in guard cells accompanying stomatal movement (MacRobbie, 1998; Blatt, 2000a; Assmann & Wang, 2001; Schroeder *et al.*, 2001). Additionally, the electro-coupling of plant ion transporters in computer models provided some concepts to explain alterations in the time course of the plasma membrane voltage in guard cells on a shorter timescale (Gradmann *et al.*, 1993; Dreyer & Hedrich, 1996; Gradmann & Hoffstadt, 1998). In the following a simple example is presented, in order to illustrate that computer models may help to understand more complex behaviours.

Oscillations in the free-running membrane potential are observed in guard cells (Fig. 6.11A; Thiel *et al.*, 1992; Gradmann *et al.*, 1993; Blatt & Thiel, 1994; Roelfsema & Prins, 1998). These action potential-like membrane potential oscillations can be simulated in computer models by combining the electrical features of the plasma membrane H^+-ATPase, the guard cell K_{in} channel, the guard cell K_{out} channel and the inactivating guard cell anion channel GCAC1 (Dreyer & Hedrich, 1996; Fig. 6.11). The computer model now allows a closer look at the different phases of the action potentials, to separate the contributions of the distinct transporters and to understand their concerted action (Fig. 6.11, a to f). Initially, the membrane potential is more negative than -150 mV. The positive current generated by proton-ATPases, pumping H^+ out of the cell, is compensated by K^+ influx through open K_{in} channels. This situation is rather stabile and represents the general case when cells accumulate relative high amounts of potassium (e.g., during stomata opening). Some disturbance, e.g., Ca^{2+} influx (Grabov & Blatt, 1998b), can destabilise the equilibrium, resulting in a negative net current, which then in turn induces a rapid membrane depolarisation (Fig. 6.11a). In the course of this depolarisation, rapid-activating anion channels GCAC1 activate and K_{in} channels deactivate. The depolarisation stops at a voltage at which the proton current of the H^+-ATPases compensates for the chloride efflux through GCAC1 (Fig. 6.11b, *white circle*). This condition is semi-stabile, since at these voltages K_{out} channels open with a delay

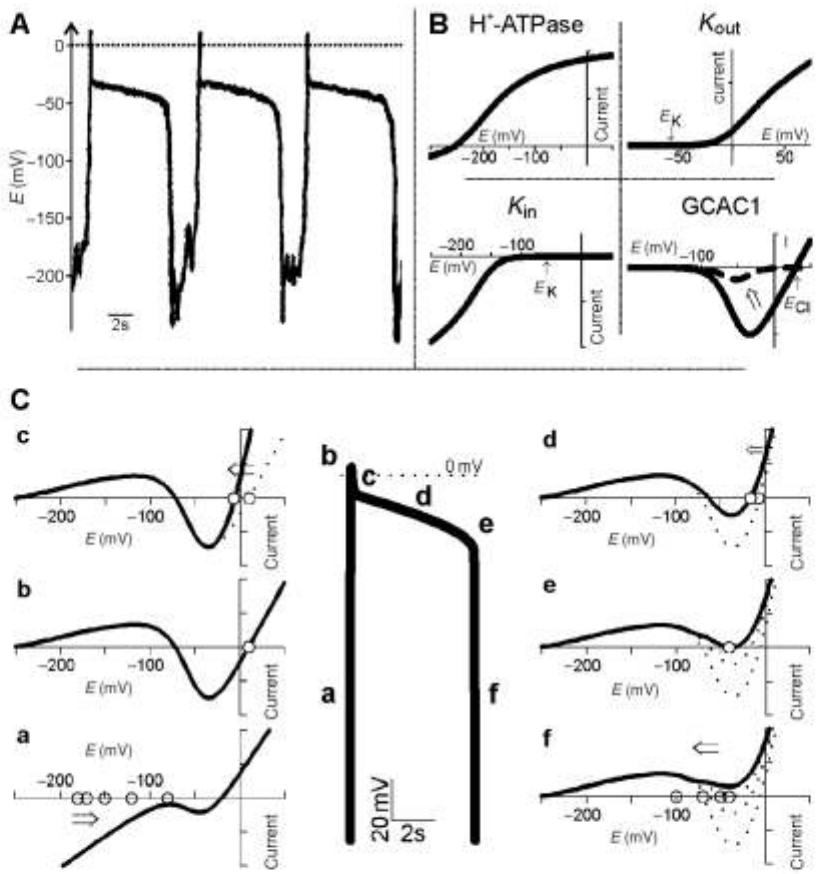

Fig. 6.11 Action potentials in guard cells. (A) In guard cells, membrane potential oscillations have been observed (data provided by G. Thiel, Darmstadt). (B) In computer simulations, the kinetical features of four guard cell plasma membrane ion transporters were combined: the proton H^+-ATPase (*top left*), the K_{out} channel (*top right*), the K_{in} channel (*bottom left*) and the inactivating rapid anion channel GCAC1 (*bottom right*). (C) The shape of computer-simulated action potentials strongly resembles the measured membrane voltage oscillations (compare C, *middle*, with A). The corresponding current–voltage curves at different phases of an action potential (a to f) are explained in the text.

and provoke a slight negative shift of the membrane potential (Fig. 6.11c). Now, a larger Cl^- efflux compensates for both, pumped H^+ and K^+ efflux. Without alterations in the activity of the ion transporters, this condition would remain stable over several minutes. GCAC1, however, inactivates slowly. In the voltage time course this inactivation is visible as a slow slight negative shift of the membrane potential (Fig. 6.11d). The electro-neutral compensation of a reduced Cl^- efflux for K^+ efflux drives the membrane potential to voltages at which K_{out} channels also show a lower

activity (plateau-phase, Fig. 6.11d). The ongoing inactivation of GCAC1 proceeds to an extent that the Cl^- efflux cannot compensate electrically anymore for H^+ and K^+ efflux (Figs. 6.11e and 6.11f). In this case, the current that flows across the membrane is positive. The positive net current induces a rapid membrane hyperpolarisation to voltages more negative than −150 mV (Fig. 6.11f). In the course of this hyperpolarisation, GCAC1 and K_{out} channels deactivate and K_{in} channels activate with a slight delay.

The prediction of the computer model that the inactivating chloride channel plays an important role in membrane potential oscillations was recently supported experimentally (Raschke *et al.*, 2003). Thus, computer models may provide valuable ideas for the understanding of more complex behaviours. At the present time the use of computer models is still an exception. In the future, however, more and detailed computer models are unavoidable. Voltage-gated ion channels, for instance, are entities of 'Ohmic networks', i.e., they are electrically coupled via the transported charges and the voltage-dependent gating. Additionally, the chemical regulation links them to further signalling cascades and even metabolic pathways. Another degree of complexity adds when taking into account that a plant cell is a multicompartment system. The comprehension of this increasing complexity with the increasing knowledge on details is certainly beyond the limits of intuitive qualitative models.

After the reductionistic view in the past, the new beginning epoch in biology research is headlined 'Systems Biology'. Although this terminus is often misinterpreted as the systematic, massive-parallel gathering of data, the aim of systems biology is to understand biological processes as whole systems instead of as isolated parts (Kitano, 2001). This challenging goal can be achieved only by combining experimental, theoretical and modelling techniques. In the past, computational power set limits, and the creation and use of computer models, were restricted to researchers with deeper knowledge in programming. Recent developments helped to overcome these restrictions. Now new computational tools are freely accessible to the scientific community, which also allow less experienced computer users to generate really complex models and to perform computational simulations (Tomita, 2001). Electrophysiological simulations can be combined with metabolic and signalling simulations, and even the inclusion of subcompartments does not cause any problem (in contrast to self-made computer-based models). Two modelling environments should be mentioned here explicitly. The first one is the 'E-Cell Project' developed by the Institute for Advanced Biosciences in Japan (http://www.e-cell.org). And the second one is the Virtual Cell developed by the National Resource for Cell Analysis and Modelling (http://www.nrcam.uchc.edu). With these tools, a first detailed computer model for a plant cell comes some large steps closer.

References

Ache, P., Becker, D., Deeken, R., *et al.* (2001) VFK1, a *Vicia faba* K^+ channel involved in phloem unloading. *Plant J.*, **27**, 571–580.

Ache, P., Becker, D., Ivashikina, N., Dietrich, P., Roelfsema, M.R. & Hedrich, R. (2000) GORK, a delayed outward rectifier expressed in guard cells of *Arabidopsis thaliana*, is a K^+-selective, K^+-sensing ion channel, *FEBS Lett.*, **486**, 93–98.

Aharon, G.S., Gelli, A., Snedden, W.A. & Blumwald, E. (1998) Activation of a plant plasma membrane Ca^{2+} channel by TGalpha1, a heterotrimeric G protein alpha-subunit homologue, *FEBS Lett.*, **424**, 17–21.

Alexandre, J., Lassalles, J.P. & Kado, R.T. (1990) Opening of Ca^{2+} channels in isolated red beet vacuole membrane by inositol 1,4,5-trisphosphate, *Nature*, **343**, 567–570.

Allen, G.J. & Sanders, D. (1994) Two voltage-gated, calcium release channels coreside in the vacuolar membrane of broad bean guard cells, *Plant Cell*, **6**, 685–694.

Allen, G.J. & Sanders, D. (1995) Calcineurin, a type 2B protein phosphatase, modulates the Ca^{2+}-permeable slow vacuolar ion channel of stomatal guard cells, *Plant Cell*, **7**, 1473–1483.

Allen, G.J. & Sanders, D. (1996) Control of ionic currents in guard cell vacuoles by cytosolic and luminal calcium, *Plant J.*, **10**, 1055–1069.

Anderson, J.A., Huprikar, S.S., Kochian, L.V., Lucas, W.J. & Gaber, R.F. (1992) Functional expression of a probable *Arabidopsis thaliana* potassium channel in *Saccharomyces cerevisiae*, *Proc. Natl. Acad. Sci. U.S.A.*, **89**, 3736–3740.

Armstrong, F. & Blatt, M.R. (1995) Evidence for K^+ channel control in *Vicia* guard cells coupled by G-proteins to a 7TMS receptor mimetic, *Plant J.*, **8**, 187–198.

Armstrong, F., Leung, J., Grabov, A., Brearley, J., Giraudat, J. & Blatt, M.R. (1995) Sensitivity to abscisic acid of guard cell K^+ channels is suppressed by *abi1-1*, a mutant *Arabidopsis* gene encoding a putative protein phosphatase, *Proc. Natl. Acad. Sci. U.S.A.*, **92**, 9520–9524.

Assmann, S.M. (2002) Heterotrimeric and unconventional GTP binding proteins in plant cell signaling, *Plant Cell*, **14** (Suppl.), S355–S373.

Assmann, S.M. & Wang, X.Q. (2001) From milliseconds to millions of years: guard cells and environmental responses, *Curr. Opin. Plant Biol.*, **4**, 421–428.

Barbara, J.G., Stoeckel, H. & Takeda, K. (1994) Hyperpolarization-activated inward chloride current in protoplasts from suspension-cultured carrot cells, *Protoplasma*, **180**, 136–144.

Barbier-Brygoo, H., Ephritikhine, G., Klämbt, D., *et al.* (1991) Perception of the auxin signal at the plasma membrane of tobacco mesophyll protoplasts, *Plant J.*, **1**, 83–93.

Barbier-Brygoo, H., Vinauger, M., Colcombet, J., Ephritikhine, G., Frachisse, J.M. & Maurel, C. (2000) Anion channels in higher plants: functional characterization, molecular structure and physiological role, *Biochim. Biophys. Acta*, **1465**, 199–218.

Bauer, C.S., Hoth, S., Haga, K., Philippar, K., Aoki, N. & Hedrich, R. (2000) Differential expression and regulation of K^+ channels in the maize coleoptile: molecular and biophysical analysis of cells isolated from cortex and vasculature, *Plant J.*, **24**, 139–145.

Becker, D., Dreyer, I., Hoth, S., *et al.* (1996) Changes in voltage activation, Cs^+ sensitivity, and ion permeability in H5 mutants of the plant K^+ channel KAT1, *Proc. Natl. Acad. Sci. U.S.A.*, **93**, 8123–8128.

Bertl, A., Blumwald, E., Coronado, R., *et al.* (1992) Electrical measurements on endomembranes, *Science*, **258**, 873–874.

Bethke, P.C. & Jones, R.L. (1994) Ca^{2+}-calmodulin modulates ion channel activity in storage protein vacuoles of barley aleurone cells, *Plant Cell*, **6**, 277–285.

Bethke, P.C. & Jones, R.L. (1997) Reversible protein phosphorylation regulates the activity of the slow-vacuolar ion channel, *Plant J.*, **11**, 1227–1235.

Bewell, M.A., Maathuis, F.J., Allen, G.J. & Sanders, D. (1999) Calcium-induced calcium release mediated by a voltage-activated cation channel in vacuolar vesicles from red beet, *FEBS Lett.*, **458**, 41–44.

Blatt, M.R. (1988) Potassium-dependent bipolar gating of potassium channels in guard cells, *J. Membr. Biol.*, **102**, 235–246.

Blatt, M.R. (1991) Ion channel gating in plants: physiological implications and integration for stomatal function, *J. Membr. Biol.*, **124**, 95–112.

Blatt, M.R. (1992) K^+ channels of stomatal guard cells. Characteristics of the inward rectifier and its control by pH, *J. Gen. Physiol.*, **99**, 615–644.

Blatt, M.R. (2000a) Ca^{2+} signalling and control of guard-cell volume in stomatal movements, *Curr. Opin. Plant Biol.*, **3**, 196–204.

Blatt, M.R. (2000b) Cellular signaling and volume control in stomatal movements in plants, *Annu. Rev. Cell Dev. Biol.*, **16**, 221–241.

Blatt, M.R. & Armstrong, F. (1993) K^+ channels of stomatal guard cells: abscisic-acid-evoked control of the outward rectifier mediated by cytoplasmic pH, *Planta*, **191**, 330–341.

Blatt, M.R. & Gradmann, D. (1997) K^+-sensitive gating of the K^+ outward rectifier in *Vicia* guard cells, *J. Membr. Biol.*, **158**, 241–256.

Blatt, M.R. & Thiel, G. (1993) Hormonal control of ion channel gating, *Annu. Rev. Plant Physiol. Plant Mol. Biol.*, **44**, 543–567.

Blatt, M.R. & Thiel, G. (1994) K^+ channels of stomatal guard cells: bimodal control of the K^+ inward-rectifier evoked by auxin, *Plant J.*, **5**, 55–68.

Blatt, M.R., Thiel, G. & Trentham, D.R. (1990) Reversible inactivation of K^+ channels of *Vicia* stomatal guard cells following the photolysis of caged inositol 1,4,5-trisphosphate, *Nature*, **346**, 766–769.

Bogre, L., Okresz, L., Henriques, R. & Anthony, R.G. (2003) Growth signalling pathways in *Arabidopsis* and the AGC protein kinases, *Trends Plant Sci.*, **8**, 424–431.

Booij, P.P., Roberts, M.R., Vogelzang, S.A., Knaayenhof, R. & de Boer, A.H. (1999) 14-3-3 proteins double the number of outward-rectifying K^+ channels available for activation in tomato cells, *Plant J.*, **20**, 673–683.

Bruggemann, L.I., Dietrich, P., Becker, D., Dreyer, I., Palme, K. & Hedrich, R. (1999a) Channel-mediated high-affinity K^+ uptake into guard cells from *Arabidopsis*, *Proc. Natl. Acad. Sci. U.S.A.*, **96**, 3298–3302.

Bruggemann, L.I., Dietrich, P., Dreyer, I. & Hedrich, R. (1999b) Pronounced differences between the native K^+ channels and KAT1 and KST1 alpha-subunit homomers of guard cells, *Planta*, **207**, 370–376.

Bruggemann, L.I., Pottosin, I.I. & Schonknecht, G. (1999c) Selectivity of the fast activating vacuolar cation channel, *J. Exp. Bot.*, **50**, 873–876.

Bruggemann, L.I., Pottosin, I.I. & Schonknecht, G. (1998) Cytoplasmic polyamines block the fast-activating vacuolar cation channel, *Plant J.*, **16**, 101–105.

Bunney, T.D., van den Wijngaard, P.W., & de Boer, A.H. (2002) 14-3-3 protein regulation of proton pumps and ion channels, *Plant Mol. Biol.*, **50**, 1041–1051.

Carpaneto, A., Cantu, A.M. & Gambale, F. (1999) Redox agents regulate ion channel activity in vacuoles from higher plant cells, *FEBS Lett.*, **442**, 129–132.

Carpaneto, A., Cantu, A.M. & Gambale, F. (2001) Effects of cytoplasmic Mg^{2+} on slowly activating channels in isolated vacuoles of *Beta vulgaris*, *Planta*, **213**, 457–468.

Cerana, R., Giromini, L. & Colombo, R. (1995) Malate-regulated channels permeable to anions in vacuoles of *Arabidopsis thaliana*, *Aust. J. Plant Physiol.*, **22**, 115–121.

Cherel, I., Michard, E., Platet, N., *et al.* (2002) Physical and functional interaction of the *Arabidopsis* K^+ channel AKT2 and phosphatase AtPP2CA, *Plant Cell*, **14**, 1133–1146.

Cho, M.H. & Spalding, E.P. (1996) An anion channel in *Arabidopsis* hypocotyls activated by blue light, *Proc. Natl. Acad. Sci. U.S.A.*, **93**, 8134–8138.

Colcombet, J., Thomine, S., Guern, J., Frachisse, J.M. & Barbier-Brygoo, H. (2001) Nucleotides provide a voltage-sensitive gate for the rapid anion channel of *Arabidopsis* hypocotyl cells, *J. Biol. Chem.*, **276**, 36139–36145.

Colombo, R., Cerana, R., Lado, P. & Peres, A. (1988) Voltage-dependent channels permeable to K^+ and Na^+ in the membrane of *Acer pseudoplatanus* vacuoles, *J. Membr. Biol.*, **103**, 227–236.

Colquhoun, D. & Hawkes, A.G. (1995) The principles of the stochastic interpretation of ion-channel mechanisms, in *Single-Channel Recording*, 2nd edn (eds B. Sakmann & E. Neher), Plenum Press, New York, pp. 397–482.

Coursol, S., Fan, L.M., Le Stunff, H., Spiegel, S., Gilroy, S. & Assmann, S.M. (2003) Sphingolipid signalling in *Arabidopsis* guard cells involves heterotrimeric G proteins, *Nature*, **423**, 651–654.
Czempinski, K., Frachisse, J.M., Maurel, C., Barbier-Brygoo, H. & Mueller-Roeber, B. (2002) Vacuolar membrane localization of the *Arabidopsis* "two-pore" K^+ channel KCO1, *Plant J.*, **29**, 809–820.
Daram, P., Urbach, S., Gaymard, F., Sentenac, H. & Cherel, I. (1997) Tetramerization of the AKT1 plant potassium channel involves its C-terminal cytoplasmic domain, *EMBO J.*, **16**, 3455–3463.
Deeken, R., Geiger, D., Fromm, J., *et al.* (2002) Loss of the AKT2/3 potassium channel affects sugar loading into the phloem of *Arabidopsis*, *Planta*, **216**, 334–344.
Dietrich, P., Dreyer, I., Wiesner, P. & Hedrich, R. (1998) Cation sensitivity and kinetics of guard-cell potassium channels differ among species, *Planta*, **205**, 277–287.
Dietrich, P. & Hedrich, R. (1994) Interconversion of fast and slow gating modes of GCAC1, a guard-cell anion channel, *Planta*, **195**, 301–304.
Dietrich, P. & Hedrich, R. (1998) Anions permeate and gate GCAC1, a voltage-dependent guard cell anion channel, *Plant J.*, **15**, 479–487.
Doyle, D.A., Morais, C.J., Pfuetzner, R.A., *et al.* (1998) The structure of the potassium channel: molecular basis of K^+ conduction and selectivity, *Science*, **280**, 69–77.
Dreyer, I., Antunes, S., Hoshi, T., *et al.* (1997) Plant K^+ channel alpha-subunits assemble indiscriminately, *Biophys. J.*, **72**, 2143–2150.
Dreyer, I., Becker, D., Bregante, M., *et al.* (1998) Single mutations strongly alter the K^+-selective pore of the K_{in} channel KAT1, *FEBS Lett.*, **430**, 370–376.
Dreyer, I. & Hedrich, R. (1996) Action potentials in guard cells – the molecular basis of oscillations, Botanikertagung, 25.8.–31.8., Düsseldorf, Germany, p. P-9.060.
Dreyer, I., Michard, E., Lacombe, B., & Thibaud, J.B. (2001) A plant Shaker-like K^+ channel switches between two distinct gating modes resulting in either inward-rectifying or "leak" current, *FEBS Lett.*, **505**, 233–239.
Edwards, M.C., Smith, G.N. & Bowling, D.J.F. (1988) Guard cells extrude protons prior to stomatal opening. A study using fluorescence microscopy and pH-micro-electrode, *J. Exp. Bot.*, **39**, 1541–1547.
Elzenga, J.T. & Van Volkenburgh, E. (1997) Kinetics of Ca^{2+}- and ATP-dependent, voltage-controlled anion conductance in the plasma membrane of mesophyll cells of *Pisum sativum*, *Planta*, **201**, 415–423.
Fairley-Grenot, K.A. & Assmann, S.M. (1991) Evidence for G-protein regulation of inward K^+ channel current in guard cells of *Fava* bean, *Plant Cell*, **3**, 1037–1044.
Felle, H.H. (1988) Short-term pH regulation in plants, *Physiol. Plant.*, **74**, 583–591.
Frachisse, J.M., Colcombet, J., Guern, J. & Barbier-Brygoo, H. (2000) Characterization of a nitrate-permeable channel able to mediate sustained anion efflux in hypocotyl cells from *Arabidopsis thaliana*, *Plant J.*, **21**, 361–371.
Frachisse, J.M., Thomine, S., Colcombet, J., Guern, J. & Barbier-Brygoo, H. (1999) Sulfate is both a substrate and an activator of the voltage-dependent anion channel of *Arabidopsis* hypocotyl cells, *Plant Physiol.*, **121**, 253–262.
Furuichi, T., Cunningham, K.W. & Muto, S. (2001) A putative two pore channel AtTPC1 mediates Ca^{2+} flux in *Arabidopsis* leaf cells, *Plant Cell Physiol.*, **42**, 900–905.
Gambale, F., Bregante, M., Stragapede, F. & Cantu, A.M. (1996) Ionic channels of the sugar beet tonoplast are regulated by a multi-ion single-file permeation mechanism, *J. Membr. Biol.*, **154**, 69–79.
Garcia-Mata, C., Gay, R., Sokolovski, S., Hills, A., Lamattina, L. & Blatt, M.R. (2003) Nitric oxide regulates K^+ and Cl^- channels in guard cells through a subset of abscisic acid-evoked signaling pathways, *Proc. Natl. Acad. Sci. U.S.A.*, **100**, 11116–11121.
Gaxiola, R.A., Fink, G.R. & Hirschi, K.D. (2002) Genetic manipulation of vacuolar proton pumps and transporters, *Plant Physiol.*, **129**, 967–973.
Gaymard, F., Pilot, G., Lacombe, B., *et al.* (1998) Identification and disruption of a plant shaker-like outward channel involved in K^+ release into the xylem sap, *Cell*, **94**, 647–655.

Gehring, C.A., Irving, H.R. & Parish, R.W. (1990) Effects of auxin and abscisic acid on cytosolic calcium and pH in plant cells, *Proc. Natl. Acad. Sci. U.S.A.*, **87**, 9645–9649.
Gelli, A. & Blumwald, E. (1993) Calcium retrieval from vacuolar pools (characterization of a vacuolar calcium channel), *Plant Physiol.*, **102**, 1139–1146.
Gelli, A. & Blumwald, E. (1997) Hyperpolarization-activated Ca^{2+}-permeable channels in the plasma membrane of tomato cells, *J. Membr. Biol.*, **155**, 35–45.
Gelli, A., Higgins, V.J. & Blumwald, E. (1997) Activation of plant plasma membrane Ca^{2+}-permeable channels by race-specific fungal elicitors, *Plant Physiol.*, **113**, 269–279.
Gilroy, S., Read, N.D. & Trewavas, A.J. (1990) Elevation of cytoplasmic calcium by caged calcium or caged inositol triphosphate initiates stomatal closure, *Nature*, **346**, 769–771.
Glasstone, S., Laidler, K.J. & Eyring, H. (1941) *The Theory of Rate Processes*, McGraw-Hill, New York.
Grabov, A. & Blatt M.R. (1997) Parallel control of the inward-rectifier K^+ channel by cytosolic-free Ca^{2+} and pH in *Vicia* guard cells, *Planta*, **201**, 84–95.
Grabov, A. & Blatt, M.R. (1998a) Co-ordination of signalling elements in guard cell ion channel control, *J. Exp. Bot.*, **49**, 351–360.
Grabov, A. & Blatt, M.R. (1998b) Membrane voltage initiates Ca^{2+} waves and potentiates Ca^{2+} increases with abscisic acid in stomatal guard cells, *Proc. Natl. Acad. Sci. U.S.A.*, **95**, 4778–4783.
Grabov, A. & Blatt, M.R. (1999) A steep dependence of inward-rectifying potassium channels on cytosolic free calcium concentration increase evoked by hyperpolarization in guard cells, *Plant Physiol.*, **119**, 277–288.
Grabov, A., Leung, J., Giraudat, J. & Blatt, M.R. (1997) Alteration of anion channel kinetics in wild-type and *abi1-1* transgenic *Nicotiana benthamiana* guard cells by abscisic acid, *Plant J.*, **12**, 203–213.
Gradmann, D., Blatt, M.R. & Thiel, G. (1993) Electrocoupling of ion transporters in plants, *J. Membr. Biol.*, **136**, 327–332.
Gradmann, D. & Hoffstadt, J. (1998) Electrocoupling of ion transporters in plants: interaction with internal ion concentrations, *J. Membr. Biol.*, **166**, 51–59.
Hafke, J.B., Hafke, Y., Smith, J.A., Luttge, U. & Thiel, G. (2003) Vacuolar malate uptake is mediated by an anion-selective inward rectifier, *Plant J.*, **35**, 116–128.
Hamilton, D.W., Hills, A. & Blatt, M.R. (2001) Extracellular Ba^{2+} and voltage interact to gate Ca^{2+} channels at the plasma membrane of stomatal guard cells, *FEBS Lett.*, **491**, 99–103.
Hamilton, D.W., Hills, A., Kohler, B. & Blatt, M.R. (2000) Ca^{2+} channels at the plasma membrane of stomatal guard cells are activated by hyperpolarization and abscisic acid, *Proc. Natl. Acad. Sci. U.S.A.*, **97**, 4967–4972.
Hechenberger, M., Schwappach, B., Fischer, W.N., Frommer, W.B., Jentsch, T.J. & Steinmeyer, K. (1996) A family of putative chloride channels from *Arabidopsis* and functional complementation of a yeast strain with a CLC gene disruption, *J. Biol. Chem.*, **271**, 33632–33638.
Hedrich, R., Busch, H. & Raschke, K. (1990) Ca^{2+} and nucleotide dependent regulation of voltage dependent anion channels in the plasma membrane of guard cells, *EMBO J.*, **9**, 3889–3892.
Hedrich, R. & Kurkdjian, A. (1988) Characterization of an anion-permeable channel from sugar beet vacuoles: effect of inhibitors, *EMBO J.*, **7**, 3661–3666.
Hedrich, R. & Marten, I. (1993) Malate-induced feedback regulation of plasma membrane anion channels could provide a CO_2 sensor to guard cells, *EMBO J.*, **12**, 897–901.
Hedrich, R., Marten, I., Lohse, G., *et al.* (1994) Malate-sensitive anion channels enable guard cells to sense changes in the ambient CO_2 concentration, *Plant J.*, **6**, 741–748.
Hedrich, R., Moran, O., Conti, F., *et al.* (1995) Inward rectifier potassium channels in plants differ from their animal counterparts in response to voltage and channel modulators, *Eur. Biophys. J.*, **24**, 107–115.
Hedrich, R. & Neher, E. (1987) Cytoplasmic calcium regulates voltage-dependent ion channels in plant vacuoles, *Nature*, **329**, 833–835.
Hodgkin, A.L. & Huxley, A.F. (1952) A quantitative description of membrane current and its application to conduction and excitation in nerve, *J. Physiol.*, **117**, 500–544.

Hoshi, T. (1995) Regulation of voltage dependence of the KAT1 channel by intracellular factors, *J. Gen. Physiol.*, **105**, 309–328.

Hosoi, S., Lino, M. & Shimozaki, K. (1988) Outward-rectifying K^+ channels in stomatal guard cell protoplasts, *Plant Cell Physiol.*, **29**, 907–911.

Hosy, E., Vavasseur, A., Mouline, K., *et al.* (2003) The *Arabidopsis* outward K^+ channel GORK is involved in regulation of stomatal movements and plant transpiration, *Proc. Natl. Acad. Sci. U.S.A.*, **100**, 5549–5554.

Hoth, S., Dreyer, I., Dietrich, P., Becker, D., Mueller-Roeber, B. & Hedrich, R. (1997) Molecular basis of plant-specific acid activation of K^+ uptake channels, *Proc. Natl. Acad. Sci. U.S.A.*, **94**, 4806–4810.

Ilan, N., Schwartz, A. & Moran, N. (1994) External pH effects on the depolarization-activated K channels in guard cell protoplasts of *Vicia faba*, *J. Gen. Physiol.*, **103**, 807–831.

Irving, H.R., Gehring, C.A. & Parish, R.W. (1992) Changes in cytosolic pH and calcium of guard cells precede stomatal movements, *Proc. Natl. Acad. Sci. U.S.A.*, **89**, 1790–1794.

Iwasaki, I., Arata, H., Kijima, H. & Nishimura, M. (1992) Two types of channels involved in the malate ion transport across the tonoplast of a crassulacean acid metabolism plant, *Plant Physiol.*, **98**, 1494–1497.

Jiang, Y., Lee, A., Chen, J., *et al.* (2003) X-ray structure of a voltage-dependent K^+ channel, *Nature*, **423**, 33–41.

Johannes, E., Brosnan, J.M. & Sanders, D. (1992) Parallel pathways for intracellular Ca^{2+} release from the vacuole of higher plants, *Plant J.*, **2**, 97–102.

Johannes, E. & Sanders, D. (1995) Lumenal calcium modulates unitary conductance and gating of a plant vacuolar calcium release channel, *J. Membr. Biol.*, **146**, 211–224.

Kaldewey, H. (1976) Considerations of geotropism in plants, *Life Sci. Space Res.*, **14**, 21–36.

Keller, B.U., Hedrich, R. & Raschke, K. (1989) Voltage-dependent anion channels in the plasma-membrane of guard-cells, *Nature*, **341**, 450–453.

Kelly, W.B., Esser, J.E. & Schroeder, J.I. (1995) Effects of cytosolic calcium and limited, possible dual, effects of G protein modulators on guard cell inward potassium channels, *Plant J.*, **8**, 479–489.

Kiegle, E., Gilliham, M., Haseloff, J. & Tester, M. (2000) Hyperpolarisation-activated calcium currents found only in cells from the elongation zone of *Arabidopsis thaliana* roots, *Plant J.*, **21**, 225–229.

Kitano, H. (2001) *Foundations of Systems Biology*, 1st edn, The MIT Press, Cambridge, MA.

Klusener, B., Boheim, G., Liss, H., Engelberth, J. & Weiler, E.W. (1995) Gadolinium-sensitive, voltage-dependent calcium release channels in the endoplasmic reticulum of a higher plant mechanoreceptor organ, *EMBO J.*, **14**, 2708–2714.

Klusener, B., Boheim, G. & Weiler, E.W. (1997) Modulation of the ER Ca^{2+} channel BCC1 from tendrils of *Bryonia dioica* by divalent cations, protons and H_2O_2, *FEBS Lett.*, **407**, 230–234.

Klusener, B. & Weiler, E.W. (1999) A calcium-selective channel from root-Tip endomembranes of garden cress, *Plant Physiol.*, **119**, 1399–1406.

Klusener, B., Young, J.J., Murata, Y., *et al.* (2002) Convergence of calcium signaling pathways of pathogenic elicitors and abscisic acid in *Arabidopsis* guard cells, *Plant Physiol.*, **130**, 2152–2163.

Kohler, B. & Blatt, M.R. (2002) Protein phosphorylation activates the guard cell Ca^{2+} channel and is a prerequisite for gating by abscisic acid, *Plant J.*, **32**, 185–194.

Kohler, B., Hills, A. & Blatt, M.R. (2003) Control of guard cell ion channels by hydrogen peroxide and abscisic acid indicates their action through alternate signaling pathways, *Plant Physiol.*, **131**, 385–388.

Köhler, B. & Raschke, K. (2000) The delivery of salts to the xylem. Three types of anion conductance in the plasmalemma of the xylem parenchyma of roots of barley, *Plant Physiol.*, **122**, 243–254.

Köhler, B., Wegner, L.H., Osipov, V. & Raschke, K. (2002) Loading of nitrate into the xylem: apoplastic nitrate controls the voltage dependence of X-QUAC, the main anion conductance in xylem-parenchyma cells of barley roots, *Plant J.*, **30**, 133–142.

Kolb, H.A., Kohler, K. & Martinoia, E. (1987) Single potassium in the membrane of isolated mesophyll barley vacuoles, *J. Membr. Biol.*, **95**, 163–169.

Kollmeier, M., Dietrich, P., Bauer, C.S., Horst, W.J. & Hedrich, R. (2001) Aluminum activates a citrate-permeable anion channel in the aluminum-sensitive zone of the maize root apex. A comparison between an aluminum-sensitive and an aluminum-resistant cultivar, *Plant Physiol.*, **126**, 397–410.

Krawczyk, S. (1978) Ionic channel formation in a living cell membrane, *Nature*, **273**, 56–57.

Krol, E. & Trebacz, K. (2000) Ways of ion channel gating in plant cells, *Ann. Bot. (Lond.)*, **86**, 449–469.

Lacombe, B., Pilot, G., Michard, E., Gaymard, F., Sentenac, H. & Thibaud, J.B. (2000) A shaker-like K^+ channel with weak rectification is expressed in both source and sink phloem tissues of *Arabidopsis*, *Plant Cell*, **12**, 837–851.

Lagarde, D., Basset, M., Lepetit, M., *et al.* (1996) Tissue-specific expression of *Arabidopsis* AKT1 gene is consistent with a role in K^+ nutrition, *Plant J.*, **9**, 195–203.

Lee, Y., Lee, H.J., Crain, R.C., Lee, A. & Korn, S.J. (1994) Polyunsaturated fatty acids modulate stomatal aperture and two distinct K^+ channel currents in guard cells, *Cell. Signal.*, **6**, 181–186.

Leigh, R.A. & Wyn Jones, R.G. (1984) A hypothesis relating critical potassium concentrations for growth to the distribution and functions of this ion in the plant cell, *New Phytol.*, **97**, 1–13.

Lemtiri-Chlieh, F. & MacRobbie, E.A. (1994) Role of calcium in the modulation of *Vicia* guard cell potassium channels by abscisic acid: a patch-clamp study, *J. Membr. Biol.*, **137**, 99–107.

Lemtiri-Chlieh, F., MacRobbie, E.A. & Brearley, C.A. (2000) Inositol hexakisphosphate is a physiological signal regulating the K^+-inward rectifying conductance in guard cells, *Proc. Natl. Acad. Sci. U.S.A.*, **97**, 8687–8692.

Lemtiri-Chlieh, F., MacRobbie, E.A., Webb, A.A., *et al.* (2003) Inositol hexakisphosphate mobilizes an endomembrane store of calcium in guard cells, *Proc. Natl. Acad. Sci. U.S.A.*, **100**, 10091–10095.

Leonhardt, N., Vavasseur, A. & Forestier, C. (1999) ATP binding cassette modulators control abscisic acid-regulated slow anion channels in guard cells, *Plant Cell*, **11**, 1141–1152.

Leyser, O. (2002) Molecular genetics of auxin signaling, *Annu. Rev. Plant Biol.*, **53**, 377–398.

Li, J. & Assmann, S.M. (1996) An abscisic acid-activated and calcium-independent protein kinase from guard cells of *Fava* bean, *Plant Cell*, **8**, 2359–2368.

Li, J., Lee, Y.R. & Assmann, S.M. (1998) Guard cells possess a calcium-dependent protein kinase that phosphorylates the KAT1 potassium channel, *Plant Physiol.*, **116**, 785–795.

Li, J., Wang, X.Q., Watson, M.B. & Assmann, S.M. (2000) Regulation of abscisic acid-induced stomatal closure and anion channels by guard cell AAPK kinase, *Science*, **287**, 300–303.

Li, W. & Assmann, S.M. (1993) Characterization of a G-protein-regulated outward K^+ current in mesophyll cells of *Vicia faba* L., *Proc. Natl. Acad. Sci. U.S.A.*, **90**, 262–266.

Li, W., Luan, S., Schreiber, S.L. & Assmann, S.M. (1994) Evidence for protein phosphatase 1 and 2A regulation of K^+ channels in two types of leaf cells, *Plant Physiol.*, **106**, 963–970.

Linder, B. & Raschke, K. (1992) A slow anion channel in guard-cells, activating at large hyperpolarization, may be principal for stomatal closing, *FEBS Lett.*, **313**, 27–30.

Luan, S., Kudla, J., Rodriguez-Concepcion, M., Yalovsky, S. & Gruissem, W. (2002) Calmodulins and calcineurin B-like proteins: calcium sensors for specific signal response coupling in plants, *Plant Cell*, **14** (Suppl.), S389–S400.

Luan, S., Li, W., Rusnak, F., Assmann, S.M. & Schreiber, S.L. (1993) Immunosuppressants implicate protein phosphatase regulation of K^+ channels in guard-cells, *Proc. Natl. Acad. Sci. U.S.A.*, **90**, 2202–2206.

Luttge, U., Pfeifer, T., Fischer-Schliebs, E. & Ratajczak, R. (2000) The role of vacuolar malate-transport capacity in crassulacean acid metabolism and nitrate nutrition. Higher malate-transport capacity in ice plant after crassulacean acid metabolism-induction and in tobacco under nitrate nutrition, *Plant Physiol.*, **124**, 1335–1348.

Maathuis, F.J., Ichida, A.M., Sanders, D. & Schroeder, J.I. (1997) Roles of higher plant K^+ channels, *Plant Physiol.*, **114**, 1141–1149.

Maathuis, F.J. & Sanders, D. (1995) Contrasting roles in ion transport of two K^+-channel types in root cells of *Arabidopsis thaliana*, *Planta*, **197**, 456–464.

MacRobbie, E.A. (1998) Signal transduction and ion channels in guard cells, *Philos. Trans. R. Soc. Lond. B Biol. Sci.*, **353**, 1475–1488.

Maeshima, M. (2001) Tonoplast transporters: organization and function, *Annu. Rev. Plant Physiol. Plant Mol. Biol.*, **52**, 469–497.

Marten, I., Hoth, S., Deeken, R., *et al.* (1999) AKT3, a phloem-localized K^+ channel, is blocked by protons, *Proc. Natl. Acad. Sci. U.S.A.*, **96**, 7581–7586.

Marten, I., Lohse, G. & Hedrich, R. (1991) Plant growth hormones control voltage-dependent activity of anion channels in plasma membrane of guard cells, *Nature*, **353**, 758–762.

Martinoia, E., Massonneau, A. & Frangne, N. (2000) Transport processes of solutes across the vacuolar membrane of higher plants, *Plant Cell Physiol.*, **41**, 1175–1186.

McAinsh, M.R., Brownlee, C. & Hetherington, A.M. (1990) Abscisic acid-induced elevation of guard cell cytosolic Ca^{2+} precedes stomatal closure, *Nature*, **343**, 186–188.

Miedema, H. & Assmann, S.M. (1996) A membrane-delimited effect of internal pH on the K^+ outward rectifier of *Vicia faba* guard cells, *J. Membr. Biol.*, **154**, 227–237.

Miedema, H., Bothwell, J.H., Brownlee, C. & Davies, J.M. (2001) Calcium uptake by plant cells – channels and pumps acting in concert, *Trends Plant Sci.*, **6**, 514–519.

Miedema, H. & Pantoja, O. (2001) Anion modulation of the slowly activating vacuolar channel, *J. Membr. Biol.*, **183**, 137–145.

Moran, N. (1996) Membrane-delimited phosphorylation enables the activation of the outward-rectifying K channels in motor cell protoplasts of *Samanea saman*, *Plant Physiol.*, **111**, 1281–1292.

Moran, N., Ehrenstein, G., Iwasa, K., Bare, C. & Mischke, C. (1984) Ion channels in plasmalemma of wheat protoplasts, *Science*, **226**, 835–838.

Mouline, K., Very, A.A., Gaymard, F., *et al.* (2002) Pollen tube development and competitive ability are impaired by disruption of a Shaker K(+) channel in *Arabidopsis*, *Genes Dev.*, **16**, 339–350.

Mueller-Roeber, B., Ellenberg, J., Provart, N., *et al.* (1995) Cloning and electrophysiological analysis of KST1, an inward rectifying K^+ channel expressed in potato guard cells, *EMBO J.*, **14**, 2409–2416.

Mueller-Roeber, B. & Pical, C. (2002) Inositol phospholipid metabolism in *Arabidopsis*. Characterized and putative isoforms of inositol phospholipid kinase and phosphoinositide-specific phospholipase C, *Plant Physiol.*, **130**, 22–46.

Murata, Y., Pei, Z.M., Mori, I.C. & Schroeder, J.I. (2001) Abscisic acid activation of plasma membrane Ca^{2+} channels in guard cells requires cytosolic NAD(P)H and is differentially disrupted upstream and downstream of reactive oxygen species production in *abi1-1* and *abi2-1* protein phosphatase 2C mutants, *Plant Cell*, **13**, 2513–2523.

Nakamura, R.L., Anderson, J.A. & Gaber, R.F. (1997) Determination of key structural requirements of a K^+ channel pore, *J. Biol. Chem.*, **272**, 1011–1018.

Nakamura, R.L., McKendree, W.L., Hirsch, R.E., Sedbrook, J.C., Gaber, R.F. & Sussman, M.R. (1995) Expression of an *Arabidopsis* potassium channel gene in guard-cells, *Plant Physiol.*, **109**, 371–374.

Neher, E. & Sakmann, B. (1976) Single-channel currents recorded from membrane of denervated frog muscle fibres, *Nature*, **260**, 799–802.

Ng, C.K., Carr, K., McAinsh, M.R., Powell, B. & Hetherington, A.M. (2001) Drought-induced guard cell signal transduction involves sphingosine-1-phosphate, *Nature*, **410**, 596–599.

Noda, M., Shimizu, S., Tanabe, T., *et al.* (1984) Primary structure of *Electrophorus electricus* sodium channel deduced from cDNA sequence, *Nature*, **312**, 121–127.

Pantoja, O., Gelli, A. & Blumwald, E. (1992a) Characterization of vacuolar malate and K^+ channels under physiological conditions, *Plant Physiol*, **100**, 1137–1141.

Pantoja, O., Gelli, A. & Blumwald, E. (1992b) Voltage-dependent calcium channels in plant vacuoles, *Science*, **255**, 1567–1570.

Pantoja, O. & Smith, J.A. (2002) Sensitivity of the plant vacuolar malate channel to pH, Ca^{2+} and anion-channel blockers, *J. Membr. Biol.*, **186**, 31–42.

Pei, Z.M., Murata, Y., Benning, G., *et al.* (2000) Calcium channels activated by hydrogen peroxide mediate abscisic acid signalling in guard cells, *Nature*, **406**, 731–734.

Pei, Z.M., Ward, J.M., Harper, J.F. & Schroeder, J.I. (1996) A novel chloride channel in *Vicia faba* guard cell vacuoles activated by the serine/threonine kinase, CDPK, *EMBO J.*, **15**, 6564–6574.

Pei, Z.M., Ward, J.M. & Schroeder, J.I. (1999) Magnesium sensitizes slow vacuolar channels to physiological cytosolic calcium and inhibits fast vacuolar channels in *Fava* bean guard cell vacuoles, *Plant Physiol.*, **121**, 977–986.

Perozo, E., MacKinnon, R., Bezanilla, F. & Stefani, E. (1993) Gating currents from a nonconducting mutant reveal open-closed conformations in Shaker K^+ channels, *Neuron*, **11**, 353–358.

Philippar, K., Fuchs, I., Luthen, H., *et al.* (1999) Auxin-induced K^+ channel expression represents an essential step in coleoptile growth and gravitropism, *Proc. Natl. Acad. Sci. U.S.A.*, **96**, 12186–12191.

Pilot, G., Lacombe, B., Gaymard, F., *et al.* (2001) Guard cell inward K^+ channel activity in *Arabidopsis* involves expression of the twin channel subunits KAT1 and KAT2, *J. Biol. Chem.*, **276**, 3215–3221.

Pineros, M.A., Magalhaes, J.V., Carvalho, A.V. & Kochian, L.V. (2002) The physiology and biophysics of an aluminum tolerance mechanism based on root citrate exudation in maize, *Plant Physiol.*, **129**, 1194–1206.

Pineros, M. & Tester, M. (1997) Calcium channels in higher plant cells: selectivity, regulation and pharmacology, *J. Exp. Bot.*, **48**, 551–577.

Plant, P.J., Gelli, A. & Blumwald, E. (1994) Vacuolar chloride regulation of an anion-selective tonoplast channel, *J. Membr. Biol.*, **140**, 1–12.

Pottosin, I.I. & Martinez-Estevez, M. (2003) Regulation of the fast vacuolar channel by cytosolic and vacuolar potassium, *Biophys. J.*, **84**, 977–986.

Pottosin, I.I., Martinez-Estevez, M., Dobrovinskaya, O.R. & Muniz, J. (2003) Potassium-selective channel in the red beet vacuolar membrane, *J. Exp. Bot.*, **54**, 663–667.

Pottosin, I.I., Tikhonova, L.I., Hedrich, R. & Schonknecht, G. (1997) Slowly activating vacuolar channels can not mediate Ca^{2+}-induced Ca^{2+} release, *Plant J.*, **12**, 1387–1398.

Pusch, M. (2004) Structural insights into chloride and proton-mediated gating of CLC chloride channels, *Biochemistry*, **43**, 1135–1144.

Raschke, K. (2003) Alternation of the slow with the quick anion conductance in whole guard cells effected by external malate, *Planta*, **217**, 651–657.

Raschke, K., Shabahang, M. & Wolf, R. (2003) The slow and the quick anion conductance in whole guard cells: their voltage-dependent alternation, and the modulation of their activities by abscisic acid and CO_2, *Planta*, **271**, 639–650.

Rea, P.A. & Sanders, D. (1987) Tonoplast energization: two pumps, one membrane, *Physiol. Plant.*, **71**, 131–141.

Reintanz, B., Szyroki, A., Ivashikina, N., *et al.* (2002) AtKC1, a silent *Arabidopsis* potassium channel alpha-subunit modulates root hair K+ influx, *Proc. Natl. Acad. Sci. U.S.A.*, **99**, 4079–4084.

Roberts, M.R. (2003) 14-3-3 proteins find new partners in plant cell signalling, *Trends Plant Sci.*, **8**, 218–223.

Roelfsema, M.R. & Prins, H.B. (1998) The membrane potential of *Arabidopsis thaliana* guard cells; depolarizations induced by apoplastic acidification, *Planta*, **205**, 100–112.

Ryan, P.R., Skerrett, M., Findlay, G.P., Delhaize, E. & Tyerman, S.D. (1997) Aluminum activates an anion channel in the apical cells of wheat roots, *Proc. Natl. Acad. Sci. U.S.A.*, **94**, 6547–6552.

Saalbach, G., Schwendel, M., Natura, G., Buschmann, P., Christov, V. & Dahse, I. (1997) Over-expression of plant 14-3-3 proteins in tobacco: enhancement of the plasmalemma K^+ conductance of mesophyll cells, *FEBS Lett.*, **413**, 294–298.

Sanders, D., Brownlee, C. & Harper, J.F. (1999) Communicating with calcium, *Plant Cell*, **11**, 691–706.

Sanders, D., Pelloux, J., Brownlee, C. & Harper, J.F. (2002) Calcium at the crossroads of signaling, *Plant Cell*, **14** (Suppl.), S401–S417.

Sather, W.A. & McCleskey, E.W. (2003) Permeation and selectivity in calcium channels, *Annu. Rev. Physiol.*, **65**, 133–159.

Schauf, C.L. & Wilson, K.J. (1987) Properties of single K^+ and Cl^- channels in *Asclepias tuberosa* protoplasts, *Plant Physiol.*, **85**, 413–418.

Schmidt, C., Schelle, I., Liao, Y.J. & Schroeder, J.I. (1995) Strong regulation of slow anion channels and abscisic acid signaling in guard cells by phosphorylation and dephosphorylation events, *Proc. Natl. Acad. Sci. U.S.A.*, **92**, 9535–9539.

Schonknecht, G., Spoormaker, P., Steinmeyer, R., *et al.* (2002) KCO1 is a component of the slow-vacuolar (SV) ion channel, *FEBS Lett.*, **511**, 28–32.
Schroeder, J.I. (1988) K^+ transport properties of K^+ channels in the plasma membrane of *Vicia faba* guard cells, *J. Gen. Physiol.*, **92**, 667–683.
Schroeder, J.I., Allen, G.J., Hugouvieux, V., Kwak, J.M. & Waner, D. (2001) Guard cell signal transduction, *Annu. Rev. Plant Physiol. Plant Mol. Biol.*, **52**, 627–658.
Schroeder, J.I. & Hagiwara, S. (1989) Cytosolic calcium regulates ion channels in the plasma membrane of *Vicia faba* guard cells, *Nature*, **338**, 427–430.
Schroeder, J.I. & Hagiwara, S. (1990) Repetitive increases in cytosolic Ca^{2+} of guard cells by abscisic acid activation of nonselective Ca^{2+} permeable channels, *Proc. Natl. Acad. Sci. U.S.A.*, **87**, 9305–9309.
Schroeder, J.I., Hedrich, R. & Fernandez, J.M. (1984) Potassium-selective single channels in guard cell protoplasts of *Vicia faba*, *Nature*, **312**, 361–362.
Schroeder, J.I. & Keller, B.U. (1992) Two types of anion channel currents in guard cells with distinct voltage regulation, *Proc. Natl. Acad. Sci. U.S.A.*, **89**, 5025–5029.
Schroeder, J.I., Raschke, K. & Neher, E. (1987) Voltage dependence of K^+ channels in guard-cell protoplasts, *Proc. Natl. Acad. Sci. U.S.A.*, **84**, 4108–4112.
Schulz-Lessdorf, B. & Hedrich, R. (1995) Protons and calcium modulate SV-type channels in the vacuolar-lysosomal compartment – channel interaction with calmodulin inhibitors, *Planta*, **197**, 655–671.
Schulz-Lessdorf, B., Lohse, G. & Hedrich, R. (1996) GCAC1 recognizes the pH gradient across the plasma membrane: a pH-sensitive and ATP-dependent anion channel links guard cell membrane potential to acid and energy metabolism, *Plant J.*, **10**, 993–1004.
Sentenac, H., Bonneaud, N., Minet, M., *et al.* (1992) Cloning and expression in yeast of a plant potassium ion transport system, *Science*, **256**, 663–665.
Skerrett, M. & Tyerman, S.D. (1994) A channel that allows inwardly directed fluxes of anions in protoplasts derived from wheat roots, *Planta*, **192**, 295–305.
Spalding, E.P., Slayman, C.L., Goldsmith, M., Gradmann, D. & Bertl, A. (1992) Ion channels in *Arabidopsis* plasma membrane – transport characteristics and involvement in light-induced voltage changes, *Plant Physiol.*, **99**, 96–102.
Stevens, C.F. (1978) Interactions between intrinsic membrane protein and electric field. An approach to studying nerve excitability, *Biophys. J.*, **22**, 295–306.
Stoelzle, S., Kagawa, T., Wada, M., Hedrich, R. & Dietrich, P. (2003) Blue light activates calcium-permeable channels in *Arabidopsis* mesophyll cells via the phototropin signaling pathway, *Proc. Natl. Acad. Sci. U.S.A.*, **100**, 1456–1461.
Szyroki, A., Ivashikina, N., Dietrich, P., *et al.* (2001) KAT1 is not essential for stomatal opening, *Proc. Natl. Acad. Sci. U.S.A.*, **98**, 2917–2921.
Terry, B.R., Tyerman, S.D. & Findlay, G.P. (1991) Ion channels in the plasma membrane of *Amaranthus* protoplasts: one cation and one anion channel dominate the conductance, *J. Membr. Biol.*, **121**, 223–236.
Thiel, G. & Blatt, M.R. (1994) Phosphatase antagonist okadaic acid inhibits steady-state K^+ currents in guard-cells of *Vicia faba*, *Plant J.*, **5**, 727–733.
Thiel, G., Blatt, M.R., Fricker, M.D., White, I.R. & Millner, P. (1993) Modulation of K^+ channels in *Vicia* stomatal guard cells by peptide homologs to the auxin-binding protein C terminus, *Proc. Natl. Acad. Sci. U.S.A.*, **90**, 11493–11497.
Thiel, G., MacRobbie, E.A. & Blatt, M.R. (1992) Membrane transport in stomatal guard cells: the importance of voltage control, *J. Membr. Biol.*, **126**, 1–18.
Thomine, S., Guern, J. & Barbier-Brygoo, H. (1997) Voltage-dependent anion channel of *Arabidopsis* hypocotyls: nucleotide regulation and pharmacological properties, *J. Membr. Biol.*, **159**, 71–82.
Thomine, S., Zimmermann, S., Guern, J. & Barbier-Brygoo, H. (1995) ATP-dependent regulation of an anion channel at the plasma membrane of protoplasts from epidermal cells of *Arabidopsis* hypocotyls, *Plant Cell*, **7**, 2091–2100.

Thuleau, P., Moreau, M., Schroeder, J.I. & Ranjeva, R. (1994a) Recruitment of plasma membrane voltage-dependent calcium-permeable channels in carrot cells, *EMBO J.*, **13**, 5843–5847.
Thuleau, P., Ward, J.M., Ranjeva, R. & Schroeder, J.I. (1994b) Voltage-dependent calcium-permeable channels in the plasma membrane of a higher plant cell, *EMBO J.*, **13**, 2970–2975.
Tikhonova, L.I., Pottosin, I.I., Dietz, K.J. & Schonknecht, G. (1997) Fast-activating cation channel in barley mesophyll vacuoles. Inhibition by calcium, *Plant J.*, **11**, 1059–1070.
Tomita, M. (2001) Whole-cell simulation: a grand challenge of the 21st century, *Trends Biotechnol.*, **19**, 205–210.
Trewavas, A.J. & Malho, R. (1998) Ca^{2+} signalling in plant cells: the big network!, *Curr. Opin. Plant Biol.*, **1**, 428–433.
Uozumi, N., Gassmann, W., Cao, Y. & Schroeder, J.I. (1995) Identification of strong modifications in cation selectivity in an *Arabidopsis* inward rectifying potassium channel by mutant selection in yeast, *J. Biol. Chem.*, **270**, 24276–24281.
Uozumi, N., Nakamura, T., Schroeder, J.I. & Muto, S. (1998) Determination of transmembrane topology of an inward-rectifying potassium channel from *Arabidopsis thaliana* based on functional expression in *Escherichia coli*, *Proc. Natl. Acad. Sci. U.S.A.*, **95**, 9773–9778.
van den Wijngaard, P.W., Bunney, T.D., Roobeek, I., Schonknecht, G. & de Boer, A.H. (2001) Slow vacuolar channels from barley mesophyll cells are regulated by 14-3-3 proteins, *FEBS Lett.*, **488**, 100–104.
Very, A.A. & Davies, J.M. (2000) Hyperpolarization-activated calcium channels at the tip of *Arabidopsis* root hairs, *Proc. Natl. Acad. Sci. U.S.A.*, **97**, 9801–9806.
Very, A.A. & Sentenac, H. (2002) Cation channels in the *Arabidopsis* plasma membrane, *Trends Plant Sci.*, **7**, 168–175.
Very, A.A. & Sentenac, H. (2003) Molecular mechanisms and regulation of K^+ transport in higher plants, *Annu. Rev. Plant Biol.*, **54**, 575–603.
Walker, D.J., Leigh, R.A. & Miller, A.J. (1996) Potassium homeostasis in vacuolate plant cells, *Proc. Natl. Acad. Sci. U.S.A.*, **93**, 10510–10514.
Wang, X.Q., Ullah, H., Jones, A.M. & Assmann, S.M. (2001) G protein regulation of ion channels and abscisic acid signaling in *Arabidopsis* guard cells, *Science*, **292**, 2070–2072.
Wang, X.Q., Wu, W.H. & Assmann, S.M. (1998) Differential responses of abaxial and adaxial guard cells of broad bean to abscisic acid and calcium, *Plant Physiol.*, **118**, 1421–1429.
Ward, J.M. & Schroeder, J.I. (1994) Calcium-activated K^+ channels and calcium-induced calcium release by slow vacuolar ion channels in guard cell vacuoles implicated in the control of stomatal closure, *Plant Cell*, **6**, 669–683.
Weber, H. (2002) Fatty acid-derived signals in plants, *Trends Plant Sci.*, **7**, 217–224.
Wegner, L.H. & de Boer, A.H. (1997) Two inward K^+ channels in the xylem parenchyma cells of barley roots are regulated by G-protein modulators through a membrane-delimited pathway, *Planta*, **203**, 506–516.
Weiser, T., Blum, W. & Bentrup, F.W. (1991) Calmodulin regulates the Ca^{2+}-dependent slow-vacuolar ion channel in the tonoplast of *Chenopodium rubrum* suspension cells, *Planta*, **185**, 440–442.
White, P.J. (1998) Calcium channels in the plasma membrane of root cells, *Ann. Bot. (Lond.)*, **81**, 173–183.
White, P.J. (2000) Calcium channels in higher plants, *Biochim. Biophys. Acta*, **1465**, 171–189.
White, P.J., Bowen, H., Demidchik, V., Nichols, C. & Davies, J. (2002) Genes for calcium-permeable channels in the plasma membrane of plant root cells, *Biochim. Biophys. Acta*, **1564**, 299.
White, P.J. & Broadley, M.R. (2001) Chloride in soils and its uptake and movement within the plant: a review, *Ann. Bot.*, **88**, 967–988.
Worrall, D., Ng, C.K. & Hetherington, A.M. (2003) Sphingolipids, new players in plant signaling, *Trends Plant Sci.*, **8**, 317–320.
Wu, W.H. & Assmann, S.M. (1994) A membrane-delimited pathway of G-protein regulation of the guard-cell inward K^+ channel, *Proc. Natl. Acad. Sci. U.S.A.*, **91**, 6310–6314.

Zhang, W.H., Skerrett, M., Walker, N.A., Patrick, J.W. & Tyerman, S.D. (2002) Nonselective currents and channels in plasma membranes of protoplasts from coats of developing seeds of bean, *Plant Physiol.*, **128**, 388–399.

Zhou, Y., Morais-Cabral, J.H., Kaufman, A. & MacKinnon, R. (2001) Chemistry of ion coordination and hydration revealed by a K^+ channel-Fab complex at 2.0 A resolution, *Nature*, **414**, 43–48.

Zimmermann, S., Thomine, S., Guern, J. & Barbier-Brygoo, H. (1994) An anion current at the plasma membrane of tobacco protoplasts shows ATP-dependent voltage regulation and is modulated by auxin, *Plant J.*, **6**, 707–716.